Following the trails of India's Atmospheric Lead (Pb): Source Identification, Apportionment, Bioavailability and Remediation

THESIS SUBMITTED

FOR THE DEGREE OF

DOCTOR OF PHILOSOPHY (ENGINEERING)

To

JADAVPUR UNIVERSITY

2025

By

IRAVATI RAY

Registration No.: 1022220001 of 2022

SCHOOL OF ENVIRONMENTAL STUDIES

JADAVPUR UNIVERSITY, KOLKATA: 700032, INDIA

To

The Periodic Table,

The map of elements

And

To

Professor Clair Patterson,

Who uncovered the perilous stories of Pb

Details of Thesis

1. **Index No. and Date of Registration:** 1022220001 registered on March 3, 2022
2. **Title of the Thesis:** Following the trails of India's Atmospheric Lead (Pb): Source Identification, Apportionment, Bioavailability and Remediation
3. **Name, Designation of the Supervisors**: (i) **Dr. Reshmi Das**

UGC Assistant Professor

School of Environmental Studies

Jadavpur University

Kolkata-700032, India

(ii) Dr. Sambuddha Misra

Associate Professor

Centre for Earth Sciences

Indian Institute of Science

Bangalore-560012, India

1. **E-mail ID of the Supervisors:** reshmidas.sest@jadavpuruniversity.in; sambuddha@iisc.ac.in
2. **List of Publications:**

a) Publications related to Doctoral work:

i. **Ray, Iravati**, Reshmi Das, Song Lin Chua, and Xianfeng Wang. "Seasonal variation of atmospheric Pb sources in Singapore-Elemental and lead isotopic compositions of PM10 as source tracer." *Chemosphere* 307 (2022): 136029. Doi: https://doi.org/10.1016/j.chemosphere.2022.136029

ii. **Ray, Iravati**, and Reshmi Das. "A lingering legacy of leaded gasoline in Southeast Asia." *Communications Earth & Environment* 4, no. 1 (2023): 468. Doi: https://doi.org/10.1038/s43247-023-01135-3

iii. **Ray, Iravati**, Sambuddha Misra, Mengli Chen, Xianfeng Wang, and Reshmi Das. "Entrapment of atmospheric particle bound heavy metals by ferns as evidenced by lead (Pb) isotope and MixSIAR: Implications for improving air quality." *Journal of Hazardous Materials* 469 (2024): 134014. Doi: https://doi.org/10.1016/j.jhazmat.2024.134014

iv. Lahiri, Divyangana, **Iravati Ray**, Rupam Ray, Ilindra Venkata Satya Chanakya, Mohd Tarique, Sambuddha Misra, Waliur Rahaman, Manish Tiwari, Xianfeng Wang, and Reshmi Das. "Source apportionment and emission projections of heavy metals from traffic sources in India: Insights from elemental and Pb isotopic compositions." *Journal of Hazardous Materials* 480 (2024): 135810. Doi: https://doi.org/10.1016/j.jhazmat.2024.135810

v. **Ray, Iravati**, Shoumick Mitra, Jariya Kayee, Shufang Yuan, SM Shiva Nagendra, Xianfeng Wang, and Reshmi Das. "Dominance of open burning signatures in PM2. 5 near coal plant should redefine pollutant priorities of India." *npj Climate and Atmospheric Science* 7, no. 1 (2024): 284. Doi: https://doi.org/10.1038/s41612-024-00836-6

b) Other Publications during the period of Doctoral Research:

i. Rahaman, Waliur, IV Satya Chanakya, **Iravati Ray**, Mohd Tarique, A. A. Fousiya, Reshmi Das, and Sambuddha Misra. "Anthropogenic Lead (Pb) deposition history of the western Indian Ocean from coral-based Pb/Ca ratio and Pb isotope records." *Science of The Total Environment* 955 (2024): 177312. Doi: https://doi.org/10.1016/j.scitotenv.2024.177312

3. List of Patents: Nil

4. List of Presentations in National/International Conferences:

i. **Ray, Iravati**, Reshmi DAS, and Sambuddha Misra. "Efficient Uptake of Atmospheric Lead (Pb) by Ferns Quantified through Pb Concentrations and Isotope Ratios." In *AGU Fall Meeting Abstracts*, vol. 2022, pp. A34B-03. 2022.

ii. Mitra, Arijeet, **Iravati Ray**, Reshmi Das, and Sambuddha Misra. "Accurate and Precise determination of Pb isotope ratio by single collector QQQ-ICP-MS: Application to environmental samples." In *Goldschmidt 2023 Conference*. GOLDSCHMIDT, 2023.

iii. **Ray, Iravati**, Sambuddha Misra, and Reshmi Das. "Source delineation of bioaccumulated Lead (Pb) in plants through isotope fingerprinting: Soil vs dry Deposition." In *Goldschmidt 2023 Conference*. GOLDSCHMIDT, 2023.

iv. **Ray, Iravati** and Reshmi Das. “Resuspension of legacy lead (Pb) still a major contributing source of atmospheric Pb in South East Asian countries?” In ACS Fall Meeting 2023

v. **Ray, Iravati**, Reshmi DAS, Shoumick Mitra, Jariya Kayee, and Xianfeng Wang. "Lead (Pb) Isotopes and Elemental Concentrations for Identification of Multiple Sources of Particulate Matter in Coal-Fired Power Plants." In *AGU Fall Meeting Abstracts*, vol. 2023, pp. A02-06. 2023.

5. Participation in Workshops, Seminars and Symposium:

i. Global online certificate course on "Demystifying Climate Change Data and Maps for Communication in the 21st century" organized by Centre for Science and Environment, Delhi, India, held on 8th – 22nd December 2023.

Certificate from Supervisors

This is to certify that the thesis entitled **"Following the trails of India's Atmospheric Lead (Pb): Source Identification, Apportionment, Bioavailability and Remediation",** prepared and submitted by **Ms. Iravati Ray,** registered as a Ph.D. scholar on **3rd March 2022** with registration no: **1022220001**, for the award of **PhD (Emgineering)** degree from **Jadavpur University**, is absolutely based upon her own work under the supervision of **Dr. Reshmi Das and Dr. Sambuddha Misra** and that neither this thesis nor any part of it has been submitted for either any degree/diploma or any other academic award anywhere before.

Sambuddha Misra

Associate Professor
Centre for Earth Sciences
Indian Institute of Science
Bangalore - 560 012, INDIA

Date: 27/1/25

Place: KOLKATA

(Signature of the Supervisor and Official Seal)

Reshmi Das
27/1/25

Reshmi Das, PhD
UGC Assistant Professor
School of Environmental Studies
Jadavpur University
Kolkata-700 032, India

Date: 27/1/25

Place: KOLKATA

(Signature of the Supervisor and Official Seal)

Statement of Originality

I, **Iravati Ray** (Reg. No. **1022220001**), registered on **March 3rd, 2022** do hereby declare that this thesis entitled "**Following the trails of India's Atmospheric Lead (Pb): Source Identification, Apportionment, Bioavailability and Remediation**" contains a literature survey and original research work done by the undersigned candidate as part of doctoral studies.

All information in this thesis has been obtained and presented in accordance with existing academic rules and ethical conduct. I declare that, as required by thesis rules and conduct, I have fully cited and referred to all materials and results that are not original to this work.

I also declare that I have checked this thesis as per the "Policy on Anti-Plagiarism, Jadavpur University, 2019," and the level of similarity as checked by iThenticate software is **5** %.

Iravati Ray 27.01.2025

Signature of the candidate with date:

Reshmi Das
27/1/25

Reshmi Das, PhD
UGC Assistant Professor
School of Environmental Studies
Jadavpur University
Kolkata-700 032, India

Aambuddha Mitra
27/1/25

Associate Professor
Centre for Earth Sciences
Indian Institute of Science
Bangalore - 560 012, INDIA

Signature of the Supervisors with date and seal:

Declaration

I hereby declare that this thesis represents my own work and has not been previously included in my thesis or any other institution for a degree, diploma, or other academic qualifications. Further, I have acknowledged all sources used and have cited these in the reference section.

I hereby submit the record of my observations for evaluation for the award of the degree of Doctor of Philosophy in Engineering.

Iravati Ray

Date: 27.01.2025

Place: KOLKATA

(Iravati Ray)

Acknowledgements

First and foremost, I extend my heartfelt gratitude to my supervisor, Dr. Reshmi Das for her unwavering guidance and encouragement throughout this journey. She has been more than a mentor—a trusted friend whose belief in me surpassed even my own confidence. Her support has been a cornerstone, and I will always cherish her invaluable role in my life.

I am deeply thankful to my co-supervisor, Dr. Sambuddha Misra for always reminding me that I got to " transcend knowledge into wisdom". His mentorship has profoundly shaped my perspective, and I am truly grateful for his generosity in always keeping his lab open for me, fostering an environment of learning and exploration.

I also express my sincere thanks to all the teachers in my department for their guidance, with special appreciation to the director, Prof. Joydeep Mukherjee for his invaluable support and encouragement throughout this journey.

I am indebted to all my teachers at school, who laid the foundational knowledge and values that shaped me from a very tender age. Their dedication and hard work have had a lasting impact on my life and continue to inspire me.

I am grateful to all the research scholars (Shayontani di, Arup da, Tanaya di, Chiradeep da, Shantanu da, Ankita di, Hamidul, Meenakshi di) in my lab at the School of Environmental Studies, Jadavpur University, for their camaraderie and assistance. A special mention goes to Arup Da and Chiradeep Da for being my gaming partners and for bringing moments of joy into my days.

My heartfelt thanks go to the scholars at the Geochemical Research Unit at Indian Institute of Science, Bangalore, whose immense support was invaluable. I am particularly thankful to Pratyusha Di, Satya Chanakya, Juzer Shaikh, Kribina Pathak, and Arijeet Mitra for their support and cooperation during my stays at the lab.

I also thank the team at Nanyang Technological University for their assistance, especially Prof. Xianfeng Wang, whose constant support has been instrumental, and my senior Jariya Kayee for her guidance.

I am deeply grateful to my friend Sayan Basak for the entertainment and laughter he brought during my PhD journey. I also fondly thank Rik for our mischievous moments and gaming sessions, and I look forward to being a tad more mischievous in the coming years.

Even my laptop deserves recognition for enduring years of relentless use and proving to be a reliable companion through this challenging journey.

I am thankful to Hiru Da and Basu Da for their prompt assistance and support in maintaining the lab.

Finally, my deepest gratitude goes to my mother and grandmother, whose unconditional love, sacrifices, and unwavering belief in me made all of this possible.

To everyone who contributed to this journey, in ways big or small, I extend my sincerest thanks.

Table of Contents

List of Tables xiii

List of Figures xv

List of Abbreviations xxv

ABSTRACT xxvi

CHAPTER 1: INTRODUCTION AND GENERAL OVERVIEW 1

1.1. Ambient air pollution: A brief history 1

1.2. Ambient air pollution: Present scenario 5

1.3. Metals present in particulate matter 8

1.4. A brief history of Pb pollution across the world 10

1.5. The recent scenario of atmospheric Pb pollution in India 14

1.6. Current understanding of sources of atmospheric Pb in India 14

1.7. Addressing atmospheric Pb pollution 16

CHAPTER 2: AIMS AND OBJECTIVES 18

CHAPTER 3: MATERIALS AND METHODS 21

3.1. Collection of PM_{10} and $PM_{2.5}$ aerosol samples and dustfall (DF) samples 21

3.2. Collection and pre-processing of traffic emission samples 21

3.3. Collection of vehicular and ship fuel samples 22

3.4. Collection and pre-processing of fern and associated samples 22

3.4.1. Gravimetric quantifications and determination of leaf surface area 22

3.4.2. Microscopic observations of leaf-surface PM by SEM-EDX 23

3.5. Sample processing for extraction of elements 23

3.5.1. PM_{10} and $PM_{2.5}$ aerosol and dustfall samples 23

3.5.2. Lignite, fly ash, soil, solid waste ash, biomass burning ash and galena samples 23

3.5.3. Brake wear, tire wear, vehicular exhaust, road pitch and road dust samples 24

3.5.4. Vehicular and ship fuel samples 24

3.5.5. Fern and associated samples 24

3.6. Sample processing for purification of Pb 25

3.7. Determination of elemental concentrations 26

3.8. Determination of Pb isotopes 30
3.9. Statistical analyses and modelling studies 32
3.9.1. Air mass back trajectory analyses 32
3.9.2. Mixing polygon simulation 32
3.9.3. Linear mixing model performed for literature data of India and SEA countries 33
3.9.4. Bayesian mixing model, MixSIAR (Stable isotope analysis in R) 34
3.9.5. Quantification of Metal Emissions from Traffic Sources 35
CHAPTER 4: SOURCES OF ATMOSPHERIC Pb IN INDIA AND SOUTH EAST ASIAN COUNTRIES IN THE LAST DECADE 37
4.1. Introduction 37
4.2. Sources of atmospheric Pb in Singapore 40
4.2.1. Study site and origin of airmasses 40
4.2.2. Particulate matter and metal concentration, enrichment factor and elemental ratios 42
4.2.3. Pb isotopic composition and its sources 51
4.2.4. Anthropogenic sources of atmospheric Pb 55
4.3. Quantitative assessment of atmospheric Pb sources in India and SEA countries in the last decade using statistical modeling 61
4.3.1. Evaluating source applicability of aerosol Pb using 3D Mixing Polygon Simulation 62
4.3.2. Contribution of sources as quantified by linear mixing model 67
4.3.3. Contribution of sources as quantified by Bayesian mixing model MixSIAR 70
4.3.4. Implications from the model results 81
CHAPTER 5: ELEMENTAL CONCENTRATION AND Pb ISOTOPIC COMPOSITION OF DIFFERENT END MEMBERS 84
5.1. Introduction 84
5.2. Elemental concentration 85
5.3. Pb isotopic composition 87
CHAPTER 6: SOURCE APPORTIONMENT AND EMISSION PROJECTIONS OF HEAVY METALS FROM TRAFFIC SOURCES IN INDIA 91
6.1. Introduction 91
6.2. Elemental concentration of exhaust and non – exhaust sources 95
6.2.1. Exhaust emission (EE) sources 97
6.2.2. Non – exhaust emission (NEE) sources 98
6.3. Elemental ratios 100
6.4. Pb isotopic signatures for source delineation 102

6.5. MixSIAR Model based approach for source apportionment 105
6.6. Metal emissions from traffic sources 108
6.7. Implications 113
CHAPTER 7: SOURCES OF ATMOSPHERIC Pb IN AND AROUND A COAL-FIRED POWER PLANT IN INDIA 118
7.1. Introduction 118
7.2. Study area 122
7.3. Elemental concentration and $PM_{2.5}$ load 123
7.4. Enrichment factors and airmass back trajectories 129
7.5. Elemental ratios as source tracers 132
7.6. Pb isotopic compositions as source tracers 133
7.7. Quantifying relevance of sources 141
7.8. Quantification of end member contributions 144
7.9. Implications 145
CHAPTER 8: TRACING ATMOSPHERIC Pb SOURCES IN INDIA'S PRISTINE REGION: A CASE STUDY FROM THE ANDAMAN AND NICOBAR ISLANDS 150
8.1. Introduction 150
8.2. Study area 152
8.3. Elemental concentrations 153
8.4. Enrichment factors and potential source regions 160
8.5. Elemental ratios 163
8.6. Pb isotopic evidences 166
8.7. Quantification of end member contributions 170
8.7.1. Quantifying the relevance of sources 170
8.7.2. Source contributions towards atmospheric Pb 172
8.8. Implications 175
CHAPTER 9: REMEDIATION OF ATMOSPHERIC Pb 176
9.1. Introduction 176
9.2. Atmospheric PM_{10} concentration and dustfall (DF) flux 178
9.3. Leaf surface dust load and SEM-EDX observations 179
9.4. Elemental concentration & enrichment factor (EF) 181
9.4.1. Aerosol (PM_{10}) and Dust fall (DF) 182
9.4.2. Soil 182

9.4.3. Foliar dusts (LD and WD) and Fern Tissues (Roots and Leaves) 182
9.5. Elemental ratios as source tracers of foliar dusts 193
9.6. Pb isotopic compositions as source tracers of foliar dusts and tissues 194
9.6.1. Aerosol (PM_{10}) and Dust fall (DF) 194
9.6.2. Soil 194
9.6.3. Fern tissues (roots and leaves) 196
9.6.4. Quantification of source contribution using mixing model (MixSIAR) 200
9.7. Ferns as air purifying agents 202
9.7.1. Suitability of fern species 202
9.7.2. Practical use and applicability of the ferns in botanical biofiltration units 203
9.8. Novelty and challenges 206
9.9. Comparison with other air purification technologies 207
CHAPTER 10: CONCLUSIONS 209
REFERENCES 212
CHAPTER 11: PUBLICATIONS AND CONFERENCES 241

List of Tables

Table 1.1: Sources of exposure to Pb and its effects from 18th to 19th century across the world as compiled from Jonasson and Afshari, 2018 13
Table 3.1: Digestion mixtures used for different types of samples 25
Table 3.2: iCAP Q ICP-MS Operating Conditions 27
Table 3.3: ICP - OES Operating Condition 27
Table 3.4: Figures of merit for ICP – OES Analysis 28
Table 3.5: ICPMS - QQQ Operating Condition 29
Table 3.6: Figures of merit for ICP MS – QQQ Analysis 29
Table 3.7: Mean concentrations of NIST SRM 2704(mg/kg), NIST SRM 2783 (ng/cm^2) and NIST SRM 1573A (mg/kg) 29
Table 3.8: Mean Pb isotopic composition of NIST SRM 981and procedural blanks during different sessions 31
Table 4.1: Metal concentration (ng/m^3) and PM_{10} concentration (µg/m^3) in Singapore aerosol 44
Table 4.2: Pb isotopic composition of Singapore aerosols 52
Table 4.3: Statistical summary of metal concentration (ng/m^3) and PM_{10} concentration (µg/m^3) in Singapore aerosols 54
Table 4.4: Individual sources of Atmospheric Pb in SEA countries and India 66
Table 4.5: MixSIAR input for concentration-dependent model 76
Table 4.6: Inputs for concentration-dependent linear model for India 79
Table 5.1: Elemental concentration of different end members of atmospheric metal emission in India 85
Table 5.2: Pb isotopic composition of different end members of atmospheric metal emission in India 87
Table 6.1: Elemental concentrations of vehicular exhausts, tire wear, brake wear, road pitch and road paint in mg/kg 96
Table 6.2: The individual and mean Pb isotopic compositions of vehicular exhaust, vehicular fuel, tire wear, brake wear, road pitch and road paint samples 103
Table 6.3: Inputs for Pb isotopic composition and Pb concentration in the MixSIAR model 107
Table 6.4 Parameters for emission calculation 115
Table 6.5: Mileage (km/L) and fuel consumption data (L) for emission analysis of ICEVs 115
Table 6.6: Total ICEV Emission (tons/year) 116
Table 6.7: Total EV Emission (tons/year) 116
Table 6.8: Total non-exhaust emissions (NEE) (ICEV + EV) (tons/year) 117
Table 6.9: Total metal emissions from NEE and EE sources (tons/year) 117

Table 7.1: Typical elemental concentrations in lignite and solid waste burning ash from different countries compiled from previous literature. 120
Table 7.2: Elemental concentrations of NLCIL coal, fly ash, solid waste and biomass burning ash, topsoil, (mg/kg), $PM_{2.5}$ aerosols (ng/m^3) 125
Table 7.3: Mean Pb isotopic composition of NLCIL coal & fly ash, local solid waste & biomass burning ashes, NLCIL topsoil, ore and $PM_{2.5}$ aerosols sampled in the years 2020, 2021 and 2022. 134
Table 7.4: Pb isotopic concentrations of NLCIL coal, fly ash, solid waste and biomass burning ash, topsoil and $PM_{2.5}$ aerosols 136
Table 7.5: Mean Pb isotopic composition, and standard deviation inputs for MixSIAR and polygon simulations. 143
Table 8.1: Elemental concentrations of PM10, PM2.5 aerosols (ng/m^3), road dust, dustfall, moss, local soil, limestone, mud volcano, Pb ore, Cu ore (ng/mg), vehicular fuel and ship emission samples (ng/mL) 154
Table 8.2: MixSIAR inputs of Pb isotopic composition and concentration of sources 174
Table 9.1: Elemental concentration in PM_{10} aerosols (ng/m^3) 186
Table 9.2: Elemental concentration in soil samples (mg/kg) 187
Table 9.3: Elemental concentration in dustfall samples(mg/kg) 188
Table 9.4: Elemental concentration in loose dust (LD) samples(mg/kg) 189
Table 9.5: Elemental concentration in wax bound dust (WD) samples(mg/kg) 190
Table 9.6: Elemental concentration in leaf samples(mg/kg) 191
Table 9.7: Elemental concentration in root samples(mg/kg) 192
Table 9.8: Mean Pb isotopic composition of PM_{10} aerosol, Dustfall (DF), Loose Dust (LD), Wax Dust (WD), Leaf, Root and Soil samples 198
Table 9.9: Pb isotopic composition of individual samples 199
Table 9.10: Viability estimation of fern species to be utilized as indoor air purifier 205

List of Figures

Figure 1.1: A detailed timeline for episodes of air pollution in the pre-industrial era 2

Figure 1.2: A detailed timeline of events related to air pollution in the industrial era 4

Figure 1.3: A schematic representation of the present-day sources of PM pollution in India 6

Figure 1.4: (a) Population weighted average level of exposure to PM2.5 across the world in 2019 (b) Relationship between PM2.5 concentration and death rate from PM pollution in 2019. Data source: Our World in Data 7

Figure 1.5: A heat map representing the number of children having BLL > 5 ug/dL in the world. Data has been adopted from UNICEF and Pure Earth report, 2020**.** 10

Figure 1.6: A detailed account of use of Pb and its effects upon humankind 11

Figure 1.7: Gasoline Pb emissions in India and other SEA countries as compiled from Lee et al., 2014 . 12

Figure 4.1: Location of Singapore in South East Asia. The coal and base metal mines of the neighbouring countries are marked for reference. (b) Sampling location within Singapore and probable local pollution sources. The base maps are adopted from the open-source online repository Opendatasoft (https://public.opendatasoft.com/explore/dataset/world-administrative-boundaries/export/) 40

Figure 4.2: 72 hours backward wind trajectory at 500 m above ground level compiled for the sampling period (June 2017 to May 2018) using [HYSPLIT (Hybrid Single Particle Lagrangian Integrated Trajectory) data from the U.S. National Oceanic and Atmospheric Administration's (NOAA) website]. The base map is adopted from the open-source online repository Opendatasoft (https://public.opendatasoft.com/explore/dataset/world-administrative-boundaries/export/) 41

Figure 4.3: (a) Box plots depicting the PM_{10} concentrations of NE, SW and Inter monsoon seasons. The maximum, minimum, 25 and 75 percentile, and mean values for the PM_{10} concentrations are labelled for reference. (b) Temporal variation in PM_{10} concentration in NE, SW and Inter monsoon winds. 42

Figure 4.4: Average annual emission of total particulate matter, $PM_{2.5}$ and organic carbon from equatorial Asia as an indicator of fire activity in the region (data source Global Fire Emission Database). Average annual $PM_{2.5}$ of Singapore is plotted for comparison (data source-Singapore NEA archive data). During the sampling period (June 2017-May 2018) there were no significant fire activities in the region 43

Figure 4.6: Enrichment factors of metals in NE, SW and IM seasons 49

Figure 4.5: Box plots depicting the concentrations of the measured elements in NE, SW and IM seasons. The horizontal lines within the boxes, upper and lower edges of the boxes specify median, 25th, and 75th percentile respectively. The mean values are specified by small solid boxes within. The upper and lower edges of the whiskers indicate maximum and minimum values 49

Figure 4.7: Pearson's correlation coefficients determined for 8 metals with Enrichment Factor>10 measured during (a) NE, (b) SW and (c) inter monsoon seasons. All coefficients above 0.6 have p values < 0.05 50

Figure 4.8: $^{206}Pb/^{207}$ Pb isotopic signatures of plausible end members and Singapore aerosols during NE, SW and Inter monsoon seasons. The inset plot shows $^{206}Pb/^{207}Pb$ ratios for NE, SW and Inter monsoon seasons 55

Figure 4.9: Triple isotope plot of Pb for (a) NE and (b) SW & IM seasons with reference to different plausible end members. The mixing line between legacy lead (LL) and Indonesian coal (IC) is shown in red. References: Indonesian coal & aerosols and Vietnamese coal & fuel (Bollhöfer and Rosman, 2000; Díaz-Somoano et al., 2009 and Chifflet et al., 2018); Chinese diesel, unleaded gasoline and coal (Bi et al., 2017); Singapore leaded gasoline and incinerator ash (Carrasco et al., 2018). 57

Figure 4.10: Seasonal variations in (a) V/Pb and (b) V/Ni ratios in Singapore aerosols. Elemental ratios for Indonesian coal and Vietnamese coal have been adopted from Belkin et al. (2009) and Chifflet et al. (2018) respectively. V/Ni ratios for ship emissions were adopted from Wu and Huang (2021) and traffic emissions from Chifflet et al. (2018). Both the elemental ratios of Singapore incineration dust were adopted from Yin et al. (2008). 58

Figure 4.11: Ni/V vs Pb/V ratios of Singapore PM10 aerosol samples in comparison to plausible anthropogenic end members. References: Indonesian coal (Belkin et al., 2009); Vietnamese coal and gasoline & diesel (Chifflet et al., 2018); Singapore incineration dust (Yin et al., 2008) 60

Figure 4.12: Three – isotope plots of the aerosol mixtures from India, Singapore, Thailand, Vietnam and their initial sources from previous literatures in (a) 208Pb/207Pb vs 206Pb/207Pb space and $^{206}Pb/^{204}Pb$ vs $^{208}Pb/^{204}Pb$ space. (c) Three – isotope plots of the aerosol mixtures from India, Singapore, Thailand, Vietnam and their initial sources along with the additional sources in $^{208}Pb/^{207}Pb$ vs $^{206}Pb/^{207}Pb$ space and (d) $^{206}Pb/^{204}Pb$ vs $^{208}Pb/^{204}Pb$ space 62

Figure 4.13: Trends in (a) Na/Mg ratios in aerosol mixtures from Singapore, Thailand and Vietnam; (b) V/Ni ratios in India, Singapore, Thailand and Vietnam. The shaded regions illustrate the ranges observed in sources for which these ratios serve as representative indicators 63

Figure 4.14: Geometric mixing lines constructed in three – isotope space between two extreme sources for SEA country aerosols and Indian aerosols segregated into divisions of 20 %. The sources considered for SEA countries are leaded gasoline on one side and coal/crust on the other. For India the sources are Indian ore on one side and coal/crust on the other. The traditional mixing line for leaded gasoline is depicted in red, constructed with the isotopic compositions of Broken Hill and Mississippi Valley ores.. 67

Figure 4.15: Source contributions determined from simple linear mixing model, represented as bar plots for each source within insets in the three – isotope plots of aerosols and sources for (a) SEA countries and (b) India in 208Pb/207Pb vs 206Pb/207Pb space. Sources considered are 5 for India (coal, crust, Indian ore, leaded gasoline and intermediate) and 4 for SEA countries (coal, crust, leaded gasoline and intermediate). The intermediate source represents mean of tertiary coal, unleaded fuel, ship soot, solid waste & biomass burning and SEA ore for SEA countries and tertiary coal, unleaded fuel, ship soot and SEA ore for India. 68

Figure 4.16: Median contribution of individual sources towards atmospheric Pb in (a) SEA countries and (b) India determined from MixSIAR simulation. The percentages on left-hand side and right-hand side of the bars represents the minimum and maximum contributions from each source respectively. 71

Figure 4.17: Median contribution range of individual sources towards atmospheric Pb in Singapore determined from MixSIAR simulation in $^{206}Pb/^{204}Pb$, 207Pb/204Pb and $^{208}Pb/^{204}Pb$ space 73

Figure 4.18: MixSIAR model results as contribution ranges for (a) concentration independent case and (b) concentration dependent case. Comparison of concentration dependent MixSIAR model results considering mean and median coal concentration for (c) Singapore and (d) Thailand. The largest variation observed for coal and crust are highlighted in grey. 77

Figure 4.19: Comparative illustration of contribution ranges obtained from concentration independent and concentration dependent linear mixing models. The aerosol mixture and sources are plotted in three isotope space in the background for reference 80

Figure 6.1: Bar plots depicting the total fuel demand in China, Asia, Other Asian countries and Asia Pacific for the years 2022, 2025, 2030, 2035, 2040 and 2045, The percentage increase in fuel demand from 2022 to 2045 is depicted by a dotted line with the percentages for respective regions indicated above the line as $Growth_{fuel}$. The total number of cars (passenger cars, commercial vehicles and electric vehicles) on road for each region is presented as line and symbol (diamond) plot. The percentage increase in the total number of cars is indicated above as $Growth_{car}$. The pie charts illustrate the percentage of internal combustion engine vehicles (ICEV) and electric vehicles (EV) in the years 2022 and 2045 for each region. 92

Figure 6.2: Location of the sites from where the end members (tire wear, brake wear, road pitch and road paint) and road dusts were sampled in eastern India. The locations for the road dusts samples have been adopted from Das et al., 2018 and Ray et al., 2024 95

Figure 6.3: Box plots depicting the elemental concentrations in (a) vehicular exhaust, (b) tire wear and brake wear and (c) road pitch and road paint samples from eastern India. The lower and the upper limits of the boxes represent 25th and 75th percentile data respectively. The black boxes represent the mean

while the lines represent the median values. The whiskers extend to the smallest and largest values within 1.5 times the interquartile range (IQR) from the first and third quartile. Data points beyond these whiskers are considered outliers depicted as black diamonds. 97

Figure 6.4: Comparison of elemental concentrations of (a) tire wear (b) brake wear (c) road pitch and (d) road paint from London and South Korea with respect to India. The data for London and South Korea has been adopted from Dong et al., 2017 and Jeong et al., 2022 respectively 99

Figure 6.5: Elemental ratios plotted as (a) bivariate plot of Mo/Pb vs Ba/Pb and (b) ternary plot of Pb/Mn, Cu/Zn and Fe/Al demonstrates that the characteristic ratios of road dusts lie between those of the EE and NEE sources. The vehicular exhaust, tire wear, brake wear and road pitch are depicted as fields in grey, blue, red and green colours respectively 101

Figure 6.6: (a) Three-isotope plots of $^{208}Pb/^{207}Pb$ vs $^{206}Pb/^{207}Pb$ for Indian fuel, vehicular exhaust, road dusts, tire wear, brake wear, road pitch and road paint. The fuel, vehicular exhaust, tire wear, brake wear and road pitch are depicted as fields in pink, dark grey, blue, red and green colours respectively. The right-hand panel provides an enlarged view of the squared section from the left-hand panel. (b) Comparison of the 206Pb/207Pb ratios in tire wear, brake wear, road pitch, and road paint from London and South Korea with those from the present study in India. The 206Pb/207Pb compositions of road dust from respective countries are shown as background fields. The data for London and South Korea has been adopted from Dong et al., 2017 and Jeong et al., 2022 respectively. The road dust data for India is adopted from Das et al., 2018 and Ray and Das 2024. 104

Figure 6.7: MixSIAR results for mean contribution of Pb towards crust, exhaust emission, tire wear, brake wear, road pitch and road paint towards road dusts from eastern India. All the samples demonstrate consistent contributions from the sources except sample “S8”, from Sagar island, a pristine location having heavy influence from natural crust 106

Figure 6.8: Stacked area plots representing total emissions of vehicular exhaust, tire wear, brake wear and road abrasions in tons/year. The stacked bar plots depict the percentage contribution of each source towards total metal emissions from traffic sources for (a) Ni (b) Cu (c) Zn and (d) Pb in the years 2022, 2025, 2030, 2035, 2040 and 2045. About 60 % - 70 % of the emissions of Ni and Cu are from brake wears while the major source of Zn emission is tire wear particles. The NEE (tire wear, brake wear, road abrasions) sources contribute more towards Pb emission than EE sources 108

Figure 6.9: Stacked area plots representing total emissions of diesel, petrol, tire wear, brake wear and road abrasions in tons/year. 109

Figure 7. 1:(a) Stacked bars representing emissions of PM_{10} and $PM_{2.5}$ (shaded bars) from different anthropogenic sources as compiled form “GAINS South Asia online,” 2020. For the past one and a half

decades, open biomass burning has been the largest emitter of PM_{10} and $PM_{2.5}$, while coal combustion emissions have steadily decreased due to the stricter emission standards implemented in 2015; (b) Particulate matter (PM) emission factors of open burning coal combustion, non-ferrous smelters and vehicular fuel. The emission factors for open burning are orders of magnitude higher than other processes. The emission factors have been compiled from (Akbari et al., 2021; Raparthi and Phuleria, 2021; Saud et al., 2011; Zhang et al., 2022; Zhu et al., 2022) 118

Figure 7. 2: Map showing the location of the state of Tamil Nadu and Cuddalore district within the state housing the largest lignite fired power plant Neyveli Lignite Corporation India Limited (NLCIL). The SIPCOT industrial estate housing different types of industries and the number of villages in the district are marked for reference. The base maps are adopted from the open-source online repository: Opendatasoft (https://public.opendatasoft.com/explore/dataset/world-administrative-boundaries/export/) 123

Figure 7. 3: (a) Temporal variation in concentrations of $PM_{2.5}$ (top panel) and elemental concentrations. The $PM_{2.5}$ loads increased in the months of April – June compared to October – December. Concentrations of all the elements witnessed a sharp decrease in the month of May (b) The top panel depicts the mean enrichment factors (EF) of each element in $PM_{2.5}$ aerosols across the sampling period with significant enrichment in Cu, Zn, Cd and Pb (EFs > 10). The lower panels illustrate the temporal variation in EFs. All the enriched elements exhibited lowest EFs in the months of April-June, indicating a reduced anthropogenic contribution during these months 124

Figure 7. 4: Comparison of elemental concentrations in Indian aerosols from previous studies across India with that of the present study at Neyveli lignite-fired power plant. The solid black lines represent the median concentration of each element 127

Figure 7. 5: Concentration of Pb in atmospheric particulates compiled from previous literatures and this study. The national ambient air quality standards (NAAQS) annual average is marked for reference..... 128

Figure 7. 6: The 72 hr airmass back trajectory clusters for an entire year computed using geographic information system (GIS) based software TrajStat (version: 1.5.3), which utilises the HYSPLIT model for trajectory calculation..... 129

Figure 7. 7: The 72h airmass back trajectories for the sampling days coupled with their corresponding EFs of Pb for (a) October 2020 (b) November 2020 (c) December 2020 (d) April 2021 (e) May 2021 (f) June 2021 (g) October 2021 (h) November 2021 (i) December 2021 (j) February 2022. The trajectories have been computed using geographic information system (GIS) based software TrajStat (version: 1.5.3). The airmasses with EFs < 32 are marked in blue while higher EFs are marked in red. (k) The monthly average rainfall in India (green bars) along with observed local fire events (yellow circles) around NLCIL

and EFs of Pb (red diamonds) in $PM_{2.5}$ aerosols sampled at NLCIL. The red dotted line represents EF = 10. (l) Spearman Correlation between the number of local fire events versus elemental EFs in $PM_{2.5}$ aerosols. The data for the fire events has been acquired from MODIS Terra and Aqua satellites available at NASA Fire Information for Resource Management System (FIRMS) 130

Figure 7. 8: Spearman correlations between $PM_{2.5}$ concentration versus the concentration (conc) of the enriched elements Cd, Pb and Zn ($p = 0.02 – 0.09$) as well as the enrichment factors (EF) of the enriched elements 131

Figure 7. 9: Elemental ratios plotted as (a) V/Pb vs Cu/Pb (b) Pb/Al vs Pb/Fe indicate that the $PM_{2.5}$ aerosols are a mixture of crust, coal & fly ash, solid waste & biomass burning and industrial smelting (depicted as ore in the figure). The characteristic V/Pb ratios for industrial, traffic and coal/crustal sources (Das et al., 2018) are marked as shaded regions for reference. The October-February aerosols have V/Pb<<1 and hence plot in the region of industrial emissions. The open waste burning aerosols from Delhi's Okhla landfill site (Kumar et al., 2018) overlapping with April-June aerosols is plotted in V/Pb vs Cu/Pb space for reference. The April-June aerosols seem to be more influenced by solid waste & biomass burning and crustal sources with decreased Pb/Fe and Pb/Al ratios than the October-February aerosols. The elemental concentration data for crust has been adopted from Rudnick and Gao 2003. 132

Figure 7. 10: The Pb isotopic compositions of the $PM_{2.5}$ aerosols and relevant end members illustrated in three-isotope space ($^{208}Pb/^{206}Pb$ vs $^{206}Pb/^{207}Pb$). Two distinct mixing lines are observed, each with crust at one end: one extends to Neyveli lignite (blue dotted line), while the other extends to Indian ore (black dotted lines). The Pb isotopic compositions of the PMs lie along the mixing line between Indian ore and crust, rather than local lignite and fly ashes. The aerosols lie close to vehicular exhaust emissions (traffic) and seawater, with less radiogenic local crust also plotting close to the aerosols compared to UCC. There is a considerable overlap between the aerosols and Indian fuelwood, local solid waste & biomass burning signatures. Isotopic signatures of previously sampled aerosols from Delhi's Okhla landfill, overlap with the Neyveli aerosols. The enclosure formed by the red dotted line signifies the mixing envelope formed using the relevant end members. The data for Indian fuelwood and OWB aerosols have been adopted from Mitra et al., 2021 and Kumar et al., 2018 respectively. Data for traffic emissions, Indian ore, crust, seawater, and local crust have been compiled from Ray and Das 2023, Deb et al., 1989, Lee et al., 2015 and Chakraborty et al., 2021 respectively 138

Figure 7. 11: Comparison of $^{208}Pb/^{206}Pb$ ratios of Indian aerosols from previous studies across various settings (urban, rural, industrial, and waste-burning) with the ratios observed in the present study. The solid black squares and lines represent mean and median values respectively. The outliers are represented by solid black diamonds. The upper and lower extremes of the boxes represent 75^{th} and 25^{th} percentile

values respectively while the upper and lower extremes of the whiskers represent 90^{th} and 10^{th} percentiles respectively. 140

Figure 7. 12: (a) Bar plots depicting the median probability of the aerosol mixtures to fall inside the mixing envelope constructed by the initial and additional sources with each source added successively. The probabilities are determined with the help of 3 – dimensional mixing polygon simulation in $^{206}Pb/^{207}Pb$, $^{208}Pb/^{207}Pb$ and $^{208}Pb/^{206}Pb$ space. Same letters above the bars indicate that the probabilities are not significantly different, as determined by Tukey's method. Addition of transboundary aerosols and leaded gasoline significantly increased the median probability. Exclusion of Neyveli coal & fly ash does not affect the results. (b) Median contribution of individual sources towards atmospheric Pb determined from MixSIAR simulation. The percentages over/beside the bars represent the range of contributions from each source. MixSIAR results indicate negligible influence of coal and fly ash throughout the year in the vicinity of lignite fired powerplant. Open burning of solid waste and biomass emerges as the major anthropogenic contributor, even in a region of coal combustion. (c) Field photographs of solid waste & biomass burning at Neyveli. 142

Figure 7. 13: Map illustrating the aerosol sampling sites and nearby coal-fired thermal power plants. The available V/Pb ratios were compiled from key locations, including Madhya Pradesh (Singrauli), Jharkhand (Jharia), Assam (Jorhat), West Bengal (Bandel and Kolaghat), Odisha (Bhubaneshwar), Andhra Pradesh (Vizag), Telangana (Hyderabad), Maharashtra (Trombay), Chhattisgarh (Raipur), Delhi, and Uttar Pradesh (Kanpur). The red dotted line indicates V/Pb > 1. Aerosols demonstrating V/Pb > 1 can be sourced from coal combustion while those having V/Pb < 1 and << 1 can be sourced from vehicular exhaust and high temperature industrial processes[1]. The base map has been adopted from the open-source online repository Opendatasoft (https://public.opendatasoft.com/explore/dataset/world-administrative-boundaries/export/) and the locations have been illustrated using ArcGIS Pro 10.8. The V/Pb ratios were plotted using Origin Pro 2024a and all the components were compiled in Adobe Illustrator 2021, to form the final illustration**.** 147

Figure 8. 1: (a) PM concentrations at Andaman and Nicobar Islands, Lakshadweep Islands, Indian mainland and South East Asian (SEA) countries from 1998 – 2000 as compiled from https://sites.wustl.edu/acag/datasets/surface-pm2-5/ (b) Cluster analysis determining the percentage of airmasses received from different directions at Andaman and Nicobar Islands and Lakshadweep Islands. The cluster analysis has been performed in TrajStat software with inputs of meteorological data downloaded from HYSPLIT gui. 150

Figure 8. 2: Elemental concentrations in $PM_{2.5}$ fraction at Andaman and Nicobar Islands, Lakshadweep Islands, Indian mainland and South East Asian (SEA) countries 157

Figure 8. 3: 72 hour airmass back trajectory at the study site for the sampling periods in winter and monsoon 158
Figure 8. 4: Median elemental concentrations in ship oil and vehicular fuel samples 159
Figure 8. 5: Mean enrichment factors of (a) $PM_{2.5}$ (b) PM_{10} (c) Dustfall and (d) soil samples 161
Figure 8. 6: Potential source hotspots for Cu, Zn, Cd and Pb in (A) $PM_{2.5}$ and (B) PM_{10} 162
Figure 8. 7: (a) Na/Mg and (b) V/Ni ratios in $PM_{2.5}$ and PM_{10} during winter and monsoon. The range of V/Ni ratios for ship oil and vehicular fuel are plotted for reference. 163
Figure 8. 8: Bivariate plots of V/Ni vs Pb/Ni illustrating aerosol as well as their potential sources in (a) winter and (b) monsoon seasons 164
Figure 8. 9: Three isotope plot illustrating the Pb isotopic composition of aerosols as well as their potential sources in (a) winter and (b) monsoon seasons 166
Figure 8. 10: Three isotope plot illustrating the Pb isotopic composition of aerosols, the conventional end members as well as bullets from different regions in (a) winter and (b) monsoon seasons 169
Figure 8. 11: Results of mixing polygon simulation depicting the probability of the aerosols to lie inside the envelope formed by the end members considered 171
Figure 8. 12: Contribution of different sources towards atmospheric Pb in A & N Islands as quantified using MixSIAR 172
Figure 9. 1: Location of the sites from where the ferns were sampled in Eastern India 177
Figure 9. 2: (a) Box plots depicting PM_{10} aerosol concentration, dust fall (DF) and foliar dusts (loose dust (LD) and wax dust (WD)). The NAAQs 24 hrs average limit for PM10 concentration is marked for reference; (b) Box plots depicting a comparison of dust fall fall fluxes between this study, industrial and urban settings. The upper and lower extremes of the boxes represent 75 and 25 percentile values respectively. The whiskers represent the highest and lowest values. Squares and lines inside boxes indicate mean and median values respectively. (c) Total leaf surface dust load (LD + WD) on the fern samples (n = 22). Foliar surface dust loads from previous studies conducted in urban and industrial settings are plotted for comparison. The ferns from this study demonstrates higher median dust loads compared to the previous studies. The lines represent the median dust loads. The values of the medians are indicated on the right-hand side of the plots. 179
Figure 9. 4: EDX spectra of selected areas from (a) adaxial and (b) abaxial surfaces of fern leaves. The tables for weight and atomic percentage of metals identified on the surface are included as insets. EDX study reveals the presence of heavy metals like Fe, Mn, Pb, Co, Ni, Cu, Zn and Cr. 180
Figure 9. 3: Representative scanning electron micrographs of (a) adaxial and (b) abaxial surface. The adaxial surface has greater accumulation of dust particles compared to abaxial surface. 180

Figure 9. 5: Bars with 1 SD depicting mean enrichment factors (EFs) of (a) PM10 aerosols, PDs, soil and (b) LD & WD. The dotted lines represent the threshold EF values (5 for soil and 10 for PM10, PD, LD and WD). Samples recording EFs beyond the threshold EFs are considered to have anthropogenic inputs. For each type of sample, the elements, Ni, Cd and Pb were observed to be enriched consistently, suggesting anthropogenic inputs. PM_{10} aerosols, LD and WD exhibits high EFs for Cr 181

Figure 9. 6: Concentrations of (a) Cr, (b) Ni, (c) Cd and (d) Pb in LD, WD, leaf, root and soil of the fern samples. The figures on the right-hand side of the symbols indicate the median concentrations illustrated by a solid black line. 183

Figure 9. 7: Leaf elemental concentration of samples having high foliar dust load represented by dark grey bars and low foliar dust samples represented by light grey bars. Samples having higher foliar dust loads had elevated concentrations of Mg, Al, Ca, Ti, V, Mn, Fe, Co, Ba and Pb. The y-axis is presented in logarithmic scale. 184

Figure 9. 9: Correlation between total foliar dust load (LD +WD) vs leaf elemental concentrations and root elemental concentration vs leaf elemental concentration for (a) Al, (b) Ca, (c) V, (d) Mn, (e) Ni and (f) Ba. The bottom x axis represents total foliar dust loads and top x axis represents elemental concentration of root. Both the axes are linked to left y axis representing leaf elemental concentration. The [leaf] vs foliar load data are plotted in green circles while the [root] vs [leaf] data are plotted in reddish brown circles (n = 12 each). All these 6 elements demonstrate moderate to strong correlation between foliar dust vs [leaf], while demonstrating weak to no correlation between [root] vs [leaf], indicating dominance of foliar translocation**.** 185

Figure 9. 8: Correlation between total foliar dust load (LD +WD) vs leaf elemental concentrations and root elemental concentration vs leaf elemental concentration for (a) Ti, (b) Fe and (c) Co. The bottom x axis represents total foliar dust loads and top x axis represents elemental concentration of root. Both the axes are linked to left y axis representing leaf elemental concentration. The [leaf] vs foliar load data are plotted in green circles while the [root] vs [leaf] data are plotted in reddish brown circles (n = 12 each). All these 3 elements demonstrate simultaneous moderate to strong correlation between foliar dust vs [leaf] and [root] vs [leaf], indicating bidirectional translocation of these metals from root to leaf and foliar surface to leaf. 185

Figure 9. 10: Elemental ratios plotted as (a) Pb/Ti vs Cd/Ti (b) Ni/Cd vs Pb/Cd and (c) Cu/Ti vs Cu/Mn. Pb/Ti vs Cd/Ti demonstrates that the characteristic ratios of LDs and WDs lie between those of soil, PDs and PM_{10}, with some of WDs overlapping with PM10 aerosols. Thus, the leaf surface dusts were a mixture of soil, PD and PM10. Overlapping of LD and WD with PM10 aerosols in Ni/Cd vs Pb/Cd

suggests that these elements in the leaf surface dusts were primarily sourced from the atmosphere. Cu/Ti vs Cu/Mn suggests that these elements were primarily of crustal origin. 193
Figure 9. 11: Bivariate plot depicting the relationship between soil Pb concentration and $^{206}Pb/^{207}Pb$ isotopic composition. Lower $^{206}Pb/^{207}Pb$ signature was associated with higher Pb concentrations 195
Figure 9. 12: (a) $^{206}Pb/^{207}Pb$ composition of soil, PM10, DF, root, leaf, WD and LD. SE, SC, SR and SS are exchangeable, carbonate, reducible and silicate fraction of soil respectively. LDs showed a higher $^{206}Pb/^{207}Pb$ signature compared to WDs, indicating the contribution of Pb from regional soil in LD. Conversely, WDs displayed a stronger association with PM_{10}. Isotopic composition of root is comparable to SE, SC and SR, which in turn are similar to DF. (b) Triple isotope plots of $^{208}Pb/^{207}Pb$ vs $^{206}Pb/^{207}Pb$ for the exchangeable (SE), carbonate (SC), reducible (SR), silicate (SS) fractions of the sequentially leached soil samples. The mixing line between SR and SS are plotted as red dashed line. The Pb isotopic compositions for corresponding root sample and atmospheric fallout samples (DF and PM_0) compositions are plotted for comparison 195
Figure 9. 13: Triple isotope plots of $^{208}Pb/^{207}Pb$ vs $^{206}Pb/^{207}Pb$ for PM_{10} aerosols, DF, LD, WD, leaf, root and soil. The soil, PM10, DF, leaf and roots are depicted as fields in grey, light red, blue, green and brown colours. The open black and red squares represent LD and WD respectively. The triple isotope plots demonstrate that the sources of Pb in WD, roots and leaves are primarily a mixture of PM_{10} and DFs, while LD demonstrates partial influence from soil along with PM_{10} and DF. 197
Figure 9. 14: MixSIAR results for mean contribution of soil, DF and PM^{10} aerosols towards (a) leaf and (b) root Pb of the fern samples. The dominant sources of Pb in leaves were DF and PM10 aerosols, whereas Pb within fern roots primarily originated from soil and DF 201
Figure 9. 15: (a) Tolerated concentrations of Cd, Cr, Cu, Ni and Pb in roots of Pteridium aquilinum and Pteris vittata demonstrated in previous studies. The concentrations of Cd, Cr, Cu, Ni and Pb in soil (open black squares) and DF (open blue triangles) from this study are also plotted for reference. (b) Box plots depicting the number of days a $1m^2$ fern cover can remain viable for Cr, Ni, Cu and Pb capture in a small $10m^2$ residential room as calculated from the leaf surface dust load data from the present study. The upper and lower extremes of the boxes represent maximum and minimum values respectively. Squares and lines inside boxes indicate mean and median values respectively. The values of each parameter are indicated on the right-hand side of the boxes in the order of maximum, mean, median and minimum (from top to bottom). The data for indoor PM_{10} concentrations, volume of air in a room and air change rate were adopted from previous literatures 203

List of Abbreviations

µg/m³	Microgram per meter cube
AGL	Above ground level
BC	Black carbon
BCE	Before common era
BLL	Blood lead level
DF	Dustfall
EDX	Energy dispersive X-ray
EE	Exhaust emission
EF	Enrichment factor
EV	Electric vehicle
GUI	Graphical User Interface
HEPA	High-energy particulate air
ICEV	Internal combustion engine vehicles
ICP – MS	Inductively coupled Plasma Mass Spectrometer
ICP – OES	Inductively coupled plasma - optical emission spectrometer
IQ	Intelligence quotient
IQR	Inter quartile range
L/min	liters/minute
LD	Loose dust
NEE	Non-exhaust emission
NIST	National Institute of Standards and Technology
NLCIL	Neyveli Lignite Corporation India Limited
OC	Organic carbon
PBL	Planetary boundary layer
PM	Particulate matter
PTFE	Polytetrafluoroethylene
SEA	South East Asia
SEM	Scanning electron microscope
SRM	Standard reference material
TEL	Tetraethyl lead
UVGI	Ultraviolet germicidal irradiation
WD	Wax Dust
WHO	World Health Organization

ABSTRACT

Atmospheric pollution, particularly particulate matter (PM), poses a significant threat to environment and public health due to its widespread impacts. India is one of the worst affected countries in terms of PM pollution. Among the toxic constituents of PM, lead (Pb) remains a critical concern, despite the global phase-out of leaded gasoline. This thesis provides a comprehensive investigation into the identification of sources, their contribution towards atmospheric Pb, seasonal variations, across urban, industrial, and pristine environments in India followed by study on remediation strategies. By analyzing elemental and Pb isotopic compositions of aerosols and several sources (end members), this study identifies both conventionally recognized and previously underdetermined sources of Pb. Key findings reveal that Pb resuspension from legacy leaded gasoline remains a significant source in South East Asia (SEA), and also to a lesser extent in India. Ship emissions emerge as a major, underexplored contributor towards atmospheric Pb and other metals in India. In India, industrial emissions and coal combustion historically dominated Pb sources in the last decade. However, their contribution has declined with stricter regulations presently. Contrarily, open burning of biomass and solid waste even in coal-dominated regions, calls for urgent mitigation measures. In urban areas, non-exhaust emissions (NEE) from tire and brake wear and road surface abrasion contribute significantly to road dust Pb levels, along with exhaust emissions (EE). Projections suggest that despite increasing electric vehicle adoption, Pb emissions from fuel combustion will persist due to the dominance of internal combustion engine vehicles over the next two decades. In pristine settings like the Andaman and Nicobar Islands, anthropogenic sources such as military activities and ship emissions were identified as dominant contributors, with natural sources such as seawater and crustal inputs always being present. To address the challenges of atmospheric heavy metal pollution, the study investigates the use of ferns as biofilters for capture of Pb along with other heavy metals. Fern species demonstrated high efficiency in accumulating Pb and other metals from indoor environments.

CHAPTER 1: INTRODUCTION AND GENERAL OVERVIEW

1.1. Ambient air pollution: A brief history

The history of air pollution can be traced back to the ancient world, with one of the earliest mentions found in the writings of Greek physician and philosopher, Hippocrates around 400 BCE. Hippocrates, often regarded as the father of medicine, noted the adverse effects of inhaling foul air on health, though the term "air pollution" as we understand it today was not in existence (Hippocrates, 400BCE). Both natural as well as anthropogenic activities have led to release of air pollutants since long. The Romans, started to recognize the detrimental effects of smoke in urban environments as early as 1st century AD. The 6th century AD eruption of a volcano in Iceland triggered a decade long climatic disturbance, contributing to poor air quality and widespread crop failures. The use of coal, began to emit gaseous pollutants in Europe, China and central Asia in the early phases of the last millennium. By the 13th century, London's deforestation and usage of "sea coal" led to the first environmental law: the 1273 Smoke Abatement Act. The 16th century witnessed coal dominate as a fuel source in Britain, further escalating air pollution (Fowler et al., 2020; Gibbons, 2018). A detailed timeline outlining the key events and developments that contributed to the air quality issues and growing awareness over time in the pre-industrial era is presented in **Figure 1.1**.

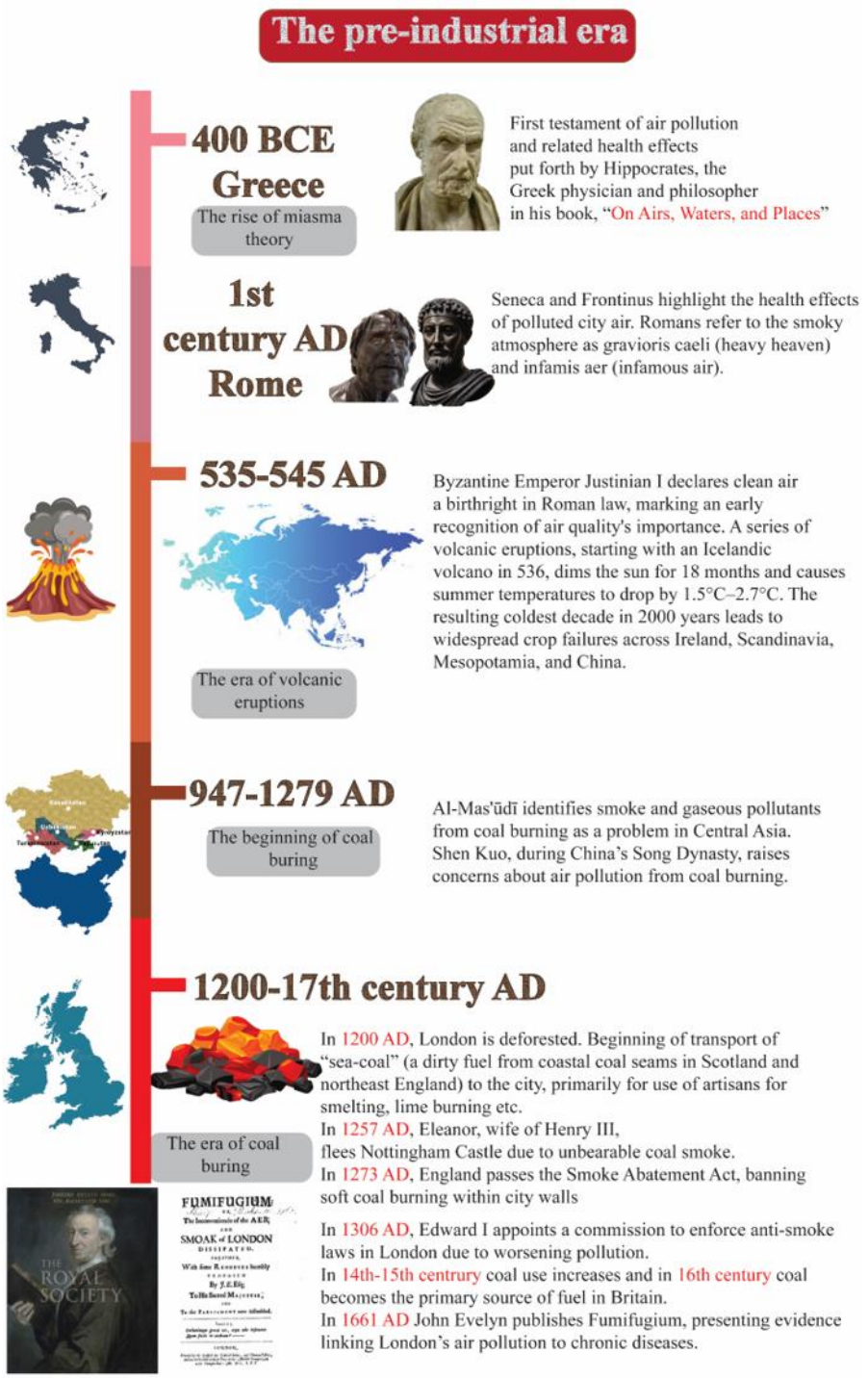

Figure 1.1: *A detailed timeline for episodes of air pollution in the pre-industrial era*

As industrialization progressed in the 18th – 19th century, aided by invention of steam engines, the detrimental effects of coal combustion in the form of "city fog" and acid rain became undeniable,

leading to scientific inquiry and legislative action. Thick, smoky fogs, often referred to as "pea-soupers" (a term coined by John Sartain) due to their yellowish color, were particularly prominent in stories of Sherlock Holmes by Sir Arthur Conan Doyle, emphasizing its impact upon human lives. The smoky fog events led to the coining of the term "smog" by Antoine des Voeux in 1905, a term that is widely used today (Corton, 2021; Fowler et al., 2020).

The 20th century witnessed numerous fatal smog events across the globe which led to global awareness of uncontrolled industrialization's health impacts. India passed her first anti-pollution law in 1905 in the form of "Bengal Smoke-Nuisances Act" to curb pollution from fireplaces and furnaces (Fowler et al., 2020). After world war there was a boom in automobile use in the mid-20th century which introduced new sources of air pollution, leading to severe smog events in USA and Europe (Fowler et al., 2020). In the 1950s, the renovation of 10 Downing Street, the residence of the Prime Minister of the United Kingdom, revealed the extent of industrial pollution through 2 centuries. It was discovered that the black façade of the building had originally been yellow, a striking representation of how industrial pollutants cloaked the cities in thick gray smog (Barnwell, 2022).

Severe health and environmental concerns led to efforts in controlling air pollution, triggering the establishment of stricter regulations and the development of new technologies aimed at reducing emissions. However, the challenge of balancing industrial growth with environmental protection continues to be a major issue in the modern era. A detailed timeline outlining the key events and developments that contributed to the air quality issues and growing awareness over time in the industrial era is presented in **Figure 1.2**.

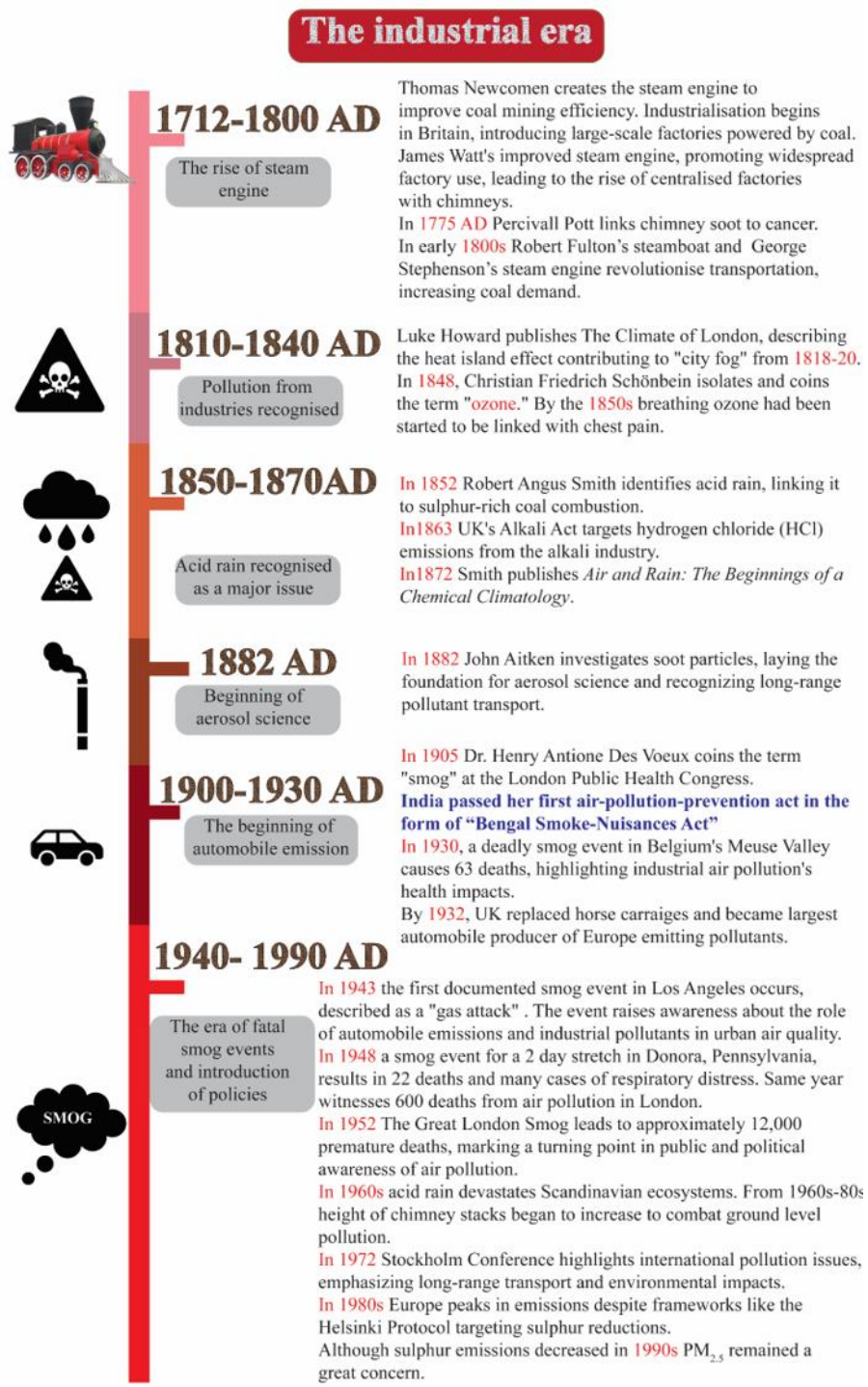

Figure 1.2: *A detailed timeline of events related to air pollution in the industrial era*

1.2. Ambient air pollution: Present scenario

In present days ambient air pollution still remains a global threat. Particulate matter (PM) is a critical component of ambient air pollution and exerts significant impacts on human health, ecosystems, and climate. A mixture of solid particles and liquid droplets suspended in the air forms these PMs, that varies in size and composition. It can be broadly categorized into coarse particles (PM_{10}, particles with diameters less than 10 micrometers) and fine particles ($PM_{2.5}$, particles with diameters less than 2.5 micrometers) (Guevara, 2016). Among these, $PM_{2.5}$ is of particular concern due to its ability to penetrate deep into the respiratory tract and subsequently to the bloodstream, causing severe health problems such as respiratory diseases, cardiovascular diseases, cancer and even premature death (Roser, 2021). As of 2019, 99 % of the global population lived in places where the air quality guidelines exceed the World Health Organization (WHO) prescribed limits. In the same year, WHO estimated that exposure to high levels of PM led to the premature death of as many as 4.2 million people worldwide (WHO, 2024).

Particulate matter originates from a complex and diverse mixture of sources that vary greatly depending on the region, land use, and prevailing economic and climatic conditions. Coarse particles primarily originate from mechanical processes and natural sources. Agricultural activities contribute significantly to coarse PM through the disturbance of soil during tilling, harvesting, and plowing, releasing organic carbon (OC) and mineral dust in the form of aerosols (Telloli et al., 2014). Vehicular traffic induced resuspension from road dust, tire, and brake wear generates urban coarse PM, especially in areas with high vehicle density (Fussell et al., 2022). Similarly, windblown dust, construction activities, mining operations play significant roles in elevating coarse PM concentrations (Muleski et al., 2005; Nieder et al., 2018). In coastal and marine regions, sea spray contributes to PM_{10}, as sea salt is carried inland by wind (Kayee et al., 2021, 2020). Events such as wildfires release OC, while volcanic activity adds ash as particulates to the atmosphere. Biological sources such as plant debris and fungal spores also contribute to coarse particles, particularly during seasonal changes in regions with extensive vegetation.

Fine particulates are more commonly associated with combustion processes and high-temperature activities. In urban settings, diesel and gasoline fueled vehicle engines along with small portions of non - exhaust emissions (NEE) are major sources, contributing significantly to PM emissions. Combustion processes involving coal, coke, and heavy oil, release fine particles rich in metals,

black carbon (BC) and OC. Biomass burning, such as agricultural stubble burning, wood burning for heating or cooking, and emissions from maritime traffic, especially from heavy fuel oil combustion, contribute significantly in specific regions. Industrial activities, such as metal processing and other industrial processes, further add to fine PM in urban-industrial regions (Harrison, 2020). A schematic representation of the present-day sources of PM are illustrated in **Figure 1.3**.

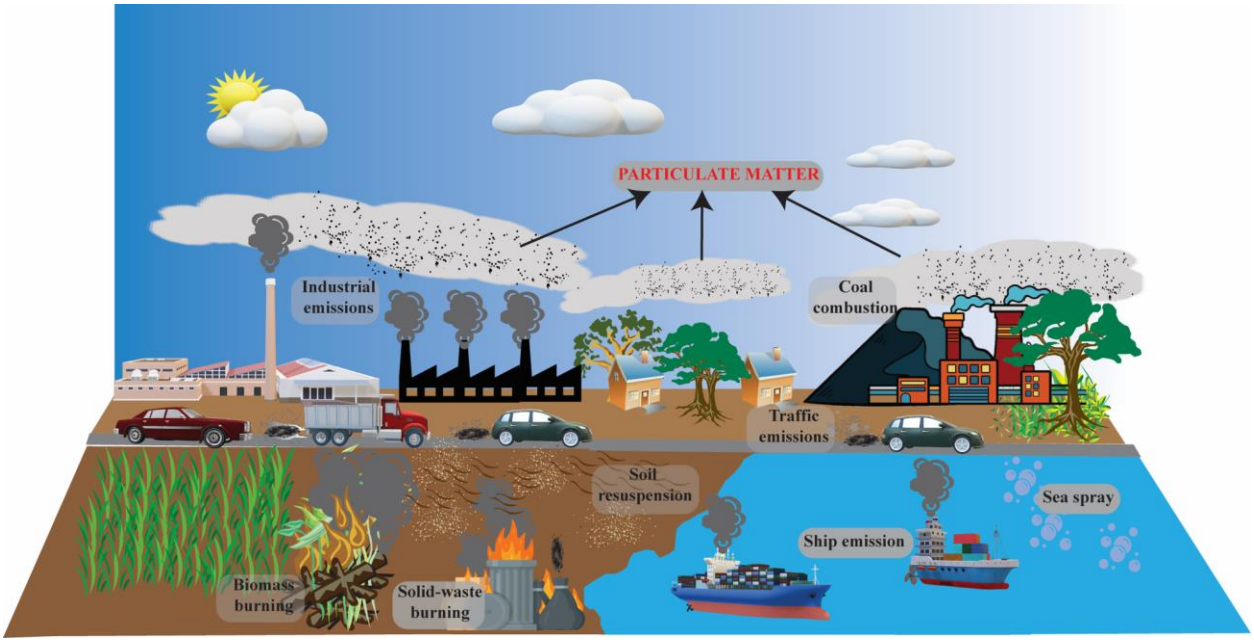

Figure 1.3: *A schematic representation of the present-day sources of PM pollution in India*

India faces severe PM pollution driven by rapid industrialization, urbanization, and population growth in the present millennium. Major sources include vehicular emissions, industrial activities, and biomass burning, particularly during winter for heating and cooking in rural areas (Venkataraman et al., 2018). Agricultural residue burning, notably in northern states like Punjab and Haryana, contributes heavily to seasonal PM spikes, exacerbating pollution in cities like Delhi (Bhuvaneshwari et al., 2019). Construction dust and unpaved roads also contribute towards atmospheric PM load. Despite efforts to promote cleaner energy, coal remains a dominant fuel for power generation, contributing to significant PM emissions.

India being one of the countries, most severely affected by PM pollution, experiences levels of $PM_{2.5}$ exceeding national and international air quality standards on majority of the days in a year. As of 2019, the population-weighted annual average concentration of $PM_{2.5}$ was ≥ 50 µg/m³, which is significantly higher than the WHO recommended annual limit of 5 µg/m³ (**Figure 1.4a**). This severe exposure to $PM_{2.5}$ in India is directly linked to one of the highest death rates in the world, with the country experiencing 94.4 deaths per 100,000 people (**Figure 1.4b**) (Our World in Data, 2024).

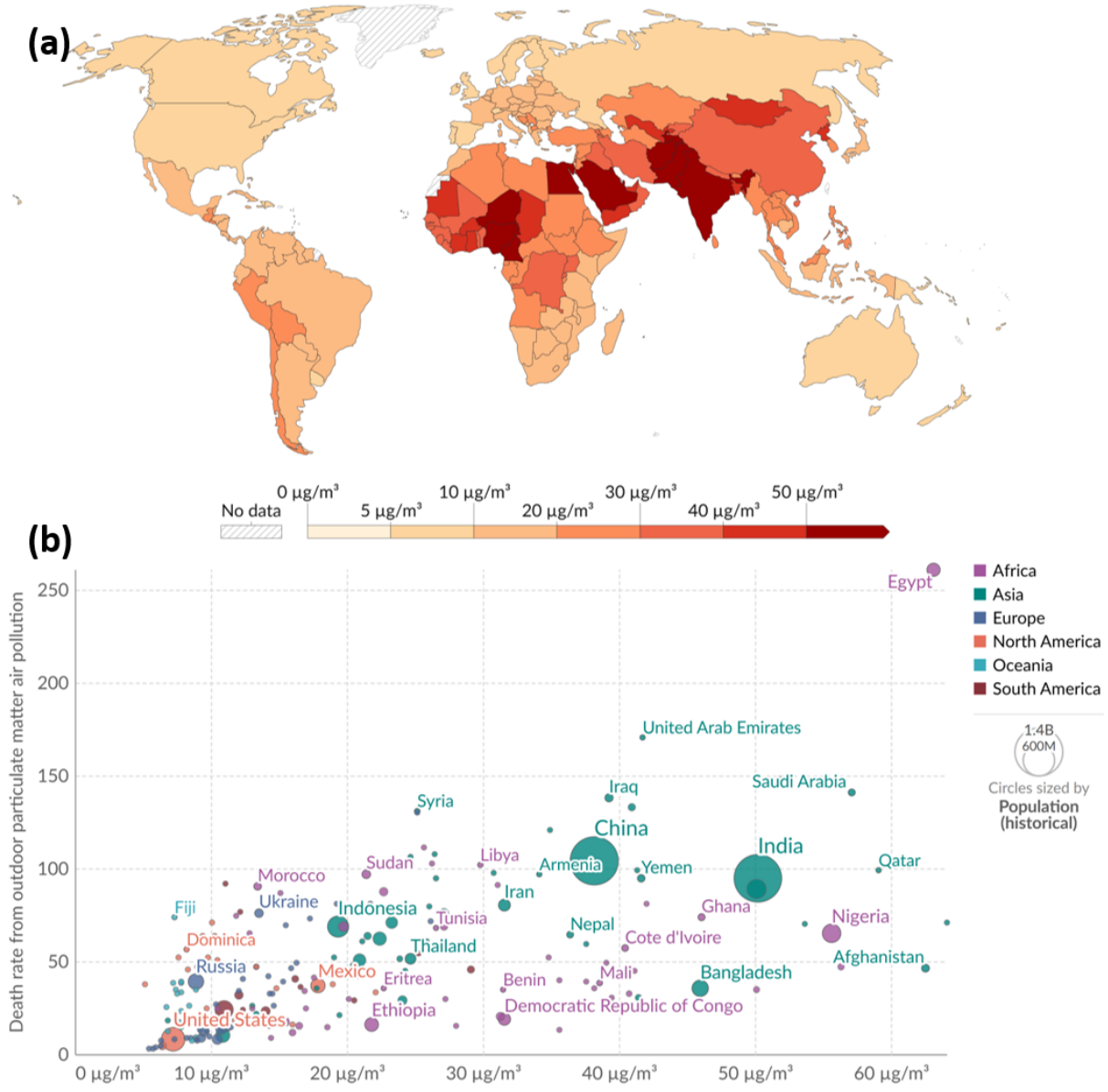

Figure 1.4: *(a) Population weighted average level of exposure to PM2.5 across the world in 2019 (b) Relationship between PM2.5 concentration and death rate from PM pollution in 2019. Data source: Our World in Data*

In India, the extensive reliance on fossil fuels for energy production significantly contributes to PM emissions, posing a severe health risk to her population. Data from 2015 reveals that India accounted for nearly 0.7 million deaths attributed to PM emissions from fossil fuel burning, an alarming share of the 3.6 million global fossil fuel deaths. (Roser, 2021). However, in 2015, India laid down strict environmental norms for coal-based thermal power plants to reduce pollution. The revised standards, notified on December 7, 2015, aim to lower emissions of PM_{10}, sulfur dioxide, and nitrogen oxides, to improve ambient air quality (PIB, 2015). However, it remains essential to monitor and evaluate whether these norms are being effectively implemented and restricting the emissions within targets. In 2019, modelling estimates revealed that combustion of solid fuels, especially in residential sector is the leading contributor towards mortality from ambient $PM_{2.5}$ (Chatterjee et al., 2023).

1.3. Metals present in particulate matter

Particulate matter from all the above-mentioned natural and anthropogenic sources serves as a significant carrier of metals and metalloids, with their concentrations and distribution varying by particle size and source. Coarser particles (PM_{10}) are typically enriched with elements which are abundant in natural sources such as crust and sea-spray that includes aluminum (Al), calcium (Ca), and iron (Fe), magnesium (Mg), potassium (K), sodium (Na) (Chester, 1990; Rudnick and Gao, 2003). In contrast, fine particles ($PM_{2.5}$) are highly enriched with toxic trace metals, including lead (Pb), cadmium (Cd), arsenic (As), mercury (Hg), zinc (Zn), and nickel (Ni), which predominantly arise from coal & biomass burning, vehicular emissions, and industrial activities such as metal smelting and waste incineration.

Fossil fuel combustion, particularly coal, is a major source of metals such as As, chromium (Cr), Hg, manganese (Mn), molybdenum (Mo), antimony (Sb), selenium (Se), tin (Sn), and zinc (Zn) while oil combustion significantly contributes to Ni and vanadium (V) emissions. Non-ferrous metal production is a key contributor of metals such as As, Cd, Cu, In, Sb, Pb, Se, and Zn into the atmosphere. Although the global phase-out of leaded gasoline has reduced Pb emissions, trace amounts of Pb in fuel still contribute to atmospheric pollution. Once emitted, these metals can travel vast distances through the atmosphere, ultimately depositing in terrestrial and aquatic ecosystems. This long-range atmospheric transport is evident in remote regions like the Arctic,

where elevated metal levels disrupt local geochemical cycles and pose risks to both ecosystems and human health (Pacyna, 1995; Pacyna and Pacyna, 2001; Schroeder et al., 1987).

In India, the widespread reliance on coal-fired power plants, industrial activities, and vehicular emissions makes the PM metal burden particularly significant. Studies have shown that metals such as Ni, Pb, V, and Zn are present at elevated concentrations in urban areas. Additionally, biomass burning, a prevalent practice in rural and agricultural regions, contributes to the release of K, Mg, and other metals (Boreddy et al., 2021; Chakraborty et al., 2023; Jain et al., 2020; Khobragade and Ahirwar, 2022; Kulshrestha et al., 2009; Mehra et al., 2020; Pandey et al., 2013; Police et al., 2016, 2018; Rabha et al., 2022).

Among these metals, particularly concerning is Pb. Majority of the anthropogenic as well as natural sources contain Pb in variable concentrations. Some anthropogenic sources of Pb, particularly those related to industrial activities such as smelting, waste incineration, Pb acid battery recycling and manufacturing can release vast quantities of this toxic metal into the environment. The anthropogenic Pb flux of 4309 ± 72 Gg/yr to the surface environment is approximately ten times higher than its natural flux (Sen et al., 2016). Among all the environmental compartments, the atmosphere is the major initial recipient of Pb.

This toxic non-essential metal is a criteria air pollutant that wreaks its havoc silently and insidiously and hence often goes unrecognized. Blood Pb levels (BLL) exceeding 5 μg/dL are affecting about 815 million children worldwide. India is one of the worst affected countries with the highest number of children having alarming BLLs. In India, more than 60 million children have BLL > 10 μg/dL and more than 250 million children have BLL > 5 μg/dL (UNICEF and Pure Earth, 2020) (**Figure 1.5**).

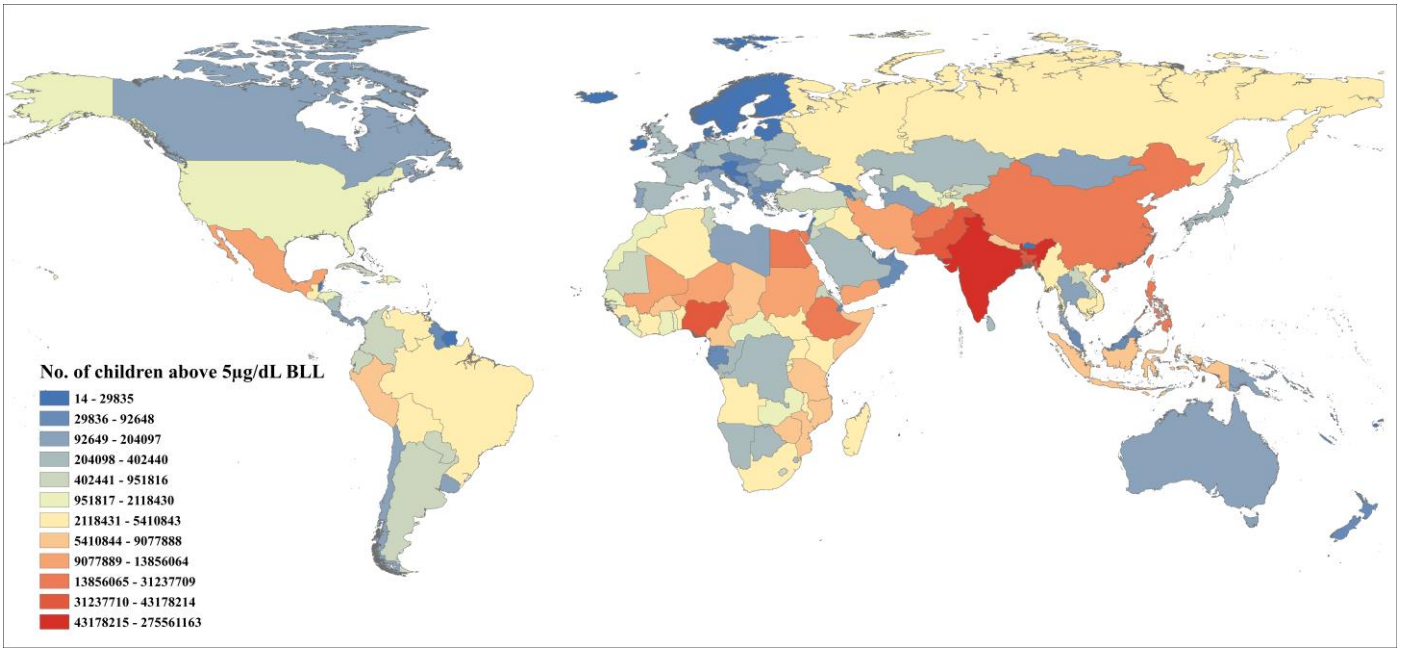

Figure 1.5: *A heat map representing the number of children having BLL > 5 ug/dL in the world. Data has been adopted from UNICEF and Pure Earth report, 2020.*

A meta-analysis examining children's blood Pb levels (BLL) in India revealed alarming findings. The study reveals that on average, children could lose up to 4 intelligence quotient (IQ) points from exposure to Pb. This analysis consolidated data from 31 studies, encompassing the BLLs of 5,472 individuals across nine Indian states. The findings demonstrated a mean BLL of 6.86 µg/dL for children and 7.52 µg/dL for adults with no known occupational exposure (Ericson et al., 2018). These elevated BLLs are a stark indicator of widespread environmental Pb contamination in India.

1.4. A brief history of Pb pollution across the world

Mining and use of Pb by humans has been going on for over 6,000 years, with its toxic effects documented for nearly 2,500 years. A detailed account of usage of Pb and its effects is presented in **Figure 1.5** as compiled from previous literatures (Hernberg, 2000; Jonasson and Afshari, 2018; Lessler, 1988; Patterson, 1987, 1965). The people of ancient Rome, were heavily exposed to Pb through various products like utensils, cosmetics, medicines, wine, and food sweetened with lead acetate or "sugar of lead." Roman plumbing systems also comprised of Pb, contributing to further exposure. Historical studies, including ice core analyses, show a significant rise in atmospheric lead during the Pax Romana period, linked to lead smelting and mining, with estimates suggesting cognitive declines in the population due to elevated Pb exposure (McConnell et al., 2025).

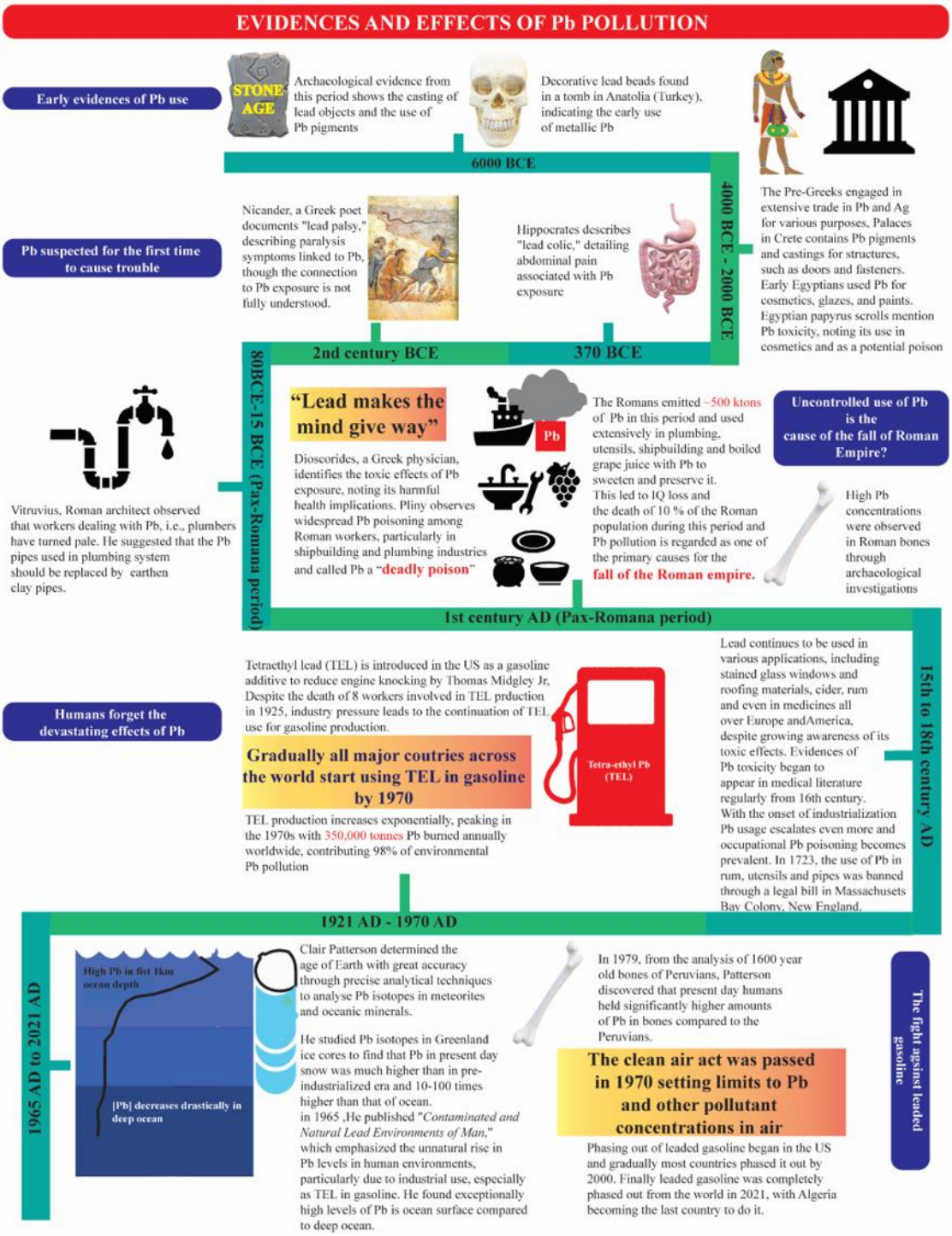

Figure 1.6: *A detailed account of use of Pb and its effects upon humankind*

Even though the toxic effects of Pb were known to humankind, its use continued extensively during the 15th to 19th century all over the world. A brief summary of the use and toxic effects of Pb during the 18th -19th century is presented in **Table 1.1**. Finally, in the 1920s tetraethyl Pb (TEL) doped gasoline was marketed in the USA, releasing tonnes of Pb into the atmosphere. By 1970 all major countries, including India adopted leaded gasoline and emission of Pb peaked during this time, releasing about 350,000 tonnes of Pb into the atmosphere. In India emission of Pb from gasoline peaked during 1980s – 1990s. **Figure 1.6** illustrates the gasoline Pb emission in India and other SEA countries (Lee et al., 2014).

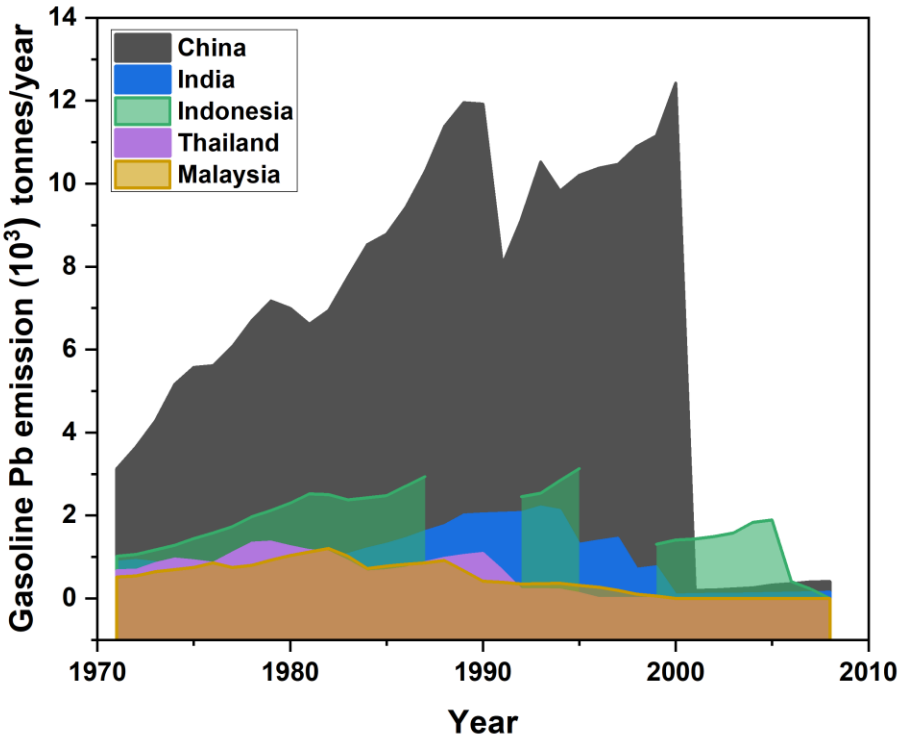

Figure 1.7: *Gasoline Pb emissions in India and other SEA countries as compiled from Lee et al., 2014*

Clair Patterson started his battle against use of TEL and his analysis of ice cores from polar regions provided critical evidence of the increase in Pb concentrations, correlating directly with the TEL into gasoline in the 1920s (Patterson, 1965). Patterson's measurements on Peruvian bones from 1600 years ago, demonstrated that present day Pb in human bones are much higher compared to the Peruvian people. He also demonstrated that the surface of North Atlantic Ocean has significantly higher Pb concentrations compared to deep waters and antient seawater. Isotopes of

Pb in the ocean indicated that the ratios have shifted from fluvial Pb discharge signatures to that of leaded gasoline in the surface ocean (Patterson, 1987). All evidences of Pb pollution put together led to the gradual phase-out of leaded gasoline, starting from the 1970s. Leaded gasoline in India was phased out in the year 2000. Finally, worldwide phase-out of leaded gasoline was achieved in 2021, with Algeria being the last country. Today, while Pb emissions from gasoline have been largely eliminated, Pb remains a persistent environmental issue, with ongoing concerns regarding its presence in emissions from different sources, especially coal (Lee et al., 2014).

***Table 1.1**: Sources of exposure to Pb and its effects from 18th to 19th century across the world as compiled from Jonasson and Afshari, 2018.*

Category	Source	Symptoms	Reasons for Use
Occupational Exposure	White Pb producing factories, pottery, coloured glass, tinfoil, dyes, miners, brass, steel, suitcase cloth, artificial rubies	Blue gum line, paralysis, colic, anemia	White lead: Used as a pigment in paints for its durability and opacity. Red lead: Used as a corrosion-resistant primer for metals and glass production.
Drinking Water	Lead pipes, contaminated wells	Sterility, spontaneous abortion	Lead pipes: Chosen for plumbing due to malleability and resistance to corrosion, ensuring long-term use in water distribution.
Food Contamination	Candies, flour, black pepper, cider, vinegar, tinned foods, rum, wine, beer, confectionaries and beverages	Chronic poisoning	Candies and flour: Pb salts added to enhance color. Black pepper: A mixture of Pb and Sn was mistaken for pepper. Tinned foods: Pb solder used to seal cans. Rum and wine: Pb used as a sweetener and precipitate hops bitters in beer.
Cosmetics and Fabrics	Lead-based cosmetics, silk soaked in lead acetate	Dermal absorption leading to Pb poisoning symptoms	Pb acetate: Used in cosmetics for its smooth texture and in fabrics to enhance weight, improving perceived quality.
Medical Uses of Lead	Lead acetate in treating cholera, diarrhea, pulmonary diseases, yellow fever, uterine disorders, abdominal issues, epilepsy etc.	Fatal poisoning	Lead acetate, believed to have therapeutic properties was used as a medicine extensively.
Kitchen Utensils and Containers	Lead-lined jars, earthenware containers, acidic food storage	Chronic poisoning	Lead linings: Used for corrosion resistance in jars and utensils; helped prevent leaks and extended the lifespan of these items.
Spices and Syrups	Contaminated cayenne pepper, grape syrup	Chronic poisoning	Added for color enhancement and sweetening precipitate hops bitters in beer.
Storage Practices	Butter, lard, and oily foods stored in lead containers	Chronic poisoning	Lead readily mixes with fats, leading to contamination.

1.5. The recent scenario of atmospheric Pb pollution in India

National Ambient Air Quality Standards (NAAQS) limits for Pb concentration in ambient air should not exceed 500 and 1000 ng/m^3 annually and daily (24 hours) respectively, in industrial, residential, rural, and other area and ecologically sensitive areas. In India, few studies investigated atmospheric aerosol Pb before the year 2000, that marked the phase out of leaded gasoline in the country. However, post 2000, there have been numerous reports of atmospheric Pb over Indian cities (Arun et al., 2019; Balachandran et al., 2000; Bandhu et al., 2000; Basha et al., 2010; Bhuyan et al., 2018; Bikkina et al., 2015; Boreddy et al., 2021; Botle et al., 2020; Chelani et al., 2001; Das et al., 2015; R. Das et al., 2018; Das, 2022; Dubey et al., 2012; Gaghate and Hasan, 1999; Gajghate et al., 2012; Gajghate and Bhanarkar, 2004, 2005; Gaonkar et al., 2020; Gokhale and Patil, 2004; Gummeneni et al., 2011; Jain et al., 2020; Jena et al., 2019; Karar and Gupta, 2006; Khare and Baruah, 2010; Khillare et al., 2004; Khillare and Sarkar, 2012; Kulshrestha et al., 2009; Mishra and Padmanabhamutry, 2003; Negi et al., 1986; Panda et al., 2021; Pant et al., 2015; Panwar et al., 2020; Perrino et al., 2011; Pipalatkar et al., 2014; Police et al., 2016; Sah, 2023; Sen et al., 2016; Shridhar et al., 2010; Shukkur et al., 2021; Singh and Sharma, 2012; Sudheer and Rengarajan, 2012; Yadav and Satsangi, 2013). From the literatures, it can be summarized that before banning of leaded gasoline, industrial emissions were significant sources of atmospheric Pb in smaller cities whereas automobile exhaust dominated atmospheric Pb release in the metro cities of India which had a large fleet of vehicles on road (Chelani et al., 2001; Gokhale and Patil, 2004). Interestingly, even after banning of leaded gasoline, in many of the urban and industrial centers, atmospheric Pb exceeded the NAAQS annual Pb concentration limit of 500 ng/m^3 (**Figure 1.7**) in ambient air. India's coal-based power generation has expanded significantly in the past three decades, with Pb emissions from coal now comparable to those from leaded gasoline exhausts (Lee et al., 2014). This suggests that shifts in the emission of Pb, from gasoline to coal, are key to understanding current levels of atmospheric Pb pollution in India. Thus, from the BLLs and atmospheric Pb concentrations in India, it is quite evident that even after the phase-out of leaded gasoline, the presence of Pb in atmosphere from other sources is still wreaking havoc especially to the children. As no level of Pb exposure can be considered safe, delineating the sources and their respective contributions must be comprehensively studied.

1.6. Current understanding of sources of atmospheric Pb in India

It is difficult to differentiate Pb sources solely based on elemental concentration studies. Thus, ratios between isotopes of Pb (^{204}Pb, ^{206}Pb, ^{207}Pb, ^{208}Pb) is commonly used as a ‘‘fingerprinting’’

tool to study Pb contamination (Komárek et al., 2008). Isotopes of Pb are the result of radioactive decay chains. Specifically, ^{206}Pb, ^{207}Pb, and ^{208}Pb are formed through the decay of uranium (U) and thorium (Th) with ^{206}Pb decaying from ^{238}U, ^{207}Pb from ^{235}U and ^{208}Pb from ^{232}Th, while ^{204}Pb is a stable isotope not involved in decay. The isotopes of Pb in a particular component, vary in their natural abundances depending on their initial U and Th concentrations and hence each component demonstrates unique Pb isotopic composition. For example, Pb from leaded gasoline and will have distinct isotopic signatures compared to Pb from coal combustion. This distinct isotopic composition is particularly useful in identifying anthropogenic contamination from different sources.

There have been very few studies in India (Bollhöfer and Rosman, 2001; R. Das et al., 2018; Kumar et al., 2016, 2018; Sen et al., 2016) on atmospheric Pb isotopes to understand the anthropogenic sources. From these studies it was observed that, the Indian aerosol $^{206}Pb/^{207}Pb$ ratio varies between 1.1155–1.1681. The only study that measured Pb isotope ratio before leaded gasoline phase out was in 1995 ($^{206}Pb/^{207}Pb$ = 1.137) by Bollhöfer and Rosman, 2001. This study identified automobile exhaust to be the primary source of atmospheric Pb. After one and half decades of gasoline ban in India, Pb isotopes were measured in aerosols from Kanpur, Delhi and Kolkata. The isotopic ratios identified industrial emission and "legacy lead" from leaded gasoline recirculating in the environment as the plausible source of anthropogenic Pb in the atmosphere of Kanpur (Sen et al., 2016). In Delhi, aerosols were collected during, before and after a dust storm event. The $^{206}Pb/^{207}Pb$ ratios were 1.1311 ± 0.0022, 1.1244 ± 0.0017 and 1.1233 ± 0.0016 during dust storm, post dust storm and winter aerosol samples respectively. A distinct difference in Pb isotopic composition between dust storm and urban aerosols were reported. Transported dust aerosols from Middle East demonstrated more radiogenic Pb with respected to $^{206}Pb/^{207}Pb$ (Kumar et al., 2016). In spite of presence of numerous medium and small-scale industries in and around Delhi, it was inferred that coal combustion was unlikely to contribute significantly to aerosol Pb. Instead, the Pb isotope ratios were closer to unleaded gasoline and probably a potential source. In Kolkata, samples were collected at three locations along a 150 Km N-S stretch with distinctive environmental settings; a pristine river island (Sagar Island on Bay of Bengal), a megacity (Kolkata), and an industrial town (Bandel) all in West Bengal. The Pb isotope ratios ($^{206}Pb/^{207}Pb$ =1.1155–1.1681) measured in this study had a wider range and are mostly higher than previously

measured in Indian aerosols. Das et al., 2018 observed that post leaded gasoline phase-out, the atmospheric Pb emissions in India are dominated by Indian coal combustion and ore processing.

1.7. Addressing atmospheric Pb pollution

Various systems are employed for ambient air PM reduction, primarily using mechanical and electronic filtration technologies. Portable air cleaners with high-efficiency particulate air (HEPA) filters are widely used to capture fine particulate matter ($PM_{2.5}$) with an efficiency of 99.97% for particles as small as 0.3 microns (CARB, 2020). Activated carbon filters, while primarily designed to adsorb gaseous pollutants, also capture PM to some extent. Advanced systems, such as hybrid air cleaners combining HEPA filtration with activated carbon or ultraviolet germicidal irradiation (UVGI), address both particulate and microbial pollutants. Some ionizer-based devices are claimed to reduce PM by generating charged particles that settle on surfaces, though their efficiency in ambient settings can be limited. However, these systems typically focus on reducing PM mass concentrations and may not specifically target PM-bound heavy metals (US EPA, 2014).

Biological systems, such as plants and microorganisms, have shown potential in reducing particulate matter (PM), yet their application has been limited to monitoring and assessing air quality, rather than active sequestration. The use of moss in studying atmospheric pollutants was first developed in the 1960s (Ruehling and Tyler, 1969). Since the last three decades, there has been an increased emphasis on biomonitoring of atmospheric trace metals using mosses and lichens. While in some studies mosses and lichens have been observed for their ability to accumulate heavy metals and absorb PM, few studies focus on their use in long-term sequestration or air purification. It has been observed that a close-set, single cell-walled moss leaves allow for close contact with the ambient air while also filtering the air during the nutrient uptake process (Ruehling, 1995)(Rühling, 1994). Mosses, particularly in high-traffic areas, have demonstrated significant PM trapping capabilities (Kayee et al., 2015), with moss turfs in Australia capturing 3.8 times more PM than vascular plants (Haynes et al., 2019). In Germany, a combination of vascular plants and moss substratum showed a synergistic effect, reducing PM by up to 25% (Sänger and Splittgerber, 2016).

In India, biomonitoring of atmospheric heavy metals using mosses and lichens has been going on for a few years. Mosses and lichens in sites with heavy traffic and nearby industries accumulate more heavy metal than those growing in relatively cleaner regions (Majumdar et al., 2019; Vats et

al., 2010). Kar et al., 2014 identified lichen species in Kolkata which were particularly resistant to heavy metal stress and also assessed their efficiency in accumulating certain heavy metals. The lichen *P. caperata*, growing in a region with heavy traffic volume, accumulated an annual average of 287 ± 12.5 μ/g Pb. Highest metal uptake was observed in winter. The efficiency of *P. caperata* in accumulating metal can be attributed to its rough surface. Thus, *P. caperata* with its high longevity and ability to withstand heavy metal stress was delineated to be a suitable sequestering agent (Kar et al., 2014). Similarly in Delhi *Physcomitrium cyathicarpum* and *Barbula constricta* was found out to be metal tolerant moss species. However, no studies on bioremediation of atmospheric pollutants using such tolerant mosses and lichens have been undertaken in India

A few plant-based air purification systems have been developed across the globe with varying focuses (Ibrahim et al., 2021; Pettit et al., 2021, 2017). Some systems use bacterial colonies in hydroponic setups to break down organic pollutants however, do not address heavy metal removal. Other systems utilize bonsai plants to absorb organic pollutants, However, they do not measure particulate matter or heavy metal removal efficiency. Some technologies focus on $PM_{2.5}$ removal during haze, although they do not quantify heavy metal removal (Chen, 1994; Darlington, 2014; Liu, 2016; Renzhengang and Li, 2015).

CHAPTER 2: AIMS AND OBJECTIVES

Despite efforts to reduce Pb emissions through the phasing out of leaded gasoline and stricter industrial regulations, significant sources of atmospheric Pb persist that includes coal combustion, vehicular emissions, and industrial activities. Additionally, the resuspension of Pb from road dust and other environmental reservoirs exacerbates the issue, particularly in urban areas. Many sources of atmospheric Pb remain poorly identified or undocumented, leading to gaps in our understanding of its distribution and behavior. Limited/no data on the elemental and Pb isotopic compositions of certain anthropogenic sources hinders precise source attribution, especially in regions with diverse pollution sources. Furthermore, the development of sustainable solutions, in mitigating Pb pollution is necessary. Thus, there is a need to bridge these knowledge gaps by identifying, characterizing and quantifying known and unknown Pb sources, evaluating the effectiveness of existing regulatory measures, and exploring innovative remediation approaches. The following aims outline the comprehensive structure of this thesis:

- To identify and quantify the sources of atmospheric Pb pollution in India and SEA countries over the last decade, using data from existing literature.
- To determine the elemental and Pb isotopic compositions of undocumented anthropogenic end members, improving the precision of source attribution in atmospheric studies.
- To quantify toxic metal emissions, particularly Pb, from road transport emissions (both exhaust emissions [EE] and non-exhaust emissions [NEE]), and determine their contribution to Indian road dust.
- To evaluate whether stricter emission norms introduced post-2015 has led to decrease in Pb emissions from coal combustion in India.
- To investigate the sources of Pb in a pristine environment by selecting a control site with minimal anthropogenic influence, such as the Andaman and Nicobar Islands, where coal-based power generation and industrial activities are absent.
- To explore the potential ferns for the removal of atmospheric Pb and other toxic metals, particularly in indoor environments

To fulfil these aims, the research is structured around the following well-defined objectives:

- To compile Pb isotopic compositions and elemental ratios from existing literature for India and SEA over the last decade, identifying overlooked/underdetermined sources of atmospheric Pb pollution.
- To apply a Bayesian source apportionment model on the compiled literature to accurately quantify contributions from various sources in the region for the past decade.
- To determine the Pb isotopic and elemental compositions of poorly documented sources such as ship fuel, vehicular fuel (particularly Indian fuel), and non-exhaust emissions (NEE) from tire wear, brake dust, and road pitch, by performing extensive sample collection and analysis.
- To revisit and analyze Pb ore samples, such as galena, which were last characterized in the 1990s, and update their Pb isotopic and elemental profiles for source attribution studies.
- To determine the sources of heavy metals in urban and semi-urban road dusts of eastern India using elemental concentration coupled with Pb isotopic compositions of exhaust emissions (EE) and non – exhaust (NEE
- To quantify the relative contributions of individual EE and NEE sources (vehicular exhaust, brake wear, tire wear, road pitch, road paint and crust) towards the road dusts using Bayesian stable isotope mixing model (MixSIAR)
- To conduct an emission analysis of heavy metals from both EE and NEE sources, using the analyzed elemental concentrations, and establish statistics for present and future metal emission scenario from traffic between the time period of 2022 and 2045
- To collect seasonally resolved $PM_{2.5}$ aerosol samples from the Neyveli lignite-fired power plant, the largest in South India
- To analyze end members in the power plant that includes feed lignite, fly ash, solid waste ash, crop ash, and local soil to perform source apportionment of atmospheric Pb from this region of coal combustion
- To collect PM_{10} and $PM_{2.5}$ aerosol samples over two seasons (winter and summer) from the Andaman and Nicobar Islands

- To investigate whether the seasonal reversal of wind patterns affects the sources of Pb and to quantify contributions from natural and minimal anthropogenic sources in a pristine environment compared to the polluted Indian mainland
- To identify fern species growing in highly polluted cities that exhibit high tolerance to PM exposure, based on field survey
- To determine the elemental concentrations of metals accumulated in ferns and use Pb isotopic compositions to trace whether the captured metals originate from the atmosphere or soil
- To evaluate the potential of ferns as effective bio-capture devices for atmospheric Pb and other toxic metals in indoor environments

CHAPTER 3: MATERIALS AND METHODS

3.1. Collection of PM_{10} and $PM_{2.5}$ aerosol samples and dustfall (DF) samples

The PM_{10} aerosol samples at Kolkata were collected for 14 days using a personal modular impactor PM_{10} (PMI, SKC Inc., USA) connected to a Deployable Particulate Sampler (DPS, Leland Legacy Pump, SKC Inc., USA) with a pumping efficiency of 10L/min. At Andaman and Nicobar Islands PM_{10} and $PM_{2.5}$ aerosol samples were collected by a two-stage inertial SKC IMPACT $PM_{10-2.5}$ and $PM_{2.5}$ sampler (SKC Inc., USA) connected to a Deployable Particulate Sampler (DPS, Leland Legacy Pump, SKC Inc., USA) with a pumping efficiency of 10 L/min. The PM_{10} samples were collected upon 47mm Polytetrafluoroethylene (PTFE) filters. At Neyveli the $PM_{2.5}$ sampling was performed with Envirotech APM 550 MFC sampler at a constant flow rate of 1 m^3/hr. The samples were collected in pre-weighed 46.2mm Whatman PTFE filters with a pore size of 2 μm. All filter papers for aerosol sample collection were pre-washed with 1N HCl at 140°C before being rinsed several times with ultrapure water. The filters were dried in an oven at 60°C, weighed, and sealed in pre-cleaned petri dishes before sampling. The samplers were placed on the roofs of buildings approximately 12 m above ground level (AGL). The concentrations of PM were determined gravimetrically by weighing then after sampling.

Dust fall samples were collected on acid washed polystyrene Petri dishes (90 mm diameter) exposed for 7 days. Pre-weighed petri dishes (n = 6) were fixed on roofs of buildings using double sided tapes to avoid any disturbance due to wind during dust settling (Gulson et al., 1995). No rainfall event occurred during the period of sampling. The petri dishes were sealed and kept inside airtight zipper bags before being processed for analysis.

3.2. Collection and pre-processing of traffic emission samples

All the traffic emission samples were collected from different locations in the city of Kolkata. The surfaces of the collected tire segments (n = 5) and brake pads (n = 3) were collected from local car repairing shops. sonicated in Milli-Q water to remove loose contaminants. Following cleaning, the tires were cut and homogenized into small pieces. The brake pads were scraped to generate loose homogenized brake wear particles. Samples of yellow and white road paint (n = 2) were applied and dried on polypropylene sheets, following which they were scraped off as dry particles (Jeong et al., 2022). Road pitch samples (n = 7) were collected from road, crushed and homogenized into finer particles. Vehicular exhaust samples (both petrol and diesel) (n = 5), along with vehicular

exhaust from tailpipes, were also collected. The soot from tailpipes were scrapped off using plastic knifes directly into Ziploc bags.

3.3. Collection of vehicular and ship fuel samples

Vehicular fuel samples of petrol and diesel (n = 5) were collected rom petrol pumps in Kolkata. High-speed diesel, along with lubricant samples (15W40, OMD 113) from the gearbox, and coolant samples (Havoline and Primax), were collected as ship oil samples. A total of three diesel samples, five lubricant samples, and three coolant samples were obtained for analysis. The engine was of a large survey vessel named Sandhayak with 4 strokes and 9 cylinders, built and maintained by Garden Reach Shipbuilders & Engineers Limited (GRSE). The engine has 270 mm bore and 380 mm stroke size and operates at a speed of 800 rpm with a maximum power of 3285 kW.

3.4. Collection and pre-processing of fern and associated samples

Pteris vittata and *Pteridium aquilinum* were observed to be widely distributed species of ferns throughout the region. Both species were sampled from 12 sites, from about 1 – 1.5 m above the ground. All the plants were in good condition and none were shaded by overhead vegetation, ensuring that the leaves were fully exposed to the atmospheric fallouts. Leaves were hand-plucked and samples from each site were sealed in separate acid-washed plastic containers to prevent cross contamination and minimize PM loss from the leaf surface. The roots of corresponding plants along with the rhizosphere soils of individual sample were sealed in separate ziploc bags. Plants of similar age determined by their appearance (height, sori development) and identified by surveying local people were selected for the study. Samples were collected at each site on the same days under rainless conditions.

3.4.1. Gravimetric quantifications and determination of leaf surface area

Foliar dusts were categorized as: (i) Loose dust (LD) and (ii) Wax bound dust (WD). The loads of dust on the leaves were determined gravimetrically using washing and weighing method (Dzierżanowski et al., 2011). A total of 22 leaves were weighed and submerged in ultrapure water (Resistivity = 18 MΩ.cm) in a 50 mL centrifuge tube and hand-shaken for 10 mins to remove the LD. The same leaf was removed from the water and submerged in trace metal grade chloroform in a separate pre-weighed Teflon beaker and shaken for 10 mins to remove the WD. The water was transferred into pre-weighed Teflon beakers and both the water and chloroform were evaporated. After evaporation the beakers were reweighed to quantify the amount of LD and WD captured by

each leaf. The cleaned leaves were photographed against a white backdrop and a digital file was created. The images were analyzed by Image-J software to calculate the individual leaf surface areas (O'Neal et al., 2002). The cleaned leaves, roots and rhizosphere soils were dried at 60 °C until constant weight and ground in agate mortar and pestle for further processing.

3.4.2. Microscopic observations of leaf-surface PM by SEM-EDX

A dusty leaf from each species were dried at 60°C until constant weights. The samples were sputter coated with platinum. The adaxial and abaxial surface PM of the leaves were examined using the ESEM (SEM: ZEISS EVO-MA 10; Carl Zeiss Pvt. Ltd., Oberkochen, Centre for Research in Nanoscience and Nanotechnology, University of Calcutta) at 500x and 200x magnifications. Energy Dispersive X-Ray Analysis (EDX) (SmartEDX, Carl Zeiss) was performed to observe the elemental content of elements present on the surface of the leaves.

3.5. Sample processing for extraction of elements

All samples were processed in clean chemistry laboratory using Milli-Q water, having resistivity > 18.2 MΩ-cm and acids purified by sub-boiling distillation of concentrated reagent grades.

3.5.1. PM_{10} and $PM_{2.5}$ aerosol and dustfall samples

The aerosol and dustfall samples were subjected to hot plate digestion in screw cap Teflon beakers (Savillex^{TM}) for 24 hours at 120°C in a mixture of concentrated 3:1 HNO_3 and HF. The digested samples were evaporated to dryness. The dried samples were redissolved and refluxed twice in concentrated HNO_3 to remove traces of HF. The solutions were dried down and redissolved in 2 mL of 2 % HNO_3, half of which was utilized for determination of elemental concentration and the other half was stored for performing anion exchange chromatography to separate Pb.

3.5.2. Lignite, fly ash, soil, solid waste ash, biomass burning ash and galena samples

Initially, the lignite samples were ashed in a muffle furnace at 300°C for 1 hour and 500°C for the next two hours before subjecting them to acid digestion (Díaz-Somoano et al., 2009). About 20 mg of the ashed lignite, top soil, SW burning ash, biomass burning ash, fly ash samples were weighed and subjected to hot plate acid digestion for 24 hours at 120°C in a mixture of concentrated 3:1 HNO_3 and HF. The digested samples were evaporated to dryness. The dried samples were redissolved and refluxed twice in concentrated HNO_3 to remove traces of HF. The solutions were dried down and redissolved in 2 mL of 2 % HNO_3, half of which was utilized for

determination of elemental concentration and the other half was stored for performing anion exchange chromatography to separate Pb.

3.5.3. Brake wear, tire wear, vehicular exhaust, road pitch and road dust samples

The homogenized brake wear, tire wear, road pitch, and road paint samples were weighed (~30 mg) and digested for 24 hours at 120°C in screw cap Teflon beakers (Savillex^{TM}) using a concentrated acid mixture of HNO_3 and H_2O_2 in 2:1 ratio. The vehicular exhaust samples were digested in concentrated HNO_3 at 120°C for 24 hrs in screw cap Teflon beakers (Savillex^{TM}). The solutions were dried down and redissolved in 2 mL of 2 % HNO_3, half of which was utilized for determination of elemental concentration and the other half was stored for performing anion exchange chromatography to separate Pb.

3.5.4. Vehicular and ship fuel samples

The ship and vehicular oil samples (1 mL each) were ashed using a muffle furnace in high-temperature-resistant Pyrex tubes, plugged with quartz wool. Prior to use, the Pyrex tubes were acid-washed. The ashing process was conducted at approximately 500°C for several hours until visible ash residues accumulated at the bottom of the tubes. To prevent combustion, the temperature was gradually increased in small increments throughout the process (10°C every 5 mins). The ashes were digested in a mixture of aqua regia and hydrogen peroxide (1:1) (Sugiyama and Williams-Jones, 2018). All the digested samples were evaporated to dryness. The dried samples were then dissolved in 2 mL of 2% HNO_3, with one half used for elemental concentration analyses and the other half reserved for anion exchange chromatography to isolate Pb.

3.5.5. Fern and associated samples

All samples were digested in Teflon beakers at 120 °C using different mixtures of acid necessary for maximum elemental extractions as reported in **Table 3.1**.

***Table 3.1**: Digestion mixtures used for different types of samples*

Sample Type	Acid Mixture	References
PM_{10} aerosols	HNO_3 : HF = 50% of 3 : 1	(Kayee et al., 2021); USEPA 3052, 1996)
Dust fall	HNO_3 : HF = 3 : 1	
Loose dusts	HNO_3 : HF = 3 : 1	
Wax bound dusts	Aqua regia : H_2O_2 = 1: 1 followed by HNO_3 : HF = 3 : 1	
Cleaned leaves	HNO_3 : H_2O_2 = 2 : 1	(Lamble and Hill, 1998)
Roots	HNO_3 : H_2O_2 = 2 : 1	(Lamble and Hill, 1998) USEPA 3052, 1996
Soils	HNO_3 : HF = 3 : 1	

The WDs were subjected to iterative treatment using HCl, HNO_3 and H_2O_2 to fully digest the wax. The sequential leaching steps for the selected soil sample included reflux of dried leached fractions in concentrated HNO_3 after extraction of (i) exchangeable fraction (SE) by 1 M Sodium Acetate at pH 7.8; (ii) carbonate fraction (SC) by 1 M Sodium Acetate adjusted to pH 5 with Acetic acid; (iii) reducible/Fe-Mn fraction (SR) in 0.04 M Hydroxylamine hydrochloride dissolved in 25% (v/v) acetic acid; and (iv) dissolution of silicate fraction (SS) in concentrated Nitric and Hydrofluoric acid mixture (3:1) (Tessier et al., 1979).

The acid mixtures for all types of samples were evaporated following digestion for 24 h. The samples containing HF were refluxed twice using concentrated HNO_3 and evaporated to remove any traces of HF. Finally, the dried samples were dissolved in 2 mL of gravimetrically prepared 2% HNO_3. From this 2 mL, half was utilised for concentration analyses and the other half for Pb isotope determination.

3.6. Sample processing for purification of Pb

For separation of Pb, the samples in 2 % HNO_3 were dried down and redissolved in ultrapure 1.1 N HBr. The column elution acids were 1.1 N HBr, 2 N and 6 N HCl which were prepared volumetrically and titrated against 1.0 N NaOH to determine their exact normality. Elution was performed in shrinkable Teflon columns packed till neck with pre-cleaned anion exchange resin

(Eichrom AG-1X8 chloride form, 200 – 400 mesh). The resin cleaning process involved sequential centrifugation at 3000 rpm for 6 minutes first in Milli-Q water, followed by 2 N HCl and subsequently with 6 N HCl. The columns were fitted with acetate membrane frits. The column-loaded resin is cleaned by passing double-distilled 6 N HCl twice. The columns filled with resin were conditioned with 400 µL of 1.1 N HBr before loading the samples (100 – 200 µL). This step was followed by elution usi ng 600 µL of 1.1 N HBr and 400 µL of 2 N HCl. Finally Pb was eluted in 600 µL of 6N HCl (Reuer et al., 2003). The Pb eluted in HCl was evaporated and redissolved in 2 % HNO_3.

3.7. Determination of elemental concentrations

All aerosol and DF samples from Neyveli, Andaman and Nicobar Islands and end member samples including, lignite, fly ash, solid waste and biomass burning ash, soil, galena, chalcopyrite road emission samples were analysed using the Thermo Scientific iCAP Q ICP-MS at Earth Observatory of Singapore, Nanyang Technological University, Singapore. For elements having high concentrations in the road emission samples (Al, Ba, Ca, Fe, Mg, Mn, Cu and Zn), measurements were initially performed on an Thermo Scientific^{TM} iCAP 7000 inductively coupled plasma - optical emission spectrometer (ICP – OES) at the Paleothermometry Laboratory of National Centre for Polar and Ocean Research (NCPOR), Goa, India. For standard sample bracketing, a multi element standard (Merck ICP ME IV) of 5 ppm was used. The obtained intensities of the samples were drift corrected and normalized with respect to the intensity of the bracketing standard.

The sample introduction setup for iCAP Q ICP-MS included a Peltier cooled quartz cyclonic spray chamber, a PFA concentric nebulizer (100µL/min), and a demountable quartz torch with a quartz injector. Platinum sampler and skimmer cones were employed at the quadrupole – torch interface. All the samples and standards were diluted in 2 % HNO_3. The instrument was operated in a single collision cell mode with kinetic energy discrimination (KED), employing pure helium (He) as the collision cell gas to remove polyatomic interferences. The instrument was tuned in iCAP Q tuning solution comprising of 1 µg/L of Ba, Bi, Ce, Co, In, Li and U. Multi element calibration standards ranging from 0.1 ppb to 500 ppb were freshly prepared gravimetrically and analyzed to obtain linear calibration curves. A multi element standard of 10 ppb was used for standard – sample bracketing. Drift corrections and normalization of the obtained raw counts per second (cps) were

performed with respect to the bracketing standard. The instrumental operating conditions are presented in **Table 3.2**.

***Table 3.2**: iCAP Q ICP-MS Operating Conditions*

RF Power	1550 W
Sample depth	5.0 mm
Nebulizer Gas	1.04 L/min
Nebulizer Pump	40 rpm
S/C T	2.7 °C
Dilution Gas	0.41 L/min
He flow	5.32 ml/min

All the PM_{10} aerosol samples from Kolkata and fern and associated samples were initially measured for elements having high concentrations (Al, Ba, Ca, Fe, Mg, and Mn) on an Agilent 5800 Inductively coupled plasma - optical emission spectrometer (ICP – OES). Analytes having lower concentrations (Ti, V, Cr, Ni, Co, Cu, Cd and Pb) were measured on an Agilent 8900 Triple Quadrupole Inductively coupled Plasma Mass Spectrometer (ICP – MS, Agilent Technologies, Santa Clara, CA, USA). Thus, concentrations of 14 elements (Mg, Al, Ca, Ti, V, Cr, Mn, Fe, Co, Ni, Cu, Cd, Ba, and Pb) were determined for all the samples using the above – mentioned instruments at Centre for Earth Sciences, Indian Institute of Science, Bangalore.

The sample introduction system of the ICP – OES includes a peristaltic pump, with a micro mist concentric nebulizer (800-900 µL/ min), and a quartz double pass spray chamber. The wavelengths selected for the analytes on the ICP – OES had the highest sensitivity and lowest spectral interferences from other elements. Multi-element calibration standards ranging from 0.1 ppm to 20 ppm were freshly prepared gravimetrically and analysed. A multi-element standard of 1 ppm was utilised for standard – sample – standard bracketing. Drift corrections and normalisations of the raw data were performed with respect to the intensities of the bracketing standard. The instrumental operating conditions and figures of merit are reported in **Table 3.3** and **Table 3.4** respectively.

***Table 3.3**: ICP - OES Operating Condition*

RF Power (kW)	1.2
Plasma Gas flow (L/min)	12
Auxiliary Gas flow (L/min)	1

Nebulizer Flow (L/min)	0.70
Pump Speed (RPM)	12
Uptake Delay (s)	18
Stabilization Time (s)	8
Read Time (s)	3
Replicates	4
Rinse Time between every sample (s)	80
Plasma viewing position	Axial

***Table 3.4**: Figures of merit for ICP – OES Analysis*

Parameters	**Mg**	**Al**	**Ca**	**Mn**	**Fe**	**Ba**
Average 1 ppb Sensitivity (cps)	53750	11336	8940	98761	32371	873690
Average Blank (cps)	24	46	16	23	21	136
Signal/Noise	2231	244	563	4222	1515	6431
Limit of Detection (ppb)	0.33	2.57	1.64	0.16	0.80	0.10

The sample introduction system of Agilent 8900 Triple Quadrupole Inductively coupled Plasma Mass Spectrometer consists of self-aspirating ESI nebulizer (uptake rate 100 µL/min), temperature controlled (+2°C) scott type quartz spray chamber, quartz torch and nickel sampler and skimmer cones. All the samples were diluted in 1ppb Y doped 2% HNO_3. Concentrations were measured in hot plasma in collision reaction cell (CRC) mode to remove the polyatomic interferences. Two sets of multi-element calibration standards ranging from 0.1 ppb to 20 ppb were freshly prepared gravimetrically and analysed. A multi-element standard of 1 ppb was utilised for standard – sample – standard bracketing. Drift corrections and normalisations of the raw data were performed with respect to the counts per second (cps) of the bracketing standard. The procedural blanks were also analysed in ICP MS and were subtracted from the total concentration of the elements. The instrumental operating conditions and figures of merit are reported in **Table 3.5** and **Table 3.6** respectively.

To determine the extraction efficiency and analytical precision, standard reference materials (SRM) from National Institute of Standards and Technology (NIST) were digested following procedures exactly same as similar types of samples. The details of the concentration and extraction percentages of the elements are reported in **Table 3.7**.

***Table 3.5**: ICPMS - QQQ Operating Condition*

RF Power	1500 W
RF Matching	1.14 V
Sample depth	4.0 mm
Nebulizer Gas	0.61 L/min
Nebulizer Pump	0.10 rps
S/C T	2 °C
Dilution Gas	0.41 L/min
He flow	3.5 ml/min
H_2 flow	2.5 ml/min

***Table 3.6:** Figures of merit for ICP MS – QQQ Analysis*

Parameters	Ti	V	Cr	Ni	Co	Cu	Cd	Pb
Average 1 ppb Sensitivity (cps)	11676	375212	441192	293751	599704	165490	104291	638198
Average Blank (cps)	155	72	2172	18822	934	1883	14	167
Signal/Noise	76	5216	203	16	642	88	7662	3815
Limit of Detection (ppt)	22	1.35	10	373	10	34	0.545	0.968

***Table 3.7:** Mean concentrations of NIST SRM 2704(mg/kg), NIST SRM 2783 (ng/cm^2) and NIST SRM 1573A (mg/kg)*

Sample/Sampling date	Sample type	Mg	Al	Ca	V	Cr	Mn	Fe	Co	Ni	Cu	Zn	Cd	Ba	Pb
NIST SRM 2704 (Buffalo River Sediment)	**Standards**	8013 (104%)	61280 (100%)	26582 (102%)		124 (92%)	552 (99%)	39293 (96%)	13.5 (97%)	44 (100%)	105 (106%)	462 (106%)	3.28 (95%)	430 (104%)	156 (97%)
NIST SRM 2783 (Urban $PM_{2.5}$)		8394 (97%)	21100 (91%)	12623 (96%)	47.1 (97%)	116 (86%)	336 (105%)	25830 (97%)	7.4 (96%)	65 (95%)	396 (98%)	1582 (88%)			316 (100%)
NIST SRM 1573A (Tomato leaf powder)		11088 (92%)	56006 (92%)	51016 (101%)		2.17 (109%)	260 (106%)	371 (101%)	0.60 (104%)		4.82 (103%)	32 (105%)	1.65 (109%)	60 (95%)	

The percentages within parentheses for the standards indicate recovery percentages

3.8. Determination of Pb isotopes

Pb isotopes were analysed by Multi-collector ICP – MS (Neptune Plus MC ICP-MS, Thermo-Fisher, Germany) at Earth Observatory of Singapore, Nanyang Technological University, Singapore, equipped with Aridus II desolvating nebulizer (100 µL/min). Instrumental mass fractionation correction involved Thalium (Tl) (NIST SRM 997) internal normalisation ($^{203}Tl/^{205}Tl$ ratio of 0.418911). Bracketing with NIST SRM-981 was adopted to normalise the obtained ratios with respect to the true value (Baker et al., 2004; White et al., 2000).

All the samples were concentration matched with standard and anaysed at comparable Pb/Tl ratios, to minimize the mass bias generated from counting statistics. The precision and accuracy of the measurements were ensured by analysing NIST SRM-981 multiple times between samples as well as at the beginning and end of sessions reported in **Table 3.8**. The contribution of the procedural blank to the total measured concentration were determined as [Pb]procedural blank/[Pb]Total. Consequently, the blank subtracted $^{206}Pb/^{207}Pb$ and $^{208}Pb/^{207}Pb$ values were determined by mass balance represented by the following equation (Gelwicks and Hayes, 1990): The Pb isotopic composition of procedural blanks in different sessions are reported in **Table 3.8**

$$\left(\frac{20x}{20y}\right)_{sample} = \left[n_T \left(\frac{20x}{20y}\right)_{total} - n_B \left(\frac{20x}{20y}\right)_{blank}\right] / (n_T - n_B) \quad \text{.....3.1}$$

Where, x = 6, 8; y= 7, 6; n is the fractional amount of substance and the subscripts T, and B refers to total and blank respectively.

***Table 3.8**: Mean Pb isotopic composition of NIST SRM 981and procedural blanks during different sessions*

Sample	$^{206}Pb/^{204}Pb$	2SD	$^{207}Pb/^{204}Pb$	2SD	$^{208}Pb/^{204}Pb$	2SD	$^{206}Pb/^{207}Pb$	2SD	$^{208}Pb/^{207}Pb$	2SD
NIST 981 (True value)	**16.9371**						**1.0933**		**2.3704**	
NIST 981 (n=29)	16.9242	0.01301	15.4730	0.01418	36.6211	0.08900	1.0937	0.00037	2.3668	0.00449
NIST 981 (n=40)	16.9307	0.02969	15.4794	0.02789	36.6677	0.06663	1.0937	0.00047	2.3688	0.00056
NIST 981 (n=12)	16.9590	0.04254	15.5116	0.04135	36.7165	0.08025	1.0933	0.00037	2.3670	0.00181
NIST 981 (n=19)	16.9411	0.03658	15.4663	0.03061	36.6493	0.07266	1.0953	0.00078	2.3696	0.00086
Blank 1	17.4950	0.06070	15.3433	0.05832	36.8284	0.12389	1.1291	0.00825	2.4042	0.00249
Blank 2	17.5633	007488	15.5037	0.06943	37.2755	0.15883	1.1323	0.00990	2.4034	0.00285
Blank 3	17.9495	0.08548	15.5931	0.07400	37.9045	0.17847	1.1510	0.01094	2.4305	0.00161
Blank 4	17.8614	0.02019	15.5067	0.01804	37.6854	0.04188	1.1520	0.00264	2.4304	0.00080
Blank 5	17.8019	0.13981	15.6047	0.03365	37.7277	0.15447	1.1408	0.00867	2.4177	0.00833
Blank 6	18.0392	0.15922	15.8088	0.24971	38.2592	0.43821	1.1411	0.00795	2.4201	0.01051
Blank 7	17.7778	0.6369	15.6326	0.5539	37.7506	1.28222	1.1365	0.00442	2.4129	0.00328

3.9. Statistical analyses and modelling studies

3.9.1. Air mass back trajectory analyses

Air-mass back trajectory statistics were obtained using meteorological data for the sampling dates, extending up to 72 hours prior. The meteorology data, that included wind speed, wind direction, temperature, humidity, and precipitation, was compiled using the Hybrid Single-Particle Lagrangian Integrated Trajectory (HYSPLIT) model through its graphical user interface (GUI)(Draxler, 1998; NOAA, 2021). This meteorological data was provided as an input into the geographic information system (GIS) based software TrajStat to generate 72-hour airmass back trajectories at 500 meters above sea level. These trajectories were then converted into a polylineZ shapefile format for spatial representation(Wang et al., 2009).

3.9.2. Mixing polygon simulation

The mixing polygon simulation is conducted in Pb isotope space involving three ratios: $^{206}Pb/^{207}Pb$, $^{208}Pb/^{207}Pb$, and $^{208}Pb/^{206}Pb$. It assesses whether majority of the aerosol mixtures fall within the mixing envelope of the considered end members. It is a Monte Carlo simulation performed in R 4.2.2 (http://www.famer.unsw.edu.au/downloads.html). As inputs for sources of the aerosol mixtures the mean Pb isotopic compositions ($^{206}Pb/^{207}Pb$, $^{208}Pb/^{207}Pb$, and $^{208}Pb/^{206}Pb$ ratios or $^{206}Pb/^{204}Pb$, $^{207}Pb/^{204}Pb$ and $^{208}Pb/^{204}Pb$ ratios) along with 1 standard deviations (SD) of the sources were fed. The Pb isotopic compositions ($^{206}Pb/^{207}Pb$, $^{208}Pb/^{207}Pb$, and $^{208}Pb/^{206}Pb$ ratios or $^{206}Pb/^{204}Pb$, $^{207}Pb/^{204}Pb$ and $^{208}Pb/^{204}Pb$ ratios) of all the aerosols were fed to the model as mixture parameters. The model performs iterations (n = 1500) that generate mixing envelopes based on the distribution of the considered sources and their SDs. The number of such envelopes that include within them the aerosols, represent the probability of the aerosols for lying inside the mixing envelope (Smith et al., 2013). The mixing polygon simulation is based on the principle that the isotopic composition of the mixture (aerosols for this study) can be explained by the isotopic compositions of the sources forming the mixing envelope only if the mixture doesn't fall outside 5 % of the generated polygons. The sample(s) with less than 5 % probabilities has/ve sources other than the considered end members and hence the selected sources cannot explain the composition of that particular mixture.

3.9.3. Linear mixing model performed for literature data of India and SEA countries

The aerosol mixtures of India, and SEA countries from the past decade as compiled from previous literatures were primarily visualized along a two-end member geometric mixing line, partitioned into intervals of 20 %. The proximity of the aerosol mixture to each source on the line provides the relative contribution between the two considered sources (Phillips and Gregg, 2003). Since, such an approach cannot consider more than 2 sources, following this, the aerosol mixture and the source Pb isotopic data were subjected to conventional mass balance based linear mixing model based on the principle of IsoSource by employing the following equations (Phillips et al., 2005):

$$\left(\frac{206}{207}Pb\right)_{mix} = \left[f_a\left(\frac{206}{207}Pb\right)_a + f_b\left(\frac{206}{207}Pb\right)_b + \cdots + f_n\left(\frac{206}{207}Pb\right)_n\right] \quad \text{.....3.2}$$

$$\left(\frac{208}{207}Pb\right)_{mix} = \left[f_a\left(\frac{208}{207}Pb\right)_a + f_b\left(\frac{208}{207}Pb\right)_b + \cdots + f_n\left(\frac{208}{207}Pb\right)_n\right] \quad \text{.....3.3}$$

$$f_a + f_b + \cdots + f_n = 1 \quad \text{.....3.4}$$

where $\left(\frac{206}{207}Pb\right)_{mix}$ and $\left(\frac{208}{207}Pb\right)_{mix}$ are isotopic compositions of the aerosol mixtures; $\left(\frac{206}{207}Pb\right)_{a,b,\ldots,n}$ and $\left(\frac{208}{207}Pb\right)_{a,b,\ldots,n}$ are isotopic compositions of the sources and $f_{a,\ b,\ \ldots,\ n}$ is the unknown proportional contribution for each source towards the aerosol mixture. It is worth noting that these equations are approximations that work because of the limited fractional variance of Pb isotope data. This system using two isotope ratios can provide unique solution for each f, up to n = 3. However, when n > 3, this becomes an underdetermined system with no unique solution (Phillips and Gregg, 2003) To estimate the source proportions ($f_{a,\ b,\ \ldots,\ n}$) from such an underdetermined system, iterative approach as followed in traditional models like IsoSource was employed (Phillips and Gregg, 2003). The linear model was made to perform an optimization process to find the optimal value for mixture of sources that matches given target aerosol mixture values. The optimization process performs ten restarts, each starting with a set of randomly assigned initial values for source proportions for the five sources. This process of conducting 10 restarts in the model was repeated 10 times to yield a set of 10 distinct sets of best results. The goal is to achieve an average deviation of 0.5‰ or less between the predicted and target mixture values. Two target aerosol mixtures, one with most radiogenic signature and the other with least, were selected. This selection is based on the fact that the source contribution towards the aerosols, lying

between these extremes, will fall within the range of source contributions obtained for these extreme target aerosols. The model then identifies the best solution based on the lowest deviation. The potential combinations of source proportions sum up to 100%. (Phillips and Gregg, 2003).

3.9.4. Bayesian mixing model, MixSIAR (Stable isotope analysis in R)

Bayesian statistics based mixing models integrates the mean and uncertainty of the data into its framework. It is based on Markov Chain Monte Carlo (MCMC) simulation that produces plausible source proportion results based upon probability densities of the fed data (Parnell et al., 2010). This is particularly useful for analyzing complex mixing problems where there are many more sources compared to isotope systems. Source apportionment of atmospheric Pb over a region requires consideration of isotopic compositions of multiple endmembers in which the Pb isotopic composition of each endmember may be spread over a significantly large range. Thus, it is preferable to apply robust Bayesian models such as MixSIAR to these kinds of data set where we can consider multiple endmembers along with their uncertainty for determination of the proportion of contribution by the sources.

The means and 1SDs of $^{206}Pb/^{207}Pb$, $^{208}Pb/^{207}Pb$ and $^{208}Pb/^{206}Pb$ of the sources, and the isotopic composition of the aerosols were fed to the model framework in R (Stock et al., 2018). Due to limited number of source data in literature, with respect to ^{204}Pb, the comprehensive modelling was always conducted using ^{206}Pb, ^{207}Pb, and ^{208}Pb isotopes. With inadequate data, the standard deviations may not accurately represent the true heterogeneity in sources. Consequently, it can compromise the accuracy and reliability of MixSIAR results by generating higher uncertainties in source contributions and ambiguous source identifications. However, as the ratios relative to ^{204}Pb stem from distinct decay chains and possess the ability to discern source ages, the utilization of ^{204}Pb contributes to improved source apportionment accuracy (Baron et al., 2014; Longman et al., 2018). Thus, in order to validate the reliability of the modelling, results derived from ^{206}Pb, ^{207}Pb and ^{208}Pb isotopes, the aerosol mixture from Singapore for the last decade and its potential end members were subjected to MixSIAR analysis specifically considering the ^{204}Pb isotope as well. While compiling the source data from literature and this study, the values that were greater/less than 2SD of the mean were treated as outliers and eliminated. This reduces the overlapping of sources and increases model accuracy (Longman et al., 2022). The large mixture datasets the mixture Pb isotope ratios were combined every 5‰ with respect to $^{206}Pb/^{207}Pb$ ratios. The model

was run using 3 parallel chains with a "long" MCMC chain length of 300,000 iterations. To ensure that the chains reached equilibrium, the first 200,000 iterated values were discarded/"burned". The remaining samples were "thinned" by keeping every 100th iterated value (Stock and Semmens, 2016). The model convergence was checked using Gelman Rubin diagnostics.

This model can be executed in both concentration-dependent and concentration-independent versions. Concentration-dependent stable isotope mixing models are important in source apportionment studies, particularly when dealing with multiple sources having differences in elemental concentrations (Cox et al., 2023; Phillips and Koch, 2002). Accurate concentration data for the sources is a necessity for effectively utilizing concentration-dependent stable isotope mixing models. This accuracy can only be achieved when isotope and elemental concentration data of the same sample set are available. While compiling data for India and SEA countries from the past decade such comprehensive concentration data for sources were not available. Hence the concentration-independent model was relied upon. However, to test the validity of the concentration-independent model, the concentration-dependent model was applied in case of Indian aerosol mixture. For rest of the objectives, as most of source data were analyzed in this study itself, the concentration-dependent model was utilized.

3.9.5. Quantification of Metal Emissions from Traffic Sources

The calculations for emissions of each metal were performed separately for EE, NEEs from internal combustion engines (ICEVs), and NEEs from EVs. Non-exhaust emission has been categorized into tire wear, brake wear and road abrasion. The two resultant NEE data from ICEVs and EVs were added to get the total NEE (ton/yr). The estimated metal concentrations were incorporated in the emission equations (Tian et al., 2015). The equations utilized for the calculations are as follows:

$$E_{ICEV} = EF_{ICEV} \times [X] \times M \times C \quad \text{..... 3.5}$$

Where, E_{ICEV} is the metal emitted in tons/year; EF_{ICEV} is the emission factor (g/km) for fuels when calculating EEs and for NEEs, EF_{ICEV} denotes the emission factors (g/km) for brake wear, tire wear, or road abrasions as applicable; [X] is the average concentration of the concerned element in mg/kg for vehicular exhaust, brake wear, tire wear or road abrasion as applicable; M is the average mileage in km/L and C is the fuel consumption of total car population in liter (L).

$$E_{EV} = EF_{EV} \times [X] \times M \times N_{EV} \ldots\ldots\ldots\

CHAPTER 4: SOURCES OF ATMOSPHERIC Pb IN INDIA AND SOUTH EAST ASIAN COUNTRIES IN THE LAST DECADE

4.1. Introduction

South and southeast Asia have become a hotspot of anthropogenic PM emissions due to increased coal combustion, high-temperature industrial operations, vehicular traffic, and agricultural biomass burning. Atmospheric Pb has been detected in the environment at hazardous levels even after the global phase out of leaded gasoline. The use of leaded gasoline dates back to the early 20th century when tetraethyl lead (TEL) was first introduced as a petroleum additive to improve the performance of internal combustion engines. During the combustion process, gasoline Pb was partially oxidized and PbO deposits caused engine fouling. To overcome this issue, dichloroethane and dibromoethane were added to leaded gasoline to act as Pb scavengers. The Pb oxides were converted to volatile Pb species such as lead chloride and lead bromide that were emitted into the atmosphere. The atmosphere was thus, the first recipient of the gasoline exhaust in the form of volatile Pb halogenides (Radojevic and Harrison, 1987). US leaded gasoline phasing out was completed in 1986 and it took 20 years for another 120 countries including Indonesia, Australia and South Africa to achieve the target. Post 2006 only five countries (Algeria, Yemen, Afghanistan, Iraq and Myanmar) were using leaded gasoline and in 2021, Algeria became the last country to ban leaded gasoline marking the success story of a global collaboration. However, along with the feat, a grave concern about the fate of the already released Pb compounds from automobile exhaust loomed. As Indonesia used leaded gasoline until 2006 (Walsh, 2007), and Myanmar until 2016 (Dumitrescu, 2017), historic Pb recirculation may contribute significantly towards atmospheric Pb in the SEA region. Once emitted, Pb has an atmospheric residence time of 5-10 days (Sturges and Barrie, 1987) before getting deposited. After several days the emitted Pb compounds settle on the top soil. Residence time of Pb in soil is 100 – 200 years (Erel, 1998). Hence it was presumed that the legacy Pb from the global use of leaded gasoline will prevail in the environment. Indeed, a strong evidence of recirculating legacy Pb in the atmosphere from soil resuspension was reported from different corners of the world. Pristine areas of the Central Himalayas still have legacy Pb as the major source of atmospheric Pb pollution. Although during the winter months, the contribution of coal combustion emissions towards atmospheric Pb increases, the contribution from resuspension of historic leaded gasoline remains stable (Mitra et al., 2021). The fingerprinting of

the source was done by the immutable Pb isotopic signature (Mitra et al., 2021; Morton-Bermea et al., 2011; Resongles et al., 2021; Sen et al., 2016).

The late phase out of leaded gasoline in South and Southeast Asian countries along with increasing coal combustion (Overland et al., 2021), high temperature industrial activities and agricultural biomass burning have made the region a hotspot of anthropogenic emissions. Atmospheric Pb has been detected in Southeast Asian nations, showing that local sources such as vehicular traffic, incineration, as well as transboundary movement of coal and high temperature metallurgical emissions play major roles in increasing atmospheric metal concentrations (Carrasco et al., 2018; Chifflet et al., 2018; George et al., 2020; Kayee et al., 2020). In highly urbanized regions and areas close to industrialized zones, emissions from vehicles and non-coal burning industries are most likely to have a significant contribution in increasing the atmospheric Pb concentration (Kumar et al., 2016; Sen et al., 2016). Singapore, one of the most developed nations among the Southeast Asian countries phased out leaded gasoline completely in July 1998 (OECD and UNEP, 1999). Since then, there has been a drastic decrease in the roadside Pb levels. Natural gas accounts for the vast bulk (95 %) of Singapore's energy generation, while coal accounts for only 1.2 % (Singapore Energy Market Authority, 2022). As a result, metals in the atmosphere from coal burning can primarily come from transboundary sources. Indonesia, and China have a large number of coal mines and recorded the biggest rise in coal output (47.06 % and 18.94 % respectively) in 2018 (British Petroleum, 2019). Vehicular traffic, solid waste incinerators and heavy industries in the island are the local factors contributing to the high PM concentrations and eventually undesirable atmospheric metal levels (George et al., 2020; Velasco and Roth, 2012). Along with local sources, transboundary Pb sources driven by seasonal wind patterns raise atmospheric Pb concentrations of Singapore (Carrasco et al., 2018).

South and South East Asian countries have recently come under scrutiny of Pb pollution due to several reasons. In India, Thailand and Vietnam, more than 250 million children have blood lead level > 5 microgram/deciliter (ug/dL) (Ericson et al., 2021). Additionally, present day Pb emissions have surpassed past century emission from leaded gasoline used in these countries (Lee et al., 2014).

Recent source apportionment studies of atmospheric Pb over Singapore, Thailand, Vietnam (referred to as SEA countries herein) and India by utilizing Pb isotopic compositions and elemental

ratios of aerosols (Carrasco et al., 2018; R. Das et al., 2018; Hoàng-Hòa et al., 2015; Kayee et al., 2020, 2021; Kumar et al., 2016; Mitra et al., 2021; Sen et al., 2016) have identified the potential sources to be crust, sea spray, coal combustion, high temperature industrial activities, vehicular and ship traffic, solid waste incineration and biomass burning. In addition to these modern sources, historic Pb deposited on top soil from leaded gasoline emissions still recirculates in the atmosphere (Carrasco et al., 2018; Mitra et al., 2021; Resongles et al., 2021). All past studies considered linear 2 or 3 endmember mixing models that may lead to oversimplification of the dynamics of atmospheric Pb pollution by exclusion of potential contributors. Moreover, a complete dataset for Pb isotopic composition of Singapore aerosols is unavailable.

Thus, this study is divided into two parts. Firstly, this study uses a year of time-series data (June 2017-May 2018) for Pb isotopes in conjunction with elemental composition of PM_{10}, interpreted in the framework of seasonal variations of wind patterns, to understand the drivers of seasonal patterns of atmospheric Pb transport to Singapore. Secondly, the study compiles all the available Pb isotope data for the SEA countries (Singapore, Thailand and Vietnam) and India (n = 341) to perform a comprehensive source apportionment study. This study performs a quantitative retrospective analysis of Pb isotope data of aerosols from the past two decades and their potential endmembers using mixing polygon simulation followed by MixSIAR analysis to distinctly understand the sources of atmospheric Pb. Utilizing MixSIAR for source apportionment of atmospheric Pb over SEA countries and India will lead to discerning the sources that require revisiting and identification of any probable underdetermined source that should be prioritized in future studies. To overcome the issue of multiple end members, Bayesian stable isotope mixing models such as MixSIR, SIAR and MixSIAR has been widely used in the field of ecology to study food webs and infer the diets of consumers based on stable isotope systems such as $\delta^{13}C$, $\delta^{15}N$ and $\delta^{34}S$ (Drucker et al., 2018; Parnell et al., 2013). Recently, MixSIAR has also been used in few source apportionment studies concerning Pb pollution that utilizes Pb isotopic compositions of pollution sources (H. Chen et al., 2023; Dietrich et al., 2021; Koffman et al., 2022; Longman et al., 2018, 2022). Isotopic systems such as $\delta^{13}C$, $\delta^{15}N$, and $\delta^{34}S$ permit the integration of concentration data within the MixSIAR framework, owing to the distinct concentrations associated with each element. For Pb isotopic system also the concentration-dependent model can be utilized where including concentration data results in identical concentrations for each ratio However, it may not be effective to execute concentration-dependent mixing models by utilizing Pb

concentration data solely, as it has large orders of magnitude variations across sources. Some of the sources may have concentration in percentage range compared to ppm or ppb range of other sources, that will introduce bias in model results. Thus, to avoid such biases, techniques, such as normalization is useful. Normalization of Pb concentration of the sources with a crustal element such as Al, Fe, Ti etc. can be an effective strategy.

4.2. Sources of atmospheric Pb in Singapore

4.2.1. Study site and origin of airmasses

Singapore is situated near the southern point of the Malay Peninsula, bordered by Malaysia to the north and Indonesia to the south **(Figure 4.1).** The island is positioned at the crossroads of ship traffic between Europe and Southeast Asia, as well as the US West Coast and Southeast Asia (Gordon et al., 2005).

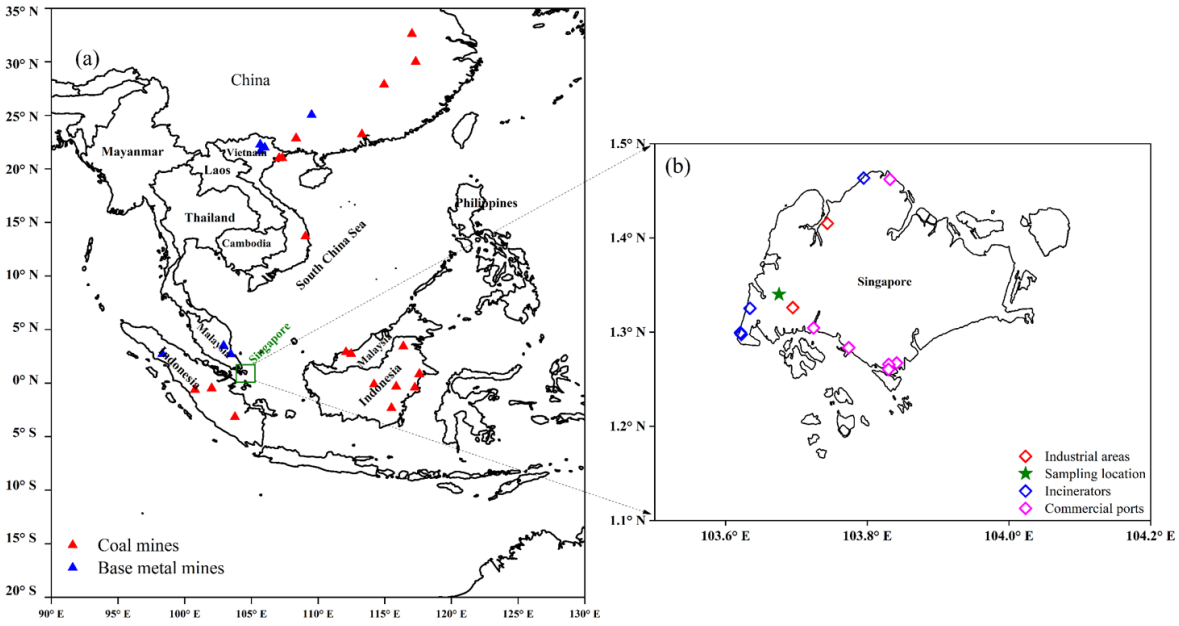

Figure 4.1: *Location of Singapore in South East Asia. The coal and base metal mines of the neighbouring countries are marked for reference. (b) Sampling location within Singapore and probable local pollution sources. The base maps are adopted from the open-source online repository Opendatasoft (https://public.opendatasoft.com/explore/dataset/world-administrative-boundaries/export/).*

Singapore has a tropical climate with two monsoon seasons that are separated by inter-monsoonal intervals. Northeast (NE) monsoons (December to March) are characterized by strong winds blowing from the north and northeast. During the Southwest Monsoon (SW), winds blow from the

south and southeast (June to September). Inter-monsoon (IM) months (April, May, October, and November) are transitional seasons between the two monsoons, with weaker and more varied winds (Meteorological Service Singapore, 2020). PM_{10} aerosol samples were collected (30 m above ground level) on the roof of Earth Observatory of Singapore, Nanyang Technological University, Singapore between June 2017 and May 2018. The sampling site is located near Jurong island, which houses a number of refineries (McNeill et al., 2020). Three solid waste incinerators are located within 12 km of the site (Singapore National Environment Agency, 2020) **(Figure 4.1**). Forty-five aerosol samples (16 during NE monsoon, 15 during SW monsoon and 14 during inter-monsoon seasons) were collected. Each sample was collected for 24 h starting at 6 AM. The 72 hours air mass back trajectory at 500 m above ground level using HYSPLIT (https://www.ready.noaa.gov/HYSPLIT_traj.php) (Stein et al., 2015) masses can help to understand the possible long range sources of pollution **(Figure 4.2).** During the NE Monsoon season, majority of the air masses originated from the South China Sea. A small cluster of the air

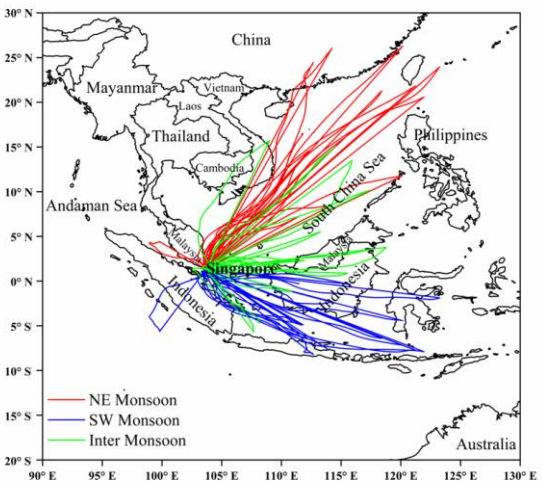

Figure 4.2: *72 hours backward wind trajectory at 500 m above ground level compiled for the sampling period (June 2017 to May 2018) using [HYSPLIT (Hybrid Single Particle Lagrangian Integrated Trajectory) data from the U.S. National Oceanic and Atmospheric Administration's (NOAA) website]. The base map is adopted from the open-source online repository Opendatasoft (https://public.opendatasoft.com/explore/dataset/world-administrative-boundaries/export/).*

masses travelled from Southern China, Vietnam, Cambodia and Malaysia. Coal and base metal mines in southern and south eastern parts of the countries, thus, may contribute to the atmospheric pollution in Singapore during the NE monsoon. A bulk of the air cluster during the SW monsoon

arrived from Kalimantan and Sulawesi islands of Indonesia. Some air masses formed over the Java Sea and the island of Java. Pollutants emitted from numerous open pit coal mines in Kalimantan **(Figure 4.1**) and coal fired plants in Indonesia, might contribute towards pollutant sources in Singapore's atmosphere. During the IM seasons air masses primarily originated from over the South China Sea and northern part of Borneo Island.

4.2.2. Particulate matter and metal concentration, enrichment factor and elemental ratios

The PM_{10} concentrations of 45 aerosol samples (**Table 4.1**) measured during all three monsoon seasons of Singapore did not show any significant difference ($p = 0.469$) upon performing Analysis of Variance (ANOVA) ($F_{2,41} = 0.77$, significance level: $p < 0.001$). The mean PM_{10} concentrations during NE, SW and IM seasons were comparable (**Figure 4.3a**) and varied from 44 to 46.6 ng/m^3 (**Figure 4.3b**). During the SW monsoon season (June to September 2017) air masses originated from over Indonesia **(Figure 4.2).** However, as no major biomass burning events were reported during the time period **(Figure 4.4),** the PM_{10} concentrations of the SW monsoon winds were not significantly different from the other two seasons.

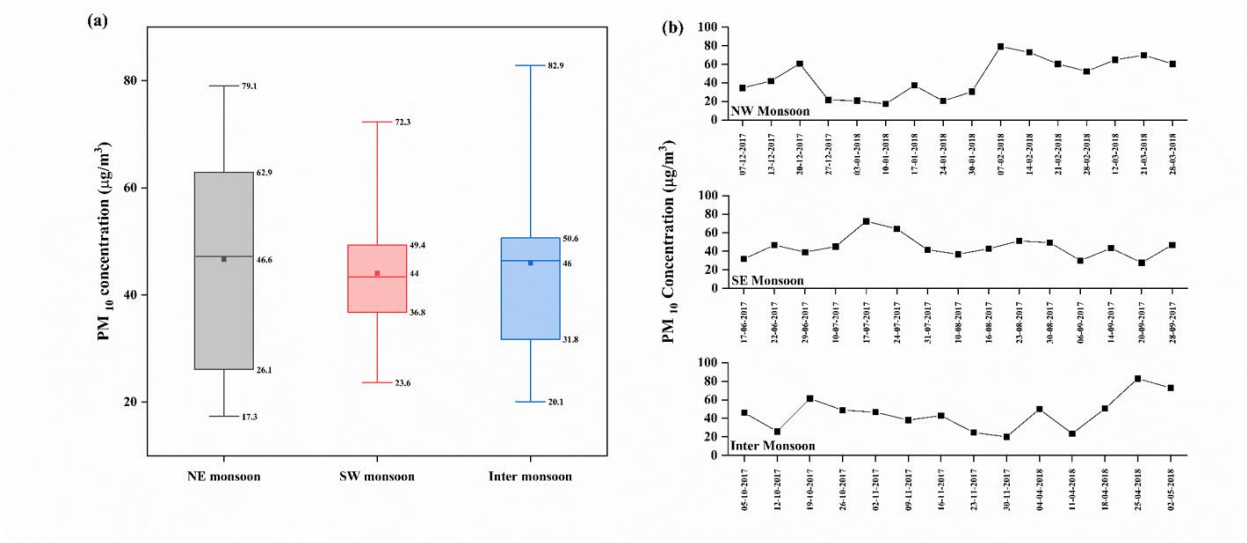

Figure 4.3: *(a) Box plots depicting the PM_{10} concentrations of NE, SW and Inter monsoon seasons. The maximum, minimum, 25 and 75 percentile, and mean values for the PM_{10} concentrations are labelled for reference. (b) Temporal variation in PM_{10} concentration in NE, SW and Inter monsoon winds.*

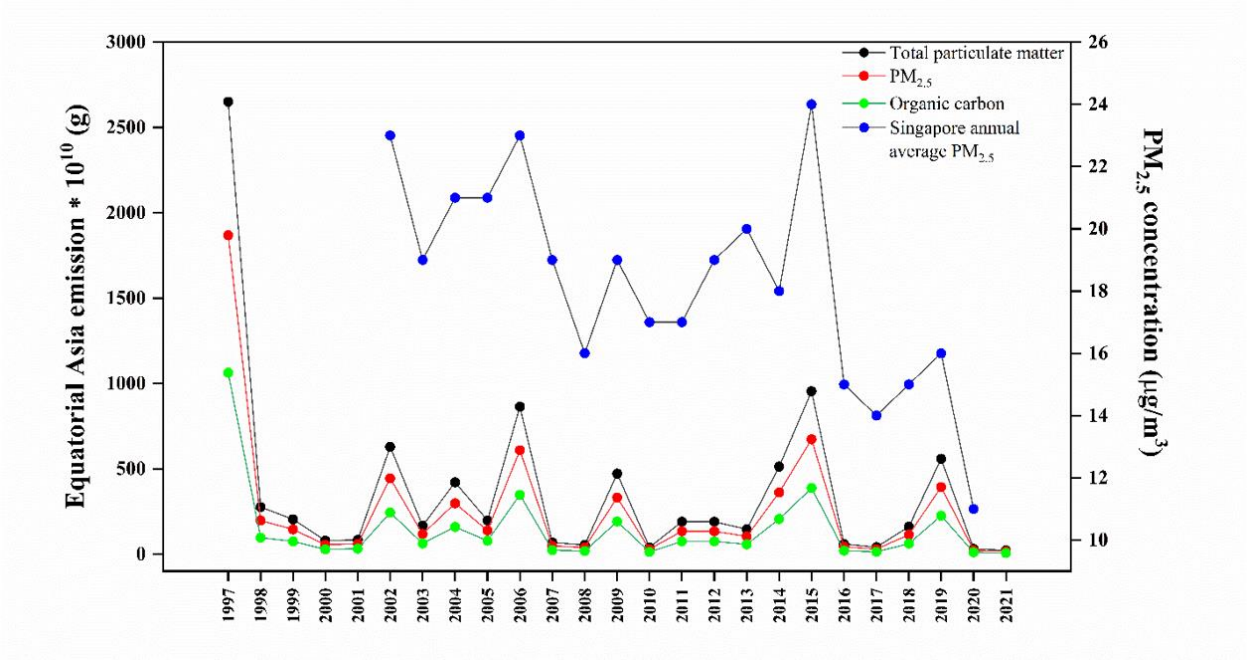

Figure 4.4: *Average annual emission of total particulate matter, $PM_{2.5}$ and organic carbon from equatorial Asia as an indicator of fire activity in the region (data source Global Fire Emission Database). Average annual $PM_{2.5}$ of Singapore is plotted for comparison (data source-Singapore NEA archive data). During the sampling period (June 2017-May 2018) there were no significant fire activities in the region*

Table 4.1: *Metal concentration (ng/m^3) and PM_{10} concentration ($\mu g/m^3$) in Singapore aerosol*

Sample	Season	Date	Al	Ba	Ca	Co	Cr	Cu	Fe	Mg	Mn	Ni	Pb	Sr	Ti	V	Zn	PM_{10}
1	SWM	17/06/2017	70	3.9	343	0.25	4.9	6.8	264	79	11	8.5	4.4	1.1	5.1	31	51	32
2	SWM	22/06/2017	130	12	207	0.34	8.0	37	363	113	15	12	15	2.7	7.2	34	63	47
3	SWM	29/06/2017	88	6.2	192	0.20	5.0	35	173	104	7.1	7.0	15	2.4	5.0	24	26	39
4	SWM	10/07/2017	110	4.1	256	0.38	7.6	5.1	284	101	8.9	8.0	1.9	1.8	5.5	22	21	45
5	SWM	17/07/2017	142	5.5	308	0.41	12	10	619	220	60	17	23	2.1	10	68	485	72
6	SWM	24/07/2017	92	3.8	188	0.26	3.6	4.2	288	192	7.9	6.5	3.0	1.8	6.3	25	32	64
7	SWM	31/07/2017	79	4.4	195	0.31	5.0	10.5	307	-	20	10	6.4	2.1	5.9	38	201	42
8	SWM	10/08/2017	66	3.9	192	0.32	5.6	15	334	91	9.3	9.8	3.5	1.1	5.2	36	41	37
9	SWM	16/08/2017	128	6.7	267	0.39	4.5	10	395	157	14	9.1	4.7	1.9	9.5	36	62	43
10	SWM	23/08/2017	133	4.9	316	0.35	4.6	10	379	-	15	8.7	5.9	2.8	8.8	37	104	51
11	SWM	30/08/2017	147	11	343	0.34	5.2	18	456	107	19	7.7	12	2.4	10	26	117	49

12	SWM	06/09/2017	114	5.8	211	0.36	5.5	9.0	432	111	23	12	11	1.3	8.2	50	171	30
13	SWM	14/09/2017	103	7.2	252	0.48	6.3	40	419	115	15	13	14	2.4	9.0	51	87	43
14	SWM	20/09/2017	59	6.0	185	0.34	6.2	17	425	87	16	9.7	4.4	1.2	5.7	36	94	28
15	SWM	28/09/2017	111	11	101	0.25	4.5	12	326	68	12	7.1	9.3	2.0	12	32	70	47
16	IM	05/10/2017	168	11	275	0.30	4.5	17	431	59	15	8.2	16	3.2	12	30	106	46
17	IM	12/10/2017	61	4.5	74	0.37	6.4	14	391	59	10	8.1	3.5	1.2	9.5	33	50	26
18	IM	19/10/2017	160	18	399	0.87	3.0	19	536	146	11	10	20	11	14	34	410	61
19	IM	26/10/2017	154	6.7	374	0.57	3.1	30	471	105	6.9	4.9	20	8.2	15	20	480	49
20	IM	02/11/2017	80	3.1	335	0.49	2.9	18	255	51	2.9	5.5	9.3	6.2	5.7	15	354	47
21	IM	09/11/2017	30	1.4	516	0.55	1.3	2.8	274	66	1.8	2.8	1.6	8.0	4.6	6.4	479	38
22	IM	16/11/2017	73	7.7	368	0.57	3.6	10	393	107	11	6.8	7.8	6.6	15	30	360	43
23	IM	23/11/2017	27	2.1	303	0.34	1.1	2.7	192	54	2.2	1.9	2.0	4.9	2.1	1.3	299	25

24	IM	30/11/2017	34	2.4	332	0.38	0.86	6.1	217	112	1.7	4.3	5.2	5.8	3.1	6.3	330	20
25	NEM	07/12/2017	133	5.8	354	0.48	2.9	4.3	304	146	7.4	4.6	5.9	6.5	9.7	6.3	359	35
26	NEM	13/12/2017	98	7.0	350	0.51	3.2	17	400	160	8.1	3.7	19	7.3	9.3	4.6	418	42
27	NEM	20/12/2017	105	2.7	345	0.71	2.4	8.8	140	266	6.6	0.05	13	2.2	9.1	0.13	32	61
28	NEM	27/12/2017	69	0.50	135	3.7	2.6	3.2	329	103	8.3	8.7	4.5	2.2	4.6	1.2	38	22
29	NEM	03/01/2018	92	6.7	196	0.84	2.5	6.6	159	140	6.0	2.1	8.2	2.7	4.7	2.7	61	21
30	NEM	10/01/2018	58	1.9	224	3.8	2.1	3.6	52	95	2.5	1.8	1.4	1.6	2.0	1.8	31	17
31	NEM	17/01/2018	114	3.9	279	0.19	2.5	7.2	183	211	4.7	2.1	5.5	2.2	6.4	4.5	66	37
32	NEM	24/01/2018	99	4.4	159	5.4	1.7	6.3	139	103	6.4	2.8	7.6	3.0	4.8	6.9	43	20
33	NEM	30/01/2018	133	5.9	283	0.90	2.7	10	219	171	6.5	3.8	5.5	2.7	9.7	9.3	45	31
34	NEM	07/02/2018	161	5.8	476	2.2	4.7	8.2	228	224	7.5	4.4	8.4	3.4	8.3	5.3	96	79
35	NEM	14/02/2018	196	7.8	288	0.82	2.1	8.5	230	419	7.1	2.1	7.0	4.8	9.9	3.3	30	73

36	NEM	21/02/2018	147	4.8	330	5.8	2.0	5.9	200	345	6.7	2.7	5.6	3.3	10	6.6	47	60
37	NEM	28/02/2018	175	11	397	0.41	16	13	530	312	16	14	7.6	4.2	11	13	74	52
38	NEM	12/03/2018	129	6.2	242	4.2	1.9	8.4	200	429	7.6	2.6	6.6	3.8	9.8	3.8	34	65
39	NEM	21/03/2018	312	6.2	326	0.81	20	8.3	398	188	9.7	9.5	12	3.0	9.5	7.9	127	70
40	NEM	28/03/2018	437	12	371	7.3	6.1	19	396	266	16	5.3	6.1	4.0	12	7.4	66	60
41	IM	04/04/2018	287	8.3	453	0.25	4.6	16	500	469	22	7.4	14	5.4	17	15	82	50
42	IM	11/01/2018	176	7.4	239	4.8	3.5	9.7	295	184	7.1	3.6	7.0	2.9	11	7.6	43	24
43	IM	18/04/2018	125	6.5	193	0.31	3.0	9.8	177	127	7.4	4.3	11	1.9	7.2	7.5	53	51
44	IM	25/04/2018	194	8.7	336	4.2	4.6	13	347	124	16	9.7	15	3.2	11	24	83	83
45	IM	02/05/2018	303	14	335	0.29	5.7	22	503	105	21	9.8	12	2.6	13	23	102	73

Meteorological conditions can influence the PM concentrations. Singapore is situated one degree north of the equator and experiences yearlong rainfall due to the two monsoon seasons and afternoon and evening thunderstorms caused by intense surface heating and sea breeze circulation. However, no correlation was observed between PM_{10} concentrations and rainfall amount during the sampled period thus, negating the possibility of a washout effect. Vertical mixing and thus dilution of near-surface pollutants are often regulated by the planetary boundary layer (PBL) height over the sampled region. In Singapore PBL height does not vary much across the months due to small variance of average daily temperature coupled with high humidity. No correlation ($r=-0.21$, $p=0.17$) was observed between PM_{10} and PBL height over Singapore for the sampled period.

Concentration of 15 elements (Al, Ba, Ca, Co, Cr, Cu, Fe, Mg, Mn, Ni, Pb, Sr, Ti, V and Zn) were measured in this study. Often elemental concentration alone is insufficient to determine the sources. Hence, we use crustal enrichment factor (EF) and elemental ratios in conjunction with concentrations to understand the sources of the PM_{10} metals.

The crustal enrichment factor (EF) is defined as the enrichment of a particular element relative to their natural abundance in crustal soil. The EF is generally calculated with respect to a reference element, usually Al or Fe and is expressed as

$$\mathrm{EF} = \left(\frac{\left(\frac{X}{Ref}\right)_{Sample}}{\left(\frac{X}{Ref}\right)_{Crust}} \right)$$

Where x is the element of interest and Ref is the reference element, which is Al for this study. The average chemical composition of crust is taken from Rudnick and Gao, 2003. EF = 1 indicate crustal source, and elements with EF ≤ 10 are considered to originate from crustal source to accommodate local and regional variations in soil chemical composition (Kaya and Tuncel, 1997).

The 15 elements analysed from the PM_{10} aerosol samples demonstrated variations in concentrations across seasons (**Table 4.1**). The concentration distribution of the elements can be used to track the sources of the pollutants. In all the three seasons the mean concentrations of Al, Ca, Fe, Mg and Zn were an order of magnitude higher than that of Pb, Ti, Ba, Cu, Cr, Co, Mn, Ni, Sr and V (**Figure 4.5**). Al, Ca, Fe and Mg are some of the most abundant elements in earth's crust after oxygen and silicon. Hence their high concentrations (105—364 ng/m^3) as compared to the

other elements (≤ 36 ng/m^3) can be attributed to the natural background of crustal dust. Besides crustal dust, Ca and Mg can have sea spray origin (Xiao et al., 2017). EFs of Ca, Fe and Mg are <10 for all the seasons confirming crustal source (**Figure 4.6**). Among the low concentration element group, Ti, Ba and Sr have crustal origin with EF < 10. EF of Mn is also < 10 for NE and IM winds but is slightly higher than 10 (EF=17) for SW winds (**Figure 4.6**).

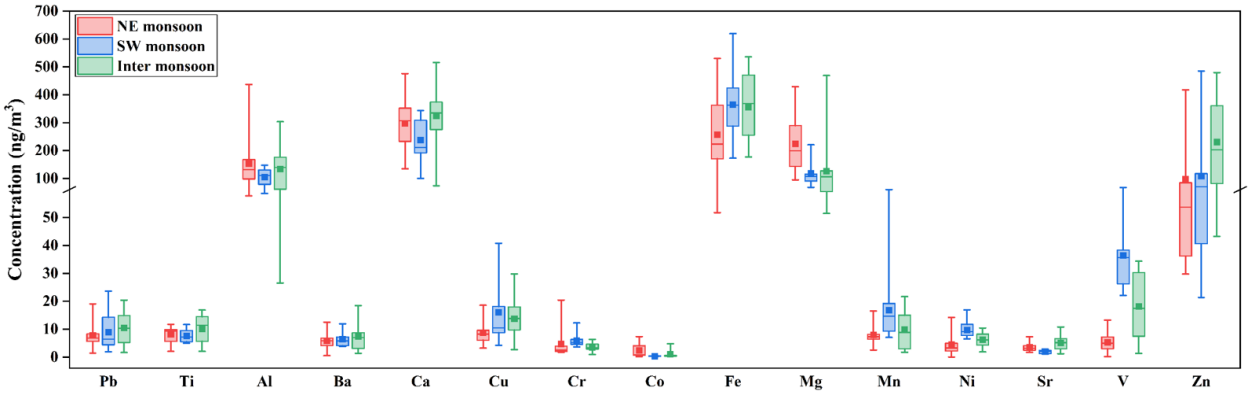

Figure 4.6: *Box plots depicting the concentrations of the measured elements in NE, SW and IM seasons. The horizontal lines within the boxes, upper and lower edges of the boxes specify median, 25th, and 75th percentile respectively. The mean values are specified by small solid boxes within. The upper and lower edges of the whiskers indicate maximum and minimum values*

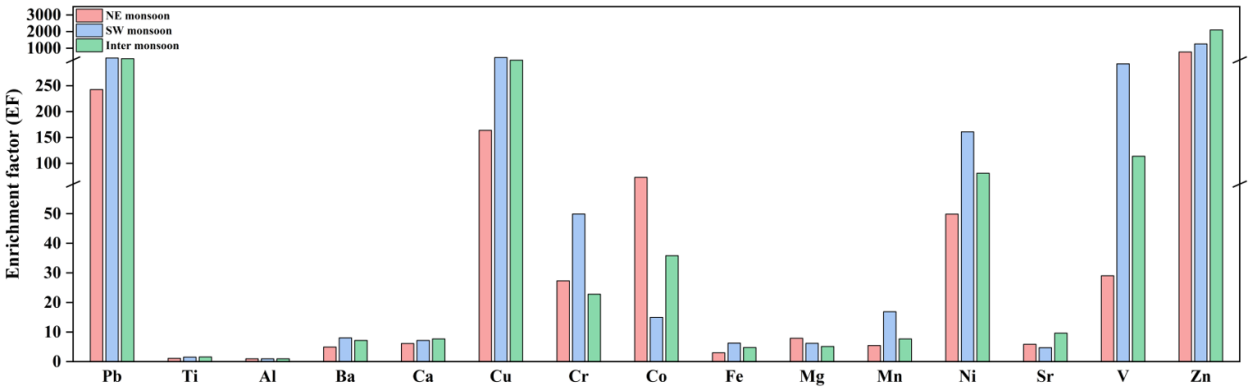

Figure 4.5: *Enrichment factors of metals in NE, SW and IM seasons*

EF indicated that the elements Pb, Zn, Cu, V, Ni, Cr, and Co were enriched by factors of 15 to 2112 implying anthropogenic origin. Out of these metals, Pb, Cu and Zn had extremely high EFs (>100 for all three seasons). The highest EFs of these metals (except Co and Zn) were observed in the SW monsoon winds. To qualitatively assess anthropogenic sources of these metals, Pearson

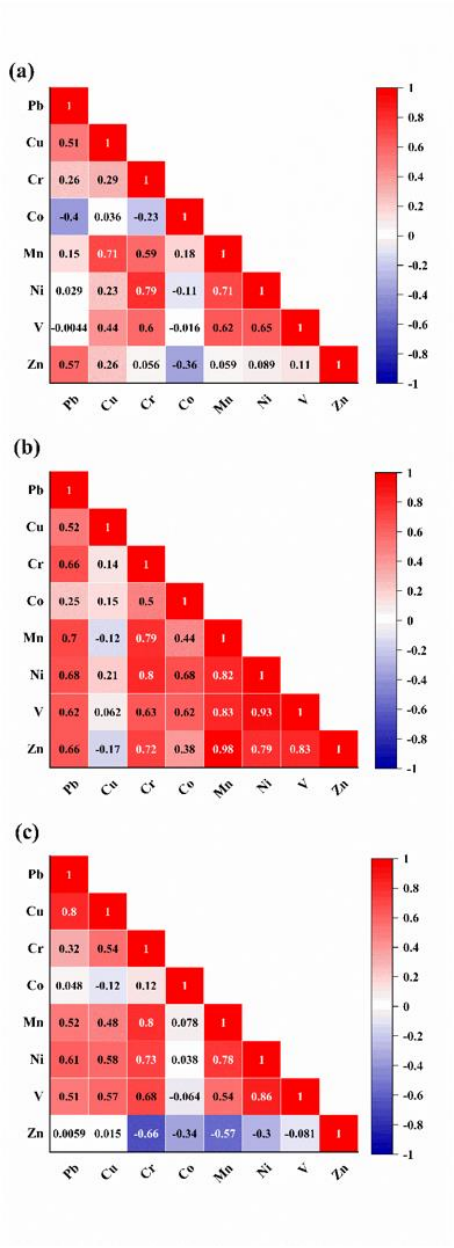

Figure 4.7:*Pearson's correlation coefficients determined for 8 metals with Enrichment Factor>10 measured during (a) NE, (b) SW and (c) inter monsoon seasons. All coefficients above 0.6 have p values < 0.05*

correlation coefficient ($p < 0.05$) indicating association between two metals were used (**Figure 4.7**). Additionally, certain elemental ratios distinctive of different sources are investigated.

In the NW monsoon winds Pb moderately correlates with Zn (0.57) and Cu (0.51). Strong and moderate correlation is observed between Ni and Cr (0.79) and Ni and V (0.65). In contrast, moderate to strong correlation between many elemental pairs were observed during SW monsoon season. Pb correlates well with Zn, Cu, V, Ni, Mn and Cr (0.52 — 0.70). Strong mutual correlation is observed between Zn, Mn and V and Ni. In the IM season Pb correlates well with Ni (0.61) and Cu (0.80). Mutual significant correlations are observed between V, Ni and Cr in the IM winds. Strong correlations between elemental pairs can be indicative of the common sources of atmospheric Pb pollution.

Elemental ratios serve as reliable tracers for contaminants in the atmosphere (Chifflet et al., 2018; R. Das et al., 2018; Kayee et al., 2021). For example, V/Pb and V/Ni ratios can act as tracers for coal and oil combustion respectively (Wu and Huang, 2021). Generally, coals are rich in V and the V/Pb > 1 indicates coal combustion emission and V/Pb < 1 indicates vehicle exhaust emission. Non coal burning industrial wastes and emissions have V/Pb << 1. V/Pb ratios of SW monsoon (5.72 ± 3.11) and IM (2.25 ± 2.31) show significant difference with that of NE (0.81 ± 0.51) monsoon [ANOVA ($F_{2,42} = 19.55$, significance level: $p < 0.001$)]. Previous studies reported V/Ni ratios between 3 - 4 in heavy oil combustion (Mazzei et al., 2008), ratio between 2.5 — 5 from

ship emissions (Salameh et al., 2015; Viana et al., 2009), whereas additional Ni from oil combustion (Peltier et al., 2009) results in lower ratio. V/Ni ratios of NE monsoon (1.52 ± 0.72) are also significantly different from that of SW (3.73 ± 0.46) and inter monsoons (2.67 ± 1.10) ($F_{2,42} = 29.60$, $p < 0.001$). During the SW monsoon season, both the V/Pb and V/Ni ratios were the highest. The significant differences in these ratios, indicate that pollution sources differ across seasons.

4.2.3. Pb isotopic composition and its sources

Average Pb concentrations in all the three seasons were comparable (7.8 – 10.4 ng/m^3) with inter monsoon > SW monsoon > NE monsoon (**Table 4.1**). Pb isotope ratios ($^{206/207}$Pb and $^{208/207}$Pb) for all 45 aerosol samples (**Table 4.2**) were determined to delineate the potential sources of pollution-derived metal in the atmosphere. NE monsoon had the highest mean $^{206/207}$Pb and $^{208/207}$Pb ratios (1.1503 ± 0.0046 and 2.4283 ± 0.006 respectively). The mean $^{206/207}$Pb and $^{208/207}$Pb ratios for SW (1.1471 ± 0.0054 and 2.4206 ± 0.0066) and inter monsoon (1.1481 ± 0.0056 and 2.4259 ± 0.0069) seasons were relatively close (**Table 4.3**).

Table 4.2: *Pb isotopic composition of Singapore aerosols*

Sample	Season	Date	$^{206}Pb/^{204}Pb$	2se	$^{207}Pb/^{204}Pb$	2se	$^{208}Pb/^{204}Pb$	2se	$^{206}Pb/^{207}Pb$	2se	$^{208}Pb/^{207}Pb$	2se	[Pb] (ng/m^3)
1	SWM	17/06/2017	17.7928	0.00393	15.5533	0.00496	37.6284	0.01618	1.1440	0.00062	2.4194	0.00074	4.4
2	SWM	22/06/2017	17.9776	0.00322	15.5823	0.00396	37.8573	0.01349	1.1538	0.00050	2.4294	0.00059	15
3	SWM	29/06/2017	17.9593	0.00273	15.5842	0.00305	37.8193	0.01124	1.1524	0.00040	2.4268	0.00050	15
4	SWM	10/07/2017	17.9127	0.00262	15.5806	0.00288	37.7855	0.01011	1.1497	0.00038	2.4254	0.00044	1.9
5	SWM	17/07/2017	17.6104	0.00254	15.5315	0.00308	37.3544	0.01065	1.1338	0.00039	2.4051	0.00048	23
6	SWM	24/07/2017	17.8725	0.00337	15.5486	0.00383	37.6956	0.01235	1.1494	0.00050	2.4241	0.00051	3.0
7	SWM	31/07/2017	17.9377	0.00324	15.5807	0.00397	37.7684	0.01341	1.1513	0.00050	2.4241	0.00062	6.4
8	SWM	10/08/2017	17.9526	0.00076	15.5668	0.00083	37.7745	0.00283	1.1533	0.00011	2.4267	0.00014	3.5
9	SWM	16/08/2017	17.8547	0.00171	15.5736	0.00208	37.6557	0.00726	1.1465	0.00026	2.4179	0.00034	4.7
10	SWM	23/08/2017	17.8496	0.00218	15.5769	0.00249	37.6779	0.00864	1.1459	0.00032	2.4188	0.00039	5.9
11	SWM	30/08/2017	17.8117	0.00092	15.5715	0.00108	37.6196	0.00363	1.1439	0.00014	2.4159	0.00016	12
12	SWM	06/09/2017	17.7199	0.00116	15.5401	0.00139	37.4776	0.00470	1.1403	0.00018	2.4117	0.00021	11
13	SWM	14/09/2017	17.9565	0.00143	15.5894	0.00184	37.8160	0.00645	1.1518	0.00023	2.4258	0.00029	14
14	SWM	20/09/2017	17.8044	0.00309	15.5374	0.00392	37.5415	0.01296	1.1459	0.00049	2.4161	0.00062	4.4
15	SWM	28/09/2017	17.8310	0.00053	15.5694	0.00052	37.7148	0.00150	1.1452	0.00007	2.4224	0.00008	9.3
16	IM	05/10/2017	17.8099	0.00051	15.5655	0.00062	37.6837	0.00180	1.1442	0.00008	2.4210	0.00008	16
17	IM	12/10/2017	17.9513	0.00049	15.5846	0.00050	37.8433	0.00129	1.1519	0.00007	2.4283	0.00005	3.5
18	IM	19/10/2017	17.8473	0.00061	15.5779	0.00074	37.7723	0.00240	1.1457	0.00009	2.4247	0.00012	20
19	IM	26/10/2017	17.9957	0.00063	15.6018	0.00071	37.9543	0.00227	1.1534	0.00009	2.4327	0.00010	20
20	IM	02/11/2017	18.1490	0.00105	15.6268	0.00114	38.1787	0.00327	1.1614	0.00015	2.4431	0.00014	9.3
21	IM	09/11/2017	17.9338	0.00059	15.5802	0.00058	37.8365	0.00148	1.1511	0.00008	2.4285	0.00007	1.6
22	IM	16/11/2017	17.9207	0.00089	15.5891	0.00075	37.8398	0.00229	1.1496	0.00011	2.4274	0.00010	7.8
23	IM	23/11/2017	17.8990	0.00071	15.5772	0.00063	37.7726	0.00151	1.1491	0.00009	2.4249	0.00005	2.0

24	IM	30/11/2017	17.8159	0.00062	15.5788	0.00058	37.7405	0.00161	1.1436	0.00008	2.4225	0.00006	5.2
25	NEM	07/12/2017	17.8802	0.00037	15.5750	0.00038	37.7758	0.00111	1.1480	0.00005	2.4254	0.00004	5.9
26	NEM	13/12/2017	17.9738	0.00094	15.5971	0.00095	37.9235	0.00286	1.1524	0.00013	2.4314	0.00012	19
27	NEM	20/12/2017	18.0783	0.00102	15.6010	0.00102	38.0954	0.00259	1.1589	0.00014	2.4419	0.00011	13
28	NEM	27/12/2017	17.8359	0.00060	15.5730	0.00057	37.7124	0.00137	1.1453	0.00008	2.4216	0.00005	4.5
29	NEM	03/01/2018	17.8543	0.00290	15.5522	0.00340	37.6997	0.01110	1.1480	0.00044	2.4241	0.00012	8.2
30	NEM	10/01/2018	17.8861	0.00216	15.5537	0.00188	37.7382	0.00423	1.1499	0.00028	2.4263	0.00010	1.4
31	NEM	17/01/2018	17.9467	0.00057	15.5859	0.00077	37.8608	0.00241	1.1515	0.00009	2.4292	0.00015	5.5
32	NEM	24/01/2018	17.7907	0.00034	15.5667	0.00042	37.6849	0.00123	1.1429	0.00005	2.4209	0.00006	7.6
33	NEM	30/01/2018	17.9492	0.00054	15.5861	0.00049	37.8683	0.00134	1.1516	0.00007	2.4295	0.00005	5.5
34	NEM	07/02/2018	18.0685	0.00030	15.6023	0.00032	38.0383	0.00089	1.1581	0.00004	2.4380	0.00005	8.4
35	NEM	14/02/2018	17.9468	0.00046	15.5906	0.00045	37.9164	0.00126	1.1511	0.00006	2.4320	0.00006	7.0
36	NEM	21/02/2018	17.9493	0.00051	15.5821	0.00051	37.8558	0.00125	1.1519	0.00007	2.4294	0.00006	5.6
37	NEM	28/02/2018	17.9930	0.00042	15.5919	0.00042	37.9097	0.00110	1.1540	0.00006	2.4314	0.00005	7.6
38	NEM	12/03/2018	17.7897	0.00046	15.5655	0.00047	37.6695	0.00125	1.1429	0.00006	2.4201	0.00007	6.6
39	NEM	21/03/2018	17.8598	0.00034	15.5810	0.00034	37.7580	0.00088	1.1463	0.00005	2.4233	0.00003	12
40	NEM	28/03/2018	17.9561	0.00047	15.5880	0.00045	37.8476	0.00116	1.1519	0.00006	2.4280	0.00006	6.1
41	IM	04/04/2018	17.8924	0.00330	15.6213	0.00420	37.9416	0.01390	1.1454	0.00052	2.4288	0.00004	14
42	IM	11/01/2018	17.7018	0.00048	15.5479	0.00044	37.5234	0.00119	1.1385	0.00006	2.4134	0.00005	7.0
43	IM	18/04/2018	17.8597	0.00032	15.5831	0.00031	37.7470	0.00092	1.1461	0.00004	2.4223	0.00005	11
44	IM	25/04/2018	17.7838	0.00033	15.5669	0.00032	37.6591	0.00093	1.1424	0.00004	2.4192	0.00004	15
45	IM	02/05/2018	17.9333	0.00031	15.5857	0.00034	37.8076	0.00090	1.1506	0.00004	2.4258	0.00004	12

***Table 4.3**: Statistical summary of metal concentration (ng/m^3) and PM_{10} concentration (µg/m^3) in Singapore aerosols*

Season	N	Parameter	Al	Ba	Ca	Co	Cr	Cu	Fe	Mg	Mn	Ni	Pb	Sr	Ti	V	Zn	PM_{10}
NE monsoon	16	Mean	154	5.8	297	2.4	4.7	8.6	257	224	7.9	4.4	7.8	3.5	8.2	5.3	98	47
		Min	58	0.50	135	0.19	1.7	3.2	52	95	2.5	0.05	1.4	1.6	2.0	0.13	30	17
		Max	437	12	476	7.3	20	18	530	429	16	14	19	7.3	11.8	13	418	79
		SD	96	3.0	90	2.3	5.4	4.3	125	107	3.6	3.6	4.1	1.6	2.8	3.3	117	21
SW monsoon	15	Mean	105	6.5	237	0.33	5.9	16	364	119	17	9.7	8.9	1.9	7.5	36	108	45
		Min	59	3.8	100	0.20	3.6	4.2	173	68	7.0	6.5	1.9	1.1	5.0	22	21	28
		Max	147	12	343	0.48	12	41	619	220	60	17	23.7	2.8	12	68	485	72
		SD	28	2.8	69	0.07	2.1	12	104	45	13	2.8	6.1	0.57	2.2	12	116	12
Inter monsoon	14	Mean	134	7.4	324	1.0	3.4	14	356	126	9.8	6.3	10.4	5.1	10	18	231	45
		Min	26	1.4	74	0.25	0.86	2.7	177	51	1.7	1.8	1.6	1.2	2.0	1.3	43	20
		Max	303	18.5	516	4.7	6.4	30	536	469	22	10	20	11	17	34	479	83
		SD	89	4.9	108	1.5	1.6	7.6	122	106	6.8	2.7	6.3	2.7	4.8	11	170	18

4.2.4. Anthropogenic sources of atmospheric Pb

The possible anthropogenic end members contributing to the atmospheric Pb concentration can be coal combustion, high temperature industrial processes, incineration of wastes, vehicular exhaust (Carrasco et al., 2018; Komárek et al., 2008) and recirculation of historical leaded gasoline exhaust particles as has been observed in Mexico (Morton-Bermea et al., 2011) and Kanpur , India (Sen et al., 2016).

Singapore completely phased out leaded gasoline in 1998 (OECD and UNEP, 1999), hence it is improbable that historic Pb from Singapore's leaded gasoline is still contaminating the atmosphere. Carrasco et al. (2018) examined the Pb isotope ratios for Singapore's leaded gasoline using local gas station soils as a proxy and found the ratios to be $^{206/207}Pb = 1.124 \pm 0.013$ and $^{208/206}Pb = 2.131 \pm 0.015$. Leaded gasoline had a substantially lower $^{206/207}Pb$ ratio than the aerosols measured in this study (**Figure 4.8).** Indonesia continued to use leaded gasoline until 2006 (Walsh, 2007) with less radiogenic Pb isotopic signature of the alkyllead closer to the Australian Broken Hill type Pb ore deposit (Bollhöfer and Rosman, 2000). The Pb isotopic signature of Indonesian atmospheric

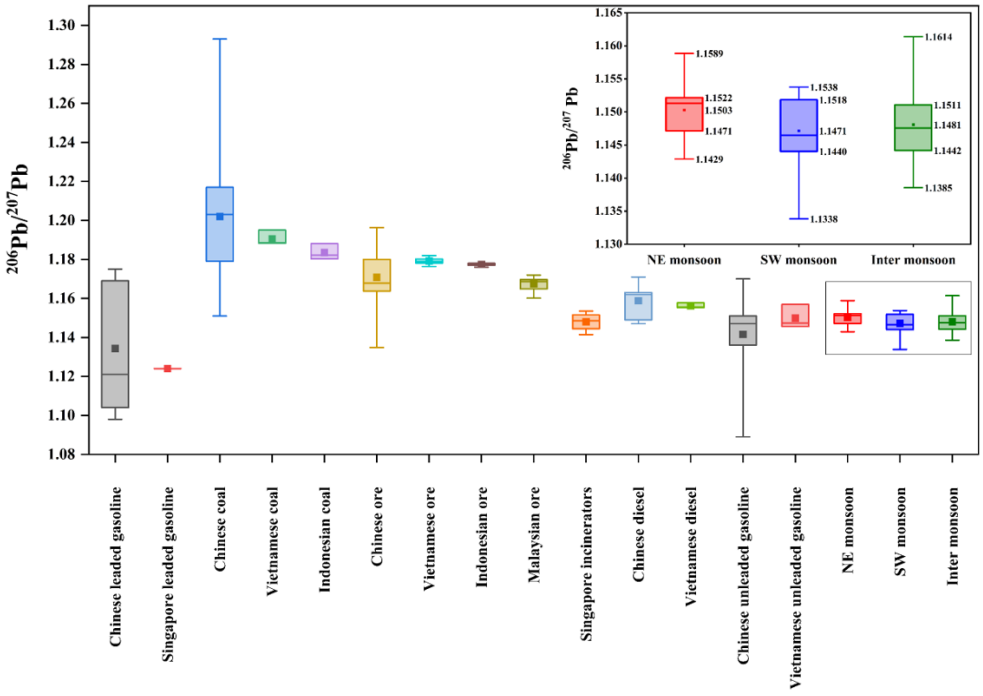

Figure 4.8: *$^{206}Pb/^{207}$ Pb isotopic signatures of plausible end members and Singapore aerosols during NE, SW and Inter monsoon seasons. The inset plot shows $^{206}Pb/^{207}Pb$ ratios for NE, SW and Inter monsoon seasons*

PM measured in 1990 had lower $^{206/207}$Pb values, (1.091-1.131) as the primary source of atmospheric Pb was found to be dominated by leaded gasoline emission (Bollhöfer and Rosman, 2000).

The $^{206/207}$Pb values of Chinese and Vietnamese unleaded gasoline vary from 1.089 to 1.170 (Bi et al., 2017) and 1.147 to 1.157 (Chifflet et al., 2018), respectively, which coincide with the $^{206/207}$Pb range of Singapore PM_{10} samples **(Figure 4.8).** The isotopic signatures of diesel from some parts of China (Yao et al., 2015) are very similar to that of Singapore PM_{10} **(Figure 4.8),** indicating probably a long range transport of Pb from diesel emissions during the NE monsoon season.

Southern Chinese, Vietnamese and Indonesian coals are enriched in radiogenic Pb with $^{206/207}$Pb values ranging from 1.16 – 1.29 in Chinese coals and $^{206/207}$Pb > 1.18 in Vietnamese and Indonesian coals (Bi et al., 2017; Chifflet et al., 2018; Díaz-Somoano et al., 2009). Despite the fact that the NE and SW monsoon winds carry air masses from Southern China and Indonesia, the Pb isotopic ratios of Singapore PM_{10} are less radiogenic than those of Chinese or Indonesian coals **(Figure 4.8).**

The Siding mine in Southern China, which is within the air mass transit range, possesses radiogenic galena ($^{206/207}$Pb = 1.16 – 1.19) (Hsu, 2019a). Similarly, Malaysian Pb-Zn ores have $^{206/207}$Pb > 1.162 (Basori et al., 2017). As a result, transboundary contamination from ore mining and coal combustion cannot be the sole source for less radiogenic Pb in Singapore PM_{10} samples. However, the radiogenic values of Pb isotopes in Indonesian coal along with less radiogenic Pb in historic leaded gasoline from Indonesia can form mixing end members in SW monsoon.

The component having the closest $^{206/207}$Pb values with that of the aerosols were incineration dust from local waste incinerators **(Figure 4.8).** Singapore's solid waste disposal infrastructure consists of 4 incinerator plants: Tuas, Senoko, Tuas South, and Keppel Seghers, with Senoko around 25 km from the sampling location and Keppel Seghers, Tuas and Tuas South approximately 12 km. The ash from the incinerators is dumped at the Samakau landfill, about 28 km from the sampling location (Singapore National Environment Agency, 2020). Carrasco et al. (2018) examined the fly ash released by incinerators to determine the $^{206/207}$Pb values in the range of 1.141 – 1.153, which overlaps with the aerosols measured in this study.

From the triple isotope plot (**Figure 4.9**), it is observed that several of the anthropogenic end members have overlapping Pb isotopic ratios. Hence the isotopic ratios in conjunction with the metal concentrations are used to deduce the possible end members for atmospheric Pb in all three seasons.

NE monsoon: NE monsoon air masses mostly come from the South China Sea and few originate in the southern part of China, south eastern Vietnam and Malaysia **(Figure 4.2).** The plausible long-range sources could be coal combustion and ore mining in southern China, Vietnam and Malaysia. However, it is evident that the coal and ore ratios do not overlap with that of the PM_{10} samples (**Figure 4.8 and Figure 4.9**). Furthermore, the V/Pb ratio, which is used to differentiate between traffic emissions (V/Pb < 1), coal combustion (V/Pb > 1), and industrial emissions (V/Pb << 1), is typically less than one during NE monsoon, with an average value of 0.813 ± 0.513 (Kayee et al., 2021). The V/Pb ratio of Vietnamese coal (0.927) lies close to that of NE monsoon aerosols **(Figure 4.10a).** Air masses originating from Vietnam may carry coal combustion signatures, which may have resulted in slightly elevated $^{206/207}$Pb and $^{208/207}$Pb values during the NE monsoon compared to the other two seasons. Nevertheless, contribution from Vietnamese coal should not be overwhelming as majority of the air masses originate from the sea during the NE monsoon season.

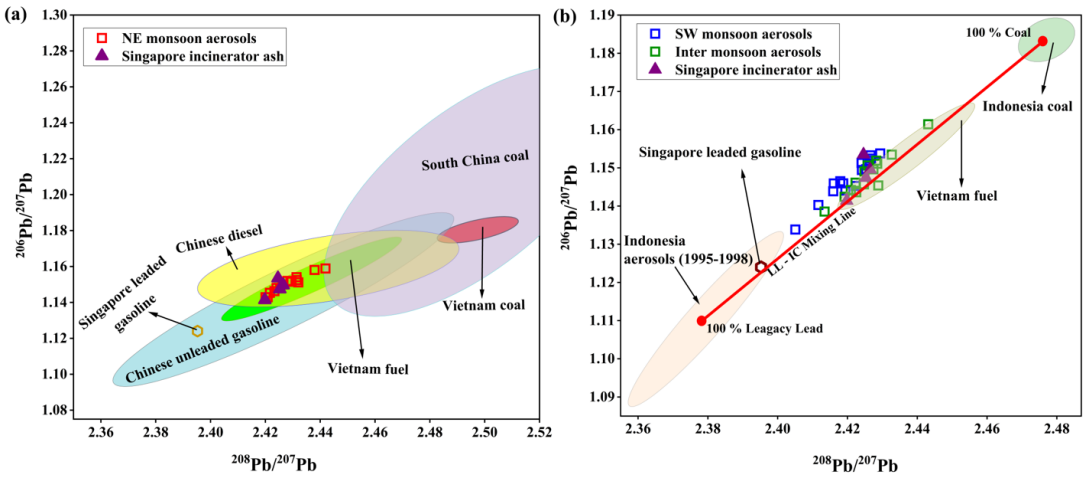

Figure 4.9: *Triple isotope plot of Pb for (a) NE and (b) SW & IM seasons with reference to different plausible end members. The mixing line between legacy lead (LL) and Indonesian coal (IC) is shown in red. References: Indonesian coal & aerosols and Vietnamese coal & fuel (Bollhöfer and Rosman, 2000; Díaz-Somoano et al., 2009 and Chifflet et al., 2018); Chinese diesel, unleaded gasoline and coal (Bi et al., 2017); Singapore leaded gasoline and incinerator ash (Carrasco et al., 2018).*

Gasoline and diesel from the region (China and Vietnam) have $^{206/207}$Pb ratios overlapping with that of the NE monsoon aerosols **(Figure 4.9).** Moreover, Singapore importing a part of its crude oil from Vietnam (Tan et al., 2010), may result in Singapore PM_{10} having similar isotopic characteristics of Vietnamese fuel. The V/Ni and V/Pb ratios during this season are quite close to the characteristic ratios of traffic emissions (Chifflet et al., 2018) along with moderate correlation between V and Ni (0.65) (**Figure 4.7a**) . Thus, vehicular emissions are the most probable sources of atmospheric Pb during NE monsoon. Few of the high $^{206/207}$Pb ratios recorded during the season could have been contributed by mixing of Vietnamese coal combustion emissions and few of the low V/Pb ratios could have resulted from fly ashes from the incinerators.

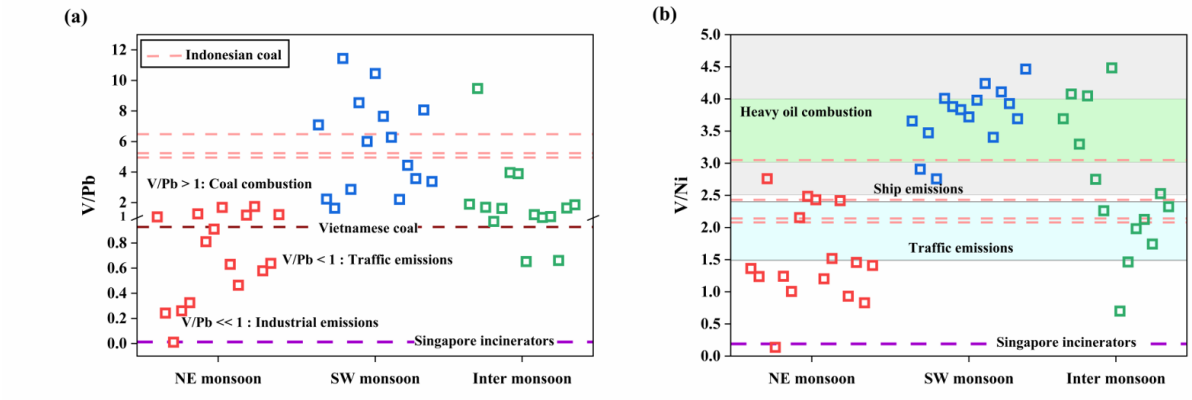

Figure 4.10: *Seasonal variations in (a) V/Pb and (b) V/Ni ratios in Singapore aerosols. Elemental ratios for Indonesian coal and Vietnamese coal have been adopted from Belkin et al. (2009) and Chifflet et al. (2018) respectively. V/Ni ratios for ship emissions were adopted from Wu and Huang (2021) and traffic emissions from Chifflet et al. (2018). Both the elemental ratios of Singapore incineration dust were adopted from Yin et al. (2008).*

SW monsoon: In SW monsoon air masses are transported from Kalimantan, Sulawesi of Indonesia and Java Sea **(Figure 4.2).** Kalimantan and Sulawesi have a large number of open pit coal mines, coal-fired power stations and Au-Pb mines. A high V/Pb ratio (5.722 ± 3.112) indicates the source of pollution to be coal combustion. V/Pb ratios in PM_{10} collected during the SW monsoon are similar to those in Indonesian coal **(Figure 4.10a)**. The Ni/V versus Pb/V plot demonstrates that the majority of the SW monsoon PM_{10} overlap with the Indonesian coals (**Figure 4.11**). However, the PM_{10} isotopic ratios do not match with the radiogenic Pb isotopic signatures of Indonesian coal

(Figure 4.8). As a result, the transboundary sources might include a mixture of radiogenic coal combustion and past Pb from less radiogenic Indonesian leaded gasoline. Indonesian atmospheric particulates collected in 1994-95 showed a dominant leaded gasoline signature ($^{206}Pb/^{207}Pb$ ranged from 1.103-1.131) and traces of the legacy Pb might still be circulating in the environment. Pearson's correlation between V — Ni (0.93) in this season was the strongest among the three seasons (**Figure 4.7b**). Moreover, V and Ni also had the highest enrichment factor **(Figure 4.6**) during this period and the V/Ni ratios of SW monsoon aerosols overlap with the characteristic V/Ni ratios of ship emissions and oil combustion **(Figure 4.10b).** This implies influence of ship and vehicular emissions on the atmospheric metal composition (Balasubramanian and Qian, 2004; Kitamura et al., 2020). A binary mixing model employing a simple mass balance equation that accounts for legacy lead and Indonesia coal reveals that legacy lead contributes 42 % — 75 % and Indonesia coal contributes 25 % — 58 % towards atmospheric Pb. The legacy lead end member is based on average $^{206/207}Pb$ and $^{208/207}Pb$ values of Singapore leaded gasoline (Carrasco et al., 2018) and Indonesia aerosols measured in 1995-1998 (Bollhöfer and Rosman, 2000). Indonesia coal end member is based on average $^{206/207}Pb$ and $^{208/207}Pb$ values from (Díaz-Somoano et al., 2009). Consequently, transboundary coal combustion mixed with legacy Pb from leaded gasoline use in Indonesia is possibly mixed with ship emissions and heavy oil combustion from local ports, in the SW monsoon winds.

Inter monsoon: In inter monsoon season, majority of the air masses originate from Java Sea and Borneo **(Figure 4.2**). The Pb isotopic fingerprints of the inter monsoon are remarkably similar to those of the SW monsoon, implying comparable end members. During the inter monsoon season, the V/Pb ratio was greater than one (2.259 ± 2.317), lying between the ratios observed during NE and SW monsoons. V/Ni ratios of Indonesian coals determined from metal data available in Belkin et al. (2009) reveal that the V/Ni ratios of the PM_{10} samples collected during the inter monsoon seasons have similar values **(Figure 4.10b).** The Ni/V versus Pb/V plot shows that the inter monsoon PM_{10} lie quite close to the Indonesian coals (**Figure 4.11**) Both these ratios suggest that coal burning emissions from Indonesia may contribute to the Pb levels in the atmosphere. However, as the $^{206/207}Pb$ ratio of Indonesian coal is substantially higher than that of Singapore PM_{10} **(Figure 4.9),** anthropogenic Pb must be generated due to a mixture of end members. The combination of radiogenic fingerprints of Pb isotopes from Indonesian coals along with historic Pb from Indonesian leaded gasoline may contribute to the less radiogenic Pb isotopic signatures

of Singapore PM_{10}. High positive correlation between V — Ni (0.86) (**Figure 4.7c**) implies vehicular traffic as a major source of pollution (Balasubramanian and Qian, 2004;). The V/Ni ratios of inter monsoon aerosols overlap with that of traffic emissions, heavy oil combustion and ship emissions **(Figure 4.10b)** (Chifflet et al., 2018; Wu and Huang, 2021). Although coal combustion emissions contributed to atmospheric Pb levels, their contribution was slightly smaller in the inter monsoon season than in the SW monsoon, as evidenced by lower V/Pb ratios (**Figure 4.10a**). Moreover, the SW monsoon air masses travel more extensively across the coal mining regions of Indonesia than the inter monsoon air masses before reaching Singapore (**Figure 4.2**). As a result, SW monsoon winds are more likely to transport Pb-laden air masses from Indonesia's coal mining regions. However, despite a probably low contribution from coal combustion, average Pb concentrations in the inter monsoon aerosols were the highest (10.42 ± 6.27 ng/m^3). A binary mixing model that accounts for legacy lead and Indonesia coal reveals that legacy lead contributes 31 % — 66 % and Indonesia coal contributes 34 % — 69 % towards atmospheric Pb. Thus, to summarize, Indonesian coal combustion, recirculating dust from historic use of leaded gasoline, heavy oil combustion and ship emissions, contributed significantly to the atmospheric Pb levels in inter monsoon season.

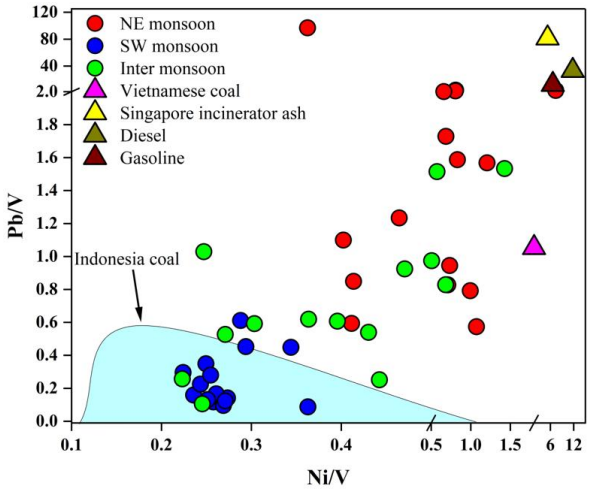

Figure 4.11: *Ni/V vs Pb/V ratios of Singapore PM10 aerosol samples in comparison to plausible anthropogenic end members. References: Indonesian coal (Belkin et al., 2009); Vietnamese coal and gasoline & diesel (Chifflet et al., 2018); Singapore incineration dust (Yin et al., 2008)*

4.3. Quantitative assessment of atmospheric Pb sources in India and SEA countries in the last decade using statistical modeling

A comprehensive literature review was conducted to gather Pb isotope and relevant elemental concentration data of aerosol samples collected from South and Southeast Asian countries over the past decade. The studied regions encompass India, and SEA countries from where a total of 341 aerosol Pb isotope data points were acquired (Carrasco et al., 2018; Chifflet et al., 2018; R. Das et al., 2018; Das et al., 2023; Kayee et al., 2020, 2021; Kumar et al., 2016; Lee et al., 2014; Mitra et al., 2021; Sen et al., 2016). These aerosol data were compiled into 4 mixture datasets, one for each country, ready, to be fed to the mixing polygon and MixSIAR modelling frameworks. The Pb isotope data of the potential sources of these aerosols available from the same and cross-referenced literatures were compiled as source datasets for India and SEA countries. The isotope data was visualized in three isotope spaces ($^{206}Pb/^{207}Pb$ vs $^{208}Pb/^{207}Pb$ and $^{206}Pb/^{204}Pb$ vs $^{208}Pb/^{204}Pb$).

Despite some overlaps, the aerosols of (a) India, (b) Singapore & Thailand and (c) Vietnam plot in 3 distinct regions, with Singapore and Thailand overlapping with each other in $^{206}Pb/^{207}Pb$ vs $^{208}Pb/^{207}Pb$ space as well as $^{206}Pb/^{204}Pb$ vs $^{208}Pb/^{204}Pb$ space (**Figure 4.12a and 4.12b**). This indicates that atmospheric Pb is either sourced from different endmembers in different regions or common sources have variable contributions in different countries. The sources are distributed along the diagonal of the three-isotope space, with certain sources bracketing the aerosol samples and others positioned at intermediate points.

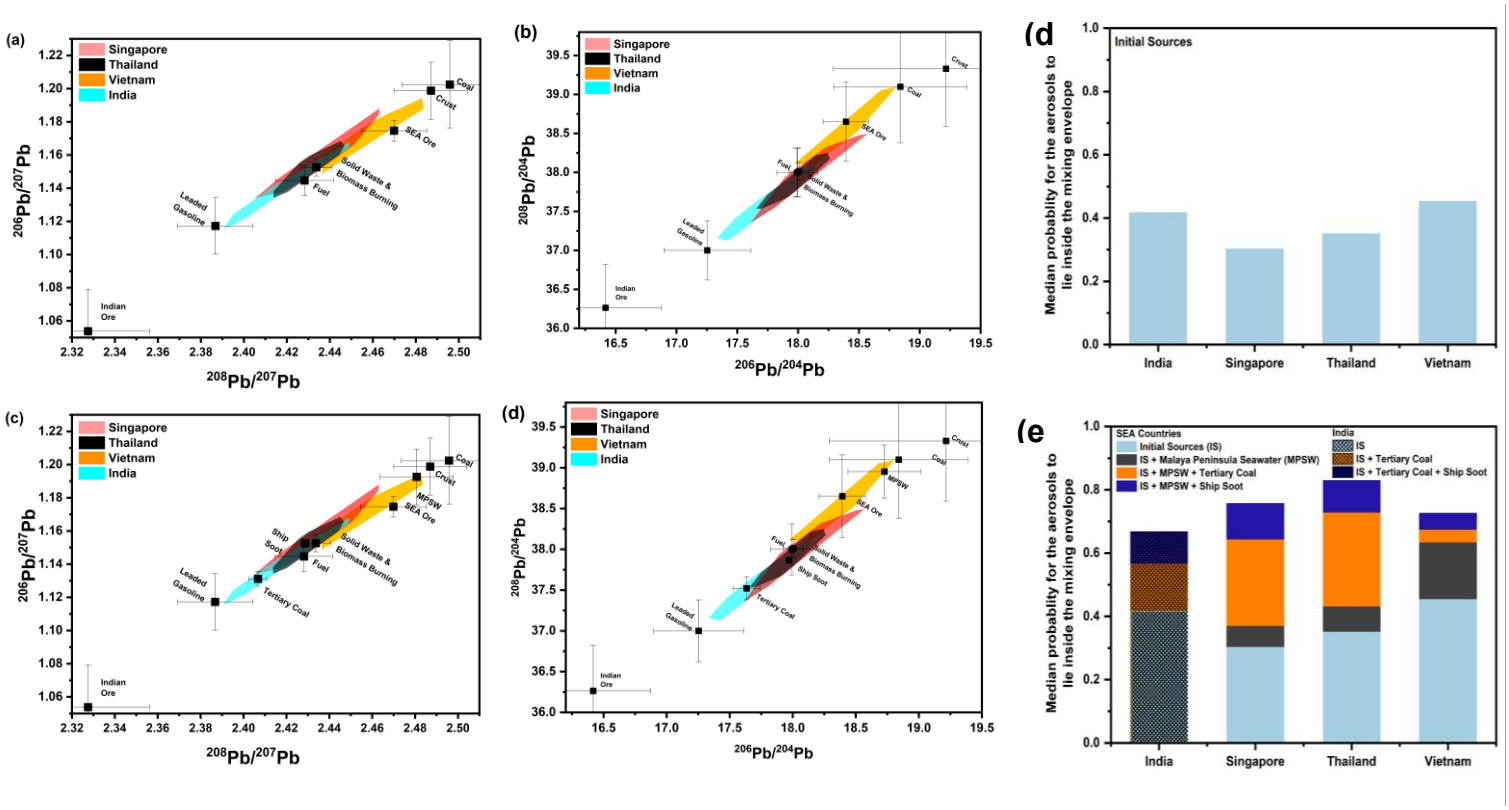

Figure 4.12: *Three – isotope plots of the aerosol mixtures from India, Singapore, Thailand, Vietnam and their initial sources from previous literatures in (a) $^{208}Pb/^{207}Pb$ vs $^{206}Pb/^{207}Pb$ space and $^{206}Pb/^{204}Pb$ vs $^{208}Pb/^{204}Pb$ space. (c) Three – isotope plots of the aerosol mixtures from India, Singapore, Thailand, Vietnam and their initial sources along with the additional sources in $^{208}Pb/^{207}Pb$ vs $^{206}Pb/^{207}Pb$ space and (d) $^{206}Pb/^{204}Pb$ vs $^{208}Pb/^{204}Pb$ space. Rresults of mixing polygon simulation with (d) initial sources and (e) additional sources*

4.3.1. Evaluating source applicability of aerosol Pb using 3D Mixing Polygon Simulation

The ability of Pb to travel long distances due to its high atmospheric residence time makes it crucial that, all natural and anthropogenic sources from the regional and local emissions are taken into consideration. Natural background contribution from upper continental crust (UCC) has been consistently observed in SEA countries (Carrasco et al., 2018; Das et al., 2023; Kayee et al., 2021) and India (R. Das et al., 2018; Kumar et al., 2016) Among the regional sources, coal combustion emissions (both Gondwana and Tertiary coal) from India (R. Das et al., 2018; Mitra et al., 2021), China (Kayee et al., 2021), Vietnam (Chifflet et al., 2018; Kayee et al., 2021), Indonesia (Ray et al., 2022) and Thailand (Kayee et al., 2021) have been proven to influence the SEA nations. Local sources include traffic emissions, high temperature metallurgy, historic leaded gasoline recirculation and solid waste incineration (Carrasco et al., 2018; Das et al., 2023; Kayee et al., 2021, 2020; Ray et al., 2022).

When analyzing in ^{206}Pb, ^{207}Pb and ^{208}Pb space, the median probability of the aerosols to fall inside the mixing envelope formed by these sources was 32 %, 36 %, 44 % and 40 % for Singapore, Thailand, Vietnam and India respectively when the conventional endmembers (coal from India, Indonesia, Vietnam and south China, SEA and Indian ore, unleaded and leaded fuel, solid waste and biomass burning in SEA and crust) were considered (Bi et al., 2017; Bollhöfer and Rosman, 2000; Carrasco et al., 2018; Chifflet et al., 2018; Das et al., 2016; R. Das et al., 2018; Das et al., 2023; Deb et al., 1989; Díaz-Somoano et al., 2009; Huang et al., 2019; Millot et al., 2004; Mitra et al., 2021; Xu et al., 2019; Yao et al., 2015) (**Figure 4.12d**). Analogous probabilities were obtained in $^{206}Pb/^{204}Pb$, $^{207}Pb/^{204}Pb$ and $^{208}Pb/^{204}Pb$ space (were 33 %, 38 %, 34 % and 53 % for Singapore, Thailand, Vietnam and India respectively), which are provided in. The data for probabilities of all the aerosols are provided in **open source data repository** (Ray and Das, 2023a). These low median probabilities observed in both the isotope spaces for all the four countries indicates that there must be sources that were not considered in previous studies.

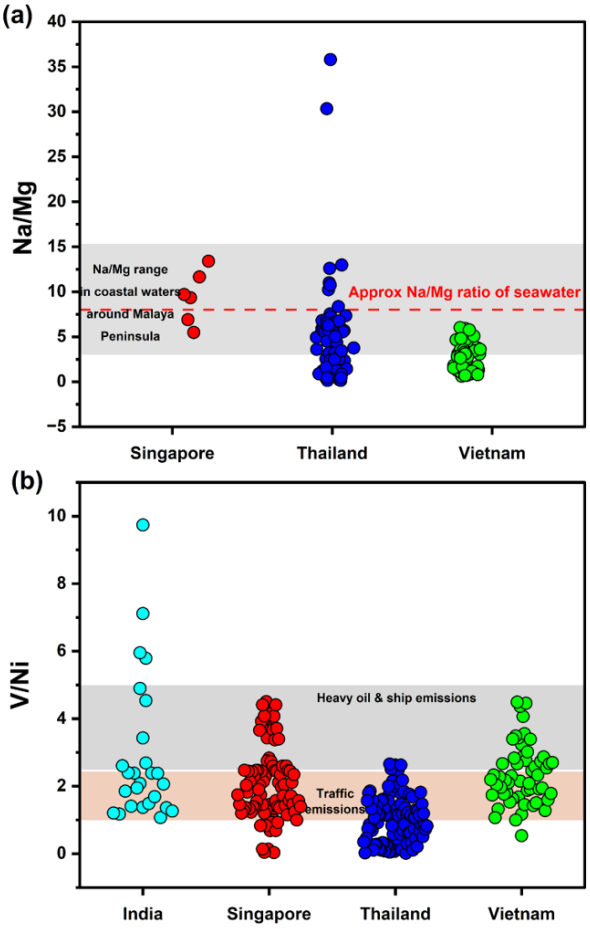

Figure 4.13: *Trends in (a) Na/Mg ratios in aerosol mixtures from Singapore, Thailand and Vietnam; (b) V/Ni ratios in India, Singapore, Thailand and Vietnam. The shaded regions illustrate the ranges observed in sources for which these ratios serve as representative indicators*

To increase the probability of the aerosols to lie inside the mixing envelope formed by the sources, the end-members mentioned in previous literatures as potential sources, although lacking Pb isotope data were tried to be incorporated by finding proper Pb isotope data through literature survey.

Ship emission, and sea spray aerosols were indicated to be probable sources in previous investigations based on elemental ratios such as V/Ni and Na/Mg respectively(R. Das et al., 2018; Kayee et al., 2021; Ray et al., 2022). Based on elemental ratios calculated from elemental concentration data provided in previous investigations, it is observed that aerosols in Singapore, Thailand and Vietnam closely align with the typical Na/Mg value of seawater (~8) (**Figure 4.13a**) (Chifflet et al., 2018; Kayee et al., 2021, 2020; See et al., 2006). The coastal waters around Malaya Peninsula have a wide range of Na/Mg values that overlap with that of the aerosols from Singapore, Thailand and Vietnam (**Figure 4.13a**) (Gasim et al., 2015; Lim et al., 2013; Looi et al., 2013). Moreover, the MPSW has higher concentration of Pb (range = 24.8 - 368 $pmol.kg^{-1}$) compared to the average Pb concentration in South China seawater (67.2 $pmol.kg^{-1}$) and Bay of Bengal (68.1 ± 10.52 $pmol.kg^{-1}$) (M. Chen et al., 2023; Lee et al., 2014). Seawaters in northern (North Atlantic, Pacific and Antarctic surface waters) and southern hemisphere (East Australian coastal shelf waters) also have lower Pb concentration ranging from 12 – 160 $pmol.kg^{-1}$ (Apte et al., 1998). This suggests that the aerosols may exhibit some degree of influence from seawater in addition to other predominant sources.

Similarly, the V/Ni ratios in aerosols from India, Singapore and Vietnam demonstrate characteristics of heavy oil and ship emissions (Chifflet et al., 2018; R. Das et al., 2018; Das et al., 2023; Khare and Baruah, 2010; Police et al., 2018; Rabha et al., 2023; Ray et al., 2022; Wu and Huang, 2021) (**Figure 4.13b**). Tertiary coal from India exhibit a distinctively lower $^{206}Pb/^{207}Pb$ (Mitra et al., 2021) composition and has not been used as an end member in previous studies. The comparable isotopic composition of tertiary coal, wood, and wood charcoal (Mitra et al., 2021), coupled with India's substantial dependence on fuelwood (Sharma, 2018), makes it necessary to consider this as an end member.

As Pb isotopic compositions of ship emissions were not measured in those studies, the sources could not be considered in linear mixing models used in the studies. From literature survey, only one Pb isotopic data representative of regional ship emissions (ship soot) in Vietnam (Hoàng-Hòa et al., 2015) was found. Since there was only one data point for regional ship soot, ship emission data available from Germany having only 10‰ and 4‰ difference in $^{206}Pb/^{207}Pb$ and $^{208}Pb/^{207}Pb$ spaces respectively was also combined (Lahd Geagea et al., 2008). Thus, as anthropogenic contributors for all the 4 countries ship soot (Hoàng-Hòa et al., 2015; Lahd Geagea et al., 2008),

leaded and unleaded gasoline, coal from Vietnam, India, Indonesia south China (referred as coal herein), and tertiary coal & wood charcoal combustion emissions from India were added (Bi et al., 2017; Bollhöfer and Rosman, 2000; Carrasco et al., 2018; Chifflet et al., 2018; Das et al., 2016; R. Das et al., 2018; Díaz-Somoano et al., 2009; Mitra et al., 2021). *A priori* grouping of Indian tertiary coal & wood charcoal isotopic compositions (referred to as tertiary coal herein) were performed as both the sources demonstrated similar ratios (Mitra et al., 2021; Phillips et al., 2014). As transboundary Pb contaminator for India ores of Indonesia, Thailand and South China (referred as SEA ore herein) were considered (Dongsheng, 2015; Hsu, 2019b; Huang et al., 2019; Xu et al., 2019). The sources were separately selected for India and SEA countries, that are listed in **Table 4.4**. We added the sources one at a time and ran the mixing polygon simulation to observe the resultant change in probability.

All the initial sources and additional sources plotted in $^{206}Pb/^{207}Pb$ vs $^{208}Pb/^{207}Pb$ $^{206}Pb/^{204}Pb$ vs $^{208}Pb/^{204}Pb$ three – isotope spaces are presented in **Figure 4.12c**. Incorporation of these previously excluded sources (sea spray, tertiary coal and ship soot) increased the area of the mixing envelope and consequently the median probability for the aerosols to lie inside the mixing envelope in $^{206}Pb/^{207}Pb$, $^{208}Pb/^{207}Pb$ and $^{208}Pb/^{206}Pb$ space to 76 %, 83 %, 73 % and in $^{207}Pb/^{204}Pb$, $^{208}Pb/^{204}Pb$ and $^{206}Pb/^{207}Pb$ space to 67 % and 64 %, 76 %, 63 % and 78 % for Singapore, Thailand, Vietnam and India respectively (**Figure 4.12e**). Data obtained from polygon simulation is provided in open source data repository (Ray and Das, 2023a)**.**

On performing Analysis of Variance (ANOVA) at 0.05 significance level, on the probability results, it was observed that addition of the MPSW resulted in significant increase in probability for Singapore, Thailand and Vietnam. Significant increases for India, Singapore and Thailand were also observed when tertiary coal and ship soot were added as sources. However, tertiary coal and ship soot had no significant effect on Vietnam aerosols.

***Table 4.4**: Individual sources of Atmospheric Pb in SEA countries and India*

India		South East Asia	
Individual Sources	References	Individual Sources	References
Crust	(Das et al., 2023; Millot et al., 2004; Mitra et al., 2021)	a. Crust	(Das et al., 2023; Millot et al., 2004; Mitra et al., 2021)
a. Gondwana Coal	(Bi et al., 2017; Chifflet et al., 2018; Das et al., 2016; R. Das et al., 2018; Díaz-Somoano et al., 2009; Mitra et al., 2021)		
b. Indian Tertiary Coal & Wood Charcoal	(Mitra et al., 2021)	b. Malaya Peninsula Seawater	(M. Chen et al., 2023)
a. Unleaded Fuel	(Bi et al., 2017; Chifflet et al., 2018; Mitra et al., 2021; Yao et al., 2015)	a. Gondwana Coal	(Bi et al., 2017; Chifflet et al., 2018; Das et al., 2016; R. Das et al., 2018; Díaz-Somoano et al., 2009; Mitra et al., 2021)
		b. Indian Tertiary Coal & Wood Charcoal	(Mitra et al., 2021)
Leaded Gasoline	(Bollhöfer and Rosman, 2000; Carrasco et al., 2018)	Unleaded Fuel	(Bi et al., 2017; Chifflet et al., 2018; Mitra et al., 2021; Yao et al., 2015)
a. Indian Ore	(Deb et al., 1989)		
b. Transboundary SEA Ore	(Dongsheng, 2015; Hsu, 2019b; Huang et al., 2019; Xu et al., 2019)	Leaded Gasoline	(Bollhöfer and Rosman, 2000; Carrasco et al., 2018)
Ship Emissions	(Hoàng-Hòa et al., 2015; Lahd Geagea et al., 2008)	SEA Ore	(Bi et al., 2017; Dongsheng, 2015; Huang et al., 2019; Xu et al., 2019)
		Solid Waste Incineration & Biomass Burning	(Carrasco et al., 2018)
		Ship Emissions	(Hoàng-Hòa et al., 2015; Lahd Geagea et al., 2008)
Aerosol Mixture	(R. Das et al., 2018; Kumar et al., 2016; Mitra et al., 2021; Sen et al., 2016)	Aerosol Mixture	(Chifflet et al., 2018; Das et al., 2016, 2023; Hoàng-Hòa et al., 2015; Kayee et al., 2021, 2020; Kumar et al., 2016; Lee et al., 2014; Mitra et al., 2021; Ray et al., 2022; Sen et al., 2016)

4.3.2. Contribution of sources as quantified by linear mixing model

From the three – isotope plot (**Figure 4.14**), it can be observed, that the aerosols do not fall on the traditional leaded gasoline mixing line constructed using Australian Broken Hill ore and USA's Mississippi Valley ore (Sangster et al., 2000). While the mean of the regional leaded gasoline data also deviates marginally from this traditional mixing line, the standard deviations exhibit alignment with it. Thus, in the three-isotope space ($^{206}Pb/^{207}Pb$ vs $^{208}Pb/^{207}Pb$), the aerosols from India are positioned between regional leaded gasoline and Indian ore on one end, and crust and coal on the other end. On the other hand, the SEA aerosols fall between local leaded gasoline and tertiary coal on one side, and crust and coal on the other side. Crust and coal are very similar in isotopic compositions and it is difficult to distinguish between their individual contribution towards aerosol Pb.

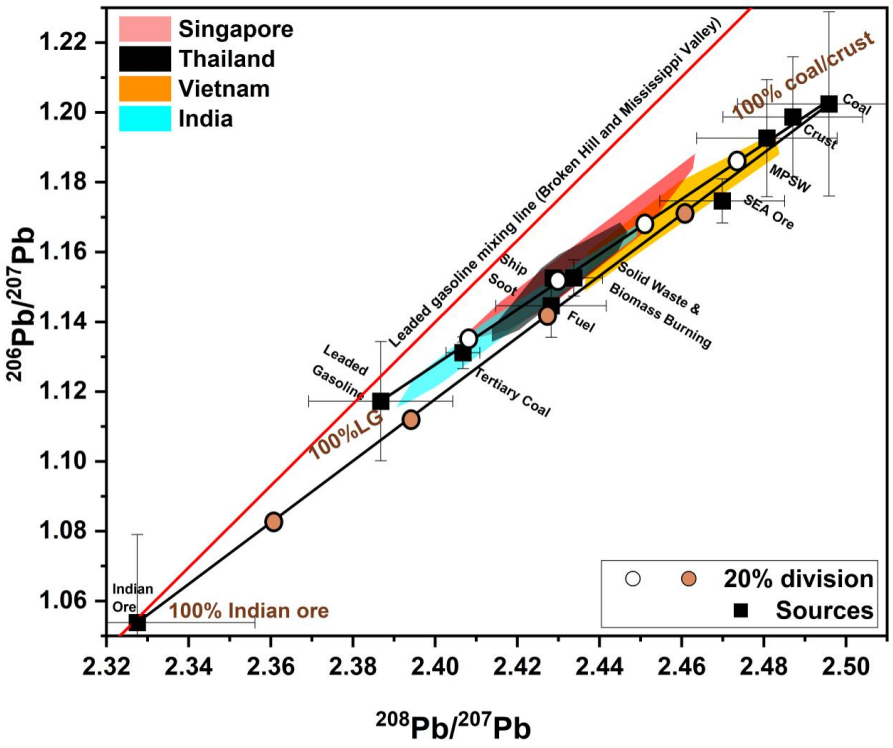

Figure 4.14: *Geometric mixing lines constructed in three – isotope space between two extreme sources for SEA country aerosols and Indian aerosols segregated into divisions of 20 %. The sources considered for SEA countries are leaded gasoline on one side and coal/crust on the other. For India the sources are Indian ore on one side and coal/crust on the other. The traditional mixing line for leaded gasoline is depicted in red, constructed with the isotopic compositions of Broken Hill and Mississippi Valley ores.*

A simple two-source geometric mixing line between leaded gasoline and crust/coal for the SEA countries (**Figure 4.14**) reveals that coal/crust contributes from 20 to 60 % towards the Singapore and Thailand aerosols while the rest from leaded gasoline. In case of Vietnam, contribution range for coal is 40 -90 % and the rest of the aerosol Pb stems from leaded gasoline. Similarly for Indian aerosols, a two-source mixing line between Indian ore and coal/crust indicates that coal/crust contributes 25 to 60 % towards the aerosol Pb and the rest is from Indian ore. In such a binary mixing system, the contribution of each source is actually weighted based on its proximity to the composition of the mixture (Phillips and Gregg, 2003, 2001). However, in this study as there are more than two sources, their relative contributions cannot be accurately represented by this binary weightage method based on proximity. Thus, for gaining primary insight about contributions of multiple sources towards the aerosol mixtures a simple two-isotope ratio linear mixing model having > 3 sources is beneficial. The optimum results derived from the iterative procedure in such an underdetermined mixing system is presented in **Figure 4.15**.

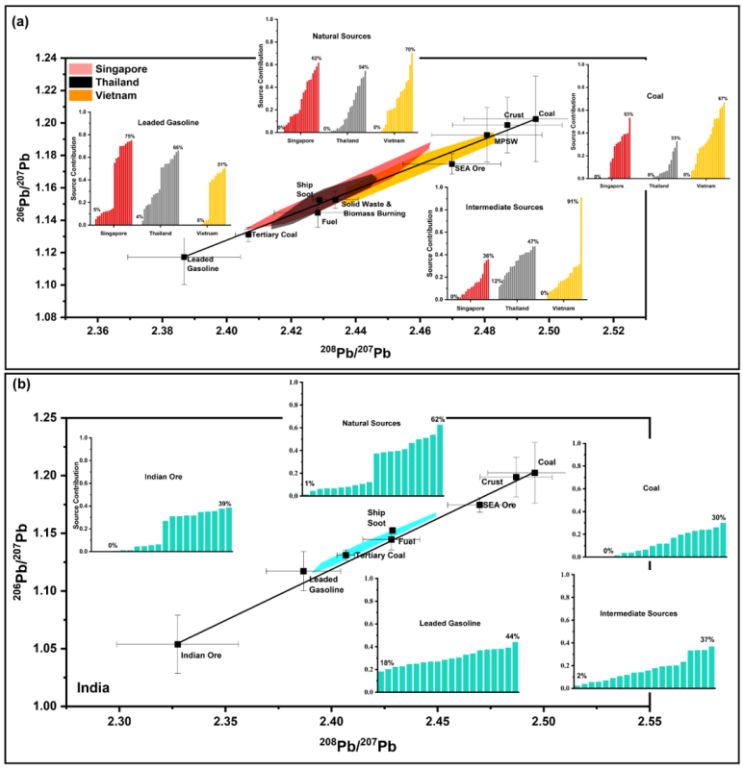

Figure 4.15*: Source contributions determined from simple linear mixing model, represented as bar plots for each source within insets in the three – isotope plots of aerosols and sources for (a) SEA countries and (b) India in 208Pb/207Pb vs 206Pb/207Pb space. Sources considered are 5 for India (coal, crust, Indian ore, leaded gasoline and intermediate) and 4 for SEA countries (coal, crust, leaded gasoline and intermediate). The intermediate source represents mean of tertiary coal, unleaded fuel, ship soot, solid waste & biomass burning and SEA ore for SEA countries and tertiary coal, unleaded fuel, ship soot and SEA ore for India.*

The entire dataset is presented in open source data repository (Ray and Das, 2023a) The model outcomes indicate considerable variability in the contributions of leaded gasoline (0 – 75 %), natural sources (1 – 70 %), coal (0 – 67 %), intermediate sources (0 – 91 %), for SEA countries. In India the contributions of leaded gasoline, natural sources, coal, intermediate sources and Indian ore range from 18 – 44 %, 1 – 62 %, 0 – 30 %, 2 – 3 7% and 0 – 39 % respectively. In fact, the extreme values of these ranges seem to be impractical. For example, zero percent contribution obtained for different sources, especially crust is not possible. Further, a contribution of up to 75% for leaded gasoline in the case of Singapore aerosols also is highly unlikely. In Singapore, where only 1.2 % of the fuel mix used for electricity generation is coal(Energy Market Authority Singapore, n.d.), it is highly unlikely that local and transboundary coal emissions will contribute up to 53 %. Such unlikely extremities may indicate overemphasis on one source, causing it to dominate the mixture, while suppressing other sources. However, some useful primary observations from this linear model can be drawn:

A. Sources demonstrating highest contribution percentages for all the four countries are leaded gasoline and natural sources (treating a spike of 91 % from intermediate sources in case of Vietnam as an outlier). Thus, these two sources can be the dominating factors controlling the Pb isotopic compositions of the aerosol mixtures.
B. Singapore demonstrating highest contribution percentage from leaded gasoline might have greater influence from the source compared to other countries.
C. Vietnam can have a greater influence from coal.
D. Among the 4 countries, India receives the least contributions from leaded gasoline.
E. The intermediate sources are the least to moderate contributing factors towards the aerosol mixtures.

However, as this linear model lacks the probabilistic framework of Bayesian models such as MixSIAR, which allows for incorporating uncertainties, the results obtained from linear model cannot be fully relied upon. The broad variation of source contributions obtained from the linear model has to be narrowed down for a more accurate estimation of the relative proportions of different sources leading to a better understanding of the underlying source dynamics and their

potential impacts. The results of the linear mixing model thus, was cross verified using MixSIAR, where overlapping sources can be better resolved with the incorporation of standard deviations.

4.3.3. Contribution of sources as quantified by Bayesian mixing model MixSIAR

Similar trends between source contribution results obtained from both linear model and MixSIAR were observed. Both approaches identify natural sources and leaded gasoline consistently as dominant contributors, indicating their substantial impact on the aerosol mixtures. Leaded gasoline contributed highest towards Singapore aerosol Pb as was observed from the linear model outcome. Similarly, coal has a greater influence on Vietnam than towards other SEA countries. Contrarily, tertiary coal emerges as a substantial contributor to aerosol Pb levels in Thailand and India, an observation not evident from the linear model.

Thus, the basic observations from the MixSIAR analysis performed on aerosol Pb samples from India and SEA countries are (**Figure 4.16**):

A. Natural background (UCC) is a prominent aerosol Pb source for India and the SEA countries

B. Tertiary Coal combustion and ore processing dominates the anthropogenic Pb emissions in India.

C. Ship emission is probably an underdetermined source in India and to some extent in Thailand.

D. In the SEA countries the largest anthropogenic source of aerosol Pb is the persistence of legacy Pb from the use of leaded gasoline in the last century.

The roughly analogous results observed between the two distinct analytical approaches (linear model and Bayesian model) lends credibility to the findings. Thus, the identified sources and their contributions are likely to be representative of the actual atmospheric Pb pollution dynamics of India and SEA countries.

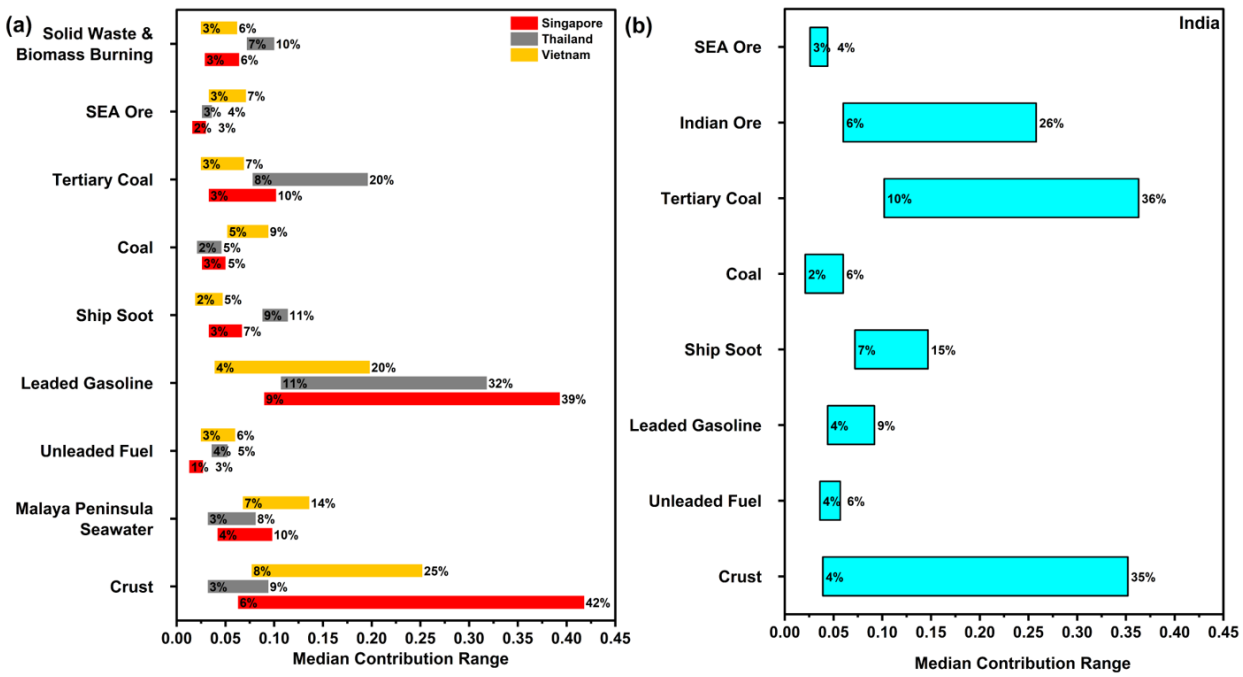

Figure 4.16: *Median contribution of individual sources towards atmospheric Pb in (a) SEA countries and (b) India determined from MixSIAR simulation. The percentages on left-hand side and right-hand side of the bars represents the minimum and maximum contributions from each source respectively.*

In detail, the resultant contributions of the individual sources obtained from the MixSIAR model (**Figure 4.16**) reveals a consistent contribution of background crustal material to all the 4 countries. This is consistent with the linear model results as well as previous investigations that demonstrated a mixture of crustal and anthropogenic contribution towards atmospheric Pb (Carrasco et al., 2018; Chifflet et al., 2018; R. Das et al., 2018; Das et al., 2023; Kayee et al., 2020, 2021). Among other natural sources in SEA, MPSW made median contribution up to 14 % in Vietnam. In Singapore and Thailand, the median contribution of Malaya Peninsula seawater was up to 10 % and 9 % respectively. Surprisingly the major anthropogenic contributor towards Pb in SEA was found to be leaded gasoline (median contribution up to 39 %), even after approximately quarter century of leaded gasoline phase out in the three countries. Tertiary coal contributed substantially to Thailand (median contribution up to 20 %). Tertiary coal fields are found in north-eastern India and there is proof of long-range transport of particulate matter from northeast India to Thailand (Amnuaylojaroen et al., 2020). Some of the endmembers such as fuel, and solid waste & biomass burning did not appear to individually contribute much (median contribution ≤ 9 %). Vietnam

atmosphere receives the least contribution from ship soot, which corroborates with finding from previous literature where insignificant impact of ship soot was observed (Hoàng-Hòa et al., 2015).

In India, ore processing (median contribution up to 26 %) and tertiary coal combustion (median contribution up to 37 %) are the major anthropogenic sources. Indian atmospheric Pb was derived from ship emissions to some extent (median contribution of up to 15 %) which was not considered in any of the previous studies. Leaded gasoline resuspension contributes relatively small (up to 9 %) proportion of atmospheric Pb in India.

4.3.3.1.MixSIAR analysis in ^{204}Pb space

To validate these results, the model was run in ^{204}Pb space for Singapore aerosols. Singapore was chosen as the country for validation as it has the highest range in aerosol Pb isotopic compositions (54‰ for ^{206}Pb/^{207}Pb ratios) compared to other countries (ranging from 34‰-52‰ for ^{206}Pb/^{207}Pb ratios). However, there are some challenges for running the model in ^{204}Pb space.

- "Solid waste and biomass burning" from SEA countries and "unleaded fuel" overlap completely, thus making it difficult to distinguish between the two. While in ^{206}Pb/^{207}Pb vs ^{208}Pb/^{207}Pb space the means of these two sources do not overlap.
- The standard deviations for all the sources in ^{204}Pb space are much larger compared to that in ^{206}Pb/^{207}Pb vs ^{208}Pb/^{207}Pb space (Supplementary Figures 1 and 3), which may make the source contribution results much more variable spanning a large range.
- For some of the sources like "leaded gasoline", "unleaded fuel", "solid waste and biomass burning" the number of data points available in ^{204}Pb space is lower compared to that in ^{206}Pb/^{207}Pb vs ^{208}Pb/^{207}Pb space.

Despite the above challenges, the overall trend of source contributions exhibited in ^{206}Pb/^{204}Pb, ^{207}Pb/^{204}Pb and ^{208}Pb/^{204}Pb space was similar to that in ^{206}Pb/^{207}Pb, ^{208}Pb/^{207}Pb and ^{208}Pb/^{206}Pb space, thus, confirming the validity of the results. Natural sources (crust+MPSW) and leaded gasoline were the largest contributors towards atmospheric Pb in Singapore. The crustal contribution obtained in ^{204}Pb space was around 20 % less possibly owing to the large standard deviations in the ratios for crust with respect to ^{204}Pb. However, we observed contribution from other sources similar showing a marginal difference ranging from 1 – 4 %. Especially the

difference in contribution percent from leaded gasoline between both spaces was a mere 1 % (**Figure 4.17**).

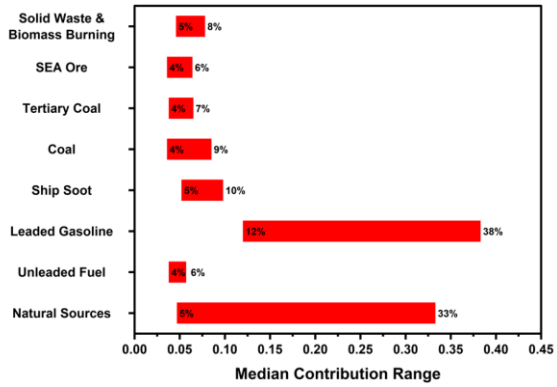

Figure 4.17: *Median contribution range of individual sources towards atmospheric Pb in Singapore determined from MixSIAR simulation in $^{206}Pb/^{204}Pb$, $207Pb/204Pb$ and $^{208}Pb/^{204}Pb$ space*

4.3.3.2. Concentration dependent MixSIAR analysis

Further validations have been performed using concentration dependent Bayesian and linear models was performed. To execute concentration-dependent linear and MixSIAR model, concentration and isotope data for the same set of aerosol and end members were required. However, several challenges were faced while compiling concentration data that are discussed below.

- The source from which tertiary coal and wood charcoal isotope data was adopted (Mitra et al., 2021) does not have Pb concentrations for the corresponding samples. Although there is elemental concentration data for Assam coal in an alternative literature (Mukherjee and Srivastava, 2005), elemental concentration data for wood charcoal is not available.
- The isotope data for solid waste incineration samples (Carrasco et al., 2018) does not have elemental concentration data for the corresponding samples.
- All the sources from where the Pb isotopic compositions of the SEA ores were adopted (Bi et al., 2017; Dongsheng, 2015; Huang et al., 2019; Xu et al., 2019) do not provide concentration data.
- One of the sources from which Pb isotope data for vehicular exhaust was adopted does not provide concentration data for the same (Mitra et al., 2021).

- The availability of Pb isotope data for ship soot is already limited (Hoàng-Hòa et al., 2015; Lahd Geagea et al., 2008). In addition to that, one of the referenced sources for this data lacks elemental concentration data (Lahd Geagea et al., 2008).

However, to validate the general findings of the concentration-independent MixSIAR model, the concentration-dependent MixSIAR model was employed for Singapore and Thailand. The concentrations for the end members were compiled from different literatures based on their availability. The approaches adopted for the compilation are outlined as follows:

- The classical literatures referred to for crustal elemental concentration data (Rudnick and Gao, 2003; Wedepohl, 1995) were consulted to extract the Pb concentration of upper continental crust (UCC). Both sources reported Pb concentration for UCC to be 17 ppm. Consequently, this concentration was utilized for the concentration-dependent MixSIAR model.

- The concentration for Malaya Peninsula Seawater corresponding to its isotope ratios is available (M. Chen et al., 2023) and was thus considered.

- The Pb content in unleaded fuel is highly variable (Bi et al., 2017; Chifflet et al., 2018; Yao et al., 2015). The concentration varies from 0.0096 to 4072 ppm (Bi et al., 2017; Chifflet et al., 2018; Yao et al., 2015). As in a dataset, the median minimizes the influence of outliers, the median of all these concentrations was determined and incorporated it in the concentration-dependent model.

- The initial Pb content in leaded gasoline (2 – 1.1 $g.gal^{-1}$ or 529 – 291 ppm), gradually decreased as the 20th century advanced due to the implementation of regulations for its phasing out (Nriagu, 1990). In Singapore the leaded gasoline concentration was brought down to 150 ppm by 1989 (Nriagu, 1990), before being phased out. Early 1990s marks the last phase of the use of leaded gasoline in the Asian countries. The aerosol data in this study spans from the years 2012 to 2017. As all the concerned countries phased out leaded gasoline by this period, recirculation of soil/road deposited particle bound Pb from leaded gasoline is the only source of airborne leaded gasoline. Thus, it is necessary to consider the concentration of Pb in resuspended soil contaminated by historic use of leaded gasoline. This concentration was calculated based on data from previous literatures that reported the mass of re-entrained dust per distance of travel ($g.km^{-1}$) (Maxwell and Nelson, 1978) and fuel economy of vehicle ($km.L^{-}$

[1] of leaded gasoline) (Marklund et al., 1990). Thus, the final concentration of resuspended Pb from leaded gasoline having a [Pb] = 150 ppm was calculated to be 48 ppm.

- The Pb concentration for ship soot corresponding to its isotope concentration is available from one of the two literatures considered for compiling isotope data. Since a single data point cannot be treated as entirely reliable, additional data points were extracted from two more literature sources, and their mean was utilized (Al-Degs et al., 2014; Popovicheva et al., 2009).

- The concentration in Gondwana coal is highly variable and ranges from 37 – 400 ppm in India (Kumar et al., 2017) and 0.41 – 60.67 in China (Bi et al., 2017). Since only two of the sources (Chifflet et al., 2018; R. Das et al., 2018), originating from India and Vietnam, provided both the Pb isotopic composition of coal and its corresponding concentration data, another literature consisting Pb concentration for Indian Gondwana coal (Das et al., 2016) was considered for better statistical significance. Their median was calculated (32 ppm) for incorporation in the modelling framework.

- In the absence of Pb concentration data corresponding to the isotope data (Mitra et al., 2021), for tertiary coal a concentration of 11 ppm was considered from alternative literature (Mukherjee and Srivastava, 2005).

- Among the four literature sources identified for compilation of Pb isotope data of SEA ores, Pb concentration data were available in two of them. The Pb concentration varied widely from 7.5 – 84.1 ppm. Consequently, the median of the data points (9.6 ppm) from these two sources were taken into consideration (Bi et al., 2017; Xu et al., 2019).

- Due to lack of Pb concentration data of solid waste incineration samples for which Pb isotopes were considered (Carrasco et al., 2018), the concentration was adopted from alternative sources (Hoàng-Hòa et al., 2015; Yin et al., 2018). The Pb concentration of the biomass burning samples having corresponding Pb isotope data is available (Das et al., 2023). The Pb content in biomass and solid waste incineration fly ash varied and consequently the average Pb content of the two kinds of samples was considered.

The details of the inputs for isotopic composition and Pb concentration data into the MixSIAR modelling framework are provided in **Table 4.5**.

Table 4.5: *MixSIAR input for concentration-dependent model*

Sources	MeanPb206 /Pb207	SDPb206/ Pb207	MeanPb208 /Pb207	SDPb208/ Pb207	MeanPb208 /Pb206	SDPb208/ Pb206	ConcPb206 /Pb207	ConcPb208 /Pb207	ConcPb208 /Pb206
Coal	1.20243	0.02639	2.49583	0.0222	2.07635	0.03487	32	32	32
SEA Ore	1.17465	0.00632	2.46987	0.0152	2.10272	0.01056	10	10	10
Unleaded Fuel	1.14592	0.01881	2.4315	0.02074	2.12313	0.02087	6	6	6
Leaded Gasoline	1.11726	0.01709	2.38677	0.01753	2.13695	0.01844	48	48	48
Solid Waste and Biomass Burning	1.15262	0.00521	2.43371	0.00702	2.11124	0.00454	102	102	102
Crust	1.19847	0.01661	2.48692	0.01689	2.07527	0.01892	17	17	17
Ship Soot	1.15255	0.00785	2.42875	0.0029	2.1065	0.01061	67	67	67
Tertiary Coal	1.13115	0.00455	2.40674	0.00411	2.12772	0.00615	11	11	11
Malay Peninsula Seawater	1.19263	0.01679	2.48073	0.01711	2.08026	0.01629	0.000076	0.000076	0.000076

All concentration data are presented in parts per million (ppm).

The conclusions drawn from the concentration-independent MixSIAR model are similar with that of the concentration-dependent MixSIAR model. Both the models identify leaded gasoline as one of the primary contributors towards atmospheric Pb pollution in Singapore and Thailand (**Figure 4.18 a,b**). Crust remains the primary contributor in Singapore. The contributions of the other sources show a similar pattern in both models, with tertiary coal contributing moderately. The differences in contribution percentages for both the models vary from 1 – 10, and the final conclusions remain consistent.

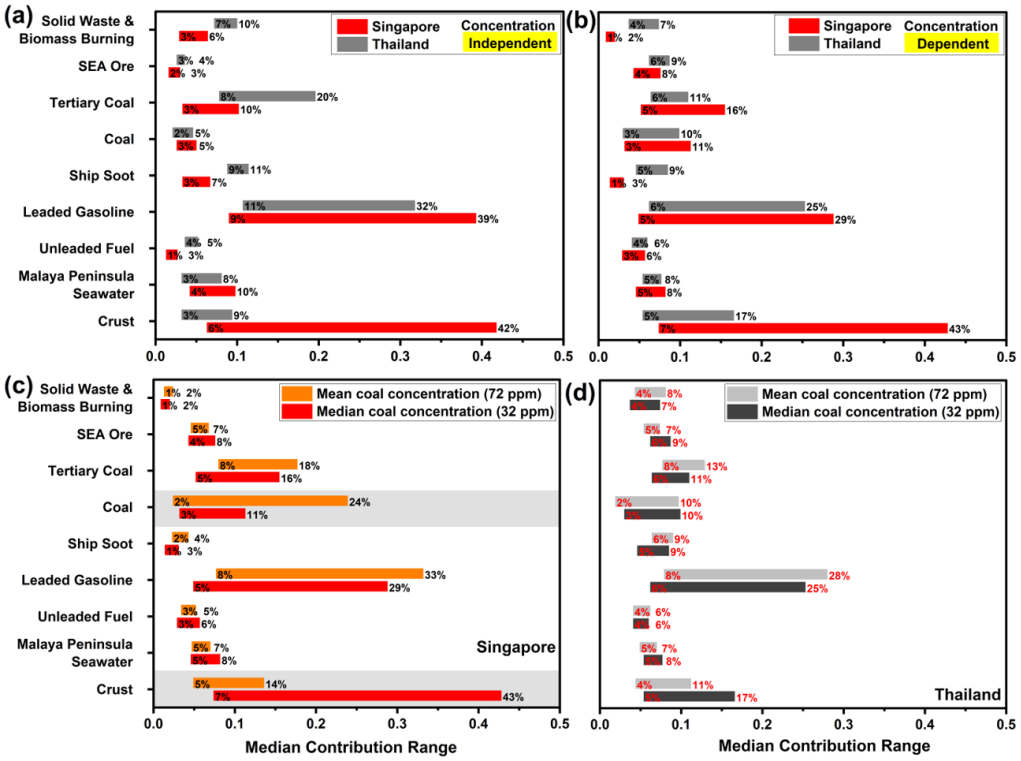

Figure 4.18: *MixSIAR model results as contribution ranges for (a) concentration independent case and (b) concentration dependent case. Comparison of concentration dependent MixSIAR model results considering mean and median coal concentration for (c) Singapore and (d) Thailand. The largest variation observed for coal and crust are highlighted in grey.*

However, for this particular study as most of the end members lack a fixed Pb concentration data corresponding to their Pb isotope ratios, the concentration-dependent model becomes less reliable. In cases, where there is large variability, median values for Pb concentration of the end members had to be considered, which might not be exact representation of the concentration of the concerned end members for the region.

As an illustration to observe the variability in the final outcomes, the concentration-dependent model was ran twice using different concentrations of Gondwana coal. In the first run, the median concentration of 32 ppm was utilized, and in a second run, the mean concentration of 72 ppm was fed as input. The outcomes remained consistent for Thailand in both scenarios (**Figure 4.18 d**). However, for Singapore, there was a significant shift, as the contribution from coal underwent a substantial increase (from 11 % to 24 %), while the contribution from crust (from 43 % to 14 %) decreased notably. (**Figure 4.18 c**). This significant shift in contributions for Singapore highlights how sensitive the model is to concentration variations. This sensitivity emphasizes the importance of having precise concentration data corresponding to the isotope ratios for the sources being considered. Otherwise, the model outcomes may not reflect the true contributions of each source accurately.

4.3.3.3. Concentration dependent linear mixing model

A concentration-dependent linear mixing model with 4 sources and two isotope ratios ($^{206}Pb/^{207}Pb$ and $^{208}Pb/^{207}Pb$) was also employed to investigate the variations of basic outcomes compared to concentration-independent models. Similar to the concentration-independent linear model, this is also an underdetermined system failing to provide unique solutions. The concentration data used for concentration-dependent MixSIAR modelling were attempted to be utilised. However, it is not effective to execute the linear mixing model by utilising Pb concentration data solely, as it has large orders of magnitude variations across sources (**Table 4.5**). If one of the sources exhibits extremely high concentration compared to others, it may dominate and overshadow the contribution from other sources. In this study, Indian ore has extremely high Pb concentration (Das et al., 2016; Deb et al., 1989) followed by solid waste incineration samples (Hoàng-Hòa et al., 2015; Yin et al., 2018) and leaded gasoline (Marklund et al., 1990; Maxwell and Nelson, 1978; Nriagu, 1990). This significant disparity in concentrations, particularly for Indian ore that has concentration in percentage range compared to ppm or ppb range of other sources will introduce bias in model results, favouring Indian ore. Thus, to avoid such biases, techniques, such as normalisation is useful. Normalisation of Pb concentration of the sources with a crustal element such as Al, Fe, Ti etc can be an effective strategy. Given the greater availability of Fe concentration data in the literature compared to other crustal elements, Fe was chosen as the element for normalisation. However, leaded gasoline lacks Fe concentration data. Consequently, India, where leaded gasoline had the least contribution, as observed from concentration-independent MixSIAR

model (Figure 5), was subjected to concentration-dependent linear mixing model. As SEA ore also has negligible contribution in India, it was excluded from the model. Thus, the sources considered for the concentration-dependent linear mixing model for India are: Indian ore, crust, coal and intermediate sources (consisting of ship soot, unleaded fuel and tertiary coal). The concentration data for both Fe and Pb was not always available simultaneously and consequently, literature survey was performed to compile the same (R. Das et al., 2018; Hoàng-Hòa et al., 2015; Popovicheva et al., 2009; Saikia et al., 2009; Sharma et al., 2005; Wang et al., 2003; Wedepohl, 1995). The details of the inputs for end member Pb isotopic composition and their corresponding Pb/Fe ratios are provided in **Table 4.6**. For the aerosol mixture, mean of the Pb isotopic ratio of the aerosols from India was calculated. The equation for the model is as follows (Upadhayay et al., 2017):

$$Mixture\left(\frac{20x}{20x}Pb\right) = \sum_1^n Source\left(\frac{20x}{20x}Pb\right) \times \pi \ldots\ldots\ldots\ldots (1)$$

$$\text{where, } \pi = \frac{f_n \times C_n}{\sum_1^n f \times C},$$

f = the source proportion,

C = concentrations of the sources, where Pb/Fe ratios are incorporated

n = the number of sources

x = 6, 7, 8

Table 4.6: *Inputs for concentration-dependent linear model for India*

Sources	MeanPb206Pb207	MeanPb208Pb207	Pb/Fe
Coal	1.20243	2.49583	0.00055
Indian Ore	1.05391	2.32759	1.44306
Crust	1.19874	2.48705	0.00182
Intermediate Sources	1.14276	2.42123	0.00955

The differences in contribution percentages between concentration-dependent and independent linear models vary from 5 – 40 (**Figure 4.19**). The largest variability is observed in case of intermediate sources. This can be due to the exclusion of leaded gasoline from the model, the contribution from which got added up in the intermediate sources. Apart from the intermediate sources, the variation between concentration-independent and dependent models ranged from 5 % to 24 %. Crust, Indian ore and coal emerged as significant contributors in both the models. Interestingly, the concentration-dependent linear mixing model aligns closely with the concentration-independent MixSIAR model results for India (**Figure 4.16 b**). Both the models highlight Indian ore and crust as significant contributors to airborne Pb, having a minor difference of 1 % to 4 % across the two model outcomes. Thus, utilising normalised concentration data as per their availability in a linear stable isotope mixing model, can provide an overview of the dominant pollution sources. However, the concentration-dependent linear model also has similar drawbacks to the independent one.

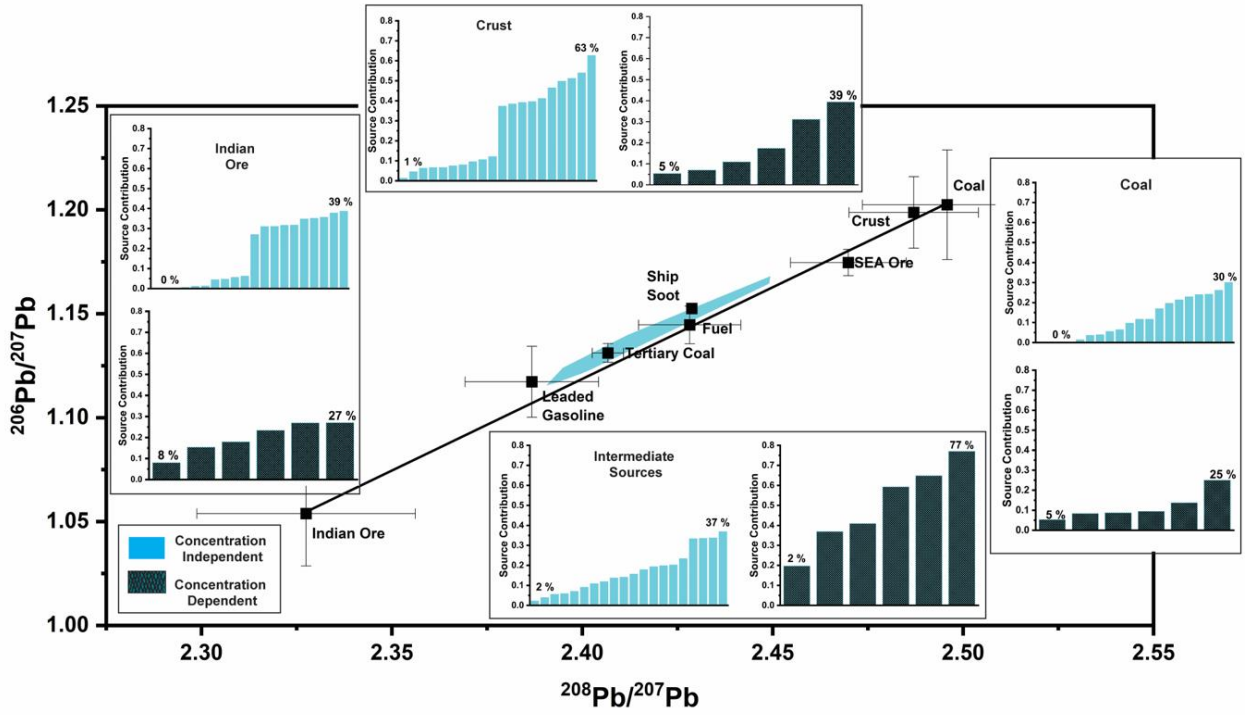

Figure 4.19: *Comparative illustration of contribution ranges obtained from concentration independent and concentration dependent linear mixing models. The aerosol mixture and sources are plotted in three isotope space in the background for reference*

4.3.4. Implications from the model results

The results for the concentration dependent models align with the concentration independent ones as demonstrated in **Figures 4.18 and 4.19**.

Tertiary coal, wood, and wood charcoal from India exhibit comparable Pb isotopic compositions, that prompted their *a priori* grouping for MixSIAR modelling. In rural, semi-urban areas, and brick kilns, of India, fuelwood still remains a predominant energy source, with consumption reaching a staggering 216.4 million tonnes annually, as of 2011 (Sharma, 2018). As radiogenic Gondwana coal dominates Indian coal reserves over less radiogenic tertiary coal (INDIAN BUREAU OF MINES, 2014), emissions from tertiary coal are likely to be less prominent. With analogous Pb isotopic composition (Mitra et al., 2021), open burning of wood and wood charcoal could potentially be the most substantial contributor to atmospheric Pb in India only second to ore processing.

Pb emission estimates in the region shows coal combustion in India emitted ~3500 tonnes of Pb in 2010 as compared to ~150 tonnes from Thailand (Lee et al., 2014). Thus, probably emissions from coal combustion, fuelwood burning and high temperature metallurgy in India has overwhelmed the leaded gasoline Pb signature which is not the case for the SEA countries.

Average concentration of Pb in UCC is 17 ppm. Thus, aerosolization of soil produced by weathering of the upper crust contains substantial Pb. Crustal dust as the natural background has been hypothesised in almost all the previous studies. MixSIAR analysis suggests, in addition to the crustal dust, sea spray also contributed towards aerosol Pb in the SEA countries (up to 8 – 14 %).

Previous studies in India showed that post leaded gasoline phase-out, the atmospheric Pb ratios plot away from the leaded gasoline mixing line and closer to the mixing line between coal combustion and ore processing (R. Das et al., 2018; Sen et al., 2016). The results obtained from MixSIAR analysis are in line with this observation. The Indian peninsula has a long coastline. Since 1992, the Asian ship traffic has increased by 200 % (Tournadre, 2014). Trace element ratios (V/Ni) indicated ship emission to be a plausible source of heavy metals in Singapore and Vietnam aerosols (Chifflet et al., 2018; Ray et al., 2022) (**Figure 4.13 b**). However, Pb isotopic composition of this source was not measured. None of the studies on Indian aerosol postulated ship emission

as a plausible source of aerosol Pb. Insufficient Pb isotope data of Heavy Fuel Oil used by ships may have led to underestimation of source contributions towards atmospheric Pb in India.

Migration rate experiments and field observations suggest that gasoline Pb is retained in soil on generational time-span. Thus, resuspension of such soil could be an important source of atmospheric Pb. The contaminated roadside soils and dusts are often re-suspended by the turbulence created by the urban traffic (Laidlaw et al., 2012). Aerosols collected from the SEA countries in the past decade shows the largest anthropogenic source of aerosol Pb is leaded gasoline. Whether it is the result of transboundary transport from Myanmar and Indonesia who were using TEL additive till the 21st century or they are remobilization of local top soil contaminated with legacy Pb remains a moot question.

Previous research has typically focused on a limited set of end members, which may exclude important sources of Pb. In fact, it is evident from this analysis, that previously underdetermined sources such as and ship emissions contribute substantially towards atmospheric Pb. Additionally non-combustible vehicular sources like tire and brake wear have been found to be important contributors towards atmospheric Pb in other countries as they contain high concentration of Pb (10 – 55 ppm). (Jeong, 2022a; Jeong et al., 2022; Resongles et al., 2021) In fact, evidences of presence of brake wear in atmospheric aerosols can be found in Vietnam from Cu/Sb ratios (Chifflet et al., 2018). However, unfortunately no local Pb isotopic data is available for these sources. Other non-combustible vehicular sources having even higher Pb concentrations include asphalt (738 ppm) and road paint (88 ppm) dusts generated from abrasion due to traffic (Jeong et al., 2022). Subsequently, these sources must be sampled locally and analyzed for Pb isotopic compositions. Further Pb isotope data of sources such as Indian ore which is different from SEA ore is three decades old and hence is in urgent need of reanalysis. Extensive Pb isotope data of coal having high $^{206}Pb/^{207}Pb$ ratios is available globally. However, it can be observed from MixSIAR results that tertiary coal and wood charcoal having low $^{206}Pb/^{207}Pb$ ratio (from Assam, India) contributes heavily towards atmospheric Pb of Thailand and India. There are no Pb isotope data of coal from Thailand which may possess low $^{206}Pb/^{207}Pb$ ratio and contributes towards atmospheric Pb of SEA countries. Thus, to gain a comprehensive understanding of the sources and pathways of Pb in natural systems, it is important to quantify the isotopic composition of Pb in all potential end members. This is especially important in regions like India and SEA, where diverse

anthropogenic and natural sources contribute to Pb emissions. Modern industrial practices, evolving fuel compositions, and increasing vehicular activity have altered the isotopic signatures of aerosols compared to historical data. Without updated and region-specific isotopic and elemental data, source apportionment results can have significant inaccuracies. Thus, comprehensive characterization of current end members is essential to refine models and enhance our understanding of Pb dynamics in the atmosphere. The next chapter presents a comprehensive compilation of the elemental concentrations and Pb isotopic compositions determined for all the end members analyzed in this study. The subsequent chapters will utilize this dataset of elemental concentrations and Pb isotopic compositions for the end members to quantify the contributions of various pollution sectors to atmospheric Pb. By integrating these end members into source apportionment models, the thesis will separately investigate the Pb pollution scenario from road transport and coal combustion sectors to quantify their individual contributions to metal-enriched PM.

CHAPTER 5: ELEMENTAL CONCENTRATION AND Pb ISOTOPIC COMPOSITION OF DIFFERENT END MEMBERS

5.1. Introduction

This chapter provides a detailed compilation of the elemental concentrations and Pb isotopic compositions of the end members analyzed in this study. These end members represent a wide range of potential sources contributing to atmospheric Pb in the studied regions, including natural, industrial, and vehicular emissions. The data presented here will serve as a critical reference for interpreting the results of subsequent qualitative analysis and modeling implications.

5.2. Elemental concentration

***Table 5.1**: Elemental concentration of different end members of atmospheric metal emission in India*

SAMPLE	SAMPLE TYPE	LOCATION	Na	Mg	Al	Ca	Ti	V	Cr	Mn	Fe	Co	Ni	Cu	Zn	Mo	Cd	Ba	Pb
C1AA	Coal	Neyveli		24417	161087	6424		209	294	138	69332	38	126	158	431		0.60		45.77
C1AB		Neyveli		22772	202013	7054		173	331	156	54616	38	132	45	194		0.56		36.75
C1A		Neyveli		48019	142708	27599		13	12	64	1419	126	403	7.9	17		0.05		0.84
C1B		Neyveli		33190	73454	22200		8	16	87	1528	62	246	9.4	13		0.04		0.97
C2A		Neyveli		37655	71224	15204		6	22	238	115966	5.1	39	8.4	14		0.13		1.13
Coal		WB	1325	5732	127271	7439	15473	326	211	401	36270		327	128	129		0.82	557	58.80
TPS1EXP	Fly ash	Neyveli		24534	185082	13400		254	261	96	27108	85	161	112	400		0.57		39.52
TPS2		Neyveli		16109	61111	7851		57	79	180	62888	17	59	12	470		0.08		9.26
TPS2 EXP		Neyveli		19212	58829	9219		74	176	355	130135	16	95	85	283		0.27		15.36
NTPP		Neyveli		13637	166049	8388		371	346	110	40915	69	150	102	109		0.28		26.49
CROP ASH	Open burning	Neyveli		18689	13831	6474		21	23	832	9927	4.5	13	32	220		0.10		13.35
SW ASH		Neyveli		11467	17126	13132		24	37	1041	8521	4.4	20	43	614		0.65		27.62
Soil P	Soil	Neyveli		929	54655	315		86.4	139.6	241	30491	9.1	32.6	26.7	57.8		0.11		15.65
Soil M		Neyveli		1425	17916	1097		37.4	83.1	290	16965	5.9	14.2	13.2	36.9		0.06		7.93
SOIL1		ANI	11740	4978	44094	26243		85	83	758	36798	9.90	39	41	627	0.55	0.7	166	51
SOIL2		ANI	8852	1286	16316	401		146	137	234	36572	12.97	66	25	75	0.90	0.1	303	19
SOIL3		ANI	6130	2640	21512	9890		88	63	330	18361	9.82	37	20	182	1.07	0.2	261	39
SOIL5		ANI	12881	3340	29966	1787		286	527	1607	103890	74	113	137	230	0.60	0.1	20	3
SOIL7		ANI	18817	1920	19287	2306		123	123	455	28262	15	50	82	289	0.57	0.4	169	44
SOIL8		ANI	6172	2801	23326	6065		58.7	88.1	477.5	14357	8.69	41.5	21.3	36.5	0.57	0.1	172	8
Soil		WB		7938	57247	22928	1090	64	71	778	28475	10	212				0.58	1245	91
Soil		WB		7124	54036	10429	4747	67	62	461	25925	9	205				0.24	480	46
Soil		WB		7774	41578	27587	2764	63	74	523	31835	9	229				0.38	477	76
Soil		WB		9020	29821	67008	4709	63	44	602	29924	5	230				0.25	498	29
Soil		WB		6811	56246	21492	4513	73	82	502	28328	11	288				0.35	638	48
Soil		WB		5631	33207	11742	2957	54	56	387	21839	13	203				0.43	614	34
Soil		WB		12651	65218	23941	4912	99	76	647	38937	16	316				0.95	439	37
Soil		WB		14237	74627	40012	5475	125	94	962	46540	17	352				0.66	662	61
Soil		WB		12789	54175	60662	3300	62	64	844	27756	10	272				0.76	609	57
Soil		WB		5782	43437	13745	1927	39	32	297	16556	6.9	126				0.19	343	21
Soil		WB		5200	35358	10412	3285	92	53	314	17191	12	178				0.57	297	23
Soil		WB		3029	12748	5880	6088	127	106	204	9653	20	414				0.93	561	78
Limestone 1	Limestone	ANI		1627	4042	252		3	2	125	2341	2.79	3.70	12.52	9.02		0.02		2.24
Limestone 2		ANI		214	18	7331		1	1	10	221	0.14	0.55	0.35	1.02		0.01		0.19
MV1	Mud Volcano	ANI		7399	45706	367		62	59	283	23321	8.10	38.70	21.65	41.44		0.06		5.72
MV2		ANI		7456	44576	272		60	48	201	21716	7.18	36.23	15.25	37.92		0.05		5.13

GALENA1	Pb Ore	Zawar, Rajasthan	2	59	20	8	0.0	0.7	5.6	356	0.67	0.2	3.0	6776		31	0.17	6407
GALENA2		Zawar, Rajasthan	27	159	44	31	0	1	25	4823	9.45	0.5	2.6	99037		352	0.42	7586
GALENA3		Zawar, Rajasthan	8	104	11	12	0.0	2.2	8.6	628	0.26	0.2	6.2	27658		82.9		10215
CHALCO1	Cu Ore	Zawar, Rajasthan	162	18932	29036	2973	88	1402	447	130825	161	1048	29199	289		1.6	698	1147
CHALCO2		Zawar, Rajasthan	162	24202	33134	5305	131	1938	273	199369	99	937	98111	127		0.3	103	171
CHALCO3		Zawar, Rajasthan	480	48844	72313	18833	417	3401	743	404440	323	2045	34398	244		1.2	2383	1794
S1	Vehicular soot from tailpipe	WB		610	2426	235	3	31	43	2391	0.7	12	18	113		0.1	-	37
S2		WB		7006	31431	5145	46	401	483	67239	10.0	84	640	839	5.93	2.0	293.8	86
S3		WB		1069	3669	902	7	812	100	11666	2.5	66	109	1570	144	0.7	77.9	263
S4		WB		802	2182	1239	4	44	58	8841	0.8	104	79	3307	38	1.0	17.0	54
S5		WB		2570	11508	1282	18	297	133	11000	3.5	19	94	286	19	0.5	59.4	31
TW1	Tire wear	WB		1188	6022	361	8	13	62	3921	1.6	5.9	20	11490	0.71	0.36	46	37
TW2		WB		3210	17848	311	13	15	16	1779	1.0	8.2	10	16992	0.59	0.78	32	19
TW3		WB		2491	2014	266	3	9	27	2292	1.6	12.7	90	43717	0.39	1.08	42	49
TW4		WB		10334	94986	48955	-	54	95	4910	49	18	182	18324	3.73	8.39	196	233
TW6		WB		25252	26252	45489	-	10	28	1500	42	3.1	35	35640	0.60	2.41	16	21
BW1	Brake wear	WB		142550	15839	6238	25	459	709	59301	32	442	125	3205	8.86	0.54	586.48	27
BW2		WB		34631	33806	6859	10	38	267	31263	4	60	987	1661	5.45	1.71	400.30	82
BW3		WB		4299	18517	51702	-	83	828	22957	-	23	38	7228	1.12	0.28	162.05	17
RP2	Road pitch	WB		16319	36617	47316	465	260	1598	61698	59	37	89	297	1.22	0.19	53	5
RP3		WB		25313	58276	74683	-	357	2148	97427	80	52	116	349	1.31	0.22	60	3
RP4		WB		19299	32702	41379	-	242	1414	75200	59	36	101	286	1.69	0.20	96	3
RP5		WB		18104	45433	37535	-	126	1008	64139	44	9	24	155	0.99	0.14	97	4
RP6		WB		39570	78403	89778	-	239	3526	145495	124	11	37	302	1.73	0.39	328	10
RP7		WB		5241	75899	11813	-	58	1108	29656	10	4.0	13	104	0.82	0.12	236	52
RP8		WB		9396	137113	14568	-	27	1529	55655	18	10	37	162	0.41	0.22	1351	42
WHITE PAINT	Road paint	WB		816	2615	58	2.8	20	5.3	279	360	13	22	242	-	0.17	-	5908
YELLOW PAINT		WB		3058	2850	841	3.5	27830	383	42725	220	12	20	471	-	1.14	-	157584
SD1	Ship Diesel	WB	36038	27024	2493	9691	11	93	323	5268	9	143	395	29962	13	6.3	304	289
SD2		WB	15226	3664	4817	5109	10	55	282	12427	8	89	546	17373	15	2.6	224	224
SD3		WB	13584	6370	1836	4486	5	100	213	7270	10	151	595	11838	23	12	499	282
SL1	Ship Lubricant	WB	24094	528971	3527	370087	71	189	1258	10473	6	166	3364	1565341	293	13	217	862
SL2		WB	25099	482831	3832	321845	61	153	1126	8827	4	143	3645	1442414	12108	13	192	858
SL3		WB	13875	349065	2059	281339	72	96	829	6207	3	547	4963	1293164	121062	8.7	158	693

SL4		WB	4074	70498	9813	64710	34	38	270	2863	2	41	1835	189248	35623	2.8	166	192
SL5		WB	19095	26490	3448	430862	59	495	5324	15410	39	417	20217	1320998	31859	248	869	8978
SC1	Ship Coolant	WB	3537999	27517	2411	19883	1.8	22	1078	13121	1.5	31	416	398	2093	0.6	1595	322
SC2		WB	6894651	48878	4646	35609	3.6	36	1429	4336	1.9	14	766	286	1222	9.4	3471	131
SC3		WB	5186632	8205	31684	2453	94	318	3143	51387	34	168	5426	8566	11556794	303	257	267
VP1	Vehicular Petrol	WB	4289	3230	2195	796	4.86	500	180	13367	3.17	599	237	64974	34.58	1.10	199	685
VP2		WB	13460	6701	2504	1580	4.89	313	133	9379	3.35	310	339	30829	14.05	9.34	367	602
VP3		WB	52110	1169	1099	511	1.62	110	42	4035	1.56	147	112	11250	7.48	7.81	389	155
VP4		WB	12722	21151	2691	2134	5.97	106	64	2581	4.51	79	98	11035	7.95	1.57	351	133
VD1	Vehicular Diesel	WB	30434	12875	2763	4326	7.68	74	134	7449	2.98	148	93	9907	6.86	5.36	318	200
VD2		WB	15435	9683	2395	2499	8.91	102	144	8384	5.61	179	57	9356	6.20	3.31	104	134

ANI = Andaman and Nicobar islands; WB = West Bengal. Concentrations of fuel samples are in ng/mL. Units for rest of the samples are in mg/kg

5.3. Pb isotopic composition

***Table 5.2**: Pb isotopic composition of different end members of atmospheric metal emission in India*

SAMPLE	SAMPLE TYPE	LOCATION	$^{208}Pb/^{206}Pb$	$^{206}Pb/^{207}Pb$	$^{208}Pb/^{207}Pb$	$^{206}Pb/^{204}Pb$	$^{207}Pb/^{204}Pb$	$^{208}Pb/^{204}Pb$
C1AA	COAL	Neyveli	2.2298	1.1118	2.4792	17.4619	15.7053	38.9358
C1AB		Neyveli	2.2534	1.0995	2.4776	17.2638	15.7017	38.9029
C1A		Neyveli	2.2096	1.1085	2.4494	17.2615	15.5718	38.1418
C1B		Neyveli	2.2166	1.1116	2.4639	17.3359	15.5871	38.3937
C2A		Neyveli	2.2284	1.1177	2.4906	17.4687	15.6294	38.9265
Coal		WB	2.0530	1.2142	2.4927	19.0518	15.6911	39.1123
TPS1EXP	FLY ASH	Neyveli	2.32098	1.07532	2.49580	16.73714	15.56487	38.84672
TPS2		Neyveli	2.28981	1.07255	2.45594	16.66820	15.54075	38.16714
TPS2 EXP		Neyveli	2.24526	1.09719	2.46349	17.20225	15.67842	38.62360
NTPP		Neyveli	2.32054	1.07072	2.48466	16.64091	15.54183	38.61610
CROP ASH	Open burning	Neyveli	2.15117	1.12989	2.43058	17.62470	15.59859	37.91364
SW ASH		Neyveli	2.12683	1.13425	2.41236	17.76528	15.66260	37.78377

Soil P	Soil	Neyveli	2.17959	1.12919	2.46118	17.24609	15.54581	38.08832
Soil M		Neyveli	2.20852	1.10937	2.45007	17.59591	15.58271	38.35183
SOIL1		ANI	2.1305	1.1367	2.4217	17.7584	15.6228	37.8337
SOIL2		ANI	2.1010	1.1944	2.5094	18.7332	15.6848	39.3589
SOIL3		ANI	2.1137	1.1461	2.4225	17.8465	15.5712	37.7212
SOIL4		ANI	2.1031	1.1660	2.4522	18.2255	15.6313	38.3308
SOIL5		ANI	2.1023	1.1670	2.4533	18.2394	15.6295	38.3438
SOIL6		ANI	2.1305	1.1382	2.4249	17.7976	15.6370	37.9173
SOIL7		ANI	2.1194	1.1373	2.4103	17.6358	15.5073	37.3776
SOIL8		ANI	2.0889	1.1920	2.4899	18.6936	15.6832	39.0488
Soil		WB	2.12144	1.14023	2.41893	17.73664	15.55646	37.62996
Soil		WB	2.11663	1.14329	2.41992	17.76364	15.53876	37.60255
Soil		WB	2.10164	1.17085	2.46069	18.28869	15.62118	38.43894
Soil		WB	2.10582	1.15617	2.43468	18.00936	15.57783	37.92709
Soil		WB	2.11531	1.15110	2.43493	17.96039	15.60398	37.99464
Soil		WB	2.08329	1.17453	2.44689	18.34904	15.62345	38.22887
Soil		WB	2.08115	1.18510	2.46637	18.56804	15.66712	38.64091
Soil		WB	2.12028	1.14101	2.41927	17.79940	15.59950	37.73934
Soil		WB	2.08087	1.18985	2.47593	18.68902	15.70718	38.88992
Soil		WB	2.09678	1.16487	2.44246	18.22051	15.64103	38.20266
Soil		WB	2.04290	1.21498	2.48208	19.14367	15.75566	39.10686
Soil		WB	2.11589	1.14810	2.42925	17.94048	15.62733	37.96272
Limestone 1	Limestone	ANI	2.08436	1.18741	2.47499	18.58856	15.65467	38.74519
Limestone 2		ANI	2.08827	1.19447	2.49437	18.72729	15.67839	39.10770
Mud Volcano 1	Mud Volcano	ANI	2.08145	1.19373	2.48468	18.67809	15.64687	38.87751
Mud Volcano 2		ANI	2.08282	1.19328	2.48539	18.66632	15.64287	38.87868
GALENA1	Pb Ore	Zawar, Rajasthan	2.20289	1.05385	2.32152	16.51047	15.66635	36.37076

GALENA2	Cu Ore	Zawar, Rajasthan	2.20315	1.05391	2.32193	16.51310	15.66793	36.38080
GALENA3		Zawar, Rajasthan	2.20201	1.05515	2.32345	16.58567	15.71833	36.52179
CHALCOPYRITE1		Zawar, Rajasthan	2.11898	1.09435	2.31891	17.21418	15.72967	36.47659
CHALCOPYRITE2		Zawar, Rajasthan	1.90177	1.20562	2.29281	19.20272	15.92679	36.51913
CHALCOPYRITE3		Zawar, Rajasthan	1.80348	1.26471	2.28089	20.21728	15.98561	36.46152
S1	VEHICULAR EXHAUST	WB	2.11932	1.14120	2.41856	17.8373	15.63078	37.80295
S2		WB	2.13954	1.12558	2.40822	17.62193	15.66314	37.70284
S3		WB	2.14496	1.11719	2.39633	17.42942	15.60063	37.38541
S4		WB	2.13605	1.12795	2.40936	17.56262	15.57048	37.51469
TW1	TIRE WEAR	WB	2.13679	1.12453	2.40287	17.54948	15.60627	37.49949
TW2		WB	2.10481	1.14931	2.41908	17.94256	15.61166	37.76565
TW3		WB	2.14861	1.11250	2.39033	17.34374	15.59027	37.2649
TW4		WB	2.11592	1.14151	2.41534			
TW5		WB	2.11849	1.14097	2.41714			
TW6		WB	2.10529	1.14383	2.40809			
BW1	BRAKE WEAR	WB	2.07066	1.16270	2.40756	18.18437	15.64045	37.65357
BW2		WB	2.10688	1.14696	2.41651	17.90500	15.61076	37.72369
BW3		WB	2.11162	1.15083	2.43012			
RP2	ROAD PITCH	WB	2.12989	1.13501	2.41744			
RP3		WB	2.11600	1.15227	2.43820			
RP4		WB	2.11793	1.14844	2.43232			
RP5		WB	2.12514	1.15489	2.45430			
RP6		WB	2.13861	1.14557	2.44994			
WHITE PAINT	ROAD PAINT	WB	2.12172	1.13931	2.41729	17.75423	15.58423	37.66955
YELLOW PAINT		WB	2.14057	1.12116	2.39993	17.45329	15.56679	37.35992
SD1	Ship Diesel	WB	2.13342	1.12773	2.40592	17.59658	15.60358	37.54090
SD2		WB	2.12925	1.13123	2.40867	17.66131	15.61249	37.60529

SD3		WB	2.13925	1.12100	2.39810	17.46722	15.58179	37.36667
SL1	Ship Lubricant	WB	2.13002	1.13005	2.40703	17.61443	15.58734	37.51914
SL2		WB	2.12924	1.13023	2.40653	17.60928	15.58029	37.49447
SL3		WB	2.11365	1.15044	2.43162	17.95503	15.60713	37.95062
SL4		WB	2.11344	1.14782	2.42584	17.90408	15.59835	37.83914
SL5		WB	2.15559	1.10128	2.37390	17.12085	15.54633	36.90546
SC1	Ship Coolant	WB	2.13347	1.12793	2.40641	17.59861	15.60251	37.54605
SC2		WB	2.12472	1.13386	2.40913	17.65616	15.57179	37.51444
SC3		WB	2.13509	1.12613	2.40438	17.55133	15.58558	37.47368
VP1	Vehicular Fuel	WB	2.13540	1.12874	2.41031	17.00828	15.06834	36.31942
VD1		WB	2.11995	1.14052	2.41785	17.7929	15.60068	37.72009
VP3		WB	2.12948	1.13254	2.41172	17.44316	15.40179	37.14484
VP4		WB	2.13515	1.12682	2.40593	17.34896	15.39641	37.04266

CHAPTER 6: SOURCE APPORTIONMENT AND EMISSION PROJECTIONS OF HEAVY METALS FROM TRAFFIC SOURCES IN INDIA

6.1. Introduction

Road traffic emissions are a major source of PM in urban roadside areas and have gained significant attention over the past decade due to their substantial contribution towards environmental pollution. (Chifflet et al., 2018; Pant and Harrison, 2013; Thorpe and Harrison, 2008). Traffic emission is usually categorized as exhaust emissions (EE) and non-exhaust emissions (NEE). Incomplete combustion of fuel and lubricant volatilization are primarily responsible for EEs (Grigoratos and Martini, 2015). On the other hand, NEEs typically arise from abrasive sources such as brake wear, tire wear, road surface abrasion and resuspension of road dust due to traffic induced turbulence in combination with crustal dusts. (Denier van der Gon and Appelman, 2009; Gioia et al., 2017).

Wear of brake linings occurs due to the frictional contact between brake system components during vehicle deceleration, leading to the emission of PM. The composition of this emitted PM depends on the composition of the brake linings, that consist of fibers for providing mechanical strength, abrasives for generating friction, lubricants for inducing stability, fillers to reduce costs, and binders to render integrity (Thorpe and Harrison, 2008). Similarly, tire wears are generated from mechanical abrasion of tire treads when in contact with road surface. The tire wear debris mostly consist of rubber hydrocarbons, carbon black, hydrocarbon oils, resins, curing agents, and various additives. Frictions generated from heavy traffic movement on roads generate the third type of NEE, i.e., road surface abrasions. The abraded material is primarily asphalt, the most common surfacing agent, consisting mainly of mineral aggregates and a bituminous binder. Fillers, such as fibers, polymers, and epoxy resins are added to the asphalt to withstand heavy traffic and extreme weather conditions. Majority of these NEE sources concentrate in the coarser fractions of PMs and get eventually get deposited as road dusts. All these NEE sources consist of toxic heavy metals and contribute towards atmospheric metal loadings (Thorpe and Harrison, 2008).

Toxic elements like arsenic (As), cadmium (Cd), nickel (Ni), and lead (Pb) are often prevalent in PM depending on the sources , Upon inhalation these elements can cause severe health problems, including respiratory issues, cardiovascular diseases, and even cancer (Geiger and Cooper, 2010). Road dusts, being the first recipient of PMs from EE and NEE are often enriched in such heavy metals (R. Das et al., 2018; Pant and Harrison, 2013; Ray et al., 2024). Brake and tire wear particles, enriched in heavy metals, are present in substantial proportions in locations encountering heavy traffic (Thorpe and Harrison, 2008). A sand paper like effect on the road asphalt and bitumen can cause additional contamination by abrading road paints and the bitumen itself, containing high concentrations of metals (Adamiec et al., 2016).

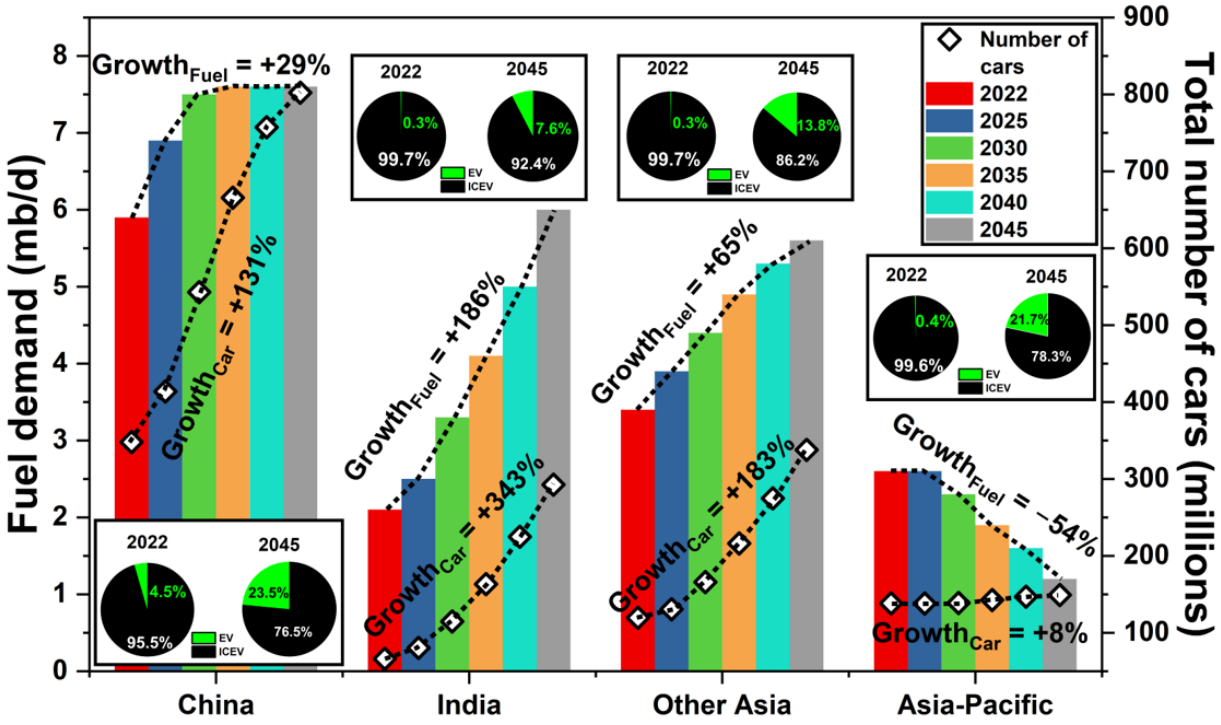

Figure 6.1: *Bar plots depicting the total fuel demand in China, Asia, Other Asian countries and Asia Pacific for the years 2022, 2025, 2030, 2035, 2040 and 2045, The percentage increase in fuel demand from 2022 to 2045 is depicted by a dotted line with the percentages for respective regions indicated above the line as Growth$_{fuel}$. The total number of cars (passenger cars, commercial vehicles and electric vehicles) on road for each region is presented as line and symbol (diamond) plot. The percentage increase in the total number of cars is indicated above as Growth$_{car}$. The pie charts illustrate the percentage of internal combustion engine vehicles (ICEV) and electric vehicles (EV) in the years 2022 and 2045 for each region.*

All nations are striving to switch to electric vehicles (EVs) as part of their efforts to combat climate change and reduce urban air pollution. While, introduction of EVs can eliminate tailpipe emissions and significantly reduce pollution, it does not address NEEs. Government of India aims for a minimum 30% market penetration of EVs in private cars and 70 % in commercial vehicles by

2030, targeting global leadership in the EV sector by 2047. However, long-term projections for oil demand in Indian transportation sector, indicate its continued rise together with the number of vehicles on road (**Figure 6.1**) (OPEC, 2023). In fact, among the Asian and Asia Pacific countries, India is expected to see the highest surge in total number of passenger cars, commercial vehicles, and EVs (343 %) as well as fuel demand (186 %) from 2022 to 2045. India's vehicle fleet (passenger cars + commercial vehicles + EVs) was 66 million as of 2022, out of which only 0.3 % was EV. This number is expected to reach 292.6 million by 2045, with only 7.6 % constituting EVs as opposed to India's targeted penetration percentages (OPEC, 2023). China and Asia Pacific countries are projected to have the highest EV penetrations by 2045 (23.5 % and 21.7 %, respectively), resulting in the lowest rise in fuel demand (**Figure 6.1**). The Asia-Pacific region is experiencing a 54 % decline in oil demand despite an 8% increase in overall vehicle growth from 2022 to 2045. This decreasing trend is driven by advances in vehicle technology and government policies promoting fuel efficiency and electric vehicles. Although passenger ICEVs are projected to decrease by 23.5%, the rise in commercial vehicles and EVs will still contribute to a gradual reduction in net fuel consumption across the region. Thus, in comparison to these regions, India's EEs appear to be steadily increasing, which is a cause for concern. Based on these forecasts, both EE and NEEs will continue to contribute to the aggravation of India's PM and metal pollution scenario. Thus, compared to these regions, India's EEs appear to be ever increasing and a concerning scenario. Based on these projections, both EE and NEEs will continue to worsen India's PM and associated metal pollution levels. The emission of metals from the traffic sources actually depends on their respective concentration in each source (fuel, brake wear, tire wear, asphalt, road paint, etc). In tire wear the most abundant element is Zn and brake dust is a significant source of Cu, Sb, Ba etc (Adamiec et al., 2016; Thorpe and Harrison, 2008). Road paints, especially yellow paints are major contributors of Cr and Pb (O'Shea et al., 2021).

Road dusts are the first recipient of the EE and NEEs in urban areas. Over the last decade a few source-apportionment studies have analyzed urban and semi-urban road dusts for elemental concentrations and Pb isotopic compositions (Das et al., 2016; R. Das et al., 2018; Ray et al., 2024). Vehicular emissions, particularly NEEs, have recently gained attention for emitting PM at levels comparable to EEs. However, source apportionment studies that quantify their contributions of heavy metals to urban atmospheric metal loading by analysis of metals in end-member samples are rare (Grigoratos and Martini, 2015; Harrison et al., 2021). Most studies have only measured

elemental concentrations in road dust, rather than in the material itself, and suggested that EEs and NEEs are significant sources of PM emissions in urban areas using tools like positive matrix factorization (PMF), chemical mass balance (CMB) etc. (Cunha-Lopes et al., 2022; Demir et al., 2022; Harrison et al., 2012; Lopez et al., 2023; Zhang et al., 2020). Over the past 15 years, some studies have focused on elemental concentrations in end members. These studies have primarily highlighted the high metal content in NEE sources subsequently providing a guideline following which specific elements can be used as qualitative tracers for NEE sources. (Adachi and Tainosho, 2004; Adamiec et al., 2016; Hjortenkrans et al., 2007; Jeong et al., 2019; Thorpe and Harrison, 2008). However, in India, studies specifically focusing on atmospheric metal pollution from vehicular components are scarce (Sethupathi et al., 2021; Singh et al., 2020). Most importantly, globally, all these studies have solely focused on metals which single-handedly is not a robust proxy for source apportionment. This highlights the need to determine isotopic composition of the end members, which is largely unavailable worldwide. Currently, Pb isotopic composition data for NEE sources are available only from South Korea and London (Dong et al., 2017; Jeong, 2022b; Jeong et al., 2022; O'Shea et al., 2021). The ability to accurately trace and quantify sources of vehicular pollution is limited by the scarcity of such data. South Korea has reported Cu and Zn isotopic signatures of NEE sources in addition to Pb isotopes. Isotope ratios of trace metals such as Zn, Cu, Ni, Cd etc. can trace contamination sources, similar to Pb isotopes. However, the effectiveness depends on the distinctness of isotopic signatures of end members and whether fractionation (mass-dependent or mass-independent) occurs during physicochemical processes which might complicate source apportionment studies.

Thus, it is crucial to quantify the extent of metal emitted from the EE and NEE sources and their respective contribution towards urban road dust. This road dust can become resuspended, contributing significantly to the atmospheric metal load and impacting air quality. While electric vehicles significantly reduce tailpipe emissions (EEs), a holistic approach requires considering NEEs to achieve environmental goals. As governments worldwide set stringent emission standards to combat air pollution, understanding NEEs become essential. Policymakers need to consider these emissions when developing regulations and incentives for EV adoption to ensure environmental benefits. As different sources (EE and NEEs) exhibit enrichment in specific elements, developing an elemental concentration profile can be useful in source apportionment as

well as emission calculation for each element. All the traffic emission samples were collected from different locations as presented in **Figure 6.2**.

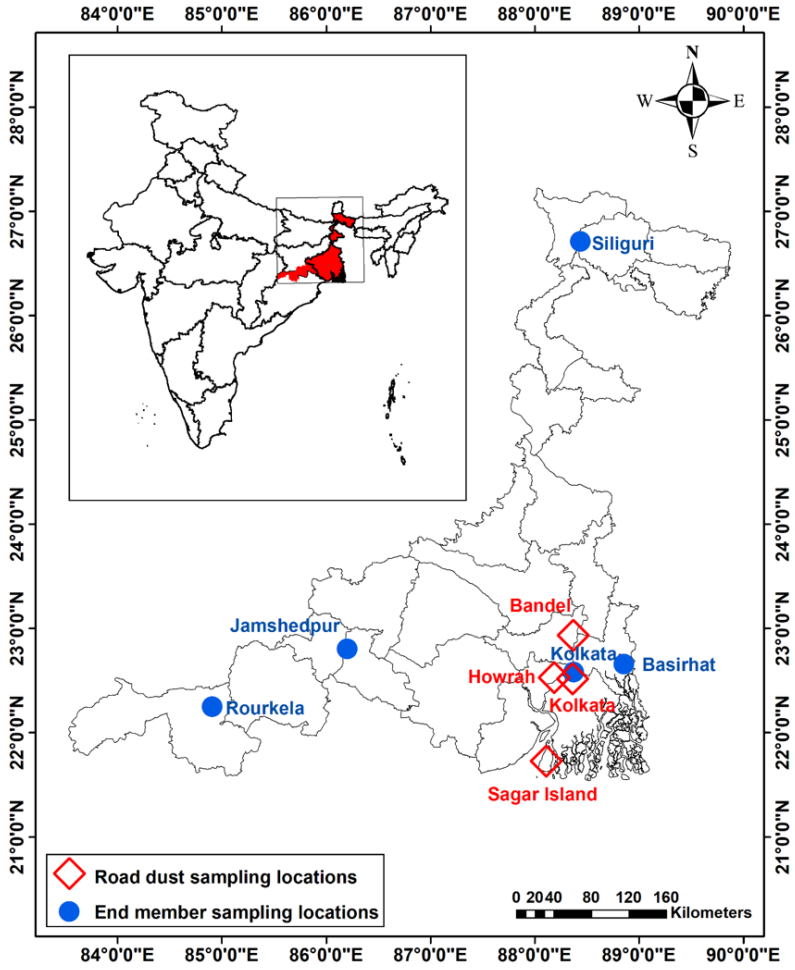

Figure 6.2: *Location of the sites from where the end members (tire wear, brake wear, road pitch and road paint) and road dusts were sampled in eastern India. The locations for the road dusts samples have been adopted from Das et al., 2018 and Ray et al., 2024*

6.2. Elemental concentration of exhaust and non – exhaust sources

The elemental concentrations of various non-exhaust sources such as tire, brake, road pitch, road paint, along with soot from tail pipe representing exhaust emission is presented in **Figure 6.3** and **Table 6.1**.

Table 6.1: *Elemental concentrations of vehicular exhausts, tire wear, brake wear, road pitch and road paint in mg/kg*

SAMPLE	SAMPLE CODE	Mg	Al	Ca	Cr	Mn	Fe	Co	Ni	Cu	Zn	Mo	Cd	Sb	Ba	Pb
VEHICULAR EXHAUST	S1	610	2426	235	31	43	2391	1	12	18	113	-	0.1	-	-	37
	S2	7006	31431	5145	401	483	67239	10	84	640	839	5.93	2.0	6.0	293	86
	S3	1069	3669	902	812	100	11666	3	66	109	1570	144	0.7	2.4	77.9	263
	S4	802	2182	1239	44	58	8841	1	104	79	3307	38	1.0	0.4	17.0	54
	S5	2570	11508	1282	297	133	11000	4	19	94	286	19	0.5	0.6	59.4	31
TIRE WEAR	TW1	1188	6022	361	13	62	3921	2	6	20	11490	0.71	0.36	0.80	46	37
	TW2	3210	17848	311	15	16	1779	1	8	10	16992	0.59	0.78	1.35	32	19
	TW3	2491	2014	266	9	27	2292	2	13	90	43717	0.39	1.08	0.88	42	49
	TW4	10334	94986	48955	54	95	4910	49	18	182	18324	3.73	8.39	98	196	233
	TW6	25252	26252	45489	10	28	1500	42	3	35	35640	0.60	2.41	2.96	16	21
BRAKE WEAR	BW1	142550	15839	6238	459	709	59301	32	442	125	3205	8.86	0.54	3.87	586	27
	BW2	34631	33806	6859	38	267	31263	4	60	987	1661	5.45	1.71	4.58	400	82
	BW3	4299	18517	51702	83	828	22957	-	23	38	7228	1.12	0.28	0.88	162	17
ROAD PITCH	RP2	16319	36617	47316	260	1598	61698	59	37	89	297	1.22	0.19	0.09	53	5
	RP3	25313	58276	74683	357	2148	97427	80	52	116	349	1.31	0.22	0.07	60	3
	RP4	19299	32702	41379	242	1414	75200	59	36	101	286	1.69	0.20	0.09	96	3
	RP5	18104	45433	37535	126	1008	64139	44	9	24	155	0.99	0.14	0.08	97	4
	RP6	39570	78403	89778	239	3526	145495	124	11	37	302	1.73	0.39	0.09	328	10
	RP7	5241	75899	11813	58	1108	29656	10	4	13	104	0.82	0.12	0.11	236	52
	RP8	9396	137113	14568	27	1529	55655	18	10	37	162	0.41	0.22	2.91	1351	42
ROAD PAINT	WHITE PAINT	816	2615	58	20	5.3	279	360	13	22	242	-	0.17	-	-	5908
	YELLOW PAINT	3058	2850	841	27830	383	42725	220	12	20	471	-	1.14	-	-	157584

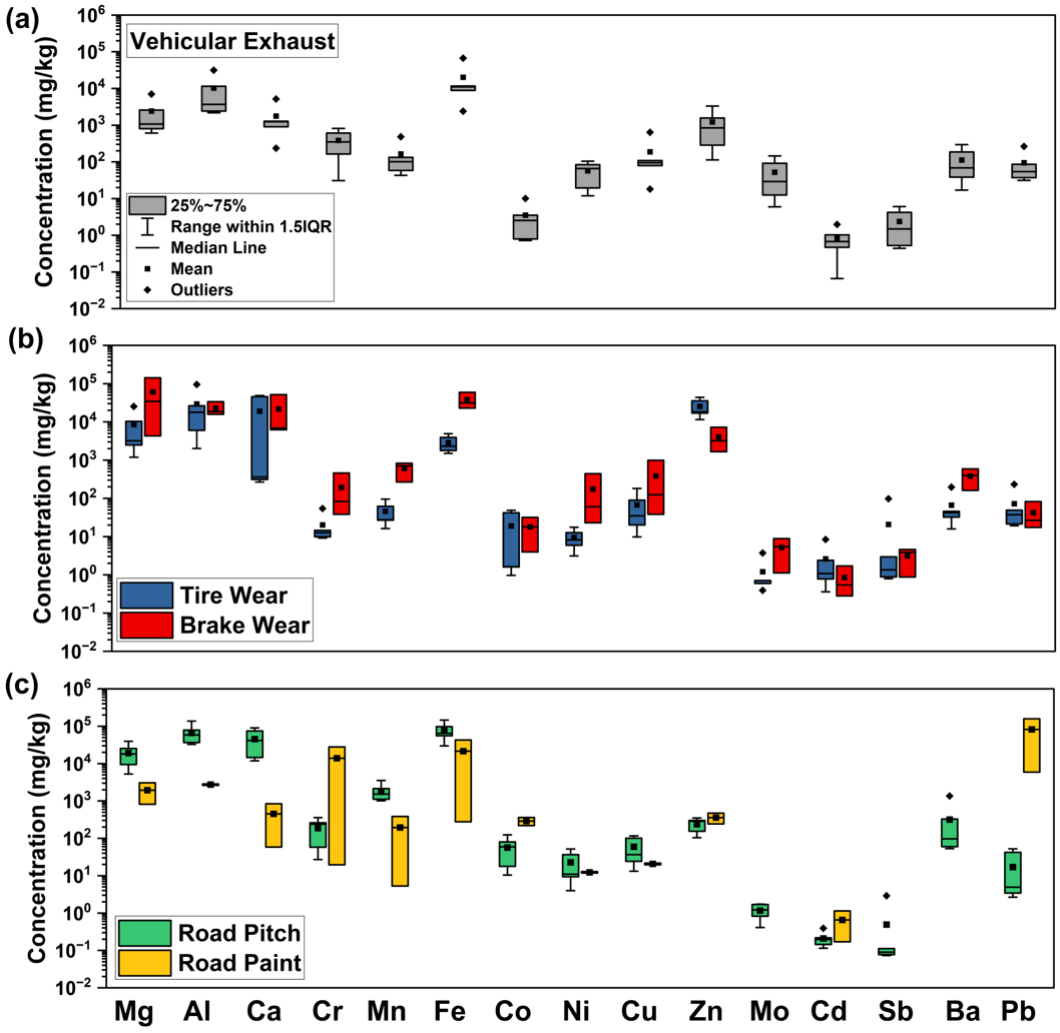

Figure 6.3: *Box plots depicting the elemental concentrations in (a) vehicular exhaust, (b) tire wear and brake wear and (c) road pitch and road paint samples from eastern India. The lower and the upper limits of the boxes represent 25th and 75th percentile data respectively. The black boxes represent the mean while the lines represent the median values. The whiskers extend to the smallest and largest values within 1.5 times the interquartile range (IQR) from the first and third quartile. Data points beyond these whiskers are considered outliers depicted as black diamonds.*

6.2.1. Exhaust emission (EE) sources

Exhaust emission sources play an important role in overall road traffic emissions (Harrison et al., 2021). Significant measures have been implemented, including the use of three-way catalytic converters in petrol vehicles and diesel particle filters to reduce PM emissions from fuel exhausts. These efforts have markedly changed the PM emissions and the associated trace metals in these emissions. (Harrison et al., 2021; Winkler et al., 2018). In this study, we have analyzed the elemental concentrations of soot from both petrol and diesel car tailpipe (referred to as vehicular exhaust herein) to obtain a clear picture of the metal emission sources from road traffic.

Vehicular exhaust predominantly consists of carbonaceous soot along with a minor fraction of non-carbonaceous, non-volatile, inorganic metal PM which is sub micrometer in size and inhalable. The elemental composition of the EE is a combination of combustion of metal additives in lubricating oil and, to a lesser extent, trace metals in the fuel (Vaaraslahti et al., 2005). In our samples the overall elemental concentration trend in the vehicular exhaust was as follows (Al, Fe) > (Mg, Ca, Zn) > (Cr, Mn, Cu, Ba, Pb) > (Ni, Mo) > (Co, Cd, Sb). Aluminum, Mg, Ca, Fe and Zn concentrations ranged from the upper μg/g to lower percent levels. The percent level concentrations of Fe and Al can result from the wear and tear of engine components, such as cylinder walls, piston rings, and bearings. The friction and heat generated during engine operation can cause small particles of Fe and Al to be released and subsequently deposited in the exhaust system. Additionally, Fe and Al can also come from the degradation of steel components within the exhaust system itself (Liati et al., 2015, 2013). Chromium, Ni, Cu can be derived from engine wear and corrosion as well. The emission of several elements such as Ca, Zn likely resulted from the use of organometallic additives in diesel fuel or lubricating oil (Dočekal et al., 1992).

6.2.2. Non – exhaust emission (NEE) sources

NEE sources primarily consist of heavy metals, such as Zn, Cu, Pb and consequently, the secondary aerosols they produce exhibit a similar chemical composition (Timmers and Achten, 2016).

Tire wear: Elemental concentration in the tire wear followed the general pattern (Mg, Al, Ca, Fe, Zn) > (Cr, Mn, Cu, Ba, Pb) > (Co, Ni, Mo, Cd, Sb) with Al, Ca and Zn ranging in the low parts per hundred level. Of all the NEE sources, Zn had the highest concentration in tires. High Zn concentrations result from addition of ZnS and ZnO in the tires during vulcanization process (Adamiec et al., 2016). Zinc concentrations of the Indian tires were found to be similar to Korean and British tires (Dong et al., 2017; Jeong, 2022b; Jeong et al., 2022) (**Figure 6.4**). Tire 4 had the highest concentration of most of the elements compared to the other tire samples. This variance in metal concentrations could be attributed to different raw materials used by different manufacturers (Jeong, 2022b). The mean concentration of Pb in tires from this study is higher than the average Pb in London tires (Dong et al., 2017) whereas it is almost similar to the concentration range of Korean tires (Jeong, 2022b) except for Tire 4 **(Figure 6.4)**.

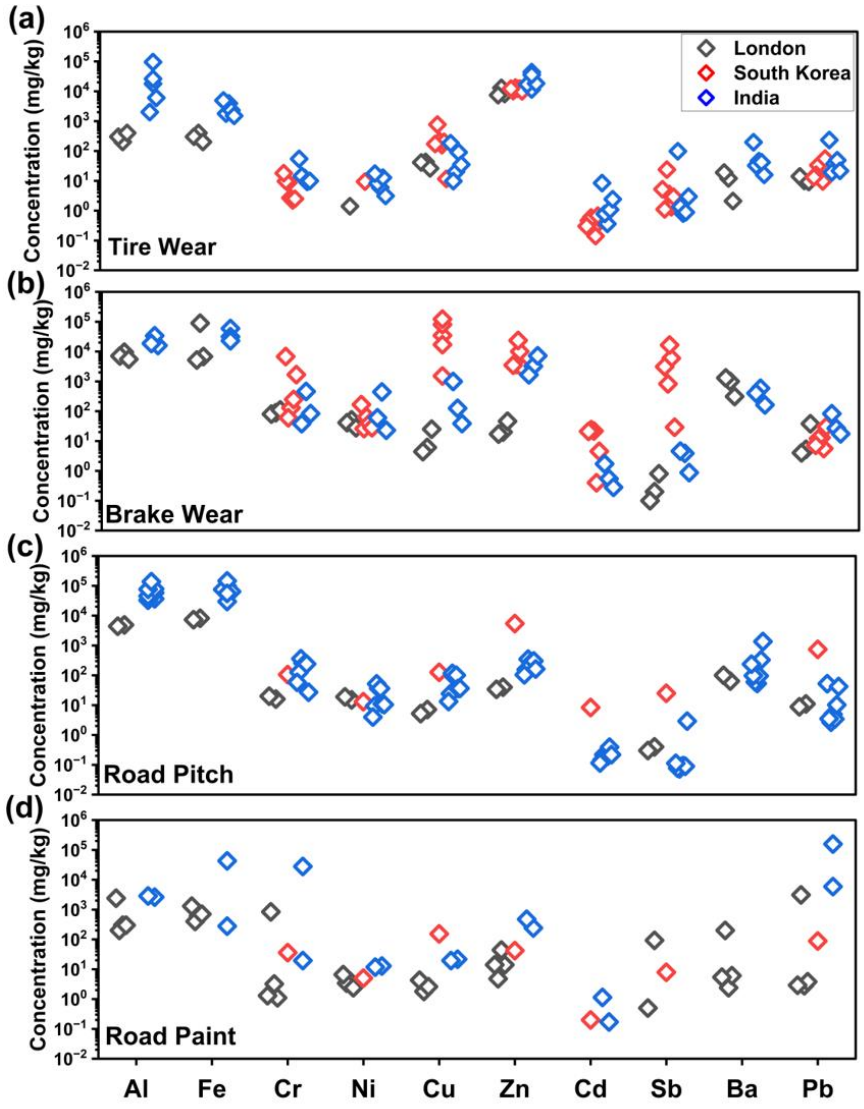

Figure 6.4: *Comparison of elemental concentrations of (a) tire wear (b) brake wear (c) road pitch and (d) road paint from London and South Korea with respect to India. The data for London and South Korea has been adopted from Dong et al., 2017 and Jeong et al., 2022 respectively*

Brake wear: Brake wear particles result from the degradation of the brake pad and the rotating disc/drum due to heat and friction. The overall pattern of break wear elemental composition followed the trend (Mg, Al, Ca, Fe) > Zn, (Cr, Mn, Ni, Cu, Ba) > (Co, Mo, Cd, Sb, Pb). Concentrations of Mg, Al, Ca and Fe were in low percent level. Aluminum oxide and iron oxides are commonly used as abrasives to increase friction material (Grigoratos and Martini, 2015).

Of all the NEE sources Ba concentrations in brake wear were the highest (**Figure 6.3**). High Ba content in brake wear can be due to the presence of barite, which is used as a filler in brake pads

due to its high specific gravity, which helps to add weight and stability to the brake pad material (Grigoratos and Martini, 2015). Lead concentrations in London and Korean brakes were comparable (approximately 15 mg/kg Pb), whereas brakes from this study had higher concentrations (47 ± 35 mg/kg).

Road Surface and paints: The bituminous road cover is a complex mixture of hydrocarbons, resins, asphaltenes, and trace metals (Samanta et al., 2022) . In road pitch samples, the concentration pattern was as follows (Mg, Al, Ca, Fe) > Mn > (Cr, Zn, Ba) > (Co, Ni, Cu, Mo, Cd, Sb, Pb). Barium concentration in road pitch samples were comparable to brake wear.

Barium is a common contaminant in oil, either naturally present in the reservoir or added as a drilling additive. Thus, the organic fraction of asphalt concrete often contains high Ba. (von Gunten et al., 2020)

In this study, we have considered road paints as a non – exhaust emission source as abraded paints can be a source of heavy metals in road dust. Two paints are widely used on Indian roads, yellow and white paint. Our study reveals that yellow paint contains high levels of Pb (157,584 µg/g) and Cr (27,830 µg/g) due to the presence of lead chromate ($PbCrO_4$) as its primary component, which imparts the yellow colour (O'Shea et al., 2021). In comparison, the white paint had a lower concentration of Cr (20 µg/g) and Pb (5908 µg/g). Although white paint had a lower Pb concentration than yellow paint, it still demonstrated significantly high Pb concentration compared to other EE and NEE sources. Other than Cr and Pb, high elemental concentrations of Mg, Al, Ca, Fe and Zn have also been observed in these paint samples. The inorganic pigments used in white-coloured paints include rutile calcium composite pigment (TiO_2 + $CaSO_4$), zinc oxide (ZnO), leaded zinc oxide (ZnO + $2PbSO_4$) (O'Shea et al., 2021) which might explain high Ca, Zn, Pb concentrations in white paints.

However, it is difficult to ascertain heavy metal sources of road dust based on concentration alone.

6.3. Elemental ratios

Elemental ratios are often used for source apportionment of metals. We have used Mo/Pb and Ba/Pb ratios, as Mo and Ba are commonly used as tracers for tires and brake emissions, respectively **(Figure 6.5 a)**. The combination of Mo and Cr is used as a heat-resistant material to coat the tires to prevent corrosion and to withstand temperature increases brought on by road friction, particularly in highways (Harrison et al., 2003; Wiseman et al., 2021). Brake wear and road pitch are characterized by high Ba/Pb ratios ranging from 4.5 to 32, whereas tire wear and

exhaust emissions have Ba/Pb < 3.5. Road dusts do not overlap with the field of the EE or NEEs and plot in between the fields indicating that, road dust consists of mixture of elements generated through variety of emission sources **(Figure 6.5 a**).

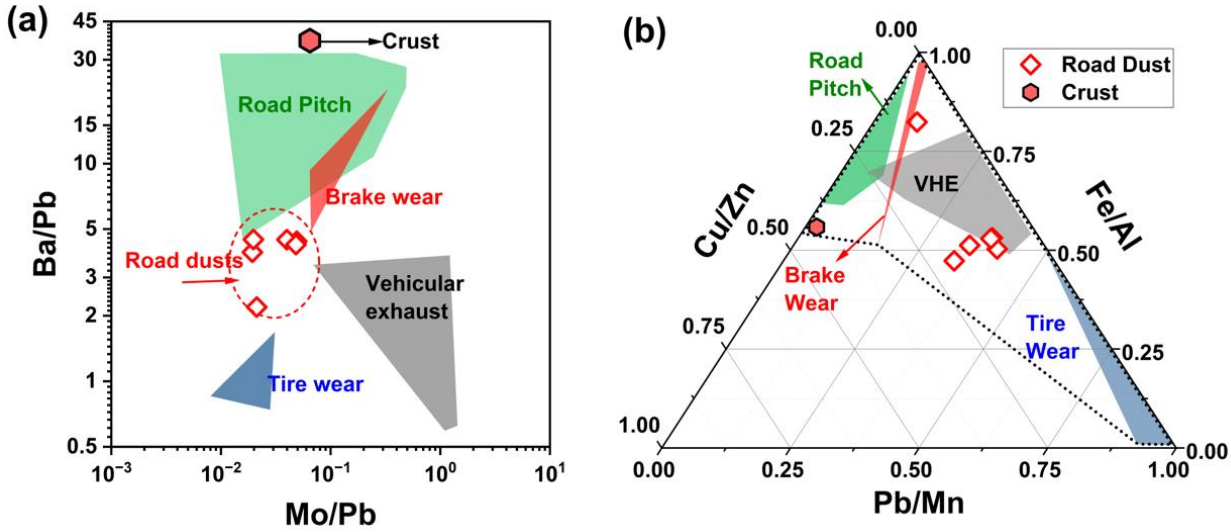

Figure 6.5: *Elemental ratios plotted as (a) bivariate plot of Mo/Pb vs Ba/Pb and (b) ternary plot of Pb/Mn, Cu/Zn and Fe/Al demonstrates that the characteristic ratios of road dusts lie between those of the EE and NEE sources. The vehicular exhaust, tire wear, brake wear and road pitch are depicted as fields in grey, blue, red and green colours respectively*

Non-exhaust emission sources are highly enriched with Cu, Zn and Pb. Copper serves as a tracer for wear abrasions, and the Cu/Zn ratio is often used as an indicator for assessing non-exhaust emission contributions to the elemental concentration in road dust and aerosols (Budai and Clement, 2018; Lin et al., 2015). The elemental composition patterns of the EE and NEE sources follow a general pattern, with Mg, Al, Ca, and Fe having the highest concentrations in low parts per hundred levels. We have used Fe/Al ratio to distinguish between EE and NEE sources. Generally Fe is high in car exhaust due to presence of brake dust and corrosion particles from cast iron manifolds in car exhaust systems (Salazar et al., 2020). Thus, the average Fe/Al ratio of EE is higher than the NEE sources though some of the brake wears show high Fe/Al ratios due the presence of Fe and Al in brake disc (Miler, 2021). Pb/Mn ratios to distinguish between different end members have been previously used (Li et al., 2018). The Pb/Mn ratios are highest in tire wears (1.36 ± 0.76) and lowest in road pitch (0.012 ± 0.017). Thus, we use the Cu/Zn, Fe/Al and Pb/Mn ratios in a ternary plot to understand the relative influence of different sources of road dust **(Figure 6.5 b).** Majority of the road dust clusters in the vehicular exhaust field with one sample

plotting close to the brake wear. However, none of the road dust samples plot close to the crust in both the plots. From the binary and ternary plot of the elemental ratios it is difficult to decisively discern the proportion of EE and NEE end member contributions. However, it is evident that resuspension of weathered crust has little contribution in the metal composition of road dusts that are heavily influenced by traffic related emissions.

6.4. Pb isotopic signatures for source delineation

The Pb isotopic compositions of the exhaust emission samples (fuel and vehicular exhaust) vary from 1.126 – 1.141 and 2.396 – 2.419 in $^{206}Pb/^{207}Pb$ and $^{208}Pb/^{207}Pb$ spaces, respectively. Fuel and vehicular exhaust demonstrate almost perfect overlap, reflecting their close association, as exhaust particles originate from combusted fuels. In contrast, the NEE samples (brake wear, tire wear, road pitch and paint) have a larger spread, with $^{206}Pb/^{207}Pb$ and $^{208}Pb/^{207}Pb$ varying from 1.112 – 1.163 and 2.390 – 2.454, respectively. The road pitch and brake wear samples are slightly more radiogenic compared to the others. The mean and individual Pb isotopic compositions of all types of samples are presented in **Table 6.2**.

Table 6.2: *The individual and mean Pb isotopic compositions of vehicular exhaust, vehicular fuel, tire wear, brake wear, road pitch and road paint samples*

SAMPLE	$^{206}Pb/^{207}Pb$	$^{208}Pb/^{207}Pb$	$^{208}Pb/^{206}Pb$
VEHICULAR EXHAUST	1.1412	2.4186	2.1193
	1.1256	2.4082	2.1395
	1.1172	2.3963	2.1450
	1.1280	2.4094	2.1361
Mean	1.1280	2.4081	2.1350
SD	0.0099	0.0091	0.0111
VEHICULAR FUEL	1.1287	2.4103	2.1354
	1.1405	2.4179	2.1200
	1.1325	2.4117	2.1295
	1.1268	2.4059	2.1352
Mean	1.1322	2.4115	2.1300
SD	0.0061	0.0049	0.0072
TIRE WEAR	1.1245	2.4029	2.1368
	1.1493	2.4191	2.1048
	1.1125	2.3903	2.1486
	1.1415	2.4153	2.1159
	1.1410	2.4171	2.1185
	1.1438	2.4081	2.1053
Mean	1.1354	2.4088	2.1217
SD	0.0140	0.0109	0.0176
BRAKE WEAR	1.1627	2.4076	2.0707
	1.1470	2.4165	2.1069
	1.1508	2.4301	2.1116
Mean	1.1535	2.4181	2.0964
SD	0.0082	0.0114	0.0224
ROAD PITCH	1.1350	2.4174	2.1299
	1.1523	2.4382	2.1160
	1.1484	2.4323	2.1179
	1.1549	2.4543	2.1251
	1.1456	2.4499	2.1386
Mean	1.1472	2.4384	2.1255
SD	0.0077	0.0147	0.0092
ROAD PAINT	1.1393	2.4173	2.1217
	1.1212	2.3999	2.1406
Mean	1.1302	2.4086	2.1311
SD	0.0128	0.0123	0.0133

All the vehicular emission samples, along with Indian road dusts from India (R. Das et al., 2018; Ray et al., 2024) exhibit Pb isotopic compositions that lie along the mixing line between crust

(Millot et al., 2004) and Indian ore (Deb et al., 1989) as observed from the three – isotope plot (**Figure 6.6 a**). While there have been evidences of some crustal and industrial influences on Indian aerosols (R. Das et al., 2018; Ray and Das, 2023b; Sen et al., 2016), the road dusts actually plot within the mixing range of EE and NEE source signatures. Road dust from Sagar Island is an exception, that plots closer to crust indicating greater influence from geogenic sources. For the rest of the aerosols from urban and semi-urban areas, the three-isotope plot indicates that the road dusts are primarily a composite mixture of EE and NEE sources. Moreover, the road dusts, demonstrate significant overlaps with tire wear and EEs, indicating considerable influence from these specific sources. However, the Pb isotopic composition of the road pitch samples significantly differ (ANOVA: $p < 0.05$) from fuel exhaust, tire wear and notably from road dusts in $^{208}Pb/^{207}Pb$ space, indicating limited influence of the source on road dusts.

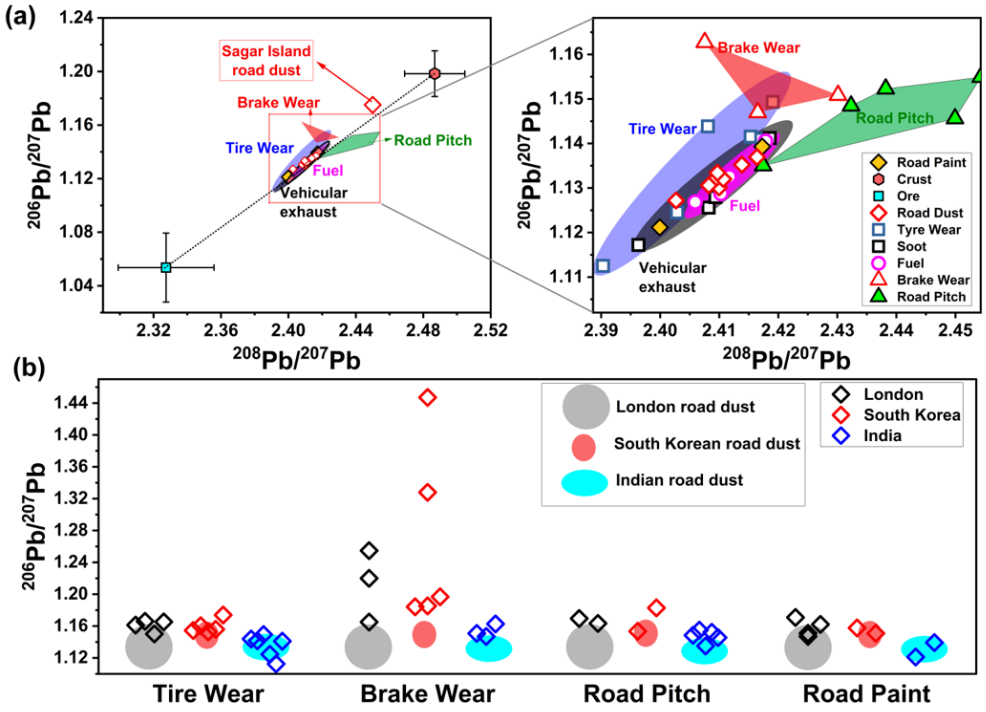

Figure 6.6: *(a) Three-isotope plots of $^{208}Pb/^{207}Pb$ vs $^{206}Pb/^{207}Pb$ for Indian fuel, vehicular exhaust, road dusts, tire wear, brake wear, road pitch and road paint. The fuel, vehicular exhaust, tire wear, brake wear and road pitch are depicted as fields in pink, dark grey, blue, red and green colours respectively. The right-hand panel provides an enlarged view of the squared section from the left-hand panel. (b) Comparison of the $^{206}Pb/^{207}Pb$ ratios in tire wear, brake wear, road pitch, and road paint from London and South Korea with those from the present study in India. The 206Pb/207Pb compositions of road dust from respective countries are shown as background fields. The data for London and South Korea has been adopted from Dong et al., 2017 and Jeong et al., 2022 respectively. The road dust data for India is adopted from Das et al., 2018 and Ray and Das 2024.*

Compared to London and South Korea (Dong et al., 2017; Jeong, 2022b; Jeong et al., 2022), the Indian NEE sources were much less radiogenic in $^{206}Pb/^{207}Pb$ space suggesting separate raw materials used for manufacturing (**Figure 6.6 b**). For all the three countries brake wears were the most radiogenic samples. However, British and South Korean brakes were about 49 ‰ and 90 ‰ more radiogenic than their Indian counterparts, respectively. The Indian brake wears demonstrated a consistent $^{206}Pb/^{207}Pb$ ratios (1SD = 0.008) while Korean (1SD = 0.117) and London (1SD = 0.045) samples varied significantly. Tire wear and road pitch samples were about 21 ‰ and 17 ‰ more radiogenic respectively in London (tire wear = 1.1607 ± 0.007; road pitch = 1.1664 ± 0.004)) and Korea (tire wear = 1.1595 ± 0.009; road pitch = 1.1682 ± 0.021) compared to India (tire wear = 1.1354 ± 0.014; road pitch = 1.1472 ± 0.008)). Similar variations were observed in $^{206}Pb/^{207}Pb$ ratios for road paints with Korean paints being 21 ‰ and London paints being 24 ‰ more radiogenic than Indian paints. Despite such high $^{206}Pb/^{207}Pb$ compositions of London NEE sources, London road dusts exhibited much lower $^{206}Pb/^{207}Pb$ ratios, similar to Indian road dusts. In South Korea, the road dusts overlap with the tire wear, road paint and to some extent road pitch samples (**Figure 6.6 b**). On the other hand, Indian road dusts have significant overlaps with all the NEE sources in $^{206}Pb/^{207}Pb$ space and also with EE sources as overserved from the three-isotope plot (**Figure 6.6 a**). Thus, South Korea and India appear to be influenced by the traffic emission sources to a greater extent than London. This can be due to a significantly lower average concentrations in most heavy metals in the NEE sources of London compared to Korea and India (**Figure 6.4**), resulting in lesser emissions. In fact, India demonstrates significantly higher concentrations of certain metals, ranging from several times to orders of magnitude higher (Al, Fe, Cr, Ni, Ba, Pb in tire wears; Cu, Zn, Sb in brake wears; Al, Fe, Cr, Cu in road pitch; Fe, Cr, Cu, Zn, Pb in road paints) compared to London. This results in Indian road dusts being more enriched in metals. To quantify contribution of each source in the Indian road dusts, Bayesian stable isotope mixing model has been utilized. Details on the mixing model results are discussed in the following section.

6.5. MixSIAR Model based approach for source apportionment

Bayesian stable isotope mixing model-based approach, MixSIAR is effective in addressing multiple endmember-based source apportionment (Longman et al., 2018; Ray and Das, 2023b; Stock, 2022). This modelling approach has been extensively used in the ecological study of food webs (Stock and Semmens, 2016). Recently, it is being utilized in source apportionment studies related to environmental pollutants based on Pb isotopic compositions (H. Chen et al., 2023;

Dietrich et al., 2021; Koffman et al., 2022; Longman et al., 2018, 2022; Ray and Das, 2023b). In this study, the concentration dependent 3D-MixSIAR model has been utilized to accurately determine the proportion of EE and each NEE source in urban road dusts (n = 10) (R. Das et al., 2018; Ray et al., 2024). Six distinct endmembers have been taken into account as components of road dust. Due to similar isotopic compositions exhibited by the exhaust emission end members (vehicular exhaust and fuel), they were averaged and combined into a single source called as EE. The other NEE sources incorporated include: tire wear, brake wear, road pitch and road paint. In case of road paint, $1/4^{th}$ of its analyzed concentration has been taken into consideration, since extant paint on the road surface contains about $1/4^{th}$ of its initial concentration (Turner and Filella, 2023). Additionally, a crustal component was incorporated as the geogenic constituent of road dust (Millot et al., 2004). Thus, the average Pb concentrations and Pb isotopic compositions of each of these end members were incorporated in the modelling framework. The input data for the model is provided in **Table 6.3**.

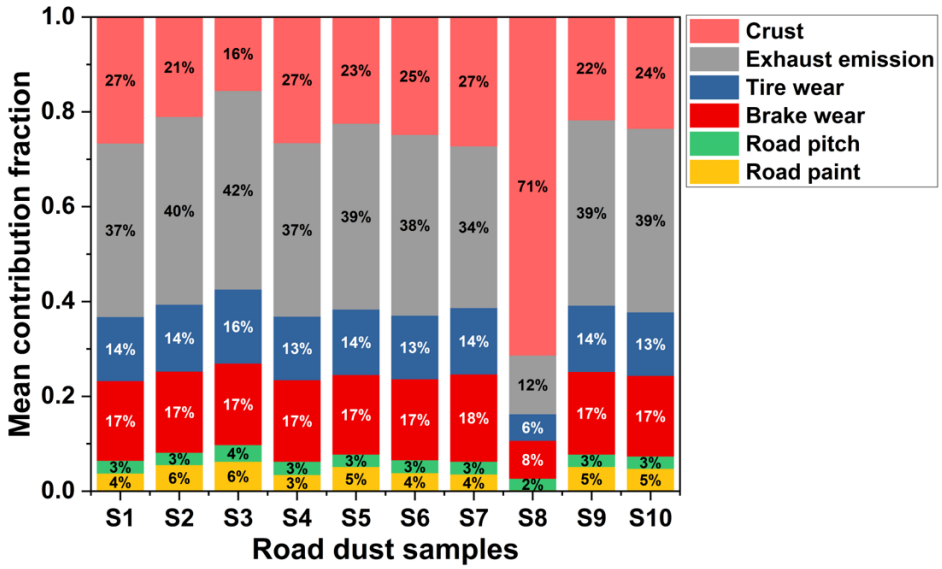

Figure 6.7: *MixSIAR results for mean contribution of Pb towards crust, exhaust emission, tire wear, brake wear, road pitch and road paint towards road dusts from eastern India. All the samples demonstrate consistent contributions from the sources except sample "S8", from Sagar island, a pristine location having heavy influence from natural crust*

MixSIAR results reveal consistent mean contributions from all six end members to the road dust samples, with one exception (sample S8 from Sagar Island) (**Figure 6.7**). Sagar Island, being a pristine location with less traffic compared to urban areas, shows the highest contribution from natural crust (71%) in its road dust. This result matches with the initial observations from the three-

isotope plot (**Figure 6.6 a**). At Sagar Island no influence of road paint could be observed, while other NEE sources (tire wear, brake wear, and road pitch) cumulatively contribute 16%, with brake wear contributing the most (8%). Exhaust emissions account for 12% of the lead (Pb) in Sagar Island's road dust. These contributions from both EE and NEE sources are the lowest among all the samples due to the heavy influence of the natural background in the region.

On the other hand, road dusts from urban and semi-urban regions consistently exhibit moderate mean contributions from natural background (16-27%). Contributions from exhaust emissions in these regions range from 34-42%. Among non-exhaust sources, road pitch and road paint contribute the least (3-6%), while tire wear and brake wear contribute significantly (14-16% and 17-18%, respectively). Thus, urban road dust shows nearly equal contributions from both EE and NEE sources (~40% each). These indicate that the road dusts are a mixture of crust, EE and NEE components with the anthropogenic sources being predominant. While EEs from combustion remain a substantial contributor in urban areas, non-exhaust sources such as brake and tire wear are also equally significant contributors to road dust composition. As there is a global urge to shift towards electric vehicles in the future, there is a potential for a reduction in atmospheric heavy metals from EEs. However, without effective control measures, NEEs from both electric and combustion engines can escalate with the increasing number of vehicles on road. Thus, it is crucial to quantitatively estimate the amount of heavy metal emitted from both exhaust and non-exhaust sources so that effective control strategies can be designed.

Table 6.3: *Inputs for Pb isotopic composition and Pb concentration in the MixSIAR model*

Sample	Mean $^{208}Pb/^{206}Pb$	SD $^{208}Pb/^{206}Pb$	Mean $^{206}Pb/^{207}Pb$	SD $^{206}Pb/^{207}Pb$	Mean $^{208}Pb/^{207}Pb$	SD $^{208}Pb/^{207}Pb$	[Pb] (mg/kg)	n
Tire wear	2.1216	0.0176	1.1354	0.0139	2.4088	0.0109	35.9	6
Brake wear	2.0964	0.0224	1.1535	0.0082	2.4181	0.0113	21.1	3
Road pitch	2.1059	0.0360	1.1744	0.0472	2.4717	0.0569	8.5	7
Road paint	2.1311	0.0133	1.1302	0.0128	2.4086	0.0122	20436	2
Vehicular exhaust	2.1324	0.0090	1.1300	0.0079	2.4097	0.0070	21.9	10
Crust*	2.0639	0.0361	1.2176	0.0210	2.5127	0.0004	26.7	2

**The data for crust (sediments of Ganga and Brahmaputra) has been adopted from Millot et al., 2004*

6.6. Metal emissions from traffic sources

The trend of annual atmospheric emissions of Ni, Cu, Zn and Pb from vehicular exhaust (only from ICEV) and various NEE sources, such as brake wear, tire wear, and road abrasions (includes the total emission from both ICEV and EV), from 2022 to 2045 is illustrated in **Figure 6.8**. Vehicular exhaust emissions are further categorized based on the fuel type, that is, petrol and diesel-driven vehicles. Statistical analysis (ANOVA, $p > 0.05$) of elemental concentration data of vehicular exhaust samples reveals no significant differences in the concentrations of Ni, Cu, Zn, and Pb between petrol and diesel samples. Therefore, the emission of these metals is primarily influenced by the fuel consumption, rather than the fuel type itself.

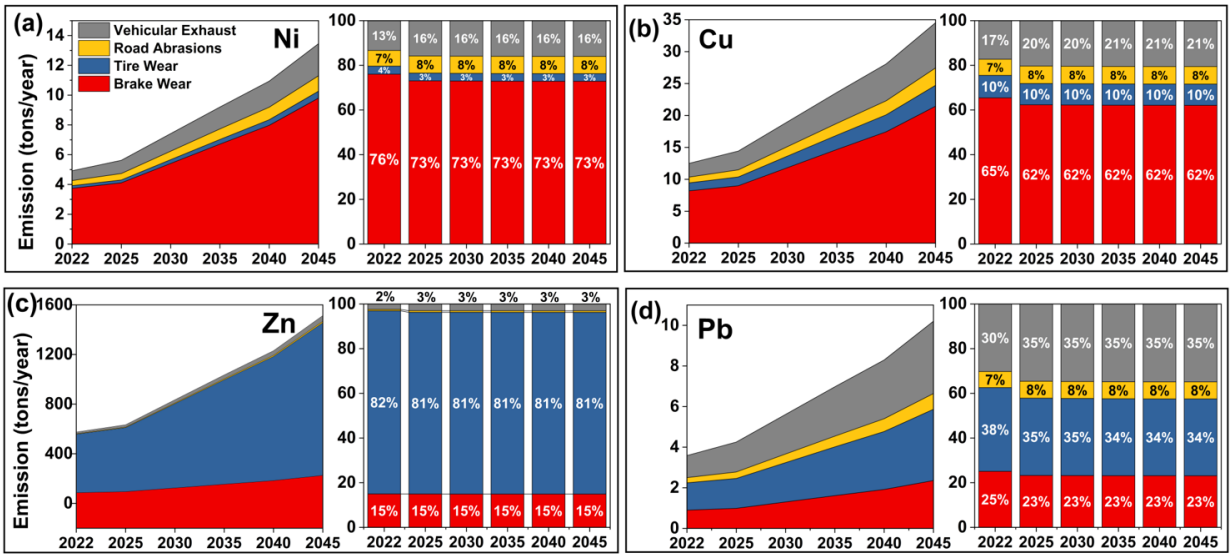

Figure 6.8: *Stacked area plots representing total emissions of vehicular exhaust, tire wear, brake wear and road abrasions in tons/year. The stacked bar plots depict the percentage contribution of each source towards total metal emissions from traffic sources for (a) Ni (b) Cu (c) Zn and (d) Pb in the years 2022, 2025, 2030, 2035, 2040 and 2045. About 60 % - 70 % of the emissions of Ni and Cu are from brake wears while the major source of Zn emission is tire wear particles. The NEE (tire wear, brake wear, road abrasions) sources contribute more towards Pb emission than EE sources*

It is challenging to differentiate between metal emissions from petrol and diesel vehicles from elemental concentration, as observed in this study and previous studies **(Dallmann et al., 2014; Pulles et al., 2012**). While diesel generally contains higher concentrations of major elements compared to petrol, trace metal concentrations are highly variable across fuels, and previous studies have not identified significant differences in trace metal content between the two fuel types (**Coufalík et al., 2019; Dallmann et al., 2014; Pulles et al., 2012**). In our study, we observed significant difference (ANOVA, $p < 0.05$) only in the concentrations of Mg and Ca in the exhaust

emissions from diesel vehicles compared to petrol vehicles. However, for metals such as Ni, Cu, Zn, and Pb, no significant difference was observed in the emissions.

To segregate the metal emissions between petrol and diesel vehicles, the projected diesel and petrol consumption data of India from U.S. Energy Information Administration website (**International Energy Outlook, 2023**) were compiled. Since there was no statistically significant difference in the concentrations of Ni, Cu, Zn, and Pb between exhaust samples from petrol and diesel vehicles (ANOVA, $p > 0.05$), the means were used to calculate the emissions of these metals for each fuel type. The emissions of Ni, Cu, Zn, and Pb from petrol and diesel vehicles were determined separately by integrating fuel consumption data for each type of vehicle (**Figure 6.9**) Thus, the difference in metal emissions is primarily dependent on the number of diesel versus gasoline vehicles on the road, rather than differences in the elemental concentrations of the fuels themselves. Therefore, fleet composition plays a critical role in determining the overall metal emissions from vehicular exhaust.

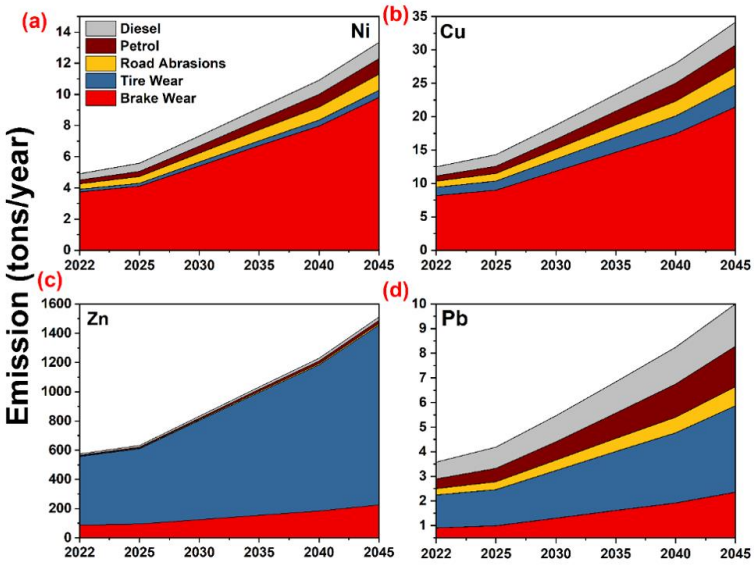

Figure 6.9: *Stacked area plots representing total emissions of diesel, petrol, tire wear, brake wear and road abrasions in tons/year.*

Primarily, emission of heavy metals from EE and NEE sources vary based on several factors including vehicle type, mileage, total vehicle population on road, and the emission factors associated with different emission sources (Tian et al., 2015). The emission factor is an essential

fraction indicating the quantity of emitted pollutants per kilometer of distance travelled in a mixed driving condition (Singh et al., 2020).

The linear increase of EE in future will be due to the steady linear growth of passenger and commercial ICEV and low adoption of EV. As NEE results from both ICEV and EVs, it is projected to increase as well following the growth curve of the vehicle growth in India.

Thus, this linear growth pattern of road transportation and hence emissions is primarily due to two reasons,

1. India's population reached 1.43 billion in 2023, surpassing China, and is projected to grow to 1.62 billion by 2045. With half of the population under 25, India's working population is expected to expand to 1.1 billion, driving economic growth. The country's GDP is projected to grow by an average of 6.1% annually between 2022 and 2045, contributing to sustained economic expansion.
2. India's urbanization rate, currently around 34%, is much lower than in developed and many developing countries, despite housing several of the world's most populous cities. Recent policy initiatives like the 'Smart Cities Mission,' affordable housing projects, and metro system expansions are expected to significantly boost urbanization during the forecast period. This urbanization will, in turn, drive increased demand for modern energy sources, including oil. Economic expansion will boost freight transport, driving increased diesel demand in road transportation. Additionally, the rapid growth of the middle class, coupled with urbanization and improved road infrastructure, is projected to more than quadruple the number of passenger vehicles, expanding the fleet from 46 million in 2022 to nearly 200 million by 2045 (excluding two-wheelers).

The present study focuses on the emission of four elements—Pb, Ni, Cu, and Zn—which are extensively used in the automobile industry and have been reported to be enriched in Indian road dust as well as aerosols. These elements are also present in significant concentrations in vehicular sources. This overlap in their prevalence in both road dust and vehicular emissions led us to focus on these elements, as it suggests they are key contributors to metal pollution from transportation sources. (A. Das et al., 2018; R. Das et al., 2018; Haritash and Kaushik, 2007; Ray et al., 2024).

Annual emission analysis over the time period of 2022 to 2045 indicates a consistent rise in the levels of Ni, Cu, Zn and Pb (**Figure 6.8 a-d**), driven by the growing vehicular population and increasing fuel consumption (**Figure 1**) (OPEC, 2023). Evidence from previous research indicate a high degree of contamination in aerosols and road dust, particularly by Cu, Pb, Ni, and Zn (Das et al., 2015; R. Das et al., 2018; Ray et al., 2024; Sen et al., 2016). Emission analysis in this study highlights the total emissions of Ni, Cu, Zn and Pb from EE and NEE sources as well as the individual percentage emission of these toxic metals from each source. Among these 4 metals, total cumulative emission for Zn (575 tons/year as of 2022) from all the traffic sources is the highest followed by Cu (12.5 tons/year as of 2022), Ni (4.9 tons/year as of 2022) and Pb (3.5 tons/year as of 2022). Results indicate that the total emissions from all the EE and NEE sources is expected to rise alarmingly by 174 %, 176 %, 163 % and 184 % for Ni, Cu, Zn and Pb from 2022 to 2045. All results for emission from NEE and EE are provided in Tables

Nickel: Brake wear is determined to be the largest emitter of Ni, contributing 76 % of total Ni emissions from traffic sources in 2022. This is followed by vehicular exhaust (13% in 2022), road abrasions (7 % in 2022) and tire wear (4 % in 2022). As of 2022 Ni emission from brake wear was estimated to be 3.73 tons, which is projected to reach 9.80 tons by 2045 (**Figure 6.8 a**). This significant contribution of brakes to Ni emissions can be attributed to the highest mean concentration of Ni in brake wear (175 mg/kg) compared to other traffic sources. Previous studies have also determined Ni concentrations in brake dust as high as 730 mg/kg (Thorpe and Harrison, 2008). To produce high wear-resistant brakes, with increased hardness, elastic modulus and oxidation resistance, Ni coatings are applied by thermal spraying or laser cladding (Aranke et al., 2019; Shi et al., 2021). Consequently, the frequent use of brakes leads to the release of Ni particles into the environment, contributing to the high emissions observed. In addition to emissions from brake wear, contributions from vehicular exhaust, tire wear and road abrasion has driven the total Ni emission to 4.9 tons in 2022. This is projected to increase progressively to 13.5 tons in 2045, if the EE and NEE sources continue to have similar Ni concentrations and emission factors (**Figure 6.8a**).

Copper: Similar to Ni, brake wear stands out as the largest emitter of Cu, contributing 65 % of total Cu emissions from traffic sources as of 2022 (**Figure 6.8 b**). Following brake wear, vehicular exhaust is the second largest emitter of Cu (17 % in 2022), followed by tire wear (10 % in 2022)

and road pitch (7% in 2022). Similar trend was also observed in China, with brake and tire wear being a significant emitter of Cu (Tian et al., 2015). In 2022, the Cu emission from brake wear was estimated at 8.18 tons, which is projected to steadily reach 21.45 tons by 2045 (**Figure 6.8 b**). Brake wears are particularly rich in Cu having the highest mean concentration (383 mg/kg) among all the EE and NEE sources as determined in this study. Copper chips are present on the surface of the brake pads to reinforce the structure as well as for lubrication during rotation. Furthermore, Cu is the chosen metal for using in brakes for quick heat dissipation. However, wearing of brakes discharges substantial amount of brake wear particles on roadside which are subsequently washed away to the waterways (US EPA, 2015). In addition to the brake pads, other EE and NEE sources emitted a total of 12.50 tons of Cu in 2022, which will go up to 34.54 tons in 2045 (**Figure 6.8 b**). If the concentrations of Cu in brakes as well as other sources are not reduced, Cu emission will continue to pose threats to urban flora and fauna and especially aquatic lives. To reduce the amount of Cu in brake pads during their manufacture, a recent initiative has been taken up by the Environmental Protection Agency (EPA) called "Copper-Free Brake Initiative", which has led to significant reduction in Cu emissions from brake pads in the US (US EPA, 2015).

Zinc: Tires are the most significant source of Zn emission among the traffic sources globally as tire threads contain about 1 wt. % of Zn (Councell et al., 2004). Similar trends were observed in this study with tire wears containing an average of 2.5 wt. % Zn (**Table 6.1**). As a result of such high concentrations Zn, emission from tire was estimated at 471 tons in 2022 and it is projected to reach 1231 tons by 2045 (**Figure 6.8 c**). These Zn emissions from tire wears actually accounts for more than 80 % of the total Zn emissions from traffic sources. While brake wears contribution is only 15 % the absolute emission per year is quite significant, with 86 tons in 2022 reaching up to 225 tons in 2045. Similarly, vehicular exhausts only accounting 2-3 % of the total Zn emissions emitted 14.06 tons in 2022 and is projected to emit 46 tons in 2045. Emission of Zn from road abrasions was about 3.59 tons in 2022, which appears to be negligible compared to tire wears (**Figure 6.8 c**). Thus, all the traffic sources emitted a cumulative of 575 tons of Zn in 2022. Without any effort to reduce the concentration of Zn in the vehicular sources this emission will reach an alarming 1513 tons in 2045.

Lead: The combined contribution from all NEE sources (tire wear, brake wear, road abrasions) surpasses that of EE. The NEEs contribute 65-70% of the total emitted Pb, while EEs account for

30-35%. (**Figure 6.8 d**). However, EE is a significant emitter of Pb among traffic emission sources despite the reduction of Pb concentration after the ban of leaded gasoline more than two decades back. Among the traffic sources, vehicular exhaust still records the highest average concentration (94 mg/kg) as determined in this study (**Table 6.1**). Furthermore, EE will continue to remain a significant emitter of Pb among traffic sources for the next two decades (**Figure 6.8 d**). In fact, the largest projected rise in Pb emission from 2022 to 2045 is expected from vehicular exhausts, increasing from 1.08 tons in 2022 to 3.56 tons in 2045 (228 % increase) This significant rise can be attributed to the increasing number of ICEV in India and least percentage of EV penetration compared to other regions (**Figure 6.1**) (OPEC, 2023). Tire wear is the most significant contributor of all NEEs contributes Pb emissions followed by brake wear and road abrasions. Thus, from all these traffic sources a total of 3.6 tons of Pb was emitted in 2022, which will go up to 10.2 tons in 2045 (**Figure 6.8 d**), if the sources continue to have similar concentrations of Pb.

6.7. Implications

Source apportionment results highlight the significant contributions of both exhaust and non-exhaust sources to the metal enriched urban road dusts, with each contributing approximately 40%. As the total emission of each metal rises, the percentage contribution of each source towards the emission of respective elements remains consistent throughout, from 2022 to 2045 (**Figure 6.8 a-d**). In this emission analysis, the concentrations of the metals in the sources have been kept constant, while the total number of cars and the percentage EVs have been modified based on projected data (OPEC, 2023). The emission factors for EVs have also been considered separately as EVs are generally heavier and hence have higher emission factors associated with tire wear, brake wear and road abrasions (OECD, 2020). Hence if there is a substantial increase in number of EVs, higher emission factor associated with them should increase the NEEs.

However, despite a 7.6% EV penetration in 2045 compared to 0.3% in 2022 (**Figure 6.1**), the percentage of emissions from vehicle exhausts remains consistent across all metals. This implies that the increased number of EVs, although having higher emission factors for NEEs than ICEVs, does not appreciably alter the overall emission profile of metals from traffic sources. According to projection data, the Indian roads will remain hugely dominated by ICEVs even in 2045, with EVs accounting for only 7.6 % of vehicles (OPEC, 2023). Emissions from EVs are directly proportional to their population and mileage (**Equation 3.6**). With an average mileage of 161 km/charge for

EVs, compared to 16.61-17.46 km/L for ICEVs, the lower number of EVs and their better mileage will lead to lower NEEs from EVs compared to ICEVs. Consequently, the majority of NEEs will originate from ICEVs, with EVs contributing only a small portion.

The total number of EVs is not substantial enough to have an impact on the overall emission profile of the metals when the vast majority are still ICEVs. Thus, the effect on the traffic emission scenario of India, due to a shift towards more EVs remains relatively negligible in context of India's total vehicle fleet.

The results presented in this chapter emphasize the significant role of road traffic emissions, in contributing to metal-enriched PM in urban environments. However, road traffic is only one piece of the broader puzzle of PM emissions. Another critical segment, particularly in regions reliant on coal for energy production, is the substantial contribution of coal combustion to emission of PM-bound metals.

Coal-fired power plants and industrial facilities are major sources of metal-laden particulates, where advancements in coal-cleaning technologies have been introduced to mitigate emissions. Despite these efforts, the extent to which these measures are effective remains uncertain.

To comprehensively address the challenges posed by PM emissions, it is vital to examine the chemical and isotopic composition of PM near coal combustion sources. This analysis will not shed light on the contribution of coal towards atmospheric metal pollution but will also provide insights into the efficacy of existing coal-cleaning practices.

Thus, the following chapter investigates the elemental and Pb isotopic composition of PM in a coal combustion energy generation plant.

Table 6.4 *Parameters for emission calculation*

(*The emission factor has been calculated by taking the weighted average based on total number of passenger cars and light commercial vehicles, each having distinct emission factors and population (OECD 2020).

Source	Metal	Average Metal Concentration (ug/g)	Emission Factor (g/km)*					
			2022	2025	2030	2035	2040	2045
Vehicular Exhaust	Ni Cu Zn Pb	57 188 1223 94	0.0057	0.006180	0.006194	0.006207	0.006211	0.0062124
Tire Wear	Ni Cu Zn Pb	9 67 25233 72	0.009229	0.008093	0.008062	0.008032	0.008024	0.008020
Brake Wear	Ni Cu Zn Pb	175 383 4031 42	0.01054	0.00928	0.00925	0.00921	0.00921	0.00920
Road Abrasions	Ni Cu Zn Pb	23 59 236 17	0.0075	0.0075	0.0075	0.0075	0.0075	0.0075

Table 6.5*: Mileage (km/L) and fuel consumption data (L) for emission analysis of ICEVs*

The mileage has been calculated by taking the weighted average based on total number of passenger cars and light commercial vehicles, each having distinct mileages and population (OECD 2020).

ICEV Mileage (km/L)**						Total ICEV Fuel Consumption (L)					
2022	2025	2030	2035	2040	2045	2022	2025	2030	2035	2040	2045
16.61	17.41	17.43	17.45	17.46	17.46	121873500000	145087500000	191515500000	237943500000	283020000000	348210000000

***Table 6.6**: Total ICEV Emission (tons/year)*

Source	Metal	2022	2025	2030	2035	2040	2045
Total Vehicular Exhaust	Ni	0.66	0.89	1.18	1.47	1.75	2.15
	Cu	2.16	2.93	3.89	4.84	5.77	7.10
	Zn	14.07	19.09	25.28	31.52	37.53	46.19
	Pb	1.08	1.47	1.95	2.43	2.89	3.56
Tire Wear	Ni	0.18	0.19	0.26	0.32	0.38	0.46
	Cu	1.26	1.38	1.81	2.24	2.67	3.28
	Zn	471	516	679	842	1000	1230
	Pb	1.34	1.47	1.94	2.40	2.85	3.51
Brake Wear	Ni	3.74	4.11	5.41	6.70	7.97	9.80
	Cu	8.18	8.99	11.84	14.67	17.44	21.45
	Zn	86	95	124	154	183	225
	Pb	0.90	0.99	1.30	1.61	1.92	2.36
Road Abrasions	Ni	0.35	0.43	0.57	0.71	0.84	1.04
	Cu	0.90	1.13	1.49	1.85	2.20	2.71
	Zn	3.59	4.48	5.92	7.36	8.76	10.77
	Pb	0.26	0.32	0.43	0.53	0.63	0.78

***Table 6.7**: Total EV Emission (tons/year)*

Source	Metal	2022	2025	2030	2035	2040	2045
Tire Wear	Ni	0.0000024	0.000007	0.000032	0.000089	0.000173	0.000262
	Cu	0.0000167	0.000050	0.000225	0.000634	0.001226	0.001859
	Zn	0.0062537	0.018761	0.084425	0.237639	0.459645	0.697284
	Pb	0.0000178	0.000054	0.000241	0.000678	0.001311	0.001989
Brake Wear	Ni	0.000012	0.000037	0.000167	0.000471	0.000912	0.001383
	Cu	0.000027	0.000081	0.000367	0.001032	0.001995	0.003027
	Zn	0.000285	0.000856	0.003854	0.010847	0.020981	0.031828
	Pb	0.000003	0.000009	0.000040	0.000113	0.000219	0.000333
Road Abrasions	Ni	0.000005	0.000016	0.000074	0.000209	0.000404	0.000612
	Cu	0.000014	0.000043	0.000194	0.000546	0.001056	0.001601
	Zn	0.000057	0.000171	0.000770	0.002168	0.004192	0.006360
	Pb	0.000004	0.000012	0.000055	0.000156	0.000302	0.000458

Table 6.8: *Total non-exhaust emissions (NEE) (ICEV + EV) (tons/year)*

		2022	2025	2030	2035	2040	2045
Source	**Metal**						
Tire Wear	Ni	0.18	0.19	0.26	0.32	0.38	0.46
	Cu	1.26	1.38	1.81	2.24	2.67	3.28
	Zn	471	516	679	842	1001	1231
	Pb	1.34	1.47	1.94	2.40	2.85	3.51
Brake Wear	Ni	3.74	4.11	5.41	6.70	7.97	9.80
	Cu	8.18	8.99	11.84	14.67	17.44	21.45
	Zn	86	95	124	154	183	226
	Pb	0.90	0.99	1.30	1.61	1.92	2.36
Road Abrasions	Ni	0.35	0.43	0.57	0.71	0.84	1.04
	Cu	0.90	1.13	1.49	1.85	2.21	2.71
	Zn	3.59	4.48	5.92	7.36	8.76	10.78
	Pb	0.26	0.32	0.43	0.53	0.63	0.78

Table 6.9*: Total metal emissions from NEE and EE sources (tons/year)*

Metal	2022	2025	2030	2035	2040	2045
Ni	4.92	5.62	7.41	9.20	10.94	13.46
Cu	12.50	14.42	19.02	23.61	28.08	34.54
Zn	575	634	835	1035	1230	1513
Pb	3.59	4.25	5.61	6.97	8.29	10.21

CHAPTER 7: SOURCES OF ATMOSPHERIC Pb IN AND AROUND A COAL-FIRED POWER PLANT IN INDIA

7.1. Introduction

Several anthropogenic sources such as coal combustion, biomass burning, vehicular fuel combustion, industrial processes etc. contribute significantly towards this elevated level of PM emission in India (**Figure 7.1a**). Comparative estimates of PM emission from these sources reveal that open burning of biomass has been the largest emitter of PM_{10} and $PM_{2.5}$ for the past one and a half decade ("GAINS South Asia online," 2020). Coal combustion emission is steadily decreasing due to implementation of stricter emission standards that was put forth in 2015 (Press Information Bureau, 2015). In contrast, PM emissions from industrial processes is projected to surpass that of coal combustion in the present decade. Apart from these sources a large collective contribution is present from other miscellaneous sources (**Figure 7.1a**).

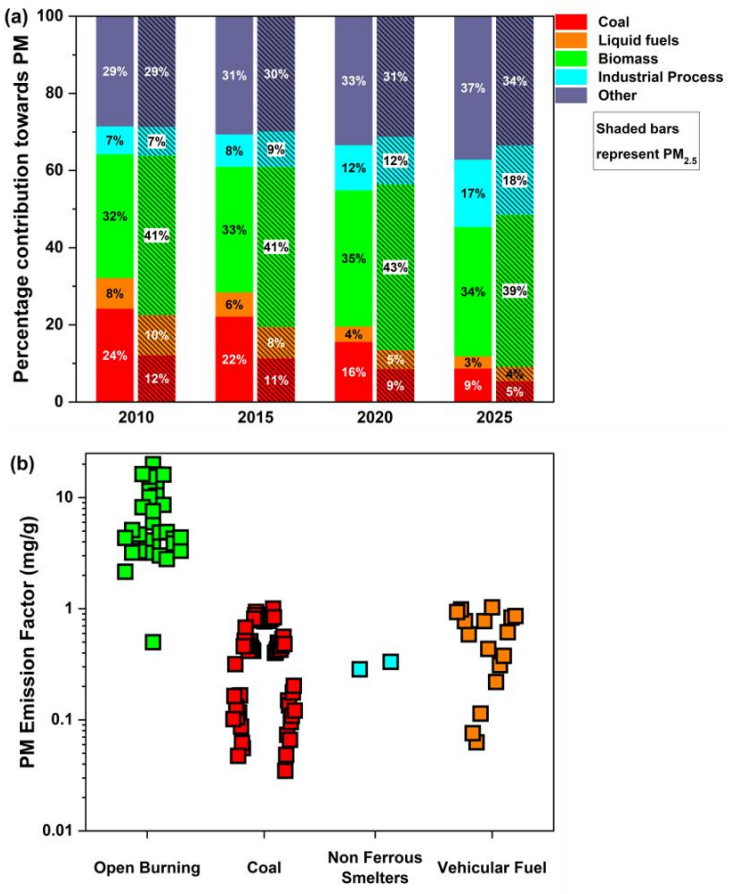

Figure 7. 1*:(a) Stacked bars representing emissions of PM_{10} and $PM_{2.5}$ (shaded bars) from different anthropogenic sources as compiled form "GAINS South Asia online," 2020. For the past one and a half decades, open biomass burning has been the largest emitter of PM_{10} and $PM_{2.5}$, while coal combustion emissions have steadily decreased due to the stricter emission standards implemented in 2015; (b) Particulate matter (PM) emission factors of open burning coal combustion, non-ferrous smelters and vehicular fuel. The emission factors for open burning are orders of magnitude higher than other processes. The emission factors have been compiled from (Akbari et al., 2021; Raparthi and Phuleria, 2021; Saud et al., 2011; Zhang et al., 2022; Zhu et al., 2022)*

India, ranks second in coal consumption, and is home to 295 coal-fired power plants (NITI Aayog, 2024; Our World in Data, 2021; Statista, 2020a, 2020b). Coal fired plants and other non-ferrous industries have emission control

systems such as cyclone separators, bag filters, electrostatic precipitators (ESP) to reduce the PM emission and metals associated with it (J. Zhang et al., 2022). On the other hand, the practice of open burning of biomass and solid wastes (SW) at open dumpsites, landfills or even individual residences, leads to uncontrolled release of PM. India ranks among the top countries globally in both waste production and open burning of wastes (Wiedinmyer et al., 2014). The mass of pollutants emitted from open burning per mass of waste (i.e. the emission factor) is an order of magnitude higher than other controlled processes (Akbari et al., 2021; Raparthi and Phuleria, 2021; Saud et al., 2011; J. Zhang et al., 2022; Zhu et al., 2022) (**Figure 7.1b**).

These emitted PMs are associated with toxic elements like Arsenic (As), Cadmium (Cd), Chromium (Cr), Cobalt (Co), Mercury (Hg), Nickel (Ni), Lead (Pb) etc that can pose significant environmental and health risks. The elements released from coal that are of highest concern, due to their high concentrations, include As, boron (B), Cd, Hg, molybdenum (Mo), Pb, and selenium (Se). Elements of moderate concern include Cr, copper (Cu), Ni, vanadium (V), and zinc (Zn) (Swaine, 2013) Non-ferrous industries and other small scale industries emit elements such as Cr, Mn, Fe, Cu, Zn, Ni, Cd and Pb (Rawat et al., 2009). On the other hand SW incineration ash consists of varying amount of trace metals of which the major concerns are Al, Cr, Cu, Zn, Cd, Pb and Hg(Wiles, 1996). These elements are often enriched in bottom and fly ashes and pose environmental risks (Jung et al., 2004). Fly ashes from SW incineration primarily consists of particles smaller than 5.5 μm, posing risk of the associated toxic metals being transferred to the human bloodstream through inhalation, if burned openly (Lee et al., 2006). The concentrations of these elements in SW ash vary across different countries (Chang and Ku, 1998; Nguyen et al., 2023; Shim et al., 2005; P. Wang et al., 2019). However, in general the trend shows very high concentrations of Mn, Cu, Zn and Pb followed by moderate concentrations of Cr, Ni and Cd. A detailed country wise comparative analysis of the elemental concentration of toxic metals in SW incineration fly ash (Chang and Ku, 1998; Greenberg et al., 1978; Nguyen et al., 2023; Shim et al., 2005; P. Wang et al., 2019) is presented in **Table 7.1**.

Table 7.1: *Typical elemental concentrations in lignite and solid waste burning ash from different countries compiled from previous literature.*

Countries	B	V	Cr	Mn	Co	Ni	Cu	Zn	As	Se	Mo	Cd	Ba	Pb	Hg	References
Lignite																
India	53.4	31.5-65.6	5.64-57.9	28.2-74.9	2.09-15.2	14.6-28.4	15.7-57.6	6.37-38.3	0.21-7.7	1.99		0.2-5.32	5.96	3-22.8	0.066-0.41	**Ram et al., 2014; Mukherjee and Srivanstava, 2005, Singh et al., 2015**
Poland		12.9-17.8	15.8-22		4.15-6.12	10.4-13.5	100-271	47.9-118					798-2046	61-85	0.06-0.665	**Burmistrz et al., 2016; Chomiak and Widera., 2020**
Bulgaria		170	130	790	23	107			60		77	22.8	1070	75		**Kortenski and Sotirov, 2002**
China		43-153	7.6-145		1.8-53.2	41-155	3.54-126	4.64-424	2.3-38		0.1-11.7	0.01-1.67	26.3-771	0.94-83		**Qi et al., 2007; Ren et al., 2004**
Czech Republic	9-104		13.6-110		2.7-16.1	26.8-115	6.7-385		0.1-757		0.6-2.7	0.3	27.7-193	3.2-16		**Bouška and Pesek, 1999**
Greece	110-188	8-170	16-423		1-32	24-664	17.2-27.8	56-93	4-366		40-98	0.4-0.72	27-443	5-22		**Filippidis et al., 1996**
USA		1-204	4-523	26-4287	0.6-92	1-306	6.8-85	0.1-278	2.3-104				24-1861			**Given and Miller, 1987; Hower et al., 2023**
This study		6.27-209	12.2-331	64.5-238	5.1-126	39.1-403	7.84-156	12.73-431				0.02-0.59		0.97-45.77		
Solid waste burning ash																
Korea	52-120		54-210	220-700		20-58	560-1700	5200-7600	12-26	6-10		220-410		2300-3600		**Shim et al., 2005**
Japan	2-32		89-160	100-260		9.4-19	230-730	1400-6500	4-20	2-6		20-95		340-3000		**Shim et al., 2005**
China			1.3-5120			1.23-555	41.8-15700	300-71600	1.1-1630			10-658		120-11300	0.05-85	**Wang et al., 2019**
Taiwan			135-324			83-243	1648-19349	16928-40711	1.1-11.7			837-1468		7645-17432	1.4-9.0	**Chang and Ku, 1998**
Germany			450			145	1050	16600	100			300		4900	8	**Chang and Ku, 1998**
Netherlands			180-715			64-110	780-1300	14200-2300	1-70			237-250		6090-7600		**Chang and Ku, 1998**
Canada			500-800			140-240	800-1400	25000-70000				400-1100		11000-26000		**Chang and Ku, 1998**
Denmark			200-1600			10-230	400-1400	2000-21000	5-80			10-300		800-13900		**Chang and Ku, 1998**
Vietnam			102-233			48.5-341	269-564	1841-3174	13.7-33.5			20.3-60.1		2.73-518		**Nguyen et al., 2022**
Egypt		110-166	1170-1900	2700-8500	26-54	580-960	300-2000	7800-13600	9.4-7.4	1.4-11		5-125		1800-5400		**Greenberg et al., 1978**
This study		24-78	37-96	1041-4180	1.4-4.4	19.9-56	42.9-111	614-1434				0.64-0.99		28-45		

These heavy metals are mostly bound to fine PM (PM < 2.5 μm) and can be transported over long distances across countries by atmospheric circulation (Rasmussen, 1998). Evidences of pollutants from Europe and North America reaching the Arctic have been reported in the past century(Pacyna, 1995) When leaded gasoline was in use, Pb compounds emitted with vehicular exhaust were transported to remote regions, including Antarctica, Greenland, Alaska, and the open ocean. This long-range transport of Pb was traced with the use of stable Pb isotopes (Sturges and Barrie, 1989). Fine particles containing Pb, Hg and Cd persist in the atmosphere for extended periods, allowing them to be deposited in areas far from their sources. Particularly, in case of Pb, the atmospheric residence time is typically 5–10 days after its emission until it gets deposited (Sturges and Barrie, 1987).

To accurately quantify these emissions, one approach is to utilize heavy metal concentrations and isotopes. These isotopes, such as Pb, can serve as tracers of PM emissions, allowing for the identification and quantification of specific sources. As there is no isotopic fractionation of Pb during physicochemical processes the isotopic signature of the source is preserved (Komárek et al., 2008). Metal concentrations are also crucial factors that supports the implications derived from isotopic compositions (R. Das et al., 2018; Sen et al., 2016). In the past decade PM bound Pb was found to be significantly enriched in Indian aerosols. This Pb is primarily sourced from coal combustion, metal ores utilised in industrial purposes and open burning of biomass and wastes (R. Das et al., 2018; Kumar et al., 2016, 2018; Sen et al., 2016). The concentration of Pb in the PM emitting sources such as, ore, Indian coal and biomass typically ranges from 1.6 to 5.5 percent, 20 to 144 ppm, and 0.2 to 28 ppm respectively (Chabukdhara and Singh, 2016; R. Das et al., 2018; Deb et al., 1989; Fulekar et al., 1983). Thus, although emission factors for coal combustion, ore smelting, and vehicular fuel combustion are less than that of open burning, the former sources have orders of magnitude higher concentrations.

The major sources of PM in the Indian atmosphere have been a subject of investigation and study. As coal combustion emission is steadily decreasing, it is crucial to investigate whether the emission norms are effective in controlling emission of heavy metals from coal combustion. Being the largest power supplying plant using lignite, Neyveli can emit significant amount of heavy metals. This makes it an ideal site for assessing how well current emission norms are controlling the release of these heavy metals to the atmosphere. A detailed country wise comparative analysis of the

elemental concentration of toxic metals in lignite (Adamidou et al., 2007; Bouška and Pešek, 1999; Burmistrz et al., 2016; Chomiak and Widera, 2020; Filippidis et al., 1996; Given and Miller, 1987; Hower et al., 2023; Kortenski and Sotirov, 2002; Mukherjee and Srivastava, 2005; Qi et al., 2007; Ram et al., 2014; Ren et al., 2004; Singh et al., 2015) is presented in **Table 7.1**. Thus, this study aims to investigate the primary sources of $PM_{2.5}$ in an area housing the major lignite fired power plant of South India using Pb isotopic compositions and elemental composition. The Indian atmosphere is additionally influenced by emissions from open burning and other large and small-scale industries. The ultimate objective is to quantify the contribution of each source towards atmospheric $PM_{2.5}$ levels by utilizing the Pb isotope and elemental concentration data of $PM_{2.5}$ so that better regulatory actions can be taken to improve air quality. In a densely populated developing country like India, where multiple sources of emission coexist, source apportionment becomes crucial for targeted mitigation strategies and implementation of stricter emission controls in specific emitting sectors.

7.2. Study area

The study was conducted in and around the largest power supplying lignite fired plant of Southern India located in the state of Tamil Nadu (Cuddalore district), and operated by Neyveli Lignite Corporation India Limited (NLCIL). Neyveli is located roughly 197 kilometres south of Chennai and 52 kilometres inland from the Bay of Bengal. It covers an area of 835 square kilometres. The Ponnaiyar River borders the town to the north, the Coleroon River to the south, and the Bay of Bengal to the east. At Neyveli there are 3 operational open cast lignite mines (Mine I, Mine IA and Mine II) with a lignite reserve of about 1357 million tons, that belongs to the tertiary geologic era (~25 MYA). The combined yearly production capacity of the mines stands at 28.5 million tonnes. At present, NLCIL operates five pit-head thermal power generation stations with a total installed capacity of 3390 MW, all fueled by the mined lignite. The total area covered by the mines and power plant is around 206 sq.km (NLCIL, 2024). In addition to the lignite mines and power plants, the region also houses several small, medium and large-scale industries ranging from chemical, pharmaceutical, textile, fertilizers, automotive etc within the State Industries Promotion Corporation of Tamil Nadu (SIPCOT) industrial complex, established in 1984 (**Figure 7.2**). In the study area, Tamil Nadu pollution control board report reveals exceedance of several air pollutants such as suspended particulate matter (SPM), PM_{10}, Gaseous Hg, SO_x and NO_x from the National Ambient Air Quality Standards (NAAQS) (TNPCB, 2023).

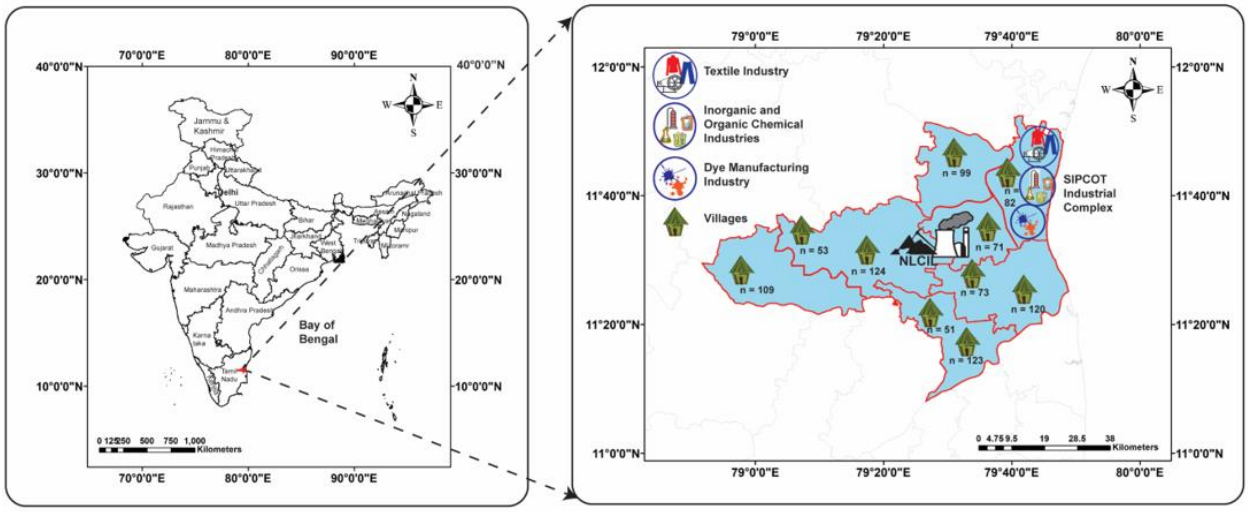

Figure 7. 2*: Map showing the location of the state of Tamil Nadu and Cuddalore district within the state housing the largest lignite fired power plant Neyveli Lignite Corporation India Limited (NLCIL). The SIPCOT industrial estate housing different types of industries and the number of villages in the district are marked for reference. The base maps are adopted from the open-source online repository: Opendatasoft (https://public.opendatasoft.com/explore/dataset/world-administrative-boundaries/export/)*

7.3. Elemental concentration and $PM_{2.5}$ load

The concentration of the 13 (Mg, Al, Ca, V, Cr, Mn, Fe, Co, Ni, Cu, Zn, Cd and Pb) elements analyzed in the $PM_{2.5}$ aerosols varied across months (**Figure 7.3a**). Across all months, the elements can be divided into three distinct groups, following the general order: (Al, Ca, Fe, Mg, Zn) > (Cr, Cu, Mn, Ni, Pb) > (Cd, Co, V). All the months witnessed orders of magnitude higher mean concentrations of Al (951 – 3525 ng/m^3), Ca (66 – 345 ng/m^3), Fe (94 – 512 ng/m^3), Mg (38 – 228 ng/m^3) and Zn (33 – 481 ng/m^3) compared to Cd (0.08 – 2.53 ng/m^3), Co (0.05 – 0.25 ng/m^3), Cr (0.90 – 13.5 ng/m^3), Cu (2.02 – 44 ng/m^3), Mn (1.96 – 68 ng/m^3), Ni (0.91 – 13.5 ng/m^3), Pb (2.32 – 79.89 ng/m^3) and V (0.41 – 2.25 ng/m^3).

Concentrations of all the elements witnessed a sharp decrease in the month of May (**Figure 7.3a**). Anthropogenically sourced elements such as Cd, Pb and Zn demonstrated a decreasing trend through the months of April – June 2021, followed by an increase in the last three months of the year. Simultaneously, there was a sharp increase in $PM_{2.5}$ load in the months of April – June compared to October – December of 2020, 2021 and February 2022 (**Figure 7.3a**). Aluminum recorded highest concentration in April.

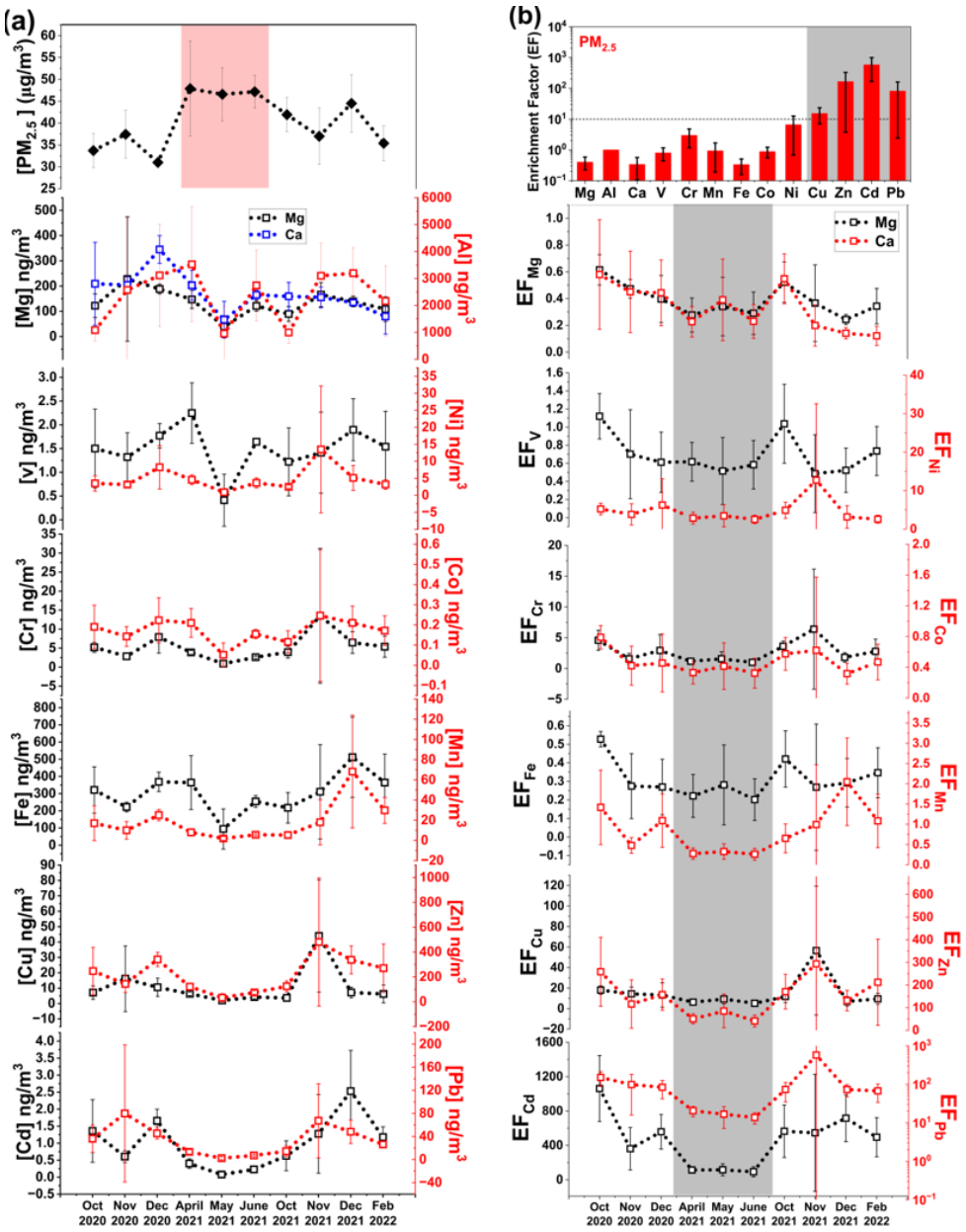

Figure 7. 3: *(a) Temporal variation in concentrations of $PM_{2.5}$ (top panel) and elemental concentrations. The $PM_{2.5}$ loads increased in the months of April – June compared to October – December. Concentrations of all the elements witnessed a sharp decrease in the month of May (b) The top panel depicts the mean enrichment factors (EF) of each element in $PM_{2.5}$ aerosols across the sampling period with significant enrichment in Cu, Zn, Cd and Pb (EFs > 10). The lower panels illustrate the temporal variation in EFs. All the enriched elements exhibited lowest EFs in the months of April-June, indicating a reduced anthropogenic contribution during these months*

In the end member samples such as soil, open waste burning ashes, coal and fly ash the general order of concentrations followed were (Al, Ca, Mg, Fe) > (Cd, Co, Cr, Cu, Mn, Ni, V, Pb, Zn). The individual concentrations of the components are presented in **Table 7.2.**

Table 7.2: *Elemental concentrations of NLCIL coal, fly ash, solid waste and biomass burning ash, topsoil, (mg/kg), $PM_{2.5}$ aerosols (ng/m^3)*

Sample/Sampling date	Sample type	Mg	Al	Ca	V	Cr	Mn	Fe	Co	Ni	Cu	Zn	Cd	Pb
C1AA	**COAL**	24417	161087	6424	209	294	138	84679	38	126	158	431	0.59	46
C1AB		22772	202013	7054	173	331	156	63544	38	132	45	194	0.46	37
C1A		48019	142708	27599	13	12	64	1462	126	403	8	17	0.03	0.8
C1B		33190	73454	22200	8	16	87	1566	62	246	9	13	0.02	1.0
C2A		37655	71224	15204	6	22	238	136798	5	39	8	14	0.11	1.1
TPS1EXP	**FLY ASH**	24534	185082	13400	254	261	96	32505	85	161	112	400	0.51	40
TPS2		16109	61111	7851	57	79	180	76739	17	59	12	470	0.06	9
TPS2 EXP		19212	58829	9219	74	176	355	144071	16	95	85	283	0.19	15
NTPP		13637	166049	8388	371	346	110	48567	69	150	102	109	0.24	26
Galena	**ORE**	98	11	10	0.05	2.22	8.84	581	0.26	0.22	5.93	26257	86	9850
Solid waste & biomass ash	**OTHERS**	18689	13831	6474	21	23	832	10052	4.5	12.9	31.9	220	0.09	13
		11467	17126	13132	24	37	1041	8142	4.4	19.9	42.9	614	0.64	28
		36904	53987	37377	78	96	4180	26608	14	56	111	1434	0.99	45
		26364	12946	6152	30	27	1137	13417	7	19	41	253	0.62	5
Soil 1		929	54656	315	86	140	241	32326	9.1	32.6	26.7	58	0.10	16
Soil 2		1426	17917	1098	37	83	291	18815	5.9	14.2	13.2	37	0.05	7.9
7th October 2020	**$PM_{2.5}$ Aerosols**	149	1040	405	1.7	4.2	7.1	313	0.19	3.7	6	164	1.07	27
8th October 2020		92	859	214	1.2	3.2	4.4	229	0.13	2.3	4	85	0.41	9
12th October 2020		68	692	39	0.8	5.3	4.5	204	0.11	1.7	4	121	0.75	21
14th October 2020		177	1825	406	3.0	5.9	49	555	0.38	7.6	15	424	2.90	70
15th October 2020		82	855	62	0.8	5.8	13	229	0.10	1.5	4	137	1.04	29
16th October 2020		164	1212	127	1.4	6.8	24	396	0.23	4.2	9	548	1.99	61
7th November 2020		512	5691	229	1.8	3.9	20	251	0.20	3.5	37	182	0.76	217
10th November 2020		92	940	216	1.4	2.4	6.3	219	0.13	3.6	5	184	0.64	19
14th November 2020		79	1082	168	0.8	2.3	3.8	195	0.10	2.3	3	64	0.42	4

6th December 2020		194	1901	408	2.0	13	31	432	0.35	15.5	17	355	1.57	51
12th December 2020		204	5299	319	1.5	6.8	21	329	0.15	5.9	7.9	388	2.03	51
15th December 2020		166	2142	308	1.9	4.4	23	343	0.17	3.3	6.6	276	1.37	34
5th April 2021		141	5903	178	2.6	4.1	7.9	327	0.21	3.6	6.9	122	0.52	17
7th April 2021		185	2923	271	2.6	4.3	12	536	0.28	6.2	7.1	146	0.43	13
11th April 2021		114	1751	160	1.5	3.3	4.4	229	0.14	3.8	5.2	96	0.25	10
19th May 2021		30	826	52	0.2	1.1	1.7	54	0.04	1.0	3.5	30	0.08	1.7
23th May 2021		86	2018	145	1.0	1.6	4.1	226	0.12	1.6	2.6	66	0.15	5.2
25th May 2021		1.20	11.05	2.58	0.01	0.04	0.06	3.23	0.002	0.04	0.05	1.55	0.002	0.06
26th June 2021		136	2478	170	1.6	2.9	6.1	268	0.15	2.3	2.9	75	0.31	8.4
28th June 2021		129	1583	180	1.6	2.6	6.1	279	0.18	3.4	4.7	90	0.24	5.4
30th June 2021		98	4165	144	1.7	2.3	4.5	215	0.13	5.2	5.1	59	0.13	7.4
14th October 2021		62	546	116	0.6	2.4	4.8	152	0.07	2.2	2.8	105	0.26	9.1
20th October 2021		121	1106	221	2.0	5.4	8.2	319	0.18	3.1	5.8	174	1.11	25
24th October 2021		85	1329	140	1.1	4.0	3.2	182	0.10	2.2	2.3	94	0.50	8.8
5th November 2021		156	3769	135	0.4	3.2	3.5	147	0.04	1.9	3.2	100	0.19	22
23th November 2021		124	3826	128	1.9	3.3	6.7	157	0.08	3.6	54	275	1.14	39
27th November 2021		218	1705	202	1.9	34	44	628	0.62	35	73	1067	2.49	141
5th December 2021	**$PM_{2.5}$ Aerosols**	144	2875	124	1.1	3.3	33	254	0.12	2.4	4	214	1.32	27
17th December 2021		157	4261	136	2.2	8.9	133	708	0.27	3.7	8	434	3.71	68
23th December 2021		116	2455	143	2.3	7.1	39	574	0.24	9.3	10	363	2.56	49
7th February 2022		200	2926	205	2.9	5.1	20	657	0.27	5.6	18	217	1.12	27
11th February 2022		65	795	19	0.9	1.5	6.9	192	0.07	1.7	3.1	76	0.50	18
11th February 2022		112	4393	46	1.2	5.8	10	301	0.13	2.4	3.1	152	0.62	19
15th February 2022		114	2181	123	2.0	4.3	42	355	0.18	2.4	6.7	218	1.21	23
15th February 2022		75	1359	33	1.1	7.5	22	242	0.24	1.9	3.3	563	1.11	25
17th February 2022		141	1487	67	1.6	10	13	420	0.18	2.8	5.2	488	1.12	30

The higher mean concentrations of Al, Ca, Fe and Mg in the months of April – May can be due to their higher crustal abundances. Previous studies have also reported high concentrations of these elements in both coarse and fine aerosols in different parts of India and attributed them to crustal sources(Boreddy et al., 2021; Das et al., 2015; Rastogi and Sarin, 2009; Yadav and Rajamani, 2004). The range of elemental concentrations observed in this study is similar to those reported in $PM_{2.5}$ aerosols from other regions of India (Boreddy et al., 2021; Chakraborty et al., 2023; Jain et al., 2020; Kulshrestha et al., 2009; Mehra et al., 2020; Pandey et al., 2013) (**Figure 7.4**).

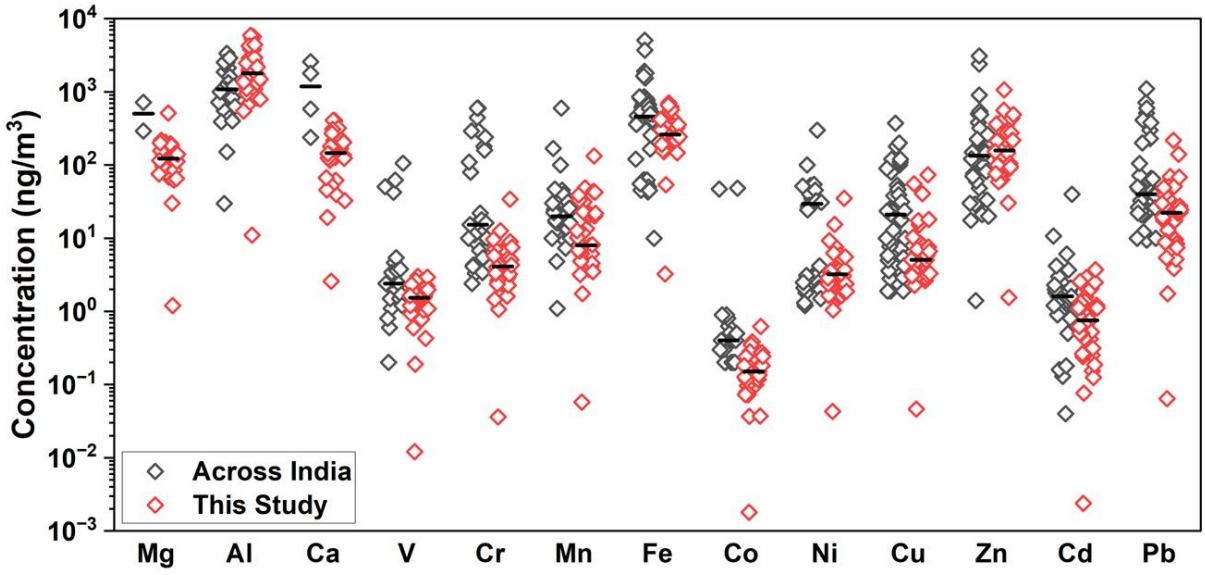

Figure 7. 4: *Comparison of elemental concentrations in Indian aerosols from previous studies across India with that of the present study at Neyveli lignite-fired power plant. The solid black lines represent the median concentration of each element*

However, when comparing median elemental concentrations specifically in $PM_{2.5}$ aerosols, Neyveli records lower median concentrations for all elements except Al and Zn. The elevated median concentration of Al, with simultaneous lower median concentrations of other elements, in the months of April – May indicates a higher contribution of crustal dust to the aerosol composition. Further insights into whether the elements have a crustal or anthropogenic origin can be inferred from the EFs, discussed later. Zinc, despite having significantly less crustal abundance compared to Ca, Fe, and Mg (Rudnick and Gao, 2003), demonstrates similar concentrations to these elements. This suggests additional anthropogenic inputs of Zn other than crust. The concentration of Pb in $PM_{2.5}$ observed in this study is lower than values reported in aerosols (TSP,

PM_{10} and $PM_{2.5}$) from urban and industrial regions of India in previous investigations (Arun et al., 2019; Balachandran et al., 2000; Bandhu et al., 2000; Basha et al., 2010; Bhuyan et al., 2018; Bikkina et al., 2015; Boreddy et al., 2021; Botle et al., 2020; Chelani et al., 2001; Das et al., 2015; R. Das et al., 2018; Dubey et al., 2012; Gaghate and Hasan, 1999; Gajghate et al., 2012; Gajghate and Bhanarkar, 2004, 2005; Gaonkar et al., 2020; Gokhale and Patil, 2004; Gummeneni et al., 2011; Jain et al., 2020; Jena et al., 2019; Karar and Gupta, 2006; Khare and Baruah, 2010; Khillare et al., 2004; Khillare and Sarkar, 2012; Kulshrestha et al., 2009; Mishra and Padmanabhamutry, 2003; Negi et al., 1986; Panda et al., 2021; Pant et al., 2015; Panwar et al., 2020; Perrino et al., 2011; Pipalatkar et al., 2014; Police et al., 2016; Sah, 2023; Sen et al., 2016; Shridhar et al., 2010; Shukkur et al., 2021; Singh and Sharma, 2012; Sudheer and Rengarajan, 2012; Yadav and Satsangi, 2013). Previous studies have reported Pb concentrations exceeding the national ambient air quality standard (NAAQS) annual average of 500 ng/m³ in industrial and major Indian cities even after the complete phase-out of leaded gasoline in the year 2000 (**Figure 7.5**). In contrast, the maximum Pb concentration recorded in this study is 79.9 ng/m³, suggesting a lower level of anthropogenic Pb pollution in the studied region compared to other parts of India.

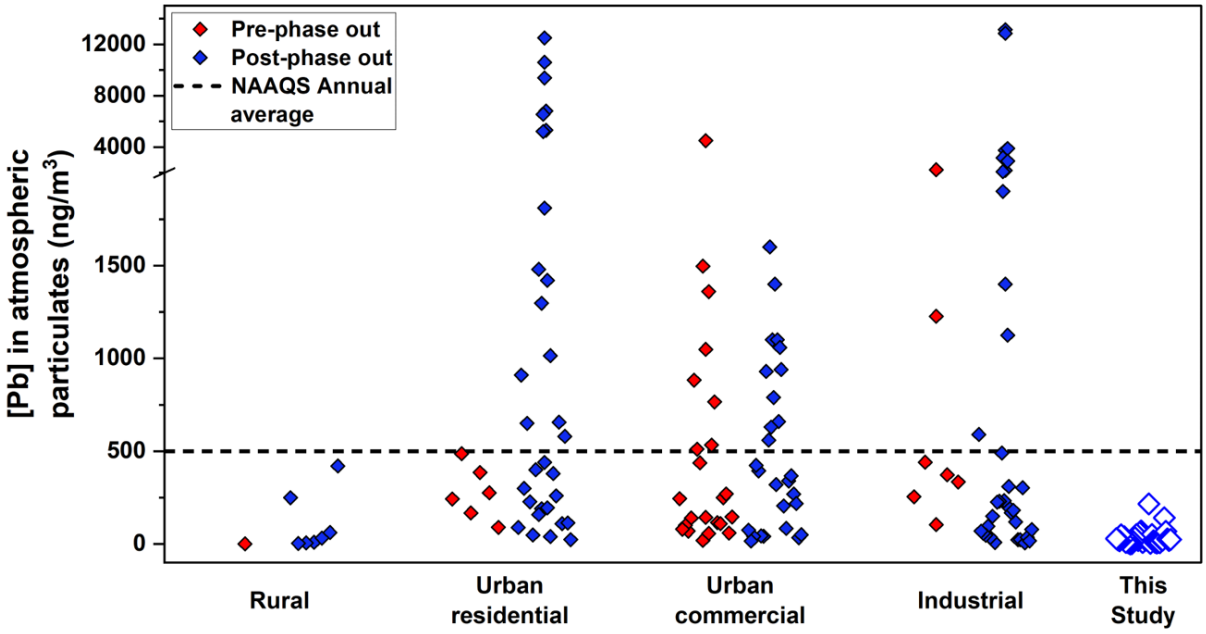

Figure 7. 5: *Concentration of Pb in atmospheric particulates compiled from previous literatures and this study. The national ambient air quality standards (NAAQS) annual average is marked for reference*

This decrease in concentration of Cr, Mn, Zn, Cd and Pb with increasing $PM_{2.5}$ load and simultaneous increase in Al concentration in the months of April – May indicate a greater influence of geogenic sources in the months of higher $PM_{2.5}$ loads. As the amount of coal combustion at the thermal power plant remained constant (A. Singh et al., 2023), it is most likely, that sources other than coal influenced the atmospheric metal concentrations of the region. To gain a better insight about the sources (geogenic or anthropogenic), of the metals the crustal EFs have been determined.

7.4. Enrichment factors and airmass back trajectories

Enrichment factors reveal that $PM_{2.5}$ aerosols were enriched in Cu, Zn, Cd and Pb (mean EF > 10) (**Figure 7.3b**), indicating anthropogenic sources. Zinc, Cd and Pb were observed to have mean EFs > 10 in all the months. Copper exhibited mean EFs < 10 in the months of April – June 2021, December 2021 and February 2022. In fact, all the enriched metals along with Mn and Co exhibited lowest EFs in the months of April – June

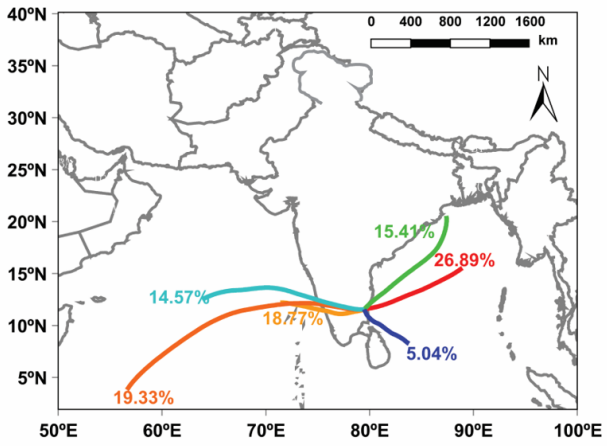

Figure 7. 6: *The 72 hr airmass back trajectory clusters for an entire year computed using geographic information system (GIS) based software TrajStat (version: 1.5.3), which utilises the HYSPLIT model for trajectory calculation*

The 72 hr airmass back trajectories for an entire year reveal that the primary origin of the airmasses are oceanic (**Figure 7.6**). From October to February, part of the airmasses originate from the land while the rest originate from the ocean. From April – June all airmasses originate from the ocean (**Figure 7.7**).

Lowest EFs in the months of April – June indicate that the atmospheric aerosols experienced a greater geogenic influence in these months. Moderate to strongly negative Spearman correlations were observed between $PM_{2.5}$ load versus the concentration of the enriched elements Cd, Pb and Zn (R = -0.56 to -0.72 and p = 0.02 – 0.09) and their EFs (R = -0.64 to -0.72 and p = 0.01 – 0.05) (**Figure 7.8**). As the operation of the lignite fired power plant was consistent throughout the sampling period (A. Singh et al., 2023), this variation in EFs must be due to other local and long-range sources.

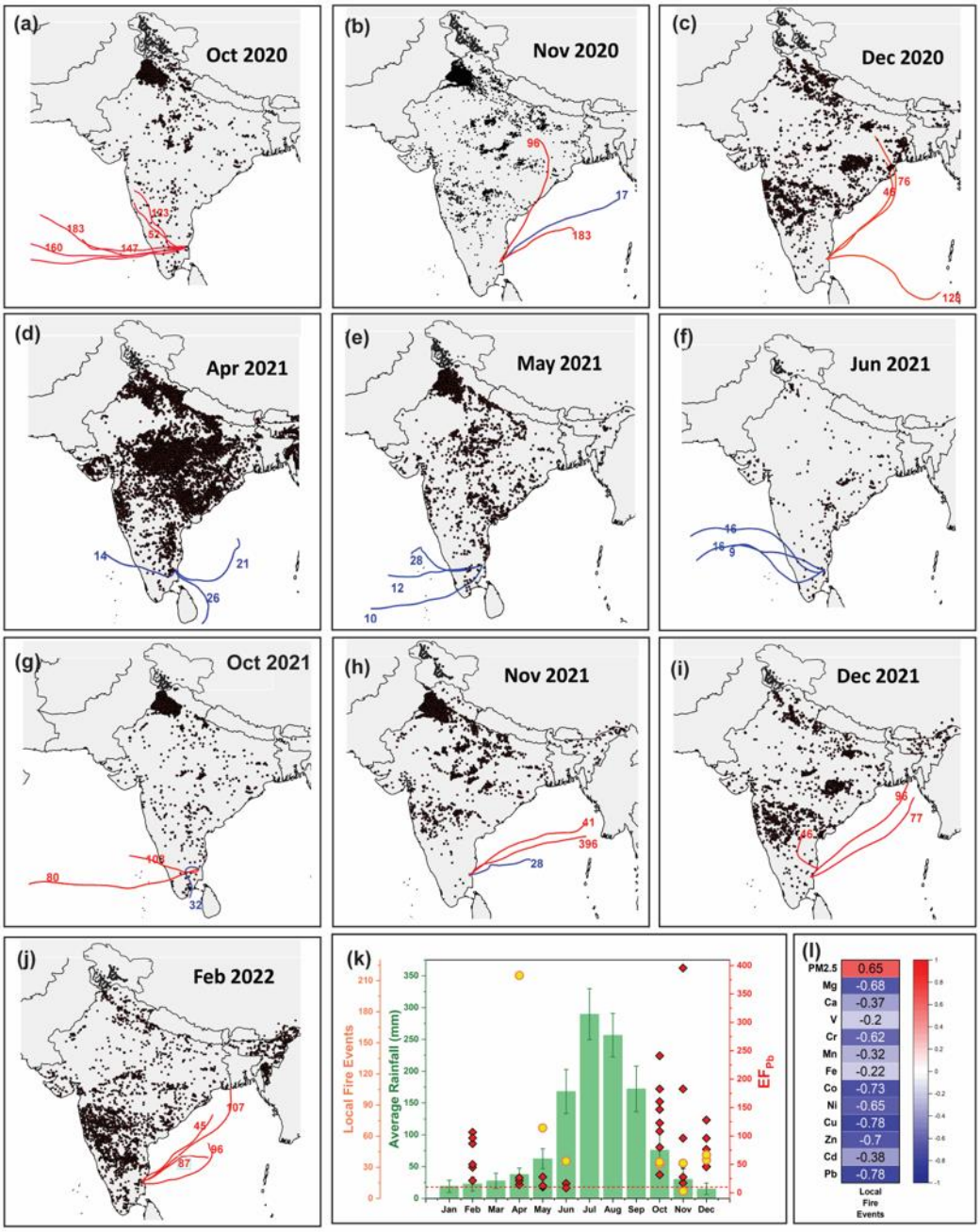

Figure 7. 7: *The 72h airmass back trajectories for the sampling days coupled with their corresponding EFs of Pb for (a) October 2020 (b) November 2020 (c) December 2020 (d) April 2021 (e) May 2021 (f) June 2021 (g) October 2021 (h) November 2021 (i) December 2021 (j) February 2022. The trajectories have been computed using geographic information system (GIS) based software TrajStat (version: 1.5.3). The airmasses with EFs < 32 are marked in blue while higher EFs are marked in red. (k) The monthly average rainfall in India (green bars) along with observed local fire events (yellow circles) around NLCIL and EFs of Pb (red diamonds) in $PM_{2.5}$ aerosols sampled at NLCIL. The red dotted line represents EF = 10. (l) Spearman Correlation between the number of local fire events versus elemental EFs in $PM_{2.5}$ aerosols. The data for the fire events has been acquired from MODIS Terra and Aqua satellites available at NASA Fire Information for Resource Management System (FIRMS)*

By coupling back trajectories with EF_{Pb}, it can be observed that the airmasses, despite having oceanic origins in the months of October – February demonstrate very high EF_{Pb} (mean = 101 ± 38). While, similar oceanic origin airmasses in the months of April – June, demonstrate $EF_{Pb} \leq 28$ (mean = 17 ± 7) in $PM_{2.5}$ (**Figure 7.7**). In India, the months of October to December mark the post-monsoon season, while April to June corresponds to the summer season. During the post-monsoon period, temperatures begin to fall, especially during the night across India, and wind patterns shift, signaling the onset of colder weather (Anu and Mohanakumar, 1996).The changing wind patterns lead to wind blowing from the land to the sea, transporting pollutants from the land surface to over the ocean. The northern Bay of Bengal (BoB) remains under the influence of airmasses from Indo Gangetic plain while the south eastern BoB receives air masses from south east Asia (Aryasree et al., 2015; Srinivas et al., 2011). Similarly, the southern Arabian Sea remains under the influence of western and southern India (Krishnamurti et al., 2009). Thus, the high EF_{Pb} in airmasses originating from the ocean during post-monsoon period can be attributed to the transport of pollutants from land to sea due to prevailing wind patterns. Further, the mean temperature is lower and as a result, temperature inversion traps cooler air beneath a layer of warmer air. This cooler air confines within it the ground-level pollution and thus, increases the pollution levels in the air masses just above the ground surface (EEA, 2016). Long-term (2010–2018) LIDAR observations and radiosonde data from Gadanki (a rural site approximately 280 km north of Neyveli), indicates that thermal inversion can fully control the vertical extent of aerosols(Prasad et al., 2022). Further research across various locations in India confirmed that thermal inversion, rather than the atmospheric boundary layer, predominantly restricts aerosol vertical distribution. In contrast to the post-monsoon months, the lower EF_{Pb} during April to June can be due to a reduced land-based pollution influence over the ocean. In fact, during the summer months there is a decrease in the EF of all the heavy metals compared to the post-monsoon period. (**Figure 7.3 b**) There was also an increase in local fire events in the months of April and May compared to October to December (**Figure 7.7 a-k**), that could have resuspended a higher amount of desiccated crustal dust resulting in an increased $PM_{2.5}$ load and simultaneous decreased EF (Das et al., 2023; Wagner et al., 2018). A Spearman

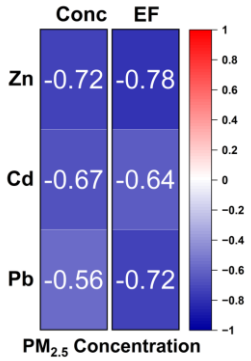

Figure 7. 8: *Spearman correlations between $PM_{2.5}$ concentration versus the concentration (conc) of the enriched elements Cd, Pb and Zn (p = 0.02 – 0.09) as well as the enrichment factors (EF) of the enriched elements*

correlation between the number of fire events versus EFs reveals strong negative correlation with anthropogenic elements and positive correlation with $PM_{2.5}$ load. (**Figure 7.7 l**). Thus, the post-monsoon months may have been influenced by both long range as well as local sources, while local sources were predominant in the summer months. A better understanding of the sources can be obtained from elemental ratios.

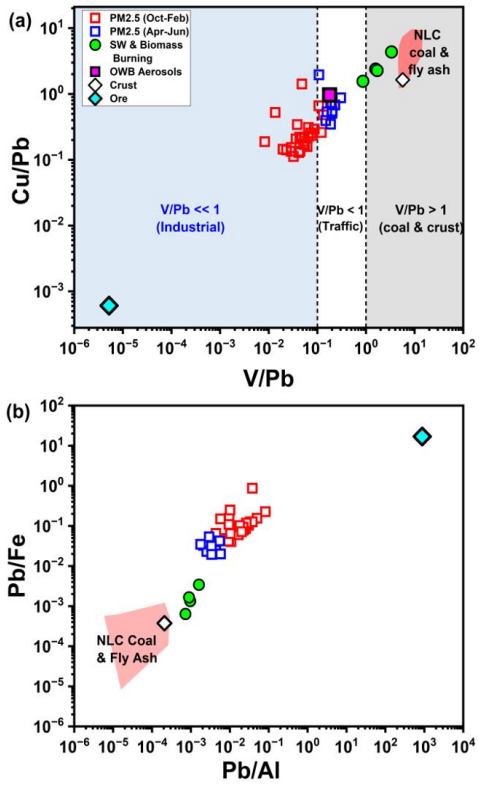

Figure 7. 9: *Elemental ratios plotted as (a) V/Pb vs Cu/Pb (b) Pb/Al vs Pb/Fe indicate that the $PM_{2.5}$ aerosols are a mixture of crust, coal & fly ash, solid waste & biomass burning and industrial smelting (depicted as ore in the figure). The characteristic V/Pb ratios for industrial, traffic and coal/crustal sources (Das et al., 2018) are marked as shaded regions for reference. The October-February aerosols have V/Pb<<1 and hence plot in the region of industrial emissions. The open waste burning aerosols from Delhi's Okhla landfill site (Kumar et al., 2018) overlapping with April-June aerosols is plotted in V/Pb vs Cu/Pb space for reference. The April-June aerosols seem to be more influenced by solid waste & biomass burning and crustal sources with decreased Pb/Fe and Pb/Al ratios than the October-February aerosols. The elemental concentration data for crust has been adopted from Rudnick and Gao 2003.*

7.5. Elemental ratios as source tracers

Elemental ratios are useful tracers for understanding pollution sources. Ratio between V and Pb (V/Pb) are tracers for coal combustion, vehicular and industrial emissions. Coal combustion typically has V/Pb ratios of > 1, in contrast to vehicle exhaust emissions, where V/Pb < 1, and industrial emissions, where V/Pb << 1(R. Das et al., 2018; Kumar et al., 2016; Sen et al., 2016). None of the aerosol samples exhibited V/Pb > 1. Instead, all the V/Pb ratios for the aerosols varied in the region of industrial and traffic emission source signatures. A bivariate plot between V/Pb and enriched elements such as Cu/Pb can provide insights about the various sources of metals in $PM_{2.5}$. The plot (**Figure 7.9 a**), reveals that the aerosols do not align with the ratios of the coal and fly ash, despite the aerosols being sampled from the vicinity of a coal fired power plant. In Cu/Pb vs V/Pb space, the crust-coal-fly ash and base metal ore (galena) depict two extreme end members with the signature of open SW & biomass burning lying in between (**Figure 7.9 a**). The $PM_{2.5}$ samples fall in between these three end members suggesting a mixture of these three sources. However, a seasonal difference in these ratios can be observed. In the months of October – February, majority of the aerosols have V/Pb << 1. In contrast, from April – June the aerosols shift towards SW & biomass burning with V/Pb ratios

typical of traffic emissions. Moreover, previously sampled aerosols from Delhi's waste dumping site Okhla also overlaps with April – June aerosols from Neyveli, indicating a strong presence of metals generated from SW & biomass burning (Kumar et al., 2018).

During the months of April – June a lower Pb/Al as well as Pb/Fe ratios were observed compared to the post-monsoon months. This suggests a greater crustal contribution during the summer months, likely due to increased pollutant dispersion resulting from absence of temperature inversion, as well as a stronger influence from local biomass burning events. Local evidences of sugarcane residue burning were observed on site. In Tamil Nadu, the primary crops are rice and sugarcane, with sugarcane being the dominant crop, produced at nearly three times the quantity of rice (Sahu et al., 2021). Of the total crop yield, approximately 13% is burnt as residue. Notably, certain areas in Tamil Nadu are also recognized as hotspots for PM emissions resulting from the burning of crop residues generated from rice, wheat, maize, and sugarcane cultivation (Sahu et al., 2021). The concentration of Pb in biomasses is typically much less than other industrial processes, that may have resulted into a lower Pb/Al and Pb/Fe ratios from April – June compared to the post-monsoon months. A bivariate plot between Pb/Al and Pb/Fe (**Figure 7.9 b**) provides similar inferences as the Cu/Pb vs V/Pb plot, with all the aerosols falling between crust, coal & fly ash, SW & biomass burning and ore. The summer aerosols lie closer to the open waste burning signatures and crust compared to post-monsoon aerosols. This suggests that, there can be a greater influence of crust in the summer aerosols compared to the post-monsoon ones. Moreover open burning of biomass and SW, together with emitting signatures from vegetation and SW also dehydrates the soil, increases local atmospheric turbulence due to fire related convective currents and subsequently mobilises the dehydrated soil particles in the air (Wagner et al., 2018). Thus, the elemental compositions during fire events may include signatures from vegetation and SW combustion, as well as contributions from crustal dust due to soil resuspension.

7.6. Pb isotopic compositions as source tracers

The mean Pb isotopic composition of the $PM_{2.5}$ samples and end members are presented in **Table 7.3**. The individual composition of each sample is presented in **Table 7.4**. The lignite and fly ash of the region are significantly different from coal samples found in other parts of India (R. Das et al., 2018). The Neyveli lignite is characterized by low $^{206}Pb/^{207}Pb$ ratios and higher $^{208}Pb/^{206}Pb$ ratios compared to other coals, indicating high Thorium contents.

Table 7.3: *Mean Pb isotopic composition of NLCIL coal & fly ash, local solid waste & biomass burning ashes, NLCIL topsoil, ore and $PM_{2.5}$ aerosols sampled in the years 2020, 2021 and 2022.*

SAMPLE	N	PARAMETER	$^{208}Pb/^{206}Pb$	$^{206}Pb/^{207}Pb$	$^{208}Pb/^{207}Pb$	$^{206}Pb/^{204}Pb$	$^{207}Pb/^{204}Pb$	$^{208}Pb/^{204}Pb$
Coal and Fly Ash	9	Mean	2.2570	1.0961	2.4734	17.1161	15.6134	38.6164
		Standard Deviation	0.0430	0.0185	0.0160	0.3375	0.0669	0.3180
Solid Waste & Biomass Burning	6	Mean	2.1451	1.1349	2.4343	17.7173	15.6116	38.0035
		Standard Deviation	0.0291	0.0058	0.0263	0.1225	0.0385	0.3701
NLCIL Topsoil	2	Mean	2.1940	1.1193	2.4556	17.4213	15.5643	38.2196
		Standard Deviation	0.0204	0.0140	0.0078	0.2472	0.0261	0.1862
Ore	3	Mean	2.2027	1.0543	2.3223	16.5364	15.6842	36.4244
		Standard Deviation	0.0006	0.0007	0.0010	0.0427	0.0296	0.0844
$PM_{2.5}$ AEROSOLS								
October 2020	6	Mean	2.1252	1.1342	2.4104	17.6910	15.5974	37.5958
		Standard Deviation	0.0082	0.0053	0.0020	0.0846	0.0069	0.0381
November 2020	3	Mean	2.1267	1.1345	2.4128	17.6925	15.5946	37.6267
		Standard Deviation	0.0043	0.0041	0.0038	0.0683	0.0166	0.0772
December 2020	3	Mean	2.1239	1.1360	2.4127	17.7188	15.5977	37.6321
		Standard Deviation	0.0039	0.0033	0.0027	0.0578	0.0062	0.0537
April 2021	3	Mean	2.1176	1.1419	2.4180	17.8250	15.6104	37.7460
		Standard Deviation	0.0026	0.0025	0.0023	0.0406	0.0046	0.0411

May 2021	3	Mean	2.1244	1.1368	2.4151	17.7476	15.6114	37.7038
		Standard Deviation	0.0013	0.0018	0.0024	0.0239	0.0088	0.0312
June 2021	3	Mean	2.1195	1.1411	2.4186	17.8177	15.6145	37.7646
		Standard Deviation	0.0095	0.0083	0.0068	0.1190	0.0131	0.0833
October 2021	3	Mean	2.1300	1.1308	2.4086	17.6277	15.5887	37.5465
		Standard Deviation	0.0066	0.0059	0.0053	0.0605	0.0298	0.0192
November 2021	3	Mean	2.1232	1.1372	2.4144	17.7247	15.5865	37.6324
		Standard Deviation	0.0074	0.0071	0.0072	0.1329	0.0190	0.1565
December 2021	3	Mean	2.1242	1.1355	2.4121	17.7092	15.5953	37.6180
		Standard Deviation	0.0077	0.0068	0.0058	0.1222	0.0164	0.1241
February 2022	6	Mean	2.1221	1.1380	2.4149	17.7583	15.6051	37.6855
		Standard Deviation	0.0028	0.0031	0.0035	0.0541	0.0067	0.0687

Table 7.4: *Pb isotopic concentrations of NLCIL coal, fly ash, solid waste and biomass burning ash, topsoil and $PM_{2.5}$ aerosols*

Sample/Sampling date	Sample Type	$^{208}Pb/^{206}Pb$	$^{206}Pb/^{207}Pb$	$^{208}Pb/^{207}Pb$	$^{206}Pb/^{204}Pb$	$^{207}Pb/^{204}Pb$	$^{208}Pb/^{204}Pb$
C1AA	**COAL**	2.2297	1.1119	2.4791	17.4622	15.7052	38.9348
C1AB		2.2533	1.0995	2.4776	17.2642	15.7016	38.9020
C1A		2.2096	1.1085	2.4494	17.2618	15.5718	38.1414
C1B		2.2165	1.1116	2.4639	17.3363	15.5871	38.3932
C2A		2.2283	1.1177	2.4905	17.4690	15.6294	38.9255
TPS1EXP	**FLY ASH**	2.3208	1.0754	2.4957	16.7379	15.5649	38.8458
TPS2		2.2897	1.0726	2.4559	16.6691	15.5408	38.1667
TPS2 EXP		2.2452	1.0972	2.4635	17.2027	15.6784	38.6229
NTPP		2.3204	1.0708	2.4846	16.6418	15.5419	38.6154
Galena 1	**ORE**	2.2028	1.0538	2.3215	16.5105	15.6663	37.3708
Galena 2		2.2031	1.0539	2.3219	16.5131	15.6679	36.3808
Galena 3		2.2020	1.0551	2.3234	16.5857	15.7183	36.5218
Solid waste & biomass ash	**OTHERS**	2.1512	1.1299	2.4306	17.6248	15.5986	37.9135
		2.1268	1.1342	2.4124	17.7653	15.6625	37.7837
		2.1407	1.1322	2.4237	17.6369	15.5771	37.7550
		2.1081	1.1461	2.4161	17.9452	15.6580	37.8310
		2.1492	1.1348	2.4390	17.6813	15.5806	38.0014
Soil 1		2.1795	1.1292	2.4611	17.2465	15.5459	38.0880
Soil 2		2.2084	1.1094	2.4500	17.5960	15.5827	38.3513
7th October 2020	**$PM_{2.5}$ Aerosols**	2.1289	1.1321	2.4100	17.6702	15.6089	37.6172
8th October 2020		2.1282	1.1324	2.4099	17.6543	15.5907	37.5713
12th October 2020		2.1322	1.1292	2.4076	17.6101	15.5957	37.5485
14th October 2020		2.1270	1.1331	2.4101	17.6704	15.5953	37.5855
15th October 2020		2.1090	1.1444	2.4136	17.8554	15.6021	37.6579
16th October 2020		2.1257	1.1343	2.4112	17.6855	15.5914	37.5944

7th November 2020	**$PM_{2.5}$ Aerosols**	2.1225	1.1386	2.4168	17.7691	15.6056	37.7155
10th November 2020		2.1265	1.1345	2.4125	17.6704	15.5756	37.5759
14th November 2020		2.1311	1.1304	2.4091	17.6379	15.6026	37.5886
6th December 2020		2.1218	1.1376	2.4138	17.7517	15.6040	37.6654
12th December 2020		2.1214	1.1382	2.4146	17.7526	15.5974	37.6608
15th December 2020		2.1284	1.1321	2.4096	17.6520	15.5917	37.5702
5th April 2021		2.1146	1.1447	2.4207	17.8706	15.6114	37.7900
7th April 2021		2.1188	1.1407	2.4170	17.8113	15.6144	37.7393
11th April 2021		2.1193	1.1402	2.4164	17.7930	15.6053	37.7085
19th May 2021		2.1252	1.1356	2.4135	17.7249	15.6080	37.6694
23th May 2021		2.1229	1.1389	2.4179	17.7726	15.6048	37.7303
25th May 2021		2.1251	1.1360	2.4141	17.7454	15.6213	37.7115
26th June 2021		2.1211	1.1388	2.4156	17.7971	15.6277	37.7500
28th June 2021		2.1094	1.1503	2.4263	17.9457	15.6015	37.8543
30th June 2021		2.1281	1.1342	2.4138	17.7102	15.6143	37.6895
14th October 2021		2.1374	1.1241	2.4027	17.5583	15.6193	37.5288
20th October 2021		2.1278	1.1327	2.4101	17.6557	15.5871	37.5670
24th October 2021		2.1248	1.1356	2.4129	17.6692	15.5597	37.5436
5th November 2021		2.1317	1.1290	2.4066	17.5722	15.5646	37.4582
23th November 2021		2.1196	1.1421	2.4208	17.8154	15.5989	37.7611
27th November 2021		2.1183	1.1405	2.4159	17.7865	15.5960	37.6777
5th December 2021		2.1244	1.1360	2.4132	17.7056	15.5865	37.6132
17th December 2021		2.1165	1.1421	2.4173	17.8331	15.6142	37.7444
23th December 2021		2.1318	1.1286	2.4059	17.5887	15.5851	37.4964
7th February 2022		2.1226	1.1365	2.4124	17.7245	15.5952	37.6219
11th February 2022		2.1184	1.1423	2.4198	17.8366	15.6152	37.7849
11th February 2022		2.1191	1.1416	2.4192	17.8184	15.6080	37.7595
15th February 2022		2.1234	1.1365	2.4131	17.7301	15.6013	37.6478
15th February 2022		2.1252	1.1354	2.4129	17.7199	15.6069	37.6583
17th February 2022		2.1242	1.1356	2.4122	17.7202	15.6043	37.6407

To identify the sources, aerosol samples and potential end members are plotted in a three-isotope space using the ratios of $^{208}Pb/^{206}Pb$ vs $^{206}Pb/^{207}Pb$ (**Figure 7.10**). Thus, in the three-isotope space two distinct mixing lines can be formed, each with the natural background crust at one end. One of the mixing lines extends to Neyveli lignite (blue dotted line), while the other extends to Indian ore (black dotted lines) at their respective ends (**Figure 7.10**).

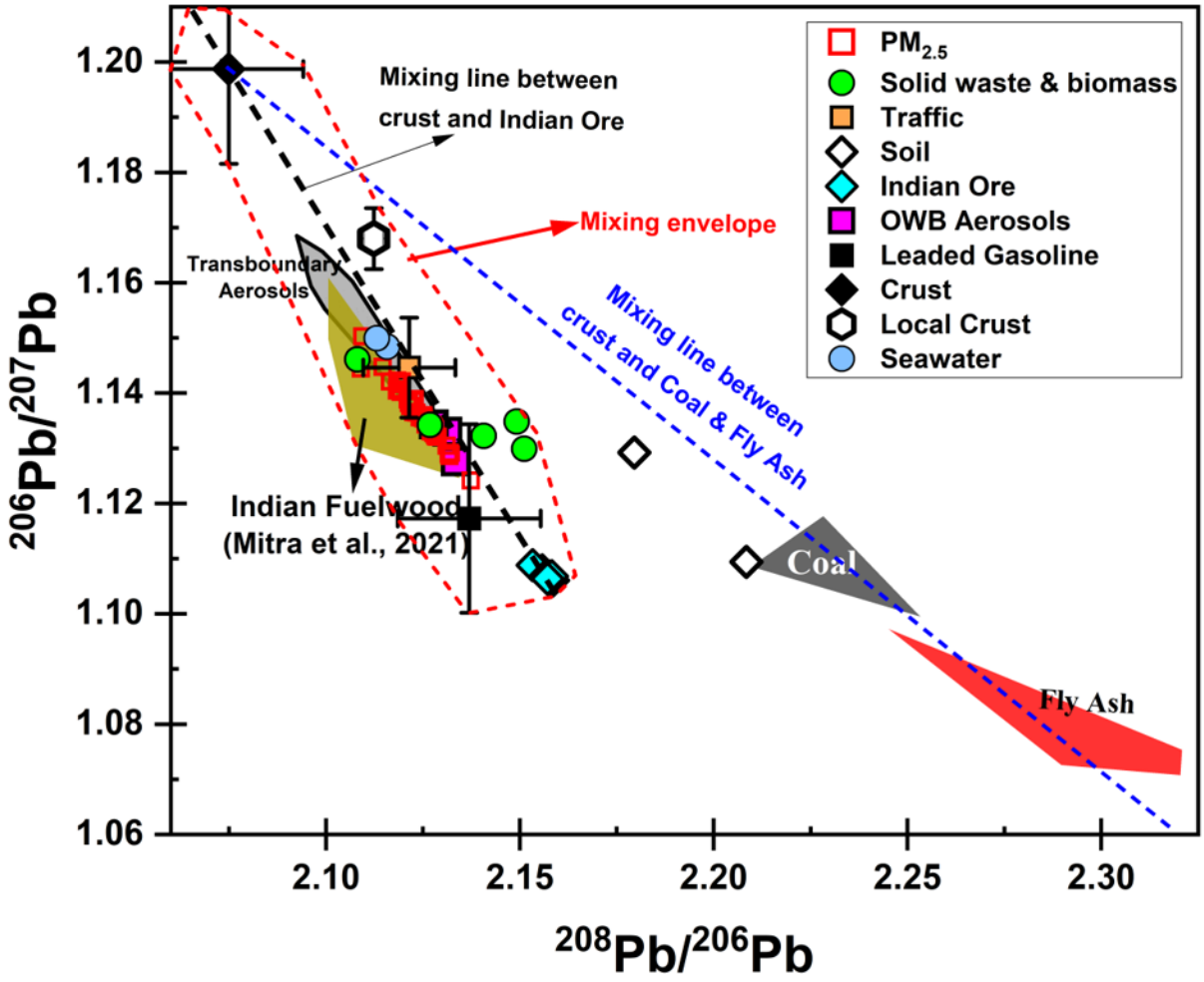

Figure 7. 10: *The Pb isotopic compositions of the $PM_{2.5}$ aerosols and relevant end members illustrated in three-isotope space ($^{208}Pb/^{206}Pb$ vs $^{206}Pb/^{207}Pb$). Two distinct mixing lines are observed, each with crust at one end: one extends to Neyveli lignite (blue dotted line), while the other extends to Indian ore (black dotted lines). The Pb isotopic compositions of the PMs lie along the mixing line between Indian ore and crust, rather than local lignite and fly ashes. The aerosols lie close to vehicular exhaust emissions (traffic) and seawater, with less radiogenic local crust also plotting close to the aerosols compared to UCC. There is a considerable overlap between the aerosols and Indian fuelwood, local solid waste & biomass burning signatures. Isotopic signatures of previously sampled aerosols from Delhi's Okhla landfill, overlap with the Neyveli aerosols. The enclosure formed by the red dotted line signifies the mixing envelope formed using the relevant end members. The data for Indian fuelwood and OWB aerosols have been adopted from Mitra et al., 2021 and Kumar et al., 2018 respectively. Data for traffic emissions, Indian ore, crust, seawater, and local crust have been compiled from Ray and Das 2023, Deb et al., 1989, Lee et al., 2015 and Chakraborty et al., 2021 respectively*

The Pb isotopic compositions of the PMs lie along the mixing line between Indian ore and crust (Bi et al., 2017; Deb et al., 1989; Mitra et al., 2021), instead of the local lignite and fly ashes (**Figure 7.10**). In fact, the $PM_{2.5}$ samples demonstrate significantly dissimilar compositions from coal and fly ash, indicating minimal influence from them. The Pb isotopic composition of the aerosols lie in the vicinity of vehicular exhaust emissions and seawater (Lee et al., 2015; Ray and Das, 2023b). Local crust being significantly less radiogenic also lies close to the aerosols compared to upper continental crust (UCC) (Chakraborty et al., 2021; Millot et al., 2004). Notably, there is a considerable overlap of the aerosols with that of Indian fuelwood (Mitra et al., 2021) and local SW & biomass burning signatures. Isotopic signatures of previously sampled aerosols from Delhi's Okhla landfill, where burning is prevalent also overlap with the Neyveli aerosols (Kumar et al., 2018). In the post-monsoon months as some of the airmasses originate from the coasts of southeast Asia, influence of transboundary aerosols can be present (**Figure 7.7 h-j**). In fact, the Neyveli $PM_{2.5}$, aerosols have substantial overlap with aerosols from Thailand, indicating presence of transboundary sources in the post-monsoon months (**Figure 7.9**). The mean Pb isotopic composition of the summer aerosols is about 6 ‰ more radiogenic in terms of $^{206}Pb/^{207}Pb$ and $^{208}Pb/^{206}Pb$ ratios than the post-monsoon aerosols indicating a seasonal shift in sources (**Table 7.3**). A higher radiogenic signature can be indicative of higher natural contributions (crust and seawater). This increase in crustal component can be due to airmasses originating from ocean (**Figure 7.7**) and soil resuspension due to burning. This increased resuspension during burning, also may mobilize the Pb deposited in the past century from leaded gasoline use. Lead emitted from leaded gasoline in the 20th century was eventually deposited onto soils, where it accumulated over time. Due to its long residence time of approximately 200 years in soil (Erel, 1998), Pb remains bound to soil particles. However, during fire events, the intense heat and turbulence cause the desiccated soil to become airborne, resuspending the previously deposited Pb back into the atmosphere. Recent studies have found evidences of such resuspended Pb contributing towards atmospheric Pb load (Ray and Das, 2023b; Resongles et al., 2021) Consequently, leaded gasoline also comes into play as a potential source. There are evidences from across the globe, demonstrating that leaded gasoline is still recirculating in the atmosphere (Carrasco et al., 2018; Ray and Das, 2023b; Resongles et al., 2021). Previous study in the Indo-Gangetic plain finds evidence of high contribution of legacy lead in biomass samples (Mitra et al., 2021). Thus, the aerosols are primarily a mixture of open waste burning, industrial smelting, traffic emissions,

natural sources (crust and seawater), and leaded gasoline, with their respective contribution varying in summer and post-monsoon period. The regional soil appears to have been contaminated by the coal combustion process.

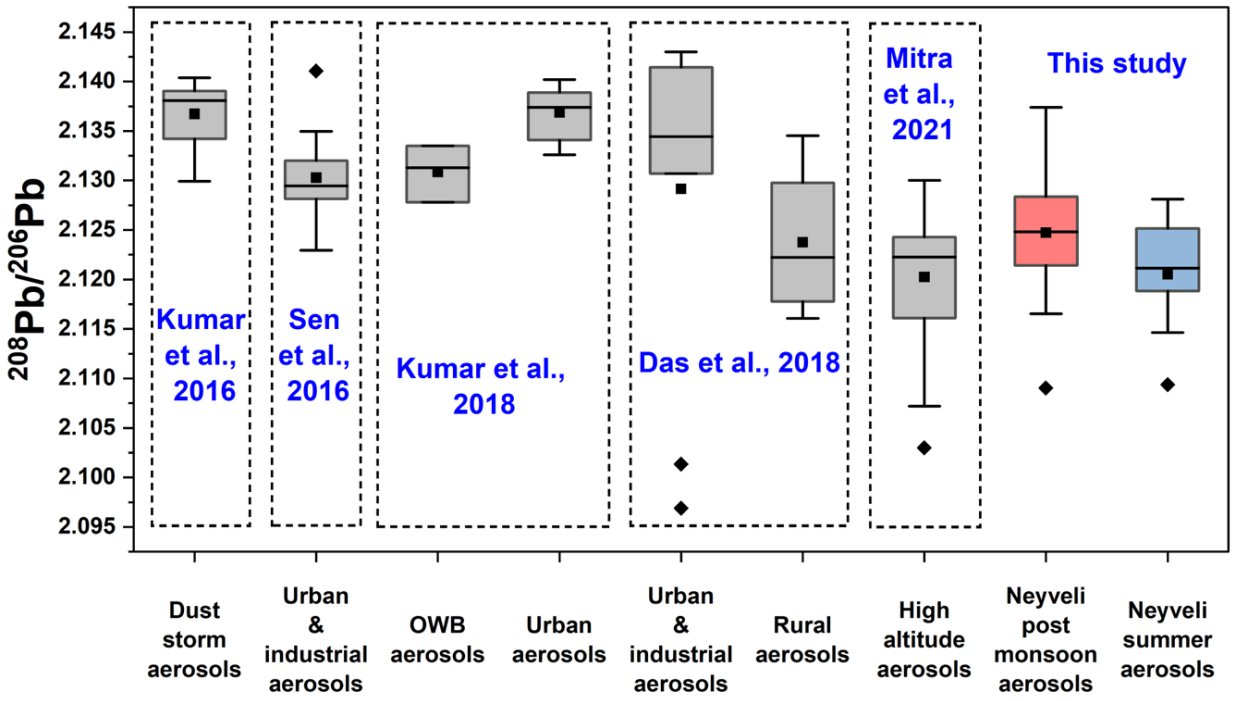

Figure 7. 11: *Comparison of $^{208}Pb/^{206}Pb$ ratios of Indian aerosols from previous studies across various settings (urban, rural, industrial, and waste-burning) with the ratios observed in the present study. The solid black squares and lines represent mean and median values respectively. The outliers are represented by solid black diamonds. The upper and lower extremes of the boxes represent 75th and 25th percentile values respectively while the upper and lower extremes of the whiskers represent 90th and 10th percentiles respectively.*

Over the past decade, only five studies have measured the Pb isotopic compositions of Indian aerosols, primarily in PM_{10} samples from diverse settings, such as urban, rural, industrial, and waste-burning sites.(R. Das et al., 2018; Kumar et al., 2016, 2018; Mitra et al., 2021; Sen et al., 2016). As Pb mostly concentrates in the finer fraction of the aerosols, Pb isotopic composition can be considered a reliable tracer of anthropogenic emissions. Thus, a comparison between Pb isotope ratios can provide insights into the distinct influences on aerosol isotopic composition in different environments. In $^{208}Pb/^{206}Pb$ space (**Figure 7.11**), aerosols linked to industrial and urban sources exhibit higher $^{208}Pb/^{206}Pb$ ratios compared to Neyveli $PM_{2.5}$ aerosols (R. Das et al., 2018; Kumar et al., 2018; Sen et al., 2016). Dust storm aerosols show significantly different median ratios due to the influence of dust from the Middle East (Mood's median test; $p < 0.0003$) (Kumar et al.,

2016). The study conducted in Delhi's open-waste burning (OWB) site and urban area records lower median $^{208}Pb/^{206}Pb$ ratios (median = 2.1313) in the OWB aerosols compared to the urban ones (median = 2.1374) (Kumar et al., 2018). Thus, the median $^{208}Pb/^{206}Pb$ ratios of the OWB aerosols plot closer to the median $^{208}Pb/^{206}Pb$ ratios of Neyveli aerosols. The closest median $^{208}Pb/^{206}Pb$ ratios to the Neyveli $PM_{2.5}$ aerosols ($median_{post\text{-}monsoon} = 2.1248$; $median_{summer} = 2.1211$) are observed in rural aerosols (median = 2.1222) and high-altitude aerosols (median = 2.1222). Rural aerosols can be under the influence of biomass burning as a source of fuelwood, while the high altitude aerosols are proven to have been influenced by wood charcoal burning (Mitra et al., 2021). In fact, the Pb isotopic compositions of the wood charcoal have significant overlap with the Neyveli aerosols in the triple isotope space (**Figure 7.10**). During the post-monsoon season the Neyveli aerosols exhibit higher $^{208}Pb/^{206}Pb$ ratios compared to the summer samples indicating increased influence from the urban and industrial sources (**Figure 7.11**).

7.7. Quantifying relevance of sources

In the 3D mixing polygon simulation, the median probabilities of all the aerosols falling inside the mixing envelope formed by sources indicate whether all sources have been considered or some are missing (Smith et al., 2013). In this simulation, polygons, that is, convex hulls (mixing envelops) are generated (1500 iterations) based on the distribution of the considered sources and their SDs. The mixing polygon simulation is based on the principle that the isotopic composition of the mixture (aerosols for this study) can be explained by the isotopic compositions of the sources forming the mixing envelope only if the mixture doesn't fall outside 5 % of the generated polygons. The sample(s) with less than 5 % probabilities has/ve sources other than the considered end members and hence the selected sources cannot explain the composition of that particular mixture. From the elemental ratios and the mixing line in the triple isotope plot, it is evident that the relevant sources are: crust, vehicle exhaust, SW & biomass burning and industrial smelting. In the post-monsoon months, significant amounts of airmass originate from the coasts of southeast Asia (**Figure 7.7**), thus, making it necessary to consider the transboundary aerosol as a source in the months of October – February. Incorporating the mean Pb isotopic composition of Thailand aerosols (Kayee et al., 2021, 2020) as a source significantly increases the median probability by 11 % (ANOVA; $p < 0.0001$). In the summer months the airmasses primarily originate from the ocean, making it a crucial component of the mixing envelope. Including seawater as a source increased the probability by 4.3 %. Leaded gasoline, though phased out in 2000, can still contribute

to $PM_{2.5}$ aerosols through soil resuspension (Carrasco et al., 2018; Mitra et al., 2021; Ray and Das, 2023b; Resongles et al., 2021). In the triple isotope space, leaded gasoline plots close to the less radiogenic $PM_{2.5}$ aerosols. Including leaded gasoline as a source significantly increases the median probability (ANOVA; $p < 0.0001$), validating it as a necessary end member. Finally, as the local crust of southern India, is significantly different from UCC, it is also considered as a source (Chakraborty et al., 2021; Millot et al., 2004).

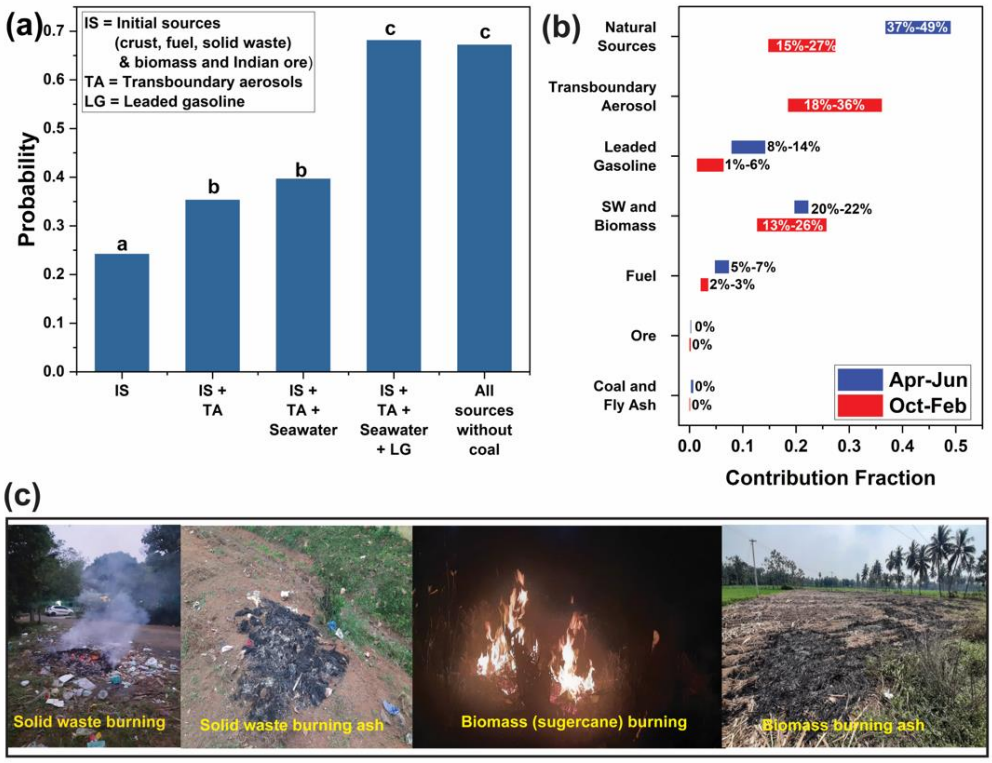

Figure 7. 12: (a) *Bar plots depicting the median probability of the aerosol mixtures to fall inside the mixing envelope constructed by the initial and additional sources with each source added successively. The probabilities are determined with the help of 3 – dimensional mixing polygon simulation in $^{206}Pb/^{207}Pb$, $^{208}Pb/^{207}Pb$ and $^{208}Pb/^{206}Pb$ space. Same letters above the bars indicate that the probabilities are not significantly different, as determined by Tukey's method. Addition of transboundary aerosols and leaded gasoline significantly increased the median probability. Exclusion of Neyveli coal & fly ash does not affect the results. (b) Median contribution of individual sources towards atmospheric Pb determined from MixSIAR simulation. The percentages over/beside the bars represent the range of contributions from each source. MixSIAR results indicate negligible influence of coal and fly ash throughout the year in the vicinity of lignite fired powerplant. Open burning of solid waste and biomass emerges as the major anthropogenic contributor, even in a region of coal combustion. (c) Field photographs of solid waste & biomass burning at Neyveli.*

Figure 7.12a illustrates all the changes in the median probabilities as each source is successively added. None of the aerosol samples demonstrated probability < 5 %. By incorporating all these sources to define the mixing envelope, the total median probability reaches 0.68. This indicates that all aerosols are a mixture of the accounted sources with varying contributions from respective

sources. Despite differing in isotopic and elemental compositions, coal and fly ash must be considered as sources, as the aerosol samples are from a lignite-fired power plant. However, the inclusion of coal & fly ash as a source does not increase the probability at all (**Figure 7.12 a**), indicating limited influence of the source on $PM_{2.5}$ aerosols. Thus, the mixing envelope (marked in red dotted line in **Figure 7.11**, comprises of UCC, local crust, seawater, vehicular fuel, SW & biomass burning, Indian fuelwood, transboundary aerosols and Indian ore. The mean Pb isotopic compositions, and Pb concentrations of all the sources fed to the simulation along with their references are listed in **Table 7.5**

Table 7.5: *Mean Pb isotopic composition, and standard deviation inputs for MixSIAR and polygon simulations.*

Sources	Mean $^{206}Pb/^{207}Pb$	SD $^{206}Pb/^{207}Pb$	Mean $^{208}Pb/^{207}Pb$	SD $^{208}Pb/^{207}Pb$	Mean $^{208}Pb/^{206}Pb$	SD $^{208}Pb/^{206}Pb$	Concentration (ppm)	n	References
Coal and Fly Ash	1.0961	0.0185	2.4733	0.0159	2.2570	0.0429	19	9	This study
Ore	1.0539	0.0260	2.3275	0.0283	2.2104	0.0263	80*	53	Deb et al., 1989; Zhang et al., 2022
Fuel	1.1459	0.0188	2.4315	0.0207	2.1231	0.0208	6	31	Ray and Das 2023
SW and biomass	1.1375	0.0101	2.4168	0.0116	2.1246	0.0153	10	18	This study and Mitra et al., 2021
Crust	1.2005	0.0267	2.4915	0.0292	2.0758	0.0268	17	4	Millot et al., 2004
Local Topsoil	1.1680	0.0055	2.4671	0.0087	2.1123	0.0025	17	2	Chakraborty et al., 2021
Leaded Gasoline	1.1172	0.0170	2.3867	0.0175	2.1369	0.0184	48	7	Ray and Das 2023
Seawater	1.1499	0.0067	2.4298	0.0069	2.1131	0.0068	0.000076	50	Lee et al., 2015
Transboundary Aerosol (Only considered for Oct-Feb aerosols)	1.1501	0.0058	2.4277	0.0063	2.1109	0.0063	0.014	95	Kayee et al., 2020, 2021

*The concentration of Pb in ore was calculated as: Pb emitted = Total [Pb] in ore × (1-Removal efficiency) (99.7 %)
The MixSIAR simulation was performed as a concentration dependent model with the concentration inputs in ppm

7.8. Quantification of end member contributions

The MixSIAR model results reveal a seasonal change in contribution percentages of the sources. The mean Pb isotopic composition of the considered sources along with their standard deviations and concentrations are presented in **Table 7.5.**

The quantification of the contribution of these sources is performed using Bayesian statistical model MixSIAR in R, presented in **Figure 7.12b**. Transboundary aerosols are only relevant in the post-monsoon months due to long range transport during the season and contributes up to 36 %. However, consistent contribution from SW and biomass burning was observed across the seasons (up to 26 % in post-monsoon season and up to 22 % in summer), indicating their significant role as a pollution source throughout the year. In both post-monsoon and summer months there are significant contributions from background natural sources. (crust + seawater). This contribution from natural sources increases in the summer months, with maximum contribution reaching up to 49 %, which is 27 % in post-monsoon. As this natural contribution increases in the summer months, so does the contribution from leaded gasoline. This increase in contribution of natural component can be explained by airmass back trajectories and their associated consequences (**Figure 7.7**). In summer, airmass back trajectories demonstrate no influence from transboundary aerosols, originating predominantly from short ranges and subsequently making the impacts of local burning such as dehydrated soil resuspension prominent. Thus, an increase in the relative crustal contribution and, consequently, the contribution of leaded gasoline from soil resuspension is observed in the summer months. Similar persistence of legacy Pb in the atmosphere has been recorded worldwide. Recent studies, utilizing Pb isotopic analyses, of aerosols in London observed long-term persistence of Pb from historically deposited leaded petrol in London's atmosphere, despite its ban in the year 2000 (MacKinnon et al., 2011; Resongles et al., 2021). Even though Pb levels in the air have significantly dropped since the ban in London, about 32 ± 10 to 43 ± 9% of airborne Pb still originates from the resuspension of Pb-contaminated dust and soil, which was initially deposited in the 20th century (Resongles et al., 2021). Similar findings have been reported from South-East Asian countries, where Pb isotopic composition of aerosols prove substantial contributions (up to 39 %) of legacy Pb (Ray and Das, 2023b). In India, similar Pb isotopic analysis revealed that over 50% of the Pb in Himalayan aerosols still comes from leaded gasoline, even 15 years after its phase-out (Mitra et al., 2021).

In post-monsoon period, transboundary aerosols become a dominating factor, reducing the relative contribution of crustal sources and subsequently that of leaded gasoline. In both seasons a modest contribution form vehicular emissions (< 10 %) can be observed. Although, the aerosols lie on the mixing line joining crust and Indian ore, negligible contribution from ore is observed from MixSIAR analysis. Most importantly, MixSIAR results indicate negligible influence of coal and fly ash throughout the year in the vicinity of lignite fired powerplant. This also confirms previous qualitative observations from elemental ratios and Pb isotopic compositions.

7.9. Implications

In the study area, the lignite storage yards, lignite transferring regions from mine to power plant and connecting roads with heavy vehicles are equipped with water sprinklers to control fugitive emissions (TNPCB, 2023). The power plants have water sprinklers and dust extraction systems in lignite handling and conveying systems to minimize dust generation. Boilers are equipped with electrostatic precipitators (ESP) in order to regulate stack emissions. The stacks are 220 m in height in 3 of the 5 power plants, while the new plant, "Neyveli New Thermal Power Plant (NNTPP)," that obtained environment clearance in 2010, has a stack of height 270 m for ensuring better pollutant dispersal. Additionally, lignite crusher houses and fly ash storages are also equipped with bag filters. Metal composition and Pb isotopes of $PM_{2.5}$ suggests minimal influence of coal emissions as a result of effective regulatory measures in the coal combustion processes, leading to reduced heavy metal contamination in the atmosphere.

The SIPCOT industrial complex in the region covers a total area of 709.31 acres, housing 21 highly polluting red, 6 orange and 3 green category industries. Emissions from chemical and petrochemical facilities include pollutants such as PM, inorganic and volatile organic compounds (VOCs), while pharmaceutical and textile dye industries additionally release various organic and inorganic compounds. There are several wood and coal fired boilers associated with these industries emitting PM on regular basis. Wood-fired boilers contribute to emissions similar to those generated by biomass burning. The industries on average have a stack height of only 24.9 m, and releases a total of around 179 kg/ day of PM (TNPCB, 2020). Majority of these industries employ dust collectors, cyclone separators, and bag filters for controlling PM emissions. The Neyveli $PM_{2.5}$ does not show influence of ore indicating industrial emission controls are effective.

Apart from thermal power plants and other industries, the region experiences emissions from open burning of crop residues, residential fuelwood burning and SW burning. The dumpsites face spontaneous or deliberate burning of municipal SW resulting in generation of organic as well as metal pollutants in the atmosphere (Peter et al., 2019). Majority of the rural households in Tamil Nadu use biofuels such as fuelwood, wood-chips and agricultural waste for cooking purposes releasing respirable PMs (Parikh et al., 2001). In the district of Cuddalore alone, there are 905 villages that shows dependence on biomass burning as their source of energy (Ranganathan et al., 2020; Velmurugan and Joseph, 2022). As per 2018, Tamil Nadu generated 31.62 MT of crop residue out of which 4.11 MT was burnt (Sahu et al., 2021). Open burning of SW and biomass have been observed at Neyveli during the sampling period (**Figure 7.12c**).

In India, the top five states with the highest power generation capacity from coal are Uttar Pradesh, Maharashtra, Chhattisgarh, Madhya Pradesh, and Gujarat, with the largest individual coal-fired power plants located in Madhya Pradesh, Gujarat, Maharashtra, Uttar Pradesh, and Odisha (NITI Aayog, 2024). Among these regions, Gujarat lacks recent literature on the elemental composition of aerosols. In the absence of Pb isotopic data, the V/Pb ratio serves as a reliable alternative tracer for coal combustion. Given the high V content in coal, the V/Pb ratio from coal combustion is consistently greater than 1. In contrast, other anthropogenic sources, such as vehicular exhaust and industrial emissions, typically exhibit V/Pb < 1 and << 1 respectively (R. Das et al., 2018; Kumar et al., 2016; Ray and Das, 2023b; Sen et al., 2016). Thus, V/Pb ratios from the literature were compiled over the last decade to gain a national perspective on whether atmospheric Pb is sourced from coal combustion. V/Pb ratios from several key locations were compiled having coal-fired power plants nearby: Madhya Pradesh (Singrauli), Jharkhand (Jharia), Assam (Jorhat), West Bengal (Bandel and Kolaghat), Odisha (Bhubaneshwar), Andhra Pradesh (Vizag), Telangana (Hyderabad), Maharashtra (Trombay), Chhattisgarh (Raipur), Delhi, and Uttar Pradesh (Kanpur)(Attri et al., 2024; Das et al., 2015; R. Das et al., 2018; Khobragade and Ahirwar, 2022; Kumar et al., 2018; Panda et al., 2021; Police et al., 2016, 2018; Rabha et al., 2022; Rout et al., 2015; Sen et al., 2016; Yadav et al., 2022).

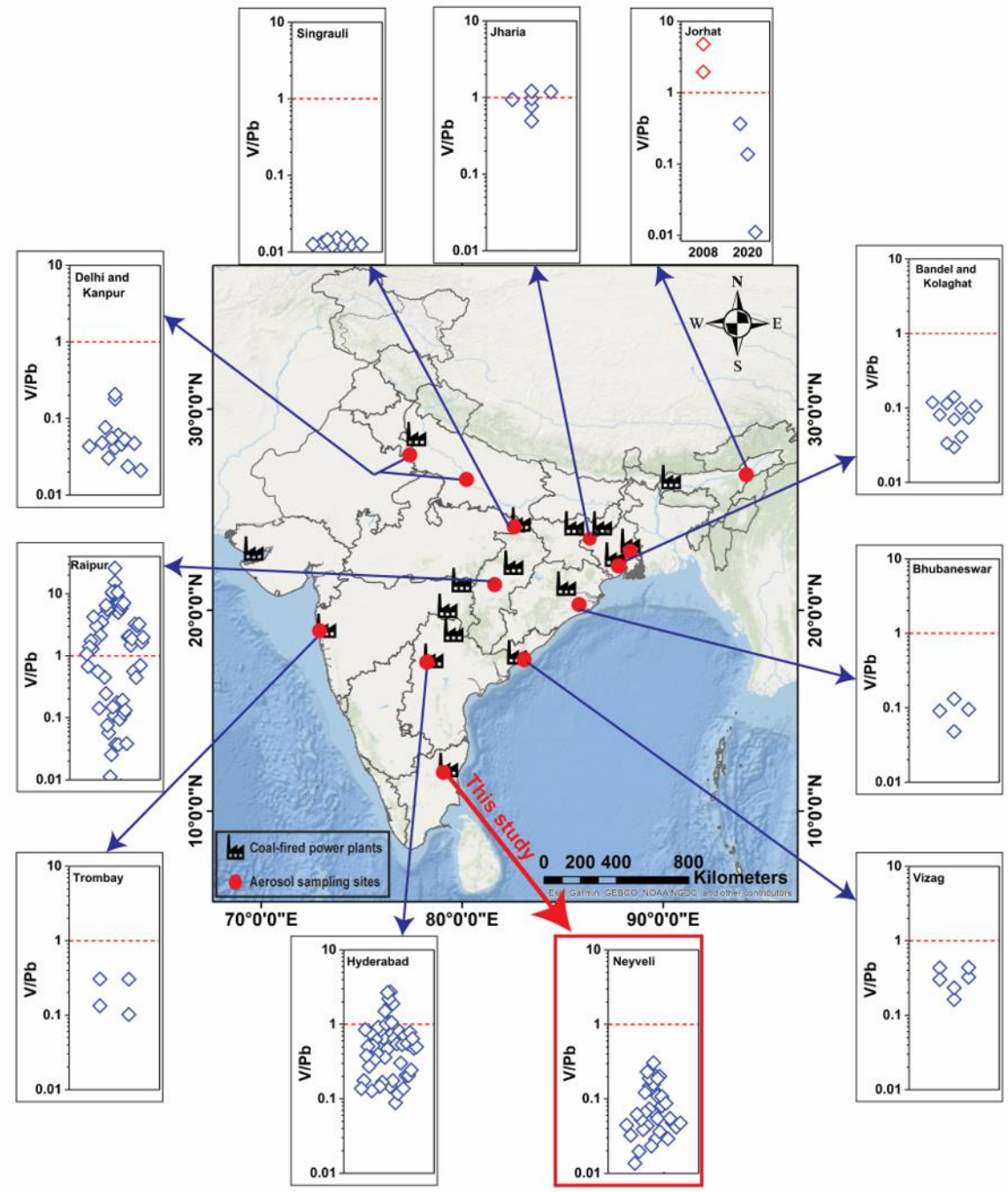

Figure 7. 13: *Map illustrating the aerosol sampling sites and nearby coal-fired thermal power plants. The available V/Pb ratios were compiled from key locations, including Madhya Pradesh (Singrauli), Jharkhand (Jharia), Assam (Jorhat), West Bengal (Bandel and Kolaghat), Odisha (Bhubaneshwar), Andhra Pradesh (Vizag), Telangana (Hyderabad), Maharashtra (Trombay), Chhattisgarh (Raipur), Delhi, and Uttar Pradesh (Kanpur). The red dotted line indicates V/Pb > 1. Aerosols demonstrating V/Pb > 1 can be sourced from coal combustion while those having V/Pb < 1 and << 1 can be sourced from vehicular exhaust and high temperature industrial processes[1]. The base map has been adopted from the open-source online repository Opendatasoft (https://public.opendatasoft.com/explore/dataset/world-administrative-boundaries/export/) and the locations have been illustrated using ArcGIS Pro 10.8. The V/Pb ratios were plotted using Origin Pro 2024a and all the components were compiled in Adobe Illustrator 2021, to form the final illustration.*

Figure 7.13 illustrates the location of the aerosol sampling sites along with the nearby thermal power plants. Majority of the locations, except Jharia, Raipur, and Hyderabad, record V/Pb < 1(Attri et al., 2024; Khobragade and Ahirwar, 2022; Rout et al., 2015). Even in Jharia, Raipur, and Hyderabad, a significant proportion of aerosols demonstrate V/Pb < 1(Attri et al., 2024; Khobragade and Ahirwar, 2022; Rout et al., 2015). Notably, in Singrauli, home to India's largest individual coal-fired power plant, all aerosols exhibit V/Pb ratios << 1(Yadav et al., 2022). Similarly, aerosols from Odisha, Uttar Pradesh, West Bengal, Andhra Pradesh, Maharashtra, and Delhi consistently record V/Pb ratios < 1 (Das et al., 2015; R. Das et al., 2018; Kumar et al., 2018; Panda et al., 2021; Police et al., 2016, 2018; Sen et al., 2016). In 2008 at Jorhat V/Pb ratios in aerosols were recorded to be > 1, which decreased to < 1 in 2020, indicating a reduced coal combustion emission over the years in the region (**Figure 7.13**). Despite India having 295 coal-fired power plants across the country(NITI Aayog, 2024), atmospheric aerosols in most regions demonstrate V/Pb ratios < 1, suggesting that coal combustion may not be the dominant source of atmospheric Pb in the country. Among these studies, the aerosols from Jorhat, Raipur, Trombay and Vizag were found to have contributions from biomass burning despite the presence of coal-fired power plants nearby (Khobragade and Ahirwar, 2022; Police et al., 2018, 2016; Rabha et al., 2022). Moreover, the only Pb isotopic study conducted near a coal-fired power plant, in Bandel, West Bengal, also identifies high-temperature industrial processes, rather than coal combustion, as the primary source of atmospheric Pb in the region (R. Das et al., 2018). Another study conducted at an industrial site in Delhi, just 56 km away from a major thermal power plant (NTPC Dadri) also finds no significant contribution of coal combustion towards atmospheric Pb (Kumar et al., 2018). Previous studies utilising Pb isotopic compositions and elemental concentrations have highlighted the contribution of biomass and SW burning at specific locations (Khobragade and Ahirwar, 2022; Kumar et al., 2018; Mitra et al., 2021; Police et al., 2018, 2016; Rabha et al., 2022; Yadav et al., 2022). Our findings also align with these results, emphasizing the need for stricter controls on open burning of SW and biomass to reduce the emission of heavy metals into the atmosphere. The dominance of open burning as a pollution source concurs with the GAINS model and highlights the pressing necessity for better waste management strategies to reduce its environmental impact. Thus, India needs to redefine her pollutant priorities and act accordingly to mitigate their effect.

The findings from this chapters and previous chapters underscore the diverse and complex nature of Pb sources across India, spanning road transport, industrial activities, coal combustion, and open burning of solid waste and biomass. These studies reveal the critical role of anthropogenic activities in shaping the profile of atmospheric metal load, with variations influenced by regional practices, energy sources, and regulatory frameworks. While these insights provide a robust understanding of Pb emissions in densely populated and industrialized regions, they leave an important gap in our knowledge: how do environments with minimum anthropogenic influence contribute to or interact with atmospheric Pb sources?

The next chapter addresses this gap by focusing on the pristine environment of the Andaman and Nicobar Islands. This region offers a unique opportunity to study the baseline elemental and Pb isotopic signatures in the absence of significant industrial and coal combustion emissions.

CHAPTER 8: TRACING ATMOSPHERIC Pb SOURCES IN INDIA'S PRISTINE REGION: A CASE STUDY FROM THE ANDAMAN AND NICOBAR ISLANDS

8.1. Introduction

The scenario of PM pollution differs significantly in remote island regions, of India such as the Lakshadweep and the Andaman and Nicobar (A & N) Islands, which are located several hundreds of kilometers away from the mainland. Due to their geographic isolation and relatively lower levels of industrial activity, these islands experience comparatively cleaner air, making them stark contrasts to the pollution levels found on the mainland. According to satellite data, from 1998 – 2022, the annual average $PM_{2.5}$ concentration in the islands of Lakshadweep and A & N have been about 50 % lower than that of Indian mainland, although it continues to exceed the WHO recommended guideline (IndiaPM25-V6GL02, 2024; Van Donkelaar et al., 2019) (**Figure 8.1a**).

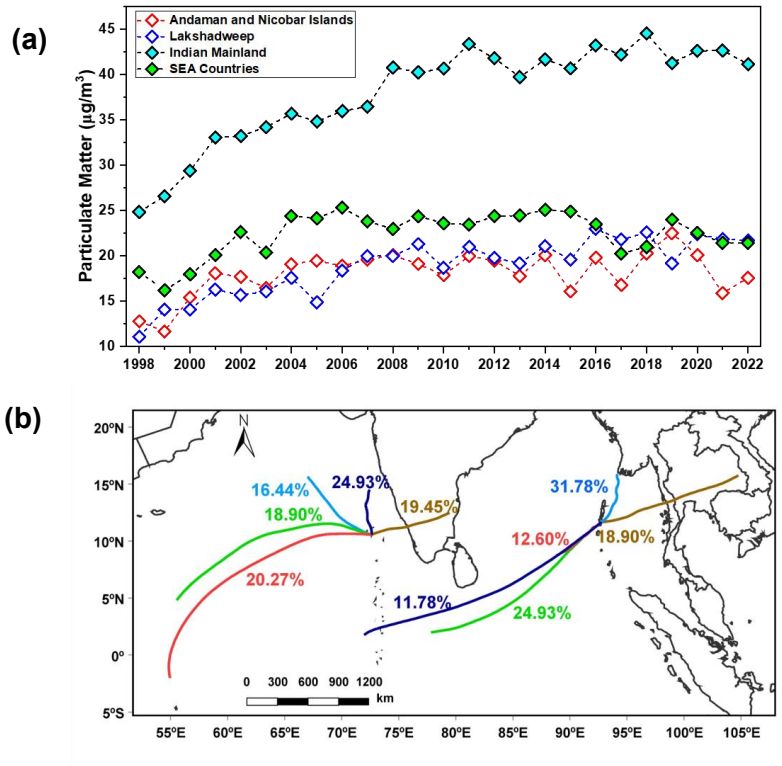

Figure 8. 1: *(a) PM concentrations at Andaman and Nicobar Islands, Lakshadweep Islands, Indian mainland and South East Asian (SEA) countries from 1998 – 2000 as compiled from https://sites.wustl.edu/acag/datasets/surface-pm2-5/ (b) Cluster analysis determining the percentage of airmasses received from different directions at Andaman and Nicobar Islands and Lakshadweep Islands. The cluster analysis has been performed in TrajStat software with inputs of meteorological data downloaded from HYSPLIT gui.*

Both local as well as long-range sources constitute significant proportions of PM. Among the long-range sources, Lakshadweep and A & N islands are predominantly influenced by airmasses from oceanic origin (> 80 %) with additional contributions from continents. While Lakshadweep receives 19.45 % of its airmasses from the Indian mainland, the A & N islands receive 18.90 % from south-east Asian (SEA) countries. Notably, the A & N Islands do not receive any direct airmass from the Indian mainland (**Figure 8.1b**). The Indian mainland experiences a significantly higher PM load than the SEA countries (**Figure 8.1a**). As a result, Lakshadweep is exposed to higher PM loads due to the airmasses carried from mainland India. In contrast, the A & N Islands, influenced by air masses from SEA countries as their only continental source of airmass, are exposed to lower PM levels due to the cleaner air in those regions. Both mainland and Lakshadweep exhibit a clear upward trend in their $PM_{2.5}$ levels from 1998 – 2022 Further, in recent years (except 2019) Lakshadweep has experienced higher $PM_{2.5}$ levels compared to A & N islands (**Figure 8.1a**). On the contrary, the A & N islands have experienced relatively consistent $PM_{2.5}$ levels from 1998 – 2022.

In addition to long-range continental sources, the lack of major industries and coal-dependent power sector in the A & N islands, eliminates the two significant pollutant sources that are prevalent in the Indian mainland (Ray and Das, 2023b). Further, with less vehicular density as well as population density and 82 % forest cover, A & N experiences much pristine environmental conditions. Thus, a stable air quality profile along with exposure to lower levels of PM make the A & N islands an ideal control site of India providing a benchmark for assessing background sources of PM in the absence of major anthropogenic contributors from the mainland.

The PMs carry variety of potentially toxic elements, such as arsenic (As), cadmium (Cd), chromium (Cr), cobalt (Co), mercury (Hg), molybdenum (Mo), nickel (Ni), lead (Pb), zinc (Zn), etc., as they are transported through the atmosphere. While these elements pose health risks to living organisms, they also serve as valuable proxies for source apportionment of pollutants in a given region. Determining elemental concentrations, and subsequently analyzing specific elemental ratios (such as V/Ni, V/Pb, Mo/Pb, etc.), provides critical tracers for identifying pollution sources such as industrial emissions, coal combustion, vehicular exhaust, geogenic sources, etc (R. Das et al., 2018; Lahiri et al., 2024; Ray et al., 2022; Ray and Das, 2023b; Sen et al., 2016). Coupling these elemental ratio tracers with stable Pb isotopic composition serves as a

robust and comprehensive tracer for the pollutants in the region. Naturally occurring, isotopes of Pb include of ^{204}Pb, ^{206}Pb, ^{207}Pb, and ^{208}Pb which ^{206}Pb, ^{207}Pb, and ^{208}Pb are radiogenic daughters of ^{238}U, ^{235}U, and ^{232}Th decay chains respectively. ^{204}Pb is the least abundant and the only non-radiogenic Pb isotope. The specific abundances of these isotopes are distinct in each source depending upon their initial U-Pb-Th composition, making the isotope ratios unique to each source. Moreover, Pb isotopes are particularly effective tracers, as there is no isotopic fractionation during physicochemical processes, which means that the isotopic signature of the source remains intact (Komárek et al., 2008). This allows for precise identification of pollution sources and helps to assess the contributions from various anthropogenic activities in a region.

Thus, this study aims to gain an overview of India's background pollution sources in the pristine location of A & N islands where major pollutants of mainland are absent by:

i. Analyzing elemental concentrations and Pb isotopic composition in atmospheric PM_{10} and $PM_{2.5}$ to identify the primary sources responsible for the presence of heavy metals in atmospheric PM in a pristine location
ii. Quantifying the relative contributions from each of the identified sources using geochemical proxies and Bayesian mixing model (MixSIAR).

8.2. Study area

The study was conducted in and around Port Blair (11.6234° N, 92.7265° E), presently known as Sri Vijaya Puram, the capital city of Andaman and Nicobar (A & N) Islands, a Union Territory of India. The city of Port Blair is approximately 1200 kms away from the major mainland cities of the eastern coast such as Kolkata and Chennai. The A & N Islands are an archipelago consisting of 572 islands, stretching across 780 kilometers in the southeastern Bay of Bengal and covering a total area of 8,249 square kilometers. Among these islands only 37 are inhabited ("DCMSME," 2015). In the islands, electricity is primarily generated by diesel-powered captive plants, located on the most inhabited islands. Waterways serve as the main mode of transport, with Port Blair acting as the central hub. Ships regularly transport passengers and goods between Port Blair and other islands, as well as to the mainland.

The Andaman and Nicobar Islands are a strategic hub for the Indian Armed Forces, hosting the only tri-service command of the country, the Andaman and Nicobar Command (ANC),

headquartered in Port Blair. This integrated command coordinates the Army, Navy, and Air Force units stationed on the islands, in this strategically critical region of the Indian Ocean. The command is equipped with extensive military infrastructure, including storage facilities for ammunition, large warships, fighter jets, and other defense equipment. Routine military activities, such as naval exercises, aerial surveillance, and training drills, are regularly conducted to ensure operational efficiency and preparedness. Additionally, the location serves as a base for missile testing (Andaman & Nicobar Command, 2022; PIB, 2023; Prakash, 2003; PTI, 2023).

8.3. Elemental concentrations

In both monsoon and winter seasons the PM_{10} and $PM_{2.5}$ followed the general order of (Na, Mg, Al, Fe) > (Ca, Cr, Mn, Ni, Cu, Zn, Ba, Pb) > (V, Co, Cd). Similar elemental concentration profiles were also observed in local soil, moss, road dust and dust fall samples with all these samples following the general order of (Na, Mg, Al, Ca, Fe) > (V, Cr, Mn, Ni, Co, Co, Zn, Cd, Ba, Pb). Elemental concentration data for all samples are provided in **Table 8.1**.

***Table 8.1**: Elemental concentrations of PM10, PM2.5 aerosols (ng/m^3), road dust, dustfall, moss, local soil, limestone, mud volcano, Pb ore, Cu ore (ng/mg), vehicular fuel and ship emission samples (ng/mL)*

Sample	Season	Sample Type	Na	Mg	Al	Ca	V	Cr	Mn	Fe	Co	Ni	Cu	Zn	Mo	Cd	Ba	Pb
AF1	**WINTER**	PM2.5	37	9	64	2	0.1	0.5	1.1	19	0.0	0.2	0.8	6	0.0704	0.05	0.3	3.0
AF2		PM2.5	34	18	67	4	0.1	0.5	0.8	36	0.0	0.3	0.9	4	0.0409	0.01	0.5	1.1
AF3		PM2.5	19	10	31	2	0.0	0.6	0.4	20	0.0	0.2	0.4	2	0.1825	0.02	0.2	10.6
AF4		PM2.5	1	0	0	0	0.0	0.0	0.0	0	0.0	0.0	0.0	0	0.1717	0.00	0.0	0.0
AF5		PM2.5	14	7	32	2	0.0	0.6	1.0	21	0.0	0.1	0.4	1	0.1718	0.01	0.2	0.8
AF6		PM2.5	30	99	58	14	0.1	0.7	7.2	116	0.1	1.2	3.5	11	0.1715	0.02	0.6	6.8
AC1		PM10	778	169	418	26	0.8	1.6	11.4	336	0.2	1.6	6.4	25	0.0044	0.18	3.6	10.5
AC2		PM10	554	124	292	19	0.6	0.9	6.1	232	0.1	0.7	2.2	15	0.2034	0.12	2.2	8.1
AC3		PM10	947	340	436	38	0.8	1.6	22.3	465	0.3	2.6	18.1	47	0.1390	0.17	3.9	18.8
AC4		PM10	916	220	829	58	1.2	1.8	11.2	503	0.2	1.1	5.1	17	0.0368	0.31	9.8	135.6
AC5		PM10	938	270	361	24	0.7	1.3	15.6	391	0.2	2.0	7.3	22	0.1390	0.12	5.6	11.6
AC6		PM10	695	186	527	34	0.9	1.6	11.0	437	0.2	1.4	3.2	21	0.2024	0.16	4.2	11.4
PD1		Dustfall	229	92	286	52	0	1	4	215	0.10	0.40	1.11	3.83	0.0114	0.01	6.20	0.39
PD2		Dustfall	468	200	710	107	1	2	9	480	0.21	0.80	2.12	9.04	0.0153	0.01	3.84	1.11
PD3		Dustfall	258	48	129	19	0	0	2	95	0.04	0.16	0.54	1.31	0.0027	0.00	0.96	0.16
PD4		Dustfall	266	68	199	31	0	1	3	146	0.06	0.22	0.41	1.87	0.0006	0.00	1.49	0.22
RDHotel		Road dust	20791	5215	20620	1578	75	82	412	29218	10.28	27.52	17.05	42.53	0.8876	0.04	136.4	3.67
RDMain road		Road dust	24951	6246	26535	2141	103	108	519	31718	15.61	34.61	93.58	40.10	0.5586	0.04	39.9	1.33
RDParking		Road dust	25627	4994	28517	2060	91	103	524	36412	13.55	35.32	32.61	48.71	4.0354	0.06	119.8	1.35
A1FC	**MONSOON**	PM2.5	63.1	34.8	119.1	3.9	0.1	2.8	3.4	62.6	0.04	1.5	2.5	9.2	0.191	0.04	0.82	1.5
A5FC		PM2.5	26.4	6.6	32.2	1.9	0.0	0.6	0.4	12.8	0.02	0.7	0.2	4.1	0.175	0.02	0.32	0.1
A9FC		PM2.5	79.4	33.6	34.9	1.6	0.0	0.2	3.7	46.9	0.03	0.9	3.7	5.9	0.039	0.02	2.715	2.1
A10FC		PM2.5	79.5	30.1	62.7	3.0	0.0	0.4	2.1	29.5	0.03	0.6	2.9	8.6	0.107	0.04	0.516	1.3
A17FC		PM2.5	18.7	9.6	61.6	1.1	0.0	0.2	0.4	13.4	0.01	0.3	0.1	1.8	0.264	0.01	12.41	0.2
A15FC		PM2.5	37.7	25.4	114.7	14.9	0.1	0.7	3.1	178.0	0.04	0.7	2.4	55.1	0.057	0.30	0.501	6.5

A2CC		PM10	6321	1269	1190	105	3.1	4.8	57.0	1183.0	0.76	10.3	27.8	77.2	0.039	0.20	4.57	32.7
A4CC		PM10	1320	277	301	25	0.6	1.2	8.3	239	0.14	1.8	5.4	13.5	0.252	0.03	1.24	3.3
A7CC		PM10	1077	162	207	15	0.6	1.0	2.9	147	0.08	0.8	0.5	3.8	0.180	0.01	0.66	0.9
A11CC		PM10	2943	465	584	43	1.5	1.7	9.7	453	0.23	1.3	4.5	14.1	0.074	0.06	1.49	2.6
A14CC		PM10	3295	464	551	52	1.3	1.4	7.0	392	0.18	1.5	1.4	33.7	0.168	0.19	2.28	2.6
A16CC		PM10	3476	503	450	37	1.2	1.1	6.0	342	0.16	1.1	0.8	4.1	0.226	0.02	2.55	0.9
PD1		Dustfall	4326	1036	1631	389	3.1	20.0	23.3	1256	0.69	3.0	4.5	47	0.11	0.0	7	3.6
PD2		Dustfall	13530	2801	4615	1034	6.9	20.6	66.4	2866	1.51	8.3	11.4	107	0.15	0.2	16	9.5
PD3		Dustfall	3132	1066	2024	317	3.3	5.4	34.5	1514	0.86	5.9	4.5	42.6	0.06	0.1	5	1.5
PD4		Dustfall	2629	670	1298	224	1.7	4.3	40.4	2819	0.60	174	4.9	19.8	0.11	0.1	6	1.1
RDM		Road dust	46719	26753	93674	14935	979	730	4259	160712	126	331	177	257	0.82	1.3	95	12.2
RDS		Road dust	55762	15415	54548	19754	634	353	2401	95207	73	166	100	136	1.16	0.3	91	3
MOSS1		Moss	2279	9710	25554	25499	48	50	442	20837	8.16	30	28	55	0.67	0.2	134	3
MOSS2		Moss	75	1239	1658	1273	7	11	44	2316	0.98	4	12	51	0.26	0.1	26	12
MOSS3		Moss	727	6956	24540	4566	69	156	500	28320	13.59	36	49	75	1.02	0.1	54	2
MOSS4		Moss	177	1571	9931	945	21	19	145	12819	3.69	16	15	63	1.51	0.0	47	15
MOSS5		Moss	158	2550	5947	2167	16	13	113	5686	2.33	11	14	22	0.90	0.1	52	2
SOIL1		Local soil	11740	4978	44094	26243	85	83	758	41132	9.90	39	43	627	0.55	0.7	166	51
SOIL2		Local soil	8852	1286	16316	401	146	137	234	40795	12.97	66	25	75	0.90	0.0	303	19
SOIL3		Local soil	6130	2640	21512	9890	88	63	330	19764	9.82	37	20	182	1.07	0.2	261	39
SOIL5		Local soil	12881	3340	29966	1787	286.1	527.3	1607.1	120250	74.22	112.7	137.7	229.8	0.60	0.1	20	3
SOIL7		Local soil	18817	1920	19287	2306	122.9	122.6	454.9	32841	15.09	50.2	82.9	288.7	0.57	0.4	169	44
SOIL8		Local soil	6172	2801	23326	6065	58.7	88.1	477.5	15809	8.69	41.5	21.6	36.5	0.57	0.1	172	8
Limestone 1		Limestone		1627	4042	252	3	2	125	2648	2.79	3.70	13.60	9.02		0.02		2.24
Limestone 2		Limestone		214	18	7331	1	1	10	216	0.14	0.55	0.36	1.02		0.01		0.19
Mud Volcano 1		Mud Volcano		7399	45706	367	62	59	283	26885	8.10	38.70	21.95	41.44		0.05		5.72
Mud Volcano 2		Mud Volcano		7456	44576	272	60	48	201	24635	7.18	36.23	15.34	37.92		0.04		5.13
GALENA1		Pb Ore	2	59	20	8	0.0	0.7	5.6	362	0.67	0.2	3.0	6776		31	0.17	6407
GALENA2		Pb Ore	27	159	44	31	0	1	25	5423	9.45	1	3	99037		359	0.42	7586
GALENA3		Pb Ore	8	104	11	12	0.0	2.2	8.6	681	0.26	0.2	6.3	27658		83.0		10215

CHALCOPYRITE1		Cu Ore	162	18932	29036	2973	88	1402	447	147670	161	1048	29344	289		1.6	698	1147
CHALCOPYRITE2		Cu Ore	162	24202	33134	5305	131	1938	273	241510	99	937	100904	127		1.0	103	171
CHALCOPYRITE3		Cu Ore	480	48844	72313	18833	417	3401	743	443977	323	2045	34184	244		1.4	2383	1794
SD1		Ship Diesel	36038	27024	2493	9691	11	93	323	5268	9	143	395	29962	13	6	304	289
SD2		Ship Diesel	15226	3664	4817	5109	10	55	282	12427	8	89	546	17373	15	3	224	224
SD3		Ship Diesel	13584	6370	1836	4486	5	100	213	7270	10	151	595	11838	23	12	499	282
SL1		Ship Lubricant	24094	528971	3527	370087	71	189	1258	10473	6	166	3364	1565341	293	13	217	862
SL2		Ship Lubricant	25099	482831	3832	321845	61	153	1126	8827	4	143	3645	1442414	12108	13	192	858
SL3		Ship Lubricant	13875	349065	2059	281339	72	96	829	6207	3	547	4963	1293164	121062	9	158	693
SL4		Ship Lubricant	4074	70498	9813	64710	34	38	270	2863	2	41	1835	189248	35623	3	166	192
SL5		Ship Lubricant	19095	26490	3448	430862	59	495	5324	15410	39	417	20217	1320998	31859	248	869	8978
SC1		Ship Coolant	3537999	27517	2411	19883	2	22	1078	13121	2	31	416	398	2093	1	1595	322
SC2		Ship Coolant	6894651	48878	4646	35609	4	36	1429	4336	2	14	766	286	1222	9	3471	131
SC3		Ship Coolant	5186632	8205	31684	2453	94	318	3143	51387	34	168	5426	8566	11556794	303	257	267
VP1		Vehicular Petrol	4289	3230	2195	796	4.86	500	180	13367	3.17	599	237	64974	34	1.10	199	685
VP2		Vehicular Petrol	13460	6701	2504	1580	4.89	313	133	9379	3.35	310	339	30829	14	9.34	367	602
VP3		Vehicular Petrol	52110	1169	1099	511	1.62	110	42	4035	1.56	147	112	11520	7.48	7.81	289	155
VP4		Vehicular Petrol	12722	21151	2691	2134	5.97	106	64	2581	4.51	79	98	11035	7.95	1.57	351	133
VD1		Vehicular Diesel	30434	12875	2763	4326	7.68	74	134	7449	2.98	148	93	9907	6.86	5.36	310	200
VD2		Vehicular Diesel	15435	9683	2395	2499	8.91	102	144	8384	5.61	179	57	9356	6.20	3.31	104	134

The higher concentration of the major elements such as Na, Mg, Al and Fe in the PM, dust fall and road dust samples indicate presence of crustal sources as these elements are abundant in the crust. The concentration of these major elements are orders of magnitude higher in PM_{10}, road dust and dust fall samples compared to $PM_{2.5}$ aerosols, indicating a greater influence of crustal sources in coarser particles. This coincides with the fact that the finer fractions of PM tend to be enriched with the anthropogenic components (Das et al., 2015). However, elemental concentrations in the $PM_{2.5}$ fraction were significantly lower by orders of magnitude compared to SEA countries such as Thailand, and especially India (Boreddy et al., 2021; Chakraborty et al., 2023; Das et al., 2015; Jain et al., 2020; Kayee et al., 2021; Khare and Baruah, 2010; Kulshrestha et al., 2009; Mehra et al., 2020; Pandey et al., 2013; Ray et al., 2024) (**Figure 8.2**).

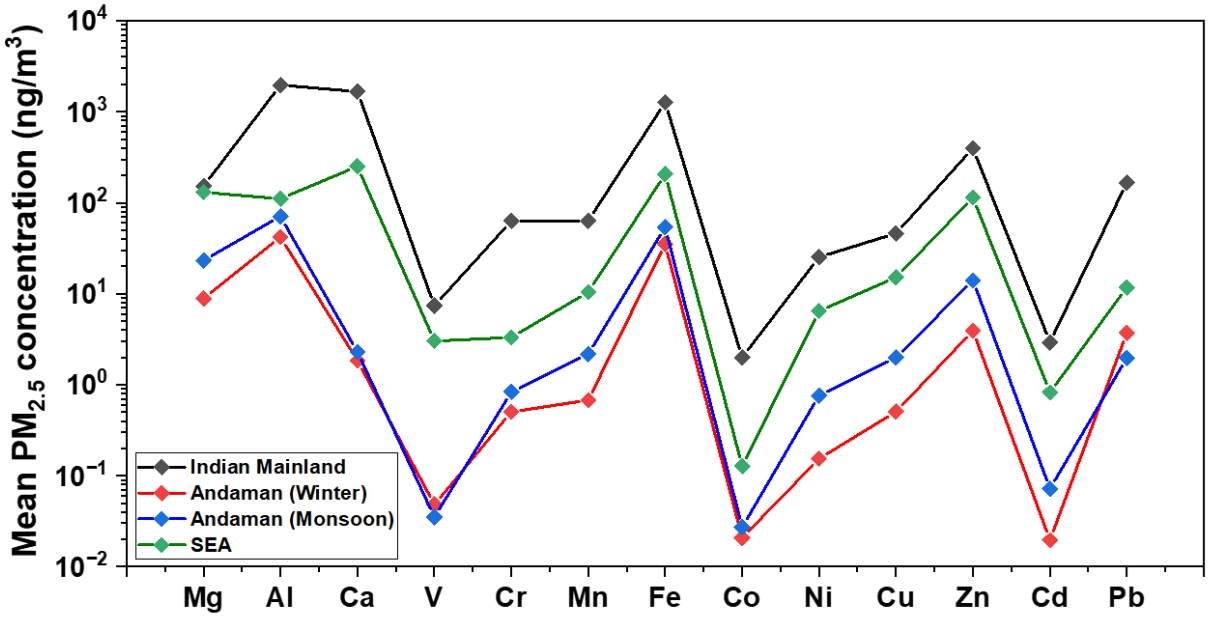

Figure 8. 2: *Elemental concentrations in $PM_{2.5}$ fraction at Andaman and Nicobar Islands, Lakshadweep Islands, Indian mainland and South East Asian (SEA) countries*

In the $PM_{2.5}$ fraction, significant seasonal variation was observed in Na, Mg, Mn, Ni, and Cu (ANOVA, $p < 0.05$), with Na, Mg, Mn and Ni concentrations higher in the monsoon, while Cu concentrations were higher in winter. Although seasonal difference for Pb concentration in $PM_{2.5}$ aerosols was not statistically significant, average Pb concentrations in the winter samples were 1.9 times those in monsoon. The PM_{10} aerosols also recorded significantly higher Na, Mg and Mn concentrations in monsoon compared to winter (ANOVA, $p < 0.05$). The significantly higher Na

and Mg concentrations in the aerosols can be due to a greater contribution of sea spray during the monsoon season. From 72 hr air-mass back trajectory analysis, it can be observed that the monsoon winds originate from the south-west direction and are of oceanic origin while the winter winds from north-east carries winds from the SEA countries (**Figure 8.3**). Thus, in the monsoon season the PMs have a greater influence of oceanic aerosols. In the coarser fraction (PM_{10}), Cd, Ba, and Pb concentrations were significantly higher in winter, suggesting that the incoming continental airmass during this season may have elevated the concentrations of these elements.

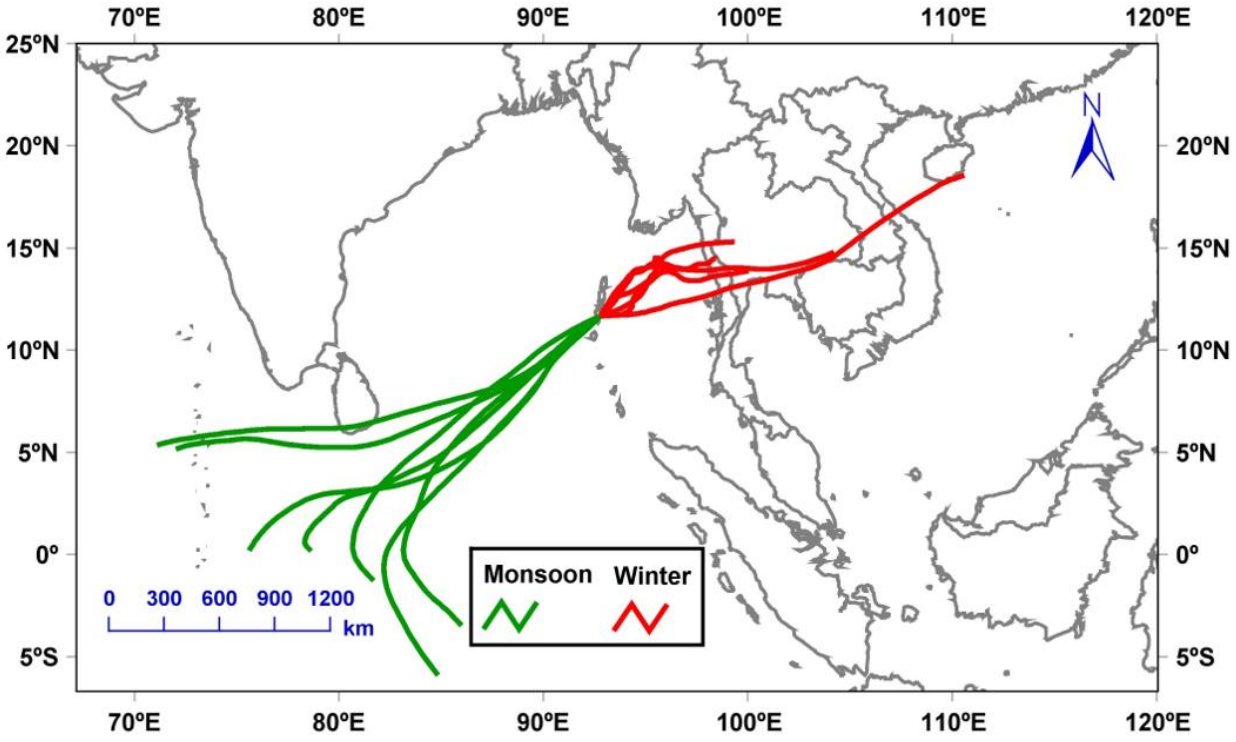

Figure 8. 3: *72 hour airmass back trajectory at the study site for the sampling periods in winter and monsoon*

Among the various fuels used in ships, distillate fuel/diesel, is one of the primary choices in India as well as globally (IMO, 2022; Ministry of Ports, Shipping & Waterways, 2023). Marine diesels have lower metal contents and consequently lower emissions of metals as well as other organic components compared to heavy fuel oil (HFO) (Corbin et al., 2018; Eichler et al., 2017; Moldanová et al., 2009; Mueller et al., 2015), whose usage is decreasing globally due to its high SOx emissions (IMO, 2022). Previous studies using ICP–OES (Inductively Coupled Plasma Optical Emission Spectroscopy) measuring metal concentrations in marine diesel have reported that heavy metals such as V, Ni, Mo, Sn, Pb etc. were below detection limits (Corbin et al., 2018).

However, with more sensitive analysis, using ICP–MS, in this study we have successfully detected these elements in marine diesel (**Table 8.1**) in significant proportions. Compared to vehicular fuels marine high-speed diesels, lubricants and coolants generally recorded higher concentrations of metals (**Figure 8.4**).

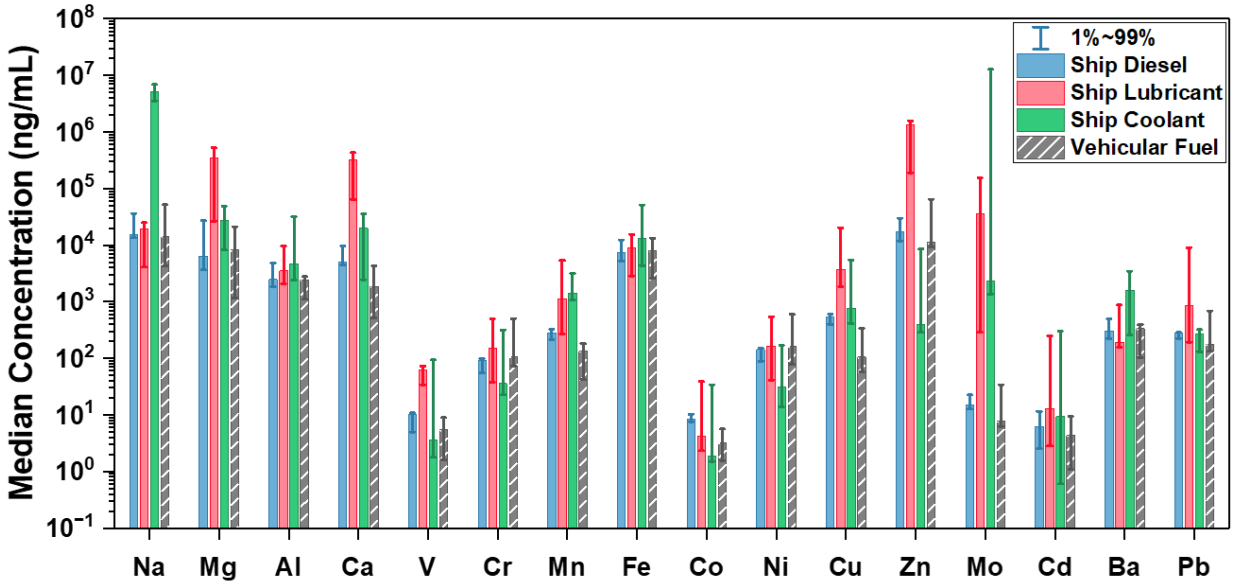

Figure 8. 4: *Median elemental concentrations in ship oil and vehicular fuel samples*

Emissions from ships are a mixture of both the fuel and the lubricants they use, while coolants are not directly involved in emissions. Previous study indicates that lubricants often dominate the composition of these emissions, highlighting their significant contribution to shipborne atmospheric pollutants (Di Natale and Carotenuto, 2015; Eichler et al., 2017; Lehtoranta et al., 2019). In this study, ship diesel recorded comparable concentrations of all elements with vehicular fuels. Ship lubricants exhibited the highest concentrations of metals, with elements such as Mg, Ca, V, Cu, Zn, and Mo being several orders of magnitude higher than in vehicular fuels (**Figure 3**). Elements such as Zn and Ca have been observed to be present in high concentrations in lubricants in previous studies and are hence recognized as markers of lube oils (Di Natale and Carotenuto, 2015). Additionally, elements such as Mn, Cd, and Pb demonstrated 3-8 times higher concentrations in lubricants compared to vehicular fuels (**Figure 8.4**). These trends reflect the distinct compositions of ship oils, containing significantly higher concentrations of metal

additives. Coolants also had extremely elevated Mo concentrations, second only to lubricants along with all other elements except Zn compared to vehicular fuel. The significantly higher concentrations of metals in ship oils, particularly in lubricants, have important implications for emissions. The elevated levels of metals such as Mo, V, Ni, Cu, Mn, and Pb in ship diesels and lubricants suggest that these metals are likely to be released into the atmosphere even in higher concentrations compared to vehicular fuels.

8.4. Enrichment factors and potential source regions

The enrichment factor (EF) is a valuable parameter for distinguishing between anthropogenically and geogenically sourced elements. The EF is a quantitative measure used to assess the relative enrichment of a specific element in a sample compared to the upper continental crust (UCC) (Rudnick and Gao, 2003). All elements are normalized against crustal elements such as Al, Fe, Ti etc. as:

$$EF = \left(\frac{\left(\frac{Element}{Reference\ element} \right)_{Sample}}{\left(\frac{Element}{Reference\ element} \right)_{Crust}} \right)$$

Due to probable anthropogenic inputs and possibility of redox reactions involving Fe in the environment, Al was selected as the normalizing element in this study. An EF > 10 indicates significant enrichment of the element of interest compared to the UCC. In the $PM_{2.5}$ samples of A & N islands Ni, Cu, Zn, Cd and Pb recorded EF > 10 in both winter and monsoon seasons. The same elements demonstrated EF > 10 in the PM_{10} samples from both seasons with the exception of Ni. This suggests that these elements are influenced by anthropogenic activities. During the monsoon season, Na recorded EF > 10 in the PM_{10} samples, indicating a higher influence of sea spray during the monsoon season. The consistent enrichment of elements such as Ni, Cu, Zn, Cd, and Pb across both seasons, despite the change in wind directions, suggests a persistent, source of these metals in the island. Despite recording higher EFs in the monsoon season, Zn and Cd showed no statistically significant difference in their mean EFs across seasons (ANOVA, $p > 0.05$). However, the variances of their EFs between seasons differed significantly, with greater variability observed during the monsoon (two sample test for variance, $p < 0.05$). Further, Pb, which also exhibited no significant seasonal difference in mean EF, recorded a notably higher (4 times) mean

EF during winter, with a significantly higher variance occurring during winter season compared to monsoon (two sample test for variance, $p < 0.05$) (**Figure 8.5**).

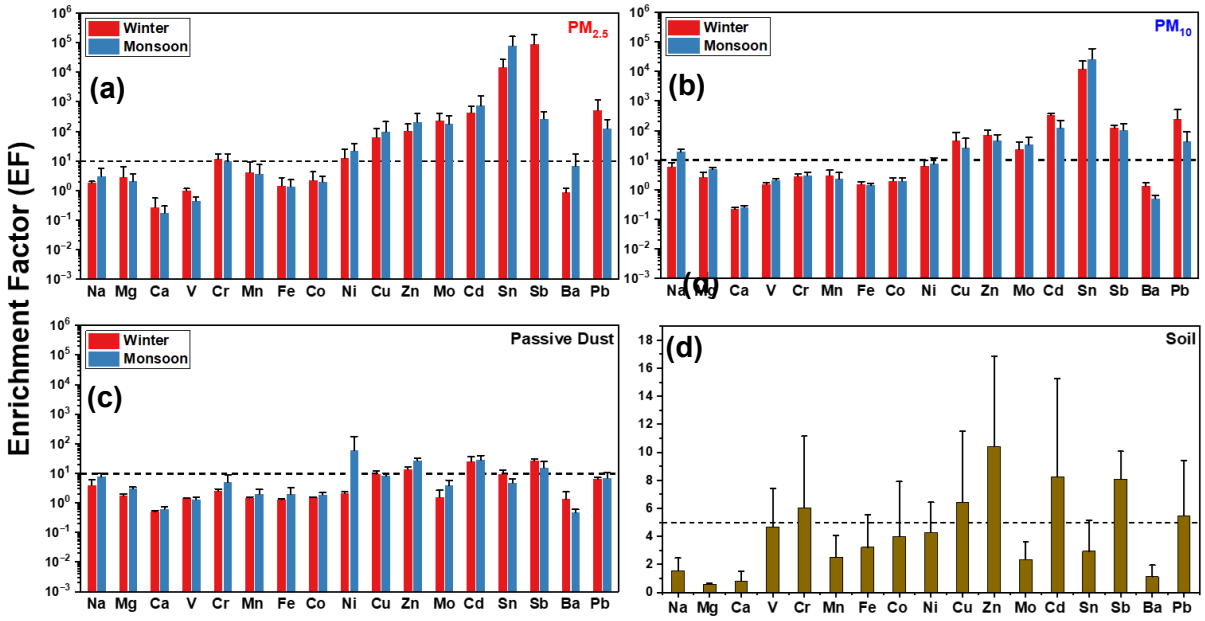

Figure 8. 5: *Mean enrichment factors of (a) $PM_{2.5}$ (b) PM_{10} (c) Dustfall and (d) soil samples*

Typically, in soil, elements having $2 < EF < 5$ are classified to be moderately enriched, primarily influenced by crustal sources, while $5 < EF < 20$ are classified to have significant non – crustal sources (Sutherland, 2000). The local soil of A & N islands recorded $EF > 5$ for Cr, Cu, Zn, Cd and Pb indicating significant anthropogenic inputs of these elements. Moderately enriched elements include V, Mn, Fe, Co, Ni and Mo, which are a mixture of crustal and minor anthropogenic sources (**Figure 8.5**).

Coupling EFs with airmass back trajectories provides valuable insights into source hotspots for enriched elements (Cu, Zn, Cd and Pb). To achieve this, a concentration-weighted trajectory (CWT) analysis was performed using the TraPSA online tool (Zhou et al., 2024). Unlike the conventional approach of using concentration data in CWT analysis, this study incorporates EFs as inputs along the trajectory lines and hence the analysis can be called enrichment factor weighted trajectory (EFWT) analysis. The incorporation of EFs, highlights regions where specific elements are significantly enriched, independently of fluctuations in absolute concentration, allowing for a more precise identification of source regions and contributions. The grids were divided into

sections of 0.5° and more weightage was provided to grids constituting higher number of trajectory terminating points. The EFWT analysis for both the seasons using same data treatment methods reveals that transboundary sources of Cu, Zn, Cd and Pb were present in significantly higher proportions in both PM_{10} and $PM_{2.5}$ samples during the winter season (**Figure 8.6**). In contrast, the monsoon season demonstrated limited influence from transboundary sources. This suggests that

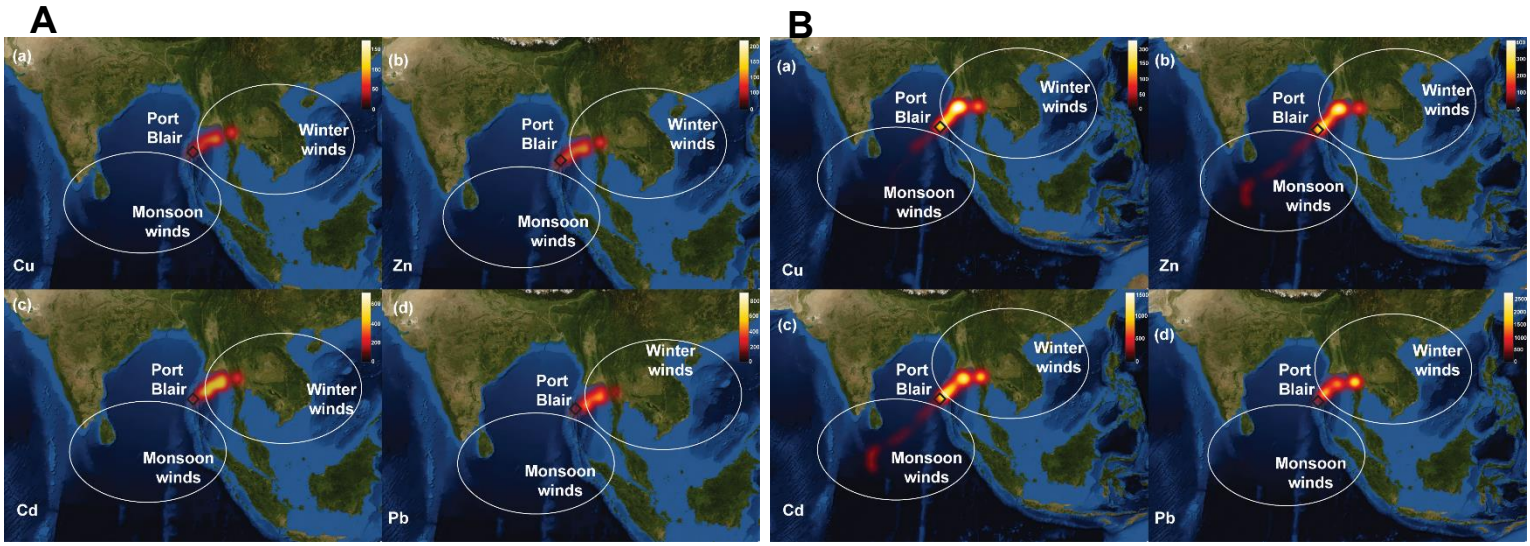

Figure 8. 6: *Potential source hotspots for Cu, Zn, Cd and Pb in (A) $PM_{2.5}$ and (B) PM_{10}*

while both transboundary and local sources contributed during winter, local sources predominantly influenced pollutant levels during the monsoon.

Thus, there is a clear dominance of local sources in the A & N islands with additional influence of long-distance sources during the winter season. As energy generated from coal combustion is not in use in the islands, one of the largest concerns for Indian mainland, coal is not a significant local source in the region. However, as of 2023, there were about 8067 total number of vehicles out of which 0.3 % were electric vehicles (Vahan Sewa, 2023). Although the total number of vehicles is only 0.03 % of the total number of vehicles running in India, it is a source of both exhaust as well as non-exhaust emission consisting of heavy metals in the island. Apart from this, an important local source whose elemental concentration data is scare is ship oil. With a total of 23 ports along the archipelago, with Port Blair being the largest and 13th largest port of India (Indian Ports Association, 2014; PIB, 2010), emissions from ship traffic can be a major contributor towards

atmospheric heavy metals in the region. The presence of these sources in A & N island's atmosphere can be better understood from characteristic elemental ratios discussed in next section.

8.5. Elemental ratios

Elemental ratios, such as V/Ni and Na/Mg, are geochemical proxies to identify and differentiate specific sources of PM. The V/Ni ratio are markers for ship emissions (Geiger and Cooper, 2010; Ray et al., 2022; Wu and Huang, 2021). Similarly, the Na/Mg ratio serves as an indicator of sea spray, providing insights about the marine influence on aerosol composition (Kayee et al., 2021). As the study location is an island hosting one of India's major ports (Port Blair), these sources are relevant.

Majority of sea-spray aerosols are composed of coarser particles in the size range of 5–10 µm (Harkel, 1997). Consequently, the seasonal variation in Na/Mg ratios was specifically evident in the PM_{10} fraction of aerosol samples (**Figure 8.7a)**. During the monsoon season, the Na/Mg ratios in PM_{10} aerosols exhibited significantly higher values (AVOVA, p = 0.011), ranging from 4.77 to 7.10 (median = 6.50), compared to the winter season, where the ratios ranged from 2.79 to 4.61 (median = 3.96). The Na/Mg ratio of seawater is typically 8.8 (Chester, 1990). During the monsoon season, PM_{10} aerosols exhibit Na/Mg ratios closer to this seawater value, suggesting a dominant marine influence primarily driven by long-range air masses originating exclusively from the open ocean. In contrast, the significantly reduced Na/Mg ratios during winter highlight a greater presence of non-marine sources.

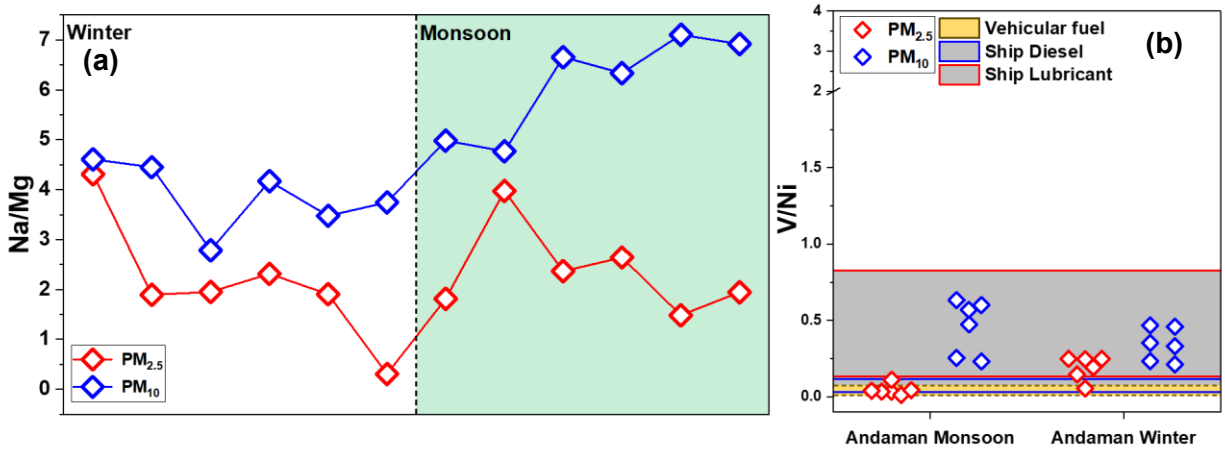

***Figure 8.** 7: (a) Na/Mg and (b) V/Ni ratios in $PM_{2.5}$ and PM_{10} during winter and monsoon. The range of V/Ni ratios for ship oil and vehicular fuel are plotted for reference.*

Ship emissions predominantly occur within a particle size range of 0.1 µm to 7 µm, corresponding to the $PM_{2.5}$ and PM_{10} aerosol fractions (Fridell et al., 2008; Moldanová et al., 2009). Metals such as V and Ni, are specifically observed within the 0.2 µm to 5 µm size range (Moldanová et al., 2009). This distribution suggests that metal signatures from ship emissions can be detected in both $PM_{2.5}$ and PM_{10} fractions.

The V/Ni ratios observed in ship oils (0.033–0.838) as measured in this study are generally higher than those reported for vehicular fuels (0.008–0.076) (Lahiri et al., 2024). The ship lubricants (range = 0.13-0.83) have distinctly higher ratios compared to the ship diesels (0.03-0.11). In V/Ni space, the lower range of ship diesel ratios shows minimal overlap with the upper range of vehicular fuel ratios. The ship lubricants which are significant components of ship emission (Di Natale and Carotenuto, 2015; Eichler et al., 2017; Lehtoranta et al., 2019), demonstrates their specific chemical signature with their distinctly high V/Ni ratios. The V/Ni ratios in PM_{10} samples from both seasons overlapped with the range observed for ship lubricants (**Figure 8.7b**). In contrast, the $PM_{2.5}$ ratios demonstrated a seasonal variation, with winter samples being more influenced by ship oils compared to those collected during the monsoon season. (**Figure 8.7b**). This suggests that the V/Ni ratios in PMs are a combination of vehicular fuel, ship fuel and

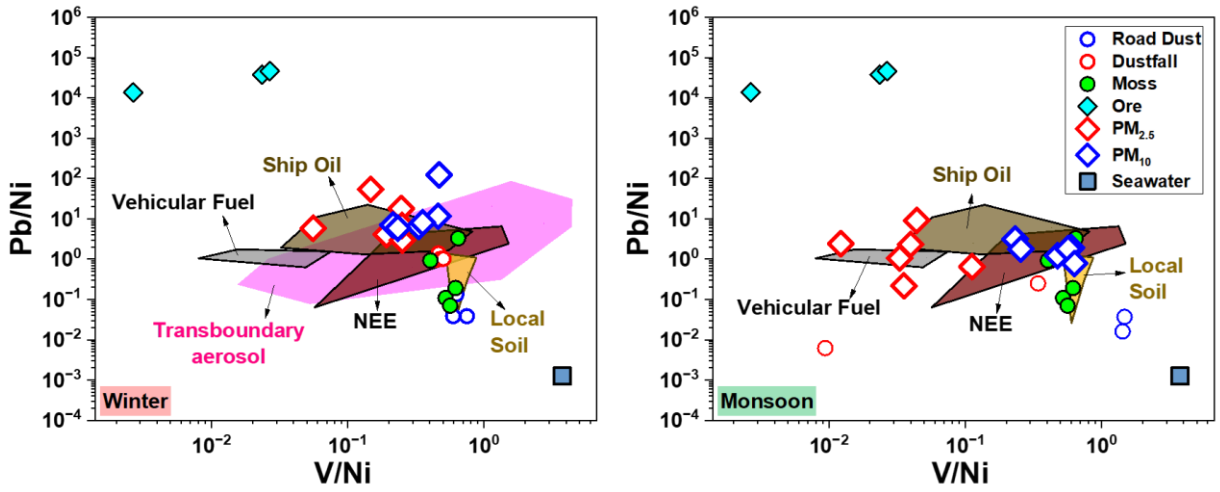

Figure 8. 8: *Bivariate plots of V/Ni vs Pb/Ni illustrating aerosol as well as their potential sources in (a) winter and (b) monsoon seasons*

lubricant emissions, with varying proportions depending on season and size fraction. The V/Ni ratios in $PM_{2.5}$ indicates a greater contribution from fuels (both vehicular and ship) while in PM_{10}, lubricants can be the dominant source of V and Ni.

The ship oil samples exhibit considerably high Pb concentrations, ranging from 0.13 ppm to 8.9 ppm (**Table 8.1**), which are higher than concentrations of V and Ni. This suggests that Pb is a dominant component in ship oil emissions and can be detected in atmospheric PM. Other end members such as transboundary aerosols during winter, NEEs and soil also contain high concentrations of Pb. By combining Pb with V and Ni, the bivariate plot of V/Ni vs. Pb/Ni reveals distinct seasonal variations in sources of PM_{10} and $PM_{2.5}$ (**Figure 8.8**). This suggests that Pb plays a pivotal role in driving the observed seasonal differences, potentially serving as a key tracer for distinguishing source contributions across seasons.

In both the seasons all the PM samples fall between two extreme sources: galena and seawater (**Figure 8.8**). In winter both the size fractions of PM have significant overlap with the ship oil samples along with transboundary aerosols. Both the Pb/Ni and V/Ni ratios were significantly higher in $PM_{2.5}$ aerosols during winter than in monsoon (Kruskal Wallis ANOVA, $p < 0.03$). The Pb/Ni ratios were also significantly higher in PM_{10} of winter samples (Kruskal Wallis ANOVA, $p < 0.004$). This consistently higher Pb/Ni ratios observed in both size fractions of aerosols during winter along with their overlap with characteristic ratios of ship oil, suggest a stronger influence of Pb-rich emissions, particularly from ship oils, during this season (**Figure 8.8**). Moreover, Thailand remains under significant influence of ship emissions (Ray and Das, 2023b) from where A & N receives substantial portion of winter airmasses. This suggests that transboundary aerosols transported from Thailand may carry elemental characteristics similar to those of ship oil samples, further supporting the observed wintertime signatures in the aerosols.

The monsoon $PM_{2.5}$ aerosols are in proximity to the ratios observed in vehicular fuel samples, while the PM_{10} aerosols align more closely with those from the NEE sources and local soil (**Figure 8.8**). This suggests that during the monsoon season, local vehicular emissions and soil resuspension play a significant role in the composition of PMs. The PM_{10} fraction aligning with NEE and local soil indicates that dust resuspension and NEE from road traffic are dominant contributors to coarser aerosols, which aligns with observation from previous study (Lahiri et al., 2024). During the monsoon season, airmass back-trajectory analysis (**Figure 8.3**) revealed that only air masses from the sea were present, with no transboundary land-based pollution. This absence of transboundary emissions, which included ship emissions and other sources from Thailand in winter (Ray and Das, 2023b), along with higher sea spray aerosols, likely resulted in

lower atmospheric Pb concentrations. The road dusts and the dustfall samples lie in the mixing range of local soil, seawater and NEE sources in both seasons. These coarse particles, typically reflect the influence of local soil resuspension and associated NEE during both dry and monsoon seasons. The local mosses also overlap with that of NEEs and local soil samples (**Figure 8.8**).

A more comprehensive understanding of the different sources contributing to atmospheric PM in the region can be obtained using Pb isotopes, as detailed in the next section.

8.6. Pb isotopic evidences

The Pb isotopic compositions of PM_{10} and $PM_{2.5}$ aerosols from the A & N Islands, along with their potential end members, were analyzed in classical three-isotope space as $^{208}Pb/^{207}Pb$ vs $^{206}Pb/^{207}Pb$ (**Figure 8.9**). No significant differences were observed between the isotopic compositions of PM_{10} and $PM_{2.5}$ aerosols in either season (ANOVA, $p>0.05$). However, distinct seasonal variations in Pb isotopic compositions indicate shifts in Pb sources between the monsoon and winter seasons. For both the size fractions, a larger spread was observed in case of the Pb isotopic compositions of the monsoon aerosols compared to the winter ones.

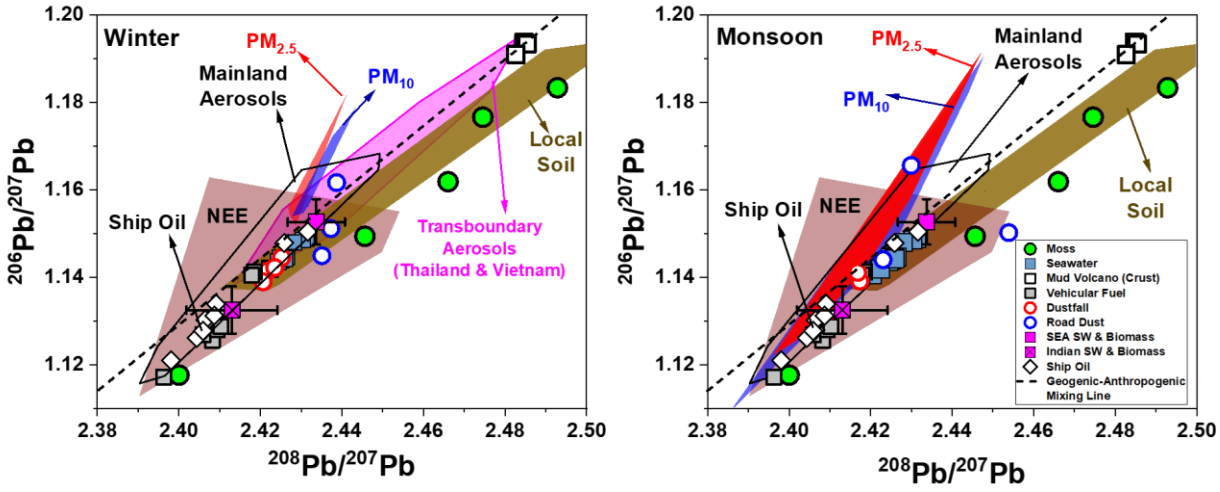

Figure 8. 9: *Three isotope plot illustrating the Pb isotopic composition of aerosols as well as their potential sources in (a) winter and (b) monsoon seasons*

Although no direct airmass transport occurs from the Indian mainland to the A & N Islands, comparing the Pb isotopic compositions of aerosols from both regions can help identify whether they share similar sources. During the winter season, the Pb isotopic compositions of mainland aerosols show minimal similarity to those of the island aerosols. However, during the monsoon

season, the less radiogenic aerosols (w.r.t. ^{206}Pb and ^{208}Pb) on the islands exhibit compositions similar to those from the Indian mainland. This similarity suggests the presence of shared sources between the island and mainland, in the absence of direct transport of mainland aerosols to the islands.

Several common sources, or end members, contribute to Pb in both the Indian mainland and the A & N Islands, including vehicular emissions (both exhaust and NEE), ship emissions, seawater, and soil as observed in elemental ratio spaces (**Figure 8.8**). During the winter season, transboundary aerosols from SEA countries also play a significant role. However, only the less radiogenic SEA aerosols show a very limited overlap with the less radiogenic aerosols (w.r.t. ^{206}Pb and ^{208}Pb) from the A & N Islands. The less radiogenic portion (w.r.t. ^{206}Pb and ^{208}Pb) of the island aerosols aligns with the isotopic range of the identified sources during the monsoon and with NEEs and transboundary SEA aerosols during the winter. However, the A & N aerosols demonstrated no overlap with SW & biomass samples. This limited overlap highlights that the conventional sources, such as vehicular emissions, ship emissions, seawater, and soil have some contribution towards atmospheric Pb of the region. However, the radiogenic aerosols of A & N islands, characterized by enrichment in ^{206}Pb (urogenic Pb) and depletion in ^{208}Pb (thorogenic Pb), do not correspond to any of the identified end members considered so far and indicate the presence of missing source(s). The radiogenic end members such as UCC or local uncontaminated crust represented by mud volcano in this study along with SEA aerosols are more radiogenic in terms of both ^{206}Pb and ^{208}Pb in contrary to the A & N aerosols, which are depleted in thorogenic Pb.

The distinct composition of the A & N aerosols creates a clear divergence between the Pb isotopic signatures of the island aerosols and those of mainland aerosols and other identified end members during both winter and monsoon seasons. Mainland aerosols, whether from India or SEA countries, along with other above-mentioned end members fall along a mixing line that connects crust and less radiogenic (w.r.t. ^{206}Pb and ^{208}Pb) sources such as Indian ore or leaded gasoline (the geogenic – anthropogenic mixing line). The local soil being less radiogenic from the mud volcano indicates contamination from anthropogenic sources. However, the local soils also lie on this traditional geogenic – anthropogenic mixing line. The road dust and the dustfall samples along with local mosses either overlap or lie in the vicinity of local soil and NEE sources. However, the A & N aerosols deviate significantly from this mixing line, suggesting a unique local source. This missing

source is distinct from the commonly identified end members such as vehicular emissions, ship emissions, seawater, soil, or transboundary aerosols and must be highly urogenic and less thorogenic to explain the Pb isotopic composition of the A & N island aerosols during both winter and monsoon seasons.

Military activities in the region release various metals into the environment through high-temperature combustions such as missile testing, gunshot residues, use of grenades etc. Gunshot residues are a significant source, containing metals such as Pb, Sb, Cu, Ba, Zn etc. from primers, bullets, and gun barrels (Skalny et al., 2021). Indoor shooting ranges have been found to have elevated airborne concentrations of metals such as Pb, Cu, Ni and Zn associated with PM, with Pb concentration being the highest reaching up to about 150 $\mu g/m^3$ (Orru et al., 2018). Exposure to Pb from firing have been reported to cause elevated BLL in military/police personnels (Greenberg et al., 2016; E. D. Rocha et al., 2014). Solid rocket motors used in defense systems also emit metal particles during combustion (Carlotti and Maggi, 2021). These emissions contribute to environmental metal contamination and pose potential health risks through inhalation or contact with airborne particulates.

Although Pb concentrations in the atmosphere of the A & N Islands are significantly lower compared to other regions (**Figure 8.2**), the Pb contribution from these local military activities, may add a distinctive isotopic signature. In the absence of substantial industrial activities and coal combustion, the continuous anthropogenic Pb contributors on the islands are road transport, shipping, along with military activities. However, even with these emissions, the concentration of Pb in the island atmosphere remains much lower compared to more industrialized or urbanized areas. While road and shipping emissions are consistently present and contribute regularly to atmospheric Pb levels, military activities, though less frequent, can be a significant source of Pb due to higher concentrations of Pb associated with missile testing and firing exercises. Extremely high concentrations of Pb have been reported in soils near firing ranges in previous studies, attributed to the accumulation of Pb from firing activities (Barker et al., 2021). Given the unique isotopic signatures and extremely high Pb concentrations associated with the bullet derived aerosols, this study also investigates military sources alongside the more consistent road and shipping emissions.

As of 2022, India imported approximately $164 million worth of ammunition, primarily from the United States of America (USA). Smaller portions of these imports originated from other countries, including Europe (Sweden, Spain, Germany, Finland, Italy, France, Czechia etc), Russia, Israel, and South Africa (KPMG, 2024; OEC, 2024). Thus, the available Pb isotopic signatures of

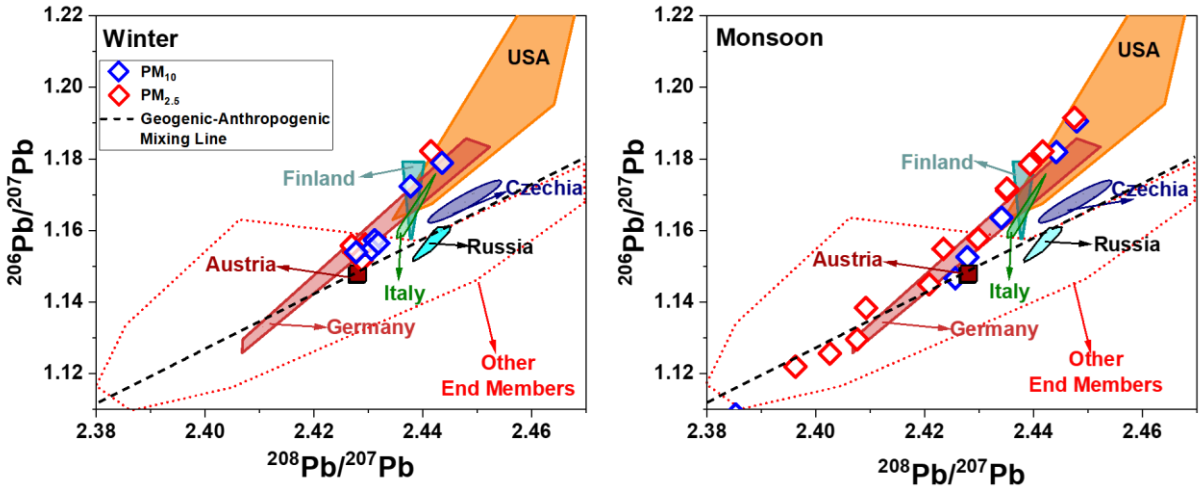

Figure 8. 10: *Three isotope plot illustrating the Pb isotopic composition of aerosols, the conventional end members as well as bullets from different regions in (a) winter and (b) monsoon seasons*

ammunition from regions were compiled (Buttigieg et al., 2003; Sjåstad et al., 2014). By comparing these isotopic compositions with that of aerosols in the A & N Islands, in three-isotope space, any potential influence of military activities in the region can be identified (**Figure 8.10**).

The available Pb isotope data includes bullets from countries such as the USA, Russia, Germany, Italy, Finland, Austria, and Czechia (Buttigieg et al., 2003; Sjåstad et al., 2014). Most bullet samples align closely with the isotopic signatures of the PM_{10} and $PM_{2.5}$ aerosols in the A & N Islands, except for those from Russia and Czechia. Bullets from Germany exhibit a broader Pb isotopic distribution in the three-isotope space compared to other bullets.

Interestingly, bullets from Finland, Italy, certain samples from Germany, and especially those from the USA are characterized by high ^{206}Pb. However, these bullets demonstrate notably lower ^{208}Pb values compared to other conventional end members with similarly high ^{206}Pb such as crust. Thus, these bullets do not plot along the conventional geogenic-anthropogenic mixing line. This pattern aligns with the unique Pb isotopic compositions observed in the A & N aerosols, suggesting these imported bullets could be a significant source of atmospheric Pb in the region. In contrast, bullet

samples from Russia, Czechia, and Austria fall along the classical geogenic-anthropogenic mixing line, resembling the isotopic range of other natural and established anthropogenic end members. The isotopic similarity between bullets from specific regions and the aerosols implies that military activities might significantly influence the local atmospheric Pb signature in the A & N Islands. To quantify whether the considered end members can adequately explain the Pb isotopic composition of aerosols in the A & N Islands, a 3D mixing polygon simulation was performed which is discussed in details in the next section (Smith et al., 2013).

8.7. Quantification of end member contributions

8.7.1. Quantifying the relevance of sources

The mixing polygon simulation assesses whether the isotopic composition of aerosols can be fully accounted for, by the isotopic composition of the identified sources. It quantifies the probability of the aerosol data points to fall within the envelope defined by the source compositions. Initially, conventional sources were considered as potential sources in the 3D mixing polygon simulation. These sources included crust, seawater, local soil, SW & biomass, vehicular fuel, ship oil, NEEs, leaded gasoline, and Indian ore. These sources, commonly observed on the Indian mainland (Lahiri et al., 2024; Ray and Das, 2023b), were examined for their potential influence on A & N aerosols through three-isotope plots (**Figure 8.9**) and elemental ratios (**Figure 8.8**). Although there are no industrial activities in the region, Indian ore was initially included to account for raw Pb ore signatures used in different processes. Transboundary aerosols from Thailand and Vietnam were incorporated as potential sources during the winter season only. Coal combustion was excluded, given its absence in the region.

The mixing polygon simulation revealed that these initial sources could only explain 28% of the aerosol Pb isotopic compositions in both winter and monsoon seasons, indicating a significant

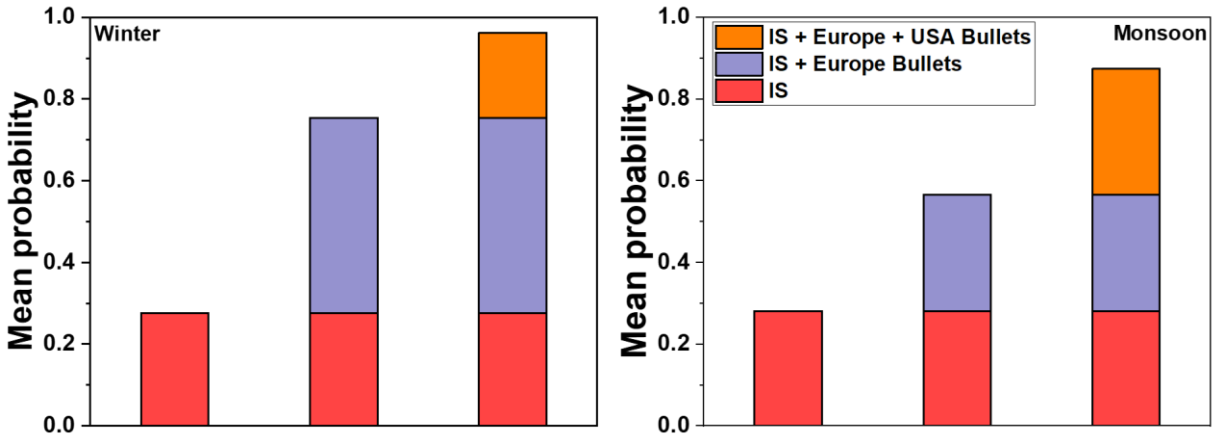

Figure 8. 11: *Results of mixing polygon simulation depicting the probability of the aerosols to lie inside the envelope formed by the end members considered*

portion of the aerosols lay outside the isotopic envelope of these sources. This suggests the presence of additional unaccounted sources (**Figure 8.10**).

As bullets were observed to be probable contributors towards aerosol Pb in the region from the three-isotope plot (**Figure 8.10**), bullets from various countries, based on import data and literature availability, were sequentially added to the polygon analysis. Incorporating European bullets (Finland, Austria, Germany, Italy) significantly increased the mean probabilities (ANOVA, $p < 0.05$) of the mixing model to 75% during winter, and 57%, during monsoon. Including bullets from the USA further raised the probabilities to 96% in winter and 87% in monsoon (**Figures 8.11a and 8.11b**). These results indicate that the Pb isotopic signatures of the aerosols could be effectively explained when bullets were included alongside conventional sources.

8.7.2. Source contributions towards atmospheric Pb

Seasonal variations in mean source contributions to atmospheric Pb were observed using Bayesian model simulations for source apportionment through MixSIAR (**Figure 8.12**). The same sources considered during the polygon simulation were considered in MixSIAR. The local topsoil exhibited varying isotopic compositions, with some samples overlapping with NEE sources (mean $^{206}Pb/^{207}Pb = 1.1396 \pm 0.0044$; n = 4). These overlapping samples were grouped with NEE, while the remaining samples, showing isotopic compositions closer to the UCC, were treated separately as local topsoil (mean $^{206}Pb/^{207}Pb = 1.1798 \pm 0.0154$). Since no significant differences in isotope ratios were observed between PM_{10} and $PM_{2.5}$ aerosol fractions (ANOVA, $p > 0.05$), the simulation was conducted separately for the two seasons while combining the two aerosol fractions. Detailed source inputs for MixSIAR are provided in **Table 8.2**.

Natural sources, such as crustal materials (local topsoil and UCC) and seawater, were significant contributors in both seasons. Crust recorded up to > 60 % contribution in both the seasons. The mean contribution from seawater increased substantially during the monsoon season, reaching up to 35%. This is consistent with higher Na/Mg ratios observed during monsoon, reflecting air masses predominantly originating from the open ocean. This elevated seawater contribution during the monsoon season results in reduced Pb enrichment in aerosols (both PM_{10} and $PM_{2.5}$) during the wet season as observed from concentration data. In contrast, during winter, air masses were primarily influenced by continental sources,

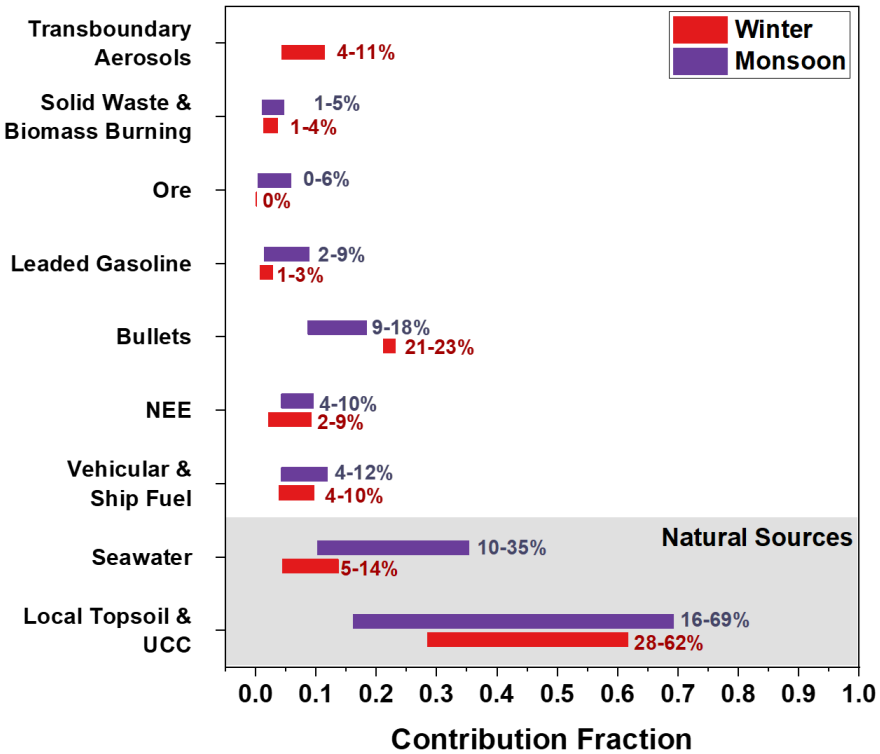

Figure 8. 12: *Contribution of different sources towards atmospheric Pb in A & N Islands as quantified using MixSIAR*

resulting in a reduced seawater contribution of up to 14%. Nevertheless, being an island, seawater contribution is always present in significant proportions in the region across seasons.

During winter, transboundary aerosols were a significant anthropogenic source, contributing up to 11% to atmospheric Pb, driven by long-range air masses originating from SEA countries. Other local anthropogenic sources recorded consistent contributions towards atmospheric Pb in the A & N islands across both the seasons. Bullets were a notable source, contributing up to 18% in winter and 23% in monsoon, suggesting a substantial influence of military activities on atmospheric Pb in the region. This was also observed qualitatively from the three-isotope plot where several aerosols overlapped with the isotopic signatures of bullets from Europe and the USA. Vehicular and ship fuel emissions were also consistent contributors, accounting for up to 10% in winter and 12% in monsoon. Non-exhaust emissions from vehicles contributed up to 9% in winter and 10% in monsoon, highlighting the persistent impact of these local sources throughout the seasons.Although leaded gasoline and Pb ore demonstrated no significant contributions during winter, minor contributions were detected in monsoon, suggesting the possibility of small-scale, localized high-temperature metallurgy activities in the region. Solid waste & biomass burning had minimal contributions in both seasons, each accounting for up to 5%.

***Table 8.2**: MixSIAR inputs of Pb isotopic composition and concentration of sources*

Sources	MeanPb206/Pb207	SDPb206/ Pb207	MeanPb208/ Pb207	SDPb208/ Pb207	MeanPb208/Pb206	SDPb208/Pb206	ConcPb206/Pb207	ConcPb208/Pb207	ConcPb208/Pb206	n
Fuel	1.130068	0.007946	2.409786	0.007015	2.132482	0.009049	94	94	94	8
SW and biomass	1.1325	0.005384	2.413	0.011133	2.1308	0.011461	10.59361	10.59361	10.59361	18
Local Topsoil	1.159689	0.023945	2.448009	0.035576	2.111164	0.014942	27	27	27	6
Seawater	1.144533	0.002647	2.425642	0.003196	2.119333	0.002249	0.000076	0.000076	0.000076	6
Ship	1.132641	0.009353	2.410362	0.010238	2.128154	0.008639	0.4856	0.4856	0.4856	8
NEE	1.141862	0.013117	2.419778	0.01749	2.119307	0.018534	40	40	40	15
USA Bullets	1.218797	0.011888	2.460972	0.005561	2.019328	0.015162	0.072	0.072	0.072	100
Europe Bullets	1.158368	0.017134	2.430361	0.011636	2.098414	0.02232	0.072	0.072	0.072	169
Crust	1.192617	0.00155	2.484248	0.001412	2.083023	0.001682	17	17	17	2
Trans	1.150122	0.005888	2.427795	0.00628	2.110933	0.006371	0.0144	0.0144	0.0144	95

Transboundary aerosol (Trans) was only considered as a source during the winter season

8.8. Implications

These observations from elemental and Pb isotopic compositions of aerosols and potential end members offer valuable insights into the sources of atmospheric Pb in the pristine A & N Islands. Notably, bullets were identified as a consistent and previously unrecognized source, reflecting the influence of military activities on local air quality. Additionally, this study determines the elemental as well as Pb isotopic signatures of ship emissions, another underexplored source, and confirms their consistent contribution to atmospheric Pb throughout the year. In the absence of widespread industrial and coal combustion activities, anthropogenic sources such as vehicular & ship emissions and military activities become the dominant and persistent sources of atmospheric Pb. The region experiences seasonal variation in sources of atmospheric Pb primarily in seawater contribution, with a marked increase during the monsoon, other anthropogenic sources remain stable across both seasons. While these sources can be equally relevant in mainland areas, they are often overshadowed by the dominance of other more significant anthropogenic activities, such as industrial emissions and open burning. In the A & N Islands, these sources become more detectable due to the absence of other major pollution sources, allowing their contribution to atmospheric Pb to be more clearly identified. The findings from this study suggest that significance of aerosol Pb from previously overlooked military sources becomes particularly pronounced in remote areas, where industrial and urban contributions to Pb pollution are negligible.

The investigation of sources of atmospheric Pb in India thus, provides a detailed assessment of its sources across varied environments, from urban, industrial and pristine. Each chapter contributes a understanding of how anthropogenic activities shape atmospheric metal pollution, particularly Pb.

The next chapter builds on these findings to focus on remediation strategies for atmospheric Pb, emphasizing on innovative and sustainable approaches. It is important to bridge the critical gap between identifying pollution sources and implementing effective control measures. The source apportionment approach applied so far can also be utilized in remediation studies to monitor and quantify the effectiveness of the mitigation efforts. If the metals removed through remediation correspond to the atmospheric sources identified, it validates the hypothesis of reducing airborne metal load. The next chapter, will provide a framework for tackling atmospheric metal contamination.

CHAPTER 9: REMEDIATION OF ATMOSPHERIC Pb

9.1. Introduction

Particulate matter serves as a primary carrier of heavy metals discharged into the atmosphere from various anthropogenic activities (Komárek et al., 2008; Li et al., 2013). Heavy metals such as manganese (Mn), cobalt (Co), chromium (Cr), nickel (Ni) and arsenic (As) bound to PM have been found to be bioaccessible and pose significant health hazards (Kumari and Bhattacharya, 2023; Roy et al., 2023; Vithanage et al., 2022; Xu et al., 2017). Inhalation of PM bound Pb elevates blood Pb levels and causes cardiovascular and neurological disorders (Lum et al., 1982; UNICEF and Pure Earth, 2020).

Plants are bioindicators and biomonitors of such PM bound pollutants. Especially, ferns being epiphytes can directly absorb nutrients and pollutants from the atmosphere, making them suitable phytomonitors and potential mitigators of atmospheric PM pollution (L. D. Rocha et al., 2014). Although ferns have been proven to be highly tolerant of heavy metals present in soil (Kachenko et al., 2007), comprehensive studies on atmospheric pollutant uptake by ferns compared to other plants are limited. The PM capture efficiency of plant species has mostly been studied and quantified utilising gravimetric techniques and surface morphological studies such as scanning electron microscopy (SEM) and energy dispersive X-ray (EDX) (Abhijith and Kumar, 2020; Beckett et al., 2000; Hrotko et al., 2020; Meravi et al., 2021; Ottelé et al., 2010; Paull et al., 2019; Redondo-Bermúdez et al., 2021; Sgrigna et al., 2015; Weerakkody et al., 2017). However, such studies cannot prove the absorption of atmospheric pollutants in plant tissues. Non-essential and toxic heavy metals such as Pb, Cd etc are internalised by various plants through foliar uptake of PM as demonstrated by elemental concentration studies (Hu et al., 2011; Schreck et al., 2012a, 2012b; Uzu et al., 2010). However, source identification of pollutants inside plant tissue solely based on elemental concentration is difficult. Stable isotope systems coupled with elemental concentration analyses are much effective is source apportionment studies. As isotopes of Pb (^{204}Pb, ^{206}Pb, ^{207}Pb and ^{208}Pb) do not undergo fractionation during physicochemical processes (Komárek et al., 2008), it is considered to be a robust geochemical tool for source tracing. Lead isotopic compositions have previously been utilised to delineate the sources of Pb inside edible (Bi et al., 2009; Cong et al., 2022; Fan et al., 2020; Gao et al., 2021; Li et al., 2012; Ma et al., 2019a, 2019b; Xiong et al., 2014; X.-Y. Zhang et al., 2022) and wild (Hu et al., 2011; Klaminder

et al., 2005) plants. From these studies, atmospheric fallout was found to be a significant contributor towards the presence of Pb inside the plants.

Indian cities are ideal locations for such studies. The densely populated Indo-Gangetic plain consists of 12 cities that are among the top 20 polluted cities in the world in terms of PM pollution (David et al., 2019). Hence, plants growing in such regions are assumed to have a high tolerance for a wide range of pollutants and can be potential remediating agents. This study has selected 2 abundantly growing fern species in densely populated regions with high traffic and small-scale industries from eastern India were selected for the present study (Gupta et al., 2008; Upadhyay et al., 2014) (**Figure 9.1**). Sampling was conducted at 12 sites in two heavily polluted Indian cities, viz., Kolkata (22.51°N, 88.63°E) and Howrah (22.52°N, 88.19°E). According to a recent report on air quality and health in global cities, Kolkata ranks the 2nd in terms of annual average $PM_{2.5}$ exposures (State of Global Air, 2022). Sampling was performed between March to May, 2022, during springtime which corresponds to the peak growth period of the ferns. Moreover, this pre monsoon period ensures the capture of highest amount of dust on the leaf surfaces.

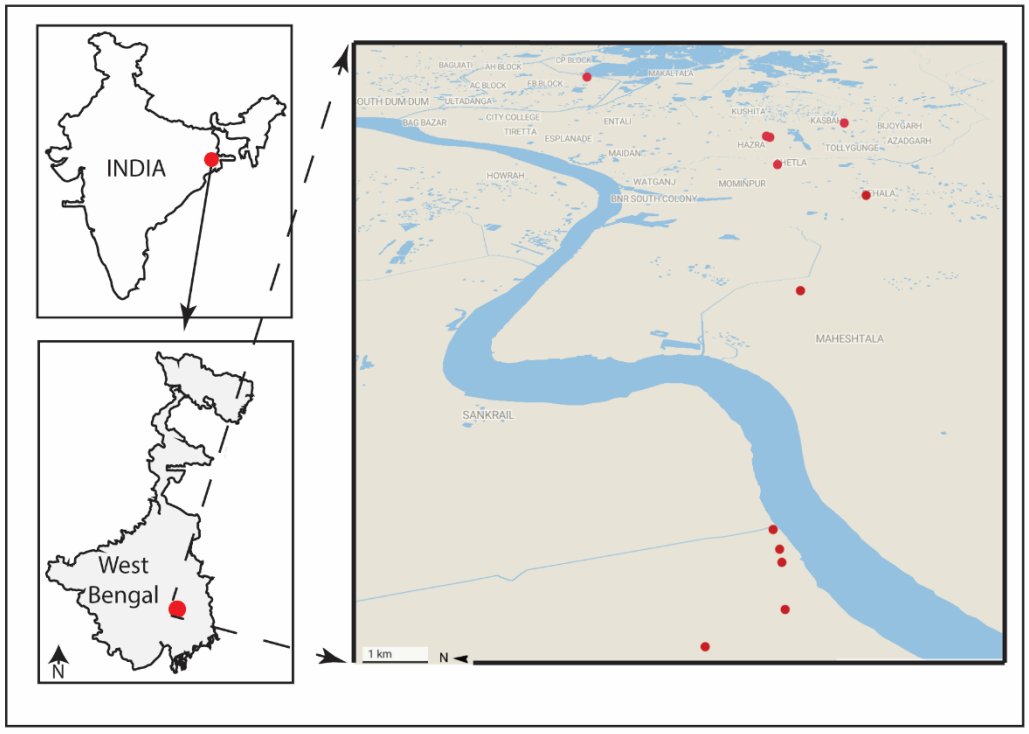

Figure 9. 1: Location of the sites from where the ferns were sampled in Eastern India

The study utilises gravimetric techniques, surface characterisations, elemental concentrations and Pb isotopic compositions to:

(i) investigate their foliar dust capture capacity
(ii) determine the sources of heavy metals on separated layers of foliar surface and inside fern tissues using elemental concentration coupled with Pb isotopic compositions
(iii) quantify the relative contribution of individual sources (soil, PM_{10}, dust fall) towards metal concentration in the plant tissues using stable isotope mixing model (MixSIAR).

Based on the results, the study hypothesises that the results obtained from this biomonitoring study can provide implications for the usage of ferns for cleaning up indoor air in polluted urban settings.

9.2. Atmospheric PM_{10} concentration and dustfall (DF) flux

The concentrations of PM_{10} aerosols ranged from 208 – 726 $\mu g/m^3$ (mean = 326 $\mu g/m^3$). Throughout all sampling days, the PM_{10} concentrations consistently exceeded the 24hr average PM_{10} concentration limits of 150 $\mu g/m^3$, specified by National Ambient Air Quality Standards (NAAQS) (US EPA, 2020). The DF flux ranged from 0.56 g/m^2/day to 2.32 g/m^2/day with an average of 1.37 g/m^2/day (**Figure 9.2a**). The observed dust flux ranges in this study conform with those recorded at industrial sites in the country, while being an order of magnitude higher than the levels recorded at urban sites (**Figure 9.2b**) (Agrawal and Singh, 2000; Majee et al., 2023; Meravi et al., 2021; Mishra and Kulshrestha, 2017; Singh and Agrawal, 2005). A high DF flux and aerosol concentration, characteristic of industrial influences can be beneficial in assessing the maximum anthropogenic particle capture efficiency, and consequently the efficiency of metal capture by the ferns.

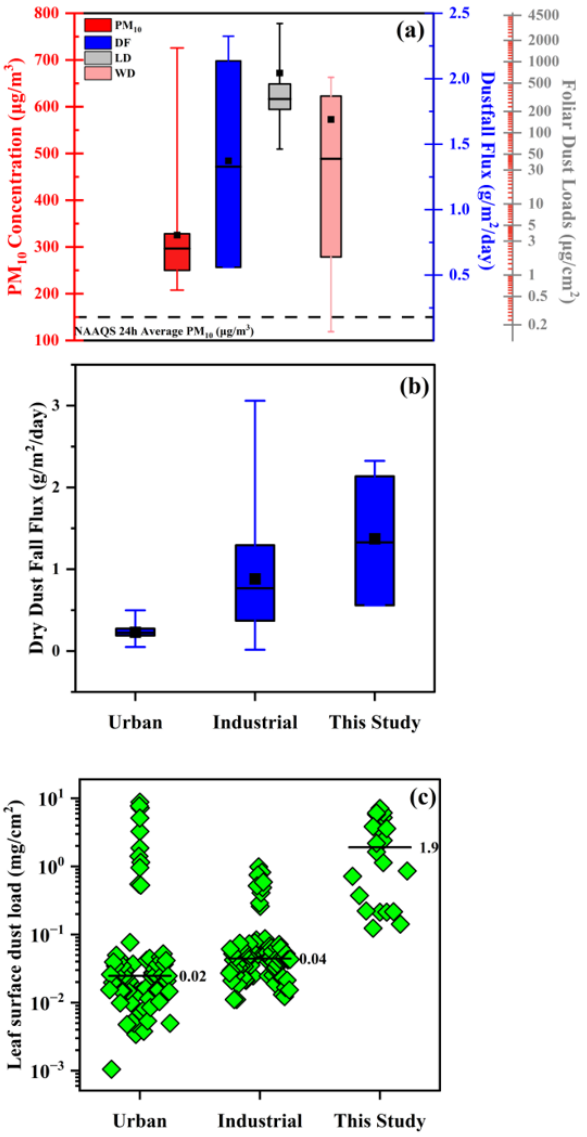

Figure 9. 2: *(a) Box plots depicting PM_{10} aerosol concentration, dust fall (DF) and foliar dusts (loose dust (LD) and wax dust (WD)). The NAAQs 24 hrs average limit for PM10 concentration is marked for reference; (b) Box plots depicting a comparison of dust fall fall fluxes between this study, industrial and urban settings. The upper and lower extremes of the boxes represent 75 and 25 percentile values respectively. The whiskers represent the highest and lowest values. Squares and lines inside boxes indicate mean and median values respectively. (c) Total leaf surface dust load (LD + WD) on the fern samples (n = 22). Foliar surface dust loads from previous studies conducted in urban and industrial settings are plotted for comparison. The ferns from this study demonstrates higher median dust loads compared to the previous studies. The lines represent the median dust loads. The values of the medians are indicated on the right-hand side of the plots.*

9.3. Leaf surface dust load and SEM-EDX observations

The loose dust (LD) and wax bound dust (WD) loads (n = 22) ranged from 0.06 – 3.59 mg/cm^2 (mean = 1.34 mg/cm^2) and 0.0002 – 4.14 mg/cm^2 (mean = 1.18 mg/cm^2), respectively. The clustering of dust on the leaf surface can be observed from the scanning electron micrographs

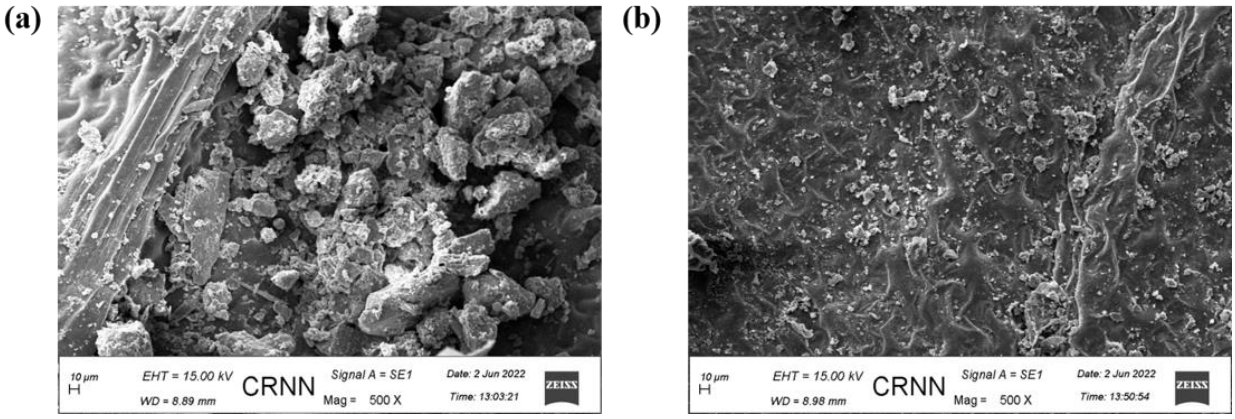

Figure 9. 3: *Representative scanning electron micrographs of (a) adaxial and (b) abaxial surface. The adaxial surface has greater accumulation of dust particles compared to abaxial surface.*

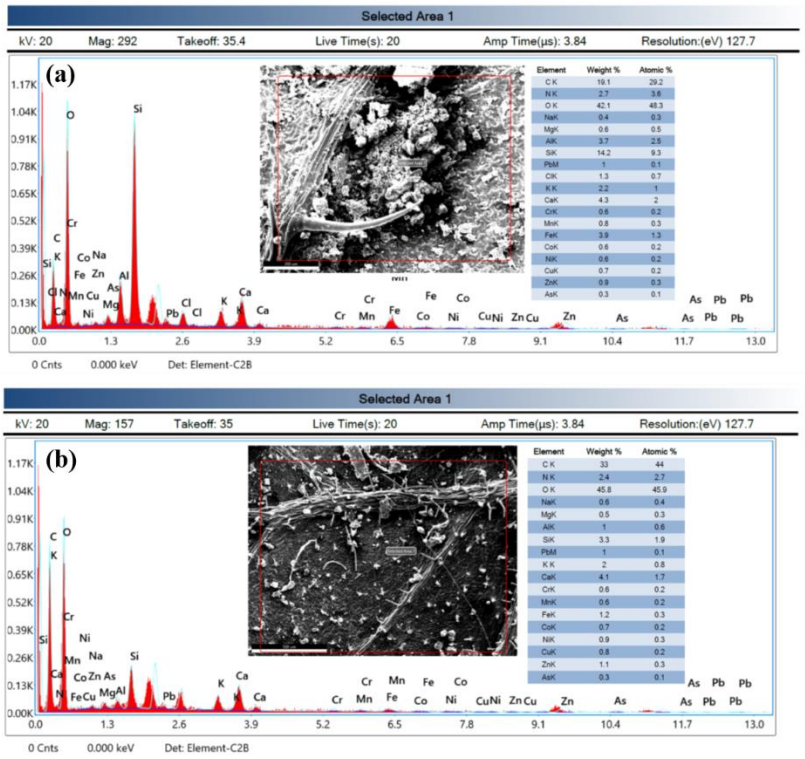

Figure 9. 4: *EDX spectra of selected areas from (a) adaxial and (b) abaxial surfaces of fern leaves. The tables for weight and atomic percentage of metals identified on the surface are included as insets. EDX study reveals the presence of heavy metals like Fe, Mn, Pb, Co, Ni, Cu, Zn and Cr.*

(**Figure 9.3**). A large quantity of dust may have formed non – stoichiometric compounds, which may have led to charge generation on the dust surface (Abubakar et al., 2020). This charged surface attracted more dusts and resulted in clustering in some regions. The adaxial surfaces had much more clustering than the abaxial surfaces. Leaf surface dust loads (LD + WD) exhibit a higher

median value, (**Figure 9.2c**) compared to previous studies in urban and industrial regions of India (Meravi et al., 2021; Prajapati and Tripathi, 2008; Prusty et al., 2005; Roy et al., 2020; S. Singh et al., 2018; Yunus et al., 1985), indicating a higher efficiency in dust capture capacity of the ferns. Initial observations from EDX indicates presence of heavy metals like Fe, Mn, Pb, Co, Ni, Cu, Zn and Cr on the leaf surfaces (**Figure 9.4**).

9.4. Elemental concentration & enrichment factor (EF)

Median concentrations are reported in this study as they are generally not influenced by extreme values or outliers. Additionally, crustal enrichment factors are calculated to understand the

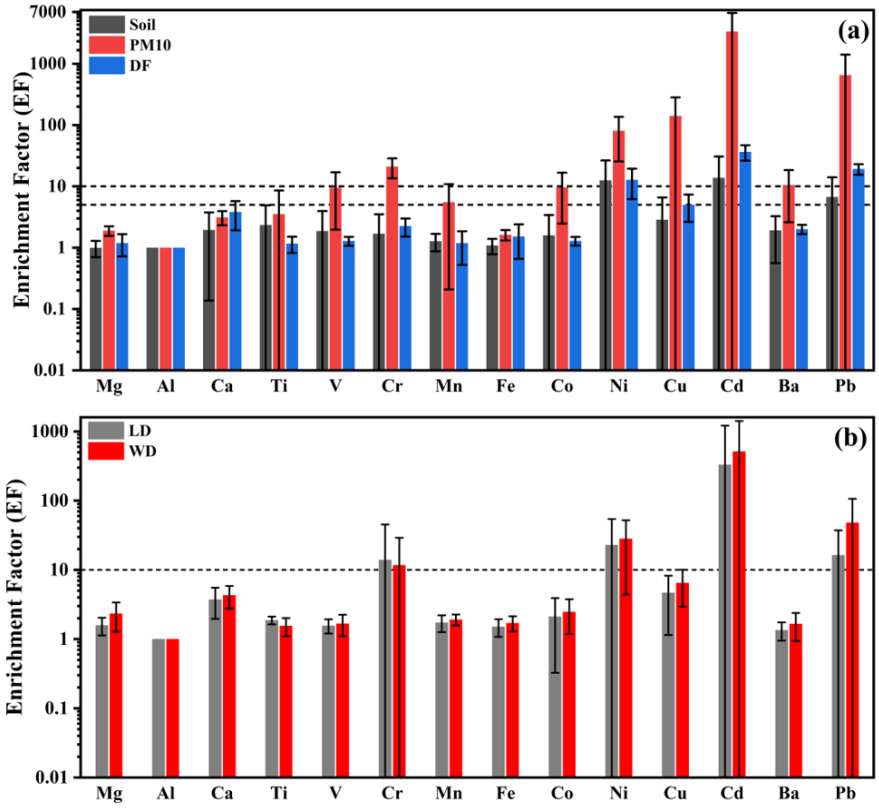

Figure 9. 5: *Bars with 1 SD depicting mean enrichment factors (EFs) of (a) PM10 aerosols, PDs, soil and (b) LD & WD. The dotted lines represent the threshold EF values (5 for soil and 10 for PM10, PD, LD and WD). Samples recording EFs beyond the threshold EFs are considered to have anthropogenic inputs. For each type of sample, the elements, Ni, Cd and Pb were observed to be enriched consistently, suggesting anthropogenic inputs. PM_{10} aerosols, LD and WD exhibits high EFs for Cr*

geogenic versus anthropogenic sources of the elements in PM_{10}, DF and soil. The crustal enrichment factors (EF) defined as $EF = \left(\frac{\left(\frac{Element}{Reference\ element} \right)_{Sample}}{\left(\frac{Element}{Reference\ element} \right)_{Crust}} \right)$ for all elements were compared

with Al as the reference element. The average elemental composition of the crust was adopted from previous literature (Rudnick and Gao, 2003).

9.4.1. Aerosol (PM_{10}) and Dust fall (DF)

Elemental compositions for individual samples are provided in **Table 9.1 – 9.7**. Median elemental concentration of PM_{10} aerosols and DF generally follow (Al, Ca, Fe, Mg) > (Ba, Cr, Cu Mn, Ni, Pb, Ti, V) > (Cd, Co). Enrichment factors for Ni, Cd and Pb are above 10, indicating anthropogenic sources (**Figure 9.5a**). Especially, Pb and Cd were heavily enriched in PM_{10} (Mean: $EF_{Pb} = 652 \pm 752$, $EF_{Cd} = 3355 \pm 3385$).

9.4.2. Soil

The median concentrations of the elements in soil generally follow the order (Al, Ba, Ca, Fe, Mg, Ti) > (Mn, Ni, V, Cr) > (Cd, Co, Cu, Pb). Soils exhibit average EFs for Mg, Ca, Ti, V, Cr, Mn, Fe, Co, Cu and Ba in the range of 0.9 – 3.8, while those of Ni, Cd and Pb were > 5 (Figure 9.5a). Elements with $2 < EF < 5$ are considered to have moderate enrichment with a dominant contribution from crustal sources, while $5 < EF < 20$ suggests significant non – crustal sources (Sutherland, 2000). Nickel, Pb and Cd were also enriched in PM_{10} and DFs (Figure 9.5a). Thus, the enrichment of these elements in soil may have resulted from the deposition of atmospheric particulates on the soil surface (Vilomet et al., 2003).

9.4.3. Foliar dusts (LD and WD) and Fern Tissues (Roots and Leaves)

The elemental concentrations of the foliar dusts were normalised with respect to the total dry weight of the leaves (mg/kg), presented in Supplementary Material 2. The LDs and WDs followed the general order of (Ti, Mg, Al, Fe, Ca) > (Ba, Ni, Mn) > (V, Pb, Cr) > (Cd, Co, Cu). The elemental concentrations of the LDs were around 1.5 – 4 times that of the WDs indicating preferential internalisation of PMs based on size (Sgrigna et al., 2015; H. Wang et al., 2019). The Mean EFs of Cr, Ni, Cd and Pb on LD and WD were ≥ ~10, indicating anthropogenic contributions (Figure 9.5b). The high EFs of Ni, Cd and Pb on PM_{10}, DF, LD, WD as well as soil indicate that these elements were sourced from atmospheric fallouts on the leaf surfaces as well as soil.

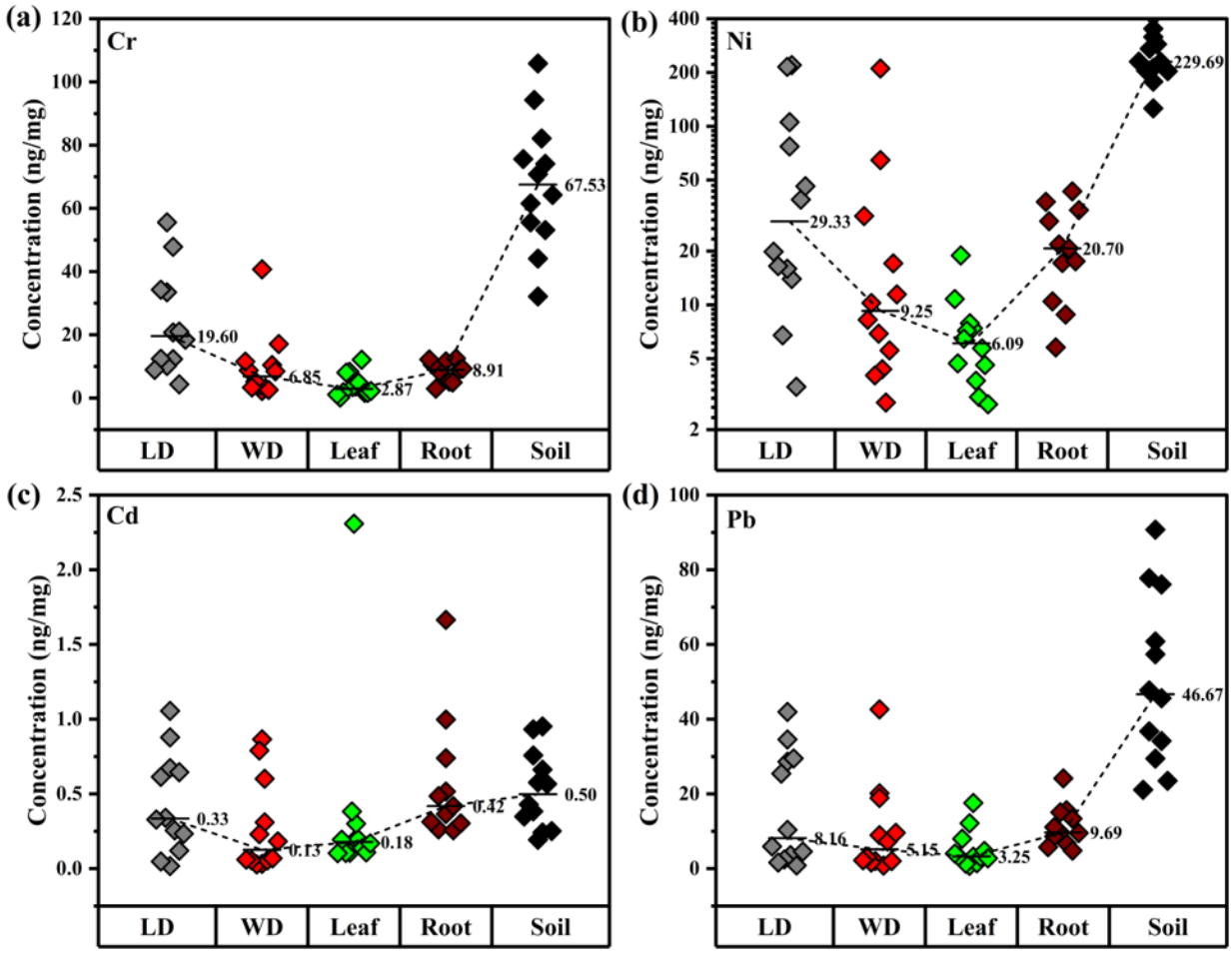

Figure 9. 6*: Concentrations of (a) Cr, (b) Ni, (c) Cd and (d) Pb in LD, WD, leaf, root and soil of the fern samples. The figures on the right-hand side of the symbols indicate the median concentrations illustrated by a solid black line.*

The median elemental concentrations in leaves and roots followed the general order (Al, Ca, Fe, Mg) > (Ba, Cr, Cu Mn, Ni, Pb, Ti, V) > (Cd, Co). The translocation of the metals within the leaf tissues can occur from foliar dust, roots or a combination of both pathways. The median concentration of the enriched metals (Cr, Ni, Cd, and Pb) follows the overall pattern LD > WD > Leaves (**Figure 9.6**). Leaf and WD demonstrated comparable concentrations of Cr, Ni, Cd and Pb (**Figure 9.6**). From soil to the leaves Cr, Ni, Cd and Pb follow Soil > Root > Leaf. Samples having high foliar dust loads (Range: 0.72 - 3.5 mg/cm^2, mean ± 1SD: 1.73 ± 1.21 mg/cm^2) had elevated concentrations of Al, Ca, Ti, V, Mn, Fe, Co, Ba and Pb (**Figure 9.7**) compared to the ones with low foliar dust loads (less than 0.4mg/cm^2, Range: 0.12 - 0.37 mg/cm^2, Mean ± 1SD: 0.22 ± 0.08

mg/cm^2). These elements also demonstrated positive correlation between foliar dust loads and leaves (**Figure 9.8, and Figure 9.9**) indicating dominance of foliar translocation. Additionally, Ti, Fe and Co demonstrated moderate to strong correlations (Pearson's r = 0.46 - 0.81; p value < ~0.05) between leaves and roots as well (**Figure 9.8**) which were not observed for Al, Ca, V, Mn and Ba (**Figure 9.8**). This implies Ti, Fe and Co were translocated to the leaves bidirectionally through both roots and foliar surface. While, Al, Ca, V, Mn and Ba having no correlation with root and leaf indicates dominance of foliar translocation of these metals. However, relying solely on elemental concentrations is inadequate for identifying the source of metals in fern tissues. Consequently, the

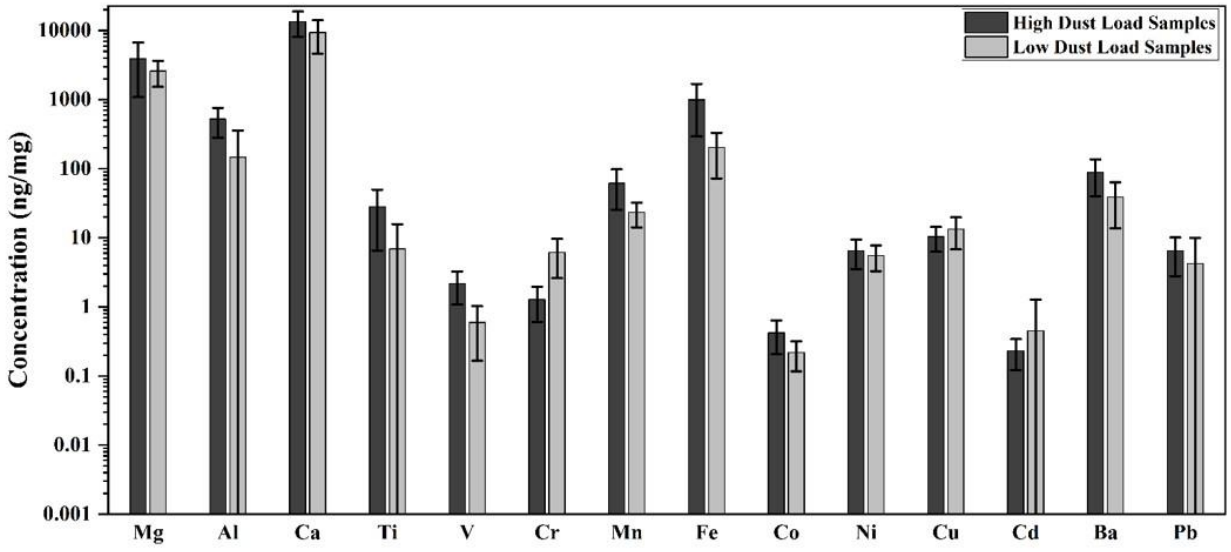

Figure 9. 7: *Leaf elemental concentration of samples having high foliar dust load represented by dark grey bars and low foliar dust samples represented by light grey bars. Samples having higher foliar dust loads had elevated concentrations of Mg, Al, Ca, Ti, V, Mn, Fe, Co, Ba and Pb. The y-axis is presented in logarithmic scale.*

inclusion of Pb isotopic compositions becomes imperative for a more accurate determination.

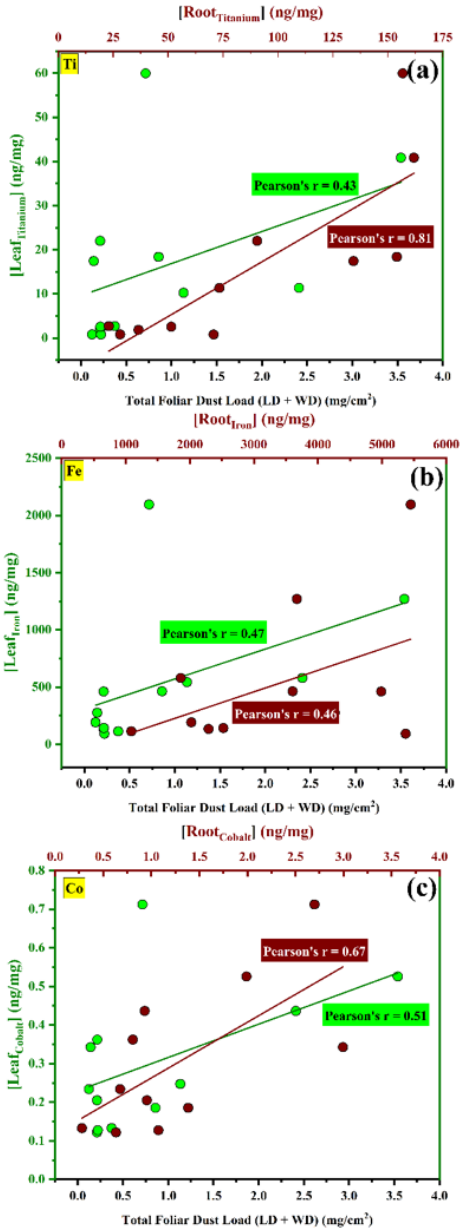

Figure 9. 8*: Correlation between total foliar dust load (LD +WD) vs leaf elemental concentrations and root elemental concentration vs leaf elemental concentration for (a) Ti, (b) Fe and (c) Co. The bottom x axis represents total foliar dust loads and top x axis represents elemental concentration of root. Both the axes are linked to left y axis representing leaf elemental concentration. The [leaf] vs foliar load data are plotted in green circles while the [root] vs [leaf] data are plotted in reddish brown circles (n = 12 each). All these 3 elements demonstrate simultaneous moderate to strong correlation between foliar dust vs [leaf] and [root] vs [leaf], indicating bidirectional translocation of these metals from root to leaf and foliar surface to leaf.*

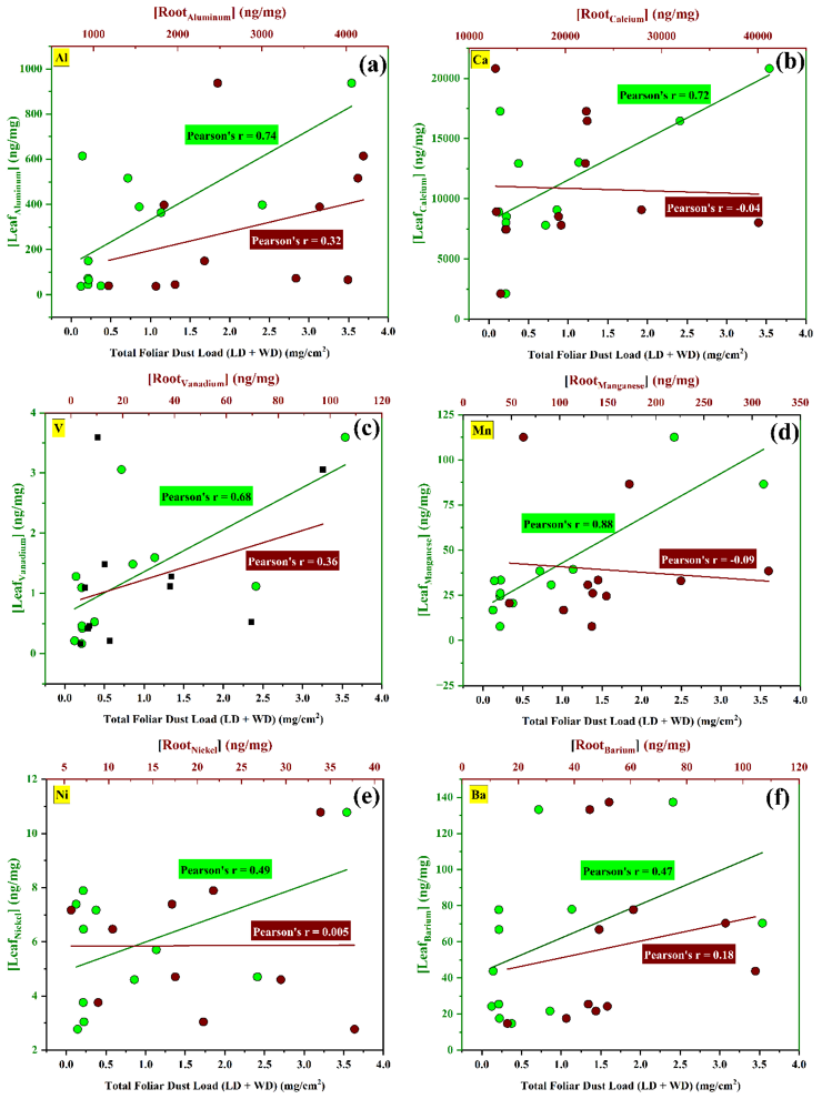

Figure 9. 9: *Correlation between total foliar dust load (LD +WD) vs leaf elemental concentrations and root elemental concentration vs leaf elemental concentration for (a) Al, (b) Ca, (c) V, (d) Mn, (e) Ni and (f) Ba. The bottom x axis represents total foliar dust loads and top x axis represents elemental concentration of root. Both the axes are linked to left y axis representing leaf elemental concentration. The [leaf] vs foliar load data are plotted in green circles while the [root] vs [leaf] data are plotted in reddish brown circles (n = 12 each). All these 6 elements demonstrate moderate to strong correlation between foliar dust vs [leaf], while demonstrating weak to no correlation between [root] vs [leaf], indicating dominance of foliar translocation.*

Table 9.1: *Elemental concentration in PM_{10} aerosols (ng/m^3)*

Sample #	Mg	Al	Ca	Ti	V	Cr	Mn	Fe	Co	Ni	Cu	Cd	Ba	Pb
1	1359	3034	5248	2192	71	124	107	2753	12	270	401	13	464	421
2	1385	3564	4084	2596	69	65	93	2617	11	230	317	7.7	447	309
3	2119	4894	4885	271	118	149	198	4505	21	423	600	21	550	774
4	1243	3522	3061	257	87	142	131	3515	13	300	228	49	452	2061
5	1035	2868	1850	102	39	62	97	1720	8.2	193	244	6.9	247	396
6	821	1834	1705	112	28	46	55	1468	5.8	153	182	14	287	178
7	1044	3242	2667	165	48	72	58	1937	9.5	174	142	8.7	341	246
8	3278	11658	13302	1152	33	253	713	12667	7.5	217	84	27	197	1512
9	1952	5744	6244	544	14	151	1273	6772	4.3	108	39	14	90	314
10	1036	3578	3213	269	10	57	164	3439	1.9	39	11	2.4	41	47
11	1574	5819	5795	682	19	140	447	6461	4.5	116	45	43	164	2086
12	1238	4072	3318	263	10	60	153	3534	2.1	47	30	2.2	644	108
13	899	3029	2409	232	16	47	114	2643	1.7	38	12	1.8	49	73
14	1254	3800	3463	275	13	58	137	3829	2.3	114	24	2.2	45	65
MEDIAN	1248	3571	3391	270	30	69	134	3477	6.7	164	113	11	267	311
MEAN	1446	4333	4375	651	41	102	267	4133	8	173	168	15	287	614
SD	645	2375	2930	792	33	60	340	2920	5	110	176	15	201	726

Table 9.2: *Elemental concentration in soil samples (mg/kg)*

Sample #	Mg	Al	Ca	Ti	V	Cr	Mn	Fe	Co	Ni	Cu	Cd	Ba	Pb
1	7938	57247	22928	1090	64	71	778	28475	10	212	39	0.58	1245	91
2	7124	54036	10429	4747	67	62	461	25925	9	205	30	0.24	480	46
3	7774	41578	27587	2764	63	74	523	31835	9	229	39	0.38	477	76
4	9020	29821	67008	4709	63	44	602	29924	5	230	15	0.25	498	29
5	6811	56246	21492	4513	73	82	502	28328	11	288	37	0.35	638	48
6	5631	33207	11742	2957	54	56	387	21839	13	203	20	0.43	614	34
7	12651	65218	23941	4912	99	76	647	38937	16	316	47	0.95	439	37
8	14237	74627	40012	5475	125	94	962	46540	17	352	44	0.66	662	61
9	12789	54175	60662	3300	62	64	844	27756	10	272	32	0.76	609	57
10	5782	43437	13745	1927	39	32	297	16556	7	126	7	0.19	343	21
11	5200	35358	10412	3285	92	53	314	17191	12	178	28	0.57	297	23
12	3029	12748	5880	6088	127	106	204	9653	20	414	64	0.93	561	78
MEDIAN	7449	46475	26320	3814	78	68	543	26913	12	252	33	0.52	572	50
MEAN	8165	46475	26320	3814	78	68	543	26913	12	252	33	0.52	572	50
SD	3431	17108	19905	1497	28	21	233	9976	4	80	15	0.26	241	23

Table 9.3: *Elemental concentration in dustfall samples(mg/kg)*

Sample #	Mg	Al	Ca	Ti	V	Cr	Mn	Fe	Co	Ni	Cu	Cd	Ba	Pb
1	3762	12889	22937	568	22	41	84	9714	4.0	84	26	0.41	199	45
2	2797	9428	16865	496	16	32	63	7401	2.9	63	28	0.33	175	39
3	3969	13952	23018	508	22	45	82	10518	3.9	82	29	0.48	187	44
4	1660	17131	7255	1443	31	38	248	9658	4.9	107	24	1.1	204	93
5	3830	27383	23162	1554	35	41	333	12072	5.2	111	23	1.1	403	103
6	5291	26588	19788	1477	31	47	585	47787	7.2	396	25	1.0	484	108
MEDIAN	3796	15542	21362	1005	26	41	166	10116	4.4	95	26	0.8	201	69
MEAN	3552	17895	18837	1007	26	41	233	16192	5	140	26	1	275	72
SD	1222	7463	6196	531	7	5	204	15552	1	126	2	0	133	33

Table 9.4: *Elemental concentration in loose dust (LD) samples(mg/kg)*

Sample #	Mg	Al	Ca	Ti	V	Cr	Mn	Fe	Co	Ni	Cu	Cd	Ba	Pb
1	347	1054	1950	101	2.06	12.36	19	896	0.44	14	1.69	0.26	19	3.63
2	596	2762	1282	242	3.91	10.16	31	1827	0.66	16	3.14	0.02	24	2.47
3	64	170	247	14	0.27	4.35	3	155	0.09	3	0.33	0.05	2	0.84
4	38	99	209	7	0.18	12.43	2	142	0.16	7	0.50	0.34	1	1.65
5	1839	5607	6753	482	10.88	18.45	91	4931	1.92	39	5.72	0.23	51	10.39
6	710	2168	3297	193	4.34	8.91	35	1880	0.77	16	2.58	0.12	21	4.57
7	2067	8245	10032	656	14.00	20.75	118	5365	2.11	46	9.74	0.67	87	28.62
8	4260	14177	22344	1095	23.73	33.46	312	9967	3.25	77	13.54	0.88	177	34.57
9	668	5470	2104	490	8.38	21.03	47	2682	1.85	20	14.19	0.33	45	5.94
10	5394	28238	20010	2814	60.57	47.84	404	20921	8.42	220	20.80	0.61	281	41.95
11	4957	18193	10284	1535	28.42	34.28	245	14545	6.03	105	8.49	1.06	158	25.43
12	10192	26537	28123	3051	80.83	55.58	512	28364	11.25	215	38.86	0.65	161	29.49
MEDIAN	1275	5539	5025	486	10	20	69	3807	1.9	29	7.1	0.33	48	8.2
MEAN	2594	9393	8886	890	20	23	152	7640	3	65	10	0.43	86	16
SD	3075	10080	9610	1057	26	16	174	9149	4	77	11	0.33	89	15

Table 9.5: *Elemental concentration in wax bound dust (WD) samples(mg/kg)*

Sample #	Mg	Al	Ca	Ti	V	Cr	Mn	Fe	Co	Ni	Cu	Cd	Ba	Pb
1	78	223	310	17	0.47	2.24	4.61	233	0.13	4.36	0.53	0.60	5.87	8.98
2	355	1025	1066	76	1.53	3.98	18.52	644	0.29	6.90	2.16	0.03	11.84	2.04
3	193	201	375	11	0.30	3.12	2.54	149	0.08	2.84	0.47	0.03	2.79	0.83
4	41	72	128	4	0.14	5.23	1.31	90	0.08	4.03	0.37	0.05	0.75	1.64
5	127	332	752	27	0.71	2.59	6.36	339	0.16	5.55	0.73	0.87	3.61	7.26
6	515	1499	1635	121	2.71	3.34	24.82	1292	0.49	10.25	1.70	0.06	13.91	3.05
7	754	1810	3374	124	3.32	10.48	36.13	1842	0.79	17.08	4.45	0.31	23.88	20.18
8	129	669	416	67	1.14	8.77	8.19	326	0.25	8.25	0.74	0.07	8.27	2.04
9	221	559	616	56	1.72	8.47	9.69	505	0.48	11.44	1.59	0.06	9.90	2.24
10	5117	18565	17219	447	14.08	11.55	359.09	19909	2.38	64.63	6.20	0.23	73.41	18.91
11	840	1782	1833	153	3.92	17.09	35.53	2012	1.24	31.43	2.88	0.18	26.50	9.59
12	7874	18686	23551	1542	61.44	40.73	452.71	23248	10.41	210	57	0.79	149	43
MEDIAN	288	847	909	72	1.6	6.8	14	574	0.38	9.2	1.6	0.13	11	5.2
MEAN	1354	3785	4273	220	8	10	80	4216	1	31	7	0.27	27	10
SD	2486	6958	7699	433	17	11	154	8167	3	59	16	0.31	43	12

Table 9.6: *Elemental concentration in leaf samples(mg/kg)*

Sample #	Mg	Al	Ca	Ti	V	Cr	Mn	Fe	Co	Ni	Cu	Cd	Ba	Pb
1	3700	37	8921	0.81	0.21	3.63	16.81	192	0.23	7.39	9.87	2.31	24.31	17.57
2	384	73	2122	22.02	1.10	3.49	7.76	461	0.21	7.89	25.16	0.19	25.46	3.21
3	2523	45	7454	1.86	0.17	4.89	24.59	134	0.12	3.76	19.00	0.11	77.79	0.76
4	3040	39	12936	2.68	0.53	8.32	20.65	113	0.13	7.17	9.94	0.20	14.79	1.43
5	2905	66	8524	0.78	0.42	12.10	33.40	93	0.13	3.04	12.07	0.10	17.63	1.28
6	2411	149	8017	2.55	0.46	8.08	26.18	143	0.36	6.47	9.66	0.14	66.81	3.06
7	4425	364	13026	10.23	1.59	1.64	39.37	543	0.25	5.71	7.64	0.30	78.04	12.14
8	1997	516	7804	59.97	3.06	1.85	38.47	2096	0.71	18.90	7.58	0.19	133.24	8.01
9	2003	389	9085	18.38	1.49	1.64	30.78	463	0.19	4.60	8.39	0.11	21.66	4.74
10	8588	397	16460	11.35	1.12	0.19	112.56	580	0.44	4.71	17.23	0.38	137.30	3.29
11	3094	614	17268	17.42	1.28	2.25	33.05	276	0.34	2.78	6.99	0.10	43.78	2.76
12	2449	937	20812	40.85	3.59	1.08	86.59	1270	0.53	10.78	10.80	0.17	70.30	4.03
MEDIAN	2714	257	9003	11	1.1	2.9	32	369	0.24	6.1	10	0.18	55	3.2
MEAN	3126	302	11036	16	1.3	4.1	39	530	0	6.9	12	0.36	59	5.2
SD	1984	287	5203	18	1.1	3.6	30	593	0	4.4	5.6	0.62	43	5.0

Table 9.7: *Elemental concentration in root samples(mg/kg)*

Sample #	Mg	Al	Ca	Ti	V	Cr	Mn	Fe	Co	Ni	Cu	Cd	Ba	Pb
1	3350	1742	12836	28	15	12	104	2023	0.68	17	20	0.52	52	7
2	2934	3404	13287	91	5	5	133	4988	0.95	22	29	0.37	45	16
3	4183	1969	13852	37	4	5	149	2293	0.63	9	23	0.74	61	10
4	2001	1180	22082	23	70	8	48	1087	0.28	6	24	0.26	16	5
5	6066	4021	19299	71	7	5	140	5369	1.07	21	22	0.26	37	9
6	2871	2318	40068	51	7	3	134	2522	0.81	10	18	0.49	49	10
7	4639	4140	19571	157	97	13	317	5447	2.70	43	28	1.00	45	15
8	2417	3685	27911	154	13	11	129	3604	1.38	29	11	0.31	48	13
9	5668	1838	22274	73	38	9	62	1858	0.93	18	10	0.30	52	6
10	3108	4205	22183	134	39	12	226	4261	2.99	38	13	0.42	104	11
11	4201	2474	12741	162	10	9	172	3671	1.99	34	37	1.66	94	24
MEDIAN	3350	2474	19571	73	13	8.9	134	3604	0.95	21	22	0.42	49	10
MEAN	3767	2816	20555	89	28	8.3	147	3375	1.31	22	21	0.57	55	11
SD	1307	1100	8147	54	31	3.3	74	1518	0.88	12	8.3	0.43	25	5.6

9.5. Elemental ratios as source tracers of foliar dusts

Elemental ratios are effective tracers for source apportionment studies (R. Das et al., 2018; Ray et al., 2022; Sen et al., 2016). As plants have differences in tolerance levels for different metals, elemental ratios are not reliable for source delineation within tissues. Thus, elemental ratios have been used to trace sources specifically for foliar surface dust. As Ti is a conservative element, with no anthropogenic influence (EF < 2) it was utilized to normalize the enriched elements such as Ni, Cd and Pb to distinguish between crustal and atmospheric deposition (Shotyk, 1996). The Pb/Ti, Cd/Ti, Ni/Cd and Pb/Cd ratios from previous literature coincide with those of the present study. This suggests that the sources of PM_{10} in the region have been similar over nearly a decade. The plot between Pb/Ti vs Cd/Ti (**Figure. 9.10a**) demonstrates that the characteristic ratios of LDs and WDs fall between those of soil, DFs and PM_{10}. This indicates that the leaf surface dusts were a mixture of soil, DF and PM_{10}. Enriched elements such as Ni, Cd and Pb when plotted as Ni/Cd vs Pb/Cd (**Figure. 9.10b**) overlap with PM_{10} samples, suggesting that these elements were primarily sourced from the atmosphere. The elemental ratios of the WDs and LDs closely align with PM_{10} and DF. In most cases, WDs exhibit a stronger association with PM_{10} aerosols, while LDs are relatively closer to the soil. Anthropogenically sourced elements like Pb and Cd that concentrate in the finer fraction of PM_{10} (Birmili et al., 2006) were significantly correlated (Pearson's correlation coefficient = 0.97; p value = 2E-8) in PM_{10} aerosols. Copper, although enriched in PM_{10}, was not

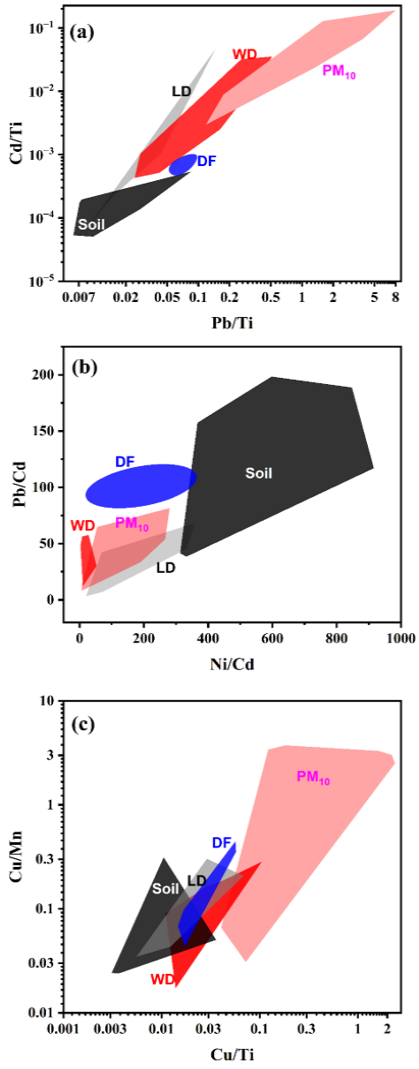

Figure 9. 10: *Elemental ratios plotted as (a) Pb/Ti vs Cd/Ti (b) Ni/Cd vs Pb/Cd and (c) Cu/Ti vs Cu/Mn. Pb/Ti vs Cd/Ti demonstrates that the characteristic ratios of LDs and WDs lie between those of soil, PDs and PM_{10}, with some of WDs overlapping with PM10 aerosols. Thus, the leaf surface dusts were a mixture of soil, PD and PM10. Overlapping of LD and WD with PM10 aerosols in Ni/Cd vs Pb/Cd suggests that these elements in the leaf surface dusts were primarily sourced from the atmosphere. Cu/Ti vs Cu/Mn suggests that these elements were primarily of crustal origin.*

observed to be enriched in LD and WD (**Figure 9.5**). A bivariate plot, normalizing Cu with crustal elements such as Ti and Mn (Cu/Ti vs Cu/Mn), indicates that both LD and WD overlap with soil and DF elemental ratios. In contrast, PM_{10} exhibits distinct ratios, indicating that Cu on the leaf surface was sourced from soil and DF rather than from PM_{10} aerosols (**Figure 9.10c**).

9.6. Pb isotopic compositions as source tracers of foliar dusts and tissues

The average Pb isotopic compositions are presented in Table 9.8. The Pb isotopic compositions of individual samples are provided in Table 9.9.

9.6.1. Aerosol (PM_{10}) and Dust fall (DF)

The average $^{206}Pb/^{207}Pb$ ratios of PM_{10} aerosols (1.1391 ± 0.0153) and DFs (1.1321 ± 0.0036) were analytically indistinguishable. The mean $^{206}Pb/^{207}Pb$ composition of Kolkata street dusts as determined by previous studies (Das et al., 2016; R. Das et al., 2018) conforms with that of the DFs from this study. The DF reflects the characteristics of the local Pb sources. The isotopic ratios of Indian aerosols (PM_{10}) from previous literature are also comparable to the ratios obtained in the present study (R. Das et al., 2018; Kumar et al., 2016; Sen et al., 2016). Similar Pb isotopic ratios over the years suggest consistent atmospheric Pb sources such as vehicle exhausts, coal combustion and industrial emissions (R. Das et al., 2018; Sen et al., 2016). This makes our rationale behind comparing the aerosol Pb isotopic composition with that of the plant tissues reasonable as absorption of elements by the plants is a continuous process rather than an instantaneous one.

9.6.2. Soil

Soil had considerably higher average $^{206}Pb/^{207}Pb$ ratios (1.1650 ± 0.0231) compared to atmospheric fallouts (both PM_{10} and DF). Crustal Pb isotope ratio is known to be radiogenic, with $^{206}Pb/^{207}Pb$ composition ranging from 1.151 – 1.232 (Allègre and Lewin, 1989; Asmerom and Jacobsen, 1993; Hemming and McLennan, 2001; Millot et al., 2004; Rudnick and Goldstein, 1990). This indicates that the soils have a strong contribution from geogenic sources. However, anthropogenic input from dust deposition on soil might have been present, as suggested by high EFs of Ni, Cd and Pb, discussed in the previous section. Atmospherically deposited Pb, associated with finer soil grains (Bi et al., 2013) has lower $^{206}Pb/^{207}Pb$ compositions and greater mobility as well as solubility (Bacon and Hewitt, 2005; Farmer et al., 2006; Kelepertzis et al., 2021; Vilomet et al., 2003). Lower $^{206}Pb/^{207}Pb$ signature was associated with higher Pb concentrations in soil,

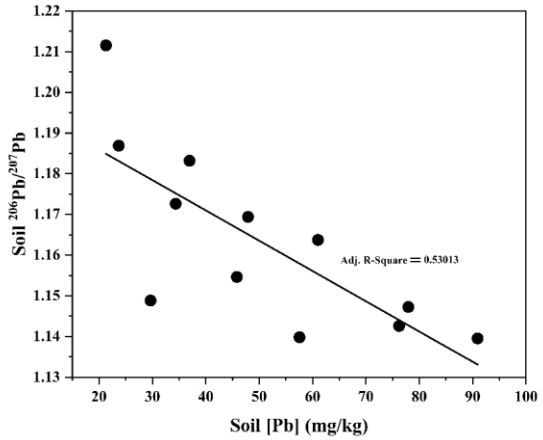

Figure 9. 11: Bivariate plot depicting the relationship *between soil Pb concentration and $^{206}Pb/^{207}Pb$ isotopic composition. Lower $^{206}Pb/^{207}Pb$ signature was associated with higher Pb concentrations*

suggesting contamination from anthropogenic sources (Wong and Li, 2004) (**Figure 9.11**). Thus, the Pb in soil can be a combination of natural and anthropogenic sources (Bacon and Hewitt, 2005). As the bulk soil Pb is isotopically distinct from the root and leaf (discussed later) we performed sequential extraction of one soil sample.

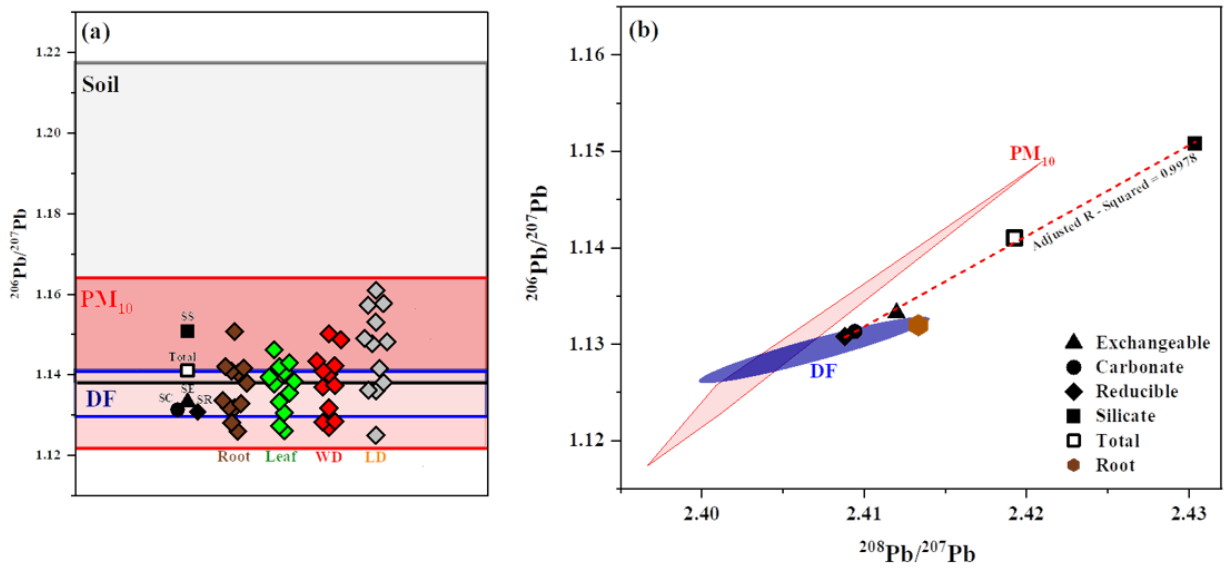

Figure 9. 12: *(a) $^{206}Pb/^{207}Pb$ composition of soil, PM10, DF, root, leaf, WD and LD. SE, SC, SR and SS are exchangeable, carbonate, reducible and silicate fraction of soil respectively. LDs showed a higher $^{206}Pb/^{207}Pb$ signature compared to WDs, indicating the contribution of Pb from regional soil in LD. Conversely, WDs displayed a stronger association with PM_{10}. Isotopic composition of root is comparable to SE, SC and SR, which in turn are similar to DF. (b) Triple isotope plots of $^{208}Pb/^{207}Pb$ vs $^{206}Pb/^{207}Pb$ for the exchangeable (SE), carbonate (SC), reducible (SR), silicate (SS) fractions of the sequentially leached soil samples. The mixing line between SR and SS are plotted as red dashed line. The Pb isotopic compositions for corresponding root sample and atmospheric fallout samples (DF and PM_0) compositions are plotted for comparison*

The sequentially leached soil sample exhibited analytically indistinguishable $^{206}Pb/^{207}Pb$ composition in exchangeable (SE), carbonate (SC) and reducible (SR) fractions, while silicate fraction (SS) displayed significantly higher $^{206}Pb/^{207}Pb$ composition compared to the bulk soil

(**Figure 9.12a**). From the triple isotope plot, it can be observed that, the bulk soil exhibited Pb isotopic composition between the silicate fraction and SE, SC & SR compositions and lies on the mixing line between SR and SS, indicating a mixing of all the fractions (**Figure 9.12b**). The Pb isotopic compositions of DFs and SE, SC & SR are closely aligned. In DF, Pb correlates with Fe and Mn (Spearman's correlation coefficient > 0.76; p value < 0.07). This indicates that at least part of the Pb is bound to Fe-Mn phases, and DF contributes to comparable Pb isotopic compositions of different soil fractions.

9.6.3. Fern tissues (roots and leaves)

Mean $^{206}Pb/^{207}Pb$ isotopic compositions of the fern tissues (leaves and roots) and WDs are closely aligned with PM_{10} and DFs. However, the soil isotopic composition was significantly different ($p < 0.0001$) from LDs, WDs, leaves and roots. These observations are also evident from the triple isotope plot of $^{206}Pb/^{207}Pb$ vs $^{208}Pb/^{207}Pb$. The triple isotope plot demonstrates that sources of Pb on the WD and inside the tissues are a mixture of PM_{10} and DF (**Figure 9.13**). No particular influence of soil is observed on the roots and leaves. All these indicate that geogenic Pb from soil is not the primary source of Pb inside the plants. Previous investigations that used Pb isotopes, to differentiate the sources of Pb inside plant tissues demonstrated that Pb in roots can be sourced from soil (Bi et al., 2009; Hu et al., 2011; Ma et al., 2021) as well as from atmospheric fallouts (Ma et al., 2019a, 2019b). Similar isotopic compositions in roots and leaves indicate a common source of absorption. Thus, the fern leaves exhibit the capacity to assimilate anthropogenic Pb from the PM, captured in the wax. From the sequentially leached soil sample, it can be observed that Pb isotopic composition of the corresponding root is comparable to SE, SC and SR, which in turn are similar to DF (**Figure 9.12**). As SE, SC and SR are more mobile and bioavailable than SS (Olajire et al., 2003), root preferentially uptakes anthropogenic Pb bound to these fractions, possibly atmospherically sourced instead of the silicate bound geogenic Pb. Consequently, it can be hypothesised that ferns have a preference for bidirectional anthropogenic Pb uptake from roots and leaves. This postulation can be tested with the help of MixSIAR results, discussed in the following section.

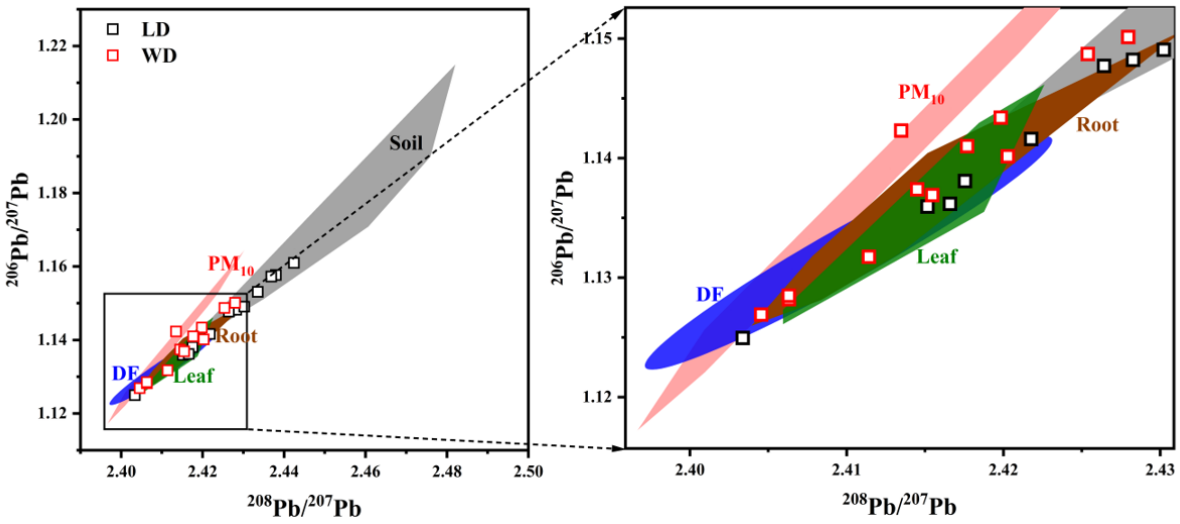

Figure 9. 13: *Triple isotope plots of $^{208}Pb/^{207}Pb$ vs $^{206}Pb/^{207}Pb$ for PM_{10} aerosols, DF, LD, WD, leaf, root and soil. The soil, PM10, DF, leaf and roots are depicted as fields in grey, light red, blue, green and brown colours. The open black and red squares represent LD and WD respectively. The triple isotope plots demonstrate that the sources of Pb in WD, roots and leaves are primarily a mixture of PM_{10} and DFs, while LD demonstrates partial influence from soil along with PM_{10} and DF.*

Table 9.8: Mean Pb isotopic composition of PM_{10} aerosol, Dustfall (DF), Loose Dust (LD), Wax Dust (WD), Leaf, Root and Soil samples

Isotope Ratio	Parameter	PM_{10} Aerosol	PD	LD	WD	Leaf	Root	Soil
$^{206}Pb/^{204}Pb$	N	14	6	12	12	12	12	12
	Mean	17.7806	17.6247	17.9250	17.7747	17.7482	17.7042	18.2057
	SD	0.272	0.054	0.181	0.134	0.102	0.146	0.429
$^{207}Pb/^{204}Pb$	N	14	6	12	12	12	12	12
	Mean	15.6087	15.5691	15.6430	15.6192	15.6161	15.5777	15.6266
	SD	0.033	0.023	0.015	0.015	0.008	0.047	0.061
$^{208}Pb/^{204}Pb$	N	14	6	12	12	12	12	12
	Mean	37.6609	37.5234	37.9478	37.7246	37.7131	37.6188	38.1970
	SD	0.249	0.089	0.205	0.140	0.094	0.211	0.488
$^{206}Pb/^{207}Pb$	N	14	6	12	12	12	12	12
	Mean	1.1391	1.1321	1.1459	1.1379	1.1367	1.1365	1.1650
	SD	0.015	0.004	0.011	0.008	0.006	0.007	0.023
$^{208}Pb/^{207}Pb$	N	14	6	12	12	12	12	12
	Mean	2.4128	2.4101	2.4259	2.4153	2.4150	2.4149	2.4443
	SD	0.011	0.005	0.011	0.007	0.005	0.008	0.022

Table 9.9: *Pb isotopic composition of individual samples*

Samples	$^{206}Pb/^{204}Pb$	$^{207}Pb/^{204}Pb$	$^{208}Pb/^{204}Pb$	$^{206}Pb/^{207}Pb$	$^{208}Pb/^{207}Pb$
PM_{10} Aerosols	18.0959	15.6486	37.9577	1.1564	2.4256
	18.0215	15.6378	37.8994	1.1524	2.4236
	17.8958	15.6425	37.8017	1.1441	2.4166
	17.5124	15.6071	37.4720	1.1221	2.4010
	18.2220	15.6492	38.0308	1.1644	2.4302
	18.1194	15.6394	37.9513	1.1586	2.4267
	17.8511	15.6273	37.7553	1.1424	2.4160
	17.4082	15.5815	37.3437	1.1172	2.3967
	17.5833	15.5770	37.4722	1.1288	2.4056
	17.6247	15.5871	37.5102	1.1307	2.4065
	17.4858	15.5747	37.3980	1.1227	2.4012
	17.6421	15.5666	37.4778	1.1333	2.4076
	17.5184	15.5626	37.3645	1.1256	2.4009
	17.9482	15.6203	37.8178	1.1489	2.4211
Dustfall (DF)	17.6811	15.5527	37.5817	1.1369	2.4164
	17.6141	15.5569	37.4855	1.1323	2.4096
	17.6612	15.5583	37.5554	1.1352	2.4138
	17.6264	15.5971	37.5884	1.1301	2.4100
	17.6387	15.6009	37.5708	1.1306	2.4082
	17.5266	15.5486	37.3585	1.1272	2.4027
Loose Dust (LD)	17.9532	15.6358	37.9678	1.1482	2.4283
	18.1308	15.6616	38.1831	1.1577	2.4380
	17.9480	15.6371	37.9423	1.1477	2.4264
	17.6002	15.6443	37.5993	1.1249	2.4034
	17.7857	15.6278	37.7810	1.1381	2.4176
	17.7599	15.6331	37.7566	1.1359	2.4152
	17.8457	15.6332	37.8601	1.1416	2.4218
	17.7449	15.6191	37.7451	1.1362	2.4166
	18.1267	15.6637	38.1703	1.1573	2.4369
	18.1822	15.6625	38.2546	1.1610	2.4424
	18.0546	15.6584	38.1054	1.1531	2.4335
	17.9683	15.6395	38.0076	1.1491	2.4302
Wax Bound Dust (WD)	17.5964	15.6160	37.5496	1.1269	2.4046
	17.9664	15.6408	37.9350	1.1487	2.4254
	17.6301	15.6250	37.5990	1.1282	2.4063
	17.7513	15.6064	37.6818	1.1374	2.4145
	17.8634	15.6239	37.8074	1.1434	2.4198
	17.8680	15.6413	37.7500	1.1423	2.4135
	17.5955	15.5907	37.5163	1.1285	2.4063
	17.8176	15.6147	37.7515	1.1410	2.4177
	17.9814	15.6333	37.9572	1.1501	2.4280
	17.8161	15.6251	37.8171	1.1401	2.4203
	17.7432	15.6045	37.6921	1.1369	2.4155
	17.6666	15.6083	37.6383	1.1317	2.4114
Leaf	17.8992	15.6198	37.8408	1.1462	2.4226
	17.6970	15.6181	37.6608	1.1333	2.4114
	17.7645	15.6167	37.7189	1.1378	2.4153
	17.8520	15.6229	37.7830	1.1430	2.4184
	17.7543	15.6002	37.6879	1.1383	2.4159
	17.6564	15.6215	37.6480	1.1305	2.4100

	17.6016	15.6138	37.5657	1.1273	2.4059
	17.5725	15.6050	37.5449	1.1261	2.4059
	17.8435	15.6261	37.8199	1.1420	2.4203
	17.8033	15.6237	37.7741	1.1394	2.4177
	17.8096	15.6145	37.7555	1.1406	2.4180
	17.7247	15.6105	37.7580	1.1355	2.4188
Root	17.7400	15.5386	37.5913	1.1416	2.4192
	17.5907	15.5295	37.4222	1.1328	2.4097
	17.6113	15.5365	37.4637	1.1336	2.4113
	17.4512	15.4998	37.2603	1.1260	2.4039
	17.7229	15.5417	37.5356	1.1404	2.4152
	17.6679	15.6080	37.5810	1.1318	2.4078
	17.7350	15.5850	37.6445	1.1379	2.4154
	17.6676	15.6071	37.6652	1.1320	2.4133
	18.0047	15.6457	38.0420	1.1507	2.4315
	17.8251	15.6239	37.8314	1.1409	2.4214
	17.8537	15.6320	37.8554	1.1420	2.4217
	17.5808	15.5845	37.5329	1.1281	2.4084
Soil	17.7366	15.5565	37.6300	1.1402	2.4189
	17.7636	15.5388	37.6025	1.1433	2.4199
	18.2887	15.6212	38.4389	1.1708	2.4607
	18.0094	15.5778	37.9271	1.1562	2.4347
	17.9604	15.6040	37.9946	1.1511	2.4349
	18.3490	15.6234	38.2289	1.1745	2.4469
	18.5680	15.6671	38.6409	1.1851	2.4664
	17.7994	15.5995	37.7393	1.1410	2.4193
	18.6890	15.7072	38.8899	1.1899	2.4759
	18.2205	15.6410	38.2027	1.1649	2.4425
	19.1437	15.7557	39.1069	1.2150	2.4821
	17.9405	15.6273	37.9627	1.1481	2.4293

9.6.4. Quantification of source contribution using mixing model (MixSIAR)

Mixing models for leaves and roots can be helpful in quantifying the contribution of DF, PM_{10} and soil towards the concentration of Pb in the fern tissues. The results of concentration dependent MixSIAR analyses are depicted in **Figure 9.14**. Soil had a greater influence on the roots (**Figure 9.15b**) (mean contribution range = 4.8 ± 5.3 to 46 ± 19%) compared to leaves (**Figure 9.14a**) (mean contribution range = 6.8 ± 7.8 to 10 ± 13%), indicating foliar dusts to be the source of Pb inside the leaves. Dust fall was revealed to be the largest contributor of Pb for both leaves (mean contribution range = 53 ± 20 to 73 ± 20%) and roots (mean contribution range = 33 ± 15 to 86 ± 18%). In fact, in some of the samples, DF demonstrated a larger influence on the roots compared to the corresponding leaves (**Figure 9.14**). This suggests that the roots sourced Pb from the soil surface, which was contaminated by atmospheric dust fall. Leaves were influenced by PM_{10}

aerosols to a greater extent compared to roots. Thus, in leaves, Pb was primarily sourced from DF and PM_{10} aerosols, while soil and DF were the primary sources of Pb inside the roots of the ferns

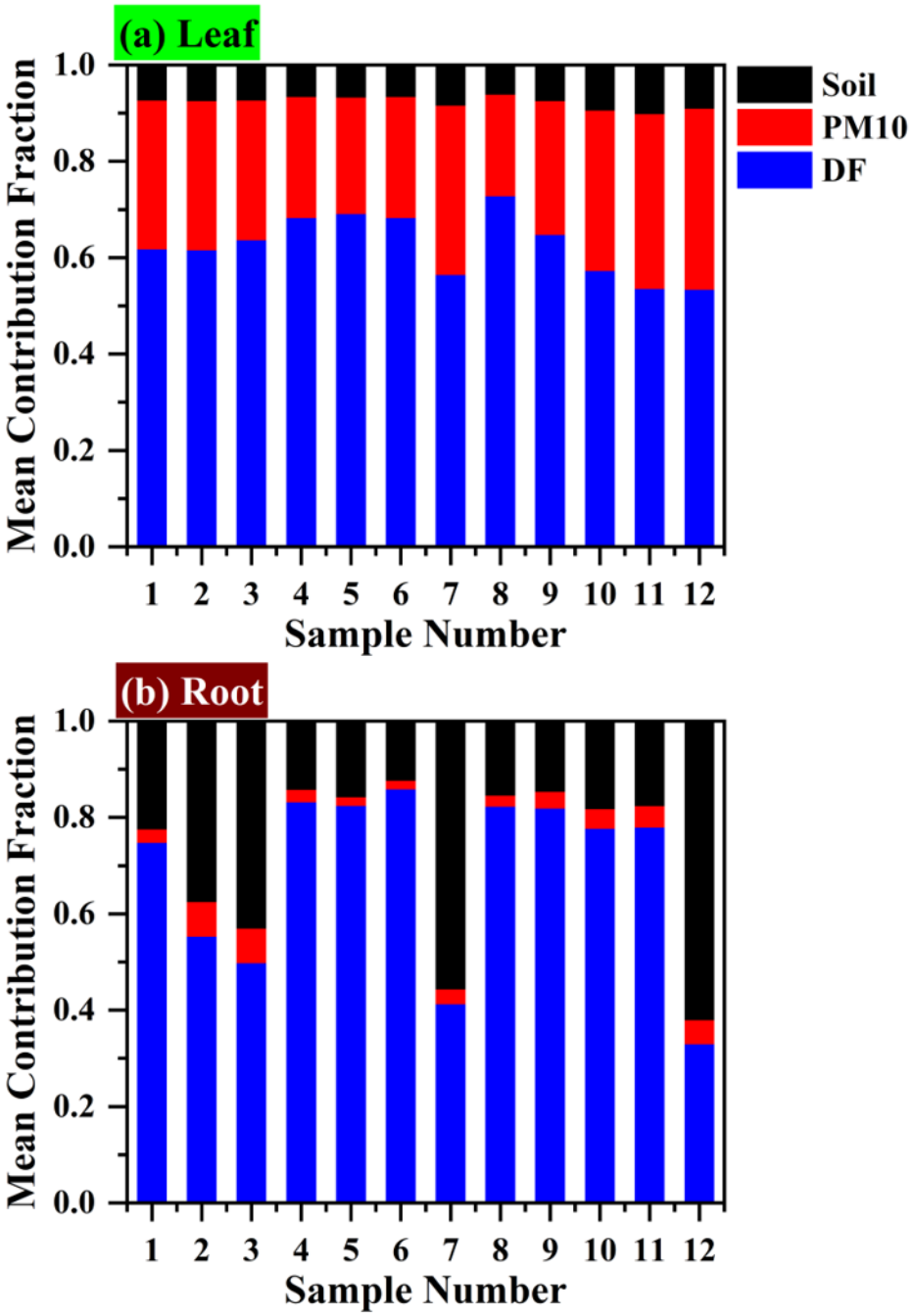

Figure 9. 14: *MixSIAR results for mean contribution of soil, DF and PM^{10} aerosols towards (a) leaf and (b) root Pb of the fern samples. The dominant sources of Pb in leaves were DF and PM10 aerosols, whereas Pb within fern roots primarily originated from soil and DF*

9.7. Ferns as air purifying agents

9.7.1. Suitability of fern species

The selection of the two fern species (*Pteris vittata* and *Pteridium aquilinum*) in this study was based on their abundant growth in the selected area. The abundance of these two particular species of fern in regions of high DF (**Figure 9.2b**) associated with metals, indicates that they likely possess resistance to metal stress. Both species have been proven to have a high tolerance for several heavy metals in previous studies. *Pteridium aquilinum* is one of the few species that is capable of naturally colonizing soils contaminated with Pb-Zn mine tailings (Shu et al., 2005). *Pteridium aquilinum* has been investigated to be tolerant to toxic heavy metals/metalloid such as As, Cd, Cr, Cu, Ni, Pb and Zn (Chang et al., 2009; Eslava-Silva et al., 2023; Gómez-Bernal et al., 2017; Kubicka et al., 2015; Olaifa and Omekam, 2014; Pratas et al., 2013; Turnau et al., 1993). Exposure to metals demonstrated no visible physiological damage to the ferns (Eslava-Silva et al., 2023; Gómez-Bernal et al., 2017; Pratas et al., 2013), although nutrient supply might be necessary when exposed to high concentrations of selected metals, such as Cu for their proper growth (Olaifa and Omekam, 2014). *Pteris vittata* has been a well-known hyperaccumulator of As for more than two decades (Ma et al., 2001). Apart from As, *Pteris vittata* also possesses tolerance to Cr, Ni, Cu, Pb and Zn and has been proven to phytostabilize metals in fly ash contaminated sites (Kumari et al., 2011; Wu et al., 2009). *Pteris vittata* was identified to be significantly tolerant to Pb with a survival rate of 93 – 100% when naturally growing at a Pb mining area containing up to 10% (w/w) soil Pb (Ha et al., 2011; Soongsombat et al., 2009; Wan et al., 2014). However, there can be a decrease in biomass when exposed to very high concentrations of metals (Fayiga et al., 2004; Wan et al., 2014; Wu et al., 2009; Y. Zheng et al., 2008). The ferns may have threshold concentrations for different metals above which they demonstrate genotoxic effects that may be expressed in the form of biomass decrease and chlorophyll content. Generally, both the fern species are tolerant to toxic heavy metals, with no indication of damage until exposed to high concentrations. The tolerable concentrations of Cd, Cr and Pb in both the species of the ferns as observed in previous literature are well above the concentrations of the respective metals in soil and DF from the present study (**Figure 9.15a**).

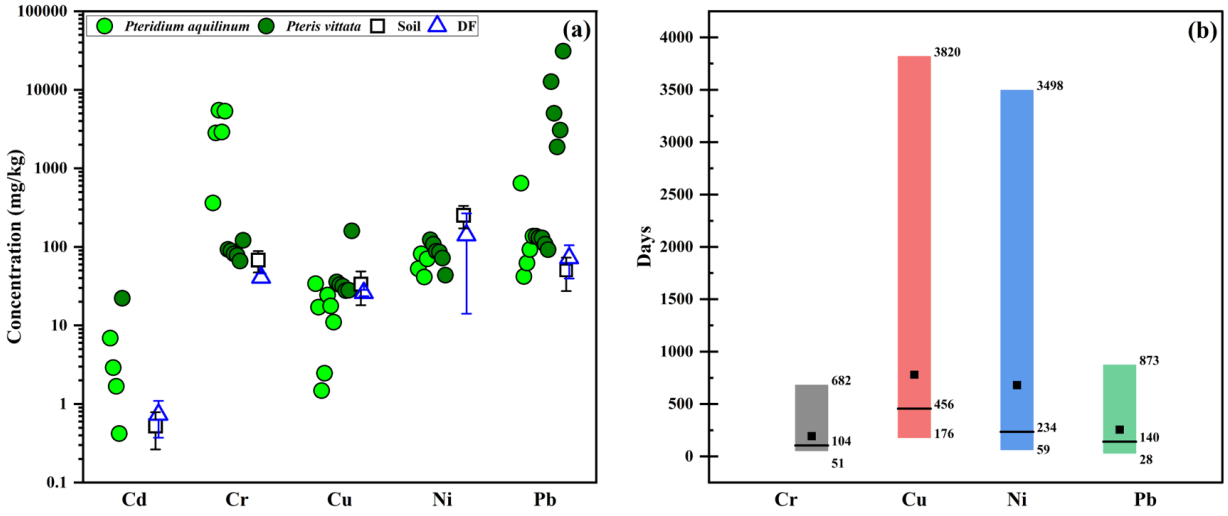

Figure 9. 15: *(a) Tolerated concentrations of Cd, Cr, Cu, Ni and Pb in roots of Pteridium aquilinum and Pteris vittata demonstrated in previous studies. The concentrations of Cd, Cr, Cu, Ni and Pb in soil (open black squares) and DF (open blue triangles) from this study are also plotted for reference. (b) Box plots depicting the number of days a 1m^2 fern cover can remain viable for Cr, Ni, Cu and Pb capture in a small 10m^2 residential room as calculated from the leaf surface dust load data from the present study. The upper and lower extremes of the boxes represent maximum and minimum values respectively. Squares and lines inside boxes indicate mean and median values respectively. The values of each parameter are indicated on the right-hand side of the boxes in the order of maximum, mean, median and minimum (from top to bottom). The data for indoor PM_{10} concentrations, volume of air in a room and air change rate were adopted from previous literatures*

This high metal tolerance of both the perennial species, surviving in tropical climatic conditions is accompanied by their adaptability to a wide range of environmental conditions (USDA, 2018; Vélez-Gavilán, 2020). *Pteridium aquilinum* can grow in slightly acidic to slightly alkaline environments while *Pteris vittata* prefers alkaline medium (Anh et al., 2018; Shu et al., 2005; Xu et al., 2022). Heavy metal absorption and biomass may decrease with decreasing pH and extreme temperatures (Anh et al., 2018; Xu et al., 2022). At regions of elevated CO_2 concentrations, the ferns demonstrate increased biomass and metal absorption (J. Zheng et al., 2008). *Pteridium aquilinum* can withstand water stress through stomatal closure, and *Pteris vittata* can grow at a wide range of moisture content (10 – 60%), thus, requiring low maintenance when used for air improvement purposes.(Tinklin and Bowling, 1969; Xu et al., 2022).

9.7.2. Practical use and applicability of the ferns in botanical biofiltration units

The duration of leaf viability for metal capture can help in optimizing the implementation of fern-based metal remediation strategies. It allows for proper timing and planning of fern planting and harvesting cycles, ensuring the most effective utilization of their metal-capturing capabilities. The

total mass of metals accumulated per unit area of the leaves in this study was used to calculate the number of days the ferns can remain viable for passive filtration in an indoor environment. The calculation was performed for Cr, Ni, Cu and Pb, based on the availability of indoor metal concentration data of PM_{10} (Kulshrestha et al., 2014) from an Indian city. The data is provided in **Table 9.10** respectively. The median number of days for which a $1m^2$ fern cover with 10 % PM capture efficiency (Budaniya and Rai, 2022) can remain viable for Cr, Ni, Cu and Pb capture in a standard small residential room of volume 26 m^3 with an air change per hour of 1.01 (Howard-Reed et al., 2002) was determined to be 104, 234, 456 and 140 respectively (**Figure 9.15b**). The species maintains its leaves for approximately 20 weeks from the emergence of a full-length leaf until the onset of senescence (Quesada, 2015; USDA, 2018). This natural process can effectively refresh a passive filtration system. Additionally, the passive filtration system when converted into an active one, can achieve a capture efficiency of up to ~90% for fern species (Pettit et al., 2017). In an active filtration system, PM is also captured on the substrate where the root grows (Mannan and Al-Ghamdi, 2021). Since this study provides evidence that roots have a preference for uptaking atmospheric particles deposited on the soil, implementing an active system would enhance the maximum amount of PM that can be assimilated by the ferns. These results indicate that these ferns can be utilized to design green walls capable of capturing heavy metal leaden PM and thus, acting as air purifying equipment. Botanical biofilters equipped with air purifying plants have been previously designed for indoor as well as outdoor environments (Irga et al., 2017; Paull et al., 2019; Pettit et al., 2017, 2021).The calculation for leaf viability presented here is for a small indoor area, that can be validated by designing a biofiltration unit with these ferns exposed to reasonable concentrations of PM bound heavy metals. The selected ferns can be arranged and maintained within a vertical framework of the botanical biofiltration unit. This framework allows the flow of air through the ferns, that effectively entraps the PM, while also housing a watering system for the optimal hydration of the ferns (Irga et al., 2017). This basic, initial design for a small indoor area can be subsequently scaled up for designing of larger green walls that can be deployed on open roads.

Table 9.10: *Viability estimation of fern species to be utilized as indoor air purifier*

Metal	[LD+WD+Clean leaf] (µg/cm^2)	Mean Concentration in PM_{10} (µg/m^3) (Kulshrestha et al., 2014)	Volume of room (m^3)	Air Change Rate (h^{-1})	Mass of metal per day (µg/day)	Number of viable days for 1m^2 leaf cover
Cr	0.064	0.197	26	1.01	124	51
	0.076					61
	0.076					61
	0.102					82
	0.108					87
	0.123					99
	0.135					109
	0.254					205
	0.307					248
	0.334					270
	0.450					363
	0.846					682
Ni	0.064	0.170	26	1.01	107	59
	0.074					69
	0.104					97
	0.107					99
	0.134					125
	0.239					223
	0.262					244
	0.276					258
	0.633					591
	0.939					877
	2.162					2018
	3.748					3498
Cu	0.041	0.037	26	1.01	23	176
	0.057					245
	0.072					312
	0.074					319
	0.080					345
	0.095					411
	0.116					501
	0.154					666
	0.158					682
	0.186					807
	0.246					1063
	0.883					3820
Pb	0.021	0.118	26	1.01	75	28
	0.022					29
	0.027					36
	0.043					58
	0.088					118
	0.089					119
	0.121					162
	0.230					309
	0.248					333
	0.291					390
	0.463					621
	0.651					873

9.8. Novelty and challenges

This study introduces an approach that involves the layered separation of dust components on the foliar surface along with different components of fern tissues and soil. Subsequently, elemental concentrations and Pb isotopic ratios are analyzed for each component. This comprehensive approach allows source apportionment of metals in the ferns and subsequently evaluates the metal uptake capacity of the selected ferns. Previous studies have analyzed isotopic compositions of either water-washed leaves or the whole leaf along with the foliar dust. This fails to wash away the wax-bound PMs and produces an isotopic signature of a combination of the foliar dust and the leaves. Consequently, determining whether the produced isotopic signature is predominantly influenced by the leaf tissue or superficial foliar dust is challenging. Separation of each dust fraction and analyzing them for elemental and Pb isotopic compositions can provide a better understanding of the sources of atmospheric fallout as well as the process of the internalization of Pb by the leaves. Moreover, most studies (except(X.-Y. Zhang et al., 2022)) relied on active PM and total suspended particulates (TSP) collection using pumping devices rather than dust fall collection to establish relationship between atmospheric fallout and foliar uptake. Analyzing dust fall without pumping systems is more representative of the foliar surface dust than active aerosols (Bollhöfer et al., 2006). Dustfall collection also leads to the measurement of the dust fall flux of a region based on gravimetric quantifications (Bruce et al., 2021).

Although the fern species can be efficient air-cleaning agents there can be certain challenges that need careful consideration. Both the selected fern species are perennial and senescence starts at about 20 weeks from the emergence of full-length leaves (Quesada, 2015; USDA, 2018). These senesced leaves will be metal-laden after their utilization in air-biofiltration system. Thus, improper disposal of the senesced leaves may lead to the transport of these heavy metals to animals and humans, which can bring about genotoxicity. Exposure to heavy metals like Cd and Pb has been known to bring about DNA damage and adverse effects on neurological, cardiovascular and renal systems in mammals (Akhavan et al., 2016; N. Singh et al., 2018). Thus, proper disposal of the contaminated biomass is of utmost importance to avoid secondary pollution. The strategies generally followed for disposal are pyrolysis, solvent/acid extraction, combustion, landfill, compaction, direct disposal etc. (Shen et al., 2022). However, these methods are not entirely capable of immobilizing or fixing the metals present in the biomass. Thermochemical methods such as pyrolysis and combustion can release the volatile metals back into the atmosphere in the

form of flue gas or pyrolysis gas, while the less volatile ones will be retained in the fly and bottom ash, leading to secondary pollution. Along with the metals, these processes also release other greenhouse gases like carbon dioxide, methane etc (Y. Singh et al., 2023). Solvent/acid extraction of the metals transforms the metals from the solid to the liquid phase. However, disposal of the metal-laden solvent/acid becomes a problem. Landfill disposal can be effective if proper confinement is achieved, without which there are chances of metal leakage into surrounding soil and groundwater. Compaction reduces the volume of the contaminated biomass and can be effective if the compacted biomass is properly sealed within impervious material (Liu and Tran, 2021; Nzihou and Stanmore, 2013; Zhang et al., 2023). An effective strategy can be mixing the compacted biomass with an impervious material like clay that will act as a barrier for the heavy metals inside (Sánchez-Jiménez et al., 2012). This clay covered compacted biomass can be utilized in making bricks for construction purposes. However, the process of firing adopted for the preparation of these bricks can release the volatile heavy metals and other greenhouse gases back into the environment. Plant-based agricultural wastes have been used in the production of sustainable and environment-friendly unfired earth bricks successfully (Lachheb et al., 2023). Thus, to immobilize the contaminants, it is most suitable to prepare unfired bricks out of the clay covered compacted biomass.

9.9. Comparison with other air purification technologies

The commonly used methods to purify indoor air are (i) fibrous filters, such as high-efficiency particulate air (HEPA) and ultra-low particulate air (ULPA) filters, (ii) electrostatic air filters and (iii) activated carbon filters (Liu et al., 2017). Although HEPA and ULPA filters are very efficient in filtering PMs, they get saturated quickly and require frequent cleaning and replacements. Clogging also increases the pressure drop across the filtration medium, thus increasing the energy consumption of the process (Kumar et al., 2023). On the other hand, while botanical biofilters may be less efficient than HEPA and ULPA in removing PM, the plants in botanical biofilters regenerate leaves periodically, which eliminates the chances of pollutant saturation. This maintains the performance of the biofilters for a longer duration and reduces the replacement costs associated with HEPA filters.

Electrostatic filters, for e.g., electrostatic precipitators rely on electrostatic charges between PM and filtration media and are > 90 % effective in terms of PM filtering (Liu et al., 2017). An

electrostatic field has to be maintained in such filters, that require a constant supply of high voltage, thus, involving high energy consumption (Kumar et al., 2023). Similar to HEPA and ULPA filters, ESPs also require frequent cleaning (every few weeks) to maintain their filtration efficiency. Moreover, due to the ionization process involved, respiratory irritants such as ozone (O_3) may be generated during filtration, which further may react with other organic compounds to produce ultrafine secondary organic aerosol (Afshari et al., 2020; Poppendieck et al., 2014). On the contrary, botanical biofilters can operate at much lower energy consumption and are also known to be effective in reducing organic pollutants (Irga et al., 2017).

Activated carbon filters are adsorption filters, that are efficient in the sorption of gaseous pollutants such as volatile organic compounds (VOC). However, they are not capable of filtering PMs (Agranovski et al., 2005).

Thus, compared to other technologies, botanical biofiltration is cost-effective and energy-efficient technique for indoor air purification. Periodic leaf generation along with heavy metal absorption capacity of the ferns makes this technique of air purification both economical and sustainable, although in particular instances it might be less efficient than HEPA or ULPA.

CHAPTER 10: CONCLUSIONS

This thesis provides a comprehensive investigation into the sources of atmospheric lead (Pb) pollution across urban, industrial, and pristine environments. Through advanced elemental and Pb isotopic composition analyses, this work has identified the dominant sources of Pb, examined the seasonal variations in its concentration, and explored the potential of innovative remediation strategies.

Starting with a detailed source apportionment of Pb emissions over the last decade, this study investigates whether there are unrecognized and underdetermined sources of atmospheric Pb in India as well as in SEA countries.

In the last decade, Pb resuspension from legacy leaded gasoline persists as a significant source, particularly in SEA. Despite its phaseout over two decades ago, its influence remains prominent in SEA and, to a lesser extent, in India. In addition to this ship emissions, which is not a much analyzed source so far were identified as a consistent and significant source of Pb, reflecting the presence of heavy metals in heavy fuel oils and other marine fuels and oils.

In India, while industrial emissions and coal combustion dominated Pb sources in the last decade, stricter environmental regulations and the implementation of cleaner technologies have markedly reduced their contribution. This is evident from coal-fired power plants, where most Pb and other heavy metals in PM are derived from other anthropogenic activities rather than from coal. Interestingly, open burning of biomass and solid waste was identified as a major contributor to Pb emissions in regions of coal combustion. The pervasive issue of open biomass and solid waste burning in coal combustion-dominated regions emerges as a critical source of atmospheric Pb.

This practice, often unregulated, contributes significantly to the heavy metal burden in the air. Addressing this issue requires the implementation of stricter waste management policies, the promotion of community-level awareness campaigns, and the enforcement of alternative, sustainable waste disposal methods. Immediate and coordinated efforts to eliminate open burning practices are essential to mitigate its adverse impacts and to foster healthier, cleaner environments in these regions.

Other than the conventionally recognized anthropogenic sources of atmospheric Pb such as coal and industrial emissions, the role of NEE in urban road pollution, was underexplored. Although EE have been studied, NEE, primarily originating from tire and brake wear, as well as road surface abrasions represents a significant component of traffic-related pollution as observed from this study. It was detected that NEE contributes almost as much Pb and other metals towards urban road dusts as EE. Emission projections indicate that even with increased EV adoption by 2045, the dominance of ICEVs in India's vehicular fleet will continue to shape the emission profile. Consequently, traffic-related Pb emissions are expected to remain largely unchanged, necessitating additional measures to address urban pollution.

Source apportionment studies in remote, pristine setting highlights how underexplored and otherwise undetectable sources become visible in the absence of larger pollution sources. In the Andaman and Nicobar Islands, where industrial and coal combustion activities are absent, the study revealed that anthropogenic sources like military activities and ship emissions are the dominant contributors to atmospheric Pb. Emissions related to military activities as determined with bullets as a proxy, emerged as a significant and previously unrecognized Pb source, while ship emissions consistently influenced Pb levels year-round. Seasonal variations with reversal in wind patterns demonstrate that seawater contributions peaking during the monsoon, with crustal and natural inputs remaining stable year-round.

Natural sources have always been dominant contributors to atmospheric Pb levels globally, a trend that persists in the findings of this study. Dust storms, soil erosion, and agricultural activities can release these materials into the atmosphere, particularly in arid and semi-arid regions. This contribution is not only localized but can also extend across continents, as observed in transcontinental dust transport events. Sea spray aerosols are another critical natural source, particularly in coastal and marine regions. The interaction between wind, waves, and seawater generates aerosols that carry marine-derived trace metals, including Pb. Seasonal variations, such as those observed during monsoon and storm seasons, can amplify this contribution, making sea spray a variable but significant factor in atmospheric Pb levels.

Building upon the understanding of natural and anthropogenic sources of atmospheric Pb, innovative remediation strategies were explored, focusing on the potential of ferns as effective biofilters for Pb capture. This approach leverages the natural metal tolerance and air-purifying

capabilities of perennial fern species, which are well-suited to tropical climates and a variety of environmental conditions. These plants have shown remarkable efficiency in capturing Pb and other heavy metals from indoor air, presenting an accessible and environmentally sustainable solution for mitigating metal exposure in urban environments.

Investigations revealed that the roots of the ferns along with the leaves also play a crucial role in metal uptake. When integrated into an active filtration system, where PM is also captured by the substrate where the fern roots grow, the overall efficiency of the system is enhanced as PM is captured by leaves, roots and the substrate.

However, the disposal of metal-laden fern leaves presents a challenge, as improper management could lead to secondary pollution. To mitigate this, safe disposal strategies, such as converting contaminated biomass into eco-friendly products like unfired earth bricks, are essential to prevent further environmental harm. Overall, fern-based biofiltration presents a promising, sustainable solution for reducing indoor metal pollution and enhancing urban air quality.

By identifying both conventional and previously overlooked sources, as well as exploring innovative solutions like fern-based biofiltration, this research provides a comprehensive framework for addressing Pb pollution. Thus, it is essential to implement stricter regulations, promote awareness, and adopt sustainable remediation practices to effectively mitigate the impact of Pb on human health and the environment.

REFERENCES

Abhijith, K.V., Kumar, P., 2020. Quantifying particulate matter reduction and their deposition on the leaves of green infrastructure. Environ. Pollut. 265, 114884. https://doi.org/10.1016/j.envpol.2020.114884

Abubakar, A.A., Yilbas, B.S., Al-Qahtani, H., Alzaydi, A., Alhelou, S., 2020. Environmental dust repelling from hydrophobic and hydrophilic surfaces under vibrational excitation. Sci. Rep. 10, 14346. https://doi.org/10.1038/s41598-020-71356-5

Adachi, K., Tainosho, Y., 2004. Characterization of heavy metal particles embedded in tire dust. Environ. Int. 30, 1009–1017. https://doi.org/10.1016/j.envint.2004.04.004

Adamidou, K., Kassoli-Fournaraki, A., Filippidis, A., Christanis, K., Amanatidou, E., Tsikritzis, L., Patrikaki, O., 2007. Chemical investigation of lignite samples and their ashing products from Kardia lignite field of Ptolemais, Northern Greece. Fuel 86, 2502–2508. https://doi.org/10.1016/j.fuel.2007.02.008

Adamiec, E., Jarosz-Krzemińska, E., Wieszała, R., 2016. Heavy metals from non-exhaust vehicle emissions in urban and motorway road dusts. Environ. Monit. Assess. 188, 369. https://doi.org/10.1007/s10661-016-5377-1

Afshari, A., Ekberg, L., Forejt, L., Mo, J., Rahimi, S., Siegel, J., Chen, W., Wargocki, P., Zurami, S., Zhang, J., 2020. Electrostatic Precipitators as an Indoor Air Cleaner—A Literature Review. Sustainability 12, 8774. https://doi.org/10.3390/su12218774

Agranovski, I.E., Moustafa, S., Braddock, R.D., 2005. Performance of Activated Carbon Loaded Fibrous Filters on Simultaneous Removal of Particulate and Gaseous Pollutants. Environ. Technol. 26, 757–766. https://doi.org/10.1080/09593332608618516

Agrawal, M., Singh, J., 2000. Impact of Coal Power Plant Emission on the Foliar Elemental Concentrations in Plants in a Low Rainfall Tropical Region. Environ. Monit. Assess. 60, 261–282. https://doi.org/10.1023/A:1006135317896

Akbari, M.Z., Thepnuan, D., Wiriya, W., Janta, R., Punsompong, P., Hemwan, P., Charoenpanyanet, A., Chantara, S., 2021. Emission factors of metals bound with PM2.5 and ashes from biomass burning simulated in an open-system combustion chamber for estimation of open burning emissions. Atmospheric Pollut. Res. 12, 13–24. https://doi.org/10.1016/j.apr.2021.01.012

Akhavan, O., Hashemi, E., Zare, H., Shamsara, M., Taghavinia, N., Heidari, F., 2016. Influence of heavy nanocrystals on spermatozoa and fertility of mammals. Mater. Sci. Eng. C 69, 52–59. https://doi.org/10.1016/j.msec.2016.06.055

Al-Degs, Y.S., Ghrir, A., Khoury, H., Walker, G.M., Sunjuk, M., Al-Ghouti, M.A., 2014. Characterization and utilization of fly ash of heavy fuel oil generated in power stations. Fuel Process. Technol. 123, 41–46. https://doi.org/10.1016/j.fuproc.2014.01.040

Allègre, C.J., Lewin, E., 1989. Chemical structure and history of the Earth: evidence from global non-linear inversion of isotopic data in a three-□ model. Earth Planet. Sci. Lett. 96, 61–88. https://doi.org/10.1016/0012-821X(89)90124-6

Amnuaylojaroen, T., Inkom, J., Janta, R., Surapipith, V., 2020. Long Range Transport of Southeast Asian PM2.5 Pollution to Northern Thailand during High Biomass Burning Episodes. Sustainability 12, 10049. https://doi.org/10.3390/su122310049

Andaman & Nicobar Command, 2022. Routine Firing Exercise from Netaji Subhash Chandra Bose Island (Ross Island). Army and Navy Components #ANC carried out a seaward joint firing drill aimed at honing interoperability. Together we are stronger #Victorythroughjointness #Alwaysbattleready https://t.co/3pLggaGCjY. Twitter.

Anh, B.T.K., Minh, N.N., Ha, N.T.H., Kim, D.D., Kien, N.T., Trung, N.Q., Cuong, T.T., Danh, L.T., 2018. Field Survey and Comparative Study of Pteris Vittata and Pityrogramma Calomelanos Grown on Arsenic Contaminated Lands with Different Soil pH. Bull. Environ. Contam. Toxicol. 100, 720–726. https://doi.org/10.1007/s00128-018-2325-5

Anu, S., Mohanakumar, K., 1996. Studies on the paratial and temporal distribution of surface meteorological parameters over Indian subcontinent (PhD Thesis). Cochin University of Science and Technology.
Apte, S.C., Batley, G.E., Szymczak, R., Rendell, P.S., Lee, R., Waite, T.D., 1998. Baseline trace metal concentrations in New South Wales coastal waters. Mar. Freshw. Res. 49, 203–214. https://doi.org/10.1071/mf96121
Aranke, O., Algenaid, W., Awe, S., Joshi, S., 2019. Coatings for Automotive Gray Cast Iron Brake Discs: A Review. Coatings 9, 552. https://doi.org/10.3390/coatings9090552
Arun, B.S., Aswini, A.R., Gogoi, M.M., Hegde, P., Kumar Kompalli, S., Sharma, P., Suresh Babu, S., 2019. Physico-chemical and optical properties of aerosols at a background site (~4 km a.s.l.) in the western Himalayas. Atmos. Environ. 218, 117017. https://doi.org/10.1016/j.atmosenv.2019.117017
Aryasree, S., Nair, P.R., Girach, I.A., Jacob, S., 2015. Winter time chemical characteristics of aerosols over the Bay of Bengal: continental influence. Environ. Sci. Pollut. Res. 22, 14901–14918. https://doi.org/10.1007/s11356-015-4700-7
Asmerom, Y., Jacobsen, S.B., 1993. The Pb isotopic evolution of the Earth: inferences from river water suspended loads. Earth Planet. Sci. Lett. 115, 245–256. https://doi.org/10.1016/0012-821X(93)90225-X
Attri, P., Tiwari, D.M., M, S., Reddy, D.V., Kumar, D., 2024. A Long-Term Study on Sources, Enrichments, and Inhalation Risk Assessments of Aerosols (Pm10) at Urban/Industrial City of Hyderabad in Southern India. https://doi.org/10.2139/ssrn.4756418
Bacon, J.R., Hewitt, I.J., 2005. Heavy metals deposited from the atmosphere on upland Scottish soils: Chemical and lead isotope studies of the association of metals with soil components. Geochim. Cosmochim. Acta 69, 19–33. https://doi.org/10.1016/j.gca.2004.06.030
Baker, J., Peate, D., Waight, T., Meyzen, C., 2004. Pb isotopic analysis of standards and samples using a 207Pb–204Pb double spike and thallium to correct for mass bias with a double-focusing MC-ICP-MS. Chem. Geol. 211, 275–303. https://doi.org/10.1016/j.chemgeo.2004.06.030
Balachandran, S., Meena, B.R., Khillare, P.S., 2000. Particle size distribution and its elemental composition in the ambient air of Delhi. Environ. Int. 26, 49–54. https://doi.org/10.1016/S0160-4120(00)00077-5
Balasubramanian, R., Qian, W.-B., 2004. Characterization and source identification of airborne trace metals in Singapore. J. Environ. Monit. 6, 813–818. https://doi.org/10.1039/B407523D
Bandhu, H.K., Puri, S., Garg, M.L., Singh, B., Shahi, J.S., Mehta, D., Swietlicki, E., Dhawan, D.K., Mangal, P.C., Singh, N., 2000. Elemental composition and sources of air pollution in the city of Chandigarh, India, using EDXRF and PIXE techniques. Nucl. Instrum. Methods Phys. Res. Sect. B Beam Interact. Mater. At. 160, 126–138. https://doi.org/10.1016/S0168-583X(99)00574-1
Barker, A.J., Clausen, J.L., Douglas, T.A., Bednar, A.J., Griggs, C.S., Martin, W.A., 2021. Environmental impact of metals resulting from military training activities: A review. Chemosphere 265, 129110. https://doi.org/10.1016/j.chemosphere.2020.129110
Barnwell, J., 2022. Finding Your Way Through the Maze: Navigating the Public and Private Spaces of Downing Street in Darkest Hour (2017 Joe Wright, PD Sarah Greenwood), in: Barnwell, J. (Ed.), Production Design & the Cinematic Home. Springer International Publishing, Cham, pp. 129–150. https://doi.org/10.1007/978-3-030-90449-4_7
Baron, S., Tămaş, C.G., Le Carlier, C., 2014. How Mineralogy and Geochemistry Can Improve the Significance of Pb Isotopes in Metal Provenance Studies. Archaeometry 56, 665–680. https://doi.org/10.1111/arcm.12037
Basha, S., Jhala, J., Thorat, R., Goel, S., Trivedi, R., Shah, K., Menon, G., Gaur, P., Mody, K.H., Jha, B., 2010. Assessment of heavy metal content in suspended particulate matter of coastal industrial town, Mithapur, Gujarat, India. Atmospheric Res. 97, 257–265. https://doi.org/10.1016/j.atmosres.2010.04.012

Basori, M.B.I., Zaw, K., Meffre, S., Large, R.R., Hassan, W.F.W., 2017. Pb-isotope compositions of the Tasik Chini volcanic-hosted massive sulfide deposit, Central Belt of Peninsular Malaysia: implication for source region and tectonic setting. Isl. Arc 26, 1–8.
Beckett, K.P., Freer-Smith, P.H., Taylor, G., 2000. The Capture of Particulate Pollution by Trees at Five Contrasting Urban Sites. Arboric. J. 24, 209–230. https://doi.org/10.1080/03071375.2000.9747273
Bhuvaneshwari, S., Hettiarachchi, H., Meegoda, J.N., 2019. Crop Residue Burning in India: Policy Challenges and Potential Solutions. Int. J. Environ. Res. Public. Health 16, 832. https://doi.org/10.3390/ijerph16050832
Bhuyan, P., Deka, P., Prakash, A., Balachandran, S., Hoque, R.R., 2018. Chemical characterization and source apportionment of aerosol over mid Brahmaputra Valley, India. Environ. Pollut. 234, 997–1010. https://doi.org/10.1016/j.envpol.2017.12.009
Bi, X., Feng, X., Yang, Y., Li, X., Shin, G.P.Y., Li, F., Qiu, G., Li, G., Liu, T., Fu, Z., 2009. Allocation and source attribution of lead and cadmium in maize (Zea mays L.) impacted by smelting emissions. Environ. Pollut. 157, 834–839. https://doi.org/10.1016/j.envpol.2008.11.013
Bi, X., Liang, S., Li, X., 2013. A novel in situ method for sampling urban soil dust: Particle size distribution, trace metal concentrations, and stable lead isotopes. Environ. Pollut. 177, 48–57. https://doi.org/10.1016/j.envpol.2013.01.045
Bi, X.-Y., Li, Z.-G., Wang, S.-X., Zhang, L., Xu, R., Liu, J.-L., Yang, H.-M., Guo, M.-Z., 2017. Lead isotopic compositions of selected coals, Pb/Zn ores and fuels in China and the application for source tracing. Environ. Sci. Technol. 51, 13502–13508.
Bikkina, S., Sarin, M.M., Chinni, V., 2015. Atmospheric 210Pb and anthropogenic trace metals in the continental outflow to the Bay of Bengal. Atmos. Environ. 122, 737–747. https://doi.org/10.1016/j.atmosenv.2015.10.044
Birmili, W., Allen, A.G., Bary, F., Harrison, R.M., 2006. Trace Metal Concentrations and Water Solubility in Size-Fractionated Atmospheric Particles and Influence of Road Traffic. Environ. Sci. Technol. 40, 1144–1153. https://doi.org/10.1021/es0486925
Bollhöfer, A., Honeybun, R., Rosman, K., Martin, P., 2006. The lead isotopic composition of dust in the vicinity of a uranium mine in northern Australia and its use for radiation dose assessment. Sci. Total Environ. 366, 579–589. https://doi.org/10.1016/j.scitotenv.2005.11.016
Bollhöfer, A., Rosman, K.J.R., 2001. Isotopic source signatures for atmospheric lead: the Northern Hemisphere. Geochim. Cosmochim. Acta 65, 1727–1740. https://doi.org/10.1016/S0016-7037(00)00630-X
Bollhöfer, A., Rosman, K.J.R., 2000. Isotopic source signatures for atmospheric lead: the Southern Hemisphere. Geochim. Cosmochim. Acta 64, 3251–3262. https://doi.org/10.1016/S0016-7037(00)00436-1
Boreddy, S.K.R., Hegde, P., Aswini, A.R., 2021. Geochemical characteristics of trace elements in size-resolved coastal urban aerosols associated with distinct air masses over tropical peninsular India: Size distributions and source apportionment. Sci. Total Environ. 763, 142967. https://doi.org/10.1016/j.scitotenv.2020.142967
Botle, A., Singhal, R.K., Basu, H., V, M., Masih, J., 2020. Health risk assessment of heavy metals associated with Coarse and Quasi-accumulative airborne particulate matter in Mumbai City situated on the Western Coast of India. Environ. Technol. Innov. 19, 100857. https://doi.org/10.1016/j.eti.2020.100857
Bouška, V., Pešek, J., 1999. Quality parameters of lignite of the North Bohemian Basin in the Czech Republic in comparison with the world average lignite. Int. J. Coal Geol. 40, 211–235. https://doi.org/10.1016/S0166-5162(98)00070-6
British Petroleum, 2019. BP - Statistical review of world energy, 2019 - Google Search [WWW Document]. URL https://www.bp.com/content/dam/bp/business-

sites/en/global/corporate/pdfs/energy-economics/statistical-review/bp-stats-review-2019-full-report.pdf (accessed 1.10.22).
Bruce, J., Smith, J., Fowler, M., 2021. Relative efficiency of passive dust samplers: Progress towards coarse dust dispersion modelling. Atmos. Environ. 244, 117872. https://doi.org/10.1016/j.atmosenv.2020.117872
Budai, P., Clement, A., 2018. Spatial distribution patterns of four traffic-emitted heavy metals in urban road dust and the resuspension of brake-emitted particles: Findings of a field study. Transp. Res. Part Transp. Environ. 62, 179–185. https://doi.org/10.1016/j.trd.2018.02.014
Budaniya, M., Rai, A.C., 2022. Effectiveness of plants for passive removal of particulate matter is low in the indoor environment. Build. Environ. 222, 109384. https://doi.org/10.1016/j.buildenv.2022.109384
Burmistrz, P., Kogut, K., Marczak, M., Zwoździak, J., 2016. Lignites and subbituminous coals combustion in Polish power plants as a source of anthropogenic mercury emission. Fuel Process. Technol. 152, 250–258. https://doi.org/10.1016/j.fuproc.2016.06.011
Buttigieg, G.A., Baker, M.E., Ruiz, J., Denton, M.B., 2003. Lead Isotope Ratio Determination for the Forensic Analysis of Military Small Arms Projectiles. Anal. Chem. 75, 5022–5029. https://doi.org/10.1021/ac0301346
CARB, 2020. Air Cleaning Devices for the Home | California Air Resources Board [WWW Document]. URL https://ww2.arb.ca.gov/resources/fact-sheets/air-cleaning-devices-home?utm_source=chatgpt.com (accessed 1.10.25).
Carrasco, G., Chen, M., Boyle, E.A., Tanzil, J., Zhou, K., Goodkin, N.F., 2018. An update of the Pb isotope inventory in post leaded-petrol Singapore environments. Environ. Pollut. 233, 925–932. https://doi.org/10.1016/j.envpol.2017.09.025
Chabukdhara, M., Singh, O.P., 2016. Coal mining in northeast India: an overview of environmental issues and treatment approaches. Int. J. Coal Sci. Technol. 3, 87–96. https://doi.org/10.1007/s40789-016-0126-1
Chakraborty, A., Gupta, T., Mandariya, A.K., Tripathi, S., 2023. Trace elements in ambient aerosols and size-resolved fog droplets: Trends, enrichment, and risk assessment. Heliyon 9, e16400. https://doi.org/10.1016/j.heliyon.2023.e16400
Chakraborty, S., Chakraborty, P., Hathorne, E., Sarkar, A., Linsy, P., Frank, M., Nath, B.N., 2021. Evidence for increasing anthropogenic Pb concentrations in Indian shelf sediments during the last century. Sci. Total Environ. 760, 143833. https://doi.org/10.1016/j.scitotenv.2020.143833
Chang, J.-S., Yoon, I.-H., Kim, K.-W., 2009. Heavy metal and arsenic accumulating fern species as potential ecological indicators in As-contaminated abandoned mines. Ecol. Indic. 9, 1275–1279. https://doi.org/10.1016/j.ecolind.2009.03.011
Chang, M.B., Ku, S., 1998. Fates and partitioning of heavy metals in municipal solid waste incineration process. Toxicol. Environ. Chem. 67, 161–169. https://doi.org/10.1080/02772249809358611
Chatterjee, D., McDuffie, E.E., Smith, S.J., Bindle, L., van Donkelaar, A., Hammer, M.S., Venkataraman, C., Brauer, M., Martin, R.V., 2023. Source Contributions to Fine Particulate Matter and Attributable Mortality in India and the Surrounding Region. Environ. Sci. Technol. 57, 10263–10275. https://doi.org/10.1021/acs.est.2c07641
Chelani, A.B., Gajghate, D.G., Hasan, M.Z., 2001. Airborne Toxic Metals in Air of Mumbai City, India. Bull. Environ. Contam. Toxicol. 66, 196–205. https://doi.org/10.1007/s0012800225
Chen, H., Yan, Y., Hu, D., Peng, L., Wang, C., 2023. High contribution of vehicular exhaust and coal combustion to PM2.5-bound Pb pollution in an industrial city in North China: An insight from isotope. Atmos. Environ. 294, 119503. https://doi.org/10.1016/j.atmosenv.2022.119503
Chen, M., Carrasco, G., Zhao, N., Wang, X., Lee, J.N., Tanzil, J.T.I., Annammala, K.V., Poh, S.C., Lauro, F.M., Ziegler, A.D., Duangnamon, D., Boyle, E.A., 2023. Boundary exchange completes the marine Pb cycle jigsaw. Proc. Natl. Acad. Sci. 120, e2213163120. https://doi.org/10.1073/pnas.2213163120

Chen Z., 1994. Natural plant decorative screen for inner wall. CN2165620Y.
Chester, R., 1990. Trace elements in the oceans, in: Chester, R. (Ed.), Marine Geochemistry. Springer Netherlands, Dordrecht, pp. 346–421. https://doi.org/10.1007/978-94-010-9488-7_11
Chifflet, S., Amouroux, D., Bérail, S., Barre, J., Van, T.C., Baltrons, O., Brune, J., Dufour, A., Guinot, B., Mari, X., 2018. Origins and discrimination between local and regional atmospheric pollution in Haiphong (Vietnam), based on metal(loid) concentrations and lead isotopic ratios in PM10. Environ. Sci. Pollut. Res. Int. 25, 26653–26668. https://doi.org/10.1007/s11356-018-2722-7
Chomiak, L., Widera, M., 2020. A comparative study of the oxide and elemental composition of ash from lignite burned at various temperatures – Konin Lignite Mine, Central Poland. Gospod. Surowcami Miner. - Miner. Resour. Manag. 145–160. https://doi.org/10.24425/gsm.2020.133942
Cong, L., Zhou, S., Niyogi, D., Wu, Y., Yan, G., Dai, L., Liu, S., Zhang, Z., Hu, Y., 2022. Concentrations and isotopic analysis for the sources and transfer of lead in an urban atmosphere-plant-soil system. J. Environ. Manage. 311, 114771. https://doi.org/10.1016/j.jenvman.2022.114771
Corbin, J.C., Mensah, A.A., Pieber, S.M., Orasche, J., Michalke, B., Zanatta, M., Czech, H., Massabò, D., Buatier de Mongeot, F., Mennucci, C., El Haddad, I., Kumar, N.K., Stengel, B., Huang, Y., Zimmermann, R., Prévôt, A.S.H., Gysel, M., 2018. Trace Metals in Soot and PM2.5 from Heavy-Fuel-Oil Combustion in a Marine Engine. Environ. Sci. Technol. 52, 6714–6722. https://doi.org/10.1021/acs.est.8b01764
Corton, C.L., 2021. London Fog as Food: From Pabulum to Poison, in: Fuller, D., Saunders, C., Macnaughton, J. (Eds.), The Life of Breath in Literature, Culture and Medicine: Classical to Contemporary. Springer International Publishing, Cham, pp. 325–343. https://doi.org/10.1007/978-3-030-74443-4_16
Coufalík, P., Matoušek, T., Křůmal, K., Vojtíšek-Lom, M., Beránek, V., Mikuška, P., 2019. Content of metals in emissions from gasoline, diesel, and alternative mixed biofuels. Environ. Sci. Pollut. Res. 26, 29012–29019. https://doi.org/10.1007/s11356-019-06144-4
Councell, T.B., Duckenfield, K.U., Landa, E.R., Callender, E., 2004. Tire-Wear Particles as a Source of Zinc to the Environment. Environ. Sci. Technol. 38, 4206–4214. https://doi.org/10.1021/es034631f
Cox, T., Laceby, J.P., Roth, T., Alewell, C., 2023. Less is more? A novel method for identifying and evaluating non-informative tracers in sediment source mixing models. J. Soils Sediments 23, 3241–3261. https://doi.org/10.1007/s11368-023-03573-0
Cunha-Lopes, I., Alves, C.A., Casotti Rienda, I., Faria, T., Lucarelli, F., Querol, X., Amato, F., Almeida, S.M., 2022. Characterisation of non-exhaust emissions from road traffic in Lisbon. Atmos. Environ. 286, 119221. https://doi.org/10.1016/j.atmosenv.2022.119221
Dallmann, T.R., Onasch, T.B., Kirchstetter, T.W., Worton, D.R., Fortner, E.C., Herndon, S.C., Wood, E.C., Franklin, J.P., Worsnop, D.R., Goldstein, A.H., Harley, R.A., 2014. Characterization of particulate matter emissions from on-road gasoline and diesel vehicles using a soot particle aerosol mass spectrometer. Atmospheric Chem. Phys. 14, 7585–7599. https://doi.org/10.5194/acp-14-7585-2014
Darlington, A.B., 2014. In-room hydroponic air cleansing unit. US20140283450A1.
Das, A., Krishna, K.V.S.S., Kumar, R., Saha, M.C., Sengupta, S., Ghosh, J.G., 2018. Lead isotopic ratios in source apportionment of heavy metals in the street dust of Kolkata, India. Int. J. Environ. Sci. Technol. 15, 159–172. https://doi.org/10.1007/s13762-017-1377-0
Das, Avijit, Krishna, K., Kumar, R., Das, Anindya, Sengupta, S., Ghosh, J.G., 2016. Tracing lead contamination in foods in the city of Kolkata, India. Environ. Sci. Pollut. Res. 23, 22454–22466. https://doi.org/10.1007/s11356-016-7409-3
Das, R., 2022. Chapter 23 - Sources of lead (Pb) in atmosphere over Indian cities and health impacts, in: Singh, R.P. (Ed.), Asian Atmospheric Pollution. Elsevier, pp. 435–452. https://doi.org/10.1016/B978-0-12-816693-2.00014-7

Das, R., Bin Mohamed Mohtar, A.T., Rakshit, D., Shome, D., Wang, X., 2018. Sources of atmospheric lead (Pb) in and around an Indian megacity. Atmos. Environ. 193, 57–65. https://doi.org/10.1016/j.atmosenv.2018.08.062

Das, R., Khezri, B., Srivastava, B., Datta, S., Sikdar, P.K., Webster, R.D., Wang, X., 2015. Trace element composition of PM2.5 and PM10 from Kolkata – a heavily polluted Indian metropolis. Atmospheric Pollut. Res. 6, 742–750. https://doi.org/10.5094/APR.2015.083

Das, R., Wang, X., Khezri, B., Webster, R.D., Itoh, M., Shiodera, S., Bin Mohamed Mohtar, A.T., Kuwata, M., 2023. Suspension of Crustal Materials from Wildfire in Indonesia as Revealed by Pb Isotope Analysis. ACS Earth Space Chem. 7, 379–387. https://doi.org/10.1021/acsearthspacechem.2c00270

David, L.M., Ravishankara, A.R., Kodros, J.K., Pierce, J.R., Venkataraman, C., Sadavarte, P., 2019. Premature Mortality Due to PM2.5 Over India: Effect of Atmospheric Transport and Anthropogenic Emissions. GeoHealth 3, 2–10. https://doi.org/10.1029/2018GH000169

DCMSME [WWW Document], 2015. URL https://dcmsme.gov.in/ (accessed 1.15.25).

Deb, M., Thorpe, R.I., Cumming, G.L., Wagner, P.A., 1989. Age, source and stratigraphic implications of Pb isotope data for conformable, sediment-hosted, base metal deposits in the Proterozoic Aravalli-Delhi orogenic belt, northwestern India. Precambrian Res. 43, 1–22. https://doi.org/10.1016/0301-9268(89)90002-8

Demir, T., Karakaş, D., Yenisoy-Karakaş, S., 2022. Source identification of exhaust and non-exhaust traffic emissions through the elemental carbon fractions and Positive Matrix Factorization method. Environ. Res. 204, 112399. https://doi.org/10.1016/j.envres.2021.112399

Denier van der Gon, H., Appelman, W., 2009. Lead emissions from road transport in Europe: A revision of current estimates using various estimation methodologies. Sci. Total Environ. 407, 5367–5372. https://doi.org/10.1016/j.scitotenv.2009.06.027

Di Natale, F., Carotenuto, C., 2015. Particulate matter in marine diesel engines exhausts: Emissions and control strategies. Transp. Res. Part Transp. Environ. 40, 166–191. https://doi.org/10.1016/j.trd.2015.08.011

Díaz-Somoano, M., Kylander, M.E., López-Antón, M.A., Suárez-Ruiz, I., Martínez-Tarazona, M.R., Ferrat, M., Kober, B., Weiss, D.J., 2009. Stable Lead Isotope Compositions In Selected Coals From Around The World And Implications For Present Day Aerosol Source Tracing. Environ. Sci. Technol. 43, 1078–1085. https://doi.org/10.1021/es801818r

Dietrich, M., Krekeler, M.P.S., Kousehlar, M., Widom, E., 2021. Quantification of Pb pollution sources in complex urban environments through a multi-source isotope mixing model based on Pb isotopes in lichens and road sediment. Environ. Pollut. 288, 117815. https://doi.org/10.1016/j.envpol.2021.117815

Dočekal, B., Krivan, V., Pelz, N., 1992. Trace and minor element characterization of diesel soot. Fresenius J. Anal. Chem. 343, 873–878. https://doi.org/10.1007/BF00321956

Dong, S., Ochoa Gonzalez, R., Harrison, R.M., Green, D., North, R., Fowler, G., Weiss, D., 2017. Isotopic signatures suggest important contributions from recycled gasoline, road dust and non-exhaust traffic sources for copper, zinc and lead in PM10 in London, United Kingdom. Atmos. Environ. 165, 88–98. https://doi.org/10.1016/j.atmosenv.2017.06.020

Dongsheng 2, 2015. **越南**东北部佐田铅锌矿床硫化物S、Pb **同位素特征及其地**质意义. **地**质通报 34, 757–768.

Draxler, R., 1998. An Overview of the HYSPLIT_4 Modelling System for Trajectories, Dispersion, and Deposition.

Drucker, D.G., Valentin, F., Thevenet, C., Mordant, D., Cottiaux, R., Delsate, D., Van Neer, W., 2018. Aquatic resources in human diet in the Late Mesolithic in Northern France and Luxembourg: insights from carbon, nitrogen and sulphur isotope ratios. Archaeol. Anthropol. Sci. 10, 351–368. https://doi.org/10.1007/s12520-016-0356-6

Dubey, B., Pal, A.K., Singh, G., 2012. Trace metal composition of airborne particulate matter in the coal mining and non–mining areas of Dhanbad Region, Jharkhand, India. Atmospheric Pollut. Res. 3, 238–246. https://doi.org/10.5094/APR.2012.026

Dumitrescu, E., 2017. Global Efforts to Promote Cleaner Used Vehicles: Focus on Solutions.

Dzierżanowski, K., Popek, R., Gawrońska, H., Sæbø, A., Gawroński, S.W., 2011. Deposition of Particulate Matter of Different Size Fractions on Leaf Surfaces and in Waxes of Urban Forest Species. Int. J. Phytoremediation 13, 1037–1046. https://doi.org/10.1080/15226514.2011.552929

EEA, 2016. Temperature inversion traps pollution at ground level — European Environment Agency [WWW Document]. URL https://www.eea.europa.eu/media/infographics/temperature-inversion-traps-pollution-at/view (accessed 5.3.24).

Eichler, P., Müller, M., Rohmann, C., Stengel, B., Orasche, J., Zimmermann, R., Wisthaler, A., 2017. Lubricating Oil as a Major Constituent of Ship Exhaust Particles. Environ. Sci. Technol. Lett. 4, 54–58. https://doi.org/10.1021/acs.estlett.6b00488

Energy Market Authority Singapore, n.d. Energy Transformation [WWW Document]. URL https://www.checkfirst.gov.sg/c/1ac4306f-4df9-4a7c-8759-00fda969d6a5 (accessed 8.11.23).

Erel, Y., 1998. Mechanisms and Velocities of Anthropogenic Pb Migration in Mediterranean Soils. Environ. Res. 78, 112–117. https://doi.org/10.1006/enrs.1997.3811

Ericson, B., Dowling, R., Dey, S., Caravanos, J., Mishra, N., Fisher, S., Ramirez, M., Sharma, P., McCartor, A., Guin, P., Taylor, M.P., Fuller, R., 2018. A meta-analysis of blood lead levels in India and the attributable burden of disease. Environ. Int. 121, 461–470. https://doi.org/10.1016/j.envint.2018.08.047

Ericson, B., Hu, H., Nash, E., Ferraro, G., Sinitsky, J., Taylor, M.P., 2021. Blood lead levels in low-income and middle-income countries: a systematic review. Lancet Planet. Health 5, e145–e153. https://doi.org/10.1016/S2542-5196(20)30278-3

Eslava-Silva, F. de J., Muñíz-Díaz de León, M.E., Jiménez-Estrada, M., 2023. Pteridium aquilinum (Dennstaedtiaceae), a Novel Hyperaccumulator Species of Hexavalent Chromium. Appl. Sci. 13, 5621. https://doi.org/10.3390/app13095621

Fan, J., Dai, W., Wang, Y., Zhang, B., Fang, J., Lou, L., Lin, Q., 2020. Seasonal disparities in airborne lead (Pb) and associated foliar uptake by ryegrass (Lolium perenne L.): A Pb isotopic approach. Sci. Total Environ. 708, 134734. https://doi.org/10.1016/j.scitotenv.2019.134734

Farmer, J.G., Graham, M.C., Yafa, C., Cloy, J.M., Freeman, A.J., MacKenzie, A.B., 2006. Use of 206Pb/207Pb ratios to investigate the surface integrity of peat cores used to study the recent depositional history and geochemical behaviour of inorganic elements in peat bogs. Glob. Planet. Change, Peatlands: records of global environmental changes 53, 240–248. https://doi.org/10.1016/j.gloplacha.2006.03.006

Fayiga, A.O., Ma, L.Q., Cao, X., Rathinasabapathi, B., 2004. Effects of heavy metals on growth and arsenic accumulation in the arsenic hyperaccumulator Pteris vittata L. Environ. Pollut. 132, 289–296. https://doi.org/10.1016/j.envpol.2004.04.020

Filippidis, A., Georgakopoulos, A., Kassoli-Fournaraki, A., Misaelides, P., Yiakkoupis, P., Broussoulis, J., 1996. Trace element contents in composited samples of three lignite seams from the central part of the Drama lignite deposit, Macedonia, Greece. Int. J. Coal Geol. 29, 219–234. https://doi.org/10.1016/0166-5162(95)00032-1

Fowler, D., Brimblecombe, P., Burrows, J., Heal, M.R., Grennfelt, P., Stevenson, D.S., Jowett, A., Nemitz, E., Coyle, M., Liu, X., Chang, Y., Fuller, G.W., Sutton, M.A., Klimont, Z., Unsworth, M.H., Vieno, M., 2020. A chronology of global air quality. Philos. Trans. R. Soc. Math. Phys. Eng. Sci. 378, 20190314. https://doi.org/10.1098/rsta.2019.0314

Fridell, E., Steen, E., Peterson, K., 2008. Primary particles in ship emissions. Atmos. Environ. 42, 1160–1168. https://doi.org/10.1016/j.atmosenv.2007.10.042

Fulekar, M.H., Naik, D.S., Dave, J.M., 1983. Heavy metals in Indian coals and corresponding fly-ash and their relationship with particulate size. Int. J. Environ. Stud. 21, 179–182. https://doi.org/10.1080/00207238308710074

Fussell, J.C., Franklin, M., Green, D.C., Gustafsson, M., Harrison, R.M., Hicks, W., Kelly, F.J., Kishta, F., Miller, M.R., Mudway, I.S., Oroumiyeh, F., Selley, L., Wang, M., Zhu, Y., 2022. A Review of Road Traffic-Derived Non-Exhaust Particles: Emissions, Physicochemical Characteristics, Health Risks, and Mitigation Measures. Environ. Sci. Technol. 56, 6813–6835. https://doi.org/10.1021/acs.est.2c01072

Gaghate, D.G., Hasan, M.Z., 1999. Ambient Lead Levels in Urban Areas. Bull. Environ. Contam. Toxicol. 62, 403–408. https://doi.org/10.1007/s001289900889

GAINS South Asia online [WWW Document], 2020. URL https://gains.iiasa.ac.at/gains/activities.INN/index.menu (accessed 6.14.23).

Gajghate, D.G., Bhanarkar, A.D., 2005. Characterisation of particulate matter for toxic metals in ambient air of Kochi City, India. Environ. Monit. Assess. 102, 119–129. https://doi.org/10.1007/s10661-005-4535-7

Gajghate, D.G., Bhanarkar, A.D., 2004. Tracking Toxic Metals in the Ambient Air of Agra City, India. Bull. Environ. Contam. Toxicol. 72, 806–812. https://doi.org/10.1007/s00128-004-0316-1

Gajghate, D.G., Talwar, B., Pipalatkar, P., Pustode, T., 2012. Chemical Characterization of PM10 for Metals in Ambient Air of Chennai, India. J. Hazard. Toxic Radioact. Waste 16, 169–174. https://doi.org/10.1061/(ASCE)HZ.1944-8376.0000079

Gao, P.-P., Xue, P.-Y., Dong, J.-W., Zhang, X.-M., Sun, H.-X., Geng, L.-P., Luo, S.-X., Zhao, J.-J., Liu, W.-J., 2021. Contribution of PM2.5-Pb in atmospheric fallout to Pb accumulation in Chinese cabbage leaves via stomata. J. Hazard. Mater. 407, 124356. https://doi.org/10.1016/j.jhazmat.2020.124356

Gaonkar, C.V., Kumar, A., Matta, V.M., Kurian, S., 2020. Assessment of crustal element and trace metal concentrations in atmospheric particulate matter over a coastal city in the Eastern Arabian Sea. J. Air Waste Manag. Assoc. 70, 78–92. https://doi.org/10.1080/10962247.2019.1680458

Gasim, M., Khalid, N.A., Muhamad, H., 2015. The influence of tidal activities on water quality of paka river Terengganu, Malaysia 19, 979–990.

Geiger, A., Cooper, J., 2010. Overview Of Airborne Metals Regulations, Exposure Limits, Health Effects, And Contemporary Research Case Study | Environmental XPRT [WWW Document]. URL https://www.environmental-expert.com/articles/overview-of-airborne-metals-regulations-exposure-limits-health-effects-and-contemporary-research-cas-450906 (accessed 6.13.24).

Gelwicks, J.T., Hayes, J.M., 1990. Carbon-isotopic analysis of dissolved acetate. Anal. Chem. 62, 535–539. https://doi.org/10.1021/ac00204a021

George, S., Chua, M.L., ZheWei, D.Z., Das, R., Bijin, V.A., Connolly, J.E., Lee, K.P., Yung, C.F., Teoh, O.H., Thomas, B., 2020. Personal level exposure and hazard potential of particulate matter during haze and non-haze periods in Singapore. Chemosphere 243, 125401. https://doi.org/10.1016/j.chemosphere.2019.125401

Gibbons, A., 2018. Why 536 was 'the worst year to be alive' [WWW Document]. URL https://www.science.org/content/article/why-536-was-worst-year-be-alive (accessed 1.8.25).

Gioia, S.M.C.L., Babinski, M., Weiss, D.J., Spiro, B., Kerr, A.A.F.S., Veríssimo, T.G., Ruiz, I., Prates, J.C.M., 2017. An isotopic study of atmospheric lead in a megacity after phasing out of leaded gasoline. Atmos. Environ. 149, 70–83. https://doi.org/10.1016/j.atmosenv.2016.10.049

Given, P.H., Miller, R.N., 1987. The association of major, minor and trace inorganic elements with lignites. III. Trace elements in four lignites and general discussion of all data from this study. Geochim. Cosmochim. Acta 51, 1843–1853. https://doi.org/10.1016/0016-7037(87)90174-8

Gokhale, S.B., Patil, R.S., 2004. Size Distribution of Aerosols (PM10) and Lead (Pb) near Traffic Intersections in Mumbai (India). Environ. Monit. Assess. 95, 311–324. https://doi.org/10.1023/B:EMAS.0000029911.81865.b6

Gómez-Bernal, J.M., Ruiz-Huerta, E.A., Armienta-Hernández, M.A., Luna-Pabello, V.M., 2017. Evaluation of the removal of heavy metals in a natural wetland impacted by mining activities in Mexico. Environ. Earth Sci. 76, 801. https://doi.org/10.1007/s12665-017-7144-1
Gordon, J.R.M., Lee, P.-M., Lucas, H.C., 2005. A resource-based view of competitive advantage at the Port of Singapore. J. Strateg. Inf. Syst. 14, 69–86. https://doi.org/10.1016/j.jsis.2004.10.001
Greenberg, N., Frimer, R., Meyer, R., Derazne, E., Chodick, G., 2016. Lead Exposure in Military Outdoor Firing Ranges. Mil. Med. 181, 1121–1126. https://doi.org/10.7205/MILMED-D-15-00454
Greenberg, R.R., Zoller, W.H., Gordon, G.E., 1978. Composition and size distributions of particles released in refuse incineration. Environ. Sci. Technol. 12, 566–573. https://doi.org/10.1021/es60141a011
Grigoratos, T., Martini, G., 2015. Brake wear particle emissions: a review. Environ. Sci. Pollut. Res. 22, 2491–2504. https://doi.org/10.1007/s11356-014-3696-8
Guevara, M., 2016. Emissions of Primary Particulate Matter.
Gulson, B.L., Davis, J.J., Mizon, K.J., Korsch, M.J., Bawden-Smith, J., 1995. Sources of lead in soil and dust and the use of dust fallout as a sampling medium. Sci. Total Environ. 166, 245–262. https://doi.org/10.1016/0048-9697(95)04505-U
Gummeneni, S., Yusup, Y.B., Chavali, M., Samadi, S.Z., 2011. Source apportionment of particulate matter in the ambient air of Hyderabad city, India. Atmospheric Res., International Conference on Nucleation and Atmospheric Aerosols (Part 2) 101, 752–764. https://doi.org/10.1016/j.atmosres.2011.05.002
Gupta, A.K., Karar, K., Ayoob, S., John, K., 2008. Spatio-temporal characteristics of gaseous and particulate pollutants in an urban region of Kolkata, India. Atmospheric Res. 87, 103–115. https://doi.org/10.1016/j.atmosres.2007.07.008
Ha, N.T.H., Sakakibara, M., Sano, S., Nhuan, M.T., 2011. Uptake of metals and metalloids by plants growing in a lead–zinc mine area, Northern Vietnam. J. Hazard. Mater. 186, 1384–1391. https://doi.org/10.1016/j.jhazmat.2010.12.020
Haritash, A.K., Kaushik, C.P., 2007. Assessment of Seasonal Enrichment of Heavy Metals in Respirable Suspended Particulate Matter of a Sub-Urban Indian City. Environ. Monit. Assess. 128, 411–420. https://doi.org/10.1007/s10661-006-9335-1
Harkel, M.J.T., 1997. The effects of particle-size distribution and chloride depletion of sea-salt aerosols on estimating atmospheric deposition at a coastal site. Atmos. Environ. 31, 417–427. https://doi.org/10.1016/S1352-2310(96)00249-X
Harrison, R.M., 2020. Airborne particulate matter. Philos. Trans. R. Soc. Math. Phys. Eng. Sci. 378, 20190319. https://doi.org/10.1098/rsta.2019.0319
Harrison, R.M., Allan, J., Carruthers, D., Heal, M.R., Lewis, A.C., Marner, B., Murrells, T., Williams, A., 2021. Non-exhaust vehicle emissions of particulate matter and VOC from road traffic: A review. Atmos. Environ. 262, 118592. https://doi.org/10.1016/j.atmosenv.2021.118592
Harrison, R.M., Jones, A.M., Gietl, J., Yin, J., Green, D.C., 2012. Estimation of the Contributions of Brake Dust, Tire Wear, and Resuspension to Nonexhaust Traffic Particles Derived from Atmospheric Measurements. Environ. Sci. Technol. 46, 6523–6529. https://doi.org/10.1021/es300894r
Harrison, R.M., Tilling, R., Callén Romero, M.S., Harrad, S., Jarvis, K., 2003. A study of trace metals and polycyclic aromatic hydrocarbons in the roadside environment. Atmos. Environ. 37, 2391–2402. https://doi.org/10.1016/S1352-2310(03)00122-5
Haynes, A., Popek, R., Boles, M., Paton-Walsh, C., Robinson, S.A., 2019. Roadside Moss Turfs in South East Australia Capture More Particulate Matter Along an Urban Gradient than a Common Native Tree Species. Atmosphere 10, 224. https://doi.org/10.3390/atmos10040224
Hemming, S.R., McLennan, S.M., 2001. Pb isotope compositions of modern deep sea turbidites. Earth Planet. Sci. Lett. 184, 489–503. https://doi.org/10.1016/S0012-821X(00)00340-X

Hernberg, S., 2000. Lead poisoning in a historical perspective. Am. J. Ind. Med. 38, 244–254. https://doi.org/10.1002/1097-0274(200009)38:3<244::AID-AJIM3>3.0.CO;2-F
Hippocrates, 400AD. The Internet Classics Archive | On Airs, Waters, and Places by Hippocrates [WWW Document]. URL https://classics.mit.edu/Hippocrates/airwatpl.1.1.html (accessed 1.8.25).
Hjortenkrans, D.S.T., Bergbäck, B.G., Häggerud, A.V., 2007. Metal Emissions from Brake Linings and Tires: Case Studies of Stockholm, Sweden 1995/1998 and 2005. Environ. Sci. Technol. 41, 5224–5230. https://doi.org/10.1021/es070198o
Hoàng-Hòa, T.B., Stille, P., Dietze, V., Guéguen, F., Perrone, T., Gieré, R., 2015. Pb, Sr and Nd isotopic composition and trace element characteristics of coarse airborne particles collected with passive samplers. Comptes Rendus Geosci., Geochemical and isotopic record of anthropogenic activities (Part 1) 347, 267–276. https://doi.org/10.1016/j.crte.2015.02.007
Howard-Reed, C., Wallace, L.A., Ott, W.R., 2002. The Effect of Opening Windows on Air Change Rates in Two Homes. J. Air Waste Manag. Assoc. 52, 147–159. https://doi.org/10.1080/10473289.2002.10470775
Hower, J.C., Warwick, P.D., Scanlon, B.R., Reedy, R.C., Childress, T.M., 2023. Distribution of rare earth and other critical elements in lignites from the Eocene Jackson Group, Texas. Int. J. Coal Geol. 275, 104302. https://doi.org/10.1016/j.coal.2023.104302
Hrotko, K., Gyeviki, M., Su¨to¨rine´, M.D., Magyar, L., Me´sza´ros, R., Honfi, P., Kardos, L., 2020. Foliar dust and heavy metal deposit on leaves of urban trees in Budapest (Hungary) | SpringerLink [WWW Document]. URL https://link.springer.com/article/10.1007/s10653-020-00769-y (accessed 3.2.22).
Hsu, Y.-K., 2019a. Chinese Lead Isotope Database. Harv. Dataverse. https://doi.org/10.7910/DVN/VID3WR
Hsu, Y.-K., 2019b. Chinese Lead Isotope Database. https://doi.org/10.7910/DVN/VID3WR
Hu, X., Zhang, Y., Luo, J., Xie, M., Wang, T., Lian, H., 2011. Accumulation and quantitative estimates of airborne lead for a wild plant (Aster subulatus). Chemosphere 82, 1351–1357. https://doi.org/10.1016/j.chemosphere.2010.11.079
Huang, C., Li, H., Lai, C.-K., 2019. Genesis of the Binh Do Pb-Zn Deposit in Northern Vietnam: Evidence from H-O-S-Pb Isotope Geochemistry. J. Earth Sci. 30, 679–688. https://doi.org/10.1007/s12583-019-0872-2
Ibrahim, I.Z., Chong, W.T., Yusoff, S., Wang, C.-T., Xiang, X., Muzammil, W.K., 2021. Evaluation of common indoor air pollutant reduction by a botanical indoor air biofilter system. Indoor Built Environ. 30, 7–21. https://doi.org/10.1177/1420326X19882080
IMO, 2022. Fuel Consumption (DCS) – IMO [WWW Document]. URL https://futurefuels.imo.org/home/latest-information/fuel-consumption-dcs/ (accessed 12.1.24).
INDIAN BUREAU OF MINES, 2014. Indian Minerals Yearbook.
Indian Ports Association, 2014. Andaman & Nicobar [WWW Document]. URL https://www.ipa.nic.in/index1.cshtml?lsid=37 (accessed 11.15.24).
IndiaPM25-V6GL02, 2024. IndiaPM25-V6GL02-Annual-REGIONAL-1998-2022-wThresFrac.csv | Powered by Box [WWW Document]. URL https://wustl.app.box.com/s/51p4t6zhmxy8i6an53hxcb2m31v04gi1 (accessed 10.18.24).
International Energy Outlook, 2023. U.S. Energy Information Administration - EIA - Independent Statistics and Analysis [WWW Document]. URL https://www.eia.gov/outlooks/aeo/data/browser/#/?id=60-IEO2023&region=0-0&cases=Reference&start=2020&end=2050&f=Q&chartindexed=2&sourcekey=1 (accessed 9.8.24).
Irga, P.J., Paull, N.J., Abdo, P., Torpy, F.R., 2017. An assessment of the atmospheric particle removal efficiency of an in-room botanical biofilter system. Build. Environ. 115, 281–290. https://doi.org/10.1016/j.buildenv.2017.01.035

Jain, S., Sharma, S.K., Vijayan, N., Mandal, T.K., 2020. Seasonal characteristics of aerosols (PM2.5 and PM10) and their source apportionment using PMF: A four year study over Delhi, India. Environ. Pollut. 262, 114337. https://doi.org/10.1016/j.envpol.2020.114337

Jena, S., Perwez, A., Singh, G., 2019. Trace element characterization of fine particulate matter and assessment of associated health risk in mining area, transportation routes and institutional area of Dhanbad, India. Environ. Geochem. Health 41, 2731–2747. https://doi.org/10.1007/s10653-019-00329-z

Jeong, C.-H., Wang, J.M., Hilker, N., Debosz, J., Sofowote, U., Su, Y., Noble, M., Healy, R.M., Munoz, T., Dabek-Zlotorzynska, E., Celo, V., White, L., Audette, C., Herod, D., Evans, G.J., 2019. Temporal and spatial variability of traffic-related PM2.5 sources: Comparison of exhaust and non-exhaust emissions. Atmos. Environ. 198, 55–69. https://doi.org/10.1016/j.atmosenv.2018.10.038

Jeong, H., 2022a. Toxic metal concentrations and Cu–Zn–Pb isotopic compositions in tires. J. Anal. Sci. Technol. 13, 2. https://doi.org/10.1186/s40543-021-00312-3

Jeong, H., 2022b. Toxic metal concentrations and Cu–Zn–Pb isotopic compositions in tires. J. Anal. Sci. Technol. 13, 2. https://doi.org/10.1186/s40543-021-00312-3

Jeong, H., Ryu, J.-S., Ra, K., 2022. Characteristics of potentially toxic elements and multi-isotope signatures (Cu, Zn, Pb) in non-exhaust traffic emission sources. Environ. Pollut. 292, 118339. https://doi.org/10.1016/j.envpol.2021.118339

Jonasson, M., Afshari, R., 2018. Historical documentation of lead toxicity prior to the 20th century in English literature. Hum. Exp. Toxicol. 37, 775–788. https://doi.org/10.1177/0960327117737146

Jung, C.H., Matsuto, T., Tanaka, N., Okada, T., 2004. Metal distribution in incineration residues of municipal solid waste (MSW) in Japan. Waste Manag. 24, 381–391. https://doi.org/10.1016/S0956-053X(03)00137-5

Kachenko, A.G., Singh, B., Bhatia, N.P., 2007. Heavy metal tolerance in common fern species. Aust. J. Bot. 55, 63–73. https://doi.org/10.1071/BT06063

Kar, S., Samal, A.C., Maity, J.P., Santra, S.C., 2014. Diversity of epiphytic lichens and their role in sequestration of atmospheric metals. Int. J. Environ. Sci. Technol. 11, 899–908. https://doi.org/10.1007/s13762-013-0270-8

Karar, K., Gupta, A.K., 2006. Seasonal variations and chemical characterization of ambient PM10 at residential and industrial sites of an urban region of Kolkata (Calcutta), India. Atmospheric Res. 81, 36–53. https://doi.org/10.1016/j.atmosres.2005.11.003

Kaya, G., Tuncel, G., 1997. Trace element and major ion composition of wet and dry depositon in Ankara, Turkey. Atmos. Environ. 31, 3985–3998. https://doi.org/10.1016/S1352-2310(97)00221-5

Kayee, J., Bureekul, S., Sompongchaiyakul, P., Wang, X., Das, R., 2021. Sources of atmospheric lead (Pb) after quarter century of phasing out of leaded gasoline in Bangkok, Thailand. Atmos. Environ. 253, 118355. https://doi.org/10.1016/j.atmosenv.2021.118355

Kayee, J., Sompongchaiyakul, P., Sanwlani, N., Bureekul, S., Wang, X., Das, R., 2020. Metal Concentrations and Source Apportionment of PM $_{2.5}$ in Chiang Rai and Bangkok, Thailand during a Biomass Burning Season. ACS Earth Space Chem. 4, 1213–1226. https://doi.org/10.1021/acsearthspacechem.0c00140

Kayee, P., Songphim, W., Parkpein, A., 2015. Using Thai Native Moss as Bio-Adsorbent for Contaminated Heavy Metal in Air. Procedia - Soc. Behav. Sci., 7th World Conference on Educational Sciences 197, 1037–1042. https://doi.org/10.1016/j.sbspro.2015.07.312

Kelepertzis, E., Chrastný, V., Botsou, F., Sigala, E., Kypritidou, Z., Komárek, M., Skordas, K., Argyraki, A., 2021. Tracing the sources of bioaccessible metal(loid)s in urban environments: A multidisciplinary approach. Sci. Total Environ. 771, 144827. https://doi.org/10.1016/j.scitotenv.2020.144827

Khare, P., Baruah, B.P., 2010. Elemental characterization and source identification of PM2.5 using multivariate analysis at the suburban site of North-East India. Atmospheric Res., Clouds, Aerosols and Radiation 98, 148–162. https://doi.org/10.1016/j.atmosres.2010.07.001
Khillare, P.S., Balachandran, S., Meena, B.R., 2004. Spatial and Temporal Variation of Heavy Metals in Atmospheric Aerosol of Delhi. Environ. Monit. Assess. 90, 1–21. https://doi.org/10.1023/B:EMAS.0000003555.36394.17
Khillare, P.S., Sarkar, S., 2012. Airborne inhalable metals in residential areas of Delhi, India: distribution, source apportionment and health risks. Atmospheric Pollut. Res. 3, 46–54. https://doi.org/10.5094/APR.2012.004
Khobragade, P.P., Ahirwar, A.V., 2022. Source identification and ambient trace element concentrations of PM10 using receptor modeling in an urban area of Chhattisgarh, India. Geocarto Int. 37, 12267–12293. https://doi.org/10.1080/10106049.2022.2066201
Kitamura, H., Dahlan, A.V., Tian, Y., Shimaoka, T., Yamamoto, T., Takahashi, F., 2020. Application of micro-scale correlation analysis to estimate metal speciation and the matrix in municipal solid waste incineration fly ash. J. Mater. Cycles Waste Manag. 22, 1081–1093. https://doi.org/10.1007/s10163-020-01001-w
Klaminder, J., Bindler, R., Emteryd, O., Renberg, I., 2005. Uptake and recycling of lead by boreal forest plants: Quantitative estimates from a site in northern Sweden. Geochim. Cosmochim. Acta 69, 2485–2496. https://doi.org/10.1016/j.gca.2004.11.013
Koffman, B.G., Saylor, P., Zhong, R., Sethares, L., Yoder, M.F., Hanschka, L., Methven, T., Cai, Y., Bolge, L., Longman, J., Goldstein, S.L., Osterberg, E.C., 2022. Provenance of Anthropogenic Pb and Atmospheric Dust to Northwestern North America. Environ. Sci. Technol. 56, 13107–13118. https://doi.org/10.1021/acs.est.2c03767
Komárek, M., Ettler, V., Chrastný, V., Mihaljevič, M., 2008. Lead isotopes in environmental sciences: A review. Environ. Int. 34, 562–577. https://doi.org/10.1016/j.envint.2007.10.005
Kortenski, J., Sotirov, A., 2002. Trace and major element content and distribution in Neogene lignite from the Sofia Basin, Bulgaria. Int. J. Coal Geol. 52, 63–82. https://doi.org/10.1016/S0166-5162(02)00133-7
KPMG, 2024. AMMO India 2024: Make in India – Make for the world [WWW Document]. KPMG. URL https://kpmg.com/in/en/insights/2024/08/ammo-india-2024-make-in-india-make-for-the-world.html (accessed 12.7.24).
Krishnamurti, T.N., Chakraborty, A., Martin, A., Lau, W.K., Kim, K.-M., Sud, Y., Walker, G., 2009. Impact of Arabian Sea pollution on the Bay of Bengal winter monsoon rains. J. Geophys. Res. Atmospheres 114. https://doi.org/10.1029/2008JD010679
Kubicka, K., Samecka-Cymerman, A., Kolon, K., Kosiba, P., Kempers, A.J., 2015. Chromium and nickel in Pteridium aquilinum from environments with various levels of these metals. Environ. Sci. Pollut. Res. 22, 527–534. https://doi.org/10.1007/s11356-014-3379-5
Kulshrestha, A., Massey, D.D., Masih, J., Taneja, A., 2014. Source Characterization of Trace Elements in Indoor Environments at Urban, Rural and Roadside Sites in a Semi Arid Region of India. Aerosol Air Qual. Res. 14, 1738–1751. https://doi.org/10.4209/aaqr.2013.05.0147
Kulshrestha, A., Satsangi, P.G., Masih, J., Taneja, A., 2009. Metal concentration of PM2.5 and PM10 particles and seasonal variations in urban and rural environment of Agra, India. Sci. Total Environ. 407, 6196–6204. https://doi.org/10.1016/j.scitotenv.2009.08.050
Kumar, A., Malyan, V., Sahu, M., 2023. Air Pollution Control Technologies for Indoor Particulate Matter Pollution: A Review. Aerosol Sci. Eng. 7, 261–282. https://doi.org/10.1007/s41810-023-00178-5
Kumar, R., Patel, S.S., Das, A., Ghosh, J.G., Sengupta, S., Krishna, K., Guha, D., 2017. Variability of Pb-isotopes in the East Indian Gondwana Coal deposits: It's influence on Kolkata street dust. Indian J. Geosci. 71, 575–588.

Kumar, S., Aggarwal, S.G., Malherbe, J., Barre, J.P.G., Berail, S., Gupta, P.K., Donard, O.F.X., 2016. Tracing dust transport from Middle-East over Delhi in March 2012 using metal and lead isotope composition. Atmos. Environ. 132, 179–187. https://doi.org/10.1016/j.atmosenv.2016.03.002

Kumar, S., Aggarwal, S.G., Sarangi, B., Malherbe, J., Barre, J.P.G., Berail, S., Séby, F., Donard, O.F.X., 2018. Understanding the Influence of Open-waste Burning on Urban Aerosols using Metal Tracers and Lead Isotopic Composition. Aerosol Air Qual. Res. 18, 2433–2446. https://doi.org/10.4209/aaqr.2017.11.0510

Kumari, A., Lal, B., Pakade, Y.B., Chand, P., 2011. Assessment of Bioaccumulation of Heavy Metal by Pteris Vittata L. Growing in the Vicinity of Fly Ash. Int. J. Phytoremediation 13, 779–787. https://doi.org/10.1080/15226514.2010.525561

Kumari, M., Bhattacharya, T., 2023. A review on bioaccessibility and the associated health risks due to heavy metal pollution in coal mines: Content and trend analysis. Environ. Dev. 46, 100859. https://doi.org/10.1016/j.envdev.2023.100859

Lachheb, M., Youssef, N., Younsi, Z., 2023. A Comprehensive Review of the Improvement of the Thermal and Mechanical Properties of Unfired Clay Bricks by Incorporating Waste Materials. Buildings 13, 2314. https://doi.org/10.3390/buildings13092314

Lahd Geagea, M., Stille, P., Gauthier-Lafaye, F., Millet, M., 2008. Tracing of Industrial Aerosol Sources in an Urban Environment Using Pb, Sr, and Nd Isotopes. Environ. Sci. Technol. 42, 692–698. https://doi.org/10.1021/es071704c

Lahiri, D., Ray, I., Ray, R., Chanakya, I.V.S., Tarique, M., Misra, S., Rahaman, W., Tiwari, M., Wang, X., Das, R., 2024. Source apportionment and emission projections of heavy metals from traffic sources in India: Insights from elemental and Pb isotopic compositions. J. Hazard. Mater. 135810. https://doi.org/10.1016/j.jhazmat.2024.135810

Laidlaw, M.A.S., Zahran, S., Mielke, H.W., Taylor, M.P., Filippelli, G.M., 2012. Re-suspension of lead contaminated urban soil as a dominant source of atmospheric lead in Birmingham, Chicago, Detroit and Pittsburgh, USA. Atmos. Environ. 49, 302–310. https://doi.org/10.1016/j.atmosenv.2011.11.030

Lamble, K.J., Hill, S.J., 1998. Microwave digestion procedures for environmental matrices . Critical Review. Analyst 123, 103R-133R. https://doi.org/10.1039/A800776D

Lee, J.-M., Boyle, E.A., Gamo, T., Obata, H., Norisuye, K., Echegoyen, Y., 2015. Impact of anthropogenic Pb and ocean circulation on the recent distribution of Pb isotopes in the Indian Ocean. Geochim. Cosmochim. Acta 170, 126–144. https://doi.org/10.1016/j.gca.2015.08.013

Lee, J.-M., Boyle, E.A., Suci Nurhati, I., Pfeiffer, M., Meltzner, A.J., Suwargadi, B., 2014. Coral-based history of lead and lead isotopes of the surface Indian Ocean since the mid-20th century. Earth Planet. Sci. Lett. 398, 37–47. https://doi.org/10.1016/j.epsl.2014.04.030

Lee, P.H., Delay, I., Nasserzadeh, V., Swithenbank, J., McLeod, C., Argent, B.B., Goodfellow, J., 2006. Characterization, decontamination and health effects of fly ash from waste incinerators. Environ. Prog. 17, 261–269. https://doi.org/10.1002/ep.670170417

Lehtoranta, K., Aakko-Saksa, P., Murtonen, T., Vesala, H., Ntziachristos, L., Rönkkö, T., Karjalainen, P., Kuittinen, N., Timonen, H., 2019. Particulate Mass and Nonvolatile Particle Number Emissions from Marine Engines Using Low-Sulfur Fuels, Natural Gas, or Scrubbers. Environ. Sci. Technol. 53, 3315–3322. https://doi.org/10.1021/acs.est.8b05555

Lessler, M.A., 1988. Lead and Lead Poisoning from Antiquity to Modern Times 88.

Li, F., Jinxu, Y., Shao, L., Zhang, G., Wang, J., Jin, Z., 2018. Delineating the origin of Pb and Cd in the urban dust through elemental and stable isotopic ratio: A study from Hangzhou City, China. Chemosphere 211, 674–683. https://doi.org/10.1016/j.chemosphere.2018.07.199

Li, F.-L., Liu, C.-Q., Yang, Y.-G., Bi, X.-Y., Liu, T.-Z., Zhao, Z.-Q., 2012. Natural and anthropogenic lead in soils and vegetables around Guiyang city, southwest China: A Pb isotopic approach. Sci. Total Environ. 431, 339–347. https://doi.org/10.1016/j.scitotenv.2012.05.040

Li, H., Qian, X., Wang, Q., 2013. Heavy Metals in Atmospheric Particulate Matter: A Comprehensive Understanding Is Needed for Monitoring and Risk Mitigation. Environ. Sci. Technol. 47, 13210–13211. https://doi.org/10.1021/es404751a

Liati, A., Pandurangi, S.S., Boulouchos, K., Schreiber, D., Arroyo Rojas Dasilva, Y., 2015. Metal nanoparticles in diesel exhaust derived by in-cylinder melting of detached engine fragments. Atmos. Environ. 101, 34–40. https://doi.org/10.1016/j.atmosenv.2014.11.014

Liati, A., Schreiber, D., Dimopoulos Eggenschwiler, P., Arroyo Rojas Dasilva, Y., 2013. Metal Particle Emissions in the Exhaust Stream of Diesel Engines: An Electron Microscope Study. Environ. Sci. Technol. 47, 14495–14501. https://doi.org/10.1021/es403121y

Lim, W.Y., Aris, A.Z., Ismail, T.H.T., Zakaria, M.P., 2013. Elemental hydrochemistry assessment on its variation and quality status in Langat River, Western Peninsular Malaysia. Environ. Earth Sci. 70, 993–1004. https://doi.org/10.1007/s12665-012-2189-7

Lin, Y.-C., Tsai, C.-J., Wu, Y.-C., Zhang, R., Chi, K.-H., Huang, Y.-T., Lin, S.-H., Hsu, S.-C., 2015. Characteristics of trace metals in traffic-derived particles in Hsuehshan Tunnel, Taiwan: size distribution, potential source, and fingerprinting metal ratio. Atmospheric Chem. Phys. 15, 4117–4130. https://doi.org/10.5194/acp-15-4117-2015

Liu, G., Xiao, M., Zhang, X., Gal, C., Chen, X., Liu, L., Pan, S., Wu, J., Tang, L., Clements-Croome, D., 2017. A review of air filtration technologies for sustainable and healthy building ventilation. Sustain. Cities Soc. 32, 375–396. https://doi.org/10.1016/j.scs.2017.04.011

Liu Q., 2016. Anti-haze plant rack. CN105993647A.

Liu, Z., Tran, K.-Q., 2021. A review on disposal and utilization of phytoremediation plants containing heavy metals. Ecotoxicol. Environ. Saf. 226, 112821. https://doi.org/10.1016/j.ecoenv.2021.112821

Longman, J., Struve, T., Pahnke, K., 2022. Spatial and Temporal Trends in Mineral Dust Provenance in the South Pacific—Evidence From Mixing Models. Paleoceanogr. Paleoclimatology 37, e2021PA004356. https://doi.org/10.1029/2021PA004356

Longman, J., Veres, D., Ersek, V., Phillips, D.L., Chauvel, C., Tamas, C.G., 2018. Quantitative assessment of Pb sources in isotopic mixtures using a Bayesian mixing model. Sci. Rep. 8, 6154. https://doi.org/10.1038/s41598-018-24474-0

Looi, L.J., Aris, A.Z., Wan Johari, W.L., Md. Yusoff, F., Hashim, Z., 2013. Baseline metals pollution profile of tropical estuaries and coastal waters of the Straits of Malacca. Mar. Pollut. Bull. 74, 471–476. https://doi.org/10.1016/j.marpolbul.2013.06.008

Lopez, B., Wang, X., Chen, L.-W.A., Ma, T., Mendez-Jimenez, D., Cobb, L.C., Frederickson, C., Fang, T., Hwang, B., Shiraiwa, M., Park, M., Park, K., Yao, Q., Yoon, S., Jung, H., 2023. Metal contents and size distributions of brake and tire wear particles dispersed in the near-road environment. Sci. Total Environ. 883, 163561. https://doi.org/10.1016/j.scitotenv.2023.163561

Lum, K.R., Betteridge, J.S., Macdonald, R.R., 1982. The potential availability of P, Al, Cd, Co, Cr, Cu, Fe, Mn, Ni, Pb and Zn in urban particulate matter. Environ. Technol. Lett. 3, 57–62. https://doi.org/10.1080/09593338209384098

Ma, C., Liu, F., Jin, K., Hu, B., Wei, M., Zhao, J., Zhang, H., Zhang, K., 2019a. Effects of Atmospheric Fallout on Lead Contamination of Wheat Tissues Based on Stable Isotope Ratios. Bull. Environ. Contam. Toxicol. 103, 676–682. https://doi.org/10.1007/s00128-019-02702-1

Ma, C., Liu, F., Xie, P., Zhang, K., Yang, J., Zhao, J., Zhang, H., 2021. Mechanism of Pb absorption in wheat grains. J. Hazard. Mater. 415, 125618. https://doi.org/10.1016/j.jhazmat.2021.125618

Ma, C., Liu, F.-Y., Hu, B., Wei, M.-B., Zhao, J.-H., Zhang, K., Zhang, H.-Z., 2019b. Direct evidence of lead contamination in wheat tissues from atmospheric deposition based on atmospheric deposition exposure contrast tests. Ecotoxicol. Environ. Saf. 185, 109688. https://doi.org/10.1016/j.ecoenv.2019.109688

Ma, L.Q., Komar, K.M., Tu, C., Zhang, W., Cai, Y., Kennelley, E.D., 2001. A fern that hyperaccumulates arsenic. Nature 409, 579–579. https://doi.org/10.1038/35054664

MacKinnon, G., MacKenzie, A.B., Cook, G.T., Pulford, I.D., Duncan, H.J., Scott, E.M., 2011. Spatial and temporal variations in Pb concentrations and isotopic composition in road dust, farmland soil and vegetation in proximity to roads since cessation of use of leaded petrol in the UK. Sci. Total Environ. 409, 5010–5019. https://doi.org/10.1016/j.scitotenv.2011.08.010

Majee, C.K., Ali, S.Y., Padhy, P.K., 2023. Effects of atmospheric dust particles on common medicinal plants in an industrial area of West Bengal, India. Environ. Monit. Assess. 195, 978. https://doi.org/10.1007/s10661-023-11573-3

Majumdar, D., Rao, P., Chelani, A., Mandal, P., Bhanarkar, A., NeelKamal, Khapade, B., 2019. PM 10 and PM 2.5 Source Apportionment Study and Development of Emission Inventory of Twin Cities Kolkata and Howrah of West Bengal. https://doi.org/10.13140/RG.2.2.33040.53765

Mannan, M., Al-Ghamdi, S.G., 2021. Active Botanical Biofiltration in Built Environment to Maintain Indoor Air Quality. Front. Built Environ. 7.

Marklund, S., Andersson, R., Tysklind, M., Rappe, C., Egebäck, K.-E., Björkman, E., Grigoriadis, V., 1990. Emissions of PCDDs and PCDFs in gasoline and diesel fueled cars. Chemosphere 20, 553–561. https://doi.org/10.1016/0045-6535(90)90111-6

Maxwell, C.M., Nelson, D.W., 1978. A LEAD EMISSION FACTOR FOR REENTRAINED DUST FROM A PAVED ROADWAY.

Mazzei, F., D'Alessandro, A., Lucarelli, F., Nava, S., Prati, P., Valli, G., Vecchi, R., 2008. Characterization of particulate matter sources in an urban environment. Sci. Total Environ. 401, 81–89. https://doi.org/10.1016/j.scitotenv.2008.03.008

McConnell, J.R., Chellman, N.J., Plach, A., Wensman, S.M., Plunkett, G., Stohl, A., Smith, N.-K., Møllesøe Vinther, B., Dahl-Jensen, D., Steffensen, J.P., Fritzsche, D., Camara-Brugger, S.O., McDonald, B.T., Wilson, A.I., 2025. Pan-European atmospheric lead pollution, enhanced blood lead levels, and cognitive decline from Roman-era mining and smelting. Proc. Natl. Acad. Sci. 122, e2419630121. https://doi.org/10.1073/pnas.2419630121

McNeill, J., Snider, G., Weagle, C.L., Walsh, B., Bissonnette, P., Stone, E., Abboud, I., Akoshile, C., Anh, N.X., Balasubramanian, R., Brook, J.R., Coburn, C., Cohen, A., Dong, J., Gagnon, G., Garland, R.M., He, K., Holben, B.N., Kahn, R., Kim, J.S., Lagrosas, N., Lestari, P., Liu, Y., Jeba, F., Joy, K.S., Martins, J.V., Misra, A., Norford, L.K., Quel, E.J., Salam, A., Schichtel, B., Tripathi, S.N., Wang, C., Zhang, Q., Brauer, M., Gibson, M.D., Rudich, Y., Martin, R.V., 2020. Large global variations in measured airborne metal concentrations driven by anthropogenic sources. Sci. Rep. 10, 21817. https://doi.org/10.1038/s41598-020-78789-y

Mehra, M., Zirzow, F., Ram, K., Norra, S., 2020. Geochemistry of PM2.5 aerosols at an urban site, Varanasi, in the Eastern Indo-Gangetic Plain during pre-monsoon season. Atmospheric Res. 234, 104734. https://doi.org/10.1016/j.atmosres.2019.104734

Meravi, N., Singh, P.K., Prajapati, S.K., 2021. Seasonal variation of dust deposition on plant leaves and its impact on various photochemical yields of plants - ScienceDirect [WWW Document]. URL https://www.sciencedirect.com/science/article/pii/S2667010021001451 (accessed 3.2.22).

Meteorological Service Singapore, 2020. Climate of Singapore | [WWW Document]. URL http://www.weather.gov.sg/climate-climate-of-singapore/ (accessed 3.20.22).

Miler, M., 2021. Airborne particles in city bus: concentrations, sources and simulated pulmonary solubility. Environ. Geochem. Health 43, 2757–2780. https://doi.org/10.1007/s10653-020-00770-5

Millot, R., Allègre, C.-J., Gaillardet, J., Roy, S., 2004. Lead isotopic systematics of major river sediments: a new estimate of the Pb isotopic composition of the Upper Continental Crust. Chem. Geol. 203, 75–90. https://doi.org/10.1016/j.chemgeo.2003.09.002

Ministry of Ports, Shipping & Waterways, 2023. Indian Shipping Statistics 2023 | Ministry of Ports,Shipping and Waterways [WWW Document]. URL https://shipmin.gov.in/content/indian-shipping-statistics-2023 (accessed 12.1.24).

Mishra, M., Kulshrestha, U., 2017. Chemical characteristics and deposition fluxes of dust-carbon mixed coarse aerosols at three sites of Delhi, NCR. J. Atmospheric Chem. 74, 399–421. https://doi.org/10.1007/s10874-016-9349-1
Mishra, V.K., Padmanabhamutry, B., 2003. Performance evaluation of CALINE3, CAL3QHC and PART5 in predicting lead concentration in the atmosphere over Delhi. Atmos. Environ. 37, 3077–3089. https://doi.org/10.1016/S1352-2310(03)00272-3
Mitra, A., Sen, I.S., Pandey, S.K., Velu, V., Reisberg, L., Bizimis, M., Cloquet, C., Nizam, S., 2021. Lead Isotope Evidence for Enhanced Anthropogenic Particle Transport to the Himalayas during Summer Months. Environ. Sci. Technol. 55, 13697–13708. https://doi.org/10.1021/acs.est.1c03830
Moldanová, J., Fridell, E., Popovicheva, O., Demirdjian, B., Tishkova, V., Faccinetto, A., Focsa, C., 2009. Characterisation of particulate matter and gaseous emissions from a large ship diesel engine. Atmos. Environ. 43, 2632–2641. https://doi.org/10.1016/j.atmosenv.2009.02.008
Morton-Bermea, O., Rodríguez-Salazar, M.T., Hernández-Alvarez, E., García-Arreola, M.E., Lozano-Santacruz, R., 2011. Lead isotopes as tracers of anthropogenic pollution in urban topsoils of Mexico City. Geochemistry 71, 189–195. https://doi.org/10.1016/j.chemer.2011.03.003
Mueller, L., Jakobi, G., Czech, H., Stengel, B., Orasche, J., Arteaga-Salas, J.M., Karg, E., Elsasser, M., Sippula, O., Streibel, T., Slowik, J.G., Prevot, A.S.H., Jokiniemi, J., Rabe, R., Harndorf, H., Michalke, B., Schnelle-Kreis, J., Zimmermann, R., 2015. Characteristics and temporal evolution of particulate emissions from a ship diesel engine. Appl. Energy 155, 204–217. https://doi.org/10.1016/j.apenergy.2015.05.115
Mukherjee, S., Srivastava, S.K., 2005. Trace Elements in High-Sulfur Assam Coals from the Makum Coalfield in the Northeastern Region of India. Energy Fuels 19, 882–891. https://doi.org/10.1021/ef049775+
Muleski, G.E., Cowherd Jr., C., Kinsey, J.S., 2005. Particulate Emissions from Construction Activities. J. Air Waste Manag. Assoc. 55, 772–783. https://doi.org/10.1080/10473289.2005.10464669
Negi, B.S., Sadasivan, S., Mishra, U.C., 1986. Aerosol composition and sources in Urban areas in India. Atmospheric Environ. 1967 21, 1259–1266. https://doi.org/10.1016/0004-6981(67)90072-8
Nguyen, T.H., Pham, Q.V., Nguyen, T.P.M., Vu, V.T., Do, T.H., Hoang, M.T., Thu Thuy Thi, N., Minh, T.B., 2023. Distribution characteristics and ecological risks of heavy metals in bottom ash, fly ash, and particulate matter released from municipal solid waste incinerators in northern Vietnam. Environ. Geochem. Health 45, 2579–2590. https://doi.org/10.1007/s10653-022-01335-4
Nieder, R., Benbi, D.K., Reichl, F.X., 2018. Soil-Borne Particles and Their Impact on Environment and Human Health, in: Nieder, R., Benbi, D.K., Reichl, F.X. (Eds.), Soil Components and Human Health. Springer Netherlands, Dordrecht, pp. 99–177. https://doi.org/10.1007/978-94-024-1222-2_3
NITI Aayog, 2024. India's Power Sector | Capacity & Generation Mix [WWW Document]. URL https://iced.niti.gov.in/energy/electricity/generation (accessed 9.21.24).
NLCIL, 2024. NLC India Limited [WWW Document]. URL https://www.nlcindia.in/new_website/index.htm (accessed 2.23.24).
NOAA, 2021. GUI Operation © [WWW Document]. URL https://www.ready.noaa.gov/documents/Tutorial_2021/html/test_gui.html (accessed 9.6.24).
Nriagu, J.O., 1990. The rise and fall of leaded gasoline. Sci. Total Environ. 92, 13–28. https://doi.org/10.1016/0048-9697(90)90318-O
Nzihou, A., Stanmore, B., 2013. The fate of heavy metals during combustion and gasification of contaminated biomass—A brief review. J. Hazard. Mater. 256–257, 56–66. https://doi.org/10.1016/j.jhazmat.2013.02.050
OEC, 2024. Explosive Ammunition in India [WWW Document]. Obs. Econ. Complex. URL https://oec.world/en/profile/bilateral-product/explosive-ammunition/reporter/ind (accessed 12.7.24).

OECD, 2020. The implications of electric vehicle uptake for non-exhaust emissions. OECD, Paris. https://doi.org/10.1787/e1bc711b-en
OECD and UNEP, 1999. Phasing lead out of gasoline: An examination of policy approaches in different countries. UNEP/Earthprint.
Olaifa, F.E., Omekam, A.J., 2014. Studies on Phytoremediation of Copper Using Pteridium Aquilinum (Bracken Fern) In the Presence of Biostimulants and Bioassay Using Clarias Gariepinus Juveniles. Int. J. Phytoremediation 16, 219–234. https://doi.org/10.1080/15226514.2013.773272
Olajire, A.A., Ayodele, E.T., Oyedirdan, G.O., Oluyemi, E.A., 2003. Levels and Speciation of Heavy Metals in Soils of Industrial Southern Nigeria. Environ. Monit. Assess. 85, 135–155. https://doi.org/10.1023/A:1023613418727
O'Neal, M.E., Landis, D.A., Isaacs, R., 2002. An inexpensive, accurate method for measuring leaf area and defoliation through digital image analysis. J. Econ. Entomol. 95, 1190–1194. https://doi.org/10.1603/0022-0493-95.6.1190
OPEC, 2023. World Oil Outlook - Chapter 3 - Oil demand [WWW Document]. URL https://woo.opec.org/chapter.php?chapterNr=1768&tableID=3000 (accessed 6.14.24).
Orru, H., Pindus, M., Harro, H.-R., Maasikmets, M., Herodes, K., 2018. Metallic Fumes at Indoor Military Shooting Ranges: Lead, Copper, Nickel, and Zinc in Different Fractions of Airborne Particulate Matter. Propellants Explos. Pyrotech. 43, 228–233. https://doi.org/10.1002/prep.201700225
O'Shea, M.J., Vigliaturo, R., Choi, J.K., McKeon, T.P., Krekeler, M.P.S., Gieré, R., 2021. Alteration of yellow traffic paint in simulated environmental and biological fluids. Sci. Total Environ. 750, 141202. https://doi.org/10.1016/j.scitotenv.2020.141202
Ottelé, M., van Bohemen, H.D., Fraaij, A.L.A., 2010. Quantifying the deposition of particulate matter on climber vegetation on living walls. Ecol. Eng., Special Issue: BioGeoCivil Engineering 36, 154–162. https://doi.org/10.1016/j.ecoleng.2009.02.007
Our World in Data, 2024. Exposure to particulate matter air pollution [WWW Document]. Our World Data. URL https://ourworldindata.org/grapher/pm25-air-pollution?time=2019 (accessed 1.5.25).
Our World in Data, 2021. Coal consumption [WWW Document]. Our World Data. URL https://ourworldindata.org/grapher/coal-consumption-by-country-terawatt-hours-twh (accessed 6.14.23).
Overland, I., Sagbakken, H.F., Chan, H.-Y., Merdekawati, M., Suryadi, B., Utama, N.A., Vakulchuk, R., 2021. The ASEAN climate and energy paradox. Energy Clim. Change 2, 100019. https://doi.org/10.1016/j.egycc.2020.100019
Pacyna, J.M., 1995. The origin of Arctic air pollutants: lessons learned and future research. Sci. Total Environ., Ecological Effects of Arctic Airborne Contaminants 160–161, 39–53. https://doi.org/10.1016/0048-9697(95)04343-Y
Pacyna, J.M., Pacyna, E.G., 2001. An assessment of global and regional emissions of trace metals to the atmosphere from anthropogenic sources worldwide. Environ. Rev. 9, 269–298. https://doi.org/10.1139/a01-012
Panda, U., Boopathy, R., Gadhavi, H.S., Renuka, K., Gunthe, S.S., Das, T., 2021. Metals in coarse ambient aerosol as markers for source apportionment and their health risk assessment over an eastern coastal urban atmosphere in India. Environ. Monit. Assess. 193, 311. https://doi.org/10.1007/s10661-021-09057-3
Pandey, P., Patel, D.K., Khan, A.H., Barman, S.C., Murthy, R.C., Kisku, G.C., 2013. Temporal distribution of fine particulates (PM2.5, PM10), potentially toxic metals, PAHs and Metal-bound carcinogenic risk in the population of Lucknow City, India. J. Environ. Sci. Health Part A 48, 730–745. https://doi.org/10.1080/10934529.2013.744613
Pant, P., Harrison, R.M., 2013. Estimation of the contribution of road traffic emissions to particulate matter concentrations from field measurements: A review. Atmos. Environ. 77, 78–97. https://doi.org/10.1016/j.atmosenv.2013.04.028

Pant, P., Shukla, A., Kohl, S.D., Chow, J.C., Watson, J.G., Harrison, R.M., 2015. Characterization of ambient PM2.5 at a pollution hotspot in New Delhi, India and inference of sources. Atmos. Environ. 109, 178–189. https://doi.org/10.1016/j.atmosenv.2015.02.074
Panwar, P., Prabhu, V., Soni, A., Punetha, D., Shridhar, V., 2020. Sources and health risks of atmospheric particulate matter at Bhagwanpur, an industrial site along the Himalayan foothills. SN Appl. Sci. 2, 632. https://doi.org/10.1007/s42452-020-2420-1
Parikh, J., Balakrishnan, K., Laxmi, V., Biswas, H., 2001. Exposure from cooking with biofuels: pollution monitoring and analysis for rural Tamil Nadu, India. Energy 26, 949–962. https://doi.org/10.1016/S0360-5442(01)00043-3
Parnell, A.C., Inger, R., Bearhop, S., Jackson, A.L., 2010. Source Partitioning Using Stable Isotopes: Coping with Too Much Variation. PLOS ONE 5, e9672. https://doi.org/10.1371/journal.pone.0009672
Parnell, A.C., Phillips, D.L., Bearhop, S., Semmens, B.X., Ward, E.J., Moore, J.W., Jackson, A.L., Grey, J., Kelly, D.J., Inger, R., 2013. Bayesian stable isotope mixing models. Environmetrics 24, 387–399. https://doi.org/10.1002/env.2221
Patterson, C., 1987. Global pollution measured by lead in mid-ocean sediments. Nature 326, 244–245. https://doi.org/10.1038/326244a0
Patterson, C.C., 1965. Contaminated and Natural Lead Environments of Man. Arch. Environ. Health Int. J. 11, 344–360. https://doi.org/10.1080/00039896.1965.10664229
Paull, N., Krix, D., Irga, P., Torpy, F., 2019. Airborne particulate matter accumulation on common green wall plants. Int. J. Phytoremediation 22, 1–13. https://doi.org/10.1080/15226514.2019.1696744
Peltier, R.E., Hsu, S.-I., Lall, R., Lippmann, M., 2009. Residual oil combustion: a major source of airborne nickel in New York City. J. Expo. Sci. Environ. Epidemiol. 19, 603–612. https://doi.org/10.1038/jes.2008.60
Perrino, C., Tiwari, S., Catrambone, M., Torre, S.D., Rantica, E., Canepari, S., 2011. Chemical characterization of atmospheric PM in Delhi, India, during different periods of the year including Diwali festival. Atmospheric Pollut. Res. 2, 418–427. https://doi.org/10.5094/APR.2011.048
Peter, A.E., Shiva Nagendra, S.M., Nambi, I.M., 2019. Environmental burden by an open dumpsite in urban India. Waste Manag. 85, 151–163. https://doi.org/10.1016/j.wasman.2018.12.022
Pettit, T., Irga, P.J., Abdo, P., Torpy, F.R., 2017. Do the plants in functional green walls contribute to their ability to filter particulate matter? Build. Environ. 125, 299–307. https://doi.org/10.1016/j.buildenv.2017.09.004
Pettit, T., Torpy, F.R., Surawski, N.C., Fleck, R., Irga, P.J., 2021. Effective reduction of roadside air pollution with botanical biofiltration. J. Hazard. Mater. 414, 125566. https://doi.org/10.1016/j.jhazmat.2021.125566
Phillips, D.L., Gregg, J.W., 2003. Source partitioning using stable isotopes: coping with too many sources. Oecologia 136, 261–269. https://doi.org/10.1007/s00442-003-1218-3
Phillips, D.L., Gregg, J.W., 2001. Uncertainty in source partitioning using stable isotopes. Oecologia 127, 171–179. https://doi.org/10.1007/s004420000578
Phillips, D.L., Inger, R., Bearhop, S., Jackson, A.L., Moore, J.W., Parnell, A.C., Semmens, B.X., Ward, E.J., 2014. Best practices for use of stable isotope mixing models in food-web studies. Can. J. Zool. 92, 823–835. https://doi.org/10.1139/cjz-2014-0127
Phillips, D.L., Koch, P.L., 2002. Incorporating concentration dependence in stable isotope mixing models. Oecologia 130, 114–125. https://doi.org/10.1007/s004420100786
Phillips, D.L., Newsome, S.D., Gregg, J.W., 2005. Combining sources in stable isotope mixing models: alternative methods. Oecologia 144, 520–527. https://doi.org/10.1007/s00442-004-1816-8
PIB, 2023. Joint Military Exercise 'Ex KAVACH' concludes at Andaman and Nicobar Command [WWW Document]. URL https://pib.gov.in/pib.gov.in/Pressreleaseshare.aspx?PRID=1914940 (accessed 12.7.24).

PIB, 2015. Environment Ministry Notifies Stricter Standards for Coal Based Thermal Power Plants to Minimise Pollution [WWW Document]. URL https://pib.gov.in/newsite/printrelease.aspx?relid=133726 (accessed 1.8.25).
PIB, 2010. English Releases [WWW Document]. URL https://pib.gov.in/newsite/erelcontent.aspx?relid=62358 (accessed 11.15.24).
Pipalatkar, P., Khaparde, V.V., Gajghate, D.G., Bawase, M.A., 2014. Source Apportionment of PM2.5 Using a CMB Model for a Centrally Located Indian City. Aerosol Air Qual. Res. 14, 1089–1099. https://doi.org/10.4209/aaqr.2013.04.0130
Police, S., Sahu, S.K., Pandit, G.G., 2016. Chemical characterization of atmospheric particulate matter and their source apportionment at an emerging industrial coastal city, Visakhapatnam, India. Atmospheric Pollut. Res. 7, 725–733. https://doi.org/10.1016/j.apr.2016.03.007
Police, S., Sahu, S.K., Tiwari, M., Pandit, G.G., 2018. Chemical composition and source apportionment of PM2.5 and PM2.5–10 in Trombay (Mumbai, India), a coastal industrial area. Particuology 37, 143–153. https://doi.org/10.1016/j.partic.2017.09.006
Popovicheva, O., Kireeva, E., Shonija, N., Zubareva, N., Persiantseva, N., Tishkova, V., Demirdjian, B., Moldanová, J., Mogilnikov, V., 2009. Ship particulate pollutants: Characterization in terms of environmental implication. J. Environ. Monit. 11, 2077–2086. https://doi.org/10.1039/B908180A
Poppendieck, D.G., Rim, D., Persily, A.K., 2014. Ultrafine Particle Removal and Ozone Generation by In-Duct Electrostatic Precipitators. Environ. Sci. Technol. 48, 2067–2074. https://doi.org/10.1021/es404884p
Prajapati, S.K., Tripathi, B.D., 2008. Seasonal Variation of Leaf Dust Accumulation and Pigment Content in Plant Species Exposed to Urban Particulates Pollution. J. Environ. Qual. 37, 865–870. https://doi.org/10.2134/jeq2006.0511
Prakash, V.A.A., 2003. Evolution of the Joint Andaman and Nicobar Command (ANC) and Defence of Our Island Territories [WWW Document]. United Serv. Inst. India. URL https://www.usiofindia.org/publication-journal/evolution-of-the-joint-andaman-and-nicobar-command-anc-and-defence-of-our-island-territories-part-ii.html (accessed 12.7.24).
Prasad, P., Basha, G., Ratnam, M.V., 2022. Is the atmospheric boundary layer altitude or the strong thermal inversions that control the vertical extent of aerosols? Sci. Total Environ. 802, 149758. https://doi.org/10.1016/j.scitotenv.2021.149758
Pratas, J., Favas, P.J.C., D'Souza, R., Varun, M., Paul, M.S., 2013. Phytoremedial assessment of flora tolerant to heavy metals in the contaminated soils of an abandoned Pb mine in Central Portugal. Chemosphere 90, 2216–2225. https://doi.org/10.1016/j.chemosphere.2012.09.079
Press Information Bureau, 2015. Environment Ministry Notifies Stricter Standards for Coal Based Thermal Power Plants to Minimise Pollution [WWW Document]. URL https://pib.gov.in/newsite/printrelease.aspx?relid=133726 (accessed 2.19.24).
Prusty, B.A.K., Mishra, P.C., Azeez, P.A., 2005. Dust accumulation and leaf pigment content in vegetation near the national highway at Sambalpur, Orissa, India. Ecotoxicol. Environ. Saf. 60, 228–235. https://doi.org/10.1016/j.ecoenv.2003.12.013
PTI, 2023. Anti-ship version of BRAHMOS missile successfully test-fired [WWW Document]. URL https://www.brahmos.com/pressRelease.php?id=102 (accessed 12.7.24).
Pulles, T., Denier van der Gon, H., Appelman, W., Verheul, M., 2012. Emission factors for heavy metals from diesel and petrol used in European vehicles. Atmos. Environ. 61, 641–651. https://doi.org/10.1016/j.atmosenv.2012.07.022
Qi, H., Hu, R., Zhang, Q., 2007. Concentration and distribution of trace elements in lignite from the Shengli Coalfield, Inner Mongolia, China: Implications on origin of the associated Wulantuga Germanium Deposit. Int. J. Coal Geol. 71, 129–152. https://doi.org/10.1016/j.coal.2006.08.005
Quesada, A.B.B., 2015. The Life and Times of Pteris vittata: Investigating Frond Life Stage and Harvest Techniques to Optimize Phytoremediation with an Arsenic Accumulating Fern - Google Search [WWW Document]. URL

https://www.google.com/search?q=The+Life+and+Times+of+Pteris+vittata%3A+Investigating+Frond+Life+Stage+and+Harvest+Techniques+to+Optimize+Phytoremediation+with+an+Arsenic+Accumulating+Fern&oq=The+Life+and+Times+of+Pteris+vittata%3A+Investigating+Frond+Life+Stage+and+Harvest+Techniques+to+Optimize+Phytoremediation+with+an+Arsenic+Accumulating+Fern&gs_lcrp=EgZjaHJvbWUyBggAEEUYOdIBBzk1N2owajeoAgCwAgA&sourceid=chrome&ie=UTF-8#ip=1 (accessed 6.29.23).

Rabha, S., Islam, N., Saikia, B.K., Singh, G.K., Qadri, A.M., Srivastava, V., Gupta, T., 2023. Year-long evaluation of aerosol chemistry and meteorological implications of PM2.5 in an urban area of the Brahmaputra Valley, India. Environ. Sci. Atmospheres 3, 196–206. https://doi.org/10.1039/D2EA00120A

Rabha, S., Subramanyam, K.S.V., Sawant, S.S., Saikia, B.K., 2022. Rare-Earth Elements and Heavy Metals in Atmospheric Particulate Matter in an Urban Area. ACS Earth Space Chem. 6, 1725–1732. https://doi.org/10.1021/acsearthspacechem.2c00009

Radojevic, M., Harrison, R.M., 1987. Concentrations and pathways of organolead compounds in the environment: A review. Sci. Total Environ., Highway Pollution 59, 157–180. https://doi.org/10.1016/0048-9697(87)90439-6

Ram, L.C., Masto, R.E., Srivastava, N.K., George, J., Selvi, V.A., Das, T.B., Pal, S.K., Maity, S., Mohanty, D., 2014. Potentially toxic elements in lignite and its combustion residues from a power plant. Environ. Monit. Assess. 187, 4148. https://doi.org/10.1007/s10661-014-4148-0

Ranganathan, K., Dhanagopalan, V., Tharumaraj, M., Annadurai, K., 2020. Fuel consumption and expenditure among rural population of Cuddalore district, Tamil Nadu: a cross sectional study. Int. J. Community Med. Public Health 7, 3630–3635. https://doi.org/10.18203/2394-6040.ijcmph20203934

Raparthi, N., Phuleria, H.C., 2021. Real-world vehicular emissions in the Indian megacity: Carbonaceous, metal and morphological characterization, and the emission factors. Urban Clim. 39, 100955. https://doi.org/10.1016/j.uclim.2021.100955

Rasmussen, P.E., 1998. Long-range atmospheric transport of trace metals: the need for geoscience perspectives. Environ. Geol. 33, 96–108. https://doi.org/10.1007/s002540050229

Rastogi, N., Sarin, M.M., 2009. Quantitative chemical composition and characteristics of aerosols over western India: One-year record of temporal variability. Atmos. Environ. 43, 3481–3488. https://doi.org/10.1016/j.atmosenv.2009.04.030

Rawat, M., Ramanathan, AL., Subramanian, V., 2009. Quantification and distribution of heavy metals from small-scale industrial areas of Kanpur city, India. J. Hazard. Mater. 172, 1145–1149. https://doi.org/10.1016/j.jhazmat.2009.07.115

Ray, I., Das, R., 2023a. Dataset for: A Lingering Legacy of Leaded Gasoline in Southeast Asia. https://doi.org/10.5281/zenodo.10101283

Ray, I., Das, R., 2023b. A lingering legacy of leaded gasoline in Southeast Asia. Commun. Earth Environ. 4, 1–11. https://doi.org/10.1038/s43247-023-01135-3

Ray, I., Das, R., Chua, S.L., Wang, X., 2022. Seasonal variation of atmospheric Pb sources in Singapore - Elemental and lead isotopic compositions of PM10 as source tracer. Chemosphere 307, 136029. https://doi.org/10.1016/j.chemosphere.2022.136029

Ray, I., Misra, S., Chen, M., Wang, X., Das, R., 2024. Entrapment of atmospheric particle bound heavy metals by ferns as evidenced by lead (Pb) isotope and MixSIAR: Implications for improving air quality. J. Hazard. Mater. 469, 134014. https://doi.org/10.1016/j.jhazmat.2024.134014

Redondo-Bermúdez, M. del C., Gulenc, I.T., Cameron, R.W., Inkson, B.J., 2021. 'Green barriers' for air pollutant capture: Leaf micromorphology as a mechanism to explain plants capacity to capture particulate matter. Environ. Pollut. 288, 117809. https://doi.org/10.1016/j.envpol.2021.117809

Ren, D., Xu, D., Zhao, F., 2004. A preliminary study on the enrichment mechanism and occurrence of hazardous trace elements in the Tertiary lignite from the Shenbei coalfield, China. Int. J. Coal Geol. 57, 187–196. https://doi.org/10.1016/j.coal.2003.10.001

Renzhengang, Li Q., 2015. Method for plant-ecologically purifying indoor air. CN104474882A.
Resongles, E., Dietze, V., Green, D.C., Harrison, R.M., Ochoa-Gonzalez, R., Tremper, A.H., Weiss, D.J., 2021. Strong evidence for the continued contribution of lead deposited during the 20th century to the atmospheric environment in London of today. Proc. Natl. Acad. Sci. 118, e2102791118. https://doi.org/10.1073/pnas.2102791118
Reuer, M.K., Boyle, E.A., Grant, B.C., 2003. Lead isotope analysis of marine carbonates and seawater by multiple collector ICP-MS. Chem. Geol. 200, 137–153. https://doi.org/10.1016/S0009-2541(03)00186-4
Rocha, E.D., Sarkis, J.E.S., Carvalho, M. de F.H., Santos, G.V. dos, Canesso, C., 2014. Occupational exposure to airborne lead in Brazilian police officers. Int. J. Hyg. Environ. Health 217, 702–704. https://doi.org/10.1016/j.ijheh.2013.12.004
Rocha, L.D., Costa, G.M.D., Gehlen, G., Droste, A., Schmitt, J.L., 2014. Morphometric differences of *Microgramma squamulosa* (Kaulf.) de la Sota (Polypodiaceae) leaves in environments with distinct atmospheric air quality. An. Acad. Bras. Ciênc. 86, 1137–1146. https://doi.org/10.1590/0001-3765201420130094
Roser, M., 2021. Data review: how many people die from air pollution? Our World Data.
Rout, T.K., Masto, R.E., Padhy, P.K., Ram, L.C., George, J., Joshi, G., 2015. Heavy metals in dusts from commercial and residential areas of Jharia coal mining town. Environ. Earth Sci. 73, 347–359. https://doi.org/10.1007/s12665-014-3429-9
Roy, A., Bhattacharya, T., Kumari, M., 2020. Air pollution tolerance, metal accumulation and dust capturing capacity of common tropical trees in commercial and industrial sites. Sci. Total Environ. 722, 137622. https://doi.org/10.1016/j.scitotenv.2020.137622
Roy, D., Kim, J., Lee, M., Park, J., 2023. Adverse impacts of Asian dust events on human health and the environment—A probabilistic risk assessment study on particulate matter-bound metals and bacteria in Seoul, South Korea. Sci. Total Environ. 875, 162637. https://doi.org/10.1016/j.scitotenv.2023.162637
Rudnick, R.L., Gao, S., 2003. 3.01 - Composition of the Continental Crust, in: Holland, H.D., Turekian, K.K. (Eds.), Treatise on Geochemistry. Pergamon, Oxford, pp. 1–64. https://doi.org/10.1016/B0-08-043751-6/03016-4
Rudnick, R.L., Goldstein, S.L., 1990. The Pb isotopic compositions of lower crustal xenoliths and the evolution of lower crustal Pb. Earth Planet. Sci. Lett. 98, 192–207. https://doi.org/10.1016/0012-821X(90)90059-7
Ruehling, A., 1995. Atmospheric heavy metal deposition in Europe estimated by moss analysis.
Ruehling, A., Tyler, G., 1969. Ecology of heavy metals - a regional and historical study. Bot Swed. 122.
Sah, D., 2023. Concentration, source apportionment and human health risk assessment of elements in PM2.5 at Agra, India. Urban Clim. 49, 101477. https://doi.org/10.1016/j.uclim.2023.101477
Sahu, S.K., Mangaraj, P., Beig, G., Samal, A., Chinmay Pradhan, Dash, S., Tyagi, B., 2021. Quantifying the high resolution seasonal emission of air pollutants from crop residue burning in India. Environ. Pollut. 286, 117165. https://doi.org/10.1016/j.envpol.2021.117165
Saikia, B.K., Goswamee, R.L., Baruah, B.P., Baruah, R.K., 2009. Occurrence of some hazardous metals in Indian coals. Coke Chem. 52, 54–59. https://doi.org/10.3103/S1068364X09020033
Salameh, D., Detournay, A., Pey, J., Pérez, N., Liguori, F., Saraga, D., Bove, M.C., Brotto, P., Cassola, F., Massabò, D., Latella, A., Pillon, S., Formenton, G., Patti, S., Armengaud, A., Piga, D., Jaffrezo, J.L., Bartzis, J., Tolis, E., Prati, P., Querol, X., Wortham, H., Marchand, N., 2015. PM2.5 chemical composition in five European Mediterranean cities: A 1-year study. Atmospheric Res. 155, 102–117. https://doi.org/10.1016/j.atmosres.2014.12.001
Salazar, J.R., Cartledge, B.T., Haynes, J.P., York-Marini, R., Robinson, A.L., Drozd, G.T., Goldstein, A.H., Fakra, S.C., Majestic, B.J., 2020. Water-soluble iron emitted from vehicle exhaust is linked to primary speciated organic compounds. Atmospheric Chem. Phys. 20, 1849–1860. https://doi.org/10.5194/acp-20-1849-2020

Samanta, S., Menzel Barraqueta, J.-L., Das, R., Roychoudhury, A.N., 2022. Source apportionment of the atmospheric Pb using a simulation-based inversion model: A case study from India uncovers bituminous road as the prime contributor of petroleum-derived Pb. Appl. Geochem. 136, 105164. https://doi.org/10.1016/j.apgeochem.2021.105164

Sánchez-Jiménez, N., Gismera, M.J., Sevilla, M.T., Cuevas, J., Rodríguez-Rastrero, M., Procopio, J.R., 2012. Clayey materials as geologic barrier in urban landfills: Comprehensive study of the interaction of selected quarry materials with heavy metals. Appl. Clay Sci. 56, 23–29. https://doi.org/10.1016/j.clay.2011.11.016

Sänger, P., Splittgerber, V., 2016. The CityTree: A Vertical Plant Filter for Enhanced Temperature Management. pp. 75–85. https://doi.org/10.1007/978-3-319-25814-0_6

Sangster, D.F., Outridge, P.M., Davis, W.J., 2000. Stable lead isotope characteristics of lead ore deposits of environmental significance. Environ. Rev. 8, 115–147. https://doi.org/10.1139/a00-008

Saud, T., Mandal, T.K., Gadi, R., Singh, D.P., Sharma, S.K., Saxena, M., Mukherjee, A., 2011. Emission estimates of particulate matter (PM) and trace gases (SO2, NO and NO2) from biomass fuels used in rural sector of Indo-Gangetic Plain, India. Atmos. Environ. 45, 5913–5923. https://doi.org/10.1016/j.atmosenv.2011.06.031

Schreck, E., Bonnard, R., Laplanche, C., Leveque, T., Foucault, Y., Dumat, C., 2012a. DECA: A new model for assessing the foliar uptake of atmospheric lead by vegetation, using Lactuca sativa as an example. J. Environ. Manage. 112, 233–239. https://doi.org/10.1016/j.jenvman.2012.07.006

Schreck, E., Foucault, Y., Sarret, G., Sobanska, S., Cécillon, L., Castrec-Rouelle, M., Uzu, G., Dumat, C., 2012b. Metal and metalloid foliar uptake by various plant species exposed to atmospheric industrial fallout: Mechanisms involved for lead. Sci. Total Environ. 427–428, 253–262. https://doi.org/10.1016/j.scitotenv.2012.03.051

Schroeder, W.H., Dobson, M., Kane, D.M., Johnson, N.D., 1987. Toxic Trace Elements Associated with Airborne Particulate Matter: A Review. JAPCA 37, 1267–1285. https://doi.org/10.1080/08940630.1987.10466321

See, S.W., Balasubramanian, R., Wang, W., 2006. A study of the physical, chemical, and optical properties of ambient aerosol particles in Southeast Asia during hazy and nonhazy days. J. Geophys. Res. Atmospheres 111. https://doi.org/10.1029/2005JD006180

Sen, I.S., Bizimis, M., Tripathi, S.N., Paul, D., 2016. Lead isotopic fingerprinting of aerosols to characterize the sources of atmospheric lead in an industrial city of India. Atmos. Environ. 129, 27–33. https://doi.org/10.1016/j.atmosenv.2016.01.005

Sethupathi, P.B., Chandradass, J., Saibalaji, M.A., 2021. Comparative study of disc brake pads sold in Indian market — Impact on safety and environmental aspects. Environ. Technol. Innov. 21, 101245. https://doi.org/10.1016/j.eti.2020.101245

Sgrigna, G., Sæbø, A., Gawronski, S., Popek, R., Calfapietra, C., 2015. Particulate Matter deposition on Quercus ilex leaves in an industrial city of central Italy. Environ. Pollut. 197, 187–194. https://doi.org/10.1016/j.envpol.2014.11.030

Sharma, J.V., 2018. Impact of wood-based energy on Forests in India | Wood Energy Catalogue | Food and Agriculture Organization of the United Nations [WWW Document]. URL https://www.fao.org/forestry/energy/catalogue/search/detail/en/c/1380965/ (accessed 8.22.23).

Sharma, M., Agarwal, A.K., Bharathi, K.V.L., 2005. Characterization of exhaust particulates from diesel engine. Atmos. Environ. 39, 3023–3028. https://doi.org/10.1016/j.atmosenv.2004.12.047

Shen, X., Dai, M., Yang, J., Sun, L., Tan, X., Peng, C., Ali, I., Naz, I., 2022. A critical review on the phytoremediation of heavy metals from environment: Performance and challenges. Chemosphere 291, 132979. https://doi.org/10.1016/j.chemosphere.2021.132979

Shi, X., Wen, D., Wang, S., Wang, G., Zhang, M., Li, J., Xue, C., 2021. Investigation on friction and wear performance of laser cladding Ni-based alloy coating on brake disc. Optik 242, 167227. https://doi.org/10.1016/j.ijleo.2021.167227

Shim, Y.-S., Rhee, S.-W., Lee, W.-K., 2005. Comparison of leaching characteristics of heavy metals from bottom and fly ashes in Korea and Japan. Waste Manag. 25, 473–480. https://doi.org/10.1016/j.wasman.2005.03.002

Shotyk, W., 1996. Peat bog archives of atmospheric metal deposition: geochemical evaluation of peat profiles, natural variations in metal concentrations, and metal enrichment factors. Environ. Rev. 4, 149–183. https://doi.org/10.1139/a96-010

Shridhar, V., Khillare, P.S., Agarwal, T., Ray, S., 2010. Metallic species in ambient particulate matter at rural and urban location of Delhi. J. Hazard. Mater. 175, 600–607. https://doi.org/10.1016/j.jhazmat.2009.10.047

Shu, W.S., Ye, Z.H., Zhang, Z.Q., Lan, C.Y., Wong, M.H., 2005. Natural Colonization of Plants on Five Lead/Zinc Mine Tailings in Southern China. Restor. Ecol. 13, 49–60. https://doi.org/10.1111/j.1526-100X.2005.00007.x

Shukkur, A.M., V.G, G., N.G, V., Mohan, M., 2021. Trace gases and PM2.5-bound metal abundance over a tropical urban environment, South India. J. Atmospheric Chem. 78, 193–208. https://doi.org/10.1007/s10874-021-09420-1

Singapore Energy Market Authority, 2022. EMA: Singapore Energy Statistics | Energy Transformation [WWW Document]. URL https://www.ema.gov.sg/singapore-energy-statistics/Ch02/index2 (accessed 1.1.22).

Singapore National Environment Agency, 2020. Solid Waste Management Infrastructure [WWW Document]. URL https://www.nea.gov.sg/our-services/waste-management/3r-programmes-and-resources/waste-management-infrastructure/solid-waste-management-infrastructure (accessed 3.20.22).

Singh, A., Raj, S.S., Panda, U., Kommula, S.M., Jose, C., Liu, T., Huang, S., Swain, B., Pöhlker, M.L., Reyes-Villegas, E., Ojha, N., Vaishya, A., Bigi, A., Ravikrishna, R., Zhu, Q., Shi, L., Allen, J., Martin, S.T., McFiggans, G., Andreae, M.O., Pöschl, U., Coe, H., Bianchi, F., Su, H., Kanawade, V.P., Liu, P., Gunthe, S.S., 2023. Rapid growth and high cloud-forming potential of anthropogenic sulfate aerosol in a thermal power plant plume during COVID lockdown in India. Npj Clim. Atmospheric Sci. 6, 1–12. https://doi.org/10.1038/s41612-023-00430-2

Singh, N., Kumar, A., Gupta, V.K., Sharma, B., 2018. Biochemical and Molecular Bases of Lead-Induced Toxicity in Mammalian Systems and Possible Mitigations. Chem. Res. Toxicol. 31, 1009–1021. https://doi.org/10.1021/acs.chemrestox.8b00193

Singh, P.K., Rajak, P.K., Singh, M.P., Naik, A.S., Singh, V.K., Raju, S.V., Ojha, S., 2015. Environmental geochemistry of selected elements in lignite from Barsingsar and Gurha mines of Rajasthan, Western India. J. Geol. Soc. India 86, 23–32. https://doi.org/10.1007/s12594-015-0277-5

Singh, R., Sharma, B.S., 2012. Composition, seasonal variation, and sources of PM10 from world heritage site Taj Mahal, Agra. Environ. Monit. Assess. 184, 5945–5956. https://doi.org/10.1007/s10661-011-2392-0

Singh, R.K., Agrawal, M., 2005. Atmospheric depositions around a heavily industrialized area in a seasonally dry tropical environment of India. Environ. Pollut. 138, 142–152. https://doi.org/10.1016/j.envpol.2005.02.009

Singh, S., Bhattacharya, P., Gupta, N.C., 2018. Dust particles characterization and innate resistance for Thevetia peruviana in different land-use pattern of urban area. Int. J. Environ. Sci. Technol. 15, 1061–1072. https://doi.org/10.1007/s13762-017-1461-5

Singh, V., Biswal, A., Kesarkar, A.P., Mor, S., Ravindra, K., 2020. High resolution vehicular PM10 emissions over megacity Delhi: Relative contributions of exhaust and non-exhaust sources. Sci. Total Environ. 699, 134273. https://doi.org/10.1016/j.scitotenv.2019.134273

Singh, Y., Negi, P., Chen, W.H., 2023. Biofuel Technologies for a Sustainable Future: India and Beyond. CRC Press.

Sjåstad, K.-E., Simonsen, S.L., Andersen, T.H., 2014. Lead isotope ratios for bullets, a descriptive approach for investigative purposes and a new method for sampling of bullet lead. Forensic Sci. Int. 244, 7–15. https://doi.org/10.1016/j.forsciint.2014.07.008
Skalny, A.V., Aschner, M., Bobrovnitsky, I.P., Chen, P., Tsatsakis, A., Paoliello, M.M.B., Buha Djordevic, A., Tinkov, A.A., 2021. Environmental and health hazards of military metal pollution. Environ. Res. 201, 111568. https://doi.org/10.1016/j.envres.2021.111568
Smith, J.A., Mazumder, D., Suthers, I.M., Taylor, M.D., 2013. To fit or not to fit: evaluating stable isotope mixing models using simulated mixing polygons. Methods Ecol. Evol. 4, 612–618. https://doi.org/10.1111/2041-210X.12048
Soongsombat, P., Kruatrachue, M., Chaiyarat, R., Pokethitiyook, P., Ngernsansaruay, C., 2009. Lead Tolerance and Accumulation in Pteris Vittata and Pityrogramma Calomelanos, and Their Potential for Phytoremediation of Lead-Contaminated Soil. Int. J. Phytoremediation 11, 396–412. https://doi.org/10.1080/15226510802565634
Srinivas, B., Kumar, A., Sarin, M.M., Sudheer, A.K., 2011. Impact of continental outflow on chemistry of atmospheric aerosols over tropical Bay of Bengal. Atmospheric Chem. Phys. Discuss. 11, 20667–20711. https://doi.org/10.5194/acpd-11-20667-2011
State of Global Air, 2022. Air Pollution and Health in Cities [WWW Document]. URL https://www.stateofglobalair.org/resources/health-in-cities (accessed 4.18.23).
Statista, 2020a. Number of coal power plants by country 2022 [WWW Document]. Statista. URL https://www.statista.com/statistics/859266/number-of-coal-power-plants-by-country/ (accessed 6.14.23).
Statista, 2020b. Proven coal reserves by country 2020 [WWW Document]. Statista. URL https://www.statista.com/statistics/237096/proven-coal-reserves-of-the-top-ten-countries/ (accessed 6.14.23).
Stein, A.F., Draxler, R.R., Rolph, G.D., Stunder, B.J.B., Cohen, M.D., Ngan, F., 2015. NOAA's HYSPLIT Atmospheric Transport and Dispersion Modeling System in: Bulletin of the American Meteorological Society Volume 96 Issue 12 (2015) [WWW Document]. URL https://journals.ametsoc.org/view/journals/bams/96/12/bams-d-14-00110.1.xml (accessed 7.19.22).
Stock, B., 2022. MixSIAR.
Stock, B., Jackson, A., Ward, E., Venkiteswaran, J., 2018. brianstock/MixSIAR 3.1.9. https://doi.org/10.5281/zenodo.1209993
Stock, B., Semmens, B., 2016. MixSIAR GUI User Manual v3.1.
Sturges, W.T., Barrie, L.A., 1989. Stable lead isotope ratios in arctic aerosols: evidence for the origin of arctic air pollution. Atmospheric Environ. 1967, Arctic Air Chemistry 23, 2513–2519. https://doi.org/10.1016/0004-6981(89)90263-1
Sturges, W.T., Barrie, L.A., 1987. Lead 206/207 isotope ratios in the atmosphere of North America as tracers of US and Canadian emissions. Nature 329, 144–146. https://doi.org/10.1038/329144a0
Sudheer, A.K., Rengarajan, R., 2012. Atmospheric Mineral Dust and Trace Metals over Urban Environment in Western India during Winter. Aerosol Air Qual. Res. 12, 923–933. https://doi.org/10.4209/aaqr.2011.12.0237
Sugiyama, I., Williams-Jones, A.E., 2018. An approach to determining nickel, vanadium and other metal concentrations in crude oil. Anal. Chim. Acta 1002, 18–25. https://doi.org/10.1016/j.aca.2017.11.040
Sutherland, R.A., 2000. Bed sediment-associated trace metals in an urban stream, Oahu, Hawaii. Environ. Geol. 39, 611–627. https://doi.org/10.1007/s002540050473
Swaine, D.J., 2013. Trace Elements in Coal. Butterworth-Heinemann.
Tan, R.B.H., Wijaya, D., Khoo, H.H., 2010. LCI (Life cycle inventory) analysis of fuels and electricity generation in Singapore. Energy, The 3rd International Conference on Sustainable Energy and

Environmental Protection, SEEP 2009 35, 4910–4916. https://doi.org/10.1016/j.energy.2010.08.036
Telloli, C., Malaguti, A., Mircea, M., Tassinari, R., Vaccaro, C., Berico, M., 2014. Properties of agricultural aerosol released during wheat harvest threshing, plowing and sowing. J. Environ. Sci. 26, 1903–1912. https://doi.org/10.1016/j.jes.2014.07.004
Tessier, A., Campbell, P.G.C., Bisson, M., 1979. Sequential extraction procedure for the speciation of particulate trace metals. Anal. Chem. 51, 844–851. https://doi.org/10.1021/ac50043a017
Thorpe, A., Harrison, R.M., 2008. Sources and properties of non-exhaust particulate matter from road traffic: A review. Sci. Total Environ. 400, 270–282. https://doi.org/10.1016/j.scitotenv.2008.06.007
Tian, H.Z., Zhu, C.Y., Gao, J.J., Cheng, K., Hao, J.M., Wang, K., Hua, S.B., Wang, Y., Zhou, J.R., 2015. Quantitative assessment of atmospheric emissions of toxic heavy metals from anthropogenic sources in China: historical trend, spatial distribution, uncertainties, and control policies. Atmospheric Chem. Phys. 15, 10127–10147. https://doi.org/10.5194/acp-15-10127-2015
Timmers, V.R.J.H., Achten, P.A.J., 2016. Non-exhaust PM emissions from electric vehicles. Atmos. Environ. 134, 10–17. https://doi.org/10.1016/j.atmosenv.2016.03.017
Tinklin, R., Bowling, D.J.F., 1969. The Water Relations of Bracken: A Preliminary Study. J. Ecol. 57, 669–671. https://doi.org/10.2307/2258491
TNPCB, 2023. BEFORE THE HON'BLE NATIONAL GREEN TRIBUNAL SOUTHERN ZONE, CHENNAI Original Application No.107 of 2023 - Google Search [WWW Document]. URL https://www.google.com/search?q=BEFORE+THE+HON%E2%80%99BLE+NATIONAL+GREEN+TRIBUNAL+SOUTHERN+ZONE%2C+CHENNAI+Original+Application+No.107+of+2023&oq=BEFORE+THE+HON%E2%80%99BLE+NATIONAL+GREEN+TRIBUNAL+SOUTHERN+ZONE%2C+CHENNAI+Original+Application+No.107+of+2023&gs_lcrp=EgZjaHJvbWUyBggAEEUYOdIBBzY2NGowajeoAgCwAgA&sourceid=chrome&ie=UTF-8 (accessed 2.23.24).
TNPCB, 2020. EVALUATION OF CEPI SCORE & ACTION PLAN FOR CEPI AREA OF TAMILNADU [WWW Document]. URL https://tnpcb.gov.in/action-plan-form.php (accessed 2.24.24).
Tournadre, J., 2014. Anthropogenic pressure on the open ocean: The growth of ship traffic revealed by altimeter data analysis. Geophys. Res. Lett. 41, 7924–7932. https://doi.org/10.1002/2014GL061786
Turnau, K., Kottke, I., Oberwinkler, F., 1993. Element localization in mycorrhizal roots of Pteridium aquilinum (L.) Kuhn collected from experimental plots treated with cadmium dust. New Phytol. 123, 313–324. https://doi.org/10.1111/j.1469-8137.1993.tb03741.x
Turner, A., Filella, M., 2023. Lead and chromium in European road paints. Environ. Pollut. 316, 120492. https://doi.org/10.1016/j.envpol.2022.120492
UNICEF and Pure Earth, 2020. The toxic truth [WWW Document]. URL https://www.unicef.org/reports/toxic-truth-childrens-exposure-to-lead-pollution-2020 (accessed 3.20.22).
Upadhayay, H.R., Bodé, S., Griepentrog, M., Huygens, D., Bajracharya, R.M., Blake, W.H., Dercon, G., Mabit, L., Gibbs, M., Semmens, B.X., Stock, B.C., Cornelis, W., Boeckx, P., 2017. Methodological perspectives on the application of compound-specific stable isotope fingerprinting for sediment source apportionment. J. Soils Sediments 17, 1537–1553. https://doi.org/10.1007/s11368-017-1706-4
Upadhyay, A., Kanchan, K., Goyal, P.G., Yerramilli, A., Gorai, A.K., 2014. Development of a Fuzzy Pattern Recognition Model for Air Quality Assessment of Howrah City. Aerosol Air Qual. Res. 14, 1639–1652. https://doi.org/10.4209/aaqr.2013.04.0118

US EPA, O., 2020. National Ambient Air Quality Standards (NAAQS) for PM [WWW Document]. URL https://www.epa.gov/pm-pollution/national-ambient-air-quality-standards-naaqs-pm (accessed 5.6.23).
US EPA, O., 2015. Copper-Free Brake Initiative [WWW Document]. URL https://www.epa.gov/npdes/copper-free-brake-initiative (accessed 6.23.24).
US EPA, O., 2014. Air Cleaners and Air Filters in the Home [WWW Document]. URL https://www.epa.gov/indoor-air-quality-iaq/air-cleaners-and-air-filters-home (accessed 1.10.25).
USDA, 2018. Pteridium aquilinum [WWW Document]. URL https://www.fs.usda.gov/database/feis/plants/fern/pteaqu/all.html#195 (accessed 6.29.23).
Uzu, G., Sobanska, S., Sarret, G., Muñoz, M., Dumat, C., 2010. Foliar Lead Uptake by Lettuce Exposed to Atmospheric Fallouts. Environ. Sci. Technol. 44, 1036–1042. https://doi.org/10.1021/es902190u
Vaaraslahti, K., Keskinen, J., Giechaskiel, B., Solla, A., Murtonen, T., Vesala, H., 2005. Effect of Lubricant on the Formation of Heavy-Duty Diesel Exhaust Nanoparticles. Environ. Sci. Technol. 39, 8497–8504. https://doi.org/10.1021/es0505503
Vahan Sewa, 2023. VAHAN SEWA| DASHBOARD [WWW Document]. URL https://vahan.parivahan.gov.in/vahan4dashboard/vahan/vahan/view/reportview.xhtml (accessed 11.15.24).
Van Donkelaar, A., Martin, R.V., Li, C., Burnett, R.T., 2019. Regional Estimates of Chemical Composition of Fine Particulate Matter Using a Combined Geoscience-Statistical Method with Information from Satellites, Models, and Monitors. Environ. Sci. Technol. 53, 2595–2611. https://doi.org/10.1021/acs.est.8b06392
Vats, S.K., Singh, A., Koul, M., Uniyal, P.L., 2010. Study on the Metal Absorption by two Mosses in Delhi Region (India).
Velasco, E., Roth, M., 2012. Review of Singapore's air quality and greenhouse gas emissions: Current situation and opportunities. J. Air Waste Manag. Assoc. 62, 625–641. https://doi.org/10.1080/10962247.2012.666513
Vélez-Gavilán, J., 2020. Pteris vittata (Chinese ladder brake fern). CABI Compend. CABI Compendium, 119837. https://doi.org/10.1079/cabicompendium.119837
Velmurugan, S., Joseph, A.A., 2022. Energy consumption of rural Households in Cuddalore district of Tamil Nadu - ProQuest [WWW Document]. URL https://www.proquest.com/openview/1f04ad64f5bbf098f85c2ff46e677e62/1?cbl=2035897&pq-origsite=gscholar (accessed 2.26.24).
Venkataraman, C., Brauer, M., Tibrewal, K., Sadavarte, P., Ma, Q., Cohen, A., Chaliyakunnel, S., Frostad, J., Klimont, Z., Martin, R.V., Millet, D.B., Philip, S., Walker, K., Wang, S., 2018. Source influence on emission pathways and ambient $PM_{2.5}$ pollution over India (2015–2050). Atmospheric Chem. Phys. 18, 8017–8039. https://doi.org/10.5194/acp-18-8017-2018
Viana, M., Amato, F., Alastuey, A., Querol, X., Moreno, T., García Dos Santos, S., Herce, M.D., Fernández-Patier, R., 2009. Chemical Tracers of Particulate Emissions from Commercial Shipping. Environ. Sci. Technol. 43, 7472–7477. https://doi.org/10.1021/es901558t
Vilomet, J.D., Veron, A., Ambrosi, J.P., Moustier, S., Bottero, J.Y., Chatelet-Snidaro, L., 2003. Isotopic Tracing of Landfill Leachates and Pollutant Lead Mobility in Soil and Groundwater. Environ. Sci. Technol. 37, 4586–4591. https://doi.org/10.1021/es010245r
Vithanage, M., Bandara, P.C., Novo, L.A.B., Kumar, A., Ambade, B., Naveendrakumar, G., Ranagalage, M., Magana-Arachchi, D.N., 2022. Deposition of trace metals associated with atmospheric particulate matter: Environmental fate and health risk assessment. Chemosphere 303, 135051. https://doi.org/10.1016/j.chemosphere.2022.135051
von Gunten, K., Konhauser, K.O., Alessi, D.S., 2020. Potential of asphalt concrete as a source of trace metals. Environ. Geochem. Health 42, 397–405. https://doi.org/10.1007/s10653-019-00370-y

Wagner, R., Jähn, M., Schepanski, K., 2018. Wildfires as a source of airborne mineral dust – revisiting a conceptual model using large-eddy simulation (LES). Atmospheric Chem. Phys. 18, 11863–11884. https://doi.org/10.5194/acp-18-11863-2018

Walsh, M.P., 2007. The global experience with lead in gasoline and the lessons we should apply to the use of MMT. Am. J. Ind. Med. 50, 853–860. https://doi.org/10.1002/ajim.20483

Wan, X., Lei, M., Chen, T., Zhou, G., Yang, J., Zhou, X., Zhang, X., Xu, R., 2014. Phytoremediation potential of Pteris vittata L. under the combined contamination of As and Pb: beneficial interaction between As and Pb. Environ. Sci. Pollut. Res. 21, 325–336. https://doi.org/10.1007/s11356-013-1895-3

Wang, H., Maher, B.A., Ahmed, I.A., Davison, B., 2019. Efficient Removal of Ultrafine Particles from Diesel Exhaust by Selected Tree Species: Implications for Roadside Planting for Improving the Quality of Urban Air. Environ. Sci. Technol. 53, 6906–6916. https://doi.org/10.1021/acs.est.8b06629

Wang, P., Hu, Y., Cheng, H., 2019. Municipal solid waste (MSW) incineration fly ash as an important source of heavy metal pollution in China. Environ. Pollut. 252, 461–475. https://doi.org/10.1016/j.envpol.2019.04.082

Wang, Y.-F., Huang, K.-L., Li, C.-T., Mi, H.-H., Luo, J.-H., Tsai, P.-J., 2003. Emissions of fuel metals content from a diesel vehicle engine. Atmos. Environ. 37, 4637–4643. https://doi.org/10.1016/j.atmosenv.2003.07.007

Wang, Y.Q., Zhang, X.Y., Draxler, R.R., 2009. TrajStat: GIS-based software that uses various trajectory statistical analysis methods to identify potential sources from long-term air pollution measurement data. Environ. Model. Softw. 24, 938–939. https://doi.org/10.1016/j.envsoft.2009.01.004

Wedepohl, K.H., 1995. The composition of the continental crust. Geochim. Cosmochim. Acta 59, 1217–1232. https://doi.org/10.1016/0016-7037(95)00038-2

Weerakkody, U., Dover, J.W., Mitchell, P., Reiling, K., 2017. Particulate matter pollution capture by leaves of seventeen living wall species with special reference to rail-traffic at a metropolitan station. Urban For. Urban Green. 27, 173–186. https://doi.org/10.1016/j.ufug.2017.07.005

White, W.M., Albarède, F., Télouk, P., 2000. High-precision analysis of Pb isotope ratios by multi-collector ICP-MS. Chem. Geol. 167, 257–270. https://doi.org/10.1016/S0009-2541(99)00182-5

WHO, 2024. Ambient (outdoor) air pollution [WWW Document]. URL https://www.who.int/news-room/fact-sheets/detail/ambient-(outdoor)-air-quality-and-health (accessed 1.5.25).

Wiedinmyer, C., Yokelson, R.J., Gullett, B.K., 2014. Global Emissions of Trace Gases, Particulate Matter, and Hazardous Air Pollutants from Open Burning of Domestic Waste. Environ. Sci. Technol. 48, 9523–9530. https://doi.org/10.1021/es502250z

Wiles, C.C., 1996. Municipal solid waste combustion ash: State-of-the-knowledge. J. Hazard. Mater., Municipal Waste Incineration 47, 325–344. https://doi.org/10.1016/0304-3894(95)00120-4

Winkler, S.L., Anderson, J.E., Garza, L., Ruona, W.C., Vogt, R., Wallington, T.J., 2018. Vehicle criteria pollutant (PM, NOx, CO, HCs) emissions: how low should we go? Npj Clim. Atmospheric Sci. 1, 1–5. https://doi.org/10.1038/s41612-018-0037-5

Wiseman, C.L.S., Levesque, C., Rasmussen, P.E., 2021. Characterizing the sources, concentrations and resuspension potential of metals and metalloids in the thoracic fraction of urban road dust. Sci. Total Environ. 786, 147467. https://doi.org/10.1016/j.scitotenv.2021.147467

Wong, C.S.C., Li, X.D., 2004. Pb contamination and isotopic composition of urban soils in Hong Kong. Sci. Total Environ. 319, 185–195. https://doi.org/10.1016/S0048-9697(03)00403-0

Wu, F.Y., Leung, H.M., Wu, S.C., Ye, Z.H., Wong, M.H., 2009. Variation in arsenic, lead and zinc tolerance and accumulation in six populations of Pteris vittata L. from China. Environ. Pollut. 157, 2394–2404. https://doi.org/10.1016/j.envpol.2009.03.022

Wu, P.-C., Huang, K.-F., 2021. Tracing local sources and long-range transport of PM10 in central Taiwan by using chemical characteristics and Pb isotope ratios. Sci. Rep. 11, 7593. https://doi.org/10.1038/s41598-021-87051-y

Xiao, H.-W., Xiao, H.-Y., Luo, L., Shen, C.-Y., Long, A.-M., Chen, L., Long, Z.-H., Li, D.-N., 2017. Atmospheric aerosol compositions over the South China Sea: temporal variability and source apportionment. Atmospheric Chem. Phys. 17, 3199–3214. https://doi.org/10.5194/acp-17-3199-2017

Xiong, T., Leveque, T., Shahid, M., Foucault, Y., Mombo, S., Dumat, C., 2014. Lead and Cadmium Phytoavailability and Human Bioaccessibility for Vegetables Exposed to Soil or Atmospheric Pollution by Process Ultrafine Particles. J. Environ. Qual. 43, 1593–1600. https://doi.org/10.2134/jeq2013.11.0469

Xu, H., Ho, S.S.H., Cao, J., Guinot, B., Kan, H., Shen, Z., Ho, K.F., Liu, S., Zhao, Z., Li, J., Zhang, N., Zhu, C., Zhang, Q., Huang, R., 2017. A 10-year observation of PM2.5-bound nickel in Xi'an, China: Effects of source control on its trend and associated health risks. Sci. Rep. 7, 41132. https://doi.org/10.1038/srep41132

Xu, J., Zhang, Z., Wu, C., Shu, Q., Zheng, C., Li, X., Jin, Z., 2019. Mineralogy, fluid inclusions, and S–Pb isotope geochemistry study of the Tuboh Pb–Zn–Ag polymetallic deposit, Lubuklinggau, Sumatra, Indonesia. Ore Geol. Rev. 112, 103032. https://doi.org/10.1016/j.oregeorev.2019.103032

Xu, W., Du, Q., Yan, S., Cao, Y., Liu, X., Guan, D.-X., Ma, L.Q., 2022. Geographical distribution of As-hyperaccumulator Pteris vittata in China: Environmental factors and climate changes. Sci. Total Environ. 803, 149864. https://doi.org/10.1016/j.scitotenv.2021.149864

Yadav, A.K., Sahoo, S.K., Patra, A.C., Thakur, V.K., Dubey, J.S., Singh, S., Lenka, P., Jha, V., Kumar, A.V., Shirin, S., Jamal, A., 2022. Enrichment Factor and Chemical Composition of Size Separated Airborne Particulate Matter of Singrauli Coalfield, India. Aerosol Sci. Eng. 6, 414–436. https://doi.org/10.1007/s41810-022-00155-4

Yadav, S., Rajamani, V., 2004. Geochemistry of aerosols of northwestern part of India adjoining the Thar desert1. Geochim. Cosmochim. Acta 68, 1975–1988. https://doi.org/10.1016/j.gca.2003.10.032

Yadav, S., Satsangi, P.G., 2013. Characterization of particulate matter and its related metal toxicity in an urban location in South West India. Environ. Monit. Assess. 185, 7365–7379. https://doi.org/10.1007/s10661-013-3106-6

Yao, P.-H., Shyu, G.-S., Chang, Y.-F., Chou, Y.-C., Shen, C.-C., Chou, C.-S., Chang, T.-K., 2015. Lead Isotope Characterization of Petroleum Fuels in Taipei, Taiwan. Int. J. Environ. Res. Public. Health 12, 4602–4616. https://doi.org/10.3390/ijerph120504602

Yin, K., Li, P., Chan, W.P., Dou, X., Wang, J.-Y., 2018. Characteristics of heavy metals leaching from MSWI fly ashes in sequential scrubbing processes. J. Mater. Cycles Waste Manag. 20, 604–613.

Yunus, Mohd., Dwivedi, A.K., Kulshreshtha, K., Ahmad, K.J., 1985. Dust loadings on some common plants near Lucknow City. Environ. Pollut. Ser. B Chem. Phys. 9, 71–80. https://doi.org/10.1016/0143-148X(85)90040-0

Zhang, C., Yang, X., Yang, S., Liu, Z., Zhang, L., He, H., Qiu, W., Zhuo, R., Xu, J., Wang, L., 2023. Valorization of heavy metal enriched phytoremediation biomass using a deep eutectic solvent (DES). Green Chem. 25, 771–778. https://doi.org/10.1039/D2GC04190A

Zhang, J., Peng, J., Song, C., Ma, C., Men, Z., Wu, J., Wu, L., Wang, T., Zhang, X., Tao, S., Gao, S., Hopke, P.K., Mao, H., 2020. Vehicular non-exhaust particulate emissions in Chinese megacities: Source profiles, real-world emission factors, and inventories. Environ. Pollut. 266, 115268. https://doi.org/10.1016/j.envpol.2020.115268

Zhang, J., Sun, X., Deng, J., Li, G., Li, Z., Jiang, J., Wu, Q., Duan, L., 2022. Emission characteristics of heavy metals from a typical copper smelting plant. J. Hazard. Mater. 424, 127311. https://doi.org/10.1016/j.jhazmat.2021.127311

Zhang, X.-Y., Geng, L.-P., Gao, P.-P., Dong, J.-W., Zhou, C., Li, H.-B., Chen, M.-M., Xue, P.-Y., Liu, W.-J., 2022. Bioimaging of Pb by LA-ICP-MS and Pb isotopic compositions reveal distributions and origins of Pb in wheat grain. Sci. Total Environ. 802, 149729. https://doi.org/10.1016/j.scitotenv.2021.149729

Zheng, J., Wang, H., Li, Z., Tang, S., Chen, Z., 2008. Using Elevated Carbon Dioxide to Enhance Copper Accumulation in Pteridium Revolutum, a Copper-Tolerant Plant, Under Experimental Conditions. Int. J. Phytoremediation 10, 161–172. https://doi.org/10.1080/15226510801913934

Zheng, Y., Xu, W., He, Z., Ma, M., 2008. Plant regeneration of the arsenic hyperaccumulator Pteris vittata L. from spores and identification of its tolerance and accumulation of arsenic and copper. Acta Physiol. Plant. 30, 249–255. https://doi.org/10.1007/s11738-007-0114-6

Zhou, C., Zhou, H., Hopke, P.K., Holsen, T.M., 2024. Overview of the Trajectory-Ensemble Potential Source Apportionment Web (TraPSA-Web) Toolkit for Atmospheric Pollutant Source Identification. Atmosphere 15, 176. https://doi.org/10.3390/atmos15020176

Zhu, J., Sun, H., Ren, W., He, X., Wang, L., Yang, Y., Shi, G., 2022. Emission Characterization of Particulate Matters from the Combustion of Pulverized Coals in a Simulated Fluidized Bed Boiler. ACS Omega 7, 37922–37932. https://doi.org/10.1021/acsomega.2c05080

CHAPTER 11: PUBLICATIONS AND CONFERENCES

Chemosphere 307 (2022) 136029

Contents lists available at ScienceDirect

Chemosphere

journal homepage: www.elsevier.com/locate/chemosphere

Seasonal variation of atmospheric Pb sources in Singapore - Elemental and lead isotopic compositions of PM_{10} as source tracer

Iravati Ray [a], Reshmi Das [a,b,*], Song Lin Chua [c], Xianfeng Wang [b,c]

[a] School of Environmental Studies, Jadavpur University, Kolkata, India
[b] Earth Observatory of Singapore, Nanyang Technological University, Singapore
[c] Asian School of Environment, Nanyang Technological University, Singapore

HIGHLIGHTS

- Pb isotope ratios and metal concentrations delineate the sources of atmospheric Pb.
- High EFs of Pb in Singapore aerosols of all 3 seasons indicate anthropogenic origin.
- Pb isotopic compositions of PM_{10} are similar across 3 seasons.
- Pb sources are car & ship exhaust, coal burning, incineration ash, past leaded fuel.

GRAPHICAL ABSTRACT

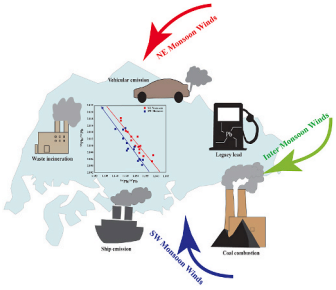

ARTICLE INFO

Handling Editor: Volker Matthias

Keywords:
PM_{10}
Source apportionment
Pb isotopes
Elemental composition

ABSTRACT

Southeast Asia has become a hotspot of anthropogenic particulate matter (PM) emissions due to increased coal combustion, high-temperature industrial operations, vehicular traffic, and agricultural biomass burning. Lead (Pb), a criteria pollutant, bound to such PM can be hazardous when inhaled, even at extremely low concentrations. Precise and accurate source apportionment of atmospheric Pb is thus, critical in order to minimize its exposure. This study investigates the sources of atmospheric Pb in Singapore aerosol samples (PM_{10}) using Pb isotopes and elemental composition as tracers of contamination sources. PM_{10} aerosol sampling was conducted over a period of 1 year from June 2017 to May 2018 to capture the seasonal variations in sources of atmospheric Pb. Elemental concentrations reveal particularly high enrichment factors for Pb, Cu, V, Ni and Zn, especially when under the influence of southwest (SW) and inter monsoon (IM) winds. Pb isotopic ratios across the three seasons ($^{206/207}Pb = 1.147–1.150$ and $^{208/207}Pb = 2.420–2.428$) are not significantly different. The Pb isotopic signatures and V/Ni ratios for all three seasons overlap with those of gasoline, diesel and ship emissions. Moreover, V/Pb values of more than unity for SW and IM winds suggest influence of transboundary coal combustion emissions particularly from Indonesia. Consequently, using Pb isotopic fingerprints and elemental ratios, we find that the primary sources of atmospheric Pb are vehicular & ship emissions, heavy oil combustion, transboundary coal combustion emissions, waste incineration and recirculation of historic leaded gasoline.

* Corresponding author. School of Environmental Studies, Jadavpur University, Kolkata, India.
E-mail address: reshmidas.sest@jadavpuruniversity.in (R. Das).

https://doi.org/10.1016/j.chemosphere.2022.136029
Received 6 April 2022; Received in revised form 22 July 2022; Accepted 8 August 2022
Available online 23 August 2022
0045-6535/© 2022 Elsevier Ltd. All rights reserved.

1. Introduction

Lead (Pb), one of the criteria air pollutants, is a neurotoxin and can be deleterious even at low levels of exposure. Evidence of serious adverse consequences reveals that no level of Pb exposure can be deemed safe (UNICEF and Pure Earth, 2020). Atmospheric Pb has been detected in the environment at hazardous levels even after the global phase out of leaded gasoline. The late phase out of leaded gasoline in Southeast Asian countries along with increasing coal combustion (Overland et al., 2021), high temperature industrial activities and agricultural biomass burning have made the region a hotspot of anthropogenic emissions. Lead has an atmospheric residence time of approximately 5–10 days and can be transferred on local, national, regional, or transcontinental scales based on the aerosol dynamics (Sturges and Barrie, 1987). Atmospheric Pb has been detected in Southeast Asian nations, showing that local sources such as vehicular traffic, incineration, as well as transboundary movement of coal and high temperature metallurgical emissions play major roles in increasing atmospheric metal concentrations (Carrasco et al., 2018; Chifflet et al., 2018; George et al., 2020; Kayee et al., 2020). In highly urbanized regions and areas close to industrialized zones, emissions from vehicles and non-coal burning industries are most likely to have a significant contribution in increasing the atmospheric Pb concentration (Kumar et al., 2016; Sen et al., 2016). Pristine areas of the Central Himalayas still have legacy Pb as the major source of atmospheric Pb pollution. Although during the winter months, the contribution of coal combustion emissions towards atmospheric Pb increases, the contribution from resuspension of historic leaded gasoline remains stable (Mitra et al., 2021).

Singapore, one of the most developed nations among the Southeast Asian countries phased out leaded gasoline completely in July 1998 (OECD and UNEP, 1999). Since then, there has been a drastic decrease in the roadside Pb levels. Natural gas accounts for the vast bulk (95%) of Singapore's energy generation, while coal accounts for only 1.2% (Singapore Energy Market Authority, 2022). As a result, metals in the atmosphere from coal burning can primarily come from transboundary sources. Indonesia, and China have a large number of coal mines and recorded the biggest rise in coal output (47.06% and 18.94% respectively) in 2018 (British Petroleum, 2019). Vehicular traffic, solid waste incinerators and heavy industries in the island are the local factors contributing to the high PM concentrations and eventually undesirable atmospheric metal levels (George et al., 2020; Velasco and Roth, 2012). Along with local sources, transboundary Pb sources driven by seasonal wind patterns raise atmospheric Pb concentrations of Singapore (Carrasco et al., 2018). The assessment of Pb isotopes and metal concentrations of PM_{10} can determine the pollution sources so that better mitigation policies can be adopted in future.

Isotope ratios have long been used to trace pollution sources as Pb isotopes do not fractionate during physicochemical processes and retain the source signature (Komárek et al., 2008). Lead isotopic ratios have extensively been used as a source tracer for Pb pollution both in the Southern and Northern Hemispheres (Bollhöfer and Rosman, 2000, 2001). However, precisely determining the origins of contaminants solely based on Pb isotope data is challenging since the pollutants can be derived from a mixture of sources where isotopic signatures of the end members are often overlapping. Emissions from coal combustion, vehicle and other industrial activities demonstrate certain distinctive elemental ratios (for e.g., V/Ni, V/Pb etc.). Thus, combining Pb isotopic data along with concentrations of metals like Cu, Ni, V, Zn etc is useful in tracing back the sources of the pollutants. There have been a few studies that have delineated the sources of atmospheric Pb in peninsular Southeast Asian nations by using isotope signatures and elemental compositions (Carrasco et al., 2018; Chifflet et al., 2018; Kayee et al., 2020, 2021). For the purpose of source apportionment, a year-long (June 2017–May 2018) PM_{10} sampling was conducted in Singapore. During the sampling period no major fire events occurred in Indonesia and thus, Singapore did not experience any biomass burning related "haze" events (Supplementary Fig. 1) that can possibly over shadow the background elemental composition of PM. Here, we use a year of time-series data for $^{208}Pb/^{207}Pb$ and $^{206}Pb/^{207}Pb$ in conjunction with elemental composition of PM_{10}, interpreted in the framework of seasonal variations of wind patterns, to understand the drivers of seasonal patterns of atmospheric Pb transport to Singapore.

2. Materials and methods

2.1. Study site and aerosol sampling

Singapore is situated near the southern point of the Malay Peninsula, bordered by Malaysia to the north and Indonesia to the south (Fig. 1). The island is positioned at the crossroads of ship traffic between Europe and Southeast Asia, as well as the US West Coast and Southeast Asia (Gordon et al., 2005). Singapore has a tropical climate with two monsoon seasons that are separated by inter-monsoonal intervals. Northeast (NE) monsoons (December to March) are characterized by strong winds blowing from the north and northeast. During the Southwest Monsoon (SW), winds blow from the south and southeast (June to September). Inter-monsoon (IM) months (April, May, October, and November) are transitional seasons between the two monsoons, with weaker and more varied winds (Meteorological Service Singapore, 2020).

PM_{10} aerosol samples were collected (30 m above ground level) on the roof of Earth Observatory of Singapore, Nanyang Technological University, Singapore between June 2017 and May 2018. The sampling site is located near Jurong island, which houses a number of refineries (McNeill et al., 2020). Three solid waste incinerators are located within 12 km of the site (Singapore National Environment Agency, 2020) (Fig. 1). Forty-five aerosol samples (16 during NE monsoon, 15 during SW monsoon and 14 during inter-monsoon seasons) were collected. Each sample was collected for 24 h starting at 6 a.m., at a pumping efficiency of 10 L/min using a personal modular impactor PM_{10} (PMI, SKC Inc., USA) linked with a Deployable Particulate Sampler (DPS, Leland Legacy Pump, SKC Inc., USA). The 47 mm PTFE filters used to capture PM_{10} were pre-washed with 1 N HCl at 140 °C, then rinsed several times with ultrapure water. The filters were oven-dried at 60 °C and sealed in petri dishes before sampling. Following sampling, the filter papers were placed on sterile petri plates and kept in a desiccator until chemical analysis could be performed. 72 h air parcel back trajectories above 500 m ground level were computed using the Hybrid Single-Particle Lagrangian Integrated Trajectory model (HYSPLIT) to detect long range pollution sources (Fig. 2).

2.2. Air mass trajectory analysis

Pb has an atmospheric residence time of 5–10 days. However, all year round high humidity and rainfall in and around Singapore effectively shortens the residence time by scavenging out the aerosols (Pandey et al., 2017). Thus, 72 h air mass back trajectory at 500 m above ground level was analysed using HYSPLIT (https://www.ready.noaa.gov/HYSPLIT_traj.php) (Stein et al., 2015) (Fig. 2). The origin of the air masses can help to understand the possible long range sources of pollution. During the NE Monsoon season, majority of the air masses originated from the South China Sea. A small cluster of the air masses travelled from Southern China, Vietnam, Cambodia and Malaysia. Coal and base metal mines in southern and south eastern parts of the countries, thus, may contribute to the atmospheric pollution in Singapore during the NE monsoon. A bulk of the air cluster during the SW monsoon arrived from Kalimantan and Sulawesi islands of Indonesia. Some air masses formed over the Java Sea and the island of Java. Pollutants emitted from numerous open pit coal mines in Kalimantan (Fig. 1) and coal fired plants in Indonesia, might contribute towards pollutant sources in Singapore's atmosphere. During the IM seasons air masses

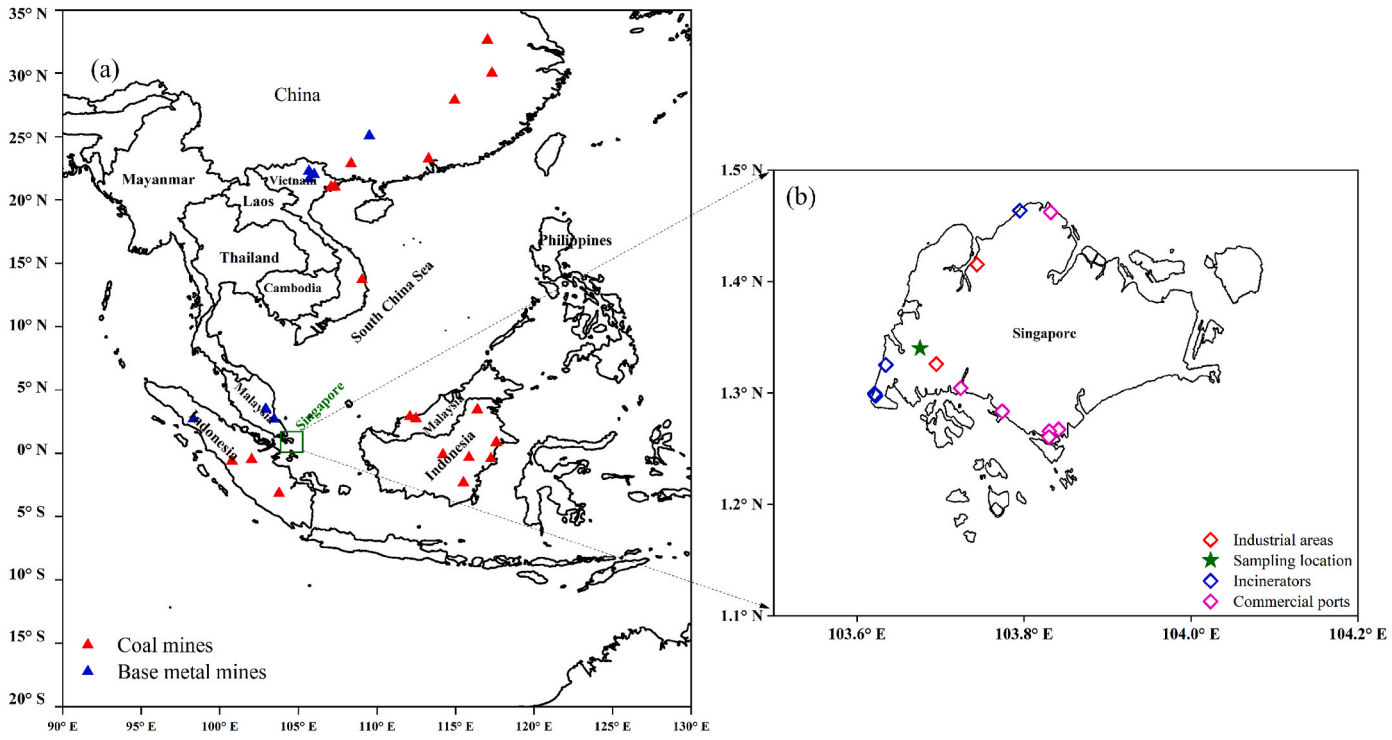

Fig. 1. Location of Singapore in South East Asia. The coal and base metal mines of the neighbouring countries are marked for reference. (b) Sampling location within Singapore and probable local pollution sources. The base maps are adopted from the open-source online repository Opendatasoft (https://public.opendatasoft.com/explore/dataset/world-administrative-boundaries/export/).

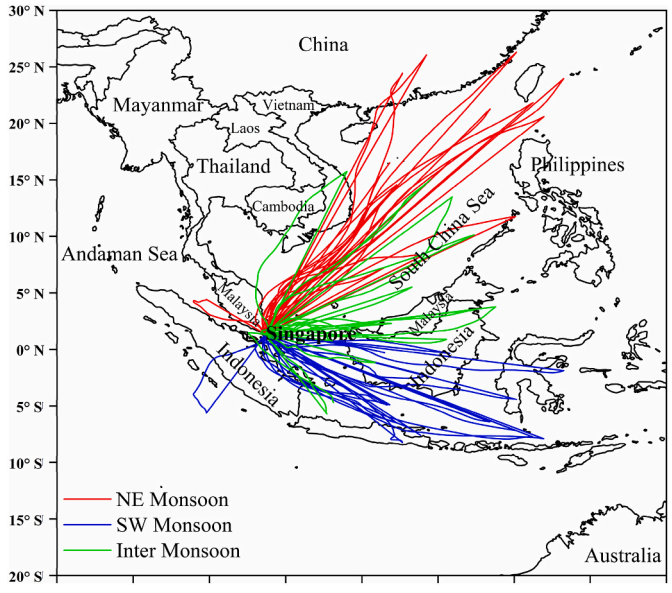

Fig. 2. 72 h backward wind trajectory at 500 m above ground level compiled for the sampling period (June 2017 to May 2018) using [HYSPLIT (Hybrid Single Particle Lagrangian Integrated Trajectory) data from the U.S. National Oceanic and Atmospheric Administration's (NOAA) website]. The base map is adopted from the open-source online repository Opendatasoft (https://public.opendatasoft.com/explore/dataset/world-administrative-boundaries/export/).

primarily originated from over the South China Sea and northern part of Borneo island.

2.3. Metal concentration analysis

Chemical extraction for determination of metal concentrations was carried out in a class 1000 clean chemistry facility at the Earth Observatory of Singapore, Nanyang Technological University. All acids used were ultrapure grade from Seastar Chemicals and ultrapure water (Super-Q, Merck Millipore) with a resistivity of 18.2 MΩ cm was used for dilution. PTFE filter samples were sliced into small pieces using a ceramic scissor and placed in Savillex Teflon beakers. After each sample, the scissor was cleaned with methanol and ultrapure water to minimize cross contamination. The filter papers were leached in a 3:1 ratio of 50 percent (v/v) HNO_3 and HF (Kayee et al., 2020, 2021). The Teflon beakers were tightly capped and sonicated at 60 °C for 1 h before being extracted at 150 °C for 24 h. The solution was evaporated to dryness at 120 °C after removing the PTFE filters using Teflon tweezers. The filters were washed with ultrapure water before being discarded. The metal extracts were repeatedly dissolved in 2 mL of 7 N HNO_3 to remove any HF residues. The dried metal salts were dissolved in 2 mL of 2% HNO_3 prior to analysis. The solution was split in two halves, with 1 mL being utilized for metal concentration analysis and the remaining 1 mL for Pb isotope analysis. Using a sector-field inductively coupled plasma mass spectrometer (SF-ICP-MS) (an Element 2 from Thermo Fisher Scientific), concentrations of 15 elements (Al, Ba, Ca, Co, Cr, Cu, Fe, Mg, Mn, Ni, Pb, Sr, Ti, V and Zn) were determined for metal analysis. One ppb of indium (instrument sensitivity ~1.8×10^6 cps/ppb) was added in the 2% HNO_3 acid matrix as an internal standard. A combination of an internal indium standard and an external bracketing multi element standard from Inorganic Ventures (IV-ICPMS- 71A) was used for instrumental drift correction. The method was validated using SRM 2783 (urban particulate matter standard). Extraction efficiency was >90% for all metals. Detection limit (LOD) ranged from 0.0023 ppb for Pb to 2.27 ppb for Ca (n = 12). Procedural blank was quantified by placing a blank filter inside the sampling pump for 5 min without turning on the pump, the approximate time taken to change filters. The blank filters (n = 4) were chemically treated in the same way as the samples. Average procedural blanks were ~0.3% of the samples' average signal intensity. Blank corrections were performed prior to reporting the metal concentrations. The elemental concentrations of the 45 aerosol samples are given in

Supplementary Table 1.

2.4. Pb isotope analysis

Pb was purified using Eichrom AG-1X8 chloride form, ion exchange resin (200–400 mesh) prior to isotope measurements. The sample solutions and blanks, were dried and re-dissolved in 1.1 N HBr before loading onto the Pb separation column. Elution of the column was achieved following Reuer et al. (2003). Briefly, the column's mobile phase comprised up of 1.1 N HBr and 2 N HCl. Pb was eluted using 6 N HCl and collected in Teflon beakers. The eluted solutions were dried at 90 °C and redissolved in 2% ultrapure HNO_3, before being analysed for Pb isotope ratios using a Multi Collector ICP-MS (Neptune Plus from Thermo Fisher Scientific). Thallium (Tl) was added to sample solutions as an internal standard (White et al., 2000). To correct for the instrumental mass fractionation, $^{203}Tl/^{205}Tl$ ratio of 0.418911 was used. To avoid any analytical bias, samples were measured at similar Pb/Tl ratios as the NBS-981 Pb standards. ^{202}Hg signal was monitored to correct for the isobaric interference of ^{204}Hg on ^{204}Pb. The isotope ratios of NIST-981 Pb standard measured during the analytical sessions and the blank values are given in Supplementary Table 2. The NBS-981 Pb standard was determined at $^{206}Pb/^{204}Pb = 16.9242 \pm 0.0130$, $^{207}Pb/^{204}Pb = 15.4730 \pm 0.0142$, $^{208}Pb/^{204}Pb = 36.6211 \pm 0.0890$, $^{208}Pb/^{207}Pb = 2.3668 \pm 0.0045$, $^{206}Pb/^{207}Pb = 1.09378 \pm 0.00037$ (2 standard deviations, n = 29).The Pb isotope ratios of the analysed samples were normalised using the difference between the measured NIST-981 Pb isotope ratio during the analysis and the real ratios provided by Baker et al. (2004).

3. Results and discussion

3.1. Particulate matter concentration

The PM_{10} concentrations of 45 aerosol samples (Supplementary Table 1) measured during all three monsoon seasons of Singapore did not show any significant difference ($p = 0.469$) upon performing Analysis of Variance (ANOVA) ($F_{2,41} = 0.77$, significance level: $p < 0.001$). The mean PM_{10} concentrations during NE, SW and IM seasons were comparable (Supplementary figure 2a) and varied from 44 to 46.6 ng/m^3 (Supplementary figure 2b). During the SW monsoon season (June to September 2017) air masses originated from over Indonesia (Fig. 2). However, as no major biomass burning events were reported during the time period (Supplementary Fig. 1), the PM_{10} concentrations of the SW monsoon winds were not significantly different from the other two seasons.

Meteorological conditions can influence the PM concentrations. Singapore is situated one degree north of the equator and experiences yearlong rainfall due to the two monsoon seasons and afternoon and evening thunderstorms caused by intense surface heating and sea breeze circulation. However, no correlation was observed between PM_{10} concentrations and rainfall amount during the sampled period thus negating the possibility of a washout effect. Vertical mixing and thus dilution of near-surface pollutants are often regulated by the planetary boundary layer (PBL) height over the sampled region. In Singapore PBL height does not vary much across the months due to small variance of average daily temperature coupled with high humidity. No correlation ($r = -0.21$, $p = 0.17$) was observed between PM_{10} and PBL height over Singapore for the sampled period.

3.1.1. Metal concentration, enrichment factor and elemental ratios

Concentrations of 15 elements (Al, Ba, Ca, Co, Cr, Cu, Fe, Mg, Mn, Ni, Pb, Sr, Ti, V and Zn) were measured in this study. Often elemental concentration alone is insufficient to determine the sources. Hence, we use crustal enrichment factor (EF) and elemental ratios in conjunction with concentrations to understand the sources of the PM_{10} metals.

The crustal enrichment factor is defined as the enrichment of a particular element relative to their natural abundance in crustal soil. The EF is generally calculated with respect to a reference element, usually Al or Fe and is expressed as

$$EF = \frac{\left(\frac{X}{Ref}\right)_{Sample}}{\left(\frac{X}{Ref}\right)_{Crust}}$$

where x is the element of interest and Ref is the reference element, which is Al for this study. The average chemical composition of crust is taken from Rudnick and Gao (2003). EF = 1 indicate crustal source, and elements with EF ≤ 10 are considered to originate from crustal source to accommodate local and regional variations in soil chemical composition (Kaya and Tuncel, 1997).

The 15 elements analysed from the PM_{10} aerosol samples demonstrated variations in concentrations across seasons (Table 1). The concentration distribution of the elements can be used to track the sources of the pollutants. In all the three seasons the mean concentrations of Al, Ca, Fe, Mg and Zn were an order of magnitude higher than that of Pb, Ti, Ba, Cu, Cr, Co, Mn, Ni, Sr and V (Supplementary Fig. 3). Al, Ca, Fe and Mg are some of the most abundant elements in earth's crust after oxygen and silicon. Hence their high concentrations (105–364 ng/m^3) as compared to the other elements (≤36 ng/m^3) can be attributed to the natural background of crustal dust. Besides crustal dust, Ca and Mg can have sea spray origin (Xiao et al., 2017). EFs of Ca, Fe and Mg are <10 for all the seasons confirming crustal source (Fig. 3). Among the low concentration element group, Ti, Ba and Sr have crustal origin with EF < 10. EF of Mn is also <10 for NE and IM winds but is slightly higher than 10 (EF = 17) for SW winds (Fig. 3).

EF indicated that the elements Pb, Zn, Cu, V, Ni, Cr, and Co were enriched by factors of 15–2112 implying anthropogenic origin. Out of these metals, Pb, Cu and Zn had extremely high EFs (>100 for all three seasons). The highest EFs of these metals (except Co and Zn) were observed in the SW monsoon winds. To qualitatively assess anthropogenic sources of these metals, Pearson correlation coefficient ($p < 0.05$) indicating association between two metals were used (Supplementary Fig. 4). Additionally, certain elemental ratios distinctive of different sources are investigated.

In the NW monsoon winds Pb moderately correlates with Zn (0.57) and Cu (0.51). Strong and moderate correlation is observed between Ni and Cr (0.79) and Ni and V (0.65). In contrast, moderate to strong correlation between many elemental pairs were observed during SW monsoon season. Pb correlates well with Zn, Cu, V, Ni, Mn and Cr (0.52–0.70). Strong mutual correlation is observed between Zn, Mn and V and Ni. In the IM season Pb correlates well with Ni (0.61) and Cu (0.80). Mutual significant correlations are observed between V, Ni and Cr in the IM winds. Strong correlations between elemental pairs can be indicative of the common sources of atmospheric Pb pollution.

Elemental ratios serve as reliable tracers for contaminants in the atmosphere (Chifflet et al., 2018; Das et al., 2018; Kayee et al., 2021). For example, V/Pb and V/Ni ratios can act as tracers for coal and oil combustion respectively (Wu and Huang, 2021). Generally, coals are rich in V and the V/Pb > 1 indicates coal combustion emission and V/Pb < 1 indicates vehicle exhaust emission. Non coal burning industrial wastes and emissions have V/Pb ≪ 1. V/Pb ratios of SW monsoon (5.72 ± 3.11) and IM (2.25 ± 2.31) show significant difference with that of NE (0.81 ± 0.51) monsoon [ANOVA ($F_{2,42} = 19.55$, significance level: $p < 0.001$)]. Previous studies reported V/Ni ratios between 3 and 4 in heavy oil combustion (Mazzei et al., 2008), ratio between 2.5 and 5 from ship emissions (Salameh et al., 2015; Viana et al., 2009), whereas additional Ni from oil combustion (Peltier et al., 2009) results in lower ratio. V/Ni ratios of NE monsoon (1.52 ± 0.72) are also significantly different from that of SW (3.73 ± 0.46) and inter monsoons (2.67 ± 1.10) ($F_{2,42} = 29.60$, $p < 0.001$). During the SW monsoon season, both the V/Pb and V/Ni ratios were the highest. The significant differences in these ratios, indicate that pollution sources differ across seasons.

Table 1
Metal concentration (ng/m^3) and PM_{10} concentration (μg/m^3) in Singapore aerosols.

Season	N	Parameter	Al	Ba	Ca	Co	Cr	Cu	Fe	Mg	Mn	Ni	Pb	Sr	Ti	V	Zn	PM_{10}
NE monsoon	16	Mean	154	5.8	297	2.4	4.7	8.6	257	224	7.9	4.4	7.8	3.5	8.2	5.3	98	47
		Min	58	0.50	135	0.19	1.7	3.2	52	95	2.5	0.05	1.4	1.6	2.0	0.13	30	17
		Max	437	12	476	7.3	20	18	530	429	16	14	19	7.3	11.8	13	418	79
		SD	96	3.0	90	2.3	5.4	4.3	125	107	3.6	3.6	4.1	1.6	2.8	3.3	117	21
SW monsoon	15	Mean	105	6.5	237	0.33	5.9	16	364	119	17	9.7	8.9	1.9	7.5	36	108	45
		Min	59	3.8	100	0.20	3.6	4.2	173	68	7.0	6.5	1.9	1.1	5.0	22	21	28
		Max	147	12	343	0.48	12	41	619	220	60	17	23.7	2.8	12	68	485	72
		SD	28	2.8	69	0.07	2.1	12	104	45	13	2.8	6.1	0.57	2.2	12	116	12
Inter monsoon	14	Mean	134	7.4	324	1.0	3.4	14	356	126	9.8	6.3	10.4	5.1	10	18	231	45
		Min	26	1.4	74	0.25	0.86	2.7	177	51	1.7	1.8	1.6	1.2	2.0	1.3	43	20
		Max	303	18.5	516	4.7	6.4	30	536	469	22	10	20	11	17	34	479	83
		SD	89	4.9	108	1.5	1.6	7.6	122	106	6.8	2.7	6.3	2.7	4.8	11	170	18

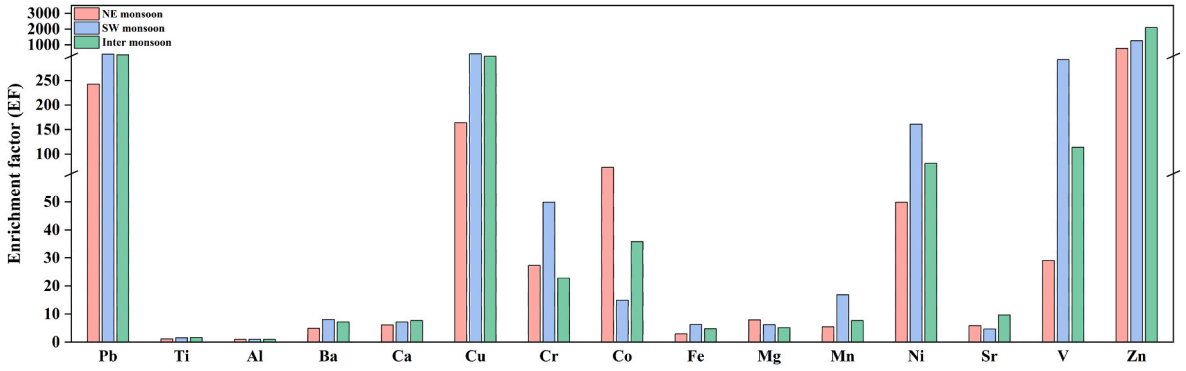

Fig. 3. Enrichment factors of metals in NE, SW and IM seasons.

3.2. Pb isotopic composition and its sources

Average Pb concentrations in all the three seasons were comparable (7.8–10.4 ng/m^3) with inter monsoon > SW monsoon > NE monsoon (Table 1). Pb isotope ratios ($^{206/207}$Pb and $^{208/207}$Pb) for all 45 aerosol samples (Supplementary table 2) were determined to delineate the potential sources of pollution-derived metal in the atmosphere. NE monsoon had the highest mean $^{206/207}$Pb and $^{208/207}$Pb ratios (1.1503 ± 0.0046 and 2.4283 ± 0.006 respectively). The $^{206/207}$Pb and $^{208/207}$Pb ratios for SW (1.1471 ± 0.0054 and 2.4206 ± 0.0066) and inter monsoon (1.1481 ± 0.0056 and 2.4259 ± 0.0069) seasons were relatively close (Table 2).

3.3. Anthropogenic sources of atmospheric Pb

The possible anthropogenic end members contributing to the atmospheric Pb concentration can be coal combustion, high temperature industrial processes, incineration of wastes, vehicular exhaust (Carrasco et al., 2018; Komárek et al., 2008) and recirculation of historical leaded gasoline exhaust particles as has been observed in Mexico (Morton--Bermea et al., 2011) and Kanpur, India (Sen et al., 2016).

Singapore completely phased out leaded gasoline in 1998 (OECD and UNEP, 1999), hence it is improbable that historic Pb from Singapore's leaded gasoline is still contaminating the atmosphere. Carrasco et al. (2018) examined the Pb isotope ratios for Singapore's leaded gasoline using local gas station soils as a proxy and found the ratios to be $^{206/207}$Pb = 1.124 ± 0.013 and $^{208/206}$Pb = 2.131 ± 0.015. Leaded gasoline had a substantially lower $^{206/207}$Pb ratio than the aerosols measured in this study (Supplementary Fig. 5). Indonesia continued to use leaded gasoline until 2006 (Walsh, 2007) with less radiogenic Pb isotopic signature of the alkyllead closer to the Australian Broken Hill type Pb ore deposit (Bollhöfer and Rosman, 2000). The Pb isotopic signature of Indonesian atmospheric PM measured in 1990 had lower $^{206/207}$Pb values, (1.091–1.131) as the primary source of atmospheric Pb was found to be dominated by leaded gasoline emission (Bollhöfer and Rosman, 2000).

The $^{206/207}$Pb values of Chinese and Vietnamese unleaded gasoline vary from 1.089 to 1.170 (Bi et al., 2017) and 1.147 to 1.157 (Chifflet et al., 2018), respectively, which coincide with the $^{206/207}$Pb range of Singapore PM_{10} samples (Supplementary Fig. 5). The isotopic signatures of diesel from some parts of China (Yao et al., 2015) are very similar to that of Singapore PM_{10} (Supplementary Fig. 5), indicating probably a long range transport of Pb from diesel emissions during the NE monsoon season.

Southern Chinese, Vietnamese and Indonesian coals are enriched in radiogenic Pb with $^{206/207}$Pb values ranging from 1.16 to 1.29 in Chinese coals and $^{206/207}$Pb > 1.18 in Vietnamese and Indonesian coals (Bi et al., 2017; Chifflet et al., 2018; Díaz-Somoano et al., 2009). Despite the fact that the NE and SW monsoon winds carry air masses from Southern China and Indonesia, the Pb isotopic ratios of Singapore PM_{10} are less radiogenic than those of Chinese or Indonesian coals (Supplementary Fig. 5).

The Siding mine in Southern China, which is within the air mass transit range, possesses radiogenic galena ($^{206/207}$Pb = 1.16–1.19) (Hsu, 2019). Similarly, Malaysian Pb–Zn ores have $^{206/207}$Pb > 1.162 (Basori et al., 2017). As a result, transboundary contamination from ore mining and coal combustion cannot be the sole source for less radiogenic Pb in Singapore PM_{10} samples. However, the radiogenic values of Pb isotopes in Indonesian coal along with less radiogenic Pb in historic leaded gasoline from Indonesia can form mixing end members in SW monsoon.

The component having the closest $^{206/207}$Pb values with that of the aerosols is incineration dust from local waste incinerators (Supplementary Fig. 5). Singapore's solid waste disposal infrastructure consists of 4 incinerator plants: Tuas, Senoko, Tuas South, and Keppel Seghers, with Senoko around 25 km from the sampling location and Keppel Seghers, Tuas and Tuas South approximately 12 km. The ash from the incinerators is dumped at the Samakau landfill, about 28 km from the sampling location (Singapore National Environment Agency, 2020).

Table 2
Pb isotopic composition of Singapore aerosols.

Season	N	Parameter	$^{206}Pb/^{204}Pb$	2se	$^{207}Pb/^{204}Pb$	2se	$^{208}Pb/^{204}Pb$	2se	$^{206}Pb/^{207}Pb$	2se	$^{208}Pb/^{207}Pb$	2se	[Pb] (ng/m^3)
NE monsoon	16	Mean	17.9224	0.00078	15.5807	0.00080	37.8346	0.00225	1.1503	0.00011	2.4283	0.00007	7.8
		Min	17.7897	0.00030	15.5522	0.00032	37.6695	0.00880	1.1429	0.00004	2.4201	0.00003	1.4
		Max	18.0783	0.00290	15.6022	0.00340	38.0954	0.01110	1.1589	0.00044	2.4419	0.00015	19
		SD	0.0861	0.00073	0.1248	0.00080	0.1248	0.00253	0.0046	0.00010	0.0060	0.00004	4.1
SW monsoon	15	Mean	17.8562	0.00223	15.5657	0.00266	37.6791	0.00903	1.1471	0.00034	2.4206	0.00041	8.9
		Min	17.6104	0.00053	15.5315	0.00052	37.3544	0.00150	1.1338	0.00007	2.4051	0.00008	1.9
		Max	17.9776	0.00393	15.5893	0.00496	37.8573	0.01618	1.1537	00062	2.4294	0.00074	23.7
		SD	0.1011	0.00108	0.0187	0.00134	0.1393	0.00446	0.0054	0.00017	0.0066	0.00020	6.1
Inter monsoon	14	Mean	17.8924	0.00077	15.5847	0.00085	37.8072	0.00255	1.1481	0.00011	2.4259	0.00007	10.4
		Min	17.7018	0.00031	15.5479	0.00031	37.5234	0.00090	1.1385	0.00004	2.4134	0.00004	1.6
		Max	18.1489	0.00330	15.6268	0.00420	38.1787	0.01390	1.1614	0.00052	2.4431	0.00014	20
		SD	0.1067	0.00076	0.0208	0.00099	0.1542	0.00334	0.0056	0.00012	0.0070	0.00003	6.3

Carrasco et al. (2018) examined the fly ash released by incinerators to determine the $^{206/207}Pb$ values in the range of 1.141–1.153, which overlaps with the aerosols measured in this study.

From the triple isotope plot (Fig. 4), it is observed that several of the anthropogenic end members have overlapping Pb isotopic ratios. Hence the isotopic ratios in conjunction with the metal concentrations are used to deduce the possible end members for atmospheric Pb in all three seasons.

3.3.1. NE monsoon

NE monsoon air masses mostly come from the South China Sea and few originate in the southern part of China, south eastern Vietnam and Malaysia (Fig. 2). The plausible long range sources could be coal combustion and ore mining in southern China, Vietnam and Malaysia. However, it is evident that the coal and ore ratios do not overlap with that of the PM_{10} samples (Fig. 4 and Supplementary Fig. 5). Furthermore, the V/Pb ratio, which is used to differentiate between traffic emissions (V/Pb $<$ 1), coal combustion (V/Pb $>$ 1), and industrial emissions (V/Pb $\ll$ 1), is typically less than one during NE monsoon, with an average value of 0.813 $\pm$ 0.513 (Kayee et al., 2021). The V/Pb ratio of Vietnamese coal (0.927) lies close to that of NE monsoon aerosols (Fig. 5a). Air masses originating from Vietnam may carry coal combustion signatures, which may have resulted in slightly elevated $^{206/207}Pb$ and $^{208/207}Pb$ values during the NE monsoon compared to the other two seasons. Nevertheless, contribution from Vietnamese coal should not be overwhelming as majority of the air masses originate from the sea during the NE monsoon season.

Gasoline and diesel from the region (China and Vietnam) have $^{206/207}Pb$ ratios overlapping with that of the NE monsoon aerosols (Fig. 4). Moreover, Singapore importing a part of its crude oil from Vietnam (Tan et al., 2010), may result in Singapore PM_{10} having similar isotopic characteristics of Vietnamese fuel. The V/Ni and V/Pb ratios during this season are quite close to the characteristic ratios of traffic emissions (Chifflet et al., 2018) along with moderate correlation between V and Ni (0.65) (Supplementary figure 4a). Thus, vehicular emissions are the most probable sources of atmospheric Pb during NE monsoon. Few of the high $^{206/207}Pb$ ratios recorded during the season could have been contributed by mixing of Vietnamese coal combustion emissions and few of the low V/Pb ratios could have resulted from fly ashes from the incinerators.

3.3.2. SW monsoon

In SW monsoon air masses are transported from Kalimantan, Sulawesi of Indonesia and Java Sea (Fig. 2). Kalimantan and Sulawesi have a large number of open pit coal mines, coal-fired power stations and Au–Pb mines. A high V/Pb ratio (5.722 $\pm$ 3.112) indicates the source of pollution to be coal combustion. V/Pb ratios in PM_{10} collected during the SW monsoon are similar to those in Indonesian coal (Fig. 5a). The Ni/V versus Pb/V plot demonstrates that the majority of the SW monsoon PM_{10} overlap with the Indonesian coals (Supplementary Fig. 6). However, the PM_{10} isotopic ratios do not match with the radiogenic Pb isotopic signatures of Indonesian coal(Fig. 4). As a result, the transboundary sources might include a mixture of radiogenic coal combustion and past Pb from less radiogenic Indonesian leaded gasoline. Indonesian atmospheric particulates collected in 1994–95 showed a dominant leaded gasoline signature ($^{206}Pb/^{207}Pb$ ranged from 1.103 to 1.131) and traces of the legacy Pb might still be circulating in the environment. Pearson's correlation between V — Ni (0.93) in this season was the strongest among the three seasons (Supplementary Fig. 4b). Moreover, V and Ni also had the highest enrichment factors (Fig. 3) during this period and the V/Ni ratios of SW monsoon aerosols overlap with the characteristic V/Ni ratios of ship emissions and oil combustion (Fig. 5b). This implies influence of ship and vehicular emissions on the atmospheric metal composition (Balasubramanian and Qian, 2004; Kitamura et al., 2020). A binary mixing model employing a simple mass balance equation that accounts for legacy lead and Indonesia coal

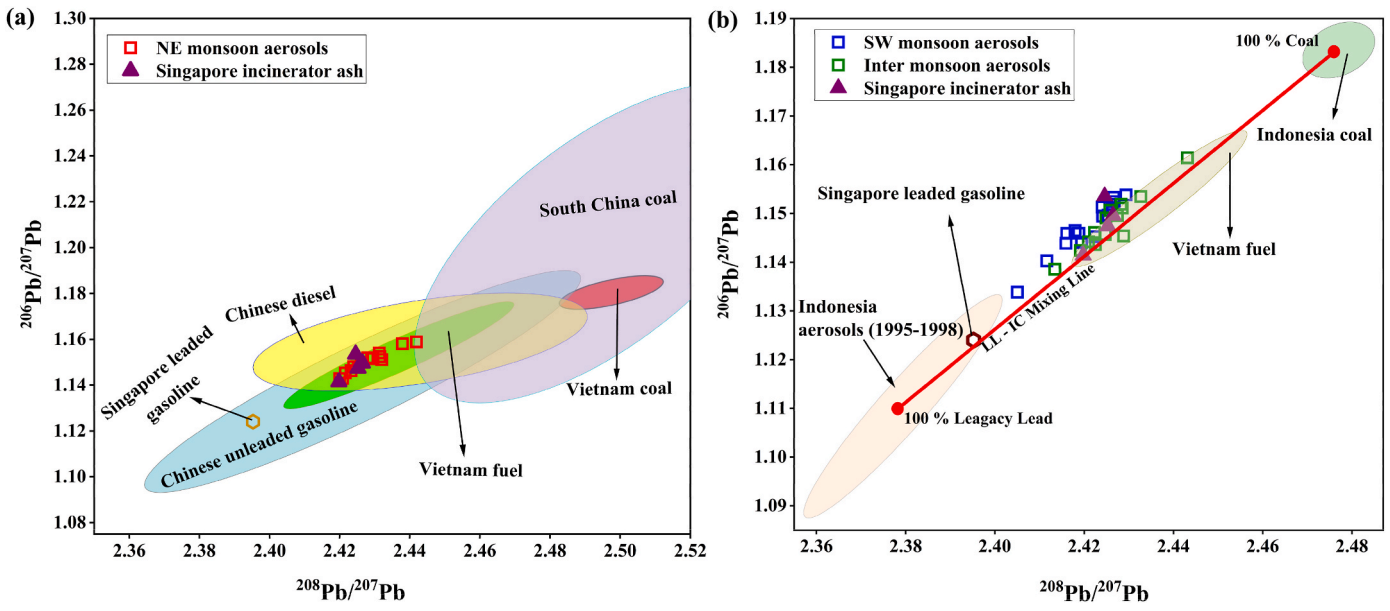

Fig. 4. Triple isotope plot of Pb for (a) NE and (b) SW & IM seasons with reference to different plausible end members. The mixing line between legacy lead (LL) and Indonesian coal (IC) is shown in red. References: Indonesian coal & aerosols and Vietnamese coal & fuel (Bollhöfer and Rosman, 2000; Díaz-Somoano et al., 2009; Chifflet et al., 2018); Chinese diesel, unleaded gasoline and coal (Bi et al., 2017); Singapore leaded gasoline and incinerator ash (Carrasco et al., 2018). (For interpretation of the references to colour in this figure legend, the reader is referred to the Web version of this article.)

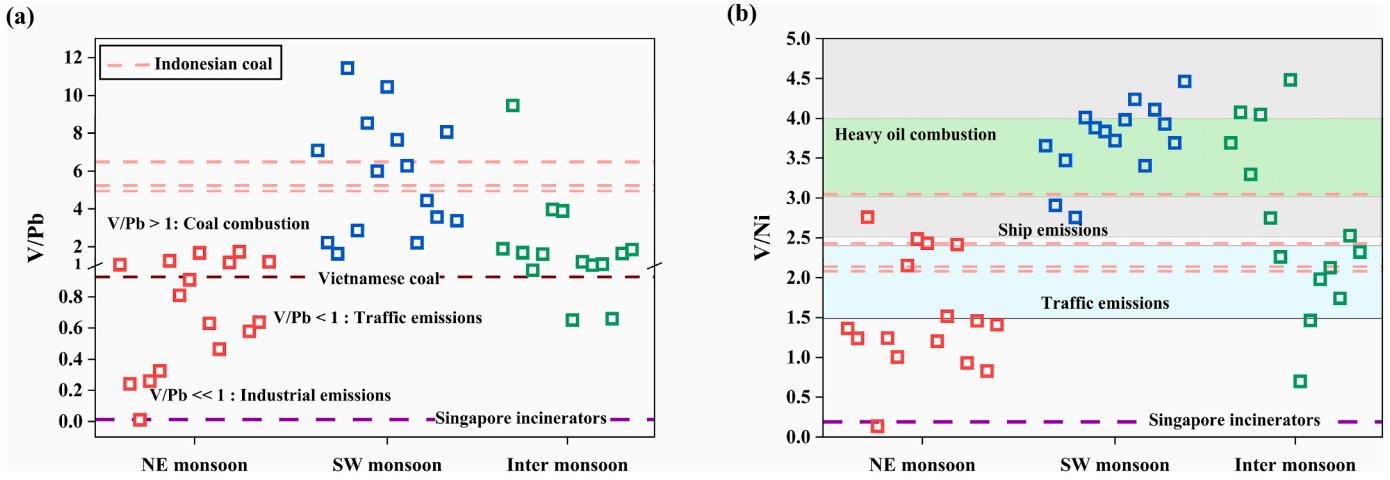

Fig. 5. Seasonal variations in (a) V/Pb and (b) V/Ni ratios in Singapore aerosols. Elemental ratios for Indonesian coal and Vietnamese coal have been adopted from Belkin et al. (2009) and Chifflet et al. (2018) respectively. V/Ni ratios for ship emissions were adopted from Wu and Huang (2021) and traffic emissions from Chifflet et al. (2018). Both the elemental ratios of Singapore incineration dust were adopted from Yin et al. (2018).

reveals that legacy lead contributes 42%–75% and Indonesia coal contributes 25%–58% towards atmospheric Pb. The legacy lead end member is based on average $^{206/207}$Pb and $^{208/207}$Pb values of Singapore leaded gasoline (Carrasco et al., 2018) and Indonesia aerosols measured in 1995–1998 (Bollhöfer and Rosman, 2000). Indonesia coal end member is based on average $^{206/207}$Pb and $^{208/207}$Pb values from (Díaz-Somoano et al., 2009). Consequently, transboundary coal combustion mixed with legacy Pb from leaded gasoline use in Indonesia is possibly mixed with ship emissions and heavy oil combustion from local ports, in the SW monsoon winds.

3.3.3. *Inter monsoon*

In inter monsoon season, majority of the air masses originate from Java Sea and Borneo (Fig. 2). The Pb isotopic fingerprints of the inter monsoon are remarkably similar to those of the SW monsoon, implying comparable end members. During the inter monsoon season, the V/Pb ratio was greater than one (2.259 ± 2.317), lying between the ratios observed during NE and SW monsoons. V/Ni ratios of Indonesian coals determined from metal data available in Belkin et al. (2009) reveal that the V/Ni ratios of the PM_{10} samples collected during the inter monsoon seasons have similar values (Fig. 5b). The Ni/V versus Pb/V plot shows that the inter monsoon PM_{10} lie quite close to the Indonesian coals (Supplementary Fig. 6) Both these ratios suggest that coal burning emissions from Indonesia may contribute to the Pb levels in the atmosphere. However, as the $^{206/207}$Pb ratio of Indonesian coal is substantially higher than that of Singapore PM_{10} (Fig. 4), anthropogenic Pb must be generated due to a mixture of end members. The combination of radiogenic fingerprints of Pb isotopes from Indonesian coals along with historic Pb from Indonesian leaded gasoline may contribute to the less radiogenic Pb isotopic signatures of Singapore PM_{10}. High positive correlation between V — Ni (0.86) (Supplementary figure 4c) implies vehicular traffic as a major source of pollution (Balasubramanian and

Qian, 2004). The V/Ni ratios of inter monsoon aerosols overlap with that of traffic emissions, heavy oil combustion and ship emissions (Fig. 5b) (Chifflet et al., 2018; Wu and Huang, 2021). Although coal combustion emissions contributed to atmospheric Pb levels, their contribution was slightly smaller in the inter monsoon season than in the SW monsoon, as evidenced by lower V/Pb ratios (Fig. 5a). Moreover, the SW monsoon air masses travel more extensively across the coal mining regions of Indonesia than the inter monsoon air masses before reaching Singapore (Fig. 2). As a result, SW monsoon winds are more likely to transport Pb-laden air masses from Indonesia's coal mining regions. However, despite a probably low contribution from coal combustion, average Pb concentrations in the inter monsoon aerosols were the highest (10.42 ± 6.27 ng/m^3). A binary mixing model that accounts for legacy lead and Indonesia coal reveals that legacy lead contributes 31%–66% and Indonesia coal contributes 34%–69% towards atmospheric Pb. Thus, to summarize, Indonesian coal combustion, recirculating dust from historic use of leaded gasoline, heavy oil combustion and ship emissions, contributed significantly to the atmospheric Pb levels in inter monsoon season.

4. Significance of the study

After global phasing out of leaded gasoline, coal combustion became the primary source of atmospheric Pb (Sen et al., 2016). However many recent studies demonstrated that substantial amount of legacy lead is still recirculating in the urban (Resongles et al., 2021; Sen et al., 2016) as well as remote pristine environment (Mitra et al., 2021). According to the UNICEF and Pure Earth report a third of the global children population have Blood Level Leads (BLLs) at or above 5 μg/dL and 50% of these children reside in South and Southeast Asia (UNICEF and Pure Earth, 2020). In the past few decades, rapid urbanization and industrialization, forced a population shift from rural to urban areas, thus increasing vehicular traffic and other commercial activities, making the urban centers hotspots for anthropogenic emissions (Wang et al., 2019). Thus, the children growing up in the urban hubs of South and Southeast Asia are at a greater risk of exposure to Pb pollution. The only sustainable solution to mitigate BLL is to stop the source. Thus, to prevent or limit the discharge of such hazardous pollutants into the atmosphere, detailed data on toxic element emissions from historic Pb and various industrial and commercial activities is required in the large cities of the region.

5. Conclusion

Pb isotopic compositions of aerosols in tandem with elemental composition are useful in discerning pollution sources. However, there was no discernible seasonal pattern in the Pb isotope ratios of Singapore PM_{10} in spite of air mass back trajectories demonstrating a clear difference in origin of SW and IM winds against the NE winds. $^{206/207}$Pb and $^{208/207}$Pb values of all the three seasons coincide with that of gasoline and diesel exhausts from China and Vietnam and incineration fly ashes from Singapore. Concentrations and EFs of hazardous metals such as Pb, Cu, Ni, V and Zn were higher under the influence of SW and IM winds compared to the NE winds. Due to the difference in air mass source, elemental ratios (V/Pb and V/Ni) differ across seasons. Winds blowing from Indonesia to Singapore cause the aerosol to exhibit substantially higher V/Pb values that are similar to Indonesian coal signatures, indicating transboundary migration of coal combustion emissions affecting the Singapore atmosphere. Despite the influence of radiogenic coal during the SW monsoon, the Pb isotopic ratios of Singapore PM_{10} are considerably less radiogenic than Indonesian coals. This suggests that coal and recirculating historic leaded gasoline may form mixing end members. The V/Ni ratios of the NE monsoon are closer to traffic emissions, whereas those of the SW monsoon are closer to ship emissions and heavy oil combustion. The IM winds carry a V/Ni signal which is a combination of vehicular exhausts, ship emissions and heavy oil combustions. Thus, during the NE monsoon, vehicular emissions and incineration dust are the primary sources of atmospheric Pb. The SW monsoon delivers Pb to the atmosphere from transboundary coal combustion, recirculating historic leaded gasoline, ship emissions, and heavy oil combustion. The sources of Pb in the IM winds are similar to those in the SW monsoon winds.

Credit author statement

Iravati Ray: Writing, Conceptualization. Reshmi Das: Conceptualization, Supervision, Analysis, Reviewing and Editing. Song Lin Chua: Sampling, Chemistry. Xianfeng Wang: Conceptualization, Supervision, Reviewing and Editing.

Declaration of competing interest

The authors declare that they have no known competing financial interests or personal relationships that could have appeared to influence the work reported in this paper.

Data availability

All data are provided in the Supplementary Material.

Acknowledgements

This research has been supported by Singapore Ministry of Education (MOE) Tier 1 grant (MOE-NTU_RG125/16-(S)) awarded to XW and RD and NRF Campus for Research Excellence and Technological Enterprise (CREATE) program (NRF2016-ITCOO1-021) awarded to XW. IR is supported by All India Council for Technical Education (AICTE) doctoral fellowship. This is Earth Observatory of Singapore contribution #467.

Appendix A. Supplementary data

Supplementary data to this article can be found online at https://doi.org/10.1016/j.chemosphere.2022.136029.

References

Baker, J., Peate, D., Waight, T., Meyzen, C., 2004. Pb isotopic analysis of standards and samples using a 207Pb–204Pb double spike and thallium to correct for mass bias with a double-focusing MC-ICP-MS. Chem. Geol. 211, 275–303. https://doi.org/10.1016/j.chemgeo.2004.06.030.

Balasubramanian, R., Qian, W.-B., 2004. Characterization and source identification of airborne trace metals in Singapore. J. Environ. Monit. 6, 813–818. https://doi.org/10.1039/B407523D.

Basori, M.B.I., Zaw, K., Meffre, S., Large, R.R., Hassan, W.F.W., 2017. Pb-isotope compositions of the Tasik Chini volcanic-hosted massive sulfide deposit, Central Belt of Peninsular Malaysia: implication for source region and tectonic setting. Isl. Arc 26, 1–8.

Belkin, H.E., Tewalt, S.J., Hower, J.C., Stucker, J.D., O'Keefe, J.M.K., 2009. Geochemistry and petrology of selected coal samples from Sumatra, Kalimantan, Sulawesi, and Papua, Indonesia. Int. J. Coal Geol. 77 (3–4), 260–268. https://doi.org/10.1016/j.coal.2008.08.001.

Bi, X.-Y., Li, Z.-G., Wang, S.-X., Zhang, L., Xu, R., Liu, J.-L., Yang, H.-M., Guo, M.-Z., 2017. Lead isotopic compositions of selected coals, Pb/Zn ores and fuels in China and the application for source tracing. Environ. Sci. Technol. 51, 13502–13508.

Bollhöfer, A., Rosman, K.J.R., 2001. Isotopic source signatures for atmospheric lead: the Northern Hemisphere. Geochem. Cosmochim. Acta 65, 1727–1740. https://doi.org/10.1016/S0016-7037(00)00630-X.

Bollhöfer, A., Rosman, K.J.R., 2000. Isotopic source signatures for atmospheric lead: the Southern Hemisphere. Geochem. Cosmochim. Acta 64, 3251–3262. https://doi.org/10.1016/S0016-7037(00)00436-1.

British Petroleum, 2019. BP - Statistical Review of World Energy, 2019 - Google Search [WWW Document]. URL. https://www.bp.com/content/dam/bp/business-sites/en/global/corporate/pdfs/energy-economics/statistical-review/bp-stats-review-2019-full-report.pdf. (Accessed 1 October 2022).

Carrasco, G., Chen, M., Boyle, E.A., Tanzil, J., Zhou, K., Goodkin, N.F., 2018. An update of the Pb isotope inventory in post leaded-petrol Singapore environments. Environ. Pollut. 233, 925–932. https://doi.org/10.1016/j.envpol.2017.09.025.

Chifflet, S., Amouroux, D., Bérail, S., Barre, J., Van, T.C., Baltrons, O., Brune, J., Dufour, A., Guinot, B., Mari, X., 2018. Origins and discrimination between local and regional atmospheric pollution in Haiphong (Vietnam), based on metal(loid)

concentrations and lead isotopic ratios in PM10. Environ. Sci. Pollut. Res. Int. 25, 26653–26668. https://doi.org/10.1007/s11356-018-2722-7.
Das, R., Bin Mohamed Mohtar, A.T., Rakshit, D., Shome, D., Wang, X., 2018. Sources of atmospheric lead (Pb) in and around an Indian megacity. Atmos. Environ. 193, 57–65. https://doi.org/10.1016/j.atmosenv.2018.08.062.
Díaz-Somoano, M., Kylander, M.E., López-Antón, M.A., Suárez-Ruiz, I., Martínez-Tarazona, M.R., Ferrat, M., Kober, B., Weiss, D.J., 2009. Stable lead isotope compositions in selected coals from around the world and implications for present day aerosol source tracing. Environ. Sci. Technol. 43, 1078–1085. https://doi.org/10.1021/es801818r.
George, S., Chua, M.L., ZheWei, D.Z., Das, R., Bijin, V.A., Connolly, J.E., Lee, K.P., Yung, C.F., Teoh, O.H., Thomas, B., 2020. Personal level exposure and hazard potential of particulate matter during haze and non-haze periods in Singapore. Chemosphere 243, 125401. https://doi.org/10.1016/j.chemosphere.2019.125401.
Gordon, J.R.M., Lee, P.-M., Lucas, H.C., 2005. A resource-based view of competitive advantage at the Port of Singapore. J. Strat. Inf. Syst. 14, 69–86. https://doi.org/10.1016/j.jsis.2004.10.001.
Hsu, Y.-K., 2019. Chinese lead isotope database. Harv. Dataverse. https://doi.org/10.7910/DVN/VID3WR.
Kaya, G., Tuncel, G., 1997. Trace element and major ion composition of wet and dry depositon in Ankara, Turkey. Atmos. Environ. 31, 3985–3998. https://doi.org/10.1016/S1352-2310(97)00221-5.
Kayee, J., Bureekul, S., Sompongchaiyakul, P., Wang, X., Das, R., 2021. Sources of atmospheric lead (Pb) after quarter century of phasing out of leaded gasoline in Bangkok, Thailand. Atmos. Environ. Times 253, 118355. https://doi.org/10.1016/j.atmosenv.2021.118355.
Kayee, J., Sompongchaiyakul, P., Sanwlani, N., Bureekul, S., Wang, X., Das, R., 2020. Metal concentrations and source apportionment of PM $_{2.5}$ in chiang rai and bangkok, Thailand during a biomass burning season. ACS Earth Space Chem 4, 1213–1226. https://doi.org/10.1021/acsearthspacechem.0c00140.
Kitamura, H., Dahlan, A.V., Tian, Y., Shimaoka, T., Yamamoto, T., Takahashi, F., 2020. Application of micro-scale correlation analysis to estimate metal speciation and the matrix in municipal solid waste incineration fly ash. J. Mater. Cycles Waste Manag. 22, 1081–1093. https://doi.org/10.1007/s10163-020-01001-w.
Komárek, M., Ettler, V., Chrastný, V., Mihaljevič, M., 2008. Lead isotopes in environmental sciences: a review. Environ. Int. 34, 562–577. https://doi.org/10.1016/j.envint.2007.10.005.
Kumar, S., Aggarwal, S.G., Malherbe, J., Barre, J.P.G., Berail, S., Gupta, P.K., Donard, O. F.X., 2016. Tracing dust transport from Middle-East over Delhi in March 2012 using metal and lead isotope composition. Atmos. Environ. 132, 179–187. https://doi.org/10.1016/j.atmosenv.2016.03.002.
Mazzei, F., D'Alessandro, A., Lucarelli, F., Nava, S., Prati, P., Valli, G., Vecchi, R., 2008. Characterization of particulate matter sources in an urban environment. Sci. Total Environ. 401, 81–89. https://doi.org/10.1016/j.scitotenv.2008.03.008.
McNeill, J., Snider, G., Weagle, C.L., Walsh, B., Bissonnette, P., Stone, E., Abboud, I., Akoshile, C., Anh, N.X., Balasubramanian, R., Brook, J.R., Coburn, C., Cohen, A., Dong, J., Gagnon, G., Garland, R.M., He, K., Holben, B.N., Kahn, R., Kim, J.S., Lagrosas, N., Lestari, P., Liu, Y., Jeba, F., Joy, K.S., Martins, J.V., Misra, A., Norford, L.K., Quel, E.J., Salam, A., Schichtel, B., Tripathi, S.N., Wang, C., Zhang, Q., Brauer, M., Gibson, M.D., Rudich, Y., Martin, R.V., 2020. Large global variations in measured airborne metal concentrations driven by anthropogenic sources. Sci. Rep. 10, 21817 https://doi.org/10.1038/s41598-020-78789-y.
Meteorological Service Singapore, 2020. Climate of Singapore [WWW Document]. URL. http://www.weather.gov.sg/climate-climate-of-singapore/, 22-3-20.
Mitra, A., Sen, I.S., Pandey, S.K., Velu, V., Reisberg, L., Bizimis, M., Cloquet, C., Nizam, S., 2021. Lead isotope evidence for enhanced anthropogenic particle transport to the Himalayas during summer months. Environ. Sci. Technol. 55, 13697–13708. https://doi.org/10.1021/acs.est.1c03830.
Morton-Bermea, O., Rodríguez-Salazar, M.T., Hernández-Alvarez, E., García-Arreola, M. E., Lozano-Santacruz, R., 2011. Lead isotopes as tracers of anthropogenic pollution in urban topsoils of Mexico City. Geochemistry 71, 189–195. https://doi.org/10.1016/j.chemer.2011.03.003.
OECD and UNEP, 1999. Phasing Lead Out of Gasoline: an Examination of Policy Approaches in Different Countries. UNEP/Earthprint.
Overland, I., Sagbakken, H.F., Chan, H.-Y., Merdekawati, M., Suryadi, B., Utama, N.A., Vakulchuk, R., 2021. The ASEAN climate and energy paradox. Energy Clim. Change 2, 100019. https://doi.org/10.1016/j.egycc.2020.100019.
Pandey, S.K., Vinoj, V., Landu, K., Babu, S.S., 2017. Declining pre-monsoon dust loading over South Asia: signature of a changing regional climate. Sci. Rep. 7, 16062 https://doi.org/10.1038/s41598-017-16338-w.
Peltier, R.E., Hsu, S.-I., Lall, R., Lippmann, M., 2009. Residual oil combustion: a major source of airborne nickel in New York City. J. Expo. Sci. Environ. Epidemiol. 19, 603–612. https://doi.org/10.1038/jes.2008.60.
Resongles, E., Dietze, V., Green, D.C., Harrison, R.M., Ochoa-Gonzalez, R., Tremper, A. H., Weiss, D.J., 2021. Strong evidence for the continued contribution of lead deposited during the 20th century to the atmospheric environment in London of today. Proc. Natl. Acad. Sci. USA 118, e2102791118. https://doi.org/10.1073/pnas.2102791118.
Reuer, M.K., Boyle, E.A., Grant, B.C., 2003. Lead isotope analysis of marine carbonates and seawater by multiple collector ICP-MS. Chem. Geol. 200, 137–153. https://doi.org/10.1016/S0009-2541(03)00186-4.
Rudnick, R.L., Gao, S., 2003. 3.01 - composition of the continental crust. In: Holland, H. D., Turekian, K.K. (Eds.), Treatise on Geochemistry. Pergamon, Oxford, pp. 1–64. https://doi.org/10.1016/B0-08-043751-6/03016-4.
Salameh, D., Detournay, A., Pey, J., Pérez, N., Liguori, F., Saraga, D., Bove, M.C., Brotto, P., Cassola, F., Massabò, D., Latella, A., Pillon, S., Formenton, G., Patti, S., Armengaud, A., Piga, D., Jaffrezo, J.L., Bartzis, J., Tolis, E., Prati, P., Querol, X., Wortham, H., Marchand, N., 2015. PM2.5 chemical composition in five European Mediterranean cities: a 1-year study. Atmos. Res. 155, 102–117. https://doi.org/10.1016/j.atmosres.2014.12.001.
Sen, I.S., Bizimis, M., Tripathi, S.N., Paul, D., 2016. Lead isotopic fingerprinting of aerosols to characterize the sources of atmospheric lead in an industrial city of India. Atmos. Environ. 129, 27–33. https://doi.org/10.1016/j.atmosenv.2016.01.005.
Singapore Energy Market Authority, 2022. EMA: Singapore Energy Statistics | Energy Transformation [WWW Document]. URL. https://www.ema.gov.sg/singapore-energy-statistics/Ch02/index2, 1-22.
Singapore National Environment Agency, 2020-3-20. Solid waste management infrastructure [WWW Document]. URL. https://www.nea.gov.sg/our-services/waste-management/3r-programmes-and-resources/waste-management-infrastructure/solid-waste-management-infrastructure, 22.
Stein, A.F., Draxler, R.R., Rolph, G.D., Stunder, B.J.B., Cohen, M.D., Ngan, F., 2015. NOAA's HYSPLIT atmospheric transport and dispersion modeling system. Bull. Am. Meteorol. Soc. 96, 12 [WWW Document]. URL2015. https://journals.ametsoc.org/view/journals/bams/96/12/bams-d-14-00110.1.xml, 22-7-19.
Sturges, W.T., Barrie, L.A., 1987. Lead 206/207 isotope ratios in the atmosphere of North America as tracers of US and Canadian emissions. Nature 329, 144–146. https://doi.org/10.1038/329144a0.
Tan, R.B.H., Wijaya, D., Khoo, H.H., 2010. LCI (life cycle inventory) analysis of fuels and electricity generation in Singapore. Energy, the 3rd international conference on sustainable energy and environmental protection. SEEP 35, 4910–4916. https://doi.org/10.1016/j.energy.2010.08.036, 2009.
UNICEF and Pure Earth, 2020. The toxic truth [WWW Document]. URL. https://www.unicef.org/reports/toxic-truth-childrens-exposure-to-lead-pollution-2020, 22-20-3.
Velasco, E., Roth, M., 2012. Review of Singapore's air quality and greenhouse gas emissions: current situation and opportunities. J. Air Waste Manag. Assoc. 62, 625–641. https://doi.org/10.1080/10962247.2012.666513.
Viana, M., Amato, F., Alastuey, A., Querol, X., Moreno, T., García Dos Santos, S., Herce, M.D., Fernández-Patier, R., 2009. Chemical tracers of particulate emissions from commercial shipping. Environ. Sci. Technol. 43, 7472–7477. https://doi.org/10.1021/es901558t.
Walsh, M.P., 2007. The global experience with lead in gasoline and the lessons we should apply to the use of MMT. Am. J. Ind. Med. 50, 853–860. https://doi.org/10.1002/ajim.20483.
Wang, Q., Kwan, M.-P., Zhou, K., Fan, J., Wang, Y., Zhan, D., 2019. The impacts of urbanization on fine particulate matter (PM2.5) concentrations: empirical evidence from 135 countries worldwide. Environ. Pollut. 247, 989–998. https://doi.org/10.1016/j.envpol.2019.01.086.
White, W.M., Albarède, F., Télouk, P., 2000. High-precision analysis of Pb isotope ratios by multi-collector ICP-MS. Chem. Geol. 167, 257–270. https://doi.org/10.1016/S0009-2541(99)00182-5.
Wu, P.-C., Huang, K.-F., 2021. Tracing local sources and long-range transport of PM10 in central Taiwan by using chemical characteristics and Pb isotope ratios. Sci. Rep. 11, 7593. https://doi.org/10.1038/s41598-021-87051-y.
Xiao, H.-W., Xiao, H.-Y., Luo, L., Shen, C.-Y., Long, A.-M., Chen, L., Long, Z.-H., Li, D.-N., 2017. Atmospheric aerosol compositions over the South China Sea: temporal variability and source apportionment. Atmos. Chem. Phys. 17, 3199–3214. https://doi.org/10.5194/acp-17-3199-2017.
Yao, P.-H., Shyu, G.-S., Chang, Y.-F., Chou, Y.-C., Shen, C.-C., Chou, C.-S., Chang, T.-K., 2015. Lead isotope characterization of Petroleum fuels in Taipei, Taiwan. Int. J. Environ. Res. Publ. Health 12, 4602–4616. https://doi.org/10.3390/ijerph120504602.
Yin, K., Li, P., Chan, W.P., Dou, X., Wang, J.Y., 2018. Characteristics of heavy metals leaching from MSWI fly ashes in sequential scrubbing processes. J. Mater. Cycles Waste Manag. 20 (1), 604–613. https://doi.org/10.1007/s10163-017-0631-3.

communications earth & environment

ARTICLE

https://doi.org/10.1038/s43247-023-01135-3 OPEN

A lingering legacy of leaded gasoline in Southeast Asia

Iravati Ray[1] & Reshmi Das[1,2]✉

Recent reports of 1 in 3 children globally having blood lead levels ≥ 5microgram decilitre^{-1} demands thorough understanding of lead (Pb) sources of the present century and the fate of legacy Pb from the past use of leaded gasoline. The present hotspot of pollution is South and Southeast Asia. To investigate this issue, here we compile Pb isotopic compositions of aerosols ($n = 341$) along with established and previously excluded sources for Singapore, Thailand, Vietnam, and India. The data was subjected to Bayesian 3D isotope mixing model simulation. Model estimates reveal consistent contributions from natural background. Leaded gasoline is the largest contributor in Southeast Asia (39%). Tertiary coal/fuelwood combustion and ore processing dominate in India, while ship emission contribute up to 15%. Thus, along with Pb from present sources, the historic use of leaded gasoline left a legacy of Pb in soil which is remobilised to the atmosphere after more than two decades of its phase-out.

[1] School of Environmental Studies, Jadavpur University, Kolkata, India. [2] Earth Observatory of Singapore, Nanyang Technological University, Singapore, Singapore. ✉email: reshmidas.sest@jadavpuruniversity.in

The use of leaded gasoline dates back to the early 20th century when tetraethyl lead (TEL) was first introduced as a petroleum additive to improve the performance of internal combustion engines. During the combustion process, gasoline lead (Pb) was partially oxidised and PbO deposits caused engine fouling. To overcome this issue, dichloroethane and dibromoethane were added to leaded gasoline to act as Pb scavengers. The Pb oxides were converted to volatile Pb species such as lead chloride and lead bromide that were emitted into the atmosphere. Once emitted, Pb has an atmospheric residence time of 5–10 days[1] before getting deposited. The Pb compounds emitted from the vehicle exhaust spread to the remote locations of the planet including Antarctica, Greenland, Alaska, and the middle of the oceans[2,3]. Patterson's identification of the automobile tailpipe as the environmental Pb source causing elevated blood lead level (BLL), endemic in the United States led to his fight against the petroleum lobby to ban TEL additive in gasoline[4]. His efforts met with success in 1972 when USEPA proposed to phase out leaded gasoline. US leaded gasoline phasing out was completed in 1986 and it took 20 years for another 120 countries including Indonesia, Australia and South Africa to achieve the target. Post 2006 only five countries (Algeria, Yemen, Afghanistan, Iraq, and Myanmar) were using leaded gasoline, and in 2021, Algeria became the last country to ban leaded gasoline marking the success story of a global collaboration. However, along with the feat, a grave concern about the fate of the already released Pb compounds from automobile exhaust loomed.

The atmosphere is the first recipient of the gasoline exhaust in the form of volatile Pb halogenides[5]. After several days the emitted Pb compounds settle on the top soil. Residence time of Pb in soil is 100–200 years[6]. Hence it was presumed that the legacy Pb from the global use of leaded gasoline will prevail in the environment. Indeed, a strong evidence of recirculating legacy lead in the atmosphere from soil resuspension were reported from different corners of the world. The fingerprinting of the source was done by the immutable Pb isotopic signature[7–10]. Pb has four naturally occurring isotopes out of which ^{206}Pb, ^{207}Pb, and ^{208}Pb are radiogenic. ^{204}Pb is the least abundant and the only non-radiogenic Pb isotope. Hence the difference in isotopic signature of Pb bearing minerals arises from the relative proportion of initial U–Th–Pb in the system and radioactive decays of ^{238}U, ^{235}U, and ^{232}Th. The relative atomic weight differences between the isotopes of Pb are minimal resulting in minimal mass-dependent Pb isotope fractionation in natural physical, chemical, and biological processes[11–13]. Pb isotopes are an effective tool for tracing Pb pollution as they do not fractionate during industrial or environmental processes and preserve the source signature even after degradation, processing, and transportation.[14].

South and South East Asian countries have recently come under scrutiny of Pb pollution due to several reasons. In India, Thailand, and Vietnam, more than 250 million children have blood lead level > 5 microgram.decilitre^{-1} (ug dL^{-1})[15]. Additionally, present day Pb emissions have surpassed past century emission from leaded gasoline used in these countries[16]. Lastly, several countries including Indonesia and Myanmar in the region were using leaded gasoline until this century.

Recent source apportionment studies of atmospheric Pb over Singapore, Thailand, Vietnam (referred to as SEA countries herein), and India by utilising Pb isotopic compositions and elemental ratios of aerosols[7,10,17–23] have identified the potential sources to be crust, sea spray, coal combustion, high temperature industrial activities, vehicular and ship traffic, solid waste incineration and biomass burning. In addition to these modern sources, historic Pb deposited on top soil from leaded gasoline emissions still recirculates in the atmosphere[7,9,17]. As Indonesia used leaded gasoline until 2006[24], and Myanmar until 2016[25], historic Pb recirculation may contribute substantially towards atmospheric Pb in the region. All past studies considered linear 2 or 3 endmember mixing models that may lead to over-simplification of the dynamics of atmospheric Pb pollution by exclusion of potential contributors. To overcome the issue of multiple end members, Bayesian stable isotope mixing models such as MixSIR, SIAR, and MixSIAR has been widely used in the field of ecology to study food webs and infer the diets of consumers based on stable isotope systems such as δ^{13}C, δ^{15}N and δ^{34}S[26,27]. Recently, MixSIAR has also been used in few source apportionment studies concerning Pb pollution that utilises Pb isotopic compositions of pollution sources[28–32]. Isotopic systems such as δ^{13}C, δ^{15}N, and δ^{34}S permit the integration of concentration data within the MixSIAR framework, owing to the distinct concentrations associated with each element. For Pb isotopic system also the concentration-dependent model can be utilised where including concentration data results in identical concentrations for each ratio However, it may not be effective to execute concentration-dependent mixing models by utilising Pb concentration data solely, as it has large orders of magnitude variations across sources. Some of the sources may have concentration in percentage range compared to ppm or ppb range of other sources, that will introduce bias in model results. Thus, to avoid such biases, techniques, such as normalisation is useful. Normalisation of Pb concentration of the sources with a crustal element such as Al, Fe, Ti, etc can be an effective strategy. This study aims to perform a quantitative retrospective analysis of Pb isotope data of aerosols from the past two decades and their potential endmembers using mixing polygon simulation followed by MixSIAR analysis to distinctly understand the sources of atmospheric Pb. Utilising MixSIAR for source apportionment of atmospheric Pb over SEA countries and India will lead to discerning the sources that require revisiting and identification of any probable underdetermined source that should be prioritised in future studies.

Results and discussion

Identifying contributing sources. Despite some overlaps, the aerosols of (a) India, (b) Singapore & Thailand and (c) Vietnam plot in 3 distinct regions, with Singapore and Thailand overlapping with each other in ^{206}Pb/^{207}Pb vs ^{208}Pb/^{207}Pb space (Fig. 1a). The aerosols also exhibit a similar arrangement in ^{206}Pb/^{204}Pb vs ^{208}Pb/^{204}Pb space (Supplementary Fig. 1). This indicates that atmospheric Pb is either sourced from different endmembers in different regions or common sources have variable contributions in different countries. The sources are distributed along the diagonal of the three-isotope space, with certain sources bracketing the aerosol samples and others positioned at intermediate points.

When analysing in ^{206}Pb, ^{207}Pb, and ^{208}Pb space, the median probabilities of the aerosols to fall inside the mixing envelope formed by these sources were 32%, 36%, 44%, and 40% for Singapore, Thailand, Vietnam, and India respectively when the conventional endmembers (coal from India, Indonesia, Vietnam and south China, SEA and Indian ore, unleaded and leaded fuel, solid waste and biomass burning in SEA and crust) were considered[7,17,18,33–43](Fig. 1b). Analogous probabilities were obtained in ^{206}Pb/^{204}Pb, ^{207}Pb/^{204}Pb and ^{208}Pb/^{204}Pb space, which is provided in Supplementary Fig. 2. The data for probabilities of all the aerosols are provided in Supplementary Data 1 [44]. These low median probabilities observed in both the isotope spaces for all the four countries indicates that there must be sources that were not considered in previous studies.

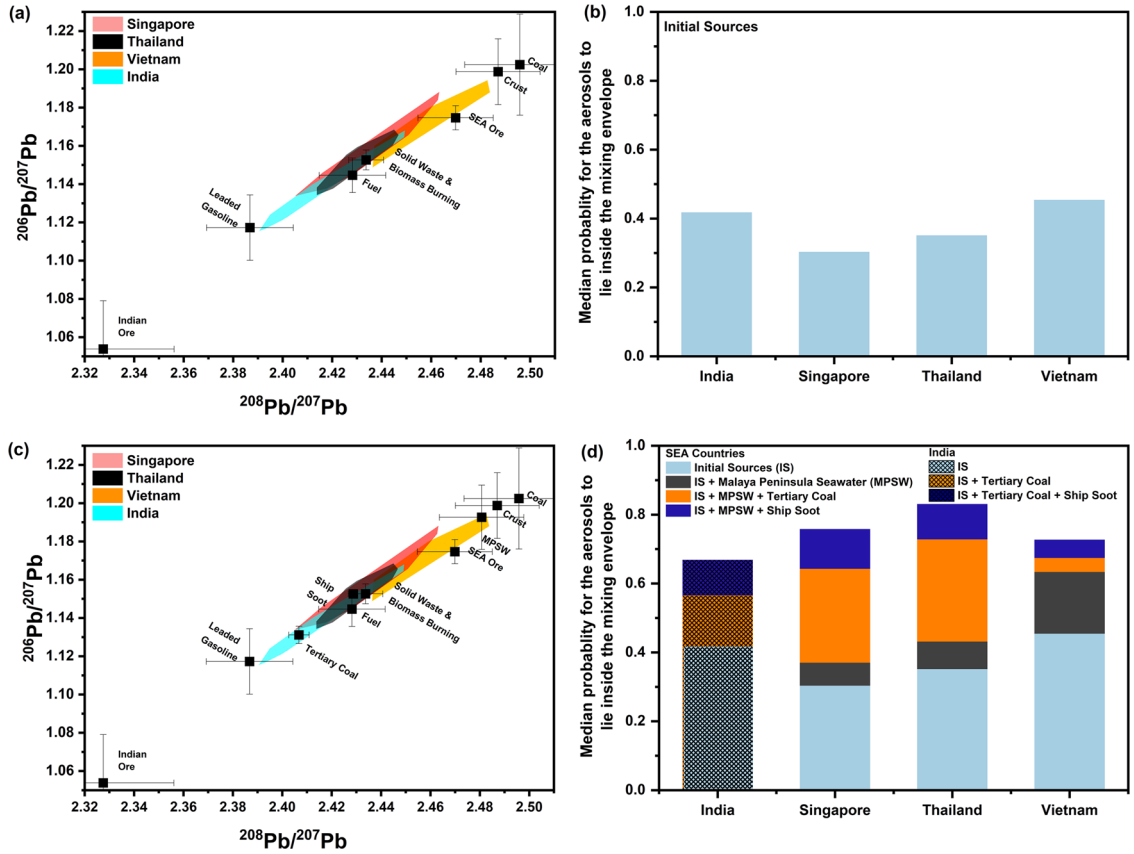

Fig. 1 Aerosol mixture and sources in three isotope space and their probability to lie inside the source defined mixing envelope. a Three—isotope plots of the aerosol mixtures from India, Singapore, Thailand, Vietnam, and their initial sources from previous literatures in $^{208}Pb/^{207}Pb$ vs $^{206}Pb/^{207}Pb$ space. The error bars signify 1 SDs of the sources and **b** Bar plots depicting the median probability of the aerosol mixtures to fall inside the mixing envelope constructed by the initial sources, determined with the help of 3 - dimensional mixing polygon simulation in $^{206}Pb/^{207}Pb$, $^{208}Pb/^{207}Pb$ and $^{208}Pb/^{206}Pb$ space **c** Three—isotope plots of the aerosol mixtures from India, Singapore, Thailand, Vietnam and their initial sources along with the additional sources in $^{208}Pb/^{207}Pb$ vs $^{206}Pb/^{207}Pb$ space and **d** Bar plots depicting the median probability of the aerosol mixtures to fall inside the mixing envelope constructed by the initial and additional sources, determined with the help of 3—dimensional mixing polygon simulation in $^{206}Pb/^{207}Pb$, $^{208}Pb/^{207}Pb$ and $^{208}Pb/^{206}Pb$ space. The aerosol mixture data for respective countries are depicted as fields, encompassing all the data points.

Based on elemental ratios calculated from elemental concentration data provided in previous investigations, it is observed that aerosols in Singapore, Thailand, and Vietnam closely align with the typical Na/Mg value of seawater (~8) (Fig. 2a)[20,21,35,45]. The coastal waters around Malaya Peninsula have a wide range of Na/Mg values that overlap with that of the aerosols from Singapore, Thailand, and Vietnam (Fig. 2a)[46–48]. Moreover, the MPSW has higher concentration of Pb (range = 24.8–368 pmol kg^{-1}) compared to the average Pb concentration in South China seawater (67.2 pmol kg^{-1}) and Bay of Bengal (68.1 ± 10.52 pmol kg^{-1})[16,49]. Seawaters in the northern (North Atlantic, Pacific, and Antarctic surface waters) and southern hemisphere (East Australian coastal shelf waters) also have lower Pb concentration ranging from 12 to 160 pmol.kg^{-1}[50]. This suggests that the aerosols may exhibit some degree of influence from seawater in addition to other predominant sources. Similarly, the V/Ni ratios in aerosols from India, Singapore, and Vietnam demonstrate characteristics of heavy oil and ship emissions[18,23,35,36,51–54] (Fig. 2b). Tertiary coal from India exhibit a distinctively lower $^{206}Pb/^{207}Pb$[7] composition and has not been used as an end member in previous studies. The comparable isotopic composition of tertiary coal, wood, and wood charcoal[7], coupled with India's substantial dependence on fuelwood[55], makes it necessary to consider this as an end member. Thus, it is imperative that all these additional sources are considered while calculating the contribution of each source towards the aerosol of these countries. All the initial sources and additional sources plotted in $^{206}Pb/^{207}Pb$ vs $^{208}Pb/^{207}Pb$ three—isotope space are presented in Fig. 1c. The three—isotope plot in $^{206}Pb/^{204}Pb$ vs $^{208}Pb/^{204}Pb$ space is presented in Supplementary Fig. 3. Incorporation of these previously excluded sources (sea spray, tertiary coal and ship soot) increased the area of the mixing envelope and consequently the median probabilities for the aerosols to lie inside the mixing envelope in $^{206}Pb/^{207}Pb$, $^{208}Pb/^{207}Pb$ and $^{208}Pb/^{206}Pb$ space to 76%, 83%, 73% and 67% for Singapore, Thailand, Vietnam, and India respectively (Fig. 1d). The results obtained from the polygon simulation performed in $^{206}Pb/^{204}Pb$, $^{207}Pb/^{204}Pb$, $^{208}Pb/^{204}Pb$ space are discussed in Supplementary Note 1 (Supplementary Fig. 4). Data is provided in Supplementary Data 1 [44].

On performing Analysis of Variance (ANOVA) at 0.05 significance level, on the probability results, it was observed that the addition of the MPSW resulted in significant increase in probabilities for Singapore, Thailand, and Vietnam. Significant increases for India, Singapore, and Thailand were also observed when tertiary coal and ship soot were added as sources. However, tertiary coal and ship soot had no significant effect on Vietnam aerosols.

Insights from linear mixing models. From the three—isotope plot (Fig. 3), it can be observed, that the aerosols do not fall on

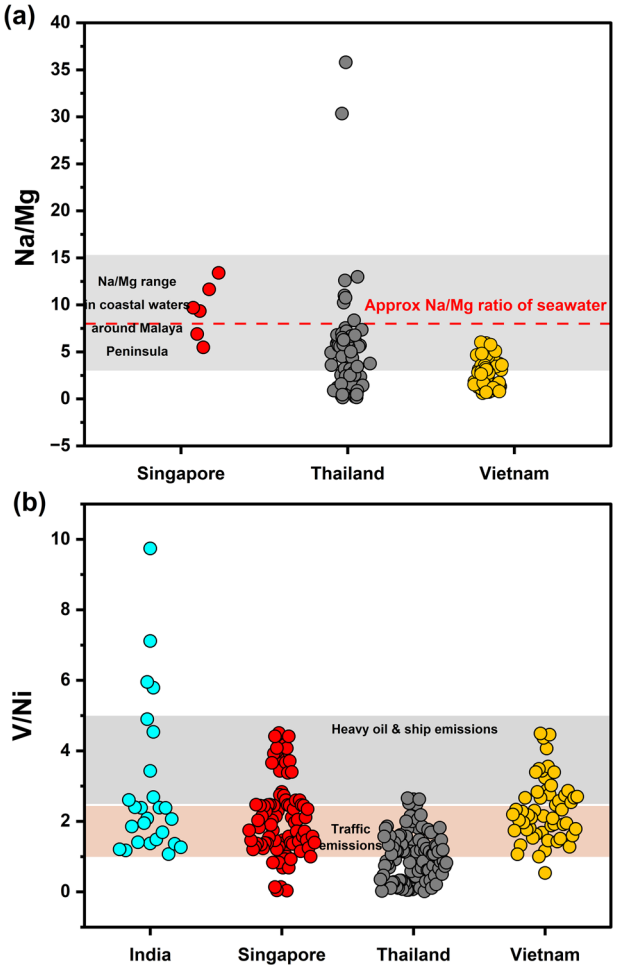

Fig. 2 Elemental ratios of aerosols demonstrating influences of sea spray and ship emissions. Trends in **a** Na/Mg ratios in aerosol mixtures from Singapore, Thailand, and Vietnam; **b** V/Ni ratios in India, Singapore, Thailand, and Vietnam. The shaded regions illustrate the ranges observed in sources for which these ratios serve as representative indicators.

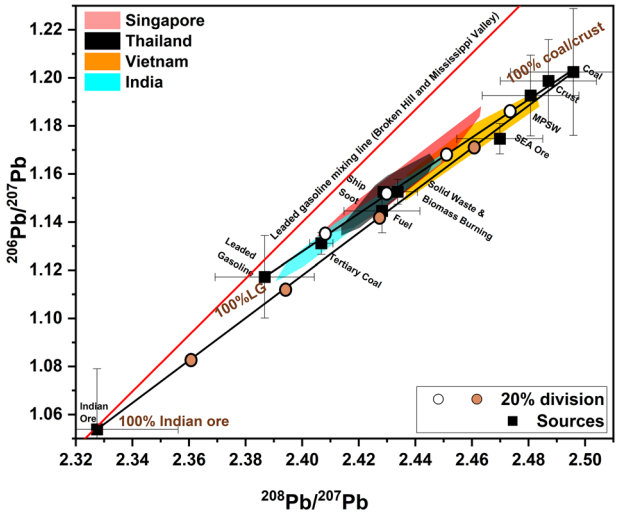

Fig. 3 Geometric mixing of sources. Geometric mixing lines constructed in three—isotope space between two extreme sources for SEA country aerosols and Indian aerosols segregated into divisions of 20%. The sources considered for SEA countries are leaded gasoline on one side and coal/crust on the other. For India, the sources are Indian ore on one side and coal/crust on the other. The traditional mixing line for leaded gasoline is depicted in red, constructed with the isotopic compositions of Broken Hill and Mississippi Valley ores. The aerosol mixture data for respective countries are depicted as fields, encompassing all the data points.

the traditional leaded gasoline mixing line constructed using Australian Broken Hill ore and USA's Mississippi Valley ore[56]. While the mean of the regional leaded gasoline data also deviates marginally from this traditional mixing line, the standard deviations exhibit alignment with it. Thus, in the three-isotope space ($^{206}Pb/^{207}Pb$ vs $^{208}Pb/^{207}Pb$), the aerosols from India are positioned between regional leaded gasoline and Indian ore on one end, and crust and coal on the other end. On the other hand, the SEA aerosols fall between local leaded gasoline and tertiary coal on one side, and crust and coal on the other side. Crust and coal are very similar in isotopic compositions and it is difficult to distinguish between their individual contribution towards aerosol Pb.

A simple two-source geometric mixing line between leaded gasoline and crust/coal for the SEA countries (Fig. 3) reveals that coal/crust contributes from 20 to 60% towards the Singapore and Thailand aerosols while the rest is from leaded gasoline. In the case of Vietnam, the contribution range for coal is 40–90% and the rest of the aerosol Pb stems from leaded gasoline. Similarly for Indian aerosols, a two-source mixing line between Indian ore and coal/crust indicates that coal/crust contributes 25–60% towards the aerosol Pb and the rest is from Indian ore. In such a binary mixing system, the contribution of each source is actually weighted based on its proximity to the composition of the mixture[57,58]. However, in this study, as there are more than two sources, their relative contributions cannot be accurately represented by this binary weightage method based on proximity. Thus, for gaining primary insight into the contributions of multiple sources towards the aerosol mixtures a simple two-isotope ratio linear mixing model having >3 sources is beneficial. The optimum results derived from the iterative procedure in such an underdetermined mixing system are presented in Fig. 4. The entire dataset is presented in Supplementary Data 2 [44] The model outcomes indicate considerable variability in the contributions of leaded gasoline (0–75%), natural sources (1–70%), coal (0–67%), intermediate sources (0–91%), for SEA countries. In India the contributions of leaded gasoline, natural sources, coal, intermediate sources, and Indian ore range from 18–44%, 1–62%, 0–30%, 2–37%, and 0–39%, respectively. In fact, the extreme values of these ranges seem to be impractical. For example, zero percent contribution obtained for different sources, especially crust is not possible. Further, a contribution of up to 75% for leaded gasoline in the case of Singapore aerosols also is highly unlikely. In Singapore, where only 1.2% of the fuel mix used for electricity generation is coal[59], it is highly unlikely that local and transboundary coal emissions will contribute up to 53%. Such unlikely extremities may indicate overemphasis on one source, causing it to dominate the mixture, while suppressing other sources. However, some useful primary observations from this linear model can be drawn:

A. Sources demonstrating the highest contribution percentages for all the four countries are leaded gasoline and natural sources (treating a spike of 91% from intermediate sources in case of Vietnam as an outlier). Thus, these two sources can be the dominating factors controlling the Pb isotopic compositions of the aerosol mixtures.
B. Singapore demonstrating the highest contribution percentage from leaded gasoline might have greater influence from the source compared to other countries.

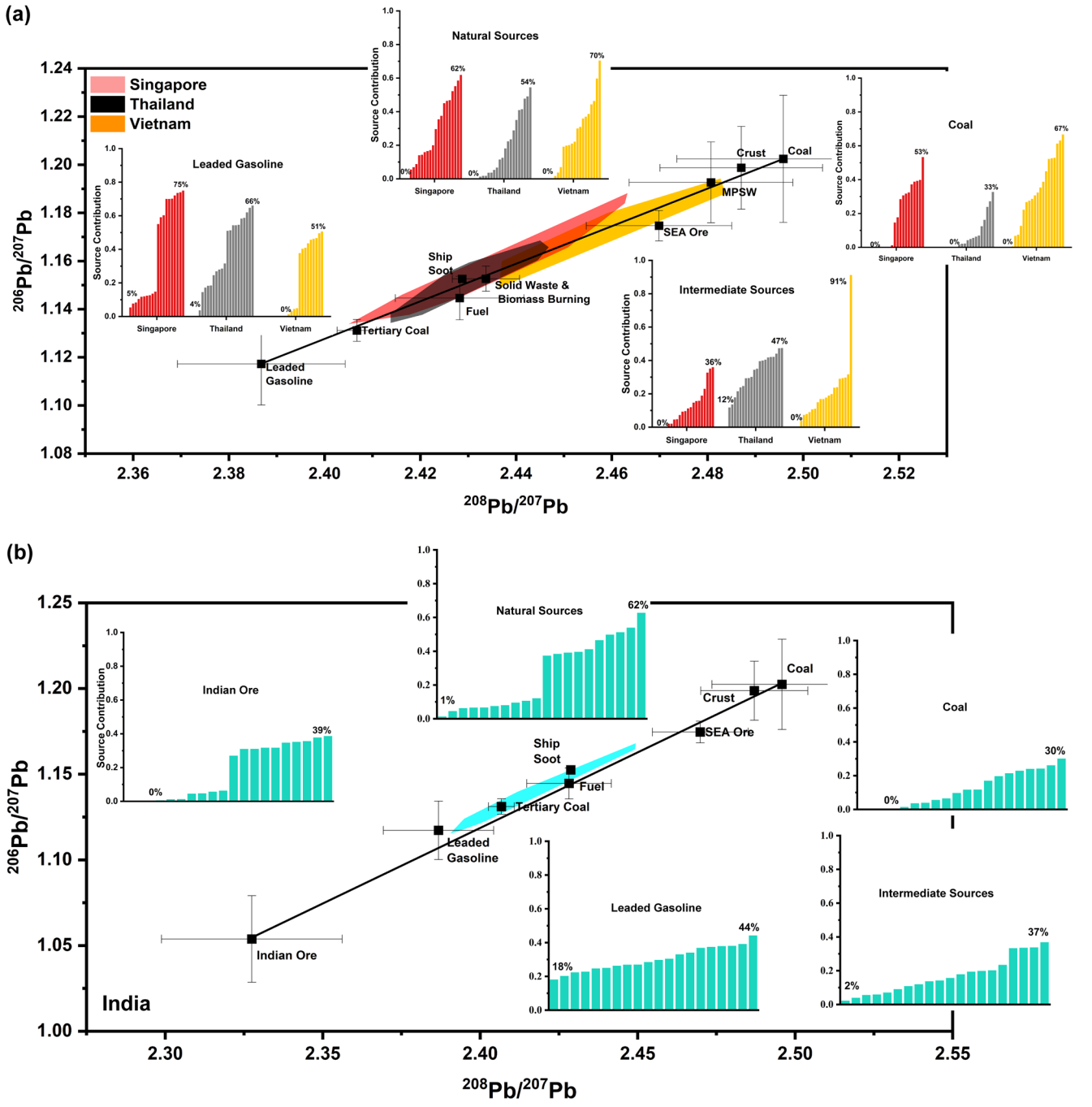

Fig. 4 Source contributions determined from simple linear mixing model. Bar plots for each source within insets in the three—isotope plots of aerosols and sources representing source contributions for **a** SEA countries and **b** India in $^{208}Pb/^{207}Pb$ vs $^{206}Pb/^{207}Pb$ space. Sources considered are 5 for India (coal, crust, Indian ore, leaded gasoline, and intermediate) and 4 for SEA countries (coal, crust, leaded gasoline, and intermediate). The intermediate source represents the mean of tertiary coal, unleaded fuel, ship soot, solid waste & biomass burning, and SEA ore for SEA countries, and tertiary coal, unleaded fuel, ship soot, and SEA ore for India. Percentages at the end of each bar depict the range of contributions, from the lowest to the highest, for each source.

C. Vietnam can have a greater influence from coal.
D. Among the 4 countries, India receives the least contributions from leaded gasoline.
E. The intermediate sources are the least to moderate contributing factors towards the aerosol mixtures.

However, as this linear model lacks the probabilistic framework of Bayesian models such as MixSIAR, which allows for incorporating uncertainties, the results obtained from the linear model cannot be fully relied upon. The broad variation of source contributions obtained from the linear model has to be narrowed down for a more accurate estimation of the relative proportions of different sources leading to a better understanding of the underlying source dynamics and their potential impacts. The results of the linear mixing model thus, were cross-verified using MixSIAR, where overlapping sources can be better resolved with the incorporation of standard deviations.

Insights from MixSIAR analysis. Similar trends between source contribution results obtained from both linear model and MixSIAR were observed. Both approaches identify natural sources

and leaded gasoline consistently as dominant contributors, indicating their substantial impact on the aerosol mixtures. Leaded gasoline contributed the highest towards Singapore aerosol Pb as was observed from the linear model outcome. Similarly, coal has a greater influence on Vietnam than towards other SEA countries. Contrarily, tertiary coal emerges as a substantial contributor to aerosol Pb levels in Thailand and India, an observation not evident from the linear model.

Thus, the basic observations from the MixSIAR analysis (Fig. 5; Supplementary Data 2)[44] performed on aerosol Pb samples from India and SEA countries are:

A. Natural background (UCC) is a prominent aerosol Pb source for India and the SEA countries.
B. Tertiary Coal combustion and ore processing dominate the anthropogenic Pb emissions in India.
C. Ship emission is probably an underdetermined source in India and to some extent in Thailand.
D. In the SEA countries, the largest anthropogenic source of aerosol Pb is the persistence of legacy Pb from the use of leaded gasoline in the last century.

The roughly analogous results observed between the two distinct analytical approaches (linear model and Bayesian model) lend credibility to the findings. Thus, the identified sources and their contributions are likely to be representative of the actual atmospheric Pb pollution dynamics of India and SEA countries.

In detail, the resultant contributions of the individual sources obtained from the MixSIAR model (Fig. 5) reveal a consistent contribution of background crustal material to all 4 countries. This is consistent with the linear model results as well as previous investigations that demonstrated a mixture of crustal and anthropogenic contributions towards atmospheric Pb[17,18,20,21,35,36]. Among other natural sources in SEA, MPSW made median contribution up to 14% in Vietnam. In Singapore and Thailand, the median contribution of Malaya Peninsula seawater was up to 10% and 9% respectively. Surprisingly the major anthropogenic contributor towards Pb in SEA was found to be leaded gasoline (median contribution up to 39%), even after approximately quarter century of leaded gasoline phase out in the three countries. Tertiary coal contributed substantially to Thailand (median contribution up to 20%). Tertiary coal fields are found in north-eastern India and there is proof of long-range transport of particulate matter from northeast India to Thailand[60]. Some of the endmembers such as fuel, and solid waste & biomass burning did not appear to individually contribute much (median contribution ≤9%). Vietnam atmosphere receives the least contribution from ship soot, which corroborates with finding from previous literature where insignificant impact of ship soot was observed[19].

In India, ore processing (median contribution up to 26%) and tertiary coal combustion (median contribution up to 37%) are the major anthropogenic sources. Indian atmospheric Pb was derived from ship emissions to some extent (median contribution of up to 15%) which was not considered in any of the previous studies. Leaded gasoline resuspension contributes relatively small (up to 9%) proportion of atmospheric Pb in India. To validate these results, the model was run in ^{204}Pb space for Singapore aerosols having the largest spread in three—isotope space, the outcomes of which are provided in Supplementary Note 2 and Supplementary Fig. 5. Further validations have been performed using concentration dependent Bayesian and linear models as discussed in Supplementary Note 3. The results for the concentration dependent model align with the concentration-independent ones as demonstrated in Supplementary Figs. 6 and 7.

Tertiary coal, wood, and wood charcoal from India exhibit comparable Pb isotopic compositions, which prompted their a priori grouping for MixSIAR modelling. In rural, semi-urban areas, and brick kilns, of India, fuelwood still remains a predominant energy source, with consumption reaching a staggering 216.4 million tonnes annually, as of 2011[55]. As radiogenic Gondwana coal dominates Indian coal reserves over less radiogenic tertiary coal[61], emissions from tertiary coal are likely to be less prominent. With analogous Pb isotopic composition[7], open burning of wood and wood charcoal could potentially be the most substantial contributor to atmospheric Pb in India only second to ore processing.

Pb emission estimates in the region show coal combustion in India emitted ~3500 tonnes of Pb in 2010 as compared to ~150 tonnes from Thailand[16]. Thus, probably emissions from coal combustion, fuelwood burning, and high-temperature metallurgy in India have overwhelmed the leaded gasoline Pb signature which is not the case for the SEA countries.

The average concentration of Pb in UCC is 17 ppm. Thus, aerosolisation of soil produced by weathering of the upper crust contains substantial Pb. Crustal dust as the natural background

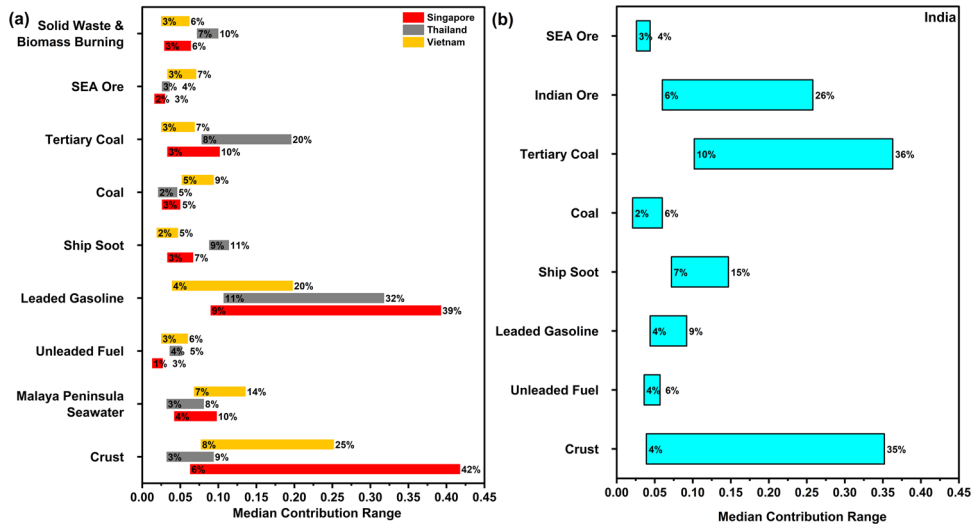

Fig. 5 MixSIAR results depicting median contributions of sources. Median contribution of individual sources towards atmospheric Pb in **a** SEA countries and **b** India determined from MixSIAR simulation. The percentages on left-hand side and right-hand side of the bars represent the minimum and maximum contributions from each source respectively.

has been hypothesised in almost all the previous studies. MixSIAR analysis suggests, that in addition to the crustal dust, sea spray also contributed towards aerosol Pb in the SEA countries (up to 8–14%).

Previous studies in India showed that post-leaded gasoline phase-out, the atmospheric Pb ratios plot away from the leaded gasoline mixing line and closer to the mixing line between coal combustion and ore processing[10,18]. The results obtained from MixSIAR analysis are in line with this observation. The Indian peninsula has a long coastline. Since 1992, the Asian ship traffic has increased by 200%[62]. Trace element ratios (V/Ni) indicated ship emission to be a plausible source of heavy metals in Singapore and Vietnam aerosols[23,35] (Fig. 2b). However, Pb isotopic composition of this source was not measured. None of the studies on Indian aerosol postulated ship emission as a plausible source of aerosol Pb. Insufficient Pb isotope data of Heavy Fuel Oil used by ships may have led to underestimation of source contributions towards atmospheric Pb in India.

Migration rate experiments and field observations suggest that gasoline Pb is retained in soil on generational time-span. Thus, resuspension of such soil could be an important source of atmospheric Pb. The contaminated roadside soils and dusts are often re-suspended by the turbulence created by the urban traffic[63]. Aerosols collected from the SEA countries in the past decade shows the largest anthropogenic source of aerosol Pb is leaded gasoline. Whether it is the result of transboundary transport from Myanmar and Indonesia using TEL additive till the 21st century or they are remobilisation of local top soil contaminated with legacy Pb remains a moot question.

Conclusion and future perspective. Pb wreaks its havoc silently and insidiously and hence often goes unrecognised. As atmosphere is the first recipient of the pollutant, identification of atmospheric Pb sources is of utmost importance. From a public health standpoint, inhalation and/or ingestion of atmospheric particles can be an important exposure pathway. Concentration of Pb bound to PM_{10} can contribute towards elevated BLL[64].

In the case of topsoil resuspension, simple yet effective abatement strategies such as covering the contaminated soils with clean soil have proved to be effective[65]. Regular and continuous monitoring of soil Pb could be performed with field portable XRF instrumentation. Future directions for research and policy to mitigate legacy Pb will require constant monitoring of soil Pb and thorough understanding of urban pedogenesis.

Previous research has typically focused on a limited set of end members, which may exclude important sources of Pb. In fact, it is evident from this analysis, that previously underdetermined sources such as and ship emissions contribute substantially towards atmospheric Pb. Additionally, non-combustible vehicular sources like tyre and brake wear have been found to be important contributors towards atmospheric Pb in other countries as they contain high concentration of Pb (10–55 ppm).[9,66,67] In fact, evidence of the presence of brake wear in atmospheric aerosols can be found in Vietnam from Cu/Sb ratios[35]. However, unfortunately, no local Pb isotopic data is available for these sources. Other non-combustible vehicular sources having even higher Pb concentrations include asphalt (738 ppm) and road paint (88 ppm) dusts generated from abrasion due to traffic[67]. Subsequently, these sources must be sampled locally and analysed for Pb isotopic compositions. Further Pb isotope data of sources such as Indian ore which is different from SEA ore is three decades old and hence is in urgent need of reanalysis. Extensive Pb isotope data of coal having high $^{206}Pb/^{207}Pb$ ratios is available globally. However, it can be observed from MixSIAR results that tertiary coal and wood charcoal having low $^{206}Pb/^{207}Pb$ ratio (from Assam, India) contributes heavily towards atmospheric Pb of Thailand and India. There are no Pb isotope data of coal from Thailand which may possess low $^{206}Pb/^{207}Pb$ ratio and contributes towards atmospheric Pb of SEA countries. Thus, to gain a comprehensive understanding of the sources and pathways of Pb in natural systems, it is important to quantify the isotopic composition of Pb in all potential end members.

Methods

Source and mixture data compilation. A comprehensive literature review was conducted to gather Pb isotope and relevant elemental concentration data of aerosol samples collected from South and Southeast Asian countries over the past decade. The studied regions encompass India, and SEA countries from where a total of 341 aerosol Pb isotope data points were acquired[7,10,16–18,20–22,35,36]. These aerosol data were compiled into 4 mixture datasets, one for each country, ready, to be fed to the mixing polygon and MixSIAR modelling frameworks. The Pb isotope data of the potential sources of these aerosols available from the same and cross-referenced literatures were compiled as source datasets for India and SEA countries. The isotope data was visualised in three isotope space ($^{206}Pb/^{207}Pb$ vs $^{208}Pb/^{207}Pb$). Further details about the source data are provided in the following section.

Constructing the mixing envelope. The ability of Pb to travel long distances due to its high atmospheric residence time makes it crucial that, all natural and anthropogenic sources from the regional and local emissions are taken into consideration. Natural background contribution from upper continental crust (UCC) has been consistently observed in SEA countries[17,20,36] and India[18,22] Among the regional sources, coal combustion emissions (both Gondwana and Tertiary coal) from India[7,18], China[20], Vietnam[20,35], Indonesia[23], and Thailand[20] have been proven to influence the SEA nations. Local sources include traffic emissions, high temperature metallurgy, historic leaded gasoline recirculation, and solid waste incineration[17,20,21,23,36].

The means and 1SDs of $^{206}Pb/^{207}Pb$, $^{208}Pb/^{207}Pb$, and $^{208}Pb/^{206}Pb$ of the well-documented sources were computed to perform a mixing polygon simulation (Monte Carlo) in 3-dimensional space in R. The simulation on the same dataset was also performed in $^{206}Pb/^{204}Pb$, $^{207}Pb/^{204}Pb$, and $^{208}Pb/^{204}Pb$ space which is discussed in Supplementary Note 1. The script for the simulation is available at http://www.famer.unsw.edu.au/downloads.html. Each iteration of the simulation generates a mixing envelope. The proportion of iterations in which the mixing envelope includes the isotopic composition of the aerosols within it, represents the probability of the aerosols ($n = 341$) for lying inside the envelope[68]. To increase this probability, the sources mentioned in previous literatures as potential sources, although lacking Pb isotope data were tried to be incorporated by finding proper Pb isotope data through literature survey.

Ship emission, and sea spray aerosols were indicated to be probable sources in previous investigations based on elemental ratios such as V/Ni and Na/Mg respectively[18,20]. As Pb isotopic compositions of these sources were not measured in those studies, the sources could not be considered in linear mixing models used in the studies. From literature survey, only one Pb isotopic data representative of regional ship emissions (ship soot) in Vietnam[19] was found. Since there was only one data point for regional ship soot, ship emission data available from Germany having only 10‰ and 4‰ difference in $^{206}Pb/^{207}Pb$ and $^{208}Pb/^{207}Pb$ spaces respectively was also combined[69]. Owing to relatively high concentration of Pb in Malaya Peninsula seawater (MPSW) compared to global average sea water, we further considered Pb

isotopic compositions of seawater around Malaya Peninsula as a natural contributor (sea spray aerosol) to SEA aerosol Pb[49]. Thus, as anthropogenic contributors for all 4 countries, we included ship soot[19,69], leaded and unleaded gasoline, coal from Vietnam, India, Indonesia south China (referred to as coal herein), and tertiary coal & wood charcoal combustion emissions from India[7,17,18,33–35,37,39]. We performed a priori grouping of Indian tertiary coal & wood charcoal isotopic compositions (referred to as tertiary coal herein) as both the sources demonstrated similar ratios[7,70]. As transboundary Pb contaminator for India we considered ores of Indonesia, Thailand, and South China (referred to as SEA ore herein)[40,42,71,72]. The sources were separately selected for India and SEA countries, which are listed in Table 1. We added the sources one at a time and ran the mixing polygon simulation to observe the resultant changes in probabilities. The probabilities obtained per aerosol were subjected to Analysis of Variance (ANOVA) at 0.05 significance level.

Linear mixing model. The aerosol mixture was primarily visualised along a two-end member geometric mixing line, partitioned into intervals of 20%. The proximity of the aerosol mixture to each source on the line provides the relative contribution between the two considered sources[57]. Since, such an approach cannot consider more than 2 sources, following this, the aerosol mixture and the source Pb isotopic data were subjected to conventional mass balance based linear mixing model based on the principle of IsoSource by employing the following equations[73]:

$$\left(\frac{206}{207}Pb\right)_{mix} = \left[f_a\left(\frac{206}{207}Pb\right)_a + f_b\left(\frac{206}{207}Pb\right)_b + \ldots + f_n\left(\frac{206}{207}Pb\right)_n\right] \quad (1)$$

$$\left(\frac{208}{207}Pb\right)_{mix} = \left[f_a\left(\frac{208}{207}Pb\right)_a + f_b\left(\frac{208}{207}Pb\right)_b + \ldots + f_n\left(\frac{208}{207}Pb\right)_n\right] \quad (2)$$

$$f_a + f_b + \ldots + f_n = 1 \quad (3)$$

where $\left(\frac{206}{207}Pb\right)_{mix}$ and $\left(\frac{208}{207}Pb\right)_{mix}$ are isotopic compositions of the aerosol mixtures; $\left(\frac{206}{207}Pb\right)_{a,b,\ldots,n}$ and $\left(\frac{208}{207}Pb\right)_{a,b,\ldots,n}$ are isotopic compositions of the sources and $f_{a,b,\ldots,n}$ is the unknown proportional contribution for each source towards the aerosol mixture. It is worth noting that these equations are approximations that work because of the limited fractional variance of Pb isotope data. This system using two isotope ratios can provide unique solution for each f, up to $n = 3$. However, when $n > 3$, this becomes an underdetermined system with no unique solution[57]. This linear model was computed for each country by considering the mean isotopic composition of the sources. For India, the considered sources consist of leaded gasoline and Indian ore as less radiogenic sources; coal and crust as the most radiogenic sources that bracketed all the Indian aerosols. An intermediate source was derived as the mean of unleaded fuel, tertiary coal, ship soot, and SEA ore that falls in the field of the aerosol mixtures. In case of SEA countries, the less radiogenic source was leaded gasoline. MPSW and upper continental crust were merged as natural sources due to their closely related isotopic compositions. Consequently, natural sources and coal constituted the radiogenic end members, while the intermediate end member was the mean of tertiary coal, unleaded fuel, solid waste & biomass burning, ship soot, and SEA ore. Thus, the total number of sources considered for India are 5 and SEA countries are 4, making the linear model framework an underdetermined system. To estimate the source proportions ($f_{a,b,\ldots,n}$) from such an underdetermined system, iterative approach as followed in traditional models like IsoSource was employed[57]. The linear model was made to perform an optimisation process to find the optimal value for mixture of sources that matches given target aerosol mixture values. The optimisation process performs ten restarts, each starting with a set of randomly assigned initial values for source proportions for the five sources. This process of conducting 10 restarts in the model was repeated 10 times to yield a set of 10 distinct sets of best results. The goal is to achieve an average deviation of 0.5‰ or less between the predicted and target mixture values. Two target aerosol mixtures, one with most radiogenic signature and the other with least, were selected. This selection is based on the fact that the source contribution towards the aerosols, lying between these extremes, will fall within the range of source contributions obtained for these extreme target aerosols. The model then identifies the best solution based on the lowest deviation. The potential combinations of source proportions sum up to 100%.[57].

Limitations of a linear model. While these linear systems can yield initial insights, their accuracy and precision are limited for a system having multiple end members. Primarily, they fail

Table 1 Individual sources of Atmospheric Pb in SEA countries and India.

India		South East Asia	
Individual Sources	**References**	**Individual Sources**	**References**
Crust	7,36,41	Crust	7,36,41
Gondwana Coal	7,18,33,35,37,39		
Indian Tertiary Coal & Wood Charcoal	7	Malaya Peninsula Seawater	49
Unleaded Fuel	7,33,35,43	Gondwana Coal	7,18,33,35,37,39
		Indian Tertiary Coal & Wood Charcoal	7
		Unleaded Fuel	7,33,35,43
Leaded Gasoline	17,34		
Indian Ore	38		
Transboundary SEA Ore	40,42,71,72	Leaded Gasoline	17,34
Ship Emissions	19,69	SEA Ore	33,40,42,71
		Solid Waste Incineration & Biomass Burning	17
		Ship Emissions	19,69
Aerosol Mixture	7,10,18,22	Aerosol Mixture	7,10,16,19–23,35–37

to yield distinct solutions when sources outnumber equations, a common occurrence in pollution apportionment studies. Furthermore, they solely account for source means without incorporating associated variability (standard deviations). Given the multiplicity and inherent heterogeneity of sources, it becomes imperative to consider both means and standard deviations in the modelling framework to achieve enhanced accuracy. Thus, the necessity of using Bayesian statistics based mixing models arises, that integrates the mean and uncertainty of the data into its framework. It is based on Markov Chain Monte Carlo (MCMC) simulation that produces plausible source proportion results based upon probability densities of the fed data[74]. This is particularly useful for analysing complex mixing problems where there are many more sources compared to isotope systems. Source apportionment of atmospheric Pb over a region requires consideration of isotopic compositions of multiple endmembers in which the Pb isotopic composition of each endmember may be spread over a large range. Thus, it is preferable to apply robust Bayesian models such as MixSIAR to these kinds of data set where we can consider multiple endmembers along with their uncertainty for determination of the proportion of contribution by the sources.

Bayesian statistics based mixing model. The means and 1SDs of $^{206}Pb/^{207}Pb$, $^{208}Pb/^{207}Pb$, and $^{208}Pb/^{206}Pb$ of the sources, listed in Table 1 and the isotopic composition of the aerosols were fed to the model framework in R[75]. Due to limited number of aerosol and source data, with respect to ^{204}Pb, the comprehensive modelling was conducted using ^{206}Pb, ^{207}Pb, and ^{208}Pb isotopes. With inadequate data, the standard deviations may not accurately represent the true heterogeneity in sources. Consequently, it can compromise the accuracy and reliability of MixSIAR results by generating higher uncertainties in source contributions and ambiguous source identifications. However, as the ratios relative to ^{204}Pb stem from distinct decay chains and possess the ability to discern source ages, the utilisation of ^{204}Pb contributes to improved source apportionment accuracy[32,76]. Thus, in order to validate the reliability of the modelling results derived from ^{206}Pb, ^{207}Pb, and ^{208}Pb isotopes, the aerosol mixture from Singapore and its potential end members were subjected to MixSIAR analysis specifically considering the ^{204}Pb isotope as well (Supplementary Note 2). The challenges for performing the analysis in ^{204}Pb space for this particular dataset are also discussed in Supplementary Note 2. While compiling the source data, the values that were greater/less than 2 SD of the mean were treated as outliers and eliminated. This reduces the overlapping of sources and increases model accuracy[31]. The mixture data was combined every 5‰ with respect to $^{206}Pb/^{207}Pb$ ratios. The model was run using 3 parallel chains with a "long" MCMC chain length of 300,000 iterations. To ensure that the chains reached equilibrium, the first 200,000 iterated values were discarded/"burned". The remaining samples were "thinned" by keeping every 100th iterated value[77]. The model convergence was checked using Gelman Rubin diagnostics.

Concentration-dependent mixing models. Concentration-dependent stable isotope mixing models are important in source apportionment studies, particularly when dealing with multiple sources having differences in elemental concentrations[78,79]. Accurate concentration data for the sources is a necessity for effectively utilising concentration-dependent stable isotope mixing models. This accuracy can only be achieved when isotope and elemental concentration data of the same sample set are available. While compiling the Pb isotope data of the south Asian and SEA aerosols along with their end members, this study identified substantial gaps in the availability of their corresponding elemental concentration data that are discussed in Supplementary Note 3.1. Hence, we could test the concentration dependent linear model for Indian aerosols only. MixSIAR model with concentration input was tested for Singapore and Thailand aerosols as they have the largest and the smallest variability in aerosol Pb isotope ratios in three isotope spaces respectively (Fig. 1a). The overarching conclusions drawn from the concentration independent model align with that of the concentration dependent model. The approaches followed for this process and the final outcomes are presented in Supplementary Notes 3.1 to 3.3. There were several challenges (discussed in Supplementary Notes 3.1) due to the unavailability of elemental concentration data in several literatures due to which concentration-dependent model outcomes cannot be entirely relied upon for this study. The dataset adopted for the concentration-dependent Bayesian and linear models are presented in Supplementary Tables 1 and 2, respectively.

Data availability

The input data for the models are adopted from previously published literature, as listed in Table 1. The probabilities from mixing polygon simulation and contribution fractions generated from linear & Bayesian model in this study are available in Supplementary Data 1 and Supplementary Data 2 respectively and also in Zenodo (https://doi.org/10.5281/zenodo.10101283).

Code availability

The R codes used for running the mixing polygon simulation and MixSIAR model are available publicly at http://www.famer.unsw.edu.au/software/polygon.html and https://zenodo.org/records/1209993, respectively.

Received: 30 May 2023; Accepted: 20 November 2023;
Published online: 12 December 2023

References

1. Sturges, W. T. & Barrie, L. A. Lead 206/207 isotope ratios in the atmosphere of North America as tracers of US and Canadian emissions. *Nature* **329**, 144–146 (1987).
2. Planchon, F. A. M. et al. One hundred fifty–year record of lead isotopes in Antarctic snow from coats land. *Geochim. Cosmochim. Acta* **67**, 693–708 (2003).
3. Sturges, W. T. & Barrie, L. A. Stable lead isotope ratios in arctic aerosols: evidence for the origin of arctic air pollution. *Atmospheric Environ.* **23**, 2513–2519 (1989).
4. Patterson, C. C. Contaminated and natural lead environments of man. *Arch. Environ. Health Int. J.* **11**, 344–360 (1965).
5. Radojevic, M. & Harrison, R. M. Concentrations and pathways of organolead compounds in the environment: a review. *Sci. Total Environ.* **59**, 157–180 (1987).
6. Erel, Y. Mechanisms and velocities of anthropogenic Pb migration in Mediterranean soils. *Environ. Res.* **78**, 112–117 (1998).
7. Mitra, A. et al. Lead isotope evidence for enhanced anthropogenic particle transport to the himalayas during summer months. *Environ. Sci. Technol.* **55**, 13697–13708 (2021).
8. Morton-Bermea, O., Rodríguez-Salazar, M. T., Hernández-Alvarez, E., García-Arreola, M. E. & Lozano-Santacruz, R. Lead isotopes as tracers of anthropogenic pollution in urban topsoils of mexico city. *Geochemistry* **71**, 189–195 (2011).
9. Resongles, E. et al. Strong evidence for the continued contribution of lead deposited during the 20th century to the atmospheric environment in London of today. *Proc. Natl. Acad. Sci. USA* **118**, e2102791118 (2021).
10. Sen, I. S., Bizimis, M., Tripathi, S. N. & Paul, D. Lead isotopic fingerprinting of aerosols to characterize the sources of atmospheric lead in an industrial city of India. *Atmos. Environ.* **129**, 27–33 (2016).
11. Doe, B. R. *Lead Isotopes*; Springer Science & Business Media (1970).
12. Flegal, A. R.; Smith, D. R. Measurements of environmental lead contamination and human exposure. In *Reviews of Environmental Contamination and Toxicology. Continuation of Residue Reviews*; Ware, G. W., Ed.; Reviews of

Environmental Contamination and Toxicology; Springer. 1–45 (Springer, New York, NY, 1995).
13. O'Nions, R. K., Frank, M., von Blanckenburg, F. & Ling, H.-F. Secular variation of Nd and Pb isotopes in ferromanganese crusts from the Atlantic, Indian and Pacific Oceans. *Earth Planet. Sci. Lett.* **155**, 15–28 (1998).
14. Komárek, M., Ettler, V., Chrastný, V. & Mihaljevič, M. Lead isotopes in environmental sciences: a review. *Environ. Int.* **34**, 562–577 (2008).
15. Ericson, B. et al. Blood lead levels in low-income and middle-income countries: a systematic review. *Lancet Planet. Health* **5**, e145–e153 (2021).
16. Lee, J.-M. et al. Coral-based history of lead and lead isotopes of the surface Indian Ocean since the mid-20th century. *Earth Planet. Sci. Lett.* **398**, 37–47 (2014).
17. Carrasco, G. et al. An update of the Pb isotope inventory in post leaded-petrol Singapore environments. *Environ. Pollut.* **233**, 925–932 (2018).
18. Das, R., Bin Mohamed Mohtar, A. T., Rakshit, D., Shome, D. & Wang, X. Sources of atmospheric lead (Pb) in and around an Indian Megacity. *Atmos. Environ.* **193**, 57–65 (2018).
19. Hoàng-Hòa, T. B. et al. Pb, Sr and Nd isotopic composition and trace element characteristics of coarse airborne particles collected with passive samplers. *Comptes Rendus Geosci.* **347**, 267–276 (2015).
20. Kayee, J., Bureekul, S., Sompongchaiyakul, P., Wang, X. & Das, R. Sources of atmospheric lead (Pb) after quarter century of phasing out of leaded gasoline in Bangkok, Thailand. *Atmos. Environ.* **253**, 118355 (2021).
21. Kayee, J. et al. Metal concentrations and source apportionment of PM $_{2.5}$ in Chiang Rai and Bangkok, Thailand during a biomass burning season. *ACS Earth Space Chem.* **4**, 1213–1226 (2020).
22. Kumar, S. et al. Tracing dust transport from middle-East over Delhi in march 2012 using metal and lead isotope composition. *Atmos. Environ.* **132**, 179–187 (2016).
23. Ray, I., Das, R., Chua, S. L. & Wang, X. Seasonal variation of atmospheric Pb sources in Singapore - elemental and lead isotopic compositions of PM10 as source tracer. *Chemosphere* **307**, 136029 (2022).
24. Walsh, M. P. The global experience with lead in gasoline and the lessons we should apply to the use of MMT. *Am. J. Ind. Med.* **50**, 853–860 (2007).
25. Dumitrescu, E. Global Efforts to Promote Cleaner Used Vehicles: Focus on Solutions (2017).
26. Drucker, D. G. et al. Aquatic resources in human diet in the late mesolithic in Northern France and Luxembourg: insights from carbon, nitrogen and sulphur isotope ratios. *Archaeol. Anthropol. Sci.* **10**, 351–368 (2018).
27. Parnell, A. C. et al. Bayesian stable isotope mixing models. *Environmetrics* **24**, 387–399 (2013).
28. Chen, H., Yan, Y., Hu, D., Peng, L. & Wang, C. High contribution of vehicular exhaust and coal combustion to PM2.5-bound Pb pollution in an industrial City in North China: an insight from isotope. *Atmos. Environ.* **294**, 119503 (2023).
29. Dietrich, M., Krekeler, M. P. S., Kousehlar, M. & Widom, E. Quantification of Pb pollution sources in complex urban environments through a multi-source isotope mixing model based on Pb isotopes in lichens and road sediment. *Environ. Pollut.* **288**, 117815 (2021).
30. Koffman, B. G. et al. Provenance of anthropogenic Pb and atmospheric dust to northwestern North America. *Environ. Sci. Technol.* **56**, 13107–13118 (2022).
31. Longman, J., Struve, T. & Pahnke, K. Spatial and temporal trends in mineral dust provenance in the South Pacific—evidence from mixing models. *Paleoceanogr. Paleoclimatology* **37**, e2021PA004356 (2022).
32. Longman, J. et al. Quantitative assessment of Pb sources in isotopic mixtures using a Bayesian mixing model. *Sci. Rep.* **8**, 6154 (2018).
33. Bi, X.-Y. et al. Lead isotopic compositions of selected coals, Pb/Zn Ores and fuels in China and the application for source tracing. *Environ. Sci. Technol.* **51**, 13502–13508 (2017).
34. Bollhöfer, A. & Rosman, K. J. R. Isotopic source signatures for atmospheric lead: the southern Hemisphere. *Geochim. Cosmochim. Acta* **64**, 3251–3262 (2000).
35. Chifflet, S. et al. Origins and discrimination between local and regional atmospheric pollution in Haiphong (Vietnam), Based on Metal(Loid) concentrations and lead isotopic ratios in PM10. *Environ. Sci. Pollut. Res. Int.* **25**, 26653–26668 (2018).
36. Das, R. et al. Suspension of crustal materials from wildfire in Indonesia as revealed by Pb isotope analysis. *ACS Earth Space Chem* **7**, 379–387 (2023).
37. Das, A. et al. Tracing lead contamination in foods in the city of Kolkata, India. *Environ. Sci. Pollut. Res.* **23**, 22454–22466 (2016).
38. Deb, M., Thorpe, R. I., Cumming, G. L. & Wagner, P. A. Age, source and stratigraphic implications of Pb isotope data for conformable, sediment-hosted, base metal deposits in the proterozoic Aravalli-Delhi orogenic belt, Northwestern India. *Precambrian Res* **43**, 1–22 (1989).
39. Díaz-Somoano, M. et al. Stable lead isotope compositions in selected coals from around the World and implications for present day aerosol source tracing. *Environ. Sci. Technol.* **43**, 1078–1085 (2009).
40. Huang, C., Li, H. & Lai, C.-K. Genesis of the Binh do Pb-Zn deposit in Northern Vietnam: evidence from H-O-S-Pb isotope geochemistry. *J. Earth Sci.* **30**, 679–688 (2019).
41. Millot, R., Allègre, C.-J., Gaillardet, J. & Roy, S. Lead isotopic systematics of major river sediments: a new estimate of the pb isotopic composition of the upper continental crust. *Chem. Geol.* **203**, 75–90 (2004).
42. Xu, J. et al. Mineralogy, fluid inclusions, and S–Pb isotope geochemistry study of the Tuboh Pb–Zn–Ag Polymetallic Deposit, Lubuklinggau, Sumatra, Indonesia. *Ore Geol. Rev.* **112**, 103032 (2019).
43. Yao, P.-H. et al. Lead isotope characterization of petroleum fuels in Taipei, Taiwan. *Int. J. Environ. Res. Public. Health* **12**, 4602–4616 (2015).
44. Ray, I.; Das, R. Dataset for: A Lingering Legacy of Leaded Gasoline in Southeast Asia (2023). https://doi.org/10.5281/zenodo.10101283.
45. See, S. W.; Balasubramanian, R.; Wang, W. A study of the physical, chemical, and optical properties of ambient aerosol particles in Southeast Asia during Hazy and Nonhazy Days. *J. Geophys. Res. Atmospher.* 111 (2006). https://doi.org/10.1029/2005JD006180.
46. Gasim, M., Khalid, N. A. & Muhamad, H. The influence of tidal activities on water quality of Paka River Terengganu. *Malaysia* **19**, 979–990 (2015).
47. Lim, W. Y., Aris, A. Z., Ismail, T. H. T. & Zakaria, M. P. Elemental hydrochemistry assessment on its variation and quality status in Langat River, Western Peninsular Malaysia. *Environ. Earth Sci.* **70**, 993–1004 (2013).
48. Looi, L. J., Aris, A. Z., Wan Johari, W. L., Md. Yusoff, F. & Hashim, Z. Baseline metals pollution profile of tropical Estuaries and Coastal waters of the straits of Malacca. *Mar. Pollut. Bull.* **74**, 471–476 (2013).
49. Chen, M. et al. Boundary exchange completes the marine Pb cycle jigsaw. *Proc. Natl. Acad. Sci. USA* **120**, e2213163120 (2023).
50. Apte, S. C. et al. Baseline trace metal concentrations in New South Wales Coastal waters. *Mar. Freshw. Res.* **49**, 203–214 (1998).
51. Wu, P.-C. & Huang, K.-F. Tracing local sources and long-range transport of PM10 in central Taiwan by using chemical characteristics and Pb isotope ratios. *Sci. Rep.* **11**, 7593 (2021).
52. Rabha, S. et al. Year-long evaluation of aerosol chemistry and meteorological implications of PM2.5 in an urban area of the Brahmaputra valley, India. *Environ. Sci. Atmospher.* **3**, 196–206 (2023).
53. Police, S., Sahu, S. K., Tiwari, M. & Pandit, G. G. Chemical composition and source apportionment of PM2.5 and PM2.5–10 in Trombay (Mumbai, India), a COASTAL INDUSTRIAL AREa. *Particuology* **37**, 143–153 (2018).
54. Khare, P. & Baruah, B. P. Elemental characterization and source identification of PM2.5 using multivariate analysis at the suburban site of North-East India. *Atmospher. Res.* **98**, 148–162 (2010).
55. Sharma, J. V. *Impact of wood-based energy on Forests in India | Wood Energy Catalogue | Food and Agriculture Organization of the United Nations*. https://www.fao.org/forestry/energy/catalogue/search/detail/en/c/1380965/ (accessed 2023-08-22).
56. Sangster, D. F., Outridge, P. M. & Davis, W. J. Stable lead isotope characteristics of lead ore deposits of environmental significance. *Environ. Rev.* **8**, 115–147 (2000).
57. Phillips, D. L. & Gregg, J. W. Source partitioning using stable isotopes: coping with too many sources. *Oecologia* **136**, 261–269 (2003).
58. Phillips, D. L. & Gregg, J. W. Uncertainty in source partitioning using stable isotopes. *Oecologia* **127**, 171–179 (2001).
59. Energy Market Authority Singapore. *Energy Transformation*. https://www.checkfirst.gov.sg/c/1ac4306f-4df9-4a7c-8759-00fda969d6a5 (accessed 2023-08-11).
60. Amnuaylojaroen, T., Inkom, J., Janta, R. & Surapipith, V. Long range transport of southeast Asian PM2.5 pollution to Northern Thailand during high biomass burning episodes. *Sustainability* **12**, 10049 (2020).
61. INDIAN BUREAU OF MINES. Indian Minerals Yearbook. (2014).
62. Tournadre, J. Anthropogenic pressure on the open ocean: the growth of ship traffic revealed by altimeter data analysis. *Geophys. Res. Lett.* **41**, 7924–7932 (2014).
63. Laidlaw, M. A. S., Zahran, S., Mielke, H. W., Taylor, M. P. & Filippelli, G. M. Re-suspension of lead contaminated urban soil as a dominant source of atmospheric lead in Birmingham, Chicago, Detroit and Pittsburgh, USA. *Atmos. Environ.* **49**, 302–310 (2012).
64. Zahran, S., Laidlaw, M. A. S., McElmurry, S. P., Filippelli, G. M. & Taylor, M. Linking source and effect: resuspended soil lead, air lead, and children's blood lead levels in Detroit, Michigan. *Environ. Sci. Technol.* **47**, 2839–2845 (2013).
65. Mielke, H. W. et al. The concurrent decline of soil lead and Children's blood lead in New Orleans. *Proc. Natl. Acad. Sci. USA* **116**, 22058–22064 (2019).
66. Jeong, H. Toxic metal concentrations and Cu–Zn–Pb isotopic compositions in tires. *J. Anal. Sci. Technol.* **13**, 2, https://doi.org/10.1186/s40543-021-00312-3 (2022).
67. Jeong, H., Ryu, J.-S. & Ra, K. Characteristics of potentially toxic elements and multi-isotope signatures (Cu, Zn, Pb) in non-exhaust traffic emission sources. *Environ. Pollut.* **292**, 118339 (2022).

68. Smith, J. A., Mazumder, D., Suthers, I. M. & Taylor, M. D. To fit or not to fit: evaluating stable isotope mixing models using simulated mixing polygons. *Methods Ecol. Evol.* **4**, 612–618 (2013).
69. Lahd Geagea, M., Stille, P., Gauthier-Lafaye, F. & Millet, M. Tracing of industrial aerosol sources in an urban environment using Pb, Sr, and Nd isotopes. *Environ. Sci. Technol.* **42**, 692–698 (2008).
70. Phillips, D. L. et al. Best practices for use of stable isotope mixing models in food-web studies. *Can. J. Zool.* **92**, 823–835 (2014).
71. Dongsheng 2. 越南东北部佐田铅锌矿床硫化物S、Pb 同位素特征及其地质意义. 地质通报, **34**, 757–768 (2015).
72. Hsu, Y.-K. Chinese Lead Isotope Database, (2019). https://doi.org/10.7910/DVN/VID3WR.
73. Phillips, D. L., Newsome, S. D. & Gregg, J. W. Combining sources in stable isotope mixing models: alternative methods. *Oecologia* **144**, 520–527 (2005).
74. Parnell, A. C., Inger, R., Bearhop, S. & Jackson, A. L. Source partitioning using stable isotopes: coping with too much variation. *PLoS ONE* **5**, e9672 (2010).
75. Stock, B.; Jackson, A.; Ward, E.; Venkiteswaran, J. Brianstock/MixSIAR 3.1.9, 2018. https://doi.org/10.5281/zenodo.1209993.
76. Baron, S., Tămaş, C. G. & Le Carlier, C. How mineralogy and geochemistry can improve the significance of Pb isotopes in metal provenance studies. *Archaeometry* **56**, 665–680 (2014).
77. Stock, B.; Semmens, B. MixSIAR GUI User Manual v3.1. (2016).
78. Phillips, D. L. & Koch, P. L. Incorporating concentration dependence in stable isotope mixing models. *Oecologia* **130**, 114–125 (2002).
79. Cox, T., Laceby, J. P., Roth, T. & Alewell, C. Less is more? A novel method for identifying and evaluating non-informative tracers in sediment source mixing models. *J. Soils Sediments* **23**, 3241–3261 (2023).

Acknowledgements

We extend their heartfelt appreciation to the three reviewers for their invaluable viewpoints in enhancing the quality of our manuscript. Reviewer 1's fundamental insights and comments have helped us provide more clarity to our article. The comprehensive overview provided by Reviewer 2 has ensured a smooth progression of the manuscript. We are grateful to Dr. Jack Longman, whose extensive work on MixSIAR analyses has significantly influenced and shaped the article. His thorough evaluation, has greatly enhanced the modelling aspects of the study. Lastly, we extend our heartfelt gratitude to the editorial board members for their constant support, positive attitude, and valuable input. We would like to thank Prof. Xianfeng Wang of Nanyang Technological University for supporting extensive atmospheric lead (Pb) research work in India and Southeast Asia for the past several years. This article would not have been possible without the insights gained from the previous work in the region by the authors. This research was supported by the Singapore Ministry of Education (MOE) Tier 1 grant (MOE-NTU_RG125/16-(S)), Department of Environment, Government of West Bengal (Grant no. ENV-29014(11)/1/2022-ACS (ENV)) and Science and Engineering Research Board (Grant no. SPG/2021/002652). RD's position is supported by UGC- Faculty Recharge Program and IR is supported by AICTE.

Author contributions

R.D. conceived, analysed, and supervised the entire study. I.R. compiled the data, performed the modelling studies, and prepared figures. Both authors wrote the manuscript.

Competing interests

The authors declare no competing interests

Additional information

Supplementary information The online version contains supplementary material available at https://doi.org/10.1038/s43247-023-01135-3.

Correspondence and requests for materials should be addressed to Reshmi Das.

Peer review information *Communications Earth & Environment* thanks Yigal Erel, Jack Longman, and the other, anonymous, reviewer(s) for their contribution to the peer review of this work. Primary Handling Editors: Yinon Rudich and Clare Davis. Peer reviewer reports are available.

Reprints and permission information is available at http://www.nature.com/reprints

Publisher's note Springer Nature remains neutral with regard to jurisdictional claims in published maps and institutional affiliations.

Open Access This article is licensed under a Creative Commons Attribution 4.0 International License, which permits use, sharing, adaptation, distribution and reproduction in any medium or format, as long as you give appropriate credit to the original author(s) and the source, provide a link to the Creative Commons licence, and indicate if changes were made. The images or other third party material in this article are included in the article's Creative Commons licence, unless indicated otherwise in a credit line to the material. If material is not included in the article's Creative Commons licence and your intended use is not permitted by statutory regulation or exceeds the permitted use, you will need to obtain permission directly from the copyright holder. To view a copy of this licence, visit http://creativecommons.org/licenses/by/4.0/.

© The Author(s) 2023

Journal of Hazardous Materials 469 (2024) 134014

Contents lists available at ScienceDirect

Journal of Hazardous Materials

journal homepage: www.elsevier.com/locate/jhazmat

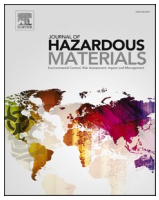

Entrapment of atmospheric particle bound heavy metals by ferns as evidenced by lead (Pb) isotope and MixSIAR: Implications for improving air quality

Iravati Ray [a,*], Sambuddha Misra [b], Mengli Chen [c,d], Xianfeng Wang [d,e], Reshmi Das [a,d,**]

[a] School of Environmental Studies, Jadavpur University, Kolkata, India
[b] Centre for Earth Sciences, Indian Institute of Sciences, Bangalore, India
[c] Tropical Marine Science Institute, National University of Singapore, Singapore
[d] Earth Observatory of Singapore, Nanyang Technological University, Singapore
[e] Asian School of Environment, Nanyang Technological University, Singapore

HIGHLIGHTS

- Mitigation of PM bound heavy metals is essential to prevent global fatalities.
- Studying PM capture capacity and sources in ferns help design remediation process.
- Pb isotopes and elemental concentration prove fern tissues capture atmospheric PM.
- Ferns hold potential to improve air quality, implying their practical use.

GRAPHICAL ABSTRACT

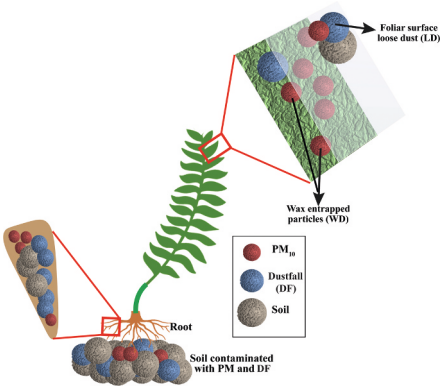

ARTICLE INFO

Keywords:
Ferns
Particulate matter trapping
Plant metal uptake
Atmospheric transfer
Pb isotope
MixSIAR

ABSTRACT

Plant metal uptake can occur through both soil-root and atmospheric transfer from leaves. The latter holds potential implications for development of biofiltration systems. To explore this potential, it is crucial to understand entrapment capacity and metal sources within plants. As ferns absorb materials from atmosphere, this study focuses on two abundant fern species growing in densely populated and highly polluted regions of Eastern India. Gravimetric quantification, elemental concentration and Pb isotopic analyses were performed by segregating the ferns into distinct components: foliage dusts (loose dust (LD) and wax-bound dust (WD)) and plant tissue (leaves and roots). To understand metal sources, the study analyzes soil, and atmospheric particulates (PM_{10} and dust fall (DF)). Results indicate that, while LDs have soil dust influence, wax entraps atmospheric particulates and translocates them inside the leaves. Furthermore, roots demonstrate dissimilar isotopic ratios from soil, while displaying close association with atmospheric particulates. Isotopic composition and subsequent

* Corresponding author.
** Corresponding author at: School of Environmental Studies, Jadavpur University, Kolkata, India.
E-mail addresses: iravatir.envs.rs@jadavpuruniversity.in (I. Ray), reshmidas.sest@jadavpuruniversity.in (R. Das).

https://doi.org/10.1016/j.jhazmat.2024.134014
Received 4 January 2024; Received in revised form 3 March 2024; Accepted 10 March 2024
Available online 16 March 2024
0304-3894/© 2024 Elsevier B.V. All rights reserved.

mixing model reveal dominant contribution from DF in leaves (53–73%) and roots (33–86%). Apart from DF, leaf Pb is sourced from PM_{10} (21–38%) with minimal contribution from soil (6–10%). Conversely, in addition to dominance from DF, roots source Pb primarily from soil (12–62%) with a meagre 2–8% contribution from PM_{10}.

1. Introduction

Prolonged exposure to particulate matter (PM) originating from anthropogenic sources causes about 4.2 million deaths globally [1]. Particulate matter serves as a primary carrier of heavy metals discharged into the atmosphere from various anthropogenic activities [2,3]. Heavy metals such as manganese (Mn), cobalt (Co), chromium (Cr), nickel (Ni) and arsenic (As) bound to PM have been found to be bioaccessible and pose significant health hazards [4–7]. Inhalation of PM bound Lead (Pb) elevates blood Pb levels and causes cardiovascular and neurological disorders [8,9].

Plants are bioindicators and biomonitors of such PM bound pollutants. Especially, ferns being epiphytes can directly absorb nutrients and pollutants from the atmosphere, making them suitable phytomonitors and potential mitigators of atmospheric PM pollution [10]. Although ferns have been proven to be highly tolerant of heavy metals present in soil [11], comprehensive studies on atmospheric pollutant uptake by ferns compared to other plants are limited. The PM capture efficiency of plant species has mostly been studied and quantified utilising gravimetric techniques and surface morphological studies such as scanning electron microscopy (SEM) and energy dispersive X-ray (EDX) [12–20]. However, such studies cannot prove the absorption of atmospheric pollutants in plant tissues. Non-essential and toxic heavy metals such as Pb, Cd etc are internalised by various plants through foliar uptake of PM as demonstrated by elemental concentration studies [21–24]. However, source identification of pollutants inside plant tissue solely based on elemental concentration is difficult. Stable isotope systems coupled with elemental concentration analyses are much effective is source apportionment studies. As isotopes of Pb (^{204}Pb, ^{206}Pb, ^{207}Pb and ^{208}Pb) do not undergo fractionation during physicochemical processes [2], it is considered to be a robust geochemical tool for source tracing. Lead isotopic compositions have previously been utilised to delineate the sources of Pb inside edible [25–33] and wild [21,34] plants. From these studies, atmospheric fallout was found to be a significant contributor towards the presence of Pb inside the plants.

Indian cities are ideal locations for such studies. The densely populated Indo-Gangetic plain consists of 12 cities that are among the top 20 polluted cities in the world in terms of PM pollution [35]. Hence, plants growing in such regions are assumed to have a high tolerance for a wide range of pollutants and can be potential remediating agents. This study has selected 2 abundantly growing fern species in densely populated regions and utilises gravimetric techniques, surface characterisations, elemental concentrations and Pb isotopic compositions to:

(i) investigate their foliar dust capture capacity
(ii) determine the sources of heavy metals on separated layers of foliar surface and inside fern tissues using elemental concentration coupled with Pb isotopic compositions
(iii) quantify the relative contribution of individual sources (soil, PM_{10}, dust fall) towards metal concentration in the plant tissues using stable isotope mixing model (MixSIAR).

Based on the results, the study hypothesises that the results obtained from this biomonitoring study can provide implications for the usage of ferns for cleaning up indoor air in polluted urban settings.

2. Materials and methods

2.1. Study area and sampling

Densely populated areas with high traffic and small-scale industries from eastern India were selected for the present study [36,37] (Supplementary Figure 1). Sampling was conducted at 12 sites in two heavily polluted Indian cities, viz., Kolkata (22.51°N, 88.63°E) and Howrah (22.52°N, 88.19°E). According to a recent report on air quality and health in global cities, Kolkata ranks the 2nd in terms of annual average $PM_{2.5}$ exposures [38]. Sampling was performed between March to May, 2022, during springtime which corresponds to the peak growth period of the ferns. Moreover, this pre monsoon period ensures the capture of highest amount of dust on the leaf surfaces. PM_{10} aerosol sampling was done for 14 days (n = 14). Samples were collected by a personal modular impactor PM_{10} (PMI, SKC Inc., USA) connected to a Deployable Particulate Sampler (DPS, Leland Legacy Pump, SKC Inc., USA) with a pumping efficiency of 10 L/min. The PM_{10} samples were collected upon 47 mm PTFE filters that had been pre-washed with 1 N HCl at 140 °C before being rinsed several times with ultrapure water. The filters were dried in an oven at 60 °C, weighed, and sealed in pre-cleaned petri dishes before sampling. The sampler was placed on the roofs of buildings approximately 12 m above ground level (AGL) [39].

For dust fall (DF) sampling, polystyrene petri dishes (90 mm dia) were cleaned using 1 N HCl followed by multiple rinsing with ultrapure water, drying, and weighing. Pre-weighed petri dishes (n = 6) were fixed on roofs of buildings using double sided tapes to avoid any disturbance due to wind during dust settling [40]. The petri dishes were kept undisturbed for ~100–150 hrs till visible dust accumulation occurred. No rainfall event occurred during the period of sampling. The petri dishes were sealed and kept inside airtight zipper bags before being processed for analysis.

Pteris vittata and *Pteridium aquilinum* were observed to be widely distributed species of ferns throughout the region. Both species were sampled from 12 sites, from about 1 – 1.5 m above the ground. All the plants were in good condition and none were shaded by overhead vegetation, ensuring that the leaves were fully exposed to the atmospheric fallouts. Leaves were hand-plucked and samples from each site were sealed in separate acid-washed plastic containers to prevent cross contamination and minimize PM loss from the leaf surface. The roots of corresponding plants along with the rhizosphere soils of individual sample were sealed in separate ziploc bags. Plants of similar age determined by their appearance (height, sori development) and identified by surveying local people were selected for the study. Samples were collected at each site on the same days under rainless conditions.

2.2. Gravimetric quantifications and determination of leaf surface area

PM_{10} (n = 14), DF (n = 6), Loose dust (LD) (n = 22) and Wax bound dust (WD) (n = 22) loads were determined gravimetrically using washing and weighing method [41]. This method separates the LD and WD from the clean leaves. A total of twelve fern samples (12 × LD, 12 × WD, 12 × cleaned leaves, 12 × soil and 12 × root) were chosen for elemental and isotopic analysis. This selection aimed to cover varying level of dust accumulation on their surfaces, ranging from low to high. This will help to compare the elemental concentration between clean leaves with high dust loads and low dust loads. The details of the method are reported in the Supplementary Material 1. The cleaned leaves were photographed against a white backdrop and a digital file was created. The images were analyzed by Image-J software to calculate the

individual leaf surface areas [42].

2.3. Analytical methods

2.3.1. Sample preparation

All samples were processed in a clean chemistry laboratory utilizing trace metal grade chemicals and double distilled acids. The samples processed for chemical analyses can be categorised into 7 types: (i) aerosols (PM_{10}; n = 14), (ii), DF (n = 6) (iii) LD (n = 12) (v) WD (n = 12) (vi) cleaned leaves (n = 12) (vii) roots (n = 12) and (viii) soils (n = 12). One of the soil samples was sequentially leached to determine the Pb isotopic compositions of exchangeable (SE), carbonate (SC), reducible (SR) and silicate fractions (SS). The details of the sequential extraction procedure are given in the Supplementary Material 1.

2.3.2. Elemental concentration analyses

Concentrations of 14 elements (Mg, Al, Ca, Ti, V, Cr, Mn, Fe, Co, Ni, Cu, Cd, Ba, and Pb) were determined for all the samples at Centre for Earth Sciences, Indian Institute of Science, Bangalore (Supplementary Material 2). Initially, measurements for elements having high concentrations (Al, Ba, Ca, Fe, Mg, and Mn) were performed on an Agilent 5800 Inductively coupled plasma - optical emission spectrometer (ICP – OES). Analytes having lower concentrations (Ti, V, Cr, Ni, Co, Cu, Cd and Pb) were measured on an Agilent 8900 Triple Quadrupole Inductively coupled Plasma Mass Spectrometer (ICP – MS, Agilent Technologies, Santa Clara, CA, USA).

In order to assess the chemical extraction efficiency and analytical precision, certified reference materials, viz., NIST SRM 1573 (Tomato Leaf Powder) and NIST SRM 2704 (Buffalo River Sediment) were digested and analyzed in accordance with the methods used for samples. Recoveries of the elements were found to be > 90% (Data provided in Supplementary Material 2).

2.3.3. Pb isotope determination

Pb isotopes (Table 1, Supplementary Material 2) were analysed on a Multi-collector ICP – MS (Neptune™ Plus, Thermo-Scientific™, Germany) at Nanyang Technological University, Singapore. Thalium (Tl) internal normalisation ($^{203}Tl/^{205}Tl$ ratio of 0.418911) followed by NIST SRM – 981 bracketing [43,44] were adopted to correct instrument fractionation.

All the samples were analysed at comparable Pb/Tl ratios to minimize any mass bias generated from beam intensity. The contribution of the procedural blank (average blank=1.6%) to the total measured concentration were determined as $[Pb]_{Procedural\ blank}/[Pb]_{Total.}$ Consequently, the blank-subtracted $^{206}Pb/^{207}Pb$ and $^{208}Pb/^{207}Pb$ values were determined by mass balance represented by the following equation [45]:

$$\left(\frac{20x}{207}\right)_{sample} = \left[n_T\left(\frac{20x}{207}\right)_{total} - n_B\left(\frac{20x}{207}\right)_{blank}\right] \Big/ (n_T - n_{B)}$$

Where, x = 6, 8; n is the fractional amount of substance; and the subscripts T, and B refers to total and blank, respectively. The blank isotope ratios and the NBS 981 ratios measured during the analytical sessions are given in Supplementary Material 2.

2.4. Statistical analyses

Differences across species were not determined as the total amount of dust per unit area on the leaf surfaces did not differ significantly between species (ANOVA at $p < 0.05$).

Bayesian statistics-based modeling package, "MixSIAR" available in R was utilized to quantify the potential source contributions towards Pb in foliage and roots. The model uses mean and standard deviations along with concentration of sources to produce model fits for user supplied data of individual samples (mixtures) through Markov Chain Monte Carlo simulations [46]. Due to mismatch in concentration units between PM_{10} aerosols and soil & DF, the Pb concentrations of the sources were normalized with Aluminum (Al) concentrations. This normalization was performed to obtain a dimensionless concentration factor [47]. This model has been previously utilized for source apportionment of Pb in peat bogs, aerosols, dusts, sediments and lichens with variable pollution sources [47–52]. The model was run with DF, PM_{10} and soil mean Pb isotope ratios and ± 1σ as sources of Pb in foliage and roots (mixtures) for each location separately to obtain a range of percent contribution. The Pb isotope ratios inputs in the model (^{206}Pb, ^{207}Pb and ^{208}Pb) of the sources and mixtures were normalized using ^{204}Pb to maximize variability in isotope signatures as each isotope originates from a different decay chain [52]. MixSIAR calculations are based upon the following equations:

$$Mixture\left(\frac{20x}{204}Pb\right) = \sum_{1}^{n} Source\left(\frac{20x}{204}Pb\right) \times \pi \quad (1)$$

where, $\pi = \frac{f_n \times C_n}{\sum_1^n f \times C}$,f = the source proportion,

C = concentrations of the sources, where Pb/Al ratios are incorporated.

n = the number of sources.

x = 6, 7, 8.

where, x = 6, 7 and 8; f_{DF}, f_{PM10} and f_{soil}, are fractions of DF, PM_{10} and soil respectively.

Table 1
Mean Pb isotopic composition of PM_{10} aerosol, Dustfall (DF), Loose Dust (LD), Wax Dust (WD), Leaf, Root and Soil samples.

Isotope Ratio	Parameter	PM_{10} Aerosol	PD	LD	WD	Leaf	Root	Soil
$^{206}Pb/^{204}Pb$	N	14	6	12	12	12	12	12
	Mean	17.7806	17.6247	17.9250	17.7747	17.7482	17.7042	18.2057
	SD	0.272	0.054	0.181	0.134	0.102	0.146	0.429
$^{207}Pb/^{204}Pb$	N	14	6	12	12	12	12	12
	Mean	15.6087	15.5691	15.6430	15.6192	15.6161	15.5777	15.6266
	SD	0.033	0.023	0.015	0.015	0.008	0.047	0.061
$^{208}Pb/^{204}Pb$	N	14	6	12	12	12	12	12
	Mean	37.6609	37.5234	37.9478	37.7246	37.7131	37.6188	38.1970
	SD	0.249	0.089	0.205	0.140	0.094	0.211	0.488
$^{206}Pb/^{207}Pb$	N	14	6	12	12	12	12	12
	Mean	1.1391	1.1321	1.1459	1.1379	1.1367	1.1365	1.1650
	SD	0.015	0.004	0.011	0.008	0.006	0.007	0.023
$^{208}Pb/^{207}Pb$	N	14	6	12	12	12	12	12
	Mean	2.4128	2.4101	2.4259	2.4153	2.4150	2.4149	2.4443
	SD	0.011	0.005	0.011	0.007	0.005	0.008	0.022

3. Results and discussion

3.1. Atmospheric PM_{10} concentration and DF flux

The concentrations of PM_{10} aerosols ranged from 208 – 726 μg/m^3 (mean = 326 μg/m^3). Throughout all sampling days, the PM_{10} concentrations consistently exceeded the 24 hr average PM_{10} concentration limits of 150 μg/m^3, specified by National Ambient Air Quality Standards (NAAQS) [53]. The DF flux ranged from 0.56 g/m^2/day to 2.32 g/m^2/day with an average of 1.37 g/m^2/day (Fig. 1a). The observed dust flux ranges in this study conform with those recorded at industrial sites in the country, while being an order of magnitude higher than the levels recorded at urban sites (Fig. 1b) [15,54–57]. A high DF flux and aerosol concentration, characteristic of industrial influences can be beneficial in assessing the maximum anthropogenic particle capture efficiency, and consequently the efficiency of metal capture by the ferns.

3.2. Leaf surface dust load and SEM-EDX observations

The LD and WD loads (n = 22) ranged from 0.06 – 3.59 mg/cm^2 (mean = 1.34 mg/cm^2) and 0.0002 – 4.14 mg/cm^2 (mean = 1.18 mg/cm^2), respectively. The clustering of dust on the leaf surface can be observed from the scanning electron micrographs (Supplementary Figure 2). A large quantity of dust may have formed non – stoichiometric compounds, which may have led to charge generation on the dust surface [58]. This charged surface attracted more dusts and resulted in clustering in some regions. The adaxial surfaces had much more clustering than the abaxial surfaces. Leaf surface dust loads (LD + WD) exhibit a higher median value, (Fig. 1c) compared to previous studies in urban and industrial regions of India [15,59–63], indicating a higher efficiency in dust capture capacity of the ferns. Initial observations from EDX indicates presence of heavy metals like Fe, Mn, Pb, Co, Ni, Cu, Zn and Cr on the leaf surfaces (Supplementary Figure 3).

3.3. Elemental concentration and enrichment factor (EF)

Median concentrations are reported in this study as they are generally not influenced by extreme values or outliers. Additionally, crustal enrichment factors are calculated to understand the geogenic versus anthropogenic sources of the elements in PM_{10}, DF and soil. The crustal enrichment factors (EF) defined as $EF = \left(\frac{\left(\frac{Element}{Reference\ element}\right)_{Sample}}{\left(\frac{Element}{Reference\ element}\right)_{Crust}}\right)$ for all elements were compared with Al as the reference element. The average elemental composition of the crust was adopted from previous literature [64].

3.3.1. Aerosol (PM_{10}) and dust fall (DF)

Elemental compositions for individual samples are provided in Supplementary Material 2. Median elemental concentration of PM_{10} aerosols and DF generally follow (Al, Ca, Fe, Mg) > (Ba, Cr, Cu Mn, Ni, Pb, Ti, V) > (Cd, Co). Enrichment Factors for Ni, Cd and Pb are above 10, indicating anthropogenic sources (Fig. 2a). Especially, Pb and Cd were heavily enriched in PM_{10} (Mean: EF_{Pb} = 652 ± 752, EF_{Cd} = 3355 ± 3385).

3.3.2. Soil

The median concentrations of the elements in soil generally follow the order (Al, Ba, Ca, Fe, Mg, Ti) > (Mn, Ni, V, Cr) > (Cd, Co, Cu, Pb). Soils exhibit average EFs for Mg, Ca, Ti, V, Cr, Mn, Fe, Co, Cu and Ba in the range of 0.9 – 3.8, while those of Ni, Cd and Pb were > 5 (Fig. 2a). Elements with 2 < EF < 5 are considered to have moderate enrichment with a dominant contribution from crustal sources, while 5 < EF < 20 suggests significant non – crustal sources [65]. Nickel, Pb and Cd were also enriched in PM_{10} and DFs (Fig. 2a). Thus, the enrichment of these

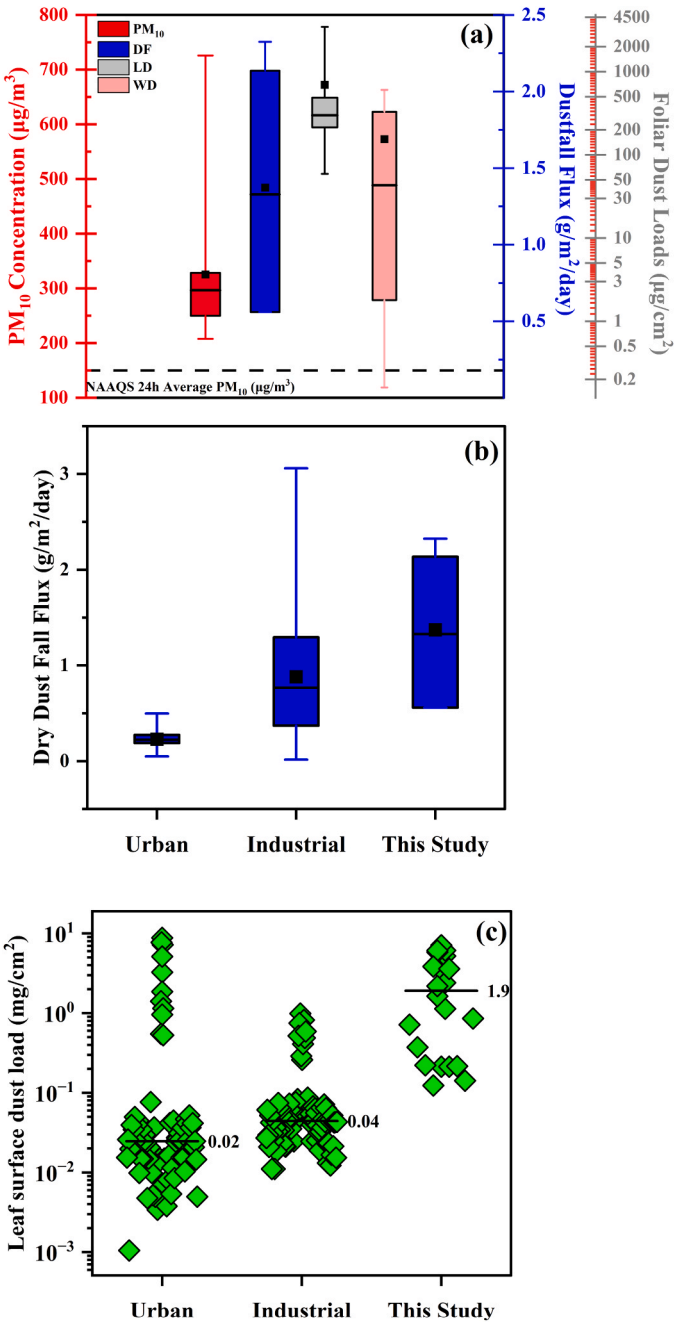

Fig. 1. **(a)** Box plots depicting PM_{10} aerosol concentration, dust fall (DF) and foliar dusts (loose dust (LD) and wax dust (WD)). The NAAQs 24 hrs average limit for PM10 concentration is marked for reference; **(b)** Box plots depicting a comparison of dust fall fluxes between this study, industrial (Uttar Pradesh [54,57], Purulia [55]) and urban settings (Delhi [15,56] of India. The upper and lower extremes of the boxes represent 75 and 25 percentile values respectively. The whiskers represent the highest and lowest values. Squares and lines inside boxes indicate mean and median values respectively. **(c)** Total leaf surface dust load (LD + WD) on the fern samples (n = 22) from this study. Foliar surface dust loads from previous studies conducted in urban (Lucknow [63], Orissa [60], Varanasi [59] and Delhi [62]) and industrial (Jharkhand [61] and Chhattisgarh [15]) settings of India are plotted for comparison. The ferns from this study demonstrates higher median dust loads compared to the previous studies. The lines represent the median dust loads. The values of the medians are indicated on the right-hand side of the plots.

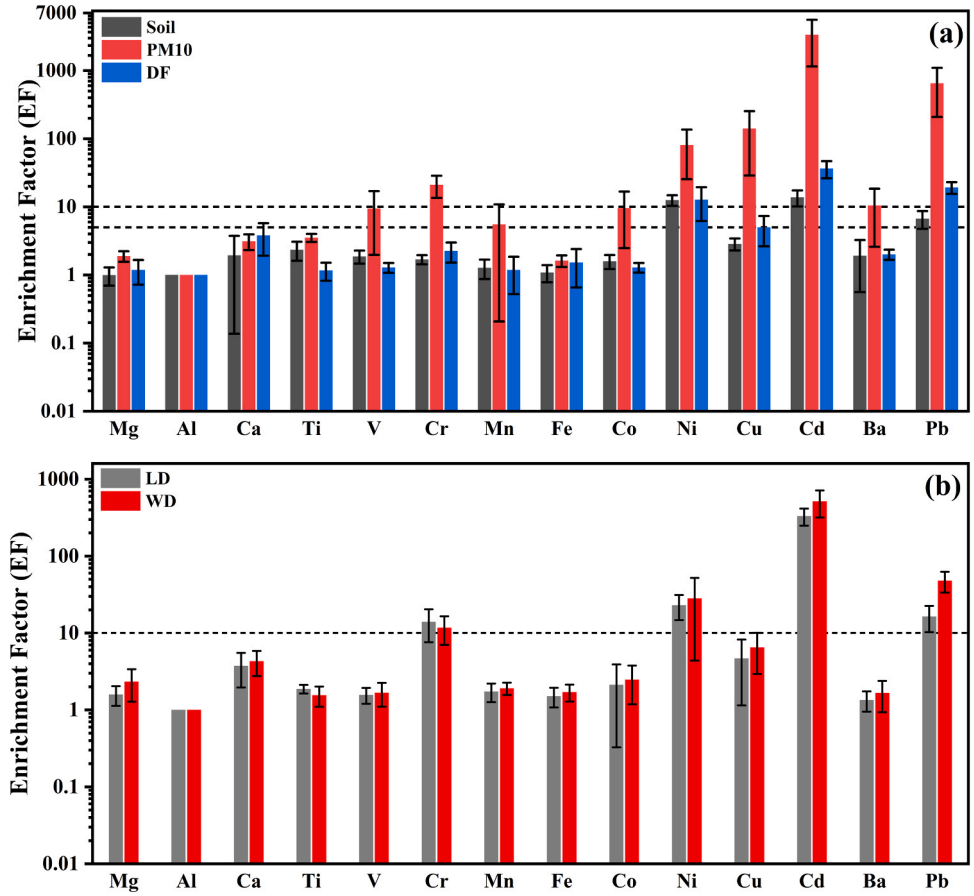

Fig. 2. : Bars with 1 SD depicting mean enrichment factors (EFs) of **(a)** PM_{10} aerosols, PDs, soil and **(b)** LD & WD. The dotted lines represent the threshold EF values (5 for soil and 10 for PM_{10}, PD, LD and WD). Samples recording EFs beyond the threshold EFs are considered to have anthropogenic inputs. For each type of sample, the elements, Ni, Cd and Pb were observed to be enriched consistently, suggesting anthropogenic inputs. PM_{10} aerosols, LD and WD exhibits high EFs for Cr.

elements in soil may have resulted from the deposition of atmospheric particulates on the soil surface [66].

3.3.3. *Foliar dusts (LD and WD) and fern tissues (roots and leaves)*

The elemental concentrations of the foliar dusts were normalised with respect to the total dry weight of the leaves (mg/kg), presented in Supplementary Material 2. The LDs and WDs followed the general order of (Ti, Mg, Al, Fe, Ca) > (Ba, Ni, Mn) > (V, Pb, Cr) > (Cd, Co, Cu). The elemental concentrations of the LDs were around 1.5 – 4 times that of the WDs indicating preferential internalisation of PMs based on size [19, 67]. The Mean EFs of Cr, Ni, Cd and Pb on LD and WD were $\geq \sim 10$, indicating anthropogenic contributions (Fig. 2b). The high EFs of Ni, Cd and Pb on PM_{10}, DF, LD, WD as well as soil indicate that these elements were sourced from atmospheric fallouts on the leaf surfaces as well as soil.

The median elemental concentrations in leaves and roots followed the general order (Al, Ca, Fe, Mg) > (Ba, Cr, Cu Mn, Ni, Pb, Ti, V) > (Cd, Co). The translocation of the metals within the leaf tissues can occur from foliar dust, roots or a combination of both pathways. The median concentration of the enriched metals (Cr, Ni, Cd, and Pb) follows the overall pattern LD > WD > Leaves (Fig. 3). Leaf and WD demonstrated comparable concentrations of Cr, Ni, Cd and Pb (Fig. 3). From soil to the leaves Cr, Ni, Cd and Pb follow Soil > Root > Leaf. Samples having high foliar dust loads (Range: 0.72 - 3.5 mg/cm^2, Mean $\pm$ 1 SD: 1.73 $\pm$ 1.21 mg/cm^2) had elevated concentrations of Al, Ca, Ti, V, Mn, Fe, Co, Ba and Pb (Supplementary Figure 4) compared to the ones with low foliar dust loads (less than 0.4 mg/cm^2, Range: 0.12 - 0.37 mg/cm^2, Mean $\pm$ 1 SD: 0.22 $\pm$ 0.08 mg/cm^2). These elements also demonstrated positive correlation between foliar dust loads and leaves(Supplementary Figure 5,6 and Fig. 5) indicating dominance of foliar translocation. Additionally, Ti, Fe and Co demonstrated moderate to strong correlations (Pearson's r = 0.46 - 0.81; p value < ~0.05) between leaves and roots as well (Supplementary Figure 5) which were not observed for Al, Ca, V, Mn and Ba (Supplementary Figure 5). This implies Ti, Fe and Co were translocated to the leaves bidirectionally through both roots and foliar surface. While, Al, Ca, V, Mn and Ba having no correlation with root and leaf indicates dominance of foliar translocation of these metals. However, relying solely on elemental concentrations is inadequate for identifying the source of metals in fern tissues. Consequently, the inclusion of Pb isotopic compositions becomes imperative for a more accurate determination.

3.4. *Elemental ratios as source tracers of foliar dusts*

Elemental ratios are effective tracers for source apportionment studies [39,68,69]. As plants have differences in tolerance levels for different metals, elemental ratios are not reliable for source delineation within tissues. Thus, elemental ratios have been used to trace sources specifically for foliar surface dust. As Ti is a conservative element, with no anthropogenic influence (EF < 2) it was utilized to normalize the enriched elements such as Ni, Cd and Pb to distinguish between crustal and atmospheric deposition [70]. The Pb/Ti, Cd/Ti, Ni/Cd and Pb/Cd ratios from previous literature coincide with those of the present study. This suggests that the sources of PM_{10} in the region have been similar over nearly a decade. The plot between Pb/Ti vs Cd/Ti (Fig. 4a) demonstrates that the characteristic ratios of LDs and WDs fall between those of soil, DFs and PM_{10}. This indicates that the leaf surface dusts were a mixture of soil, DF and PM_{10}. Enriched elements such as Ni, Cd and Pb

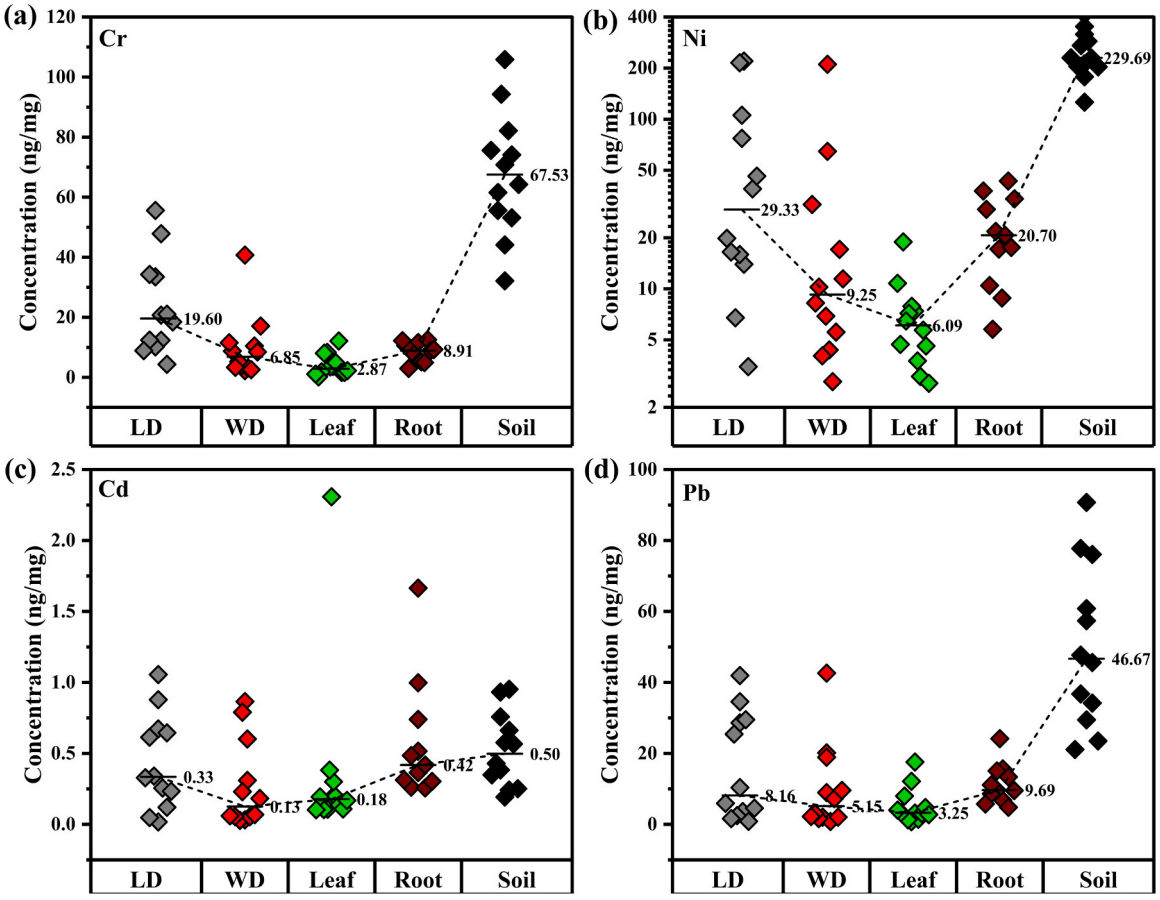

Fig. 3. : Concentrations of **(a)** Cr, **(b)** Ni, **(c)** Cd and **(d)** Pb in LD, WD, leaf, root and soil of the fern samples. The figures on the right-hand side of the symbols indicate the median concentrations, illustrated by a dotted black line.

when plotted as Ni/Cd vs Pb/Cd (Fig. 4b) overlap with PM_{10} samples, suggesting that these elements were primarily sourced from the atmosphere. The elemental ratios of the WDs and LDs closely align with PM_{10} and DF. In most cases, WDs exhibit a stronger association with PM_{10} aerosols, while LDs are relatively closer to the soil. Anthropogenically sourced elements like Pb and Cd that concentrate in the finer fraction of PM_{10} [71] were significantly correlated (Pearson's correlation coefficient = 0.97; p value = 2E-8) in PM_{10} aerosols. Copper, although enriched in PM_{10}, was not observed to be enriched in LD and WD (Fig. 2). A bivariate plot, normalizing Cu with crustal elements such as Ti and Mn (Cu/Ti vs Cu/Mn), indicates that both LD and WD overlap with soil and DF elemental ratios. In contrast, PM_{10} exhibits distinct ratios, indicating that Cu on the leaf surface was sourced from soil and DF rather than from PM_{10} aerosols (Fig. 4c).

3.5. *Pb isotopic compositions as source tracers of foliar dusts and tissues*

The average Pb isotopic compositions are presented in Table 1. The Pb isotopic compositions of individual samples are provided in Supplementary Material 2.

3.5.1. *Aerosol (PM_{10}) and Dust fall (DF)*

The average $^{206}Pb/^{207}Pb$ ratios of PM_{10} aerosols (1.1391 ± 0.0153) and DFs (1.1321 ± 0.0036) were analytically indistinguishable. The mean $^{206}Pb/^{207}Pb$ composition of Kolkata street dusts as determined by previous studies [39,72] conforms with that of the DFs from this study. The DF reflects the characteristics of the local Pb sources. The isotopic ratios of Indian aerosols (PM_{10}) from previous literature are also comparable to the ratios obtained in the present study [39,69,73]. Similar Pb isotopic ratios over the years suggest consistent atmospheric Pb sources such as vehicle exhausts, coal combustion and industrial emissions [39,69]. This makes our rationale behind comparing the aerosol Pb isotopic composition with that of the plant tissues reasonable as absorption of elements by the plants is a continuous process rather than an instantaneous one.

3.5.2. *Soil*

Soil had considerably higher average $^{206}Pb/^{207}Pb$ ratios (1.1650 ± 0.0231) compared to atmospheric fallouts (both PM_{10} and DF). Crustal Pb isotope ratio is known to be radiogenic, with $^{206}Pb/^{207}Pb$ composition ranging from 1.151 – 1.232 [74–78]. This indicates that the soils have a strong contribution from geogenic sources. However, anthropogenic input from dust deposition on soil might have been present, as suggested by high EFs of Ni, Cd and Pb, discussed in the previous section. Atmospherically deposited Pb, associated with finer soil grains [79] has lower $^{206}Pb/^{207}Pb$ compositions and greater mobility as well as solubility [66,80–82]. Lower $^{206}Pb/^{207}Pb$ signature was associated with higher Pb concentrations in soil, suggesting contamination from anthropogenic sources [83] (Supplementary Figure 7). Thus, the Pb in soil can be a combination of natural and anthropogenic sources [80]. As the bulk soil Pb is isotopically distinct from the root and leaf (discussed later) we performed sequential extraction of one soil sample.

The sequentially leached soil sample exhibited analytically indistinguishable $^{206}Pb/^{207}Pb$ composition in exchangeable (SE), carbonate (SC) and reducible (SR) fractions, while silicate fraction (SS) displayed significantly higher $^{206}Pb/^{207}Pb$ composition compared to the bulk soil (Supplementary Figure 8a). From the triple isotope plot, it can be observed that, the bulk soil exhibited Pb isotopic composition between the silicate fraction and SE, SC & SR compositions and lies on the mixing

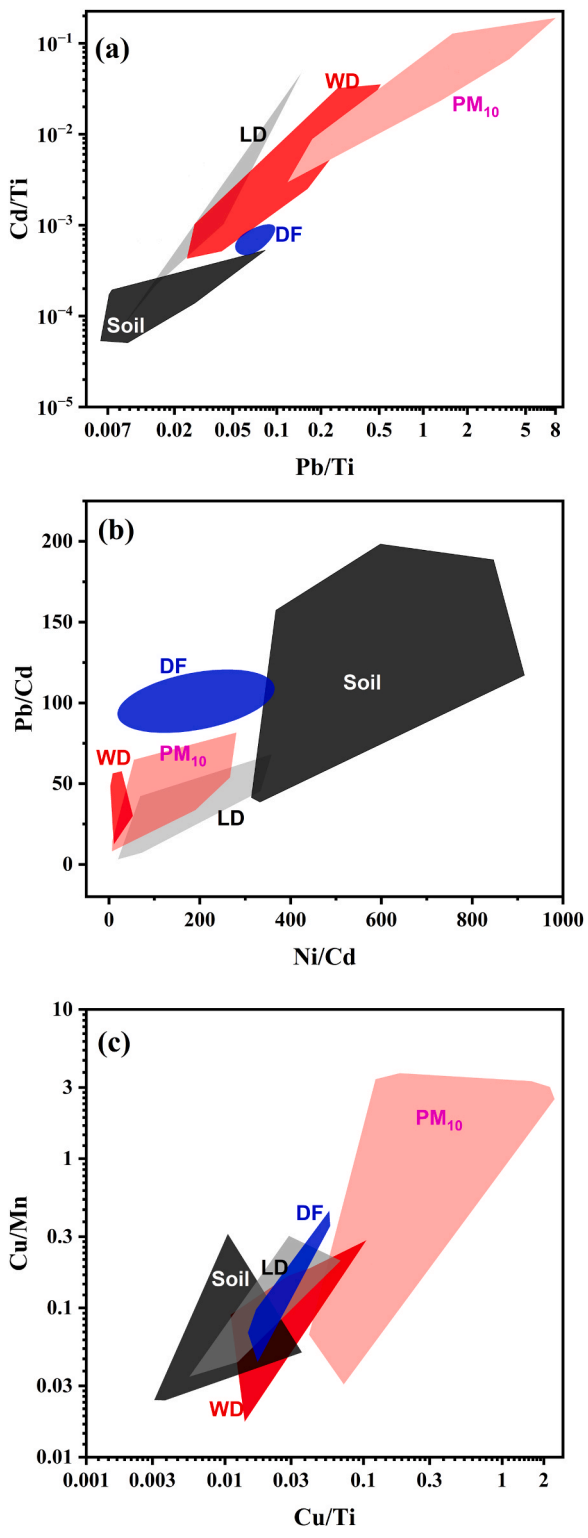

Fig. 4. : Elemental ratios plotted as **(a)** Pb/Ti vs Cd/Ti **(b)** Ni/Cd vs Pb/Cd and **(c)** Cu/Ti vs Cu/Mn. Pb/Ti vs Cd/Ti demonstrates that the characteristic ratios of LDs and WDs lie between those of soil, PDs and PM_{10}, with some of WDs overlapping with PM_{10} aerosols. Thus, the leaf surface dusts were a mixture of soil, PD and PM_{10}. Overlapping of LD and WD with PM_{10} aerosols in Ni/Cd vs Pb/Cd suggests that these elements in the leaf surface dusts were primarily sourced from the atmosphere. Cu/Ti vs Cu/Mn suggests that these elements were primarily of crustal origin.

line between SR and SS, indicating a mixing of all the fractions (Supplementary Figure 8b). The Pb isotopic compositions of DFs and SE, SC & SR are closely aligned. In DF, Pb correlates with Fe and Mn (Spearman's correlation coefficient > 0.76; p value < 0.07). This indicates that at least part of the Pb is bound to Fe-Mn phases, and DF contributes to comparable Pb isotopic compositions of different soil fractions.

3.5.3. *Foliar dusts - loose surface dust (LD) and Wax Dust (WD)*

The LD and WD samples exhibited $^{206}Pb/^{207}Pb$ signatures that were closer to DF and PM_{10} than to soil (Table 1). The LDs demonstrated a higher $^{206}Pb/^{207}Pb$ signature compared to WDs, indicating the contribution of Pb from regional soil in LDs. Conversely, WDs displayed a stronger association with PM_{10} and DF (Fig. 5). This is consistent with the observations from elemental ratios, discussed in the previous section.

3.5.4. *Fern tissues (roots and leaves)*

Mean $^{206}Pb/^{207}Pb$ isotopic compositions of the fern tissues (leaves and roots) and WDs are closely aligned with PM_{10} and DFs. However, the soil isotopic composition was significantly different ($p < 0.0001$) from LDs, WDs, leaves and roots. These observations are also evident from the triple isotope plot of $^{206}Pb/^{207}Pb$ vs $^{208}Pb/^{207}Pb$. The triple isotope plot demonstrates that sources of Pb on the WD and inside the tissues are a mixture of PM_{10} and DF (Fig. 5). No particular influence of soil is observed on the roots and leaves. All these indicate that geogenic Pb from soil is not the primary source of Pb inside the plants. Previous investigations that used Pb isotopes, to differentiate the sources of Pb inside plant tissues demonstrated that Pb in roots can be sourced from soil [21,25,84] as well as from atmospheric fallouts [30,31]. Similar isotopic compositions in roots and leaves indicate a common source of absorption. Thus, the fern leaves exhibit the capacity to assimilate anthropogenic Pb from the PM, captured in the wax. From the sequentially leached soil sample, it can be observed that Pb isotopic composition of the corresponding root is comparable to SE, SC and SR, which in turn are similar to DF (Supplementary Figure 8). As SE, SC and SR are more mobile and bioavailable than SS [85], root preferentially uptakes anthropogenic Pb bound to these fractions, possibly atmospherically sourced instead of the silicate bound geogenic Pb. Consequently, it can be hypothesised that ferns have a preference for bidirectional anthropogenic Pb uptake from roots and leaves. This postulation can be tested with the help of MixSIAR results, discussed in the following section.

3.5.5. *Quantification of source contribution using mixing model (MixSIAR)*

Mixing models for leaves and roots can be helpful in quantifying the contribution of DF, PM_{10} and soil towards the concentration of Pb in the fern tissues. The results of concentration dependent MixSIAR analyses are depicted in Fig. 6. Soil had a greater influence on the roots (Fig. 7b) (mean contribution range = 4.8 ± 5.3 to 46 ± 19%) compared to leaves (Fig. 6a) (mean contribution range = 6.8 ± 7.8 to 10 ± 13%), indicating foliar dusts to be the source of Pb inside the leaves. Dust fall was revealed to be the largest contributor of Pb for both leaves (mean contribution range = 53 ± 20 to 73 ± 20%) and roots (mean contribution range = 33 ± 15 to 86 ± 18%). In fact, in some of the samples, DF demonstrated a larger influence on the roots compared to the corresponding leaves (Fig. 6). This suggests that the roots sourced Pb from the soil surface, which was contaminated by atmospheric dust fall. Leaves were influenced by PM_{10} aerosols to a greater extent compared to roots. Thus, in leaves, Pb was primarily sourced from DF and PM_{10} aerosols, while soil and DF were the primary sources of Pb inside the roots of the ferns.

4. Ferns as air purifying agent

4.1. *Suitability of the fern species*

The selection of the two fern species (*Pteris vittata* and *Pteridium*

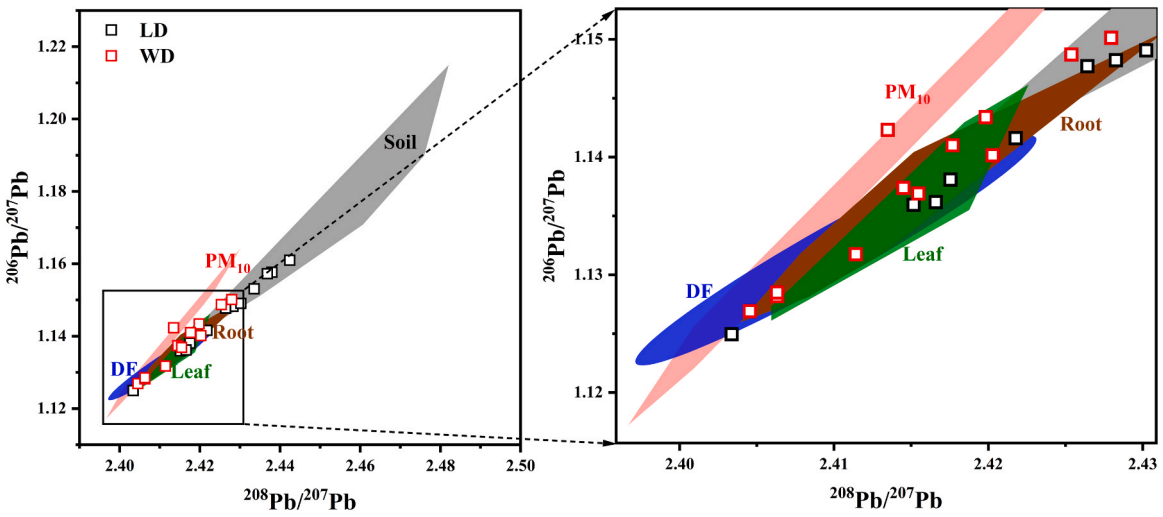

Fig. 5. : Triple isotope plots of 208Pb/207Pb vs 206Pb/207Pb for PM10 aerosols, DF, LD, WD, leaf, root and soil. The soil, PM_{10}, DF, leaf and roots are depicted as fields in grey, light red, blue, green and brown colours. The open black and red squares represent LD and WD respectively. The triple isotope plots demonstrate that the sources of Pb in WD, roots and leaves are primarily a mixture of PM_{10} and DFs, while LD demonstrates partial influence from soil along with PM_{10} and DF.

aquilinum) in this study was based on their abundant growth in the selected area. The abundances of these two particular species of fern in regions of high DF (Fig. 1b) associated with metals, indicate that they likely possess resistance to metal stress. Both species have been proven to have high tolerance for several heavy metals in previous studies. *Pteridium aquilinum* is one of the few species that is capable of naturally colonizing soils contaminated with Pb-Zn mine tailings [86]. *Pteridium aquilinum* has been investigated to be tolerant to toxic heavy metals/metalloid such as As, Cd, Cr, Cu, Ni, Pb and Zn [87–93]. Exposure to metals demonstrated no visible physiological damage to the ferns [88, 89,92], although nutrient supply might be necessary when exposed to high concentrations of selected metals, such as Cu for their proper growth [91]. *Pteris vittata* has been a well-known hyperaccumulator of As for more than two decades [94]. Apart from As, *Pteris vittata* also possesses tolerance to Cr, Ni, Cu, Pb and Zn and has been proven to phytostabilize metals in fly ash contaminated sites [95,96]. *Pteris vittata* was identified to be significantly tolerant to Pb with a survival rate of 93 – 100% when naturally growing at a Pb mining area containing up to 10% (w/w) soil Pb [97–99]. However, there can be a decrease in biomass when exposed to very high concentrations of metals [96, 99–101]. The ferns may have threshold concentrations for different metals above which they demonstrate genotoxic effects that may be expressed in the form of biomass decrease and chlorophyll content. Generally, both the fern species are tolerant to toxic heavy metals, with no indication of damage until exposed to high concentrations. The tolerable concentrations of Cd, Cr and Pb in both the species of the ferns as observed in previous literature are well above the concentrations of the respective metals in soil and DF from the present study (Fig. 7a).

This high metal tolerance of both the perennial species, surviving in tropical climatic conditions is accompanied by their adaptability to a wide range of environmental conditions [102,103]. *Pteridium aquilinum* can grow in slightly acidic to slightly alkaline environments while *Pteris vittata* prefers alkaline medium [86,104,105]. Heavy metal absorption and biomass may decrease with decreasing pH and extreme temperatures [104,105]. At regions of elevated CO_2 concentrations, the ferns demonstrate increased biomass and metal absorption [106]. *Pteridium aquilinum* can withstand water stress through stomatal closure, and *Pteris vittata* can grow at a wide range of moisture content (10 – 60%), thus, requiring low maintenance when used for air improvement purposes.[105,107].

4.2. Practical use and applicability of the ferns in botanical biofiltration units

The duration of leaf viability for metal capture can help in optimizing the implementation of fern-based metal remediation strategies. It allows for proper timing and planning of fern planting and harvesting cycles, ensuring the most effective utilization of their metal-capturing capabilities. The total mass of metals accumulated per unit area of the leaves in this study was used to calculate the number of days the ferns can remain viable for passive filtration in an indoor environment. The calculation was performed for Cr, Ni, Cu and Pb, based on the availability of indoor metal concentration data of PM_{10} [108] from an Indian city. The details of the process and data are provided in Supplementary material 1 and 3 respectively. The median number of days for which a 1 m^2 fern cover with 10% PM capture efficiency [109] can remain viable for Cr, Ni, Cu and Pb capture in a standard small residential room of volume 26 m^3 with an air change per hour of 1.01 [110] was determined to be 104, 234, 456 and 140 respectively (Fig. 7b). The species maintains its leaves for approximately 20 weeks from the emergence of a full-length leaf until the onset of senescence [102,111]. This natural process can effectively refresh a passive filtration system. Additionally, the passive filtration system when converted into an active one, can achieve a capture efficiency of up to ~90% for fern species [112]. In an active filtration system, PM is also captured on the substrate where the root grows [113]. Since this study provides evidence that roots have a preference for uptaking atmospheric particles deposited on the soil, implementing an active system would enhance the maximum amount of PM that can be assimilated by the ferns. These results indicate that these ferns can be utilized to design green walls capable of capturing heavy metal leaden PM and thus, acting as air purifying equipment. Botanical biofilters equipped with air purifying plants have been previously designed for indoor as well as outdoor environments [17,112,114,115]. The calculation for leaf viability presented here is for a small indoor area, that can be validated by designing a biofiltration unit with these ferns exposed to reasonable concentrations of PM bound heavy metals. The selected ferns can be arranged and maintained within a vertical framework of the botanical biofiltration unit. This framework allows the flow of air through the ferns, that effectively entraps the PM, while also housing a watering system for the optimal hydration of the ferns [114]. This basic, initial design for a small indoor area can be subsequently scaled up for designing of larger green walls that can be deployed on open roads.

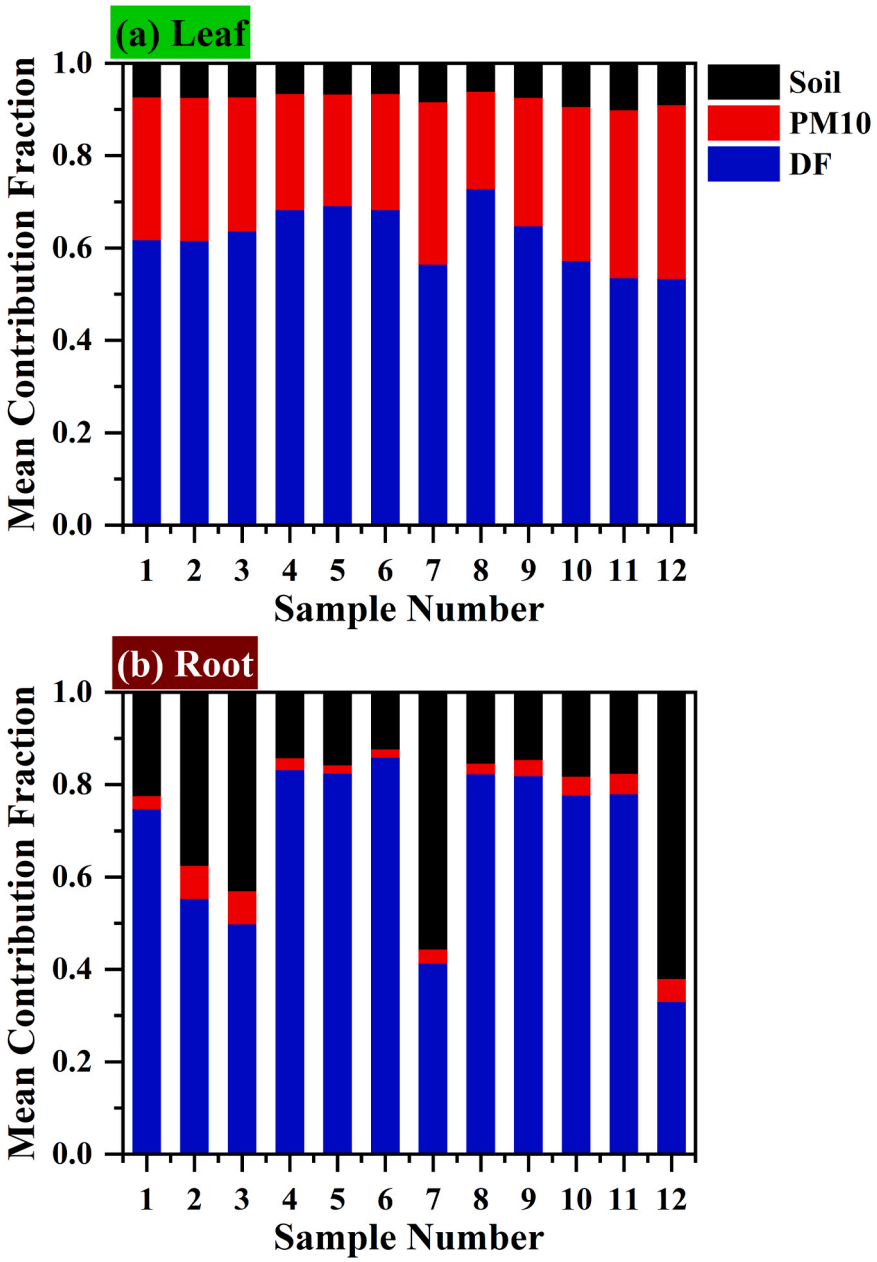

Fig. 6. : MixSIAR results for mean contribution of soil, DF and PM_{10} aerosols towards **(a)** leaf and **(b)** root Pb of the fern samples. The dominant sources of Pb in leaves were DF and PM_{10} aerosols, whereas Pb within fern roots primarily originated from soil and DF.

5. Novelty and challenges

This study introduces an approach that involves the layered separation of dust components on the foliar surface along with different components of fern tissues and soil. Subsequently, elemental concentrations and Pb isotopic ratios are analyzed for each component. This comprehensive approach allows source apportionment of metals in the ferns and subsequently evaluates the metal uptake capacity of the selected ferns. Previous studies have analyzed isotopic compositions of either water-washed leaves or the whole leaf along with the foliar dust. This fails to wash away the wax-bound PMs and produces an isotopic signature of a combination of the foliar dust and the leaves. Consequently, determining whether the produced isotopic signature is predominantly influenced by the leaf tissue or superficial foliar dust is challenging. Separation of each dust fraction and analyzing them for elemental and Pb isotopic compositions can provide a better understanding of the sources of atmospheric fallout as well as the process of the internalization of Pb by the leaves. Moreover, most studies (except [33]) relied on active PM and total suspended particulates (TSP) collection using pumping devices rather than dust fall collection to establish relationship between atmospheric fallout and foliar uptake. Analyzing dust fall without pumping systems is more representative of the foliar surface dust than active aerosols [116]. Dustfall collection also leads to the measurement of the dust fall flux of a region based on gravimetric quantifications [117].

Although the fern species can be efficient air-cleaning agents there can be certain challenges that need careful consideration. Both the selected fern species are perennial and senescence starts at about 20 weeks from the emergence of full-length leaves [102,111]. These senesced leaves will be metal-laden after their utilization in air-biofiltration system. Thus, improper disposal of the senesced leaves may lead to the transport of these heavy metals to animals and humans, which can bring about genotoxicity. Exposure to heavy metals like Cd and Pb has been known to bring about DNA damage and adverse effects on neurological,

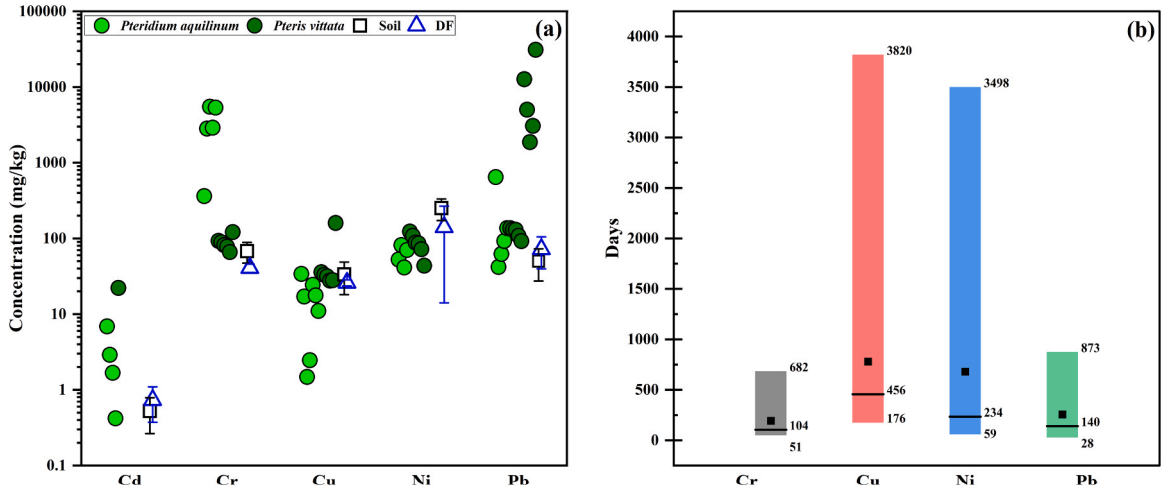

Fig. 7. : (a) Tolerated concentrations of Cd, Cr, Cu, Ni and Pb in roots of Pteridium aquilinum and Pteris vittata demonstrated in previous studies [86–93,95–99]. The concentrations of Cd, Cr, Cu, Ni and Pb in soil (open black squares) and DF (open blue triangles) from this study are also plotted for reference. **(b)** Box plots depicting the number of days a 1 m^2 fern cover can remain viable for Cr, Ni, Cu and Pb capture in a small 10 m^2 residential room as calculated from the leaf surface dust load data from the present study. The upper and lower extremes of the boxes represent maximum and minimum values respectively. Squares and lines inside boxes indicate mean and median values respectively. The values of each parameter are indicated on the right-hand side of the boxes in the order of maximum, median and minimum (from top to bottom).The data for indoor PM_{10} concentrations, volume of air in a room and air change rate were adopted from previous literatures [108–110].

cardiovascular and renal systems in mammals [118,119]. Thus, proper disposal of the contaminated biomass is of utmost importance to avoid secondary pollution. The strategies generally followed for disposal are pyrolysis, solvent/acid extraction, combustion, landfill, compaction, direct disposal etc. [120]. However, these methods are not entirely capable of immobilizing or fixing the metals present in the biomass. Thermochemical methods such as pyrolysis and combustion can release the volatile metals back into the atmosphere in the form of flue gas or pyrolysis gas, while the less volatile ones will be retained in the fly and bottom ash, leading to secondary pollution. Along with the metals, these processes also release other greenhouse gases like carbon dioxide, methane etc [121]. Solvent/acid extraction of the metals transforms the metals from the solid to the liquid phase. However, disposal of the metal-laden solvent/acid becomes a problem. Landfill disposal can be effective if proper confinement is achieved, without which there are chances of metal leakage into surrounding soil and groundwater. Compaction reduces the volume of the contaminated biomass and can be effective if the compacted biomass is properly sealed within impervious material [122–124]. An effective strategy can be mixing the compacted biomass with an impervious material like clay that will act as a barrier for the heavy metals inside [125]. This clay covered compacted biomass can be utilized in making bricks for construction purposes. However, the process of firing adopted for the preparation of these bricks can release the volatile heavy metals and other greenhouse gases back into the environment. Plant-based agricultural wastes have been used in the production of sustainable and environment-friendly unfired earth bricks successfully [126]. Thus, to immobilize the contaminants, it is most suitable to prepare unfired bricks out of the clay covered compacted biomass.

6. Comparison with other air purification technologies

The commonly used methods to purify indoor air are (i) fibrous filters, such as high-efficiency particulate air (HEPA) and ultra-low particulate air (ULPA) filters, (ii) electrostatic air filters and (iii) activated carbon filters [127]. Although HEPA and ULPA filters are very efficient in filtering PMs, they get saturated quickly and require frequent cleaning and replacements. Clogging also increases the pressure drop across the filtration medium, thus increasing the energy consumption of the process [128]. On the other hand, while botanical biofilters may be less efficient than HEPA and ULPA in removing PM, the plants in botanical biofilters regenerate leaves periodically, which eliminates the chances of pollutant saturation. This maintains the performance of the biofilters for a longer duration and reduces the replacement costs associated with HEPA filters.

Electrostatic filters, for e.g., electrostatic precipitators rely on electrostatic charges between PM and filtration media and are $>90\%$ effective in terms of PM filtering [127]. An electrostatic field has to be maintained in such filters, that require a constant supply of high voltage, thus, involving high energy consumption [128]. Similar to HEPA and ULPA filters, ESPs also require frequent cleaning (every few weeks) to maintain their filtration efficiency. Moreover, due to the ionization process involved, respiratory irritants such as ozone (O_3) may be generated during filtration, which further may react with other organic compounds to produce ultrafine secondary organic aerosol [129,130]. On the contrary, botanical biofilters can operate at much lower energy consumption and are also known to be effective in reducing organic pollutants [114].

Activated carbon filters are adsorption filters, that are efficient in the sorption of gaseous pollutants such as volatile organic compounds (VOC). However, they are not capable of filtering PMs [131].

Thus, compared to other technologies, botanical biofiltration is cost-effective and energy-efficient technique for indoor air purification. Periodic leaf generation along with heavy metal absorption capacity of the ferns makes this technique of air purification both economical and sustainable, although in particular instances it might be less efficient than HEPA or ULPA.

7. Conclusions

Based on elemental concentration, Pb isotopic compositions and subsequent mixing model analyses, it is evident that atmospheric fallout dominates as a source in both leaves and roots of ferns. The leaf surface contains aerosolized soil particles along with the atmospherically sourced particles that are internalized in the tissue. The soil which is contaminated with atmospheric fallout, still supplies crustally sourced metals to the roots and leaves. Thus, the sources of metals in soil, foliar surface and inside the fern tissues are a complex mixture of atmospheric fallouts (PM_{10} and DF) and crust (soil). This is evident from the MixSIAR analysis, where we observe minor contributions of soil in leaves, and a

more pronounced contribution from soil in roots. However, all the components analyzed in this study consistently indicate the dominance of atmospherically sourced metals both on the surface as well as within the fern tissues. The study shows that ferns, with their ability to regenerate leaves, effectively capture heavy metals from the atmosphere, making them suitable for prolonged use as metal-trapping agents. This suggests ferns could be utilized in botanical biofiltration systems for indoor air purification, offering efficiency, cost-effectiveness, and aesthetic appeal compared to mechanical purifiers like HEPA and ULPA filters. While HEPA filters are commonly used for PM filtration, they require frequent cleaning and replacement due to saturation, whereas ferns regenerate leaves, maintaining biofilter performance and reducing replacement costs.

Environmental implication

The global phase out of leaded gasoline has often been regarded as 'magnificent achievement of pollution management', accompanied by a growing feeling that the 'lead problem' has been solved. Noteworthily, this study shows that aerosol Pb in India is still 100–1000 times enriched than crustal average. All other studies reporting enriched aerosol Pb indicate that new Pb sources are present. This elevated aerosol Pb aligns with the high blood lead levels in India; and the increasing trends of Pb in paleoenvironmental records in South Asia. These indicate that there is still a need for further action and mitigation studies.

CRediT authorship contribution statement

Xianfeng Wang: Writing – review & editing, Resources. **Reshmi Das:** Writing – review & editing, Supervision, Resources, Project administration, Methodology, Funding acquisition, Formal analysis, Conceptualization. **Iravati Ray:** Writing – original draft, Visualization, Software, Methodology, Investigation, Formal analysis, Data curation, Conceptualization. **Sambuddha Misra:** Visualization, Supervision, Resources, Methodology, Investigation, Data curation. **Mengli Chen:** Writing – review & editing, Formal analysis.

Declaration of Competing Interest

The authors declare that they have no known competing financial interests or personal relationships that could have appeared to influence the work reported in this paper.

Data Availability

Data included in manuscript.

Acknowledgement

R.D. acknowledges the financial supports from the Department of Environment, Government of West Bengal (Grant no. ENV-29014(11)/1/2022-ACS (ENV)) and Science and Engineering Research Board (Grant no. SPG/2021/002652).

S.M. acknowledges Science and Engineering Research Board (SERB), Govt. of India, for financial support (Grant no. SPR\2021\000808).

X.W. acknowledges the financial support from the Earth Observatory of Singapore and the Imperial College - Nanyang Technological University Collaboration Fund (INCF-2023-015). This work comprises Earth Observatory of Singapore contribution no 587.

R.D.'s position is supported by University Gransts Commission through the Faculty Recharge Programme (FRP-74) and I.R.'s position is supported by All India Council for Technical Education (AICTE), through the AICTE Doctoral Fellow Programme (S2021280)

The authors further extend their gratitude to **Mr. Apurba Naskar** (PhD student at University of Alabama) for his invaluable assistance in the sampling process.

Appendix A. Supporting information

Supplementary data associated with this article can be found in the online version at doi:10.1016/j.jhazmat.2024.134014.

References

[1] Gakidou, E., et al., 2017. Global, regional, and national comparative risk assessment of 84 behavioural, environmental and occupational, and metabolic risks or clusters of risks, 1990–2016: a systematic analysis for the Global Burden of Disease Study 2016. Lancet 390, 1345–1422. https://doi.org/10.1016/S0140-6736(17)32366-8.

[2] Komárek, M., Ettler, V., Chrastný, V., Mihaljevič, M., 2008. Lead isotopes in environmental sciences: a review. Environ Int 34, 562–577. https://doi.org/10.1016/j.envint.2007.10.005.

[3] Li, H., Qian, X., Wang, Q., 2013. Heavy metals in atmospheric particulate matter: a comprehensive understanding is needed for monitoring and risk mitigation. Environ Sci Technol 47, 13210–13211. https://doi.org/10.1021/es404751a.

[4] Kumari, M., Bhattacharya, T., 2023. A review on bioaccessibility and the associated health risks due to heavy metal pollution in coal mines: content and trend analysis. Environ Dev 46, 100859. https://doi.org/10.1016/j.envdev.2023.100859.

[5] Roy, D., Kim, J., Lee, M., Park, J., 2023. Adverse impacts of Asian dust events on human health and the environment—A probabilistic risk assessment study on particulate matter-bound metals and bacteria in Seoul, South Korea. Sci Total Environ 875, 162637. https://doi.org/10.1016/j.scitotenv.2023.162637.

[6] Vithanage, M., Bandara, P.C., Novo, L.A.B., Kumar, A., Ambade, B., Naveendrakumar, G., et al., 2022. Deposition of trace metals associated with atmospheric particulate matter: environmental fate and health risk assessment. Chemosphere 303, 135051. https://doi.org/10.1016/j.chemosphere.2022.135051.

[7] Xu, H., Ho, S.S.H., Cao, J., Guinot, B., Kan, H., Shen, Z., et al., 2017. A 10-year observation of PM2.5-bound nickel in Xi'an, China: effects of source control on its trend and associated health risks. Sci Rep 7, 41132. https://doi.org/10.1038/srep41132.

[8] Lum, K.R., Betteridge, J.S., Macdonald, R.R., 1982. The potential availability of P, Al, Cd, Co, Cr, Cu, Fe, Mn, Ni, Pb and Zn in urban particulate matter. Environ Technol Lett 3, 57–62. https://doi.org/10.1080/09593338209384098.

[9] UNICEF and Pure Earth, The toxic truth, (2020). ⟨https://www.unicef.org/reports/toxic-truth-childrens-exposure-to-lead-pollution-2020⟩ (accessed March 20, 2022).

[10] Rocha, L.D., Costa, G.M.D., Gehlen, G., Droste, A., Schmitt, J.L., 2014. Morphometric differences of *Microgramma squamulosa* (Kaulf.) de la Sota (Polypodiaceae) leaves in environments with distinct atmospheric air quality. Acad Bras Ciênc 86, 1137–1146. https://doi.org/10.1590/0001-3765201420130094.

[11] Kachenko, A.G., Singh, B., Bhatia, N.P., 2007. Heavy metal tolerance in common fern species. Aust J Bot 55, 63–73. https://doi.org/10.1071/BT06063.

[12] Abhijith, K.V., Kumar, P., 2020. Quantifying particulate matter reduction and their deposition on the leaves of green infrastructure. Environ Pollut 265, 114884. https://doi.org/10.1016/j.envpol.2020.114884.

[13] Beckett, K.P., Freer-Smith, P.H., Taylor, G., 2000. The capture of particulate pollution by trees at five contrasting urban sites. Arboric J 24, 209–230. https://doi.org/10.1080/03071375.2000.9747273.

[14] Hrotko, K., Gyeviki, M., Sütörine, M.D., Magyar, L., Meśzaŕos, R., Honfi, P., et al., 2020. Foliar dust and heavy metal deposit on leaves of urban trees in Budapest (Hungary). | SpringerLink. ⟨https://link.springer.com/article/10.1007/s10653-020-00769-y⟩ (accessed March 2, 2022).

[15] N. Meravi, P.K. Singh, S.K. Prajapati, Seasonal variation of dust deposition on plant leaves and its impact on various photochemical yields of plants - ScienceDirect, (2021). ⟨https://www.sciencedirect.com/science/article/pii/S2667010021001451⟩ (accessed March 2, 2022).

[16] Ottelé, M., van Bohemen, H.D., Fraaij, A.L.A., 2010. Quantifying the deposition of particulate matter on climber vegetation on living walls. Ecol Eng 36, 154–162. https://doi.org/10.1016/j.ecoleng.2009.02.007.

[17] Paull, N., Krix, D., Irga, P., Torpy, F., 2019. Airborne particulate matter accumulation on common green wall plants. Int J Phytoremediat 22, 1–13. https://doi.org/10.1080/15226514.2019.1696744.

[18] Redondo-Bermúdez, M. del C., Gulenc, I.T., Cameron, R.W., Inkson, B.J., 2021. Green barriers' for air pollutant capture: Leaf micromorphology as a mechanism to explain plants capacity to capture particulate matter. Environ Pollut 288, 117809. https://doi.org/10.1016/j.envpol.2021.117809.

[19] Sgrigna, G., Sæbø, A., Gawronski, S., Popek, R., Calfapietra, C., 2015. Particulate Matter deposition on Quercus ilex leaves in an industrial city of central Italy. Environ Pollut 197, 187–194. https://doi.org/10.1016/j.envpol.2014.11.030.

[20] Weerakkody, U., Dover, J.W., Mitchell, P., Reiling, K., 2017. Particulate matter pollution capture by leaves of seventeen living wall species with special reference to rail-traffic at a metropolitan station. Urban Urban Green 27, 173–186. https://doi.org/10.1016/j.ufug.2017.07.005.

[21] Hu, X., Zhang, Y., Luo, J., Xie, M., Wang, T., Lian, H., 2011. Accumulation and quantitative estimates of airborne lead for a wild plant (Aster subulatus). Chemosphere 82, 1351–1357. https://doi.org/10.1016/j.chemosphere.2010.11.079.

[22] Schreck, E., Bonnard, R., Laplanche, C., Leveque, T., Foucault, Y., Dumat, C., 2012. DECA: a new model for assessing the foliar uptake of atmospheric lead by vegetation, using Lactuca sativa as an example. J Environ Manag 112, 233–239. https://doi.org/10.1016/j.jenvman.2012.07.006.
[23] Schreck, E., Foucault, Y., Sarret, G., Sobanska, S., Cécillon, L., Castrec-Rouelle, M., et al., 2012. Metal and metalloid foliar uptake by various plant species exposed to atmospheric industrial fallout: Mechanisms involved for lead. Sci Total Environ 427–428, 253–262. https://doi.org/10.1016/j.scitotenv.2012.03.051.
[24] Uzu, G., Sobanska, S., Sarret, G., Muñoz, M., Dumat, C., 2010. Foliar Lead Uptake by Lettuce Exposed to Atmospheric Fallouts. Environ Sci Technol 44, 1036–1042. https://doi.org/10.1021/es902190u.
[25] Bi, X., Feng, X., Yang, Y., Li, X., Shin, G.P.Y., Li, F., et al., 2009. Allocation and source attribution of lead and cadmium in maize (Zea mays L.) impacted by smelting emissions. Environ Pollut 157, 834–839. https://doi.org/10.1016/j.envpol.2008.11.013.
[26] Cong, L., Zhou, S., Niyogi, D., Wu, Y., Yan, G., Dai, L., et al., 2022. Concentrations and isotopic analysis for the sources and transfer of lead in an urban atmosphere-plant-soil system. J Environ Manag 311, 114771. https://doi.org/10.1016/j.jenvman.2022.114771.
[27] Fan, J., Dai, W., Wang, Y., Zhang, B., Fang, J., Lou, L., et al., 2020. Seasonal disparities in airborne lead (Pb) and associated foliar uptake by ryegrass (Lolium perenne L.): A Pb isotopic approach. Sci Total Environ 708, 134734. https://doi.org/10.1016/j.scitotenv.2019.134734.
[28] Gao, P.-P., Xue, P.-Y., Dong, J.-W., Zhang, X.-M., Sun, H.-X., Geng, L.-P., et al., 2021. Contribution of PM2.5-Pb in atmospheric fallout to Pb accumulation in Chinese cabbage leaves via stomata. J Hazard Mater 407, 124356. https://doi.org/10.1016/j.jhazmat.2020.124356.
[29] Li, F.-L., Liu, C.-Q., Yang, Y.-G., Bi, X.-Y., Liu, T.-Z., Zhao, Z.-Q., 2012. Natural and anthropogenic lead in soils and vegetables around Guiyang city, southwest China: a Pb isotopic approach. Sci Total Environ 431, 339–347. https://doi.org/10.1016/j.scitotenv.2012.05.040.
[30] Ma, C., Liu, F., Jin, K., Hu, B., Wei, M., Zhao, J., et al., 2019. Effects of ATmospheric Fallout on Lead Contamination of Wheat Tissues Based on Stable Isotope Ratios. Bull Environ Contam Toxicol 103, 676–682. https://doi.org/10.1007/s00128-019-02702-1.
[31] Ma, C., Liu, F.-Y., Hu, B., Wei, M.-B., Zhao, J.-H., Zhang, K., et al., 2019. Direct evidence of lead contamination in wheat tissues from atmospheric deposition based on atmospheric deposition exposure contrast tests. Ecotoxicol Environ Saf 185, 109688. https://doi.org/10.1016/j.ecoenv.2019.109688.
[32] Xiong, T., Leveque, T., Shahid, M., Foucault, Y., Mombo, S., Dumat, C., 2014. Lead and cadmium phytoavailability and human bioaccessibility for vegetables exposed to soil or atmospheric pollution by process ultrafine particles. J Environ Qual 43, 1593–1600. https://doi.org/10.2134/jeq2013.11.0469.
[33] Zhang, X.-Y., Geng, L.-P., Gao, P.-P., Dong, J.-W., Zhou, C., Li, H.-B., et al., 2022. Bioimaging of Pb by LA-ICP-MS and Pb isotopic compositions reveal distributions and origins of Pb in wheat grain. Sci Total Environ 802, 149729. https://doi.org/10.1016/j.scitotenv.2021.149729.
[34] Klaminder, J., Bindler, R., Emteryd, O., Renberg, I., 2005. Uptake and recycling of lead by boreal forest plants: Quantitative estimates from a site in northern Sweden. Geochim Cosmochim Acta 69, 2485–2496. https://doi.org/10.1016/j.gca.2004.11.013.
[35] David, L.M., Ravishankara, A.R., Kodros, J.K., Pierce, J.R., Venkataraman, C., Sadavarte, P., 2019. Premature mortality due to PM2.5 over India: effect of atmospheric transport and anthropogenic emissions. GeoHealth 3, 2–10. https://doi.org/10.1029/2018GH000169.
[36] Gupta, A.K., Karar, K., Ayoob, S., John, K., 2008. Spatio-temporal characteristics of gaseous and particulate pollutants in an urban region of Kolkata, India. Atmos Res 87, 103–115. https://doi.org/10.1016/j.atmosres.2007.07.008.
[37] Upadhyay, A., Kanchan, K., Goyal, P.G., Yerramilli, A., Gorai, A.K., 2014. Development of a Fuzzy pattern recognition model for air quality assessment of Howrah City. Aerosol Air Qual Res 14, 1639–1652. https://doi.org/10.4209/aaqr.2013.04.0118.
[38] State of Global Air, Air Pollution and Health in Cities, (2022). ⟨https://www.stateofglobalair.org/resources/health-in-cities⟩ (accessed April 18, 2023).
[39] Das, R., Bin Mohamed Mohtar, A.T., Rakshit, D., Shome, D., Wang, X., 2018. Sources of atmospheric lead (Pb) in and around an Indian megacity. Atmos Environ 193, 57–65. https://doi.org/10.1016/j.atmosenv.2018.08.062.
[40] Gulson, B.L., Davis, J.J., Mizon, K.J., Korsch, M.J., Bawden-Smith, J., 1995. Sources of lead in soil and dust and the use of dust fallout as a sampling medium. Sci Total Environ 166, 245–262. https://doi.org/10.1016/0048-9697(95)04505-U.
[41] Dzierżanowski, K., Popek, R., Gawrońska, H., Sæbø, A., Gawroński, S.W., 2011. Deposition of particulate matter of different size fractions on leaf surfaces and in waxes of urban forest species. Int J Phytoremediat 13, 1037–1046. https://doi.org/10.1080/15226514.2011.552929.
[42] O'Neal, M.E., Landis, D.A., Isaacs, R., 2002. An inexpensive, accurate method for measuring leaf area and defoliation through digital image analysis. J Econ Entomol 95, 1190–1194. https://doi.org/10.1603/0022-0493-95.6.1190.
[43] Baker, J., Peate, D., Waight, T., Meyzen, C., 2004. Pb isotopic analysis of standards and samples using a 207Pb–204Pb double spike and thallium to correct for mass bias with a double-focusing MC-ICP-MS. Chem Geol 211, 275–303. https://doi.org/10.1016/j.chemgeo.2004.06.030.
[44] White, W.M., Albarède, F., Télouk, P., 2000. High-precision analysis of Pb isotope ratios by multi-collector ICP-MS. Chem Geol 167, 257–270. https://doi.org/10.1016/S0009-2541(99)00182-5.
[45] Gelwicks, J.T., Hayes, J.M., 1990. Carbon-isotopic analysis of dissolved acetate. Anal Chem 62, 535–539. https://doi.org/10.1021/ac00204a021.
[46] B. Stock, A. Jackson, E. Ward, J. Venkiteswaran, brianstock/MixSIAR 3.1.9, (2018). https://doi.org/10.5281/zenodo.1209993.
[47] Ray, I., Das, R., 2023. A lingering legacy of leaded gasoline in Southeast Asia. Commun Earth Environ 4, 1–11. https://doi.org/10.1038/s43247-023-01135-3.
[48] Chen, H., Yan, Y., Hu, D., Peng, L., Wang, C., 2023. High contribution of vehicular exhaust and coal combustion to PM2.5-bound Pb pollution in an industrial city in North China: an insight from isotope. Atmos Environ 294, 119503. https://doi.org/10.1016/j.atmosenv.2022.119503.
[49] Dietrich, M., Krekeler, M.P.S., Kousehlar, M., Widom, E., 2021. Quantification of Pb pollution sources in complex urban environments through a multi-source isotope mixing model based on Pb isotopes in lichens and road sediment. Environ Pollut 288, 117815. https://doi.org/10.1016/j.envpol.2021.117815.
[50] Koffman, B.G., Saylor, P., Zhong, R., Sethares, L., Yoder, M.F., Hanschka, L., et al., 2022. Provenance of Anthropogenic Pb and Atmospheric Dust to Northwestern North America. Environ Sci Technol 56, 13107–13118. https://doi.org/10.1021/acs.est.2c03767.
[51] Longman, J., Struve, T., Pahnke, K., 2022. Spatial and temporal trends in mineral dust provenance in the South Pacific—evidence from mixing models. Paleoceanogr Paleoclimatology 37, e2021PA004356. https://doi.org/10.1029/2021PA004356.
[52] Longman, J., Veres, D., Ersek, V., Phillips, D.L., Chauvel, C., Tamas, C.G., 2018. Quantitative assessment of Pb sources in isotopic mixtures using a Bayesian mixing model. Sci Rep 8, 6154. https://doi.org/10.1038/s41598-018-24474-0.
[53] O. US EPA, National Ambient Air Quality Standards (NAAQS) for PM, (2020). ⟨https://www.epa.gov/pm-pollution/national-ambient-air-quality-standards-naaqs-pm⟩ (accessed May 6, 2023).
[54] Agrawal, M., Singh, J., 2000. Impact of Coal Power Plant Emission on the Foliar Elemental Concentrations in Plants in a Low Rainfall Tropical Region. Environ Monit Assess 60, 261–282. https://doi.org/10.1023/A:1006135317896.
[55] Majee, C.K., Ali, S.Y., Padhy, P.K., 2023. Effects of atmospheric dust particles on common medicinal plants in an industrial area of West Bengal, India. Environ Monit Assess 195, 978. https://doi.org/10.1007/s10661-023-11573-3.
[56] Mishra, M., Kulshrestha, U., 2017. Chemical characteristics and deposition fluxes of dust-carbon mixed coarse aerosols at three sites of Delhi, NCR. J Atmos Chem 74, 399–421. https://doi.org/10.1007/s10874-016-9349-1.
[57] Singh, R.K., Agrawal, M., 2005. Atmospheric depositions around a heavily industrialized area in a seasonally dry tropical environment of India. Environ Pollut 138, 142–152. https://doi.org/10.1016/j.envpol.2005.02.009.
[58] Abubakar, A.A., Yilbas, B.S., Al-Qahtani, H., Alzaydi, A., Alhelou, S., 2020. Environmental dust repelling from hydrophobic and hydrophilic surfaces under vibrational excitation. Sci Rep 10, 14346. https://doi.org/10.1038/s41598-020-71356-5.
[59] Prajapati, S.K., Tripathi, B.D., 2008. Seasonal Variation of Leaf Dust Accumulation and Pigment Content in Plant Species Exposed to Urban Particulates Pollution. J Environ Qual 37, 865–870. https://doi.org/10.2134/jeq2006.0511.
[60] Prusty, B.A.K., Mishra, P.C., Azeez, P.A., 2005. Dust accumulation and leaf pigment content in vegetation near the national highway at Sambalpur, Orissa, India. Ecotoxicol Environ Saf 60, 228–235. https://doi.org/10.1016/j.ecoenv.2003.12.013.
[61] Roy, A., Bhattacharya, T., Kumari, M., 2020. Air pollution tolerance, metal accumulation and dust capturing capacity of common tropical trees in commercial and industrial sites. Sci Total Environ 722, 137622. https://doi.org/10.1016/j.scitotenv.2020.137622.
[62] Singh, S., Bhattacharya, P., Gupta, N.C., 2018. Dust particles characterization and innate resistance for Thevetia peruviana in different land-use pattern of urban area. Int J Environ Sci Technol 15, 1061–1072. https://doi.org/10.1007/s13762-017-1461-5.
[63] Yunus, Mohd, Dwivedi, A.K., Kulshreshtha, K., Ahmad, K.J., 1985. Dust loadings on some common plants near Lucknow City. Environ Pollut Ser B Chem Phys 9, 71–80. https://doi.org/10.1016/0143-148X(85)90040-0.
[64] Rudnick, R.L., Gao, S., 2003. 3.01 - Composition of the Continental Crust. In: Holland, H.D., Turekian, K.K. (Eds.), Treatise Geochem. Pergamon, Oxford, pp. 1–64. https://doi.org/10.1016/B0-08-043751-6/03016-4.
[65] Sutherland, R.A., 2000. Bed sediment-associated trace metals in an urban stream, Oahu, Hawaii. Environ Geol 39, 611–627. https://doi.org/10.1007/s002540050473.
[66] Vilomet, J.D., Veron, A., Ambrosi, J.P., Moustier, S., Bottero, J.Y., Chatelet-Snidaro, L., 2003. Isotopic Tracing of Landfill Leachates and Pollutant Lead Mobility in Soil and Groundwater. Environ Sci Technol 37, 4586–4591. https://doi.org/10.1021/es010245r.
[67] Wang, H., Maher, B.A., Ahmed, I.A., Davison, B., 2019. Efficient removal of ultrafine particles from diesel exhaust by selected tree species: implications for roadside planting for improving the quality of urban air. Environ Sci Technol 53, 6906–6916. https://doi.org/10.1021/acs.est.8b06629.
[68] Ray, I., Das, R., Chua, S.L., Wang, X., 2022. Seasonal variation of atmospheric Pb sources in Singapore - Elemental and lead isotopic compositions of PM10 as source tracer. Chemosphere 307, 136029. https://doi.org/10.1016/j.chemosphere.2022.136029.
[69] Sen, I.S., Bizimis, M., Tripathi, S.N., Paul, D., 2016. Lead isotopic fingerprinting of aerosols to characterize the sources of atmospheric lead in an industrial city of India. Atmos Environ 129, 27–33. https://doi.org/10.1016/j.atmosenv.2016.01.005.

[70] Shotyk, W., 1996. Peat bog archives of atmospheric metal deposition: geochemical evaluation of peat profiles, natural variations in metal concentrations, and metal enrichment factors. Environ Rev 4, 149–183. https://doi.org/10.1139/a96-010.
[71] Birmili, W., Allen, A.G., Bary, F., Harrison, R.M., 2006. Trace Metal Concentrations and Water Solubility in Size-Fractionated Atmospheric Particles and Influence of Road Traffic. Environ Sci Technol 40, 1144–1153. https://doi.org/10.1021/es0486925.
[72] Das, A., Krishna, K., Kumar, R., Das, A., Sengupta, S., Ghosh, J.G., 2016. Tracing lead contamination in foods in the city of Kolkata, India. Environ Sci Pollut Res 23, 22454–22466. https://doi.org/10.1007/s11356-016-7409-3.
[73] Kumar, S., Aggarwal, S.G., Malherbe, J., Barre, J.P.G., Berail, S., Gupta, P.K., et al., 2016. Tracing dust transport from Middle-East over Delhi in March 2012 using metal and lead isotope composition. Atmos Environ 132, 179–187. https://doi.org/10.1016/j.atmosenv.2016.03.002.
[74] Allègre, C.J., Lewin, E., 1989. Chemical structure and history of the Earth: evidence from global non-linear inversion of isotopic data in a three-□ model. Earth Planet Sci Lett 96, 61–88. https://doi.org/10.1016/0012-821X(89)90124-6.
[75] Asmerom, Y., Jacobsen, S.B., 1993. The Pb isotopic evolution of the Earth: inferences from river water suspended loads. Earth Planet Sci Lett 115, 245–256. https://doi.org/10.1016/0012-821X(93)90225-X.
[76] Hemming, S.R., McLennan, S.M., 2001. Pb isotope compositions of modern deep sea turbidites. Earth Planet Sci Lett 184, 489–503. https://doi.org/10.1016/S0012-821X(00)00340-X.
[77] Millot, R., Allègre, C.-J., Gaillardet, J., Roy, S., 2004. Lead isotopic systematics of major river sediments: a new estimate of the Pb isotopic composition of the Upper Continental Crust. Chem Geol 203, 75–90. https://doi.org/10.1016/j.chemgeo.2003.09.002.
[78] Rudnick, R.L., Goldstein, S.L., 1990. The Pb isotopic compositions of lower crustal xenoliths and the evolution of lower crustal Pb. Earth Planet Sci Lett 98, 192–207. https://doi.org/10.1016/0012-821X(90)90059-7.
[79] Bi, X., Liang, S., Li, X., 2013. A novel in situ method for sampling urban soil dust: Particle size distribution, trace metal concentrations, and stable lead isotopes. Environ Pollut 177, 48–57. https://doi.org/10.1016/j.envpol.2013.01.045.
[80] Bacon, J.R., Hewitt, I.J., 2005. Heavy metals deposited from the atmosphere on upland Scottish soils: Chemical and lead isotope studies of the association of metals with soil components. Geochim Cosmochim Acta 69, 19–33. https://doi.org/10.1016/j.gca.2004.06.030.
[81] Farmer, J.G., Graham, M.C., Yafa, C., Cloy, J.M., Freeman, A.J., MacKenzie, A.B., 2006. Use of 206Pb/207Pb ratios to investigate the surface integrity of peat cores used to study the recent depositional history and geochemical behaviour of inorganic elements in peat bogs. Glob Planet Change 53, 240–248. https://doi.org/10.1016/j.gloplacha.2006.03.006.
[82] Kelepertzis, E., Chrastný, V., Botsou, F., Sigala, E., Kypritidou, Z., Komárek, M., et al., 2021. Tracing the sources of bioaccessible metal(loid)s in urban environments: A multidisciplinary approach. Sci Total Environ 771, 144827. https://doi.org/10.1016/j.scitotenv.2020.144827.
[83] Wong, C.S.C., Li, X.D., 2004. Pb contamination and isotopic composition of urban soils in Hong Kong. Sci Total Environ 319, 185–195. https://doi.org/10.1016/S0048-9697(03)00403-0.
[84] Ma, C., Liu, F., Xie, P., Zhang, K., Yang, J., Zhao, J., et al., 2021. Mechanism of Pb absorption in wheat grains. J Hazard Mater 415, 125618. https://doi.org/10.1016/j.jhazmat.2021.125618.
[85] Olajire, A.A., Ayodele, E.T., Oyedirdan, G.O., 2003. E.A. Oluyemi, Levels and Speciation of Heavy Metals in Soils of Industrial Southern Nigeria. Environ Monit Assess 85, 135–155. https://doi.org/10.1023/A:1023613418727.
[86] Shu, W.S., Ye, Z.H., Zhang, Z.Q., Lan, C.Y., Wong, M.H., 2005. Natural colonization of plants on five lead/zinc mine tailings in Southern China. Restor Ecol 13, 49–60. https://doi.org/10.1111/j.1526-100X.2005.00007.x.
[87] Chang, J.-S., Yoon, I.-H., Kim, K.-W., 2009. Heavy metal and arsenic accumulating fern species as potential ecological indicators in As-contaminated abandoned mines. Ecol Indic 9, 1275–1279. https://doi.org/10.1016/j.ecolind.2009.03.011.
[88] de, F., Eslava-Silva, J., Muñíz-Díaz de León, M.E., Jiménez-Estrada, M., 2023. Pteridium aquilinum (Dennstaedtiaceae), a Novel Hyperaccumulator Species of Hexavalent Chromium. Appl Sci 13, 5621. https://doi.org/10.3390/app13095621.
[89] Gómez-Bernal, J.M., Ruiz-Huerta, E.A., Armienta-Hernández, M.A., Luna-Pabello, V.M., 2017. Evaluation of the removal of heavy metals in a natural wetland impacted by mining activities in Mexico. Environ Earth Sci 76, 801. https://doi.org/10.1007/s12665-017-7144-1.
[90] Kubicka, K., Samecka-Cymerman, A., Kolon, K., Kosiba, P., Kempers, A.J., 2015. Chromium and nickel in Pteridium aquilinum from environments with various levels of these metals. Environ Sci Pollut Res 22, 527–534. https://doi.org/10.1007/s11356-014-3379-5.
[91] Olaifa, F.E., Omekam, A.J., 2014. Studies on PHytoremediation of Copper Using Pteridium Aquilinum (Bracken Fern) in the presence of biostimulants and bioassay using Clarias gariepinus Juveniles. Int J Phytoremediat 16, 219–234. https://doi.org/10.1080/15226514.2013.773272.
[92] Pratas, J., Favas, P.J.C., D'Souza, R., Varun, M., Paul, M.S., 2013. Phytoremedial assessment of flora tolerant to heavy metals in the contaminated soils of an abandoned Pb mine in Central Portugal. Chemosphere 90, 2216–2225. https://doi.org/10.1016/j.chemosphere.2012.09.079.
[93] Turnau, K., Kottke, I., Oberwinkler, F., 1993. Element localization in mycorrhizal roots of Pteridium aquilinum (L.) Kuhn collected from experimental plots treated with cadmium dust. N Phytol 123, 313–324. https://doi.org/10.1111/j.1469-8137.1993.tb03741.x.
[94] Ma, L.Q., Komar, K.M., Tu, C., Zhang, W., Cai, Y., Kennelley, E.D., 2001. A fern that hyperaccumulates arsenic, 579–579 Nature 409. https://doi.org/10.1038/35054664.
[95] Kumari, A., Lal, B., Pakade, Y.B., Chand, P., 2011. Assessment of Bioaccumulation of Heavy Metal by Pteris vittata L. Growing in the Vicinity of Fly Ash. Int J Phytoremediat 13, 779–787. https://doi.org/10.1080/15226514.2010.525561.
[96] Wu, F.Y., Leung, H.M., Wu, S.C., Ye, Z.H., Wong, M.H., 2009. Variation in arsenic, lead and zinc tolerance and accumulation in six populations of Pteris vittata L. from China. Environ Pollut 157, 2394–2404. https://doi.org/10.1016/j.envpol.2009.03.022.
[97] Ha, N.T.H., Sakakibara, M., Sano, S., Nhuan, M.T., 2011. Uptake of metals and metalloids by plants growing in a lead–zinc mine area, Northern Vietnam. J Hazard Mater 186, 1384–1391. https://doi.org/10.1016/j.jhazmat.2010.12.020.
[98] Soongsombat, P., Kruatrachue, M., Chaiyarat, R., Pokethitiyook, P., Ngernsansaruay, C., 2009. Lead Tolerance and Accumulation in Pteris vittata and Pityrogramma calomelanos, and Their Potential for Phytoremediation of Lead-Contaminated Soil. Int J Phytoremediat 11, 396–412. https://doi.org/10.1080/15226510802565634.
[99] Wan, X., Lei, M., Chen, T., Zhou, G., Yang, J., Zhou, X., et al., 2014. Phytoremediation potential of Pteris vittata L. under the combined contamination of As and Pb: beneficial interaction between As and Pb. Environ Sci Pollut Res 21, 325–336. https://doi.org/10.1007/s11356-013-1895-3.
[100] Fayiga, A.O., Ma, L.Q., Cao, X., Rathinasabapathi, B., 2004. Effects of heavy metals on growth and arsenic accumulation in the arsenic hyperaccumulator Pteris vittata L. Environ Pollut 132, 289–296. https://doi.org/10.1016/j.envpol.2004.04.020.
[101] Zheng, Y., Xu, W., He, Z., Ma, M., 2008. Plant regeneration of the arsenic hyperaccumulator Pteris vittata L. from spores and identification of its tolerance and accumulation of arsenic and copper. Acta Physiol Plant 30, 249–255. https://doi.org/10.1007/s11738-007-0114-6.
[102] USDA, Pteridium aquilinum, (2018). ⟨https://www.fs.usda.gov/database/feis/plants/fern/pteaqu/all.html#195⟩ (accessed June 29, 2023).
[103] Vélez-Gavilán, J., 2020. Pteris vittata (Chinese ladder brake fern), CABI Compend. CABI Compend, 119837. https://doi.org/10.1079/cabicompendium.119837.
[104] Anh, B.T.K., Minh, N.N., Ha, N.T.H., Kim, D.D., Kien, N.T., Trung, N.Q., et al., 2018. Field survey and comparative study of pteris vittata and pityrogramma calomelanos grown on arsenic contaminated lands with different soil pH. Bull Environ Contam Toxicol 100, 720–726. https://doi.org/10.1007/s00128-018-2325-5.
[105] Xu, W., Du, Q., Yan, S., Cao, Y., Liu, X., Guan, D.-X., et al., 2022. Geographical distribution of As-hyperaccumulator Pteris vittata in China: environmental factors and climate changes. Sci Total Environ 803, 149864. https://doi.org/10.1016/j.scitotenv.2021.149864.
[106] Zheng, J., Wang, H., Li, Z., Tang, S., Chen, Z., 2008. Using elevated carbon dioxide to enhance copper accumulation in pteridium revolutum, a copper-tolerant plant, under experimental conditions. Int J Phytoremediat 10, 161–172. https://doi.org/10.1080/15226510801913934.
[107] Tinklin, R., Bowling, D.J.F., 1969. The water relations of bracken: a preliminary study. J Ecol 57, 669–671. https://doi.org/10.2307/2258491.
[108] Kulshrestha, A., Massey, D.D., Masih, J., Taneja, A., 2014. Source characterization of trace elements in indoor environments at urban, rural and roadside sites in a semi arid region of India. Aerosol Air Qual Res 14, 1738–1751. https://doi.org/10.4209/aaqr.2013.05.0147.
[109] Budaniya, M., Rai, A.C., 2022. Effectiveness of plants for passive removal of particulate matter is low in the indoor environment. Build Environ 222, 109384. https://doi.org/10.1016/j.buildenv.2022.109384.
[110] Howard-Reed, C., Wallace, L.A., Ott, W.R., 2002. The effect of opening windows on air change rates in two homes. J Air Waste Manag Assoc 52, 147–159. https://doi.org/10.1080/10473289.2002.10470775.
[111] A.B.B. Quesada, The Life and Times of Pteris vittata: Investigating Frond Life Stage and Harvest Techniques to Optimize Phytoremediation with an Arsenic Accumulating Fern - Google Search, (2015). ⟨https://www.google.com/search?q=The+Life+and+Times+of+Pteris+vittat%3A+Investigating+Frond+Life+Stage+and+Harvest+Techniques+to+Optimize+Phytoremediation+with+an+Arsenic+Accumulating+Fern&oq=The+Life+and+Times+of+Pteris+vittat%3A+Investigating+Frond+Life+Stage+and+Harvest+Techniques+to+Optimize+Phytoremediation+with+an+Arsenic+Accumulating+Fern&gs_lcrp=EgZjaHJvbWUyBggAEEUYOdIBBzk1N2owajeoAgCwAgA&sourceid=chrome&ie=UTF-8#ip=1⟩ (accessed June 29, 2023).
[112] Pettit, T., Irga, P.J., Abdo, P., Torpy, F.R., 2017. Do the plants in functional green walls contribute to their ability to filter particulate matter? Build Environ 125, 299–307. https://doi.org/10.1016/j.buildenv.2017.09.004.
[113] Mannan, M., Al-Ghamdi, S.G., 2021. Active Botanical Biofiltration in Built Environment to Maintain Indoor Air Quality. Front Built Environ 7. https://doi.org/10.3389/fbuil.2021.672102. ⟨https://www.frontiersin.org/articles/⟩ (accessed June 29, 2023).
[114] Irga, P.J., Paull, N.J., Abdo, P., Torpy, F.R., 2017. An assessment of the atmospheric particle removal efficiency of an in-room botanical biofilter system. Build Environ 115, 281–290. https://doi.org/10.1016/j.buildenv.2017.01.035.
[115] Pettit, T., Torpy, F.R., Surawski, N.C., Fleck, R., Irga, P.J., 2021. Effective reduction of roadside air pollution with botanical biofiltration. J Hazard Mater 414, 125566. https://doi.org/10.1016/j.jhazmat.2021.125566.

[116] Bollhöfer, A., Honeybun, R., Rosman, K., Martin, P., 2006. The lead isotopic composition of dust in the vicinity of a uranium mine in northern Australia and its use for radiation dose assessment. Sci Total Environ 366, 579–589. https://doi.org/10.1016/j.scitotenv.2005.11.016.
[117] Bruce, J., Smith, J., Fowler, M., 2021. Relative efficiency of passive dust samplers: Progress towards coarse dust dispersion modelling. Atmos Environ 244, 117872. https://doi.org/10.1016/j.atmosenv.2020.117872.
[118] Akhavan, O., Hashemi, E., Zare, H., Shamsara, M., Taghavinia, N., Heidari, F., 2016. Influence of heavy nanocrystals on spermatozoa and fertility of mammals. Mater Sci Eng C 69, 52–59. https://doi.org/10.1016/j.msec.2016.06.055.
[119] Singh, N., Kumar, A., Gupta, V.K., Sharma, B., 2018. Biochemical and Molecular Bases of Lead-Induced Toxicity in Mammalian Systems and Possible Mitigations. Chem Res Toxicol 31, 1009–1021. https://doi.org/10.1021/acs.chemrestox.8b00193.
[120] Shen, X., Dai, M., Yang, J., Sun, L., Tan, X., Peng, C., et al., 2022. A critical review on the phytoremediation of heavy metals from environment: Performance and challenges. Chemosphere 291, 132979. https://doi.org/10.1016/j.chemosphere.2021.132979.
[121] Singh, Y., Negi, P., Chen, W.H., 2023. Biofuel technologies for a sustainable. Future: India and Beyond. CRC Press,.
[122] Liu, Z., Tran, K.-Q., 2021. A review on disposal and utilization of phytoremediation plants containing heavy metals. Ecotoxicol Environ Saf 226, 112821. https://doi.org/10.1016/j.ecoenv.2021.112821.
[123] Nzihou, A., Stanmore, B., 2013. The fate of heavy metals during combustion and gasification of contaminated biomass—A brief review. J Hazard Mater 256–257, 56–66. https://doi.org/10.1016/j.jhazmat.2013.02.050.
[124] Zhang, C., Yang, X., Yang, S., Liu, Z., Zhang, L., He, H., et al., 2023. Valorization of heavy metal enriched phytoremediation biomass using a deep eutectic solvent (DES). Green Chem 25, 771–778. https://doi.org/10.1039/D2GC04190A.
[125] Sánchez-Jiménez, N., Gismera, M.J., Sevilla, M.T., Cuevas, J., Rodríguez-Rastrero, M., Procopio, J.R., 2012. Clayey materials as geologic barrier in urban landfills: comprehensive study of the interaction of selected quarry materials with heavy metals. Appl Clay Sci 56, 23–29. https://doi.org/10.1016/j.clay.2011.11.016.
[126] Lachheb, M., Youssef, N., Younsi, Z., 2023. A Comprehensive Review of the Improvement of the Thermal and Mechanical Properties of Unfired Clay Bricks by Incorporating Waste Materials. Buildings 13, 2314. https://doi.org/10.3390/buildings13092314.
[127] Liu, G., Xiao, M., Zhang, X., Gal, C., Chen, X., Liu, L., et al., 2017. A review of air filtration technologies for sustainable and healthy building ventilation. Sustain Cities Soc 32, 375–396. https://doi.org/10.1016/j.scs.2017.04.011.
[128] Kumar, A., Malyan, V., Sahu, M., 2023. Air Pollution Control Technologies for Indoor Particulate Matter Pollution: A Review. Aerosol Sci Eng 7, 261–282. https://doi.org/10.1007/s41810-023-00178-5.
[129] Afshari, A., Ekberg, L., Forejt, L., Mo, J., Rahimi, S., Siegel, J., et al., 2020. Electrostatic precipitators as an indoor air cleaner—a literature review. Sustainability 12, 8774. https://doi.org/10.3390/su12218774.
[130] Poppendieck, D.G., Rim, D., Persily, A.K., 2014. Ultrafine particle removal and ozone generation by in-duct electrostatic precipitators. Environ Sci Technol 48, 2067–2074. https://doi.org/10.1021/es404884p.
[131] Agranovski, I.E., Moustafa, S., Braddock, R.D., 2005. Performance of activated carbon loaded fibrous filters on simultaneous removal of particulate and gaseous pollutants. Environ Technol 26, 757–766. https://doi.org/10.1080/09593332608618516.

Journal of Hazardous Materials 480 (2024) 135810

Contents lists available at ScienceDirect

Journal of Hazardous Materials

journal homepage: www.elsevier.com/locate/jhazmat

Source apportionment and emission projections of heavy metals from traffic sources in India: Insights from elemental and Pb isotopic compositions

Divyangana Lahiri [a], Iravati Ray [a,*,1], Rupam Ray [a], Ilindra Venkata Satya Chanakya [b], Mohd Tarique [c], Sambuddha Misra [b], Waliur Rahaman [c], Manish Tiwari [c], Xianfeng Wang [d,e], Reshmi Das [a,d,**]

[a] School of Environmental Studies, Jadavpur University, Kolkata, India
[b] Centre for Earth Sciences, Indian Institute of Sciences, Bangalore, India
[c] National Centre for Polar and Ocean Research, Ministry of Earth Sciences, Goa, India
[d] Earth Observatory of Singapore, Nanyang Technological University, Singapore
[e] Asian School of Environment, Nanyang Technological University, Singapore

HIGHLIGHTS

- Sources of metals in urban road dust identified using elemental concentration and Pb isotopes.
- Both exhaust and non-exhaust sources contribute significantly to metal-enriched urban road dust.
- Predicted metal emissions to rise by 163-184 % for Ni, Cu, Zn, Pb from 2022 to 2045.
- EV penetration in India is not sufficient to curb metal emissions from vehicle exhausts.

GRAPHICAL ABSTRACT

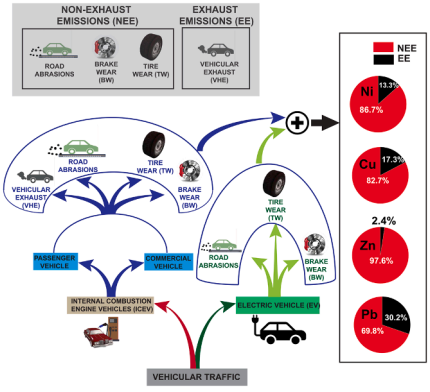

ARTICLE INFO

Keywords:
Traffic emissions
Exhaust emissions
Non-exhaust emissions
Source apportionment
Elemental concentration

ABSTRACT

The study investigates the sources of metals in urban road dusts using elemental concentration and Pb isotopic ratios. The elemental concentrations are also utilized to determine the present heavy metal emissions as well as projected emissions till 2045. Bayesian mixing model for source apportionment highlights the significant contributions of both exhaust and non-exhaust sources to the metal-enriched urban road dusts, with each contributing approximately 40 %. Emission analysis reveals that India's projected electric vehicle (EV) penetration may not be sufficient to suppress the metal emissions from vehicular exhausts. Further challenge is posed by high

* Corresponding author.
** Corresponding author at: School of Environmental Studies, Jadavpur University, Kolkata, India.
E-mail addresses: iravatir.envs.rs@jadavpuruniversity.in (I. Ray), reshmidas.sest@jadavpuruniversity.in (R. Das).
[1] Joint First Author

https://doi.org/10.1016/j.jhazmat.2024.135810
Received 26 June 2024; Received in revised form 9 September 2024; Accepted 9 September 2024
Available online 11 September 2024
0304-3894/© 2024 Elsevier B.V. All rights are reserved, including those for text and data mining, AI training, and similar technologies.

Pb isotope
MixSIAR

metal concentrations in the non-exhaust sources, that dominates the emission of some metals compared to exhaust sources. If the metal concentrations remain unchanged, the emission analysis predicts alarming increases in total emissions from all the exhaust and non-exhaust sources by 174 %, 176 %, 163 % and 184 % for Ni, Cu, Zn and Pb, respectively, from 2022 to 2045. Thus, it is crucial to reduce the metal concentrations in traffic emission sources and also impose better regulatory measures to improve the urban metal pollution scenario.

1. Introduction

Particulate matter (PM) is a complex mixture of particles of varying diameters, (total suspended PM, PM_{10}, $PM_{2.5}$, etc) carrying the signature of their sources [1]. For example, combustion processes from vehicles, power plants, and industrial activities produce soot, ash, and organic carbon. Residential sources generate PM from wood burning, cooking smoke etc. Since the industrial revolution, anthropogenic PM emission has significantly exceeded the crustal derived sources of trace metals due to rapid industrialization, urbanization, and motorization [2,3].

Road traffic emissions are a major source of PM in urban roadside areas and have gained significant attention over the past decade due to their substantial contribution towards environmental pollution [4-6]. Traffic emission is usually categorized as exhaust emissions (EE) and non-exhaust emissions (NEE). Incomplete combustion of fuel and lubricant volatilization are primarily responsible for EEs [7]. On the other hand, NEEs typically arise from abrasive sources such as brake wear, tire wear, road surface abrasion and resuspension of road dust due to traffic induced turbulence in combination with crustal dusts [8,9].

Wear of brake linings occurs due to the frictional contact between brake system components during vehicle deceleration, leading to the emission of PM. The composition of this emitted PM depends on the composition of the brake linings, that consist of fibers for providing mechanical strength, abrasives for generating friction, lubricants for inducing stability, fillers to reduce costs, and binders to render integrity [6]. Similarly, tire wears are generated from mechanical abrasion of tire treads when in contact with road surface. The tire wear debris mostly consist of rubber hydrocarbons, carbon black, hydrocarbon oils, resins, curing agents, and various additives. Frictions generated from heavy traffic movement on roads generate the third type of NEE, i.e., road surface abrasions. The abraded material is primarily asphalt, the most common surfacing agent, consisting mainly of mineral aggregates and a bituminous binder. Fillers, such as fibres, polymers, and epoxy resins are added to the asphalt to withstand heavy traffic and extreme weather conditions. Majority of these NEE sources concentrate in the coarser fractions of PMs and eventually get deposited as road dusts. All these NEE sources consist of toxic heavy metals and contribute towards atmospheric metal loadings [6].

Toxic elements like arsenic (As), cadmium (Cd), nickel (Ni), and lead (Pb) are often prevalent in PM depending on the sources, Upon inhalation these elements can cause severe health problems, including respiratory issues, cardiovascular diseases, and even cancer [10]. Road dusts, being the first recipient of PMs from EE and NEE are often enriched in such heavy metals [11,12,5,13]. Brake and tire wear particles, enriched in heavy metals, are present in substantial proportions in locations encountering heavy traffic [6,14]. A sand paper like effect on the road asphalt and bitumen can cause additional contamination by abrading road paints and the bitumen itself, containing high concentrations of metals [15].

All nations are striving to switch to electric vehicles (EVs) as part of their efforts to combat climate change and reduce urban air pollution. While, introduction of EVs can eliminate tailpipe emissions and significantly reduce pollution, it does not address NEEs. Government of India aims for a minimum 30 % market penetration of EVs in private cars and 70 % in commercial vehicles by 2030, targeting global leadership in the EV sector by 2047. However, long-term projections for oil demand in Indian transportation sector, indicate its continued rise together with the number of vehicles on road (Fig. 1) [16]. In fact, among the Asian and Asia Pacific countries, India is expected to see the highest surge in total number of passenger cars, commercial vehicles, and EVs (343 %) as well as fuel demand (186 %) from 2022 to 2045. India's vehicle fleet (passenger cars + commercial vehicles + EVs) was 66 million as of 2022, out of which only 0.3 % was EV. This number is expected to reach 292.6 million by 2045, with only 7.6 % constituting EVs as opposed to India's targeted penetration percentages [16]. China and Asia Pacific countries are projected to have the highest EV penetrations by 2045 (23.5 % and 21.7 %, respectively), resulting in the lowest rise in fuel demand (Fig. 1). The Asia-Pacific region is experiencing a 54 % decline in oil demand despite an 8 % increase in overall vehicle growth from 2022 to 2045. This decreasing trend is driven by advances in vehicle technology and government policies promoting fuel efficiency and electric vehicles. Although passenger ICEVs are projected to decrease by 23.5 %, the rise in commercial vehicles and EVs will still contribute to a gradual reduction in net fuel consumption across the region. Thus, in comparison to these regions, India's EEs appear to be steadily increasing, which is a cause for concern. Based on these forecasts, both EE and NEEs will continue to contribute to the aggravation of India's PM and metal pollution scenario. Thus, compared to these regions, India's EEs appear to be ever increasing and a concerning scenario. Based on these projections, both EE and NEEs will continue to worsen India's PM and associated metal pollution levels. The emission of metals from the traffic sources actually depends on their respective concentration in each source (fuel, brake wear, tire wear, asphalt, road paint, etc). In tire wear the most abundant element is Zn and brake dust is a significant source of Cu, Sb, Ba etc [6,15]. Road paints, especially yellow paints are major contributors of Cr and Pb [17].

1.1. Novelty and aims

Road dusts are the first recipient of the EE and NEEs in urban areas. Over the last decade a few source-apportionment studies have analysed

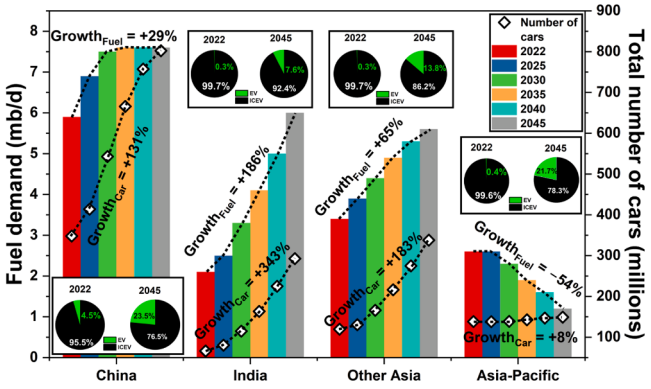

Fig. 1. Bar plots depicting the total fuel demand in China, Asia, Other Asian countries and Asia Pacific for the years 2022, 2025, 2030, 2035, 2040 and 2045, The percentage increase in fuel demand from 2022 to 2045 is depicted by a dotted line with the percentages for respective regions indicated above the line as $Growth_{fuel}$. The total number of cars (passenger cars, commercial vehicles and electric vehicles) on road for each region is presented as line and symbol (diamond) plot. The percentage increase in the total number of cars is indicated above as $Growth_{car}$. The pie charts illustrate the percentage of internal combustion engine vehicles (ICEV) and electric vehicles (EV) in the years 2022 and 2045 for each region.

urban and semi-urban road dusts for elemental concentrations and Pb isotopic compositions [18,12,13]. Vehicular emissions, particularly NEEs, have recently gained attention for emitting PM at levels comparable to EEs. However, source apportionment studies that quantify their contributions of heavy metals to urban atmospheric metal loading by analysis of metals in end-member samples are rare [7,19]. Most studies have only measured elemental concentrations in road dust, rather than in the material itself, and suggested that EEs and NEEs are significant sources of PM emissions in urban areas using tools like positive matrix factorization (PMF), chemical mass balance (CMB) etc. [20-24]. Over the past 15 years, some studies have focused on elemental concentrations in end members. These studies have primarily highlighted the high metal content in NEE sources subsequently providing a guideline following which specific elements can be used as qualitative tracers for NEE sources [25,15,26,27,6]. However, in India, studies specifically focusing on atmospheric metal pollution from vehicular components are scarce [28,29]. Most importantly, globally, all these studies have solely focused on metals, which single-handedly is not a robust proxy for source apportionment. This highlights the need to determine isotopic composition of the end members, which is largely unavailable worldwide. Currently, Pb isotopic composition data for NEE sources are available only from South Korea and London [30-32,17]. The ability to accurately trace and quantify sources of vehicular pollution is limited by the scarcity of such data. South Korea has reported Cu and Zn isotopic signatures of NEE sources in addition to Pb isotopes. Isotope ratios of trace metals such as Zn, Cu, Ni, Cd etc. can trace contamination sources, similar to Pb isotopes. However, the effectiveness depends on the distinctness of isotopic signatures of end members and whether fractionation (mass-dependent or mass-independent) occurs during physicochemical processes which might complicate source apportionment studies.

Thus, it is crucial to quantify the extent of metal emitted from the EE and NEE sources and their respective contribution towards urban road dust. This road dust can become resuspended, contributing significantly to the atmospheric metal load and impacting air quality. While electric vehicles significantly reduce tailpipe emissions (EEs), a holistic approach requires considering NEEs to achieve environmental goals. As governments worldwide set stringent emission standards to combat air pollution, understanding NEEs become essential. Policymakers need to consider these emissions when developing regulations and incentives for EV adoption to ensure environmental benefits. As different sources (EE and NEEs) exhibit enrichment in specific elements, developing an elemental concentration profile can be useful in source apportionment as well as emission calculation for each element. For source apportionment studies isotopic compositions are the most robust proxies. Especially, as isotopes of Pb do not fractionate under physicochemical processes and preserve the signature of sources, they are ideal tools in source delineation [33]. Besides isotope analysis, other tracers such as enrichment factors, trace element ratios, and chemical speciation are often used to identify sources. Each technique has its strengths and limitations, and a combination of approaches is often employed for accurate source attribution, as demonstrated in this study with Pb isotopes and trace element ratios. Stable isotopic composition coupled with elemental concentrations has proven to be a robust strategy for source apportionment in the field of air pollution research [12,34-36]. Particularly, the availability of elemental concentration and Pb isotopic composition of Indian road dusts for the last few years provides a baseline for integrating with it the end member data and performing source apportionment. Given the diverse components of exhaust and non-exhaust emissions present in road dusts, employing a Bayesian model such as MixSIAR is advantageous compared to linear models. Linear models lack the probabilistic framework of Bayesian models and fails to generate accurate and precise results when dealing with multiple end members. Linear models cannot provide distinct solutions when the number of unknowns exceeds the number of equations that can be formed using the isotope system. Further, the heterogeneity of the sources makes it crucial to incorporate the standard deviations of their isotopic compositions. This is the primary advantage of using a Bayesian model in source apportionment studies having multiple heterogenous end members. Further details about the model are available in previously publised literature [37].

Thus, this study aims to:

(i) determine the sources of heavy metals in urban and semi-urban road dusts of eastern India using elemental concentration coupled with Pb isotopic compositions of traffic emission sources
(ii) quantify the relative contributions of individual sources (vehicular exhaust, brake wear, tire wear, road pitch, road paint and crust) towards the road dusts using Bayesian stable isotope mixing model (MixSIAR)
(iii) conduct an emission analysis of heavy metals from both exhaust and non-exhaust sources, using the analyzed elemental concentrations, and establish statistics for present and future metal emission scenario from traffic between the time period of 2022 and 2045

This comprehensive source apportionment study, utilizing Pb isotopes and elemental concentrations, together with a detailed metal emission analysis, will provide an overview of how different emission sources contribute towards the metal enrichments in urban road dusts.

2. Materials and methods

2.1. Sample collection and initial processing

All the traffic emission samples were collected from different locations as presented in Supplementary Figure 1. The surfaces of the collected tire segments (n = 5) and brake pads (n = 3) were sonicated in Milli-Q water to remove loose contaminants. Following cleaning, the tires were cut and homogenized into small pieces. The brake pads were scraped to generate loose homogenized brake wear particles. Samples of yellow and white road paint (n = 2) were applied and dried on polypropylene sheets, following which they were scraped off as dry particles [32]. Road pitch samples (n = 7) were crushed and homogenized into finer particles. Vehicular exhaust samples (both petrol and diesel) (n = 5), along with vehicular exhaust from tailpipes, were also collected. The fuel samples (1 mL) were taken in Pyrex test tubes with quartz wool plugging. The samples in the tightly plugged test tubes were ashed in muffle furnace at 400 °C until ashes were visible at the bottom [38].

2.2. Elemental concentration and Pb isotope analyses

For determination of elemental concentration and Pb isotopic compositions, the samples were processed in a clean chemistry laboratory using Milli-Q water (resistivity > 18.2 MΩ-cm) and acids purified from concentrated reagent grade acid using sub-boiling distillation (Savillex™). The homogenized brake wear, tire wear, road pitch, and road paint samples were weighed (~30 mg) and digested for 24 h at 120 °C in screw cap Teflon beakers (Savillex™) using a concentrated acid mixture of HNO_3 and H_2O_2 in 2:1 ratio. The ashed fuels were digested in concentrated HNO_3 at 120 °C for 24 hrs in screw cap Teflon beakers (Savillex™). All digested samples were dried and redissolved in 2 mL of 2 % HNO_3. Half of each sample was utilized for determining elemental concentrations in ICP-OES and ICP-MS. The other half was utilized for the purification of Pb through ion exchange chromatography (resin used: Eichrom AG-1 ×8 chloride form, 200 – 400 mesh). For column chromatography, the dried samples were redissolved in 1.1 N HBr and loaded in the columns packed with resin and finally eluted in 6 N HCl [39].

Concentrations of 15 elements (Mg, Al, Ca, Cr, Mn, Fe, Co, Ni, Cu, Zn, Mo, Cd, Sb, Ba, and Pb) were determined for the samples. For elements

having high concentrations (Al, Ba, Ca, Fe, Mg, Mn, Cu and Zn), measurements were performed on an Thermo Scientific™ iCAP 7000 inductively coupled plasma - optical emission spectrometer (ICP – OES) at the Paleothermometry Laboratory of National Centre for Polar and Ocean Research (NCPOR), Goa, India. For standard sample bracketing, a multi element standard (Merck ICP ME IV) of 5 ppm was used. The obtained intensities of the samples were drift corrected and normalized with respect to the intensity of the bracketing standard. Rest of the analytes were measured on the Thermo Scientific™ iCAP Q inductively coupled plasma - mass spectrometer (ICP-MS) at the Earth Observatory of Singapore, Nanyang Technological University, Singapore. Samples were introduced through a PFA concentric nebulizer (100 μL/min), Peltier cooled quartz cyclonic spray chamber and a demountable quartz torch with a quartz injector. The interface between the torch and the quadrupole was equipped with the platinum sampler and skimmer cones. For removal of polyatomic interferences, the samples were measured in kinetic energy discrimination (KED) mode by utilizing pure helium (He) inside the single collision cell.

Tuning was performed in iCAP Q tuning solution (1 μg/L of Ba, Bi, Ce, Co, In, Li and U). Freshly prepared gravimetric multi-element calibration standards (Inorganic Ventures-ICPMS-71A and 71B) with concentrations ranging from 0.1 ppb to 500 ppb were analyzed at the beginning of the analysis to obtain linear calibration curves. For the standard sample bracketing, a multi element standard of 10 ppb was used. The obtained raw counts per second (cps) of the samples were drift corrected and normalized with respect to the cps of the bracketing standard. Chemical extraction efficiency and analytical precision were assessed using certified reference material NIST SRM 8704 (Buffalo River Sediment) which was analyzed following the same methods used for samples. Elemental recoveries were found to be > 90 %.

Multi-collectors ICP – MS (Neptune Plus MC ICP-MS, Thermo-Fisher, Germany) at Earth Observatory of Singapore, Nanyang Technological University, Singapore and Centre for Earth Sciences, IISc Bangalore, India were utilized for Pb isotope analysis. The sample introduction system is equipped with Aridus II desolvating nebulizer (100 μL/min). Thallium (Tl) internal normalization ($^{203}Tl/^{205}Tl$ ratio of 0.418911) was performed to correct instrumental mass fractionation. Standards (2.5 ppb of NIST SRM-981 with 0.65 ppb Tl) was measured several times in between samples as well as at the beginning and end. Samples were bracketed with NIST SRM-981 to normalize the raw ratios with respect to true values [40,41].

2.3. Mixing model and emission analyses

The Pb isotopic compositions along with the 1SDs ($^{206}Pb/^{207}Pb$, $^{208}Pb/^{207}Pb$, $^{208}Pb/^{206}Pb$) of the sources were fed to the Bayesian statistics-based modelling package, "MixSIAR", available in R, to estimate the contributions of each source towards the road dusts. The $^{206}Pb/^{207}Pb$, $^{208}Pb/^{207}Pb$, $^{208}Pb/^{206}Pb$ ratios of the road dusts (n = 10) were fed as the mixture data [42]. The concentration-dependent 3 – isotope model was utilized, incorporating the concentrations of Pb in the sources into the modelling framework. Three parallel "long" Markov Chain Monte Carlo (MCMC) chains were run having a length of 300000 iterations. The first 200000 iterations were discarded, and every 100th iteration from the remaining were taken into consideration to ensure that the chains reached equilibrium. Gelman Rubin diagnostics [43] was used to check the model convergence.

The calculations for emissions of each metal were performed separately for EE, NEEs from internal combustion engines (ICEVs), and NEEs from EVs for the time period of 2022 – 2045. Non-exhaust emission has been categorized into tire wear, brake wear and road abrasion. The two resultant NEE data from ICEVs and EVs were added to get the total NEE (ton/yr). The estimated metal concentrations were incorporated in the emission equations [44]. Other relevant data such as number of vehicles, fuel consumption, emission factors and mileage are summarized, and the detailed calculations are provided in Supplementary Material 2 [45].

The equations utilized for the calculations are as follows:

$$E_{ICEV} = EF_{ICEV} \times [X] \times M \times C \quad (1)$$

Where, E_{ICEV} is the metal emitted in tons/year; EF_{ICEV} is the emission factor (g/km) for fuels when calculating EEs and for NEEs, EF_{ICEV} denotes the emission factors (g/km) for brake wear, tire wear, or road abrasions as applicable; [X] is the average concentration of the concerned element in mg/kg for vehicular exhaust, brake wear, tire wear or road abrasion as applicable; M is the average mileage in km/L and C is the fuel consumption of total car population in liter (L).

$$E_{EV} = EF_{EV} \times [X] \times M \times N_{EV} \quad (2)$$

Where, E_{EV} is the metal emitted in tons/year; EF_{EV} is the emission factor (g/km) in EVs, for brake wear, tire wear, or road abrasions as applicable; [X] is the average concentration of the concerned element in mg/kg for brake wear, tire wear or road abrasion as applicable; M is the average mileage in km traveled by an EV in one full charge and N_{EV} is the population of EVs.

3. Results and Discussion:

3.1. Elemental concentration of exhaust and non-exhaust sources

The elemental concentrations of various non-exhaust sources such as tire, brake, road pitch, road paint, along with soot from tail pipe representing exhaust emission are presented in Fig. 2 and Supplementary Table 1.

3.1.1. Exhaust emission (EE) sources

Exhaust emission sources play an important role in overall road traffic emissions [19]. Significant measures have been implemented, including the use of three-way catalytic converters in petrol vehicles and diesel particle filters to reduce PM emissions from fuel exhausts. These efforts have markedly changed the PM emissions and the associated trace metals in these emissions [19,46]. In this study, we have analyzed the elemental concentrations of soot from both petrol and diesel car tailpipe (referred to as vehicular exhaust herein) to obtain a clear picture of the metal emission sources from road traffic.

Vehicular exhaust predominantly consists of carbonaceous soot along with a minor fraction of non-carbonaceous, non-volatile, inorganic metal PM which is sub micrometer in size and inhalable. The elemental composition of the EE is a combination of combustion of metal additives in lubricating oil and, to a lesser extent, trace metals in the fuel [47]. In our samples the overall elemental concentration trend in the vehicular exhaust was as follows (Al, Fe) > (Mg, Ca, Zn) > (Cr, Mn, Cu, Ba, Pb) > (Ni, Mo) > (Co, Cd, Sb). Aluminum, Mg, Ca, Fe and Zn concentrations ranged from the upper μg/g to lower percent levels. The percent level concentrations of Fe and Al can result from the wear and tear of engine components, such as cylinder walls, piston rings, and bearings. The friction and heat generated during engine operation can cause small particles of Fe and Al to be released and subsequently deposited in the exhaust system. Additionally, Fe and Al can also come from the degradation of steel components within the exhaust system itself [48,49]. Chromium, Ni, Cu can be derived from engine wear and corrosion as well. The emission of several elements such as Ca, Zn likely resulted from the use of organometallic additives in diesel fuel or lubricating oil [50].

3.1.2. Non-exhaust emission (NEE) sources

NEE sources primarily consist of heavy metals, such as Zn, Cu, Pb and consequently, the secondary aerosols they produce, exhibit a similar chemical composition [51].

Tire wear: Elemental concentration in the tire wear followed the general pattern (Mg, Al, Ca, Fe, Zn) > (Cr, Mn, Cu, Ba, Pb) > (Co, Ni, Mo, Cd, Sb) with Al, Ca and Zn ranging in the low parts per hundred

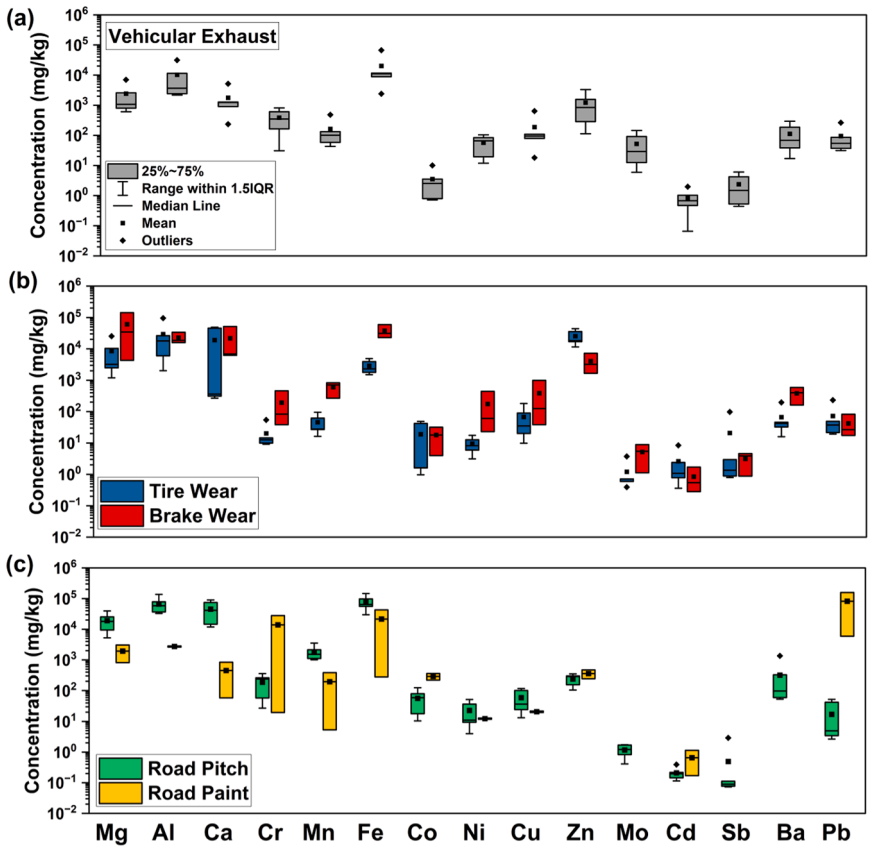

Fig. 2. Box plots depicting the elemental concentrations in (a) vehicular exhaust, (b) tire wear and brake wear and (c) road pitch and road paint samples from eastern India. The lower and the upper limits of the boxes represent 25th and 75th percentile data respectively. The black boxes represent the mean while the lines represent the median values. The whiskers extend to the smallest and largest values within 1.5 times the interquartile range (IQR) from the first and third quartile. Data points beyond these whiskers are considered outliers depicted as black diamonds.

level. Of all the NEE sources, Zn had the highest concentration in tires. High Zn concentrations result from addition of ZnS and ZnO in the tires during vulcanization process [15]. Zinc concentrations of the Indian tires were found to be similar to Korean and British tires [30-32] (Supplementary figure 2). Tire 4 had the highest concentration of most of the elements compared to the other tire samples. This variance in metal concentrations could be attributed to different raw materials used by different manufacturers [31]. The mean concentration of Pb in tires from this study is higher than the average Pb in London tires [30] whereas it is almost similar to the concentration range of Korean tires [31] except for Tire 4 (Supplementary figure 2).

Brake wear: Brake wear particles result from the degradation of the brake pad and the rotating disc/drum due to heat and friction. The overall pattern of break wear elemental composition followed the trend (Mg, Al, Ca, Fe) > Zn, (Cr, Mn, Ni, Cu, Ba) > (Co, Mo, Cd, Sb, Pb). Concentrations of Mg, Al, Ca and Fe were in low percent level. Aluminum oxide and iron oxides are commonly used as abrasives to increase friction material [7].

Of all the NEE sources Ba concentrations in brake wear were the highest (Fig. 2). High Ba content in brake wear can be due to the presence of barite, which is used as a filler in brake pads due to its high specific gravity, which helps to add weight and stability to the brake pad material [7]. Lead concentrations in London and Korean brakes were comparable (approximately 15 mg/kg Pb), whereas brakes from this study had higher concentrations (47 ± 35 mg/kg).

Road Surface and paints: The bituminous road cover is a complex mixture of hydrocarbons, resins, asphaltenes, and trace metals [52]. In road pitch samples, the concentration pattern was as follows (Mg, Al, Ca, Fe) > Mn > (Cr, Zn, Ba) > (Co, Ni, Cu, Mo, Cd, Sb, Pb). Barium concentration in road pitch samples were comparable to brake wear.

Barium is a common contaminant in oil, either naturally present in the reservoir or added as a drilling additive. Thus, the organic fraction of asphalt concrete often contains high Ba [53].

In this study, we have considered road paints as a non – exhaust emission source as abraded paints can be a source of heavy metals in road dust. Two paints are widely used on Indian roads, yellow and white paint. Our study reveals that yellow paint contains high levels of Pb (157,584 μg/g) and Cr (27,830 μg/g) due to the presence of lead chromate ($PbCrO_4$) as its primary component, which imparts the yellow colour [17]. In comparison, the white paint had a lower concentration of Cr (20 μg/g) and Pb (5908 μg/g). Although white paint had a lower Pb concentration than yellow paint, it still demonstrated significantly high Pb concentration compared to other EE and NEE sources. Other than Cr and Pb, high elemental concentrations of Mg, Al, Ca, Fe and Zn have also been observed in these paint samples. The inorganic pigments used in white-coloured paints include rutile calcium composite pigment ($TiO_2 + CaSO_4$), zinc oxide (ZnO), leaded zinc oxide ($ZnO + 2PbSO_4$) [17] which might explain high Ca, Zn, Pb concentrations in white paints.

However, it is difficult to ascertain heavy metal sources of road dust based on concentration alone.

3.2. *Elemental ratios*

Elemental ratios are often used for source apportionment of metals. We have used Mo/Pb and Ba/Pb ratios, as Mo and Ba are commonly used as tracers for tires and brake emissions, respectively (Fig. 3a). The combination of Mo and Cr is used as a heat-resistant material to coat the tires to prevent corrosion and to withstand temperature increases brought on by road friction, particularly in highways [54,55]. Brake wear and road pitch are characterized by high Ba/Pb ratios ranging from

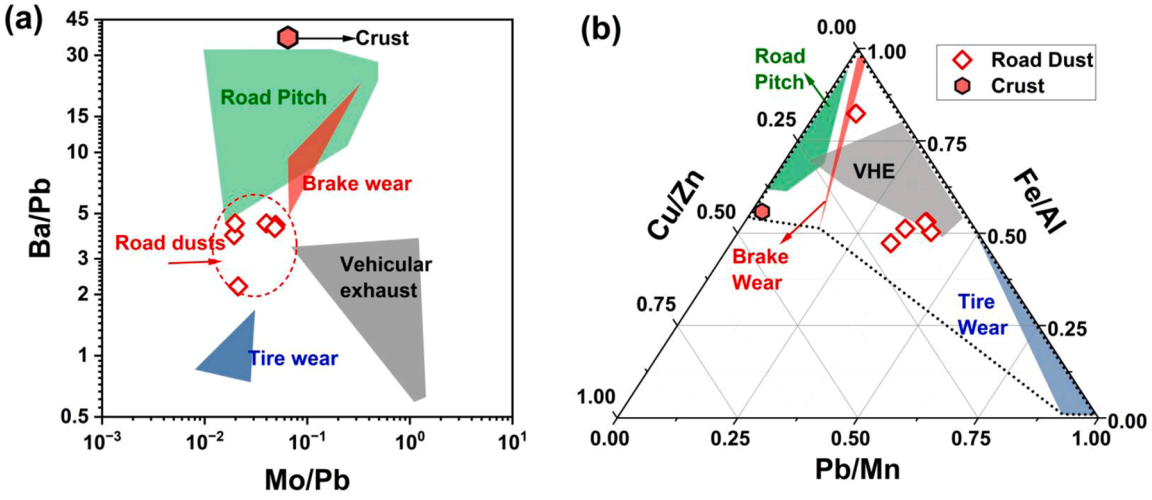

Fig. 3. Elemental ratios plotted as (a) bivariate plot of Mo/Pb vs Ba/Pb and (b) ternary plot of Pb/Mn, Cu/Zn and Fe/Al demonstrates that the characteristic ratios of road dusts lie between those of the EE and NEE sources. The vehicular exhaust, tire wear, brake wear and road pitch are depicted as fields in grey, blue, red and green colours respectively.

4.5 to 32, whereas tire wear and exhaust emissions have Ba/Pb < 3.5. Road dusts do not overlap with the field of the EE or NEEs and plot in between the fields indicating that, road dust consists of mixture of elements generated through variety of emission sources (Fig. 3a).

Non-exhaust emission sources are highly enriched with Cu, Zn and Pb. Copper serves as a tracer for wear abrasions, and the Cu/Zn ratio is often used as an indicator for assessing non-exhaust emission contributions to the elemental concentration in road dust and aerosols [56,57]. The elemental composition patterns of the EE and NEE sources follow a general pattern, with Mg, Al, Ca, and Fe having the highest concentrations in low parts per hundred levels. We have used Fe/Al ratio to distinguish between EE and NEE sources. Generally Fe is high in car exhaust due to presence of brake dust and corrosion particles from cast iron manifolds in car exhaust systems [58]. Thus, the average Fe/Al ratio of EE is higher than the NEE sources though some of the brake wears show high Fe/Al ratios due the presence of Fe and Al in brake disc [59]. Pb/Mn ratios to distinguish between different end members have been previously used [60]. The Pb/Mn ratios are highest in tire wears (1.36 ± 0.76) and lowest in road pitch (0.012 ± 0.017). Thus, we use the Cu/Zn, Fe/Al and Pb/Mn ratios in a ternary plot to understand the relative influence of different sources of road dust (Fig. 3b). Majority of the road dust clusters in the vehicular exhaust field with one sample plotting close to the brake wear. However, none of the road dust samples plot close to the crust in both the plots. From the binary and ternary plot of the elemental ratios it is difficult to decisively discern the proportion of EE and NEE end member contributions. However, it is evident that resuspension of weathered crust has little contribution in the metal composition of road dusts that are heavily influenced by traffic related emissions.

3.3. Pb isotopic signatures for source delineation

The Pb isotopic compositions of the exhaust emission samples (fuel and vehicular exhaust) vary from 1.126 – 1.141 and 2.396 – 2.419 in $^{206}Pb/^{207}Pb$ and $^{208}Pb/^{207}Pb$ spaces, respectively. Fuel and vehicular exhaust demonstrate almost perfect overlap, reflecting their close association, as exhaust particles originate from combusted fuels. In contrast, the NEE samples (brake wear, tire wear, road pitch and paint) have a larger spread, with $^{206}Pb/^{207}Pb$ and $^{208}Pb/^{207}Pb$ varying from 1.112 – 1.163 and 2.390 – 2.454, respectively. The road pitch and brake wear samples are slightly more radiogenic compared to the others. The mean and individual Pb isotopic compositions of all types of samples are presented in Supplementary Table 2.

All the vehicular emission samples, along with Indian road dusts from India [12,13] exhibit Pb isotopic compositions that lie along the mixing line between crust [61] and Indian ore [62] as observed from the three – isotope plot (Fig. 4a). While there have been evidences of some crustal and industrial influences on Indian aerosols [12,37,36], the road dusts actually plot within the mixing range of EE and NEE source signatures. Road dust from Sagar Island [12] is an exception, that plots closer to crust indicating greater influence from geogenic sources. For the rest of the aerosols from urban and semi-urban areas, the three-isotope plot indicates that the road dusts are primarily a composite mixture of EE and NEE sources. Moreover, the road dusts, demonstrate significant overlaps with tire wear and EEs, indicating considerable influence from these specific sources. However, the Pb isotopic composition of the road pitch samples significantly differ (ANOVA: $p < 0.05$) from fuel exhaust, tire wear and notably from road dusts in $^{208}Pb/^{207}Pb$ space, indicating limited influence of the source on road dusts.

Compared to London and South Korea [30-32], the Indian NEE sources were much less radiogenic in $^{206}Pb/^{207}Pb$ space suggesting separate raw materials used for manufacturing (Fig. 4b). For all the three countries brake wears were the most radiogenic samples. However, British and South Korean brakes were about 49 ‰ and 90 ‰ more radiogenic than their Indian counterparts, respectively. The Indian brake wears demonstrated a consistent $^{206}Pb/^{207}Pb$ ratios (1 SD = 0.008) while Korean (1 SD = 0.117) and London (1 SD = 0.045) samples varied significantly. Tire wear and road pitch samples were about 21 ‰ and 17 ‰ more radiogenic respectively in London (tire wear = 1.1607 ± 0.007; road pitch = 1.1664 ± 0.004)) and Korea (tire wear = 1.1595 ± 0.009; road pitch = 1.1682 ± 0.021) compared to India (tire wear = 1.1354 ± 0.014; road pitch = 1.1472 ± 0.008)). Similar variations were observed in $^{206}Pb/^{207}Pb$ ratios for road paints with Korean paints being 21 ‰ and London paints being 24 ‰ more radiogenic than Indian paints. Despite such high $^{206}Pb/^{207}Pb$ compositions of London NEE sources, London road dusts exhibited much lower $^{206}Pb/^{207}Pb$ ratios, similar to Indian road dusts. In South Korea, the road dusts overlap with the tire wear, road paint and to some extent road pitch samples (Fig. 4b). On the other hand, Indian road dusts have significant overlaps with all the NEE sources in $^{206}Pb/^{207}Pb$ space and also with EE sources as overserved from the three-isotope plot (Fig. 4a). Thus, South Korea and India appear to be influenced by the traffic emission sources to a greater extent than London. This can be due to a significantly lower average concentrations in most heavy metals in the NEE sources of London compared to Korea and India (Supplementary Figure 2), resulting in lesser emissions. In fact, India demonstrates significantly higher

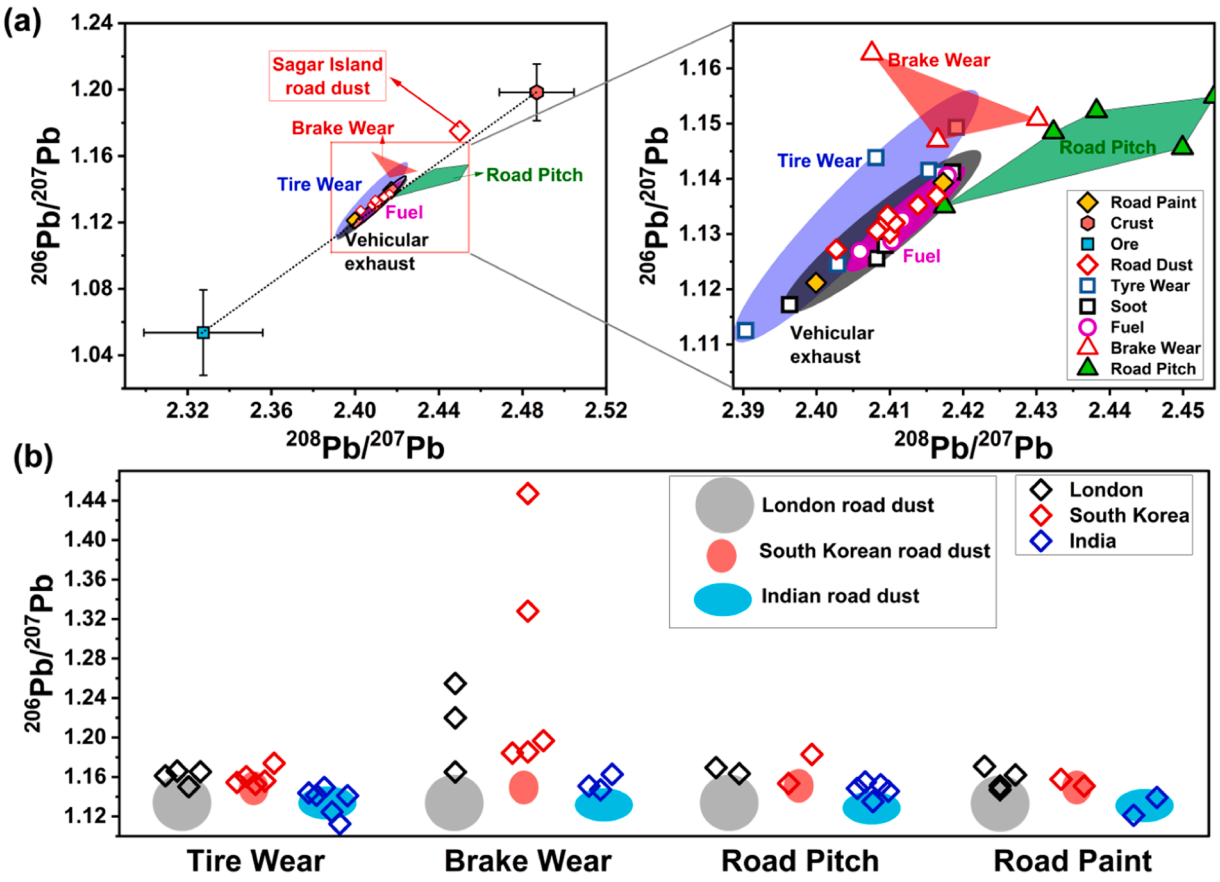

Fig. 4. (a) Three-isotope plots of $^{208}Pb/^{207}Pb$ vs $^{206}Pb/^{207}Pb$ for Indian fuel, vehicular exhaust, road dusts, tire wear, brake wear, road pitch and road paint. The fuel, vehicular exhaust, tire wear, brake wear and road pitch are depicted as fields in pink, dark grey, blue, red and green colours respectively. The right-hand panel provides an enlarged view of the squared section from the left-hand panel. (b) Comparison of the $^{206}Pb/^{207}Pb$ ratios in tire wear, brake wear, road pitch, and road paint from London and South Korea with those from the present study in India. The $^{206}Pb/^{207}Pb$ compositions of road dust from respective countries are shown as background fields.
(a) The data for London and South Korea has been adopted from [30] and [32] respectively. (b) The road dust data for India is adopted from [12] and Ray and Das 2024.

concentrations of certain metals, ranging from several times to orders of magnitude higher (Al, Fe, Cr, Ni, Ba, Pb in tire wears; Cu, Zn, Sb in brake wears; Al, Fe, Cr, Cu in road pitch; Fe, Cr, Cu, Zn, Pb in road paints) compared to London. This results in Indian road dusts being more enriched in metals. To quantify contribution of each source in the Indian road dusts, Bayesian stable isotope mixing model has been utilized. Details on the mixing model results are discussed in the following section.

3.4. MixSIAR model based approach for source apportionment

Bayesian stable isotope mixing model-based approach, MixSIAR is effective in addressing multiple endmember-based source apportionment [43,37,63]. This modelling approach has been extensively used in the ecological study of food webs [42]. Recently, it is being utilized in source apportionment studies related to environmental pollutants based on Pb isotopic compositions [64-67,43,37]. In this study, the concentration dependent 3D-MixSIAR model has been utilized to accurately determine the proportion of EE and each NEE source in urban road dusts (n = 10) [12,13]. Six distinct endmembers have been taken into account as components of road dust. Due to similar isotopic compositions exhibited by the exhaust emission end members (vehicular exhaust and fuel), they were averaged and combined into a single source called as EE. The other NEE sources incorporated include: tire wear, brake wear, road pitch and road paint. In case of road paint, 1/4th of its analyzed concentration has been taken into consideration, since extant paint on the road surface contains about 1/4th of its initial concentration [68]. Additionally, a crustal component was incorporated as the geogenic constituent of road dust [61]. Thus, the average Pb concentrations and Pb isotopic compositions of each of these end members were incorporated in the modelling framework. The input data for the model is provided in Supplementary Table 3.

MixSIAR results reveal consistent mean contributions from all six end members to the road dust samples, with one exception (sample S8 from Sagar Island (R. [12])) (Fig. 5). Sagar Island, being a pristine location with less traffic compared to urban areas, shows the highest contribution from natural crust (71 %) in its road dust. This result matches with the initial observations from the three-isotope plot (Fig. 4a). At Sagar Island no influence of road paint could be observed, while other NEE sources (tire wear, brake wear, and road pitch) cumulatively contribute 16 %, with brake wear contributing the most (8 %). Exhaust emissions account for 12 % of the lead (Pb) in Sagar Island's road dust. These contributions from both EE and NEE sources are the lowest among all the samples due to the heavy influence of the natural background in the region.

On the other hand, road dusts from urban and semi-urban regions consistently exhibit moderate mean contributions from natural background (16–27 %). Contributions from exhaust emissions in these regions range from 34–42 %. Among non-exhaust sources, road pitch and road paint contribute the least (3–6 %), while tire wear and brake wear contribute significantly (14–16 % and 17–18 %, respectively). Thus, urban road dust shows nearly equal contributions from both EE and NEE

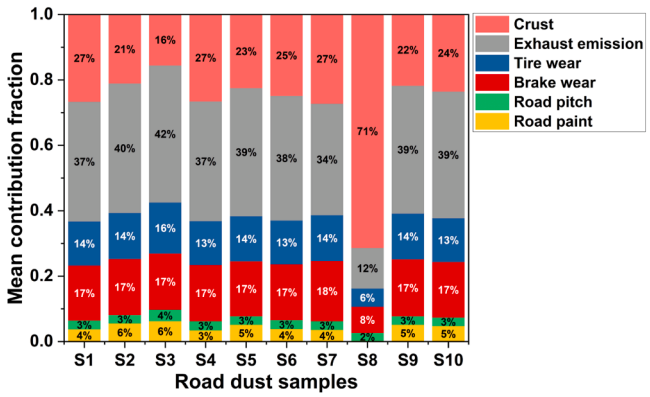

Fig. 5. MixSIAR results for mean contribution of Pb towards crust, exhaust emission, tire wear, brake wear, road pitch and road paint towards road dusts from eastern India. All the samples demonstrate consistent contributions from the sources except sample "S8″, from Sagar island, a pristine location having heavy influence from natural crust.

sources (~40 % each). These indicate that the road dusts are a mixture of crust, EE and NEE components with the anthropogenic sources being predominant. While EEs from combustion remain a substantial contributor in urban areas, non-exhaust sources such as brake and tire wear are also equally significant contributors to road dust composition. As there is a global urge to shift towards electric vehicles in the future, there is a potential for a reduction in atmospheric heavy metals from EEs. However, without effective control measures, NEEs from both electric and combustion engines can escalate with the increasing number of vehicles on road. Thus, it is crucial to quantitatively estimate the amount of heavy metal emitted from both exhaust and non-exhaust sources so that effective control strategies can be designed.

3.5. Metal emissions from traffic sources

The trend of annual atmospheric emissions of Ni, Cu, Zn and Pb from vehicular exhaust (only from ICEV) and various NEE sources, such as brake wear, tire wear, and road abrasions (includes the total emission from both ICEV and EV), from 2022 to 2045 is illustrated in Fig. 6. Vehicular exhaust emissions are further categorized based on the fuel type, that is, petrol and diesel-driven vehicles. Statistical analysis (ANOVA, $p > 0.05$) of elemental concentration data of vehicular exhaust samples reveals no significant differences in the concentrations of Ni, Cu, Zn, and Pb between petrol and diesel samples. Therefore, the emission of these metals is primarily influenced by the fuel consumption, rather than the fuel type itself. Further details are provided in **Supplementary Note 1** and the emissions of Ni, Cu, Zn and Pb are illustrated in Supplementary Figure 3. Emission of heavy metals from EE and NEE sources vary based on several factors including vehicle type, mileage, total vehicle population on road, and the emission factors associated with different emission sources [44]. The emission factor is an essential fraction indicating the quantity of emitted pollutants per kilometer of distance travelled in a mixed driving condition [29].

The linear increase of EE in future will be due to the steady linear growth of passenger and commercial ICEV and low adoption of EV. As NEE results from both ICEV and EVs, it is projected to increase as well following the growth curve of the vehicle growth in India.

Thus, this linear growth pattern of road transportation and hence emissions is primarily due to two reasons,

1. India's population reached 1.43 billion in 2023, surpassing China, and is projected to grow to 1.62 billion by 2045. With half of the population under 25, India's working population is expected to expand to 1.1 billion, driving economic growth. The country's GDP is projected to grow by an average of 6.1 % annually between 2022 and 2045, contributing to sustained economic expansion.
2. India's urbanization rate, currently around 34 %, is much lower than in developed and many developing countries, despite housing several of the world's most populous cities. Recent policy initiatives like the 'Smart Cities Mission,' affordable housing projects, and metro system expansions are expected to significantly boost urbanization during the forecast period. This urbanization will, in turn, drive increased demand for modern energy sources, including oil. Economic expansion will boost freight transport, driving increased diesel demand in road transportation. Additionally, the rapid growth of the middle class, coupled with urbanization and improved road

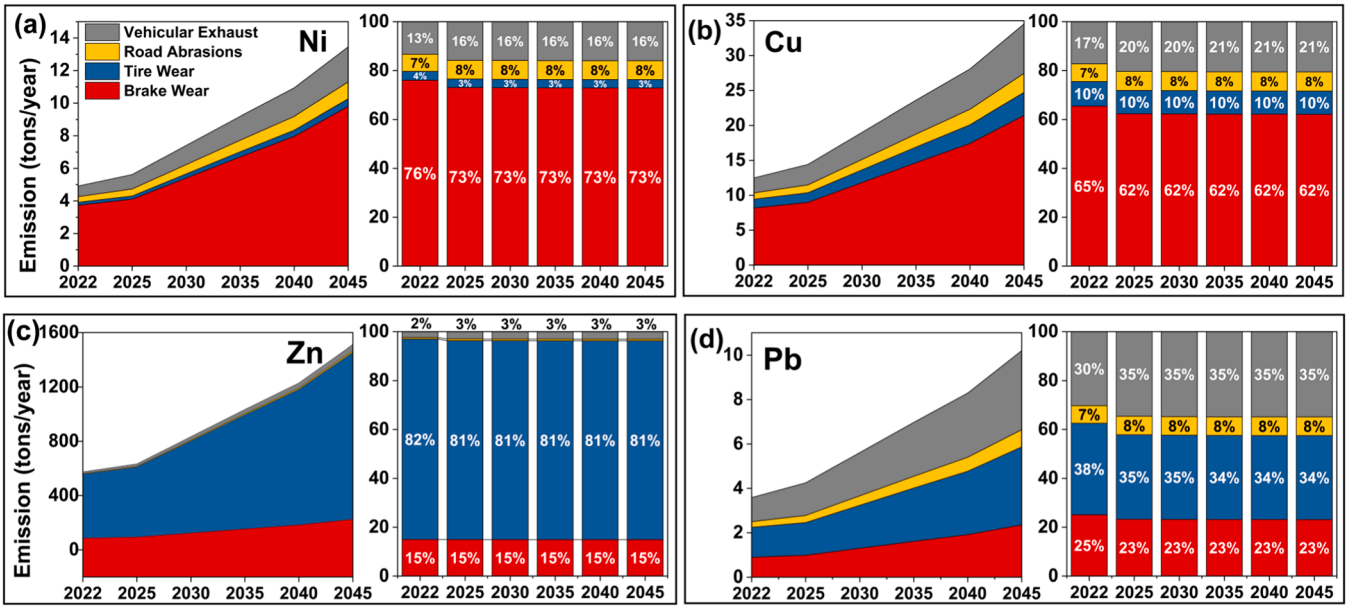

Fig. 6. Stacked area plots representing total emissions of vehicular exhaust, tire wear, brake wear and road abrasions in tons/year. The stacked bar plots depict the percentage contribution of each source towards total metal emissions from traffic sources for (a) Ni (b) Cu (c) Zn and (d) Pb in the years 2022, 2025, 2030, 2035, 2040 and 2045. About 60 % - 70 % of the emissions of Ni and Cu are from brake wears while the major source of Zn emission is tire wear particles. The NEE (tire wear, brake wear, road abrasions) sources contribute more towards Pb emission than EE sources

infrastructure, is projected to more than quadruple the number of passenger vehicles, expanding the fleet from 46 million in 2022 to nearly 200 million by 2045 (excluding two-wheelers).

The present study focuses on the emission of four elements—Pb, Ni, Cu, and Zn—which are extensively used in the automobile industry and have been reported to be enriched in Indian road dust as well as aerosols. These elements are also present in significant concentrations in vehicular sources. This overlap in their prevalence in both road dust and vehicular emissions led us to focus on these elements, as it suggests they are key contributors to metal pollution from transportation sources [12,69,13].

Annual emission analysis over the time period of 2022 to 2045 indicates a consistent rise in the levels of Ni, Cu, Zn and Pb (Fig. 6a-d), driven by the growing vehicular population and increasing fuel consumption (Fig. 1) [16]. Evidence from previous research indicate a high degree of contamination in aerosols and road dust, particularly by Cu, Pb, Ni, and Zn [12,70,13,36]. Emission analysis in this study highlights the total emissions of Ni, Cu, Zn and Pb from EE and NEE sources as well as the individual percentage emission of these toxic metals from each source. Among these 4 metals, total cumulative emission for Zn (575 tons/year as of 2022) from all the traffic sources is the highest followed by Cu (12.5 tons/year as of 2022), Ni (4.9 tons/year as of 2022) and Pb (3.5 tons/year as of 2022). Results indicate that the total emissions from all the EE and NEE sources is expected to rise alarmingly by 174 %, 176 %, 163 % and 184 % for Ni, Cu, Zn and Pb from 2022 to 2045 (Supplementary material 2).

Nickel: Brake wear is determined to be the largest emitter of Ni, contributing 76 % of total Ni emissions from traffic sources in 2022. This is followed by vehicular exhaust (13 % in 2022), road abrasions (7 % in 2022) and tire wear (4 % in 2022). As of 2022 Ni emission from brake wear was estimated to be 3.73 tons, which is projected to reach 9.80 tons by 2045 (Fig. 6a). This significant contribution of brakes to Ni emissions can be attributed to the highest mean concentration of Ni in brake wear (175 mg/kg) compared to other traffic sources. Previous studies have also determined Ni concentrations in brake dust as high as 730 mg/kg [6]. To produce high wear-resistant brakes, with increased hardness, elastic modulus and oxidation resistance, Ni coatings are applied by thermal spraying or laser cladding [71,72]. Consequently, the frequent use of brakes leads to the release of Ni particles into the environment, contributing to the high emissions observed. In addition to emissions from brake wear, contributions from vehicular exhaust, tire wear and road abrasion has driven the total Ni emission to 4.9 tons in 2022. This is projected to increase progressively to 13.5 tons in 2045, if the EE and NEE sources continue to have similar Ni concentrations and emission factors (Fig. 6a).

Copper: Similar to Ni, brake wear stands out as the largest emitter of Cu, contributing 65 % of total Cu emissions from traffic sources as of 2022 (Fig. 6b). Following brake wear, vehicular exhaust is the second largest emitter of Cu (17 % in 2022), followed by tire wear (10 % in 2022) and road pitch (7 % in 2022). Similar trend was also observed in China, with brake and tire wear being a significant emitter of Cu [44]. In 2022, the Cu emission from brake wear was estimated at 8.18 tons, which is projected to steadily reach 21.45 tons by 2045 (Fig. 6b). Brake wears are particularly rich in Cu having the highest mean concentration (383 mg/kg) among all the EE and NEE sources as determined in this study. Copper chips are present on the surface of the brake pads to reinforce the structure as well as for lubrication during rotation. Furthermore, Cu is the chosen metal for using in brakes for quick heat dissipation. However, wearing of brakes discharges substantial amount of brake wear particles on roadside which are subsequently washed away to the waterways [73]. In addition to the brake pads, other EE and NEE sources emitted a total of 12.50 tons of Cu in 2022, which will go up to 34.54 tons in 2045 (Fig. 6b). If the concentrations of Cu in brakes as well as other sources are not reduced, Cu emission will continue to pose threats to urban flora and fauna and especially aquatic lives. To reduce the amount of Cu in brake pads during their manufacture, a recent initiative has been taken up by the Environmental Protection Agency (EPA) called "Copper-Free Brake Initiative", which has led to significant reduction in Cu emissions from brake pads in the US [73].

Zinc: Tires are the most significant source of Zn emission among the traffic sources globally as tire threads contain about 1 wt% of Zn [74]. Similar trends were observed in this study with tire wears containing an average of 2.5 wt% Zn (Supplementary Table 1). As a result of such high concentrations Zn, emission from tire was estimated at 471 tons in 2022 and it is projected to reach 1231 tons by 2045 (Fig. 6c). These Zn emissions from tire wears actually accounts for more than 80 % of the total Zn emissions from traffic sources. While brake wears contribution is only 15 % the absolute emission per year is quite significant, with 86 tons in 2022 reaching up to 225 tons in 2045. Similarly, vehicular exhausts only accounting 2–3 % of the total Zn emissions emitted 14.06 tons in 2022 and is projected to emit 46 tons in 2045. Emission of Zn from road abrasions was about 3.59 tons in 2022, which appears to be negligible compared to tire wears (Fig. 6c). Thus, all the traffic sources emitted a cumulative of 575 tons of Zn in 2022. Without any effort to reduce the concentration of Zn in the vehicular sources this emission will reach an alarming 1513 tons in 2045.

Lead: The combined contribution from all NEE sources (tire wear, brake wear, road abrasions) surpasses that of EE. The NEEs contribute 65–70 % of the total emitted Pb, while EEs account for 30–35 %. (Fig. 6d). However, EE is a significant emitter of Pb among traffic emission sources despite the reduction of Pb concentration after the ban of leaded gasoline more than two decades back. Among the traffic sources, vehicular exhaust still records the highest average concentration (94 mg/kg) as determined in this study (Supplementary Table 1). Furthermore, EE will continue to remain a significant emitter of Pb among traffic sources for the next two decades (Fig. 6d). In fact, the largest projected rise in Pb emission from 2022 to 2045 is expected from vehicular exhausts, increasing from 1.08 tons in 2022 to 3.56 tons in 2045 (228 % increase) This significant rise can be attributed to the increasing number of ICEV in India and least percentage of EV penetration compared to other regions (Fig. 1) [16]. Tire wear is the most significant contributor of all NEEs contributes Pb emissions followed by brake wear and road abrasions. Thus, from all these traffic sources a total of 3.6 tons of Pb was emitted in 2022, which will go up to 10.2 tons in 2045 (Fig. 6d), if the sources continue to have similar concentrations of Pb.

As the total emission of each metal rises, the percentage contribution of each source towards the emission of respective elements remains consistent throughout, from 2022 to 2045 (Fig. 6a-d). In this emission analysis, the concentrations of the metals in the sources have been kept constant, while the total number of cars and the percentage EVs have been modified based on projected data [16]. The emission factors for EVs have also been considered separately as EVs are generally heavier and hence have higher emission factors associated with tire wear, brake wear and road abrasions [45]. Hence if there is a substantial increase in number of EVs, higher emission factor associated with them should increase the NEEs.

However, despite a 7.6 % EV penetration in 2045 compared to 0.3 % in 2022 (Fig. 1), the percentage of emissions from vehicle exhausts remains consistent across all metals. This implies that the increased number of EVs, although having higher emission factors for NEEs than ICEVs, does not appreciably alter the overall emission profile of metals from traffic sources. According to projection data, the Indian roads will remain hugely dominated by ICEVs even in 2045, with EVs accounting for only 7.6 % of vehicles [16]. Emissions from EVs are directly proportional to their population and mileage (Eq. 2). With an average mileage of 161 km/charge for EVs, compared to 16.61–17.46 km/L for ICEVs (Supplementary Material 2), the lower number of EVs and their better mileage will lead to lower NEEs from EVs compared to ICEVs. Consequently, the majority of NEEs will originate from ICEVs, with EVs contributing only a small portion.

The total number of EVs is not substantial enough to have an impact on the overall emission profile of the metals when the vast majority are still ICEVs. Thus, the effect on the traffic emission scenario of India, due to a shift towards more EVs remains relatively negligible in context of India's total vehicle fleet.

4. Limitations and concluding remarks

The results from the current study are limited by the following factors:

- India can be divided into central, northern, southern, western, and eastern regions. However, this study could perform sampling only from eastern India. Thus, to generalize the findings, and widen the database for elemental concentration and isotopic composition of end members, it is necessary to include samples from other regions of India in future studies.
- In India, there is a notable gap between the number of electric vehicles projected under the current stated policies and those under announced pledges [75]. Consequently, projections for vehicle population, fuel consumption, etc based on the stated policies scenario are subject to change if there are modifications in policies by the government. Since vehicle population, fuel consumption, mileage etc are critical variables for calculating emissions (both EE and NEE) any uncertainty in these projections will introduce corresponding uncertainty in estimates of metal emissions. Thus, the emission projections in this study are only valid for current policy scenario of India. However, the equations used for emission calculation can be utilized in future, incorporating the projected data considering future policy scenarios.
- The study is unable to differentiate between metal emissions from petrol and diesel vehicles in the case of EEs due to the lack of separate data projection on vehicle population (passenger cars and light commercial vehicles) and fuel consumption in the source [45]. To the best of our knowledge only one source separately provides data for petrol and diesel consumption consumption till the year 2050. (Supplementary Note 1) Therefore more studies are required to accurately estimate separate emissions from petrol and diesel consumption.

Despite these limitations, the study provides valuable insights into metal emissions from vehicular sources and their contributions towards urban road dust in eastern India. The study emphasizes the significant contribution of NEE sources to overall metal emissions and investigates whether India's projected EV penetration will reduce metal emissions from EE. In the current scenario, as evidenced by the elemental compositions, Pb isotopic ratios and emission analysis, a substantial portion of the traffic emissions originates from NEE sources. In fact, for some metals, the NEEs dominate. However, stringent policies to control NEEs are lacking. Legislative initiatives aimed at lowering EEs and promoting EVs are not expected to lead to high market penetration of EVs. As a result, the initiatives may not be adequate in reducing air pollution in the urban and suburban areas, as evidenced by the emission analysis. Even with substantial EV market penetration in India, like other regions of the world, the high metal concentrations observed in this study, suggest that NEE will remain significant. Electric vehicles can reduce PM pollution by eliminating tailpipe emissions and utilizing regenerative braking technologies. However, the additional weight of EV batteries raises the quantity resuspended dust, tire and road wear emissions, negating the notion of "zero impact vehicles". Technological improvements such as altering the chemical composition of brake rotors, brake pads, road pavements, and tires, as well as implementing brake dust collection devices are highly necessary to ensure the reduction of NEEs [76]. Alongside of technological improvement, efforts like street sweeping, washing, & dust suppression, effective traffic management and various regulatory actions are capable of effective reduction of non-exhaust pollutants and improve urban air quality [77,78]. Additionally, promoting alternative modes of transport, such as public transit, cycling, and walking, can further reduce the reliance on private vehicles. Reducing the number of cars and increasing carpooling can significantly reduce traffic congestion and improve urban air quality. Policies focusing on ownership of private vehicles, such as implementing stringent regulations on vehicle registration, can reduce India's total vehicle fleet and consequently mitigate traffic-related emissions.

Environmental implications

The study highlights the significant environmental impact of exhaust and non-exhaust emissions from traffic sources, in Indian urban areas. Despite policies for reductions in exhaust emissions and promoting electric vehicles (EV), exhaust emissions have still been proven in previous studies to contribute significantly towards metal emissions. Further, the non-exhaust emissions arising both from fuel-driven vehicles and EVs will continue to rise with increasing number of vehicles, without proper regulations. Identifying dominating sources in urban road dusts and quantifying the emissions from the respective sources is crucial for improving urban air quality by Implementing effective regulatory measures based on the findings.

CRediT authorship contribution statement

Reshmi Das: Writing – review & editing, Validation, Supervision, Resources, Project administration, Methodology, Investigation, Funding acquisition, Formal analysis, Conceptualization. **Xianfeng Wang:** Supervision, Investigation. **Manish Tiwari:** Supervision, Investigation. **Waliur Rahaman:** Supervision, Investigation. **Iravati Ray:** Writing – review & editing, Visualization, Software, Methodology, Funding acquisition, Formal analysis, Data curation. **Divyangana Lahiri:** Writing – review & editing, Writing – original draft, Visualization, Software. **Sambuddha Misra:** Supervision, Investigation. **Mohd Tarique:** Formal analysis. **Ilindra Venkata Satya Chanakya:** Methodology, Formal analysis. **Rupam Ray:** Methodology.

Declaration of Competing Interest

The authors declare that they have no known competing financial interests or personal relationships that could have appeared to influence the work reported in this paper.

Data availability

Data included in manuscript.

Acknowledgement

R.D. acknowledges the financial supports from the Science and Engineering Research Board (Grant no. SPG/2021/002652). S.M. acknowledges Science and Engineering Research Board (SERB), Govt. of India, for financial support (Grant no. SPR\2021\000808). X.W. acknowledges the financial support from the Earth Observatory of Singapore and the Imperial College - Nanyang Technological University Collaboration Fund (INCF-2023–015) and Singapore MOE AcRF Tier 1 (RT22/21). This work comprises Earth Observatory of Singapore contribution no 622 and NCPOR contribution number J-22/2024-25. R. D.'s position is supported by University Grants Commission through the Faculty Recharge Programme (FRP-74) and I.R.'s position is supported by All India Council for Technical Education (AICTE), through the AICTE Doctoral Fellow Programme (S2021280).

Appendix A. Supporting information

Supplementary data associated with this article can be found in the

online version at doi:10.1016/j.jhazmat.2024.135810.

References

[1] US EPA, O.., 2016. Particulate Matter (PM) Basics [WWW Document]. URL ⟨https://www.epa.gov/pm-pollution/particulate-matter-pm-basics⟩ (accessed 6.13.24).

[2] Li, G., Fang, C., Wang, S., Sun, S., 2016. The effect of economic growth, urbanization, and industrialization on fine particulate matter (PM2.5) concentrations in China. Environ Sci Technol 50, 11452–11459. https://doi.org/10.1021/acs.est.6b02562.

[3] Power, A.L., Tennant, R.K., Stewart, A.G., Gosden, C., Worsley, A.T., Jones, R., et al., 2023. The evolution of atmospheric particulate matter in an urban landscape since the Industrial Revolution. Sci Rep 13, 8964. https://doi.org/10.1038/s41598-023-35679-3.

[4] Chifflet, S., Amouroux, D., Bérail, S., Barre, J., Van, T.C., Baltrons, O., et al., 2018. Origins and discrimination between local and regional atmospheric pollution in Haiphong (Vietnam), based on metal(loid) concentrations and lead isotopic ratios in PM10. Environ Sci Pollut Res 25, 26653–26668. https://doi.org/10.1007/s11356-018-2722-7.

[5] Pant, P., Harrison, R.M., 2013. Estimation of the contribution of road traffic emissions to particulate matter concentrations from field measurements: a review. Atmos Environ 77, 78–97. https://doi.org/10.1016/j.atmosenv.2013.04.028.

[6] Thorpe, A., Harrison, R.M., 2008. Sources and properties of non-exhaust particulate matter from road traffic: a review. Sci Total Environ 400, 270–282. https://doi.org/10.1016/j.scitotenv.2008.06.007.

[7] Grigoratos, T., Martini, G., 2015. Brake wear particle emissions: a review. Environ Sci Pollut Res 22, 2491–2504. https://doi.org/10.1007/s11356-014-3696-8.

[8] Denier van der Gon, H., Appelman, W., 2009. Lead emissions from road transport in Europe: a revision of current estimates using various estimation methodologies. Sci Total Environ 407, 5367–5372. https://doi.org/10.1016/j.scitotenv.2009.06.027.

[9] Gioia, S.M.C.L., Babinski, M., Weiss, D.J., Spiro, B., Kerr, A.A.F.S., Veríssimo, T.G., et al., 2017. An isotopic study of atmospheric lead in a megacity after phasing out of leaded gasoline. Atmos Environ 149, 70–83. https://doi.org/10.1016/j.atmosenv.2016.10.049.

[10] Geiger, A., Cooper, J., 2010. Overview Of Airborne Metals Regulations, Exposure Limits, Health Effects, And Contemporary Research Case Study | Environmental XPRT [WWW Document]. URL ⟨https://www.environmental-expert.com/articles/overview-of-airborne-metals-regulations-exposure-limits-health-effects-and-contemporary-research-cas-450906⟩ (accessed 6.13.24).

[11] Das, A., Krishna, K.V.S.S., Kumar, R., Saha, M.C., Sengupta, S., Ghosh, J.G., 2018. Lead isotopic ratios in source apportionment of heavy metals in the street dust of Kolkata, India. Int J Environ Sci Technol 15, 159–172. https://doi.org/10.1007/s13762-017-1377-0.

[12] Das, R., Bin Mohamed Mohtar, A.T., Rakshit, D., Shome, D., Wang, X., 2018. Sources of atmospheric lead (Pb) in and around an Indian megacity. Atmos Environ 193, 57–65. https://doi.org/10.1016/j.atmosenv.2018.08.062.

[13] Ray, I., Misra, S., Chen, M., Wang, X., Das, R., 2024. Entrapment of atmospheric particle bound heavy metals by ferns as evidenced by lead (Pb) isotope and MixSIAR: implications for improving air quality. J Hazard Mater 469, 134014. https://doi.org/10.1016/j.jhazmat.2024.134014.

[14] Rudnick, R.L., Gao, S., 2003. 3.01 - Composition of the Continental Crust. In: Holland, H.D., Turekian, K.K. (Eds.), Treatise on Geochemistry. Pergamon, Oxford, pp. 1–64. https://doi.org/10.1016/B0-08-043751-6/03016-4.

[15] Adamiec, E., Jarosz-Krzemińska, E., Wieszała, R., 2016. Heavy metals from non-exhaust vehicle emissions in urban and motorway road dusts. Environ Monit Assess 188, 369. https://doi.org/10.1007/s10661-016-5377-1.

[16] OPEC, 2023. World Oil Outlook - Chapter 3 - Oil demand [WWW Document]. URL ⟨https://woo.opec.org/chapter.php?chapterNr=1768&tableID=3000⟩ (accessed 6.14.24).

[17] O'Shea, M.J., Vigliaturo, R., Choi, J.K., McKeon, T.P., Krekeler, M.P.S., Gieré, R., 2021. Alteration of yellow traffic paint in simulated environmental and biological fluids. Sci Total Environ 750, 141202. https://doi.org/10.1016/j.scitotenv.2020.141202.

[18] Das, Avijit, Krishna, K., Kumar, R., Das, Anindya, Sengupta, S., Ghosh, J.G., 2016. Tracing lead contamination in foods in the city of Kolkata, India. Environ Sci Pollut Res 23, 22454–22466. https://doi.org/10.1007/s11356-016-7409-3.

[19] Harrison, R.M., Allan, J., Carruthers, D., Heal, M.R., Lewis, A.C., Marner, B., et al., 2021. Non-exhaust vehicle emissions of particulate matter and VOC from road traffic: a review. Atmos Environ 262, 118592. https://doi.org/10.1016/j.atmosenv.2021.118592.

[20] Cunha-Lopes, I., Alves, C.A., Casotti Rienda, I., Faria, T., Lucarelli, F., Querol, X., et al., 2022. Characterisation of non-exhaust emissions from road traffic in Lisbon. Atmos Environ 286, 119221. https://doi.org/10.1016/j.atmosenv.2022.119221.

[21] Demir, T., Karakaş, D., Yenisoy-Karakaş, S., 2022. Source identification of exhaust and non-exhaust traffic emissions through the elemental carbon fractions and Positive Matrix Factorization method. Environ Res 204, 112399. https://doi.org/10.1016/j.envres.2021.112399.

[22] Harrison, R.M., Jones, A.M., Gietl, J., Yin, J., Green, D.C., 2012. Estimation of the contributions of brake dust, tire wear, and resuspension to nonexhaust traffic particles derived from atmospheric measurements. Environ Sci Technol 46, 6523–6529. https://doi.org/10.1021/es300894r.

[23] Lopez, B., Wang, X., Chen, L.-W.A., Ma, T., Mendez-Jimenez, D., Cobb, L.C., et al., 2023. Metal contents and size distributions of brake and tire wear particles dispersed in the near-road environment. Sci Total Environ 883, 163561. https://doi.org/10.1016/j.scitotenv.2023.163561.

[24] Zhang, J., Peng, J., Song, C., Ma, C., Men, Z., Wu, J., et al., 2020. Vehicular non-exhaust particulate emissions in Chinese megacities: source profiles, real-world emission factors, and inventories. Environ Pollut 266, 115268. https://doi.org/10.1016/j.envpol.2020.115268.

[25] Adachi, K., Tainosho, Y., 2004. Characterization of heavy metal particles embedded in tire dust. Environ Int 30, 1009–1017. https://doi.org/10.1016/j.envint.2004.04.004.

[26] Hjortenkrans, D.S.T., Bergbäck, B.G., Häggerud, A.V., 2007. Metal emissions from brake linings and tires: case studies of stockholm, Sweden 1995/1998 and 2005. Environ Sci Technol 41, 5224–5230. https://doi.org/10.1021/es070198o.

[27] Jeong, C.-H., Wang, J.M., Hilker, N., Debosz, J., Sofowote, U., Su, Y., et al., 2019. Temporal and spatial variability of traffic-related PM2.5 sources: comparison of exhaust and non-exhaust emissions. Atmos Environ 198, 55–69. https://doi.org/10.1016/j.atmosenv.2018.10.038.

[28] Sethupathi, P.B., Chandradass, J., Saibalaji, M.A., 2021. Comparative study of disc brake pads sold in Indian market — Impact on safety and environmental aspects. Environ Technol Innov 21, 101245. https://doi.org/10.1016/j.eti.2020.101245.

[29] Singh, V., Biswal, A., Kesarkar, A.P., Mor, S., Ravindra, K., 2020. High resolution vehicular PM10 emissions over megacity Delhi: Relative contributions of exhaust and non-exhaust sources. Sci Total Environ 699, 134273. https://doi.org/10.1016/j.scitotenv.2019.134273.

[30] Dong, S., Ochoa Gonzalez, R., Harrison, R.M., Green, D., North, R., Fowler, G., et al., 2017. Isotopic signatures suggest important contributions from recycled gasoline, road dust and non-exhaust traffic sources for copper, zinc and lead in PM10 in London, United Kingdom. Atmos Environ 165, 88–98. https://doi.org/10.1016/j.atmosenv.2017.06.020.

[31] Jeong, H., 2022. Toxic metal concentrations and Cu–Zn–Pb isotopic compositions in tires. J Anal Sci Technol 13, 2. https://doi.org/10.1186/s40543-021-00312-3.

[32] Jeong, H., Ryu, J.-S., Ra, K., 2022. Characteristics of potentially toxic elements and multi-isotope signatures (Cu, Zn, Pb) in non-exhaust traffic emission sources. Environ Pollut 292, 118339. https://doi.org/10.1016/j.envpol.2021.118339.

[33] Komárek, M., Ettler, V., Chrastný, V., Mihaljevič, M., 2008. Lead isotopes in environmental sciences: a review. Environ Int 34, 562–577. https://doi.org/10.1016/j.envint.2007.10.005.

[34] Das, R., Wang, X., Khezri, B., Webster, R.D., Itoh, M., Shiodera, S., et al., 2023. Suspension of crustal materials from wildfire in indonesia as revealed by Pb isotope analysis. ACS Earth Space Chem 7, 379–387. https://doi.org/10.1021/acsearthspacechem.2c00270.

[35] Ray, I., Das, R., Chua, S.L., Wang, X., 2022. Seasonal variation of atmospheric Pb sources in Singapore - Elemental and lead isotopic compositions of PM10 as source tracer. Chemosphere 307, 136029. https://doi.org/10.1016/j.chemosphere.2022.136029.

[36] Sen, I.S., Bizimis, M., Tripathi, S.N., Paul, D., 2016. Lead isotopic fingerprinting of aerosols to characterize the sources of atmospheric lead in an industrial city of India. Atmos Environ 129, 27–33. https://doi.org/10.1016/j.atmosenv.2016.01.005.

[37] Ray, I., Das, R., 2023. A lingering legacy of leaded gasoline in Southeast Asia. Commun Earth Environ 4, 1–11. https://doi.org/10.1038/s43247-023-01135-3.

[38] Sugiyama, I., Williams-Jones, A.E., 2018. An approach to determining nickel, vanadium and other metal concentrations in crude oil. Anal Chim Acta 1002, 18–25. https://doi.org/10.1016/j.aca.2017.11.040.

[39] Reuer, M.K., Boyle, E.A., Grant, B.C., 2003. Lead isotope analysis of marine carbonates and seawater by multiple collector ICP-MS. Chem Geol 200, 137–153. https://doi.org/10.1016/S0009-2541(03)00186-4.

[40] Baker, J., Peate, D., Waight, T., Meyzen, C., 2004. Pb isotopic analysis of standards and samples using a 207Pb–204Pb double spike and thallium to correct for mass bias with a double-focusing MC-ICP-MS. Chem Geol 211, 275–303. https://doi.org/10.1016/j.chemgeo.2004.06.030.

[41] White, W.M., Albarède, F., Télouk, P., 2000. High-precision analysis of Pb isotope ratios by multi-collector ICP-MS. Chem Geol 167, 257–270. https://doi.org/10.1016/S0009-2541(99)00182-5.

[42] Stock, B., Semmens, B., 2016. MixSIAR GUI User Manual v3.1.

[43] Longman, J., Veres, D., Ersek, V., Phillips, D.L., Chauvel, C., Tamas, C.G., 2018. Quantitative assessment of Pb sources in isotopic mixtures using a Bayesian mixing model. Sci Rep 8, 6154. https://doi.org/10.1038/s41598-018-24474-0.

[44] Tian, H.Z., Zhu, C.Y., Gao, J.J., Cheng, K., Hao, J.M., Wang, K., et al., 2015. Quantitative assessment of atmospheric emissions of toxic heavy metals from anthropogenic sources in China: historical trend, spatial distribution, uncertainties, and control policies. Atmos Chem Phys 15, 10127–10147. https://doi.org/10.5194/acp-15-10127-2015.

[45] OECD, 2020. The implications of electric vehicle uptake for non-exhaust emissions. OECD, Paris. https://doi.org/10.1787/e1bc711b-en.

[46] Winkler, S.L., Anderson, J.E., Garza, L., Ruona, W.C., Vogt, R., Wallington, T.J., 2018. Vehicle criteria pollutant (PM, NOx, CO, HCs) emissions: how low should we go? Npj. Clim Atmos Sci 1, 1–5. https://doi.org/10.1038/s41612-018-0037-5.

[47] Vaaraslahti, K., Keskinen, J., Giechaskiel, B., Solla, A., Murtonen, T., Vesala, H., 2005. Effect of lubricant on the formation of heavy-duty diesel exhaust nanoparticles. Environ Sci Technol 39, 8497–8504. https://doi.org/10.1021/es0505503.

[48] Liati, A., Pandurangi, S.S., Boulouchos, K., Schreiber, D., Arroyo Rojas Dasilva, Y., 2015. Metal nanoparticles in diesel exhaust derived by in-cylinder melting of detached engine fragments. Atmos Environ 101, 34–40. https://doi.org/10.1016/j.atmosenv.2014.11.014.

[49] Liati, A., Schreiber, D., Dimopoulos Eggenschwiler, P., Arroyo Rojas Dasilva, Y., 2013. Metal particle emissions in the exhaust stream of diesel engines: an electron microscope study. Environ Sci Technol 47, 14495–14501. https://doi.org/10.1021/es403121y.
[50] Dočekal, B., Krivan, V., Pelz, N., 1992. Trace and minor element characterization of diesel soot. Fresenius J Anal Chem 343, 873–878. https://doi.org/10.1007/BF00321956.
[51] Timmers, V.R.J.H., Achten, P.A.J., 2016. Non-exhaust PM emissions from electric vehicles. Atmos Environ 134, 10–17. https://doi.org/10.1016/j.atmosenv.2016.03.017.
[52] Samanta, S., Menzel Barraqueta, J.-L., Das, R., Roychoudhury, A.N., 2022. Source apportionment of the atmospheric Pb using a simulation-based inversion model: a case study from India uncovers bituminous road as the prime contributor of petroleum-derived Pb. Appl Geochem 136, 105164. https://doi.org/10.1016/j.apgeochem.2021.105164.
[53] von Gunten, K., Konhauser, K.O., Alessi, D.S., 2020. Potential of asphalt concrete as a source of trace metals. Environ Geochem Health 42, 397–405. https://doi.org/10.1007/s10653-019-00370-y.
[54] Harrison, R.M., Tilling, R., Callén Romero, M.S., Harrad, S., Jarvis, K., 2003. A study of trace metals and polycyclic aromatic hydrocarbons in the roadside environment. Atmos Environ 37, 2391–2402. https://doi.org/10.1016/S1352-2310(03)00122-5.
[55] Wiseman, C.L.S., Levesque, C., Rasmussen, P.E., 2021. Characterizing the sources, concentrations and resuspension potential of metals and metalloids in the thoracic fraction of urban road dust. Sci Total Environ 786, 147467. https://doi.org/10.1016/j.scitotenv.2021.147467.
[56] Budai, P., Clement, A., 2018. Spatial distribution patterns of four traffic-emitted heavy metals in urban road dust and the resuspension of brake-emitted particles: findings of a field study. Transp Res Part Transp Environ 62, 179–185. https://doi.org/10.1016/j.trd.2018.02.014.
[57] Lin, Y.-C., Tsai, C.-J., Wu, Y.-C., Zhang, R., Chi, K.-H., Huang, Y.-T., et al., 2015. Characteristics of trace metals in traffic-derived particles in Hsuehshan Tunnel, Taiwan: size distribution, potential source, and fingerprinting metal ratio. Atmos Chem Phys 15, 4117–4130. https://doi.org/10.5194/acp-15-4117-2015.
[58] Salazar, J.R., Cartledge, B.T., Haynes, J.P., York-Marini, R., Robinson, A.L., Drozd, G.T., et al., 2020. Water-soluble iron emitted from vehicle exhaust is linked to primary speciated organic compounds. Atmos Chem Phys 20, 1849–1860. https://doi.org/10.5194/acp-20-1849-2020.
[59] Miler, M., 2021. Airborne particles in city bus: concentrations, sources and simulated pulmonary solubility. Environ Geochem Health 43, 2757–2780. https://doi.org/10.1007/s10653-020-00770-5.
[60] Li, F., Jinxu, Y., Shao, L., Zhang, G., Wang, J., Jin, Z., 2018. Delineating the origin of Pb and Cd in the urban dust through elemental and stable isotopic ratio: a study from Hangzhou City, China. Chemosphere 211, 674–683. https://doi.org/10.1016/j.chemosphere.2018.07.199.
[61] Millot, R., Allègre, C.-J., Gaillardet, J., Roy, S., 2004. Lead isotopic systematics of major river sediments: a new estimate of the Pb isotopic composition of the Upper Continental Crust. Chem Geol 203, 75–90. https://doi.org/10.1016/j.chemgeo.2003.09.002.
[62] Deb, M., Thorpe, R.I., Cumming, G.L., Wagner, P.A., 1989. Age, source and stratigraphic implications of Pb isotope data for conformable, sediment-hosted, base metal deposits in the Proterozoic Aravalli-Delhi orogenic belt, northwestern India. Precambrian Res 43, 1–22. https://doi.org/10.1016/0301-9268(89)90002-8.
[63] Stock, B., 2022. MixSIAR.
[64] Chen, H., Yan, Y., Hu, D., Peng, L., Wang, C., 2023. High contribution of vehicular exhaust and coal combustion to PM2.5-bound Pb pollution in an industrial city in North China: an insight from isotope. Atmos Environ 294, 119503. https://doi.org/10.1016/j.atmosenv.2022.119503.
[65] Dietrich, M., Krekeler, M.P.S., Kousehlar, M., Widom, E., 2021. Quantification of Pb pollution sources in complex urban environments through a multi-source isotope mixing model based on Pb isotopes in lichens and road sediment. Environ Pollut 288, 117815. https://doi.org/10.1016/j.envpol.2021.117815.
[66] Koffman, B.G., Saylor, P., Zhong, R., Sethares, L., Yoder, M.F., Hanschka, L., et al., 2022. Provenance of Anthropogenic Pb and Atmospheric Dust to Northwestern North America. Environ Sci Technol 56, 13107–13118. https://doi.org/10.1021/acs.est.2c03767.
[67] Longman, J., Struve, T., Pahnke, K., 2022. Spatial and temporal trends in mineral dust provenance in the south pacific-evidence from mixing models. e2021PA004356 Paleoceanogr Paleoclimatology 37. https://doi.org/10.1029/2021PA004356.
[68] Turner, A., Filella, M., 2023. Lead and chromium in European road paints. Environ Pollut 316, 120492. https://doi.org/10.1016/j.envpol.2022.120492.
[69] Haritash, A.K., Kaushik, C.P., 2007. Assessment of seasonal enrichment of heavy metals in respirable suspended particulate matter of a sub-urban Indian City. Environ Monit Assess 128, 411–420. https://doi.org/10.1007/s10661-006-9335-1.
[70] Das, R., Khezri, B., Srivastava, B., Datta, S., Sikdar, P.K., Webster, R.D., et al., 2015. Trace element composition of PM2.5 and PM10 from Kolkata – a heavily polluted Indian metropolis. Atmos Pollut Res 6, 742–750. https://doi.org/10.5094/APR.2015.083.
[71] Aranke, O., Algenaid, W., Awe, S., Joshi, S., 2019. Coatings for automotive gray cast iron brake discs: a review. Coatings 9, 552. https://doi.org/10.3390/coatings9090552.
[72] Shi, X., Wen, D., Wang, S., Wang, G., Zhang, M., Li, J., et al., 2021. Investigation on friction and wear performance of laser cladding Ni-based alloy coating on brake disc. Optik 242, 167227. https://doi.org/10.1016/j.ijleo.2021.167227.
[73] US EPA, O.., 2015. Copper-Free Brake Initiative [WWW Document]. URL ⟨https://www.epa.gov/npdes/copper-free-brake-initiative⟩ (accessed 6.23.24).
[74] Councell, T.B., Duckenfield, K.U., Landa, E.R., Callender, E., 2004. Tire-wear particles as a source of zinc to the environment. Environ Sci Technol 38, 4206–4214. https://doi.org/10.1021/es034631f.
[75] International Energy Agency, 2024. Outlook for electric mobility – Global EV Outlook 2024 – Analysis [WWW Document]. IEA. URL ⟨https://www.iea.org/reports/global-ev-outlook-2024/outlook-for-electric-mobility⟩ (accessed 8.6.24).
[76] Piscitello, A., Bianco, C., Casasso, A., Sethi, R., 2021. Non-exhaust traffic emissions: sources, characterization, and mitigation measures. Sci Total Environ 766, 144440. https://doi.org/10.1016/j.scitotenv.2020.144440.
[77] Amato, F., Cassee, F.R., Denier van der Gon, H.A.C., Gehrig, R., Gustafsson, M., Hafner, W., et al., 2014. Urban air quality: the challenge of traffic non-exhaust emissions. J Hazard Mater 275, 31–36. https://doi.org/10.1016/j.jhazmat.2014.04.053.
[78] Keuken, M., Denier van der Gon, H., van der Valk, K., 2010. Non-exhaust emissions of PM and the efficiency of emission reduction by road sweeping and washing in the Netherlands. Sci Total Environ 408, 4591–4599. https://doi.org/10.1016/j.scitotenv.2010.06.052.

npj | climate and atmospheric science

Article

Published in partnership with CECCR at King Abdulaziz University

https://doi.org/10.1038/s41612-024-00836-6

Dominance of open burning signatures in $PM_{2.5}$ near coal plant should redefine pollutant priorities of India

Check for updates

Iravati Ray[1] ✉, Shoumick Mitra[2], Jariya Kayee[3], Shufang Yuan[3], S. M. Shiva Nagendra[2], Xianfeng Wang[3,4] & Reshmi Das[1,3] ✉

India, heavily reliant on coal for power generation, has been a significant emitter of particulate matter (PM) bound lead (Pb) and other heavy metals. It is crucial to understand whether implementation of stricter norms in recent years have effectively reduced emissions from coal combustion. This study aims to investigate and quantify the primary sources of $PM_{2.5}$ in an area housing a major lignite-fired power plant in South India using Pb isotopic compositions and elemental concentrations. Characteristic ratios such as V/Pb and Cu/Pb demonstrate negligible influence from coal combustion, and indicate that summer aerosols are influenced by open burning. In Pb triple-isotope space the $PM_{2.5}$ aerosols plot away from coal, overlapping with open burning signatures. These indicate that the atmosphere is predominantly influenced by open burning of solid waste and biomass rather than coal combustion, suggesting a promising decrease in coal emissions. Bayesian mixing model demonstrates that solid waste & biomass burning is the largest anthropogenic contributor towards atmospheric Pb (up to 26%), even in a region of coal combustion and presence of medium and small-scale industries. The dominance of open burning as a pollution source in the vicinity of a lignite fired power plant highlights the necessity for better waste management strategies.

Particulate matter (PM) is one of the most concerning threats among the air pollutants, as it leads to majority of premature deaths globally[1]. India is one of the worst affected countries in terms of PM exposure. Alarmingly, on 96% of the days in a year, India with her 1.42 billion people is exposed to $PM_{2.5}$ levels higher than the WHO prescribed average 24 h limit of 15 $\mu g/m^3$ [2]. In terms of fine particulate pollution, India experienced a staggering death toll of over 9.72 million in 2019, placing it in second position after China[3]. Several anthropogenic sources such as coal combustion, biomass burning, vehicular fuel combustion, industrial processes etc. contribute significantly towards this elevated level of PM emission in India (Fig. 1a). Comparative estimates of PM emission from these sources reveal that open burning of biomass has been the largest emitter of PM_{10} and $PM_{2.5}$ for the past one and a half decade[4]. Coal combustion emission is steadily decreasing due to implementation of stricter emission standards that was put forth in 2015[5]. In contrast, PM emissions from industrial processes is projected to surpass that of coal combustion in the present decade. Apart from these sources a large collective contribution is present from other miscellaneous sources (Fig. 1a).

India, ranks second in coal consumption, and is home to 295 coal-fired power plants[6–9]. Coal fired plants and other non-ferrous industries have emission control systems such as cyclone separators, bag filters, electrostatic precipitators (ESP) to reduce the PM emission and metals associated with it[10]. On the other hand, the practice of open burning of biomass and solid wastes (SW) at open dumpsites, landfills or even individual residences, leads to uncontrolled release of PM. India ranks among the top countries globally in both waste production and open burning of wastes[11]. The mass of pollutants emitted from open burning per mass of waste (i.e., the emission factor) is an order of magnitude higher than other controlled processes[10,12–15] (Fig. 1b).

These emitted PMs are associated with toxic elements like Arsenic (As), Cadmium (Cd), Chromium (Cr), Cobalt (Co), Mercury (Hg), Nickel (Ni), Lead (Pb) etc that can pose significant environmental and health risks. The elements released from coal that are of highest concern, due to their high concentrations, include As, boron (B), Cd, Hg, molybdenum (Mo), Pb, and selenium (Se). Elements of moderate concern include Cr, copper (Cu), Ni, vanadium (V), and zinc (Zn)[16] Non-ferrous industries and other small-

[1]School of Environmental Studies, Jadavpur University, Kolkata, India. [2]Department of Civil Engineering, Indian Institute of Technology Madras, Madras, India. [3]Earth Observatory of Singapore, Nanyang Technological University, Singapore, Singapore. [4]Asian School of Environment, Nanyang Technological University, Singapore, Singapore. ✉e-mail: iravatir.envs.rs@jadavpuruniversity.in; reshmidas.sest@jadavpuruniversity.in

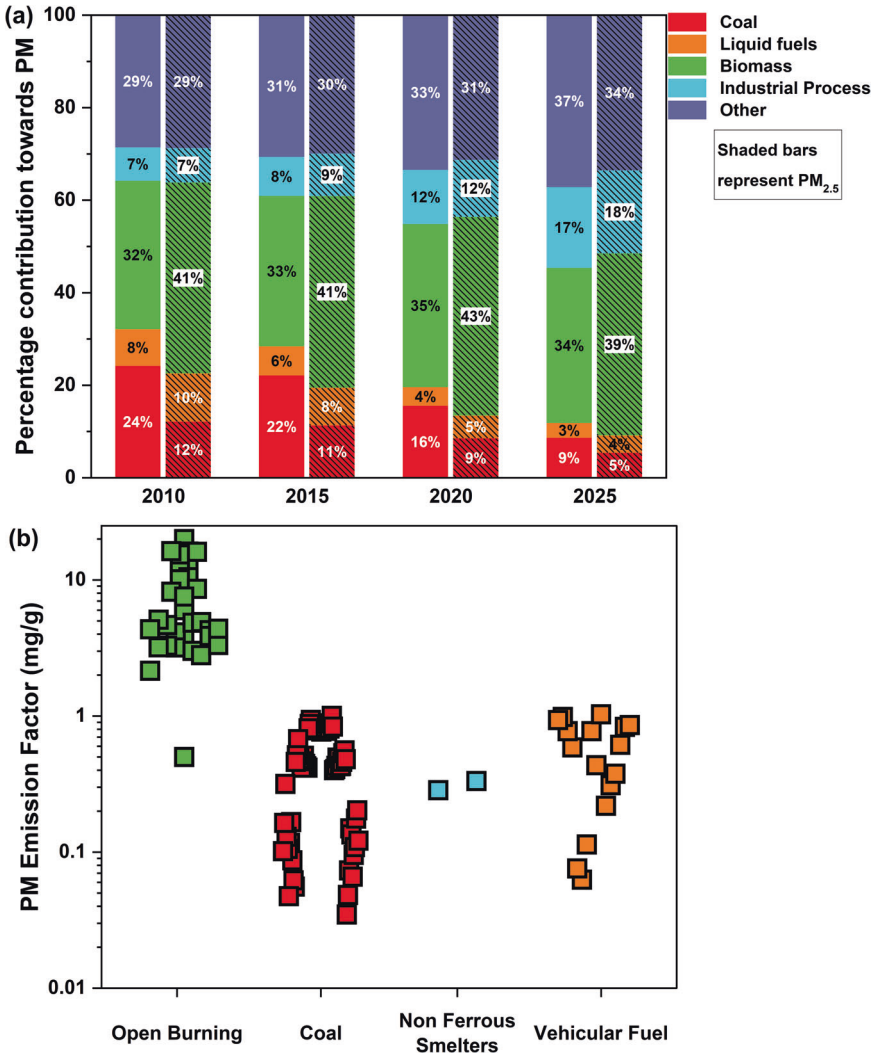

Fig. 1 | Comparative estimates of PM emission and emission factors of various anthropogenic processes. a Stacked bars representing emissions of PM_{10} and $PM_{2.5}$ (shaded bars) from different anthropogenic sources as compiled form "GAINS South Asia online," 2020. For the past one and a half decades, open biomass burning has been the largest emitter of PM_{10} and $PM_{2.5}$, while coal combustion emissions have steadily decreased due to the stricter emission standards implemented in 2015; **b** Particulate matter (PM) emission factors of open burning coal combustion, non-ferrous smelters and vehicular fuel. The emission factors for open burning are orders of magnitude higher than other processes. The emission factors have been compiled from Akbari et al.[12]; Raparthi and Phuleria[13]; Saud et al.[14]; Zhang et al.[10]; Zhu et al.[15].

scale industries emit elements such as Cr, Mn, Fe, Cu, Zn, Ni, Cd and Pb[17]. On the other hand, SW incineration ash consists of varying amount of trace metals of which the major concerns are Al, Cr, Cu, Zn, Cd, Pb and Hg[18]. These elements are often enriched in bottom and fly ashes and pose environmental risks[19]. Fly ashes from SW incineration primarily consists of particles smaller than 5.5 μm, posing risk of the associated toxic metals being transferred to the human bloodstream through inhalation, if burnt openly[20]. The concentrations of these elements in SW ash vary across different countries[21–24]. However, in general the trend shows very high concentrations of Mn, Cu, Zn and Pb followed by moderate concentrations of Cr, Ni and Cd. A detailed country wise comparative analysis of the elemental concentration of toxic metals in SW incineration fly ash[21–25] is presented in Supplementary Table 1.

These heavy metals are mostly bound to fine PM (PM < 2.5 μm) and can be transported over long distances across countries by atmospheric circulation[26]. Evidences of pollutants from Europe and North America reaching the Arctic have been reported in the past century[27] When leaded gasoline was in use, Pb compounds emitted with vehicular exhaust were transported to remote regions, including Antarctica, Greenland, Alaska, and the open ocean. This long-range transport of Pb was traced with the use of stable Pb isotopes.[28]. Fine particles containing Pb, Hg, and Cd persist in the atmosphere for extended periods, allowing them to be deposited in areas far from their sources. Particularly, in case of Pb, the atmospheric residence time is typically 5–10 days after its emission until it gets deposited[29].

To accurately quantify these emissions, one approach is to utilize heavy metal concentrations and isotopes. These isotopes, such as Pb, can serve as tracers of PM emissions, allowing for the identification and quantification of specific sources[30]. As there is no isotopic fractionation of Pb during physicochemical processes the isotopic signature of the source is preserved[31]. Metal concentrations are also crucial factors that supports the implications derived from isotopic compositions[32,33]. In the past decade PM bound Pb was found to be significantly enriched in Indian aerosols. This Pb is primarily sourced from coal combustion, metal ores utilized in industrial purposes and open burning of biomass and wastes[30,32–35]. The concentration of Pb in the PM emitting sources such as ore, Indian coal and biomass typically ranges from 1.6 to 5.5%, 20 to 144 ppm, and 0.2 to 28 ppm, respectively[32,36–38]. Thus, although emission factors for coal combustion, ore smelting, and vehicular fuel combustion are less than that of open burning, the former sources have orders of magnitude higher concentrations.

The major sources of PM in the Indian atmosphere have been a subject of investigation and study. As coal combustion emission is steadily decreasing, it is crucial to investigate whether the emission norms are effective in controlling emission of heavy metals from coal combustion. Being the largest power-supplying plant using lignite, Neyveli can emit significant amount of heavy metals. This makes it an ideal site for assessing how well current emission norms are controlling the release of these heavy metals to the atmosphere. A detailed country wise comparative analysis of the elemental concentration of toxic metals in lignite[39–51] is presented in

Supplementary Table 1. Thus, this study aims to investigate the primary sources of $PM_{2.5}$ in an area housing the major lignite-fired power plant of South India using Pb isotopic compositions and elemental composition. The Indian atmosphere is additionally influenced by emissions from open burning and other large and small-scale industries. The ultimate objective is to quantify the contribution of each source towards atmospheric $PM_{2.5}$ levels by utilizing the Pb isotope and elemental concentration data of $PM_{2.5}$ so that better regulatory actions can be taken to improve air quality. In a densely populated developing country like India, where multiple sources of emission coexist, source apportionment becomes crucial for targeted mitigation strategies and implementation of stricter emission controls in specific emitting sectors.

Results

Elemental concentration and $PM_{2.5}$ load

The concentration of the 13 (Mg, Al, Ca, V, Cr, Mn, Fe, Co, Ni, Cu, Zn, Cd and Pb) elements analyzed in the $PM_{2.5}$ aerosols varied across months (Fig. 2a). Across all months, the elements can be divided into three distinct groups, following the general order: (Al, Ca, Fe, Mg, Zn) > (Cr, Cu, Mn, Ni, Pb) > (Cd, Co, V). All the months witnessed orders of magnitude higher mean concentrations of Al (951–3525 ng/m^3), Ca (66–345 ng/m^3), Fe (94–512 ng/m^3), Mg (38–228 ng/m^3) and Zn (33–481 ng/m^3) compared to Cd (0.08–2.53 ng/m^3), Co (0.05–0.25 ng/m^3), Cr (0.90–13.5 ng/m^3), Cu (2.02–44 ng/m^3), Mn (1.96–68 ng/m^3), Ni (0.91–13.5 ng/m^3), Pb (2.32–79.89 ng/m^3) and V (0.41–2.25 ng/m^3).

Concentrations of all the elements witnessed a sharp decrease in the month of May (Fig. 2a). Anthropogenically sourced elements such as Cd, Pb and Zn demonstrated a decreasing trend through the months of April–June 2021, followed by an increase in the last three months of the year. Simultaneously, there was a sharp increase in $PM_{2.5}$ load in the months of April–June compared to October–December of 2020, 2021 and February 2022 (Fig. 2a). Aluminum recorded highest concentration in April.

In the end member samples such as soil, open waste burning ashes, coal and fly ash the general order of concentrations followed were (Al, Ca, Mg, Fe) > (Cd, Co, Cr, Cu, Mn, Ni, V, Pb, Zn). The individual concentrations of the components are presented in Supplementary Table 2.

Enrichment factors and airmass back trajectories

Enrichment factors reveal that $PM_{2.5}$ aerosols were enriched in Cu, Zn, Cd and Pb (mean EF > 10) (Fig. 2b), indicating anthropogenic sources. Zinc, Cd and Pb were observed to have mean EFs >10 in all the months. Copper exhibited mean EFs <10 in the months of April–June 2021, December 2021 and February 2022. In fact, all the enriched metals along with Mn and Co exhibited lowest EFs in the months of April–June.

The 72 h airmass back trajectories for an entire year reveal that the primary origin of the airmasses are oceanic (Supplementary Fig. 1). From October to February, part of the airmasses originate from the land while the rest originate from the ocean. From April to June all airmasses originate from the ocean (Fig. 3).

Pb isotopic compositions as source tracers

The mean Pb isotopic composition of the $PM_{2.5}$ samples and end members are presented in Table 1. The individual composition of each sample is presented in Supplementary Table 3. The lignite and fly ash of the region are significantly different from coal samples found in other parts of India[32]. The Neyveli lignite is characterized by low $^{206}Pb/^{207}Pb$ ratios and higher $^{208}Pb/^{206}Pb$ ratios compared to other coals, indicating high Thorium contents.

Quantification of end member contributions

The MixSIAR model results reveal a seasonal change in contribution percentages of the sources. The mean Pb isotopic composition of the considered sources along with their standard deviations and concentrations are presented in Supplementary Table 4.

Discussion

The higher mean concentrations of Al, Ca, Fe and Mg in the months of April–May can be due to their higher crustal abundances. Previous studies have also reported high concentrations of these elements in both coarse and fine aerosols in different parts of India and attributed them to crustal sources[52–55]. The range of elemental concentrations observed in this study is similar to those reported in $PM_{2.5}$ aerosols from other regions of India[53,56–60] (Supplementary Fig. 2). However, when comparing median elemental concentrations specifically in $PM_{2.5}$ aerosols, Neyveli records lower median concentrations for all elements except Al and Zn. The elevated median concentration of Al, with simultaneous lower median concentrations of other elements, in the months of April–May indicates a higher contribution of crustal dust to the aerosol composition. Further insights into whether the elements have a crustal or anthropogenic origin can be inferred from the EFs, discussed later. Zinc, despite having significantly less crustal abundance compared to Ca, Fe, and Mg[61], demonstrates similar concentrations to these elements. This suggests additional anthropogenic inputs of Zn other than crust. The concentration of Pb in $PM_{2.5}$ observed in this study is lower than values reported in aerosols (TSP, PM_{10} and $PM_{2.5}$) from urban and industrial regions of India in previous investigations[32,33,53,55,58,59,62–96]. Previous studies have reported Pb concentrations exceeding the national ambient air quality standard (NAAQS) annual average of 500 ng/m^3 in industrial and major Indian cities even after the complete phase-out of leaded gasoline in the year 2000 (Supplementary Fig. 3). In contrast, the maximum Pb concentration recorded in this study is 79.9 ng/m^3, suggesting a lower level of anthropogenic Pb pollution in the studied region compared to other parts of India.

This decrease in concentration of Cr, Mn, Zn, Cd and Pb with increasing $PM_{2.5}$ load and simultaneous increase in Al concentration in the months of April–May indicate a greater influence of geogenic sources in the months of higher $PM_{2.5}$ loads. As the amount of coal combustion at the thermal power plant remained constant[97], it is most likely, that sources other than coal influenced the atmospheric metal concentrations of the region. To gain a better insight about the sources (geogenic or anthropogenic), of the metals the crustal EFs have been determined.

Lowest EFs in the months of April–June indicate that the atmospheric aerosols experienced a greater geogenic influence in these months. Moderate to strongly negative Spearman correlations were observed between $PM_{2.5}$ load versus the concentration of the enriched elements Cd, Pb and Zn ($R = -0.56$ to -0.72 and $p = 0.02–0.09$) and their EFs ($R = -0.64$ to -0.72 and $p = 0.01–0.05$) (Supplementary Fig. 4). As the operation of the lignite-fired power plant was consistent throughout the sampling period[97], this variation in EFs must be due to other local and long-range sources.

By coupling back trajectories with EF_{Pb}, it can be observed that the airmasses, despite having oceanic origins in the months of October–February demonstrate very high EF_{Pb} (mean = 101 ± 38). While, similar oceanic origin airmasses in the months of April–June, demonstrate $EF_{Pb} \leq 28$ (mean = 17 ± 7) in $PM_{2.5}$ (Fig. 3). In India, the months of October to December mark the post-monsoon season, while April to June corresponds to the summer season. During the post-monsoon period, temperatures begin to fall, especially during the night across India, and wind patterns shift, signaling the onset of colder weather[98]. The changing wind patterns lead to wind blowing from the land to the sea, transporting pollutants from the land surface to over the ocean. The northern Bay of Bengal (BoB) remains under the influence of airmasses from Indo Gangetic plain while the southeastern BoB receives air masses from southeast Asia[99,100]. Similarly, the southern Arabian Sea remains under the influence of western and southern India[101]. Thus, the high EF_{Pb} in airmasses originating from the ocean during post-monsoon period can be attributed to the transport of pollutants from land to sea due to prevailing wind patterns. Further, the mean temperature is lower and as a result, temperature inversion traps cooler air beneath a layer of warmer air. This cooler air confines within it the ground-level pollution and thus, increases the pollution levels in the air masses just above the ground surface[102]. Long-term (2010–2018) LIDAR observations and radiosonde data from Gadanki (a rural site ~280 km north

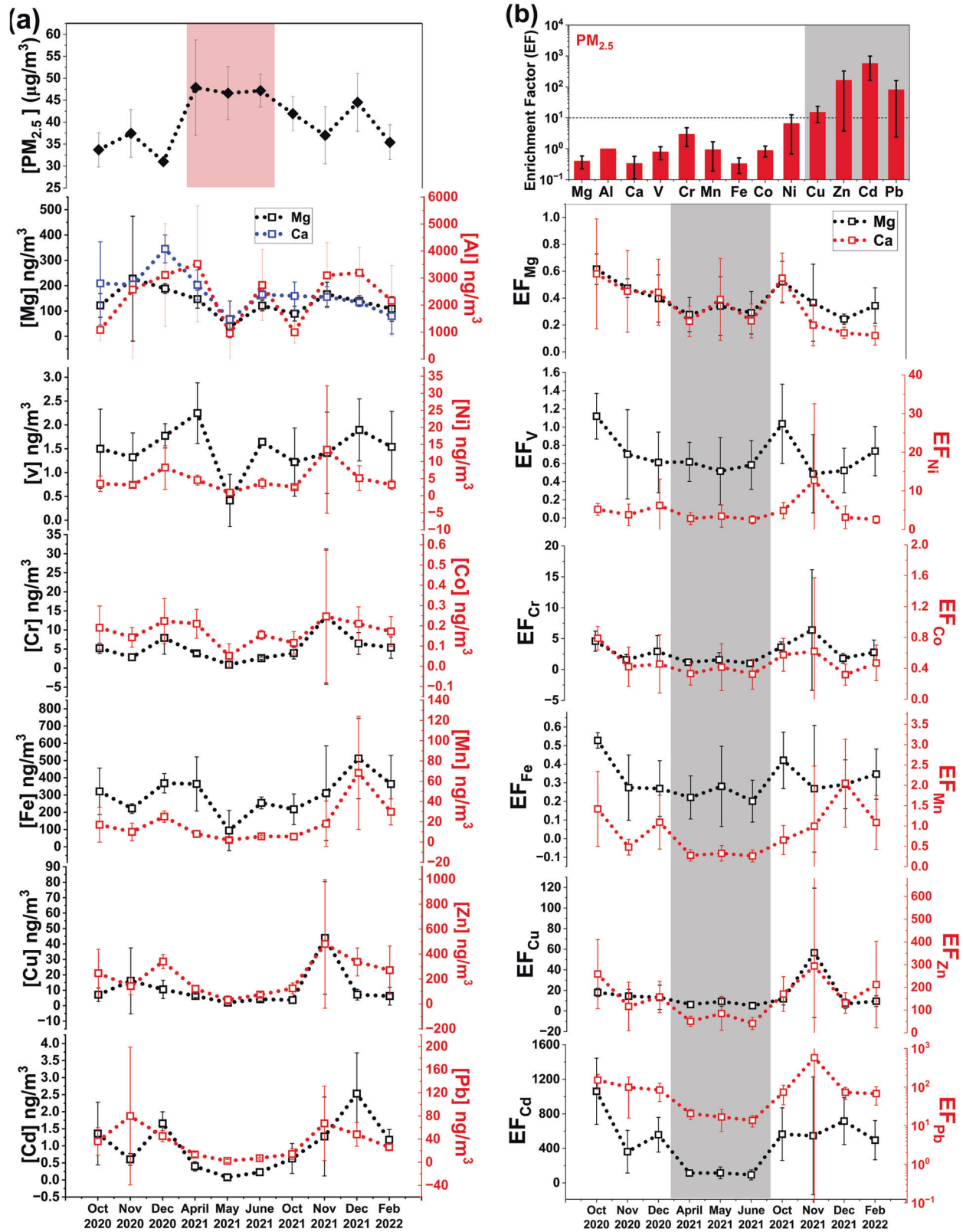

Fig. 2 | Temporal variations in $PM_{2.5}$ load, elemental concentrations and enrichment factors. a Temporal variation in concentrations of $PM_{2.5}$ (top panel) and elements. The $PM_{2.5}$ loads increased in the months of April–June compared to October–December. Concentrations of all the elements witnessed a sharp decrease in the month of May. **b** The top panel depicts the mean enrichment factors (EF) of each element in $PM_{2.5}$ aerosols across the sampling period with significant enrichment in Cu, Zn, Cd and Pb (EFs > 10). The lower panels illustrate the temporal variation in EFs. All the enriched elements exhibited lowest EFs in the months of April–June, indicating a reduced anthropogenic contribution during these months.

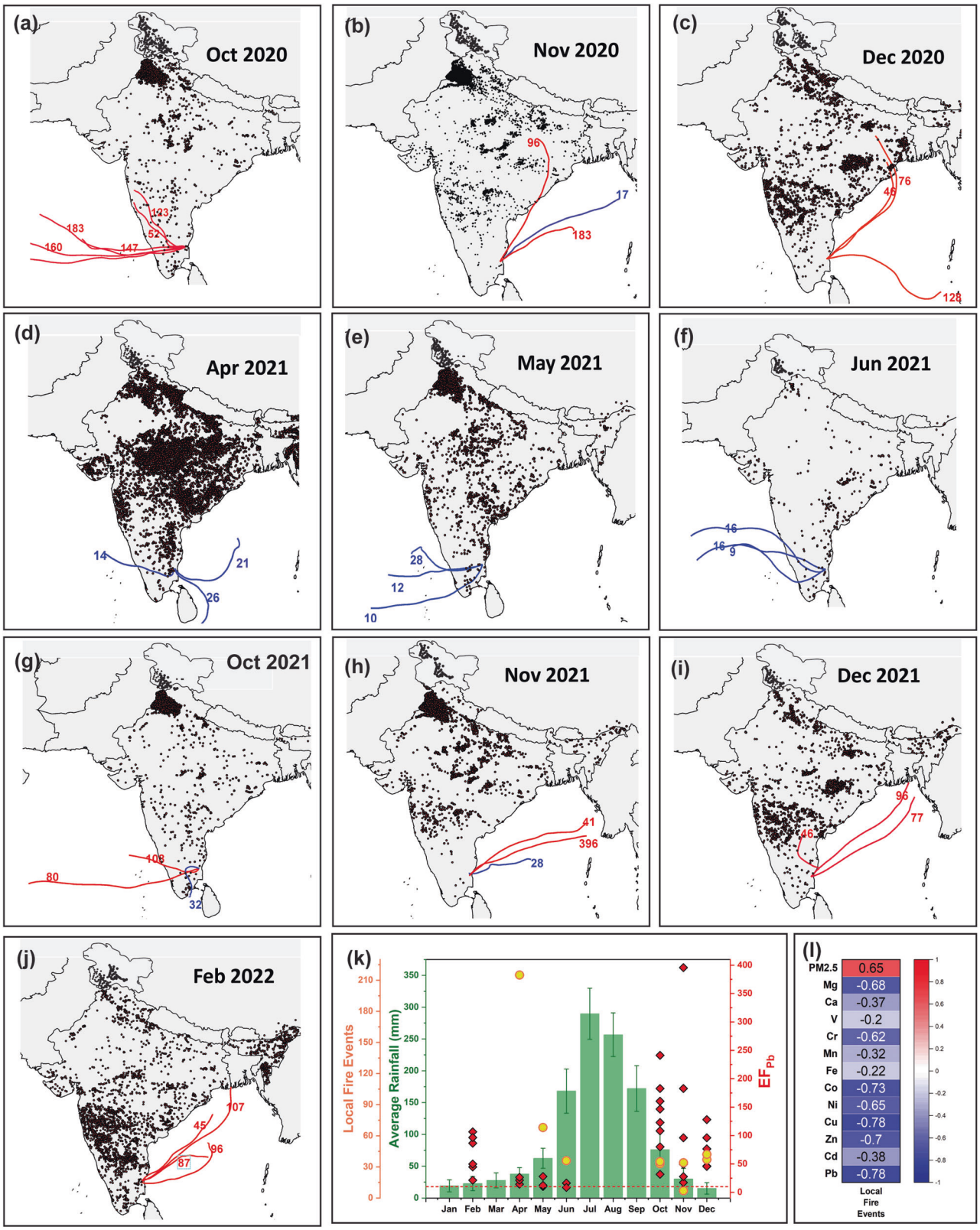

Fig. 3 | Influence of airmass back trajectories, local fire events, and rainfall over Pb enrichments in $PM_{2.5}$ aerosols across the sampling period. The 72 h airmass back trajectories for the sampling days coupled with their corresponding EFs of Pb for (**a**) October 2020 (**b**) November 2020 (**c**) December 2020 (**d**) April 2021 (**e**) May 2021 (**f**) June 2021 (**g**) October 2021 (**h**) November 2021 (**i**) December 2021 (**j**) February 2022. The trajectories have been computed using geographic information system (GIS) based software TrajStat (version: 1.5.3). The airmasses with EFs < 32 are marked in blue while higher EFs are marked in red. **k** The monthly average rainfall in India (green bars) along with observed local fire events (yellow circles) around NLCIL and EFs of Pb (red diamonds) in $PM_{2.5}$ aerosols sampled at NLCIL. The red dotted line represents EF = 10. **l** Spearman Correlation between the number of local fire events versus elemental EFs in $PM_{2.5}$ aerosols. The data for the fire events has been acquired from MODIS Terra and Aqua satellites available at NASA Fire Information for Resource Management System (FIRMS).

Table 1 | Mean Pb isotopic composition of NLCIL coal & fly ash, local solid waste & biomass burning ashes, NLCIL topsoil, ore and $PM_{2.5}$ aerosols sampled in the years 2020, 2021 and 2022

Sample	N	Parameter	$^{208}Pb/^{206}Pb$	$^{206}Pb/^{207}Pb$	$^{208}Pb/^{207}Pb$	$^{206}Pb/^{204}Pb$	$^{207}Pb/^{204}Pb$	$^{208}Pb/^{204}Pb$
Coal and fly ash	9	Mean	2.2570	1.0961	2.4734	17.1161	15.6134	38.6164
		Standard deviation	0.0430	0.0185	0.0160	0.3375	0.0669	0.3180
Solid waste & biomass burning	6	Mean	2.1451	1.1349	2.4343	17.7173	15.6116	38.0035
		Standard deviation	0.0291	0.0058	0.0263	0.1225	0.0385	0.3701
NLCIL topsoil	2	Mean	2.1940	1.1193	2.4556	17.4213	15.5643	38.2196
		Standard deviation	0.0204	0.0140	0.0078	0.2472	0.0261	0.1862
Ore	3	Mean	2.2027	1.0543	2.3223	16.5364	15.6842	36.4244
		Standard deviation	0.0006	0.0007	0.0010	0.0427	0.0296	0.0844
$PM_{2.5}$ aerosols								
October 2020	6	Mean	2.1252	1.1342	2.4104	17.6910	15.5974	37.5958
		Standard deviation	0.0082	0.0053	0.0020	0.0846	0.0069	0.0381
November 2020	3	Mean	2.1267	1.1345	2.4128	17.6925	15.5946	37.6267
		Standard deviation	0.0043	0.0041	0.0038	0.0683	0.0166	0.0772
December 2020	3	Mean	2.1239	1.1360	2.4127	17.7188	15.5977	37.6321
		Standard deviation	0.0039	0.0033	0.0027	0.0578	0.0062	0.0537
April 2021	3	Mean	2.1176	1.1419	2.4180	17.8250	15.6104	37.7460
		Standard deviation	0.0026	0.0025	0.0023	0.0406	0.0046	0.0411
May 2021	3	Mean	2.1244	1.1368	2.4151	17.7476	15.6114	37.7038
		Standard deviation	0.0013	0.0018	0.0024	0.0239	0.0088	0.0312
June 2021	3	Mean	2.1195	1.1411	2.4186	17.8177	15.6145	37.7646
		Standard deviation	0.0095	0.0083	0.0068	0.1190	0.0131	0.0833
October 2021	3	Mean	2.1300	1.1308	2.4086	17.6277	15.5887	37.5465
		Standard deviation	0.0066	0.0059	0.0053	0.0605	0.0298	0.0192
November 2021	3	Mean	2.1232	1.1372	2.4144	17.7247	15.5865	37.6324
		Standard deviation	0.0074	0.0071	0.0072	0.1329	0.0190	0.1565
December 2021	3	Mean	2.1242	1.1355	2.4121	17.7092	15.5953	37.6180
		Standard deviation	0.0077	0.0068	0.0058	0.1222	0.0164	0.1241
February 2022	6	Mean	2.1221	1.1380	2.4149	17.7583	15.6051	37.6855
		Standard deviation	0.0028	0.0031	0.0035	0.0541	0.0067	0.0687

of Neyveli), indicates that thermal inversion can fully control the vertical extent of aerosols[103]. Further research across various locations in India confirmed that thermal inversion, rather than the atmospheric boundary layer, predominantly restricts aerosol vertical distribution. In contrast to the post-monsoon months, the lower EF_{Pb} during April to June can be due to a reduced land-based pollution influence over the ocean. In fact, during the summer months there is a decrease in the EF of all the heavy metals compared to the post-monsoon period. (Fig. 2b) There was also an increase in local fire events in the months of April and May compared to October to December (Fig. 3a–k), that could have resuspended a higher amount of desiccated crustal dust resulting in an increased $PM_{2.5}$ load and simultaneous decreased EF[104,105]. A Spearman correlation between the number of fire events versus EFs reveals strong negative correlation with anthropogenic elements and positive correlation with $PM_{2.5}$ load. (Fig. 3l). Thus, the post-monsoon months may have been influenced by both long range as well as local sources, while local sources were predominant in the summer months. A better understanding of the sources can be obtained from elemental ratios.

Elemental ratios are useful tracers for understanding pollution sources. Ratio between V and Pb (V/Pb) are tracers for coal combustion, vehicular and industrial emissions. Coal combustion typically has V/Pb ratios of >1, in contrast to vehicle exhaust emissions, where V/Pb < 1, and industrial emissions, where $V/Pb \ll 1$[30,32,33,35]. None of the aerosol samples exhibited V/Pb > 1. Instead, all the V/Pb ratios for the aerosols varied in the region of industrial and traffic emission source signatures. A bivariate plot between V/Pb and enriched elements such as Cu/Pb can provide insights about the various sources of metals in $PM_{2.5}$. The plot (Fig. 4a), reveals that the aerosols do not align with the ratios of the coal and fly ash, despite the aerosols being sampled from the vicinity of a coal-fired power plant. In Cu/Pb vs V/Pb space, the crust-coal-fly ash and base metal ore (galena) depict two extreme end members with the signature of open SW & biomass burning lying in between (Fig. 4a). The $PM_{2.5}$ samples fall in between these three end members suggesting a mixture of these three sources. However, a seasonal difference in these ratios can be observed. In the months of October–February, majority of the aerosols have $V/Pb \ll 1$. In contrast, from April to June the aerosols shift towards SW & biomass burning with V/Pb ratios typical of traffic emissions. Moreover, previously sampled aerosols from Delhi's waste dumping site Okhla also overlaps with April–June aerosols from Neyveli, indicating a strong presence of metals generated from SW & biomass burning[34].

During the months of April–June a lower Pb/Al as well as Pb/Fe ratios were observed compared to the post-monsoon months. This suggests a greater crustal contribution during the summer months, likely due to increased pollutant dispersion resulting from absence of temperature inversion, as well as a stronger influence from local biomass burning events. Local evidences of sugarcane residue burning was observed on site. In Tamil Nadu, the primary crops are rice and sugarcane, with sugarcane being the dominant crop, produced at nearly three times the quantity of rice[106]. Of the total crop yield, ~13% is burnt as residue. Notably, certain areas in Tamil

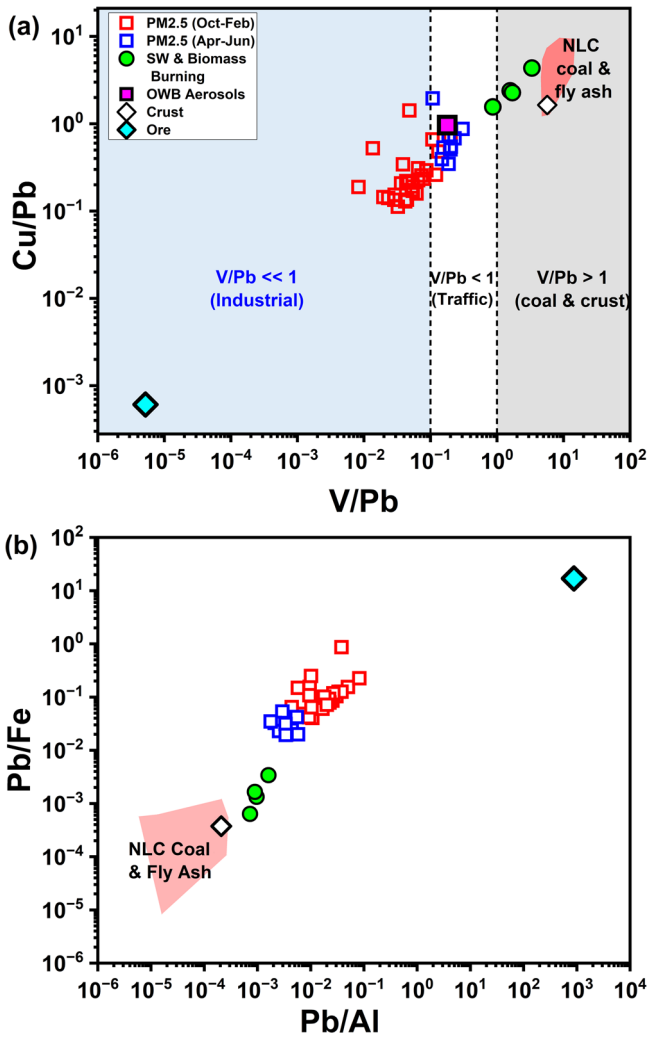

Fig. 4 | Elemental ratios in $PM_{2.5}$ aerosols depicting influence of different sources. Elemental ratios plotted as (**a**) V/Pb vs Cu/Pb (**b**) Pb/Al vs Pb/Fe indicate that the $PM_{2.5}$ aerosols are a mixture of crust, coal & fly ash, solid waste & biomass burning and industrial smelting (depicted as ore in the figure). The characteristic V/Pb ratios for industrial, traffic and coal/crustal sources (Das et al.[32]) are marked as shaded regions for reference. The October-February aerosols have V/Pb ≪ 1 and hence plot in the region of industrial emissions. The open waste burning aerosols from Delhi's Okhla landfill site (Kumar et al.[34]) overlapping with April–June aerosols is plotted in V/Pb vs Cu/Pb space for reference. The April-June aerosols seem to be more influenced by solid waste & biomass burning and crustal sources with decreased Pb/Fe and Pb/Al ratios.

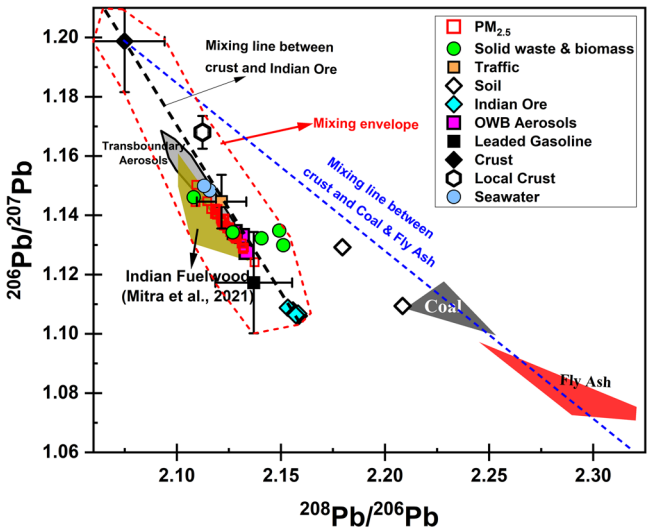

Fig. 5 | The Pb isotopic compositions of the $PM_{2.5}$ aerosols and relevant end members illustrated in three-isotope space ($^{208}Pb/^{206}Pb$ vs $^{206}Pb/^{207}Pb$). Two distinct mixing lines are observed in the tree-isotope plot, each with crust at one end: one extends to Neyveli lignite (blue dotted line), while the other extends to Indian ore (black dotted lines). The Pb isotopic compositions of the PMs lie along the mixing line between Indian ore and crust, rather than local lignite and fly ashes. The aerosols lie close to vehicular exhaust emissions (traffic) and seawater, with less radiogenic local crust also plotting close to the aerosols compared to UCC. There is a considerable overlap between the aerosols and Indian fuelwood, local solid waste & biomass burning signatures. Isotopic signatures of previously sampled aerosols from Delhi's Okhla landfill, overlap with the Neyveli aerosols. The enclosure formed by the red dotted line signifies the mixing envelope formed using the relevant end members. The data for Indian fuelwood and OWB aerosols have been adopted from Mitra et al.[108] and Kumar et al.[34] respectively. Data for traffic emissions, Indian ore, crust, seawater, and local crust have been compiled from Ray and Das[113], Deb et al.[37], Lee et al.[109] and Chakraborty et al.[110] respectively.

Nadu are also recognized as hotspots for PM emissions resulting from the burning of crop residues generated from rice, wheat, maize, and sugarcane cultivation[106]. The concentration of Pb in biomasses is typically much less than other industrial processes, that may have resulted into a lower Pb/Al and Pb/Fe ratios from April–June compared to the post-monsoon months. A bivariate plot between Pb/Al and Pb/Fe (Fig. 4b) provides similar inferences as the Cu/Pb vs V/Pb plot, with all the aerosols falling between crust, coal & fly ash, SW & biomass burning and ore. The summer aerosols lie closer to the open waste burning signatures and crust compared to post-monsoon aerosols. This suggests that there can be a greater influence of crust in the summer aerosols compared to the post-monsoon ones. Moreover, open burning of biomass and SW, together with emitting signatures from vegetation and SW also dehydrates the soil, increases local atmospheric turbulence due to fire-related convective currents, and subsequently mobilises the dehydrated soil particles in the air[105]. Thus, the elemental compositions during fire events may include signatures from vegetation and SW combustion, as well as contributions from crustal dust due to soil resuspension.

To identify the sources, aerosol samples and potential end members are plotted in a three-isotope space using the ratios of $^{208}Pb/^{206}Pb$ vs $^{206}Pb/^{207}Pb$ (Fig. 5). Thus, in the three-isotope space two distinct mixing lines can be formed, each with the natural background crust at one end. One of the mixing lines extends to Neyveli lignite (blue dotted line), while the other extends to Indian ore (black dotted lines) at their respective ends (Fig. 5). The Pb isotopic compositions of the PMs lie along the mixing line between Indian ore and crust[37,107,108], instead of the local lignite and fly ashes (Fig. 5). In fact, the $PM_{2.5}$ samples demonstrate significantly dissimilar compositions from coal and fly ash, indicating minimal influence from them. The Pb isotopic composition of the aerosols lie in the vicinity of vehicular exhaust emissions and seawater[30,109]. Local crust being significantly less radiogenic also lies close to the aerosols compared to upper continental crust (UCC)[110,111]. Notably, there is a considerable overlap of the aerosols with that of Indian fuelwood[108] and local SW & biomass burning signatures. Isotopic signatures of previously sampled aerosols from Delhi's Okhla landfill, where burning is prevalent also overlap with the Neyveli aerosols[34]. In the post-monsoon months as some of the airmasses originate from the coasts of southeast Asia, influence of transboundary aerosols can be present (Fig. 3h–j). In fact, the Neyveli $PM_{2.5}$, aerosols have substantial overlap with aerosols from Thailand, indicating presence of transboundary sources in the post-monsoon months (Fig. 5). The mean Pb isotopic composition of the summer aerosols is about 6‰ more radiogenic in terms of $^{206}Pb/^{207}Pb$ and $^{208}Pb/^{206}Pb$ ratios than the post-monsoon aerosols indicating a seasonal shift in sources (Table 1). A higher radiogenic signature can be indicative of higher natural contributions (crust and seawater). This increase in crustal component can be due to airmasses originating from ocean (Fig. 3) and soil

resuspension due to burning. This increased resuspension during burning, also may mobilise the Pb deposited in the past century from leaded gasoline use. Lead emitted from leaded gasoline in the 20th century was eventually deposited onto soils, where it accumulated over time. Due to its long residence time of ~200 years in soil[112], Pb remains bound to soil particles. However, during fire events, the intense heat and turbulence cause the desiccated soil to become airborne, resuspending the previously deposited Pb back into the atmosphere. Recent studies have found evidences of such resuspended Pb contributing towards atmospheric Pb load[113,114] Consequently, leaded gasoline also comes into play as a potential source. There are evidences from across the globe, demonstrating that leaded gasoline is still recirculating in the atmosphere[30,114,115]. Previous study in the Indo-Gangetic plain finds evidence of high contribution of legacy lead in biomass samples[108]. Thus, the aerosols are primarily a mixture of open waste burning, industrial smelting, traffic emissions, natural sources (crust and seawater), and leaded gasoline, with their respective contribution varying in summer and post-monsoon period. The regional soil appears to have been contaminated by the coal combustion process.

Over the past decade, only five studies have measured the Pb isotopic compositions of Indian aerosols, primarily in PM_{10} samples from diverse settings, such as urban, rural, industrial, and waste-burning sites[32–35,108]. As Pb mostly concentrates in the finer fraction of the aerosols, Pb isotopic composition can be considered a reliable tracer of anthropogenic emissions. Thus, a comparison between Pb isotope ratios can provide insights into the distinct influences on aerosol isotopic composition in different environments. In $^{208}Pb/^{206}Pb$ space (Supplementary Fig. 5), aerosols linked to industrial and urban sources exhibit higher $^{208}Pb/^{206}Pb$ ratios compared to Neyveli $PM_{2.5}$ aerosols[32–34]. Dust storm aerosols show significantly different median ratios due to the influence of dust from the Middle East (Mood's median test; $p < 0.0003$)[35]. The study conducted in Delhi's open-waste burning (OWB) site and urban area records lower median $^{208}Pb/^{206}Pb$ ratios (median = 2.1313) in the OWB aerosols compared to the urban ones (median = 2.1374)[34]. Thus, the median $^{208}Pb/^{206}Pb$ ratios of the OWB aerosols plot closer to the median $^{208}Pb/^{206}Pb$ ratios of Neyveli aerosols. The closest median $^{208}Pb/^{206}Pb$ ratios to the Neyveli $PM_{2.5}$ aerosols ($median_{post\text{-}monsoon}$ = 2.1248; $median_{summer}$ = 2.1211) are observed in rural aerosols (median = 2.1222) and high-altitude aerosols (median = 2.1222). Rural aerosols can be under the influence of biomass burning as a source of fuelwood, while the high altitude aerosols are proven to have been influenced by wood charcoal burning[108]. In fact, the Pb isotopic compositions of the wood charcoal have significant overlap with the Neyveli aerosols in the triple isotope space (Fig. 5). During the post-monsoon season the Neyveli aerosols exhibit higher $^{208}Pb/^{206}Pb$ ratios compared to the summer samples indicating increased influence from the urban and industrial sources (Supplementary Fig. 5).

In the 3D mixing polygon simulation, the median probabilities of all the aerosols falling inside the mixing envelope formed by sources indicate whether all sources have been considered or some are missing[116]. In this simulation, polygons, that is, convex hulls (mixing envelops) are generated (1500 iterations) based on the distribution of the considered sources and their SDs. The mixing polygon simulation is based on the principle that the isotopic composition of the mixture (aerosols for this study) can be explained by the isotopic compositions of the sources forming the mixing envelope only if the mixture doesn't fall outside 5% of the generated polygons. The sample(s) with less than 5% probabilities has/ve sources other than the considered end members and hence the selected sources cannot explain the composition of that particular mixture. From the elemental ratios and the mixing line in the triple isotope plot, it is evident that the relevant sources are: crust, vehicle exhaust, SW & biomass burning and industrial smelting. In the post-monsoon months, significant amounts of airmass originate from the coasts of southeast Asia (Fig. 3), thus, making it necessary to consider the transboundary aerosol as a source in the months of October–February. Incorporating the mean Pb isotopic composition of Thailand aerosols[117,118] as a source significantly increases the median probability by 11% (ANOVA; $p < 0.0001$). In the summer months, the airmasses primarily originate from the ocean, making it a crucial component of the mixing envelope. Including seawater as a source increased the probability by 4.3%. Leaded gasoline, though phased out in 2000, can still contribute to $PM_{2.5}$ aerosols through soil resuspension[30,108,114,115]. In the triple isotope space, leaded gasoline plots close to the less radiogenic $PM_{2.5}$ aerosols. Including leaded gasoline as a source significantly increases the median probability (ANOVA; $p < 0.0001$), validating it as a necessary end member. Finally, as the local crust of southern India, is significantly different from UCC, it is also considered as a source[110,111]. Figure 6a illustrates all the changes in the median probabilities as each source is successively added. None of the aerosol samples demonstrated probability <5%. By incorporating all these sources to define the mixing envelope, the total median probability reaches 0.68. This indicates that all aerosols are a mixture of the accounted sources with varying contributions from respective sources. Despite differing in isotopic and elemental compositions, coal and fly ash must be considered as sources, as the aerosol samples are from a lignite-fired power plant. However, the inclusion of coal & fly ash as a source does not increase the probability at all (Fig. 6a), indicating limited influence of the source on $PM_{2.5}$ aerosols. Thus, the mixing envelope (marked in red dotted line in Fig. 5), comprises of UCC, local crust, seawater, vehicular fuel, SW & biomass burning, Indian fuelwood, transboundary aerosols and Indian ore. The mean Pb isotopic compositions and Pb concentrations of all the sources fed to the simulation along with their references are listed in Supplementary Table 4.

The quantification of the contribution of these sources is performed using Bayesian statistical model MixSIAR in R, presented in Fig. 6b. Transboundary aerosols are only relevant in the post-monsoon months due to long range transport during the season and contributes up to 36%. However, consistent contribution from SW and biomass burning was observed across the seasons (up to 26% in post-monsoon season and up to 22% in summer), indicating their significant role as a pollution source throughout the year. In both post-monsoon and summer months there are significant contributions from background natural sources. (crust + seawater). This contribution from natural sources increases in the summer months, with maximum contribution reaching up to 49%, which is 27% in post-monsoon. As this natural contribution increases in the summer months, so does the contribution from leaded gasoline. This increase in contribution of natural component can be explained by airmass back trajectories and their associated consequences (Fig. 3). In summer, airmass back trajectories demonstrate no influence from transboundary aerosols, originating predominantly from short ranges and subsequently making the impacts of local burning such as dehydrated soil resuspension prominent. Thus, an increase in the relative crustal contribution and, consequently, the contribution of leaded gasoline from soil resuspension is observed in the summer months. Similar persistence of legacy Pb in the atmosphere has been recorded worldwide. Recent studies, utilizing Pb isotopic analyses, of aerosols in London observed long-term persistence of Pb from historically deposited leaded petrol in London's atmosphere, despite its ban in the year 2000[114,119]. Even though Pb levels in the air have significantly dropped since the ban in London, about 32 ± 10 to 43 ± 9% of airborne Pb still originates from the resuspension of Pb-contaminated dust and soil, which was initially deposited in the 20th century[114]. Similar findings have been reported from South-East Asian countries, where Pb isotopic composition of aerosols prove substantial contributions (up to 39%) of legacy Pb[113]. In India, similar Pb isotopic analysis revealed that over 50% of the Pb in Himalayan aerosols still comes from leaded gasoline, even 15 years after its phase-out[108].

In post-monsoon period, transboundary aerosols become a dominating factor, reducing the relative contribution of crustal sources and subsequently that of leaded gasoline. In both seasons a modest contribution form vehicular emissions (<10%) can be observed. Although, the aerosols lie on the mixing line joining crust and Indian ore, negligible contribution from ore is observed from MixSIAR analysis. Most importantly, MixSIAR results indicate negligible influence of coal and fly ash throughout the year in the vicinity of lignite-fired powerplant. This also confirms previous qualitative observations from elemental ratios and Pb isotopic compositions.

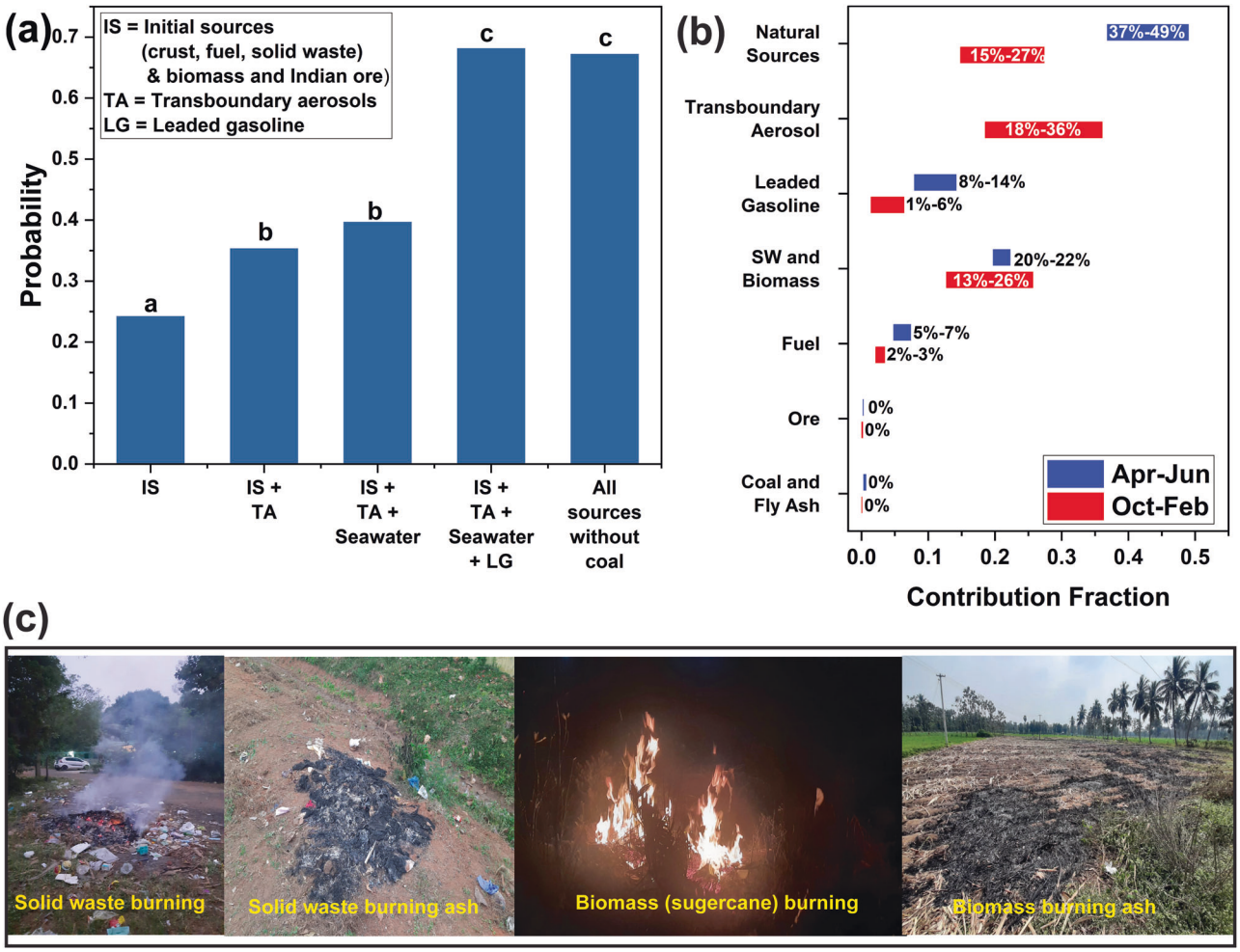

Fig. 6 | Relevance of the sources considered and the contribution of individual sources to atmospheric Pb along with field evidence of open burning. a Bar plots depicting the median probability of the aerosol mixtures to fall inside the mixing envelope constructed by the initial and additional sources with each source added successively. The probabilities are determined with the help of 3 – dimensional mixing polygon simulation in $^{206}Pb/^{207}Pb$, $^{208}Pb/^{207}Pb$ and $^{208}Pb/^{206}Pb$ space. Same letters above the bars indicate that the probabilities are not significantly different, as determined by Tukey's method. Addition of transboundary aerosols and leaded gasoline significantly increased the median probability. Exclusion of Neyveli coal & fly ash does not affect the results. **b** Median contribution of individual sources towards atmospheric Pb determined from MixSIAR simulation. The percentages over/beside the bars represent the range of contributions from each source. MixSIAR results indicate negligible influence of coal and fly ash throughout the year in the vicinity of lignite fired powerplant. Open burning of solid waste and biomass emerges as the major anthropogenic contributor, even in a region of coal combustion. **c** Field photographs of solid waste & biomass burning at Neyveli.

In the study area, the lignite storage yards, lignite transferring regions from mine to power plant and connecting roads with heavy vehicles are equipped with water sprinklers to control fugitive emissions[120]. The power plants have water sprinklers and dust extraction systems in lignite handling and conveying systems to minimize dust generation. Boilers are equipped with ESP in order to regulate stack emissions. The stacks are 220 m in height in 3 of the 5 power plants, while the new plant, "Neyveli New Thermal Power Plant (NNTPP)," that obtained environment clearance in 2010, has a stack of height 270 m for ensuring better pollutant dispersal. Additionally, lignite crusher houses and fly ash storages are also equipped with bag filters. Metal composition and Pb isotopes of $PM_{2.5}$ suggests minimal influence of coal emissions as a result of effective regulatory measures in the coal combustion processes, leading to reduced heavy metal contamination in the atmosphere.

The SIPCOT industrial complex in the region covers a total area of 709.31 acres, housing 21 highly polluting red, 6 orange and 3 green category industries. Emissions from chemical and petrochemical facilities include pollutants such as PM, inorganic and volatile organic compounds, while pharmaceutical and textile dye industries additionally release various organic and inorganic compounds. There are several wood and coal-fired boilers associated with these industries emitting PM on regular basis. Wood-fired boilers contribute to emissions similar to those generated by biomass burning. The industries on average have a stack height of only 24.9 m and releases a total of around 179 kg/ day of PM[121]. Majority of these industries employ dust collectors, cyclone separators, and bag filters for controlling PM emissions. The Neyveli $PM_{2.5}$ does not show influence of ore indicating industrial emission controls are effective.

Apart from thermal power plants and other industries, the region experiences emissions from open burning of crop residues, residential fuelwood burning and SW burning. The dumpsites face spontaneous or deliberate burning of municipal SW resulting in generation of organic as well as metal pollutants in the atmosphere[122]. Majority of the rural households in Tamil Nadu use biofuels such as fuelwood, wood-chips and agricultural waste for cooking purposes releasing respirable PMs[123]. In the district of Cuddalore alone, there are 905 villages that shows dependence on biomass burning as their source of energy[124,125]. As per 2018, Tamil Nadu generated 31.62 MT of crop residue out of which 4.11 MT was burnt[106]. Open burning of SW and biomass have been observed at Neyveli during the sampling period (Fig. 6c).

In India, the top five states with the highest power generation capacity from coal are Uttar Pradesh, Maharashtra, Chhattisgarh, Madhya Pradesh, and Gujarat, with the largest individual coal-fired power plants located in

Madhya Pradesh, Gujarat, Maharashtra, Uttar Pradesh, and Odisha[9]. Among these regions, Gujarat lacks recent literature on the elemental composition of aerosols. In the absence of Pb isotopic data, the V/Pb ratio serves as a reliable alternative tracer for coal combustion. Given the high V content in coal, the V/Pb ratio from coal combustion is consistently greater than 1. In contrast, other anthropogenic sources, such as vehicular exhaust and industrial emissions, typically exhibit V/Pb < 1 and ≪1 respectively[32,33,35,113]. Thus, V/Pb ratios from the literature were compiled over the last decade to gain a national perspective on whether atmospheric Pb is sourced from coal combustion. V/Pb ratios from several key locations were compiled having coal-fired power plants nearby: Madhya Pradesh (Singrauli), Jharkhand (Jharia), Assam (Jorhat), West Bengal (Bandel and Kolaghat), Odisha (Bhubaneshwar), Andhra Pradesh (Vizag), Telangana (Hyderabad), Maharashtra (Trombay), Chhattisgarh (Raipur), Delhi, and Uttar Pradesh (Kanpur)[32–34,55,92,95,126–131]. Figure 7 illustrates the location of the aerosol sampling sites along with the nearby thermal power plants. Majority of the locations, except Jharia, Raipur, and Hyderabad, record V/Pb < 1[128,129,131]. Even in Jharia, Raipur, and Hyderabad, a significant proportion of aerosols demonstrate V/Pb < 1[128,129,131]. Notably, in Singrauli, home to India's largest individual coal-fired power plant, all aerosols exhibit V/Pb ratios ≪1[126]. Similarly, aerosols from Odisha, Uttar Pradesh, West Bengal, Andhra Pradesh, Maharashtra, and Delhi consistently record V/Pb ratios <1[32–34,55,92,95,130]. In 2008 at Jorhat V/Pb ratios in aerosols were recorded to be >1, which decreased to <1 in 2020, indicating a reduced coal combustion emission over the years in the region (Fig. 7). Despite India having 295 coal-fired power plants across the country[9], atmospheric aerosols in most regions demonstrate V/Pb ratios <1, suggesting that coal combustion may not be the dominant source of atmospheric Pb in the country. Among these studies, the aerosols from Jorhat, Raipur, Trombay, and Vizag were found to have contributions from biomass burning despite the presence of coal-fired power plants nearby[95,127,129,130]. Moreover, the only Pb isotopic study conducted near a coal-fired power plant, in Bandel, West Bengal, also identifies high-temperature industrial processes, rather than coal combustion, as the primary source of atmospheric Pb in the region[32]. Another study conducted at an industrial site in Delhi, just 56 km away from a major thermal power plant (NTPC Dadri) also finds no significant contribution of coal combustion towards atmospheric Pb[34]. Previous studies utilizing Pb isotopic compositions and elemental concentrations have highlighted the contribution of biomass and SW burning at specific locations[34,95,108,126,127,129,130]. Our findings also align with these results, emphasizing the need for stricter controls on open burning of SW and biomass to reduce the emission of heavy metals into the atmosphere. The dominance of open burning as a pollution source concurs with the GAINS model and highlights the pressing necessity for better waste management strategies to reduce its environmental impact. Thus, India needs to redefine her pollutant priorities and act accordingly to mitigate their effect.

Methods

Study area

The study was conducted in and around the largest power supplying lignite fired plant of Southern India located in the state of Tamil Nadu (Cuddalore district) and operated by Neyveli Lignite Corporation India Limited (NLCIL). Neyveli is located roughly 197 km south of Chennai and 52 km inland from the BoB. It covers an area of 835 km^2. The Ponnaiyar River borders the town to the north, the Coleroon River to the south, and the BoB to the east. At Neyveli there are 3 operational open cast lignite mines (Mine I, Mine IA and Mine II) with a lignite reserve of about 1357 million tons, that belongs to the tertiary geologic era (~25 MYA). The combined yearly production capacity of the mines stands at 28.5 million tonnes. At present, NLCIL operates five pit-head thermal power generation stations with a total installed capacity of 3390 MW, all fueled by the mined lignite. The total area covered by the mines and power plant is around 206 km^2 [132]. In addition to the lignite mines and power plants, the region also houses several small, medium and large-scale industries ranging from chemical, pharmaceutical, textile, fertilizers, automotive etc within the State Industries Promotion Corporation of Tamil Nadu (SIPCOT) industrial complex, established in 1984 (Supplementary Fig. 6).

In the study area, Tamil Nadu pollution control board report reveals exceedance of several air pollutants such as suspended particulate matter (SPM), PM_{10}, Gaseous Hg, SO_x and NO_x from the NAAQS[120].

Sample collection

Sampling of $PM_{2.5}$ and the end members (lignite, fly ash, topsoil, crop ash and SW burning ash) took place in and around NLCIL between October 2020 and April 2022. The $PM_{2.5}$ sampling was performed with Envirotech APM 550 MFC sampler at a constant flow rate of 1 m^3/h. The samples were collected in pre-weighed 46.2 mm Whatman PTFE filters with a pore size of 2 μm. Before sampling, the filter papers were acid-washed in 1 N double-distilled HCl at 140 °C followed by multiple rinses with ultrapure water (resistivity>18.2 MΩ-cm). Finally, the filter papers were dried at 60 °C[133]. Following sampling, the filters were transferred to a desiccator and kept for 24 h, following which the final weights were recorded. Subsequently, they were carefully packed into resealable zip-lock bags for subsequent chemical analysis.

Concentration and Pb isotope determination

Sample processing was performed in clean chemistry laboratory using Milli-Q water (resistivity >18.2 MΩ-cm) and acids purified by sub-boiling distillation of concentrated reagent grade acids. The aerosol samples were subjected to hot plate digestion in screw cap Teflon beakers (Savillex™) for 24 h at 120 °C in a mixture of concentrated 3:1 HNO_3 and HF. About 20 mg of the top soil, SW burning ash, biomass burning ash, fly ash and coal samples were weighed and subjected to the same digestion procedure. Prior to acid digestion, the coals were ashed in a muffle furnace at 300 °C for 1 h and 500 °C for the next two hours[134]. The digested samples were evaporated to dryness. The dried samples were redissolved and refluxed twice in concentrated HNO_3 to remove traces of HF. The solutions were dried down and redissolved in 2 mL of 2% HNO_3, half of which was utilized for determination of elemental concentration and the other half was stored for performing anion exchange chromatography to separate Pb. For separation of Pb, the samples were dried down and redissolved in 1.1 N HBr and loaded in columns packed with anion exchange resin (Eichrom AG-1×8 chloride form, 200–400 mesh). Finally Pb was eluted in 6 N HCl[135].

The Thermo Scientific iCAP Q ICP-MS at Earth Observatory of Singapore, Nanyang Technological University, Singapore, was utilized to analyse the elemental concentrations of the samples. The sample introduction setup included a Peltier-cooled quartz cyclonic spray chamber, a PFA concentric nebulizer (100 μL/min), and a demountable quartz torch with a quartz injector. Platinum sampler and skimmer cones were employed at the quadrupole–torch interface. All the samples and standards were diluted in 2% HNO_3. The instrument was operated in a single collision cell mode with kinetic energy discrimination (KED), employing pure helium (He) as the collision cell gas to remove polyatomic interferences. The instrument was tuned in iCAP Q tuning solution comprising of 1 μg/L of Ba, Bi, Ce, Co, In, Li, and U. Multi element calibration standards ranging from 0.1 ppb to 500 ppb were freshly prepared gravimetrically and analyzed to obtain linear calibration curves. A multi-element standard of 10 ppb was used for standard–sample bracketing. Drift corrections and normalization of the obtained raw counts per second (cps) were performed with respect to the bracketing standard. The instrumental operating conditions are presented in Supplementary Table 5.

To determine the extraction efficiency and analytical precision for the measured elemental concentrations, NIST SRM-2783 (urban $PM_{2.5}$) and NIST SRM-2704 (Buffalo River sediment). were digested and analyzed using the methods similar to the corresponding samples. Recoveries of the elements were found to be >90% (Supplementary Table 2).

Pb isotopes were analyzed by Multi-collector ICP–MS (Neptune Plus MC ICP-MS, Thermo-Fisher, Germany) at Earth Observatory of Singapore, Nanyang Technological University, Singapore, equipped with Aridus II desolvating nebulizer (100 μL/min). Instrumental mass fractionation

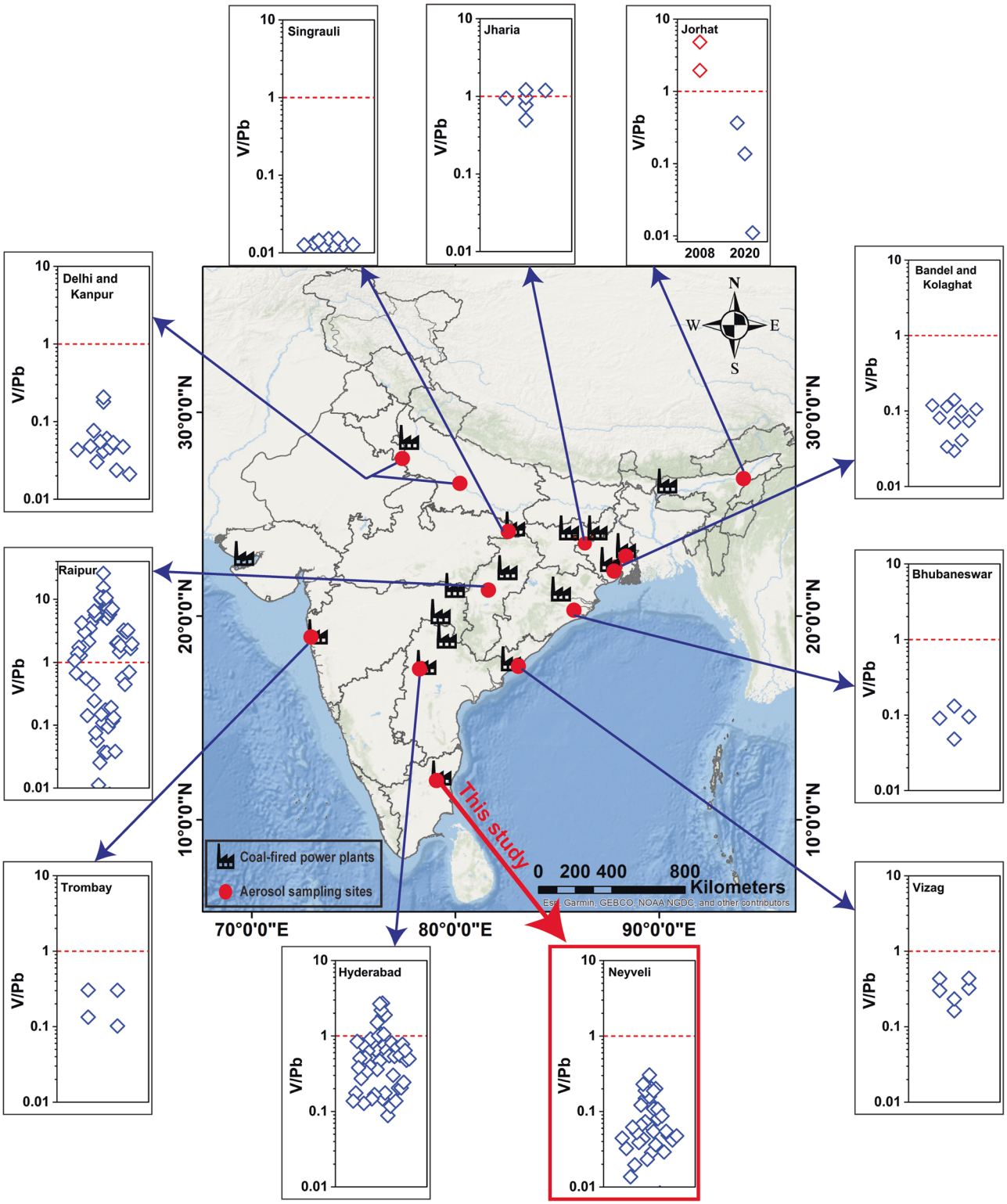

Fig. 7 | Ratios of V/Pb at various locations illustrating the influence of coal combustion towards atmospheric aerosols across India. Map illustrating the aerosol sampling sites and nearby coal-fired thermal power plants. The available V/Pb ratios were compiled from key locations, including Madhya Pradesh (Singrauli)[9], Jharkhand (Jharia)[11], Assam (Jorhat)[10], West Bengal (Bandel and Kolaghat)[1,8], Odisha (Bhubaneshwar)[12], Andhra Pradesh (Vizag)[16], Telangana (Hyderabad)[15], Maharashtra (Trombay)[14], Chhattisgarh (Raipur)[13], Delhi[4], and Uttar Pradesh (Kanpur)[2]. The red dotted line indicates V/Pb > 1. Aerosols demonstrating V/Pb > 1 can be sourced from coal combustion while those having V/Pb < 1 and ≪ 1 can be sourced from vehicular exhaust and high temperature industrial processes1. The base map has been adopted from the open-source online repository Opendatasoft (https://public.opendatasoft.com/explore/dataset/world-administrative-boundaries/export/) and the locations have been illustrated using ArcGIS Pro 10.8. The V/Pb ratios were plotted using Origin Pro 2024a and all the components were compiled in Adobe Illustrator 2021, to form the final illustration.

correction involved Thalium (Tl) (NIST SRM 997) internal normalization ($^{203}Tl/^{205}Tl$ ratio of 0.418911). Bracketing with NIST SRM-981 was adopted to normalize the obtained ratios with respect to the true value[136,137].

All the samples were concentration matched with standard and analysed at comparable Pb/Tl ratios, to minimize the mass bias generated from counting statistics. The precision and accuracy of the measurements were ensured by analysing NIST SRM-981 multiple times between samples as well as at the beginning and end of sessions. The contribution of the procedural blank (median blank = 0.07%) to the total measured concentration were determined as $[Pb]_{procedural\ blank}/[Pb]_{Total}$. Consequently, the blank subtracted $^{206}Pb/^{207}Pb$ and $^{208}Pb/^{207}Pb$ values were determined by mass balance represented by the following equation[138]:

$$\left(\frac{20x}{20y}\right)_{sample} = \left[n_T\left(\frac{20x}{20y}\right)_{total} - n_B\left(\frac{20x}{20y}\right)_{blank}\right]/(n_T - n_{B)}$$

Where, $x = 6, 8$; $y = 7, 6$; n is the fractional amount of substance and the subscripts T, and B refers to total and blank respectively.

Determination of enrichment factor and air mass back trajectories

To distinguish between crustal and anthropogenic origins, the crustal enrichment factor (EF) defined as $EF = \left(\frac{\left(\frac{Element}{Reference\ element}\right)_{Sample}}{\left(\frac{Element}{Reference\ element}\right)_{Crust}}\right)$ for all elements were compared with Al as reference element. The factor $\left(\frac{Element}{Reference\ element}\right)_{Crust}$ was calculated from the composition of UCC[61]. In aerosols, the elements typically have EF ≤ 10, when originating primarily from crustal sources[139]. In this study, both the elements Al, Fe, which are commonly used for calculation of EF were present in considerably high concentrations. However, the concentrations of Fe can have anthropogenic inputs from small-scale industries present in the vicinity. Furthermore, Fe undergoes redox reactions and can be mobilized under various environmental conditions. This mobility can skew the EF calculation, as the concentration of Fe might not accurately reflect its crustal origin due to such geochemical processes. Hence Al was selected as the reference material for calculating EF.

Air-mass back trajectory statistics were obtained using meteorological data for the sampling dates, extending up to 72- h prior. The meteorology data, that included wind speed, wind direction, temperature, humidity, and precipitation, was compiled using the Hybrid Single-Particle Lagrangian Integrated Trajectory (HYSPLIT) model through its graphical user interface[140,141]. This meteorological data was provided as an input into the geographic information system (GIS) based software TrajStat to generate 72-h airmass back trajectories at 500 m above sea level. These trajectories were then converted into a polylineZ shapefile format for spatial representation[142].

Statistical analysis

To assess whether majority of the aerosol mixtures fall within the mixing envelope of the considered end members, a 3–dimensional (3D) mixing polygon simulation (Monte Carlo) was performed in R 4.2.2 (http://www.famer.unsw.edu.au/downloads.html). The simulation was performed in $^{206}Pb/^{207}Pb$, $^{208}Pb/^{207}Pb$, and $^{208}Pb/^{206}Pb$ space where the means and 1 standard deviations (SDs) of the sources were taken into account. The iterations generate mixing envelopes and the number of such envelopes that include within them the aerosols, represent the probability of the aerosols for lying inside the mixing envelope[116].

To quantify the potential source contributions towards aerosol Pb Bayesian statistics-based modeling package, "MixSIAR" available in R was utilized. The model incorporates mean and SDs along with concentration of the end members to produce model fits for the aerosol mixtures through Markov Chain Monte Carlo simulations[143].

Data availability

Full dataset for elemental concentration and lead (Pb) isotopic compositions of $PM_{2.5}$ aerosols and end members are available in **Supplementary Information**.

Code availability

The codes for running the mixing polygon simulation and MixSIAR model in R are available publicly at http://www.famer.unsw.edu.au/software/polygon.html and https://zenodo.org/records/1209993, respectively.

Received: 21 June 2024; Accepted: 11 November 2024;
Published online: 20 November 2024

References

1. Southerland, V. A. et al. Global urban temporal trends in fine particulate matter (PM2·5) and attributable health burdens: estimates from global datasets. *Lancet Planet. Health* **6**, e139–e146, https://doi.org/10.1016/S2542-5196(21)00350-8 (2022).
2. Yu, W. et al. Global estimates of daily ambient fine particulate matter concentrations and unequal spatiotemporal distribution of population exposure: a machine learning modelling study. *Lancet Planet. Health* **7**, e209–e218, https://doi.org/10.1016/S2542-5196(23)00008-6 (2023).
3. UNEP. Air pollution note (accessed 17 June 2023). https://www.unep.org/interactive/air-pollution-note.
4. GAINS South Asia online (accessed 14 June 2023). https://gains.iiasa.ac.at/gains/activities.INN/index.menu.
5. Press Information Bureau. Environment Ministry Notifies Stricter Standards for Coal Based Thermal Power Plants to Minimise Pollution (accessed 19 February 2024). https://pib.gov.in/newsite/printrelease.aspx?relid=133726.
6. Our World in Data. Coal consumption. Our World in Data (accessed 14 June 2023) https://ourworldindata.org/grapher/coal-consumption-by-country-terawatt-hours-twh.
7. Statista. Number of coal power plants by country 2022 (accessed 14 June 2023) Statista. https://www.statista.com/statistics/859266/number-of-coal-power-plants-by-country/.
8. Statista. *Proven coal reserves by country 2020*. Statista (accessed 16 June 2023). https://www.statista.com/statistics/237096/proven-coal-reserves-of-the-top-ten-countries.
9. NITI Aayog. India's Power Sector | Capacity & Generation Mix (accessed 21 September 2024). https://iced.niti.gov.in/energy/electricity/generation.
10. Zhang, J. et al. Emission characteristics of heavy metals from a typical copper smelting plant. *J. Hazard. Mater.* **424**, 127311, https://doi.org/10.1016/j.jhazmat.2021.127311 (2022).
11. Wiedinmyer, C., Yokelson, R. J. & Gullett, B. K. Global emissions of trace gases, particulate matter, and hazardous air pollutants from open burning of domestic waste. *Environ. Sci. Technol.* **48**, 9523–9530, https://doi.org/10.1021/es502250z (2014).
12. Akbari, M. Z. et al. Emission factors of metals bound with PM2.5 and ashes from biomass burning simulated in an open-system combustion chamber for estimation of open burning emissions. *Atmos. Pollut. Res.* **12**, 13–24, https://doi.org/10.1016/j.apr.2021.01.012 (2021).
13. Raparthi, N. & Phuleria, H. C. Real-world vehicular emissions in the indian megacity: carbonaceous, metal and morphological characterization, and the emission factors. *Urban Clim.* **39**, 100955, https://doi.org/10.1016/j.uclim.2021.100955 (2021).
14. Saud, T. et al. Emission estimates of particulate matter (PM) and trace gases (SO2, NO and NO2) from biomass fuels used in rural sector of Indo-Gangetic Plain, India. *Atmos. Environ.* **45**, 5913–5923, https://doi.org/10.1016/j.atmosenv.2011.06.031 (2011).
15. Zhu, J. et al. Emission characterization of particulate matters from the combustion of pulverized coals in a simulated fluidized bed

boiler. *ACS Omega* **7**, 37922–37932, https://doi.org/10.1021/acsomega.2c05080 (2022).
16. Swaine, D. J. *Trace Elements in Coal* (Butterworth-Heinemann, 2013).
17. Rawat, M., Ramanathan, A. L. & Subramanian, V. Quantification and distribution of heavy metals from small-scale industrial areas of Kanpur City, India. *J. Hazard. Mater.* **172**, 1145–1149, https://doi.org/10.1016/j.jhazmat.2009.07.115 (2009).
18. Wiles, C. C. Municipal solid waste combustion ash: state-of-the-knowledge. *J. Hazard. Mater.* **47**, 325–344, https://doi.org/10.1016/0304-3894(95)00120-4 (1996).
19. Jung, C. H., Matsuto, T., Tanaka, N. & Okada, T. Metal distribution in incineration residues of municipal solid waste (MSW) in Japan. *Waste Manag.* **24**, 381–391, https://doi.org/10.1016/S0956-053X(03)00137-5 (2004).
20. Lee, P. H. et al. Characterization, decontamination and health effects of fly ash from waste incinerators. *Environ. Prog.* **17**, 261–269, https://doi.org/10.1002/ep.670170417 (2006).
21. Shim, Y.-S., Rhee, S.-W. & Lee, W.-K. Comparison of leaching characteristics of heavy metals from bottom and fly ashes in Korea and Japan. *Waste Manag* **25**, 473–480, https://doi.org/10.1016/j.wasman.2005.03.002 (2005).
22. Chang, M. B. & Ku, S. Fates and partitioning of heavy metals in municipal solid waste incineration process. *Toxicol. Environ. Chem.* **67**, 161–169, https://doi.org/10.1080/02772249809358611 (1998).
23. Wang, P., Hu, Y. & Cheng, H. Municipal solid waste (MSW) incineration fly ash as an important source of heavy metal pollution in China. *Environ. Pollut.* **252**, 461–475, https://doi.org/10.1016/j.envpol.2019.04.082 (2019).
24. Nguyen, T. H. et al. Distribution characteristics and ecological risks of heavy metals in bottom ash, fly ash, and particulate matter released from municipal solid waste incinerators in Northern Vietnam. *Environ. Geochem. Health* **45**, 2579–2590, https://doi.org/10.1007/s10653-022-01335-4 (2023).
25. Greenberg, R. R., Zoller, W. H. & Gordon, G. E. Composition and size distributions of particles released in refuse incineration. *Environ. Sci. Technol.* **12**, 566–573, https://doi.org/10.1021/es60141a011 (1978).
26. Rasmussen, P. E. Long-range atmospheric transport of trace metals: the need for geoscience perspectives. *Environ. Geol.* **33**, 96–108, https://doi.org/10.1007/s002540050229 (1998).
27. Pacyna, J. M. The origin of arctic air pollutants: lessons learned and future research. *Sci. Total Environ.* **160–161**, 39–53, https://doi.org/10.1016/0048-9697(95)04343-Y (1995).
28. Sturges, W. T. & Barrie, L. A. Stable lead isotope ratios in arctic aerosols: evidence for the origin of arctic air pollution. *Atmos. Environ.* **23**, 2513–2519, https://doi.org/10.1016/0004-6981(89)90263-1 (1989).
29. Sturges, W. T. & Barrie, L. A. Lead 206/207 isotope ratios in the atmosphere of North America as tracers of US and Canadian emissions. *Nature* **329**, 144–146, https://doi.org/10.1038/329144a0 (1987).
30. Ray, I. & Das, R. A lingering legacy of leaded gasoline in Southeast Asia. *Commun. Earth Environ.* **4**, 1–11, https://doi.org/10.1038/s43247-023-01135-3 (2023).
31. Komárek, M., Ettler, V., Chrastný, V. & Mihaljevič, M. Lead isotopes in environmental sciences: a review. *Environ. Int.* **34**, 562–577, https://doi.org/10.1016/j.envint.2007.10.005 (2008).
32. Das, R., Bin Mohamed Mohtar, A. T., Rakshit, D., Shome, D. & Wang, X. Sources of atmospheric lead (Pb) in and around an Indian Megacity. *Atmos. Environ.* **193**, 57–65, https://doi.org/10.1016/j.atmosenv.2018.08.062 (2018).
33. Sen, I. S., Bizimis, M., Tripathi, S. N. & Paul, D. Lead isotopic fingerprinting of aerosols to characterize the sources of atmospheric lead in an industrial city of India. *Atmos. Environ.* **129**, 27–33, https://doi.org/10.1016/j.atmosenv.2016.01.005 (2016).
34. Kumar, S. et al. Understanding the influence of open-waste burning on urban aerosols using metal tracers and lead isotopic composition. *Aerosol Air Qual. Res.* **18**, 2433–2446, https://doi.org/10.4209/aaqr.2017.11.0510 (2018).
35. Kumar, S. et al. Tracing dust transport from middle-east over Delhi in March 2012 using metal and lead isotope composition. *Atmos. Environ.* **132**, 179–187, https://doi.org/10.1016/j.atmosenv.2016.03.002 (2016).
36. Chabukdhara, M. & Singh, O. P. Coal mining in Northeast India: an overview of environmental issues and treatment approaches. *Int. J. Coal Sci. Technol.* **3**, 87–96, https://doi.org/10.1007/s40789-016-0126-1 (2016).
37. Deb, M., Thorpe, R. I., Cumming, G. L. & Wagner, P. A. Age, source and stratigraphic implications of Pb isotope data for conformable, sediment-hosted, base metal deposits in the proterozoic Aravalli-Delhi Orogenic Belt, Northwestern India. *Precambrian Res.* **43**, 1–22, https://doi.org/10.1016/0301-9268(89)90002-8 (1989).
38. Fulekar, M. H., Naik, D. S. & Dave, J. M. Heavy metals in indian coals and corresponding fly-ash and their relationship with particulate size. *Int. J. Environ. Stud.* **21**, 179–182, https://doi.org/10.1080/00207238308710074 (1983).
39. Burmistrz, P., Kogut, K., Marczak, M. & Zwoździak, J. Lignites and subbituminous coals combustion in Polish Power plants as a source of anthropogenic mercury emission. *Fuel Process. Technol.* **152**, 250–258, https://doi.org/10.1016/j.fuproc.2016.06.011 (2016).
40. Chomiak, L.; Widera, M. A comparative study of the oxide and elemental composition of ash from lignite burned at various temperatures – Konin Lignite Mine, Central Poland. *Gospod. Surowcami Miner. - Miner. Resour. Manag*. 2020, 145–160. https://doi.org/10.24425/gsm.2020.133942.
41. Ram, L. C. et al. Potentially toxic elements in lignite and its combustion residues from a power plant. *Environ. Monit. Assess.* **187**, 4148, https://doi.org/10.1007/s10661-014-4148-0 (2014).
42. Mukherjee, S. & Srivastava, S. K. Trace elements in high-sulfur assam coals from the Makum Coalfield in the Northeastern Region of India. *Energy Fuels* **19**, 882–891, https://doi.org/10.1021/ef049775+ (2005).
43. Singh, P. K. et al. Environmental geochemistry of selected elements in lignite from Barsingsar and Gurha Mines of Rajasthan, Western India. *J. Geol. Soc. India* **86**, 23–32, https://doi.org/10.1007/s12594-015-0277-5 (2015).
44. Kortenski, J. & Sotirov, A. Trace and major element content and distribution in neogene lignite from the Sofia Basin, Bulgaria. *Int. J. Coal Geol.* **52**, 63–82, https://doi.org/10.1016/S0166-5162(02)00133-7 (2002).
45. Qi, H., Hu, R. & Zhang, Q. Concentration and distribution of trace elements in lignite from the Shengli Coalfield, Inner Mongolia, China: implications on origin of the associated wulantuga germanium deposit. *Int. J. Coal Geol.* **71**, 129–152, https://doi.org/10.1016/j.coal.2006.08.005 (2007).
46. Ren, D., Xu, D. & Zhao, F. A preliminary study on the enrichment mechanism and occurrence of hazardous trace elements in the tertiary lignite from the Shenbei Coalfield, China. *Int. J. Coal Geol.* **57**, 187–196, https://doi.org/10.1016/j.coal.2003.10.001 (2004).
47. Bouška, V. & Pešek, J. Quality parameters of lignite of the North Bohemian Basin in the Czech Republic in comparison with the world average lignite. *Int. J. Coal Geol.* **40**, 211–235, https://doi.org/10.1016/S0166-5162(98)00070-6 (1999).
48. Filippidis, A. et al. Trace element contents in composited samples of three lignite seams from the central part of the drama lignite deposit, Macedonia, Greece. *Int. J. Coal Geol.* **29**, 219–234, https://doi.org/10.1016/0166-5162(95)00032-1 (1996).
49. Adamidou, K. et al. Chemical investigation of lignite samples and their ashing products from Kardia Lignite Field of Ptolemais, Northern Greece. *Fuel* **86**, 2502–2508, https://doi.org/10.1016/j.fuel.2007.02.008 (2007).

50. Given, P. H. & Miller, R. N. The association of major, minor and trace inorganic elements with lignites. III. Trace elements in four lignites and general discussion of all data from this study. *Geochim. Cosmochim. Acta* **51**, 1843–1853, https://doi.org/10.1016/0016-7037(87)90174-8 (1987).
51. Hower, J. C., Warwick, P. D., Scanlon, B. R., Reedy, R. C. & Childress, T. M. Distribution of rare earth and other critical elements in lignites from the Eocene Jackson Group, Texas. *Int. J. Coal Geol.* **275**, 104302, https://doi.org/10.1016/j.coal.2023.104302 (2023).
52. Rastogi, N. & Sarin, M. M. Quantitative chemical composition and characteristics of aerosols over Western India: one-year record of temporal variability. *Atmos. Environ.* **43**, 3481–3488, https://doi.org/10.1016/j.atmosenv.2009.04.030 (2009).
53. Boreddy, S. K. R., Hegde, P. & Aswini, A. R. Geochemical characteristics of trace elements in size-resolved coastal urban aerosols associated with distinct air masses over tropical peninsular India: size distributions and source apportionment. *Sci. Total Environ.* **763**, 142967, https://doi.org/10.1016/j.scitotenv.2020.142967 (2021).
54. Yadav, S. & Rajamani, V. Geochemistry of aerosols of Northwestern Part of India Adjoining the Thar Desert1. *Geochim. Cosmochim. Acta* **68**, 1975–1988, https://doi.org/10.1016/j.gca.2003.10.032 (2004).
55. Das, R. et al. Trace element composition of PM2.5 and PM10 from Kolkata – a heavily polluted Indian Metropolis. *Atmos. Pollut. Res.* **6**, 742–750, https://doi.org/10.5094/APR.2015.083 (2015).
56. Chakraborty, A., Gupta, T., Mandariya, A. K. & Tripathi, S. Trace elements in ambient aerosols and size-resolved fog droplets: trends, enrichment, and risk assessment. *Heliyon* **9**, e16400, https://doi.org/10.1016/j.heliyon.2023.e16400 (2023).
57. Mehra, M., Zirzow, F., Ram, K. & Norra, S. Geochemistry of PM2.5 aerosols at an urban site, Varanasi, in the Eastern Indo-Gangetic plain during pre-monsoon season. *Atmos. Res.* **234**, 104734, https://doi.org/10.1016/j.atmosres.2019.104734 (2020).
58. Jain, S., Sharma, S. K., Vijayan, N. & Mandal, T. K. Seasonal characteristics of aerosols (PM2.5 and PM10) and their source apportionment using PMF: a four year study over Delhi, India. *Environ. Pollut.* **262**, 114337, https://doi.org/10.1016/j.envpol.2020.114337 (2020).
59. Kulshrestha, A., Satsangi, P. G., Masih, J. & Taneja, A. Metal concentration of PM2.5 and PM10 particles and seasonal variations in urban and rural environment of Agra, India. *Sci. Total Environ.* **407**, 6196–6204, https://doi.org/10.1016/j.scitotenv.2009.08.050 (2009).
60. Pandey, P. et al. Temporal distribution of fine particulates (PM2.5, PM10), potentially toxic metals, PAHs and metal-bound carcinogenic risk in the population of Lucknow City, India. *J. Environ. Sci. Health Part A* **48**, 730–745, https://doi.org/10.1080/10934529.2013.744613 (2013).
61. Rudnick, R. L.; Gao, S. 3.01 - Composition of the Continental Crust. in *Treatise on Geochemistry* (eds Holland, H. D., Turekian, K. K.) 1–64 (Pergamon: Oxford, 2003). https://doi.org/10.1016/B0-08-043751-6/03016-4.
62. Khare, P. & Baruah, B. P. Elemental characterization and source identification of PM2.5 using multivariate analysis at the suburban site of North-East India. *Atmos. Res.* **98**, 148–162, https://doi.org/10.1016/j.atmosres.2010.07.001 (2010).
63. Negi, B. S., Sadasivan, S. & Mishra, U. C. Aerosol Composition and Sources in Urban Areas in India. *Atmos. Environ. 1967* **21**, 1259–1266, https://doi.org/10.1016/0004-6981(67)90072-8 (1986).
64. Gaonkar, C. V., Kumar, A., Matta, V. M. & Kurian, S. Assessment of crustal element and trace metal concentrations in atmospheric particulate matter over a coastal city in the Eastern Arabian Sea. *J. Air Waste Manag. Assoc.* **70**, 78–92, https://doi.org/10.1080/10962247.2019.1680458 (2020).
65. Arun, B. S. et al. Physico-chemical and optical properties of aerosols at a background site (~4 km a.s.l.) in the Western Himalayas. *Atmos. Environ.* **218**, 117017, https://doi.org/10.1016/j.atmosenv.2019.117017 (2019).
66. Bhuyan, P., Deka, P., Prakash, A., Balachandran, S. & Hoque, R. R. Chemical characterization and source apportionment of aerosol over mid Brahmaputra Valley, India. *Environ. Pollut.* **234**, 997–1010, https://doi.org/10.1016/j.envpol.2017.12.009 (2018).
67. Shridhar, V., Khillare, P. S., Agarwal, T. & Ray, S. Metallic species in ambient particulate matter at rural and urban location of Delhi. *J. Hazard. Mater.* **175**, 600–607, https://doi.org/10.1016/j.jhazmat.2009.10.047 (2010).
68. Balachandran, S., Meena, B. R. & Khillare, P. S. Particle size distribution and its elemental composition in the ambient air of Delhi. *Environ. Int.* **26**, 49–54, https://doi.org/10.1016/S0160-4120(00)00077-5 (2000).
69. Pant, P. et al. Characterization of ambient PM2.5 at a pollution hotspot in New Delhi, India and inference of sources. *Atmos. Environ.* **109**, 178–189, https://doi.org/10.1016/j.atmosenv.2015.02.074 (2015).
70. Bandhu, H. K. et al. Elemental composition and sources of air pollution in the city of Chandigarh, India, using EDXRF and PIXE techniques. *Nucl. Instrum. Methods Phys. Res. Sect. B Beam Interact. Mater.* **160**, 126–138, https://doi.org/10.1016/S0168-583X(99)00574-1 (2000).
71. Khillare, P. S. & Sarkar, S. Airborne inhalable metals in residential areas of Delhi, India: distribution, source apportionment and health risks. *Atmos. Pollut. Res.* **3**, 46–54, https://doi.org/10.5094/APR.2012.004 (2012).
72. Khillare, P. S., Balachandran, S. & Meena, B. R. Spatial and temporal variation of heavy metals in atmospheric aerosol of Delhi. *Environ. Monit. Assess.* **90**, 1–21, https://doi.org/10.1023/B:EMAS.0000003555.36394.17 (2004).
73. Gajghate, D. G. & Bhanarkar, A. D. Tracking toxic metals in the ambient air of Agra City, India. *Bull. Environ. Contam. Toxicol.* **72**, 806–812, https://doi.org/10.1007/s00128-004-0316-1 (2004).
74. Gajghate, D. G. & Bhanarkar, A. D. Characterisation of particulate matter for toxic metals in ambient air of Kochi City, India. *Environ. Monit. Assess.* **102**, 119–129, https://doi.org/10.1007/s10661-005-4535-7 (2005).
75. Gajghate, D. G., Talwar, B., Pipalatkar, P. & Pustode, T. Chemical characterization of PM10 for metals in ambient air of Chennai, India. *J. Hazard. Toxic. Radioact. Waste* **16**, 169–174, https://doi.org/10.1061/(ASCE)HZ.1944-8376.0000079 (2012).
76. Panwar, P., Prabhu, V., Soni, A., Punetha, D. & Shridhar, V. Sources and health risks of atmospheric particulate matter at Bhagwanpur, an industrial site along the Himalayan Foothills. *SN Appl. Sci.* **2**, 632, https://doi.org/10.1007/s42452-020-2420-1 (2020).
77. Chelani, A. B., Gajghate, D. G. & Hasan, M. Z. Airborne toxic metals in air of Mumbai City, India. *Bull. Environ. Contam. Toxicol.* **66**, 196–205, https://doi.org/10.1007/s0012800225 (2001).
78. Gaghate, D. G. & Hasan, M. Z. Ambient lead levels in urban areas. *Bull. Environ. Contam. Toxicol.* **62**, 403–408, https://doi.org/10.1007/s001289900889 (1999).
79. Karar, K. & Gupta, A. K. Seasonal variations and chemical characterization of ambient PM10 at residential and industrial sites of an urban region of Kolkata (Calcutta), India. *Atmos. Res.* **81**, 36–53, https://doi.org/10.1016/j.atmosres.2005.11.003 (2006).
80. Singh, R. & Sharma, B. S. Composition, seasonal variation, and sources of PM10 from World Heritage Site Taj Mahal, Agra. *Environ. Monit. Assess.* **184**, 5945–5956, https://doi.org/10.1007/s10661-011-2392-0 (2012).
81. Sudheer, A. K. & Rengarajan, R. Atmospheric mineral dust and trace metals over urban environment in Western India during winter. *Aerosol Air Qual. Res.* **12**, 923–933, https://doi.org/10.4209/aaqr.2011.12.0237 (2012).
82. Yadav, S. & Satsangi, P. G. Characterization of particulate matter and its related metal toxicity in an urban location in south West India.

Environ. Monit. Assess. **185**, 7365–7379, https://doi.org/10.1007/s10661-013-3106-6 (2013).
83. Shukkur, A. M., V.G, G., N.G, V. & Mohan, M. Trace gases and PM2.5-bound metal abundance over a tropical urban environment, South India. *J. Atmos. Chem.* **78**, 193–208, https://doi.org/10.1007/s10874-021-09420-1 (2021).
84. Bikkina, S., Sarin, M. M. & Chinni, V. Atmospheric 210Pb and anthropogenic trace metals in the continental outflow to the Bay of Bengal. *Atmos. Environ.* **122**, 737–747, https://doi.org/10.1016/j.atmosenv.2015.10.044 (2015).
85. Jena, S., Perwez, A. & Singh, G. Trace element characterization of fine particulate matter and assessment of associated health risk in mining area, transportation routes and institutional area of Dhanbad, India. *Environ. Geochem. Health* **41**, 2731–2747, https://doi.org/10.1007/s10653-019-00329-z (2019).
86. Gokhale, S. B. & Patil, R. S. Size distribution of aerosols (PM10) and lead (Pb) near traffic intersections in Mumbai (India). *Environ. Monit. Assess.* **95**, 311–324, https://doi.org/10.1023/B:EMAS.0000029911.81865.b6 (2004).
87. Mishra, V. K. & Padmanabhamutry, B. Performance evaluation of CALINE3, CAL3QHC and PART5 in predicting lead concentration in the atmosphere over Delhi. *Atmos. Environ.* **37**, 3077–3089, https://doi.org/10.1016/S1352-2310(03)00272-3 (2003).
88. Perrino, C. et al. Chemical characterization of atmospheric PM in Delhi, India, during different periods of the year including diwali festival. *Atmos. Pollut. Res.* **2**, 418–427, https://doi.org/10.5094/APR.2011.048 (2011).
89. Sah, D. Concentration, source apportionment and human health risk assessment of elements in PM2.5 at Agra, India. *Urban Clim.* **49**, 101477, https://doi.org/10.1016/j.uclim.2023.101477 (2023).
90. Pipalatkar, P., Khaparde, V. V., Gajghate, D. G. & Bawase, M. A. Source apportionment of PM2.5 using a CMB model for a centrally located Indian City. *Aerosol Air Qual. Res.* **14**, 1089–1099, https://doi.org/10.4209/aaqr.2013.04.0130 (2014).
91. Dubey, B., Pal, A. K. & Singh, G. Trace metal composition of airborne particulate matter in the coal mining and non–mining areas of Dhanbad Region, Jharkhand, India. *Atmos. Pollut. Res.* **3**, 238–246, https://doi.org/10.5094/APR.2012.026 (2012).
92. Panda, U. et al. Metals in coarse ambient aerosol as markers for source apportionment and their health risk assessment over an eastern coastal urban atmosphere in India. *Environ. Monit. Assess.* **193**, 311, https://doi.org/10.1007/s10661-021-09057-3 (2021).
93. Gummeneni, S., Yusup, Y. B., Chavali, M. & Samadi, S. Z. Source apportionment of particulate matter in the ambient air of Hyderabad City, India. *Atmos. Res.* **101**, 752–764, https://doi.org/10.1016/j.atmosres.2011.05.002 (2011).
94. Botle, A., Singhal, R. K., Basu, H., V, M. & Masih, J. Health risk assessment of heavy metals associated with coarse and quasi-accumulative airborne particulate matter in Mumbai City situated on the western coast of India. *Environ. Technol. Innov.* **19**, 100857, https://doi.org/10.1016/j.eti.2020.100857 (2020).
95. Police, S., Sahu, S. K. & Pandit, G. G. Chemical characterization of atmospheric particulate matter and their source apportionment at an emerging industrial coastal city, Visakhapatnam, India. *Atmos. Pollut. Res.* **7**, 725–733, https://doi.org/10.1016/j.apr.2016.03.007 (2016).
96. Basha, S. et al. Assessment of heavy metal content in suspended particulate matter of coastal industrial town, Mithapur, Gujarat, India. *Atmos. Res.* **97**, 257–265, https://doi.org/10.1016/j.atmosres.2010.04.012 (2010).
97. Singh, A. et al. Rapid growth and high cloud-forming potential of anthropogenic sulfate aerosol in a thermal power plant plume during COVID lockdown in India.*NPJ Clim. Atmos. Sci.* **6**, 1–12, https://doi.org/10.1038/s41612-023-00430-2 (2023).
98. Anu, S.; Mohanakumar, K. *Studies on the Paratial and Temporal Distribution of Surface Meteorological Parameters over Indian Subcontinent*. PhD Thesis, Cochin University of Science and Technology, 1996. https://events.cusat.ac.in/xmlui/handle/purl/3160.
99. Aryasree, S., Nair, P. R., Girach, I. A. & Jacob, S. Winter time chemical characteristics of aerosols over the Bay of Bengal: continental influence. *Environ. Sci. Pollut. Res.* **22**, 14901–14918, https://doi.org/10.1007/s11356-015-4700-7 (2015).
100. Srinivas, B., Kumar, A., Sarin, M. M. & Sudheer, A. K. Impact of continental outflow on chemistry of atmospheric aerosols over tropical Bay of Bengal. *Atmos. Chem. Phys. Discuss.* **11**, 20667–20711, https://doi.org/10.5194/acpd-11-20667-2011 (2011).
101. Krishnamurti, T. N. et al. Impact of Arabian Sea Pollution on the Bay of Bengal winter monsoon rains. *J. Geophys. Res. Atmos.* 2009, 114. https://doi.org/10.1029/2008JD010679.
102. EEA. *Temperature inversion traps pollution at ground level — European Environment Agency* (accessed 03 May 2024). https://www.eea.europa.eu/media/infographics/temperature-inversion-traps-pollution-at/view.
103. Prasad, P., Basha, G. & Ratnam, M. V. Is the atmospheric boundary layer altitude or the strong thermal inversions that control the vertical extent of aerosols? *Sci. Total Environ.* **802**, 149758, https://doi.org/10.1016/j.scitotenv.2021.149758 (2022).
104. Das, R. et al. Suspension of crustal materials from wildfire in indonesia as revealed by Pb isotope analysis. *ACS Earth Space Chem.* **7**, 379–387, https://doi.org/10.1021/acsearthspacechem.2c00270 (2023).
105. Wagner, R., Jähn, M. & Schepanski, K. Wildfires as a source of airborne mineral dust – revisiting a conceptual model using large-Eddy simulation (LES). *Atmos. Chem. Phys.* **18**, 11863–11884, https://doi.org/10.5194/acp-18-11863-2018 (2018).
106. Sahu, S. K. et al. Quantifying the high resolution seasonal emission of air pollutants from crop residue burning in India. *Environ. Pollut.* **286**, 117165, https://doi.org/10.1016/j.envpol.2021.117165 (2021).
107. Bi, X.-Y. et al. Lead isotopic compositions of selected coals, Pb/Zn Ores and fuels in China and the application for source tracing. *Environ. Sci. Technol.* **51**, 13502–13508 (2017).
108. Mitra, A. et al. Lead isotope evidence for enhanced anthropogenic particle transport to the Himalayas during summer months. *Environ. Sci. Technol.* **55**, 13697–13708, https://doi.org/10.1021/acs.est.1c03830 (2021).
109. Lee, J.-M. et al. Impact of anthropogenic Pb and ocean circulation on the recent distribution of Pb isotopes in the Indian Ocean. *Geochim. Cosmochim. Acta* **170**, 126–144, https://doi.org/10.1016/j.gca.2015.08.013 (2015).
110. Chakraborty, S. et al. Evidence for increasing anthropogenic Pb concentrations in indian shelf sediments during the last century. *Sci. Total Environ.* **760**, 143833, https://doi.org/10.1016/j.scitotenv.2020.143833 (2021).
111. Millot, R., Allègre, C.-J., Gaillardet, J. & Roy, S. Lead isotopic systematics of major river sediments: a new estimate of the Pb isotopic composition of the upper continental crust. *Chem. Geol.* **203**, 75–90, https://doi.org/10.1016/j.chemgeo.2003.09.002 (2004).
112. Erel, Y. Mechanisms and velocities of anthropogenic Pb migration in Mediterranean soils. *Environ. Res.* **78**, 112–117, https://doi.org/10.1006/enrs.1997.3811 (1998).
113. Ray, I.; Das, R. *Dataset for: A Lingering Legacy of Leaded Gasoline in Southeast Asia*. 2023. https://doi.org/10.5281/zenodo.10101283.
114. Resongles, E. et al. Strong evidence for the continued contribution of lead deposited during the 20th century to the atmospheric environment in London of today. *Proc. Natl Acad. Sci.* **118**, e2102791118, https://doi.org/10.1073/pnas.2102791118 (2021).

115. Carrasco, G. et al. An update of the Pb isotope inventory in post leaded-petrol Singapore environments. *Environ. Pollut.* **233**, 925–932, https://doi.org/10.1016/j.envpol.2017.09.025 (2018).
116. Smith, J. A., Mazumder, D., Suthers, I. M. & Taylor, M. D. To fit or not to fit: evaluating stable isotope mixing models using simulated mixing polygons. *Methods Ecol. Evol.* **4**, 612–618, https://doi.org/10.1111/2041-210X.12048 (2013).
117. Kayee, J., Bureekul, S., Sompongchaiyakul, P., Wang, X. & Das, R. Sources of atmospheric lead (Pb) after quarter century of phasing out of leaded gasoline in Bangkok, Thailand. *Atmos. Environ.* **253**, 118355, https://doi.org/10.1016/j.atmosenv.2021.118355 (2021).
118. Kayee, J. et al. Metal concentrations and source apportionment of $PM_{2.5}$ in Chiang Rai and Bangkok, Thailand during a biomass burning season. *ACS Earth Space Chem.* **4**, 1213–1226, https://doi.org/10.1021/acsearthspacechem.0c00140 (2020).
119. MacKinnon, G. et al. Spatial and temporal variations in Pb concentrations and isotopic composition in road dust, farmland soil and vegetation in proximity to roads since cessation of use of leaded petrol in the UK. *Sci. Total Environ.* **409**, 5010–5019, https://doi.org/10.1016/j.scitotenv.2011.08.010 (2011).
120. TNPCB. *Before the Hon'ble NATIONAL GREEN TRIBUNAL SOUTHERN ZONE, CHENNAI Original Application No.107 of 2023 - Google Search* (accessed 23 February 2024). https://www.google.com/search?q=BEFORE+THE+HON%E2%80%99BLE+NATIONAL+GREEN+TRIBUNAL+SOUTHERN+ZONE%2C+CHENNAI+Original+Application+No.107+of+2023&oq=BEFORE+THE+HON%E2%80%99BLE+NATIONAL+GREEN+TRIBUNAL+SOUTHERN+ZONE%2C+CHENNAI+Original+Application+No.107+of+2023&gs_lcrp=EgZjaHJvbWUyBggAEEUYOdIBBzY2NGowajeoAgCwAgA&sourceid=chrome&ie=UTF-8.
121. TNPCB. *Evaluation of CEPI Score & action plan for CEPI area of Tamilnadu*. https://tnpcb.gov.in/action-plan-form.php (accessed 24 February 2024).
122. Peter, A. E., Shiva Nagendra, S. M. & Nambi, I. M. Environmental burden by an open dumpsite in urban India. *Waste Manag.* **85**, 151–163, https://doi.org/10.1016/j.wasman.2018.12.022 (2019).
123. Parikh, J., Balakrishnan, K., Laxmi, V. & Biswas, H. Exposure from cooking with biofuels: pollution monitoring and analysis for rural Tamil Nadu, India. *Energy* **26**, 949–962, https://doi.org/10.1016/S0360-5442(01)00043-3 (2001).
124. Ranganathan, K., Dhanagopalan, V., Tharumaraj, M. & Annadurai, K. Fuel consumption and expenditure among rural population of Cuddalore District, Tamil Nadu: a cross sectional study. *Int. J. Community Med. Public Health* **7**, 3630–3635, https://doi.org/10.18203/2394-6040.ijcmph20203934 (2020).
125. Velmurugan, S.; Joseph, A. A. *Energy consumption of rural Households in Cuddalore district of Tamil Nadu - ProQuest* (accessed 26 February 2024). https://www.proquest.com/openview/1f04ad64f5bbf098f85c2ff46e677e62/1?cbl=2035897&pq-origsite=gscholar.
126. Yadav, A. K. et al. Enrichment factor and chemical composition of size separated airborne particulate matter of Singrauli Coalfield, India. *Aerosol Sci. Eng.* **6**, 414–436, https://doi.org/10.1007/s41810-022-00155-4 (2022).
127. Rabha, S., Subramanyam, K. S. V., Sawant, S. S. & Saikia, B. K. Rare-earth elements and heavy metals in atmospheric particulate matter in an urban area. *ACS Earth Space Chem.* **6**, 1725–1732, https://doi.org/10.1021/acsearthspacechem.2c00009 (2022).
128. Rout, T. K. et al. Heavy metals in dusts from commercial and residential areas of Jharia coal mining town. *Environ. Earth Sci.* **73**, 347–359, https://doi.org/10.1007/s12665-014-3429-9 (2015).
129. Khobragade, P. P. & Ahirwar, A. V. Source identification and ambient trace element concentrations of PM10 using receptor modeling in an urban area of Chhattisgarh, India. *Geocarto Int.* **37**, 12267–12293, https://doi.org/10.1080/10106049.2022.2066201 (2022).
130. Police, S., Sahu, S. K., Tiwari, M. & Pandit, G. G. Chemical composition and source apportionment of PM2.5 and PM2.5–10 in Trombay (Mumbai, India), a coastal industrial area. *Particuology* **37**, 143–153, https://doi.org/10.1016/j.partic.2017.09.006 (2018).
131. Attri, P. et al. *A Long-Term Study on Sources, Enrichments, and Inhalation Risk Assessments of Aerosols (Pm10) at Urban/Industrial City of Hyderabad in Southern India*. Rochester, NY, 2024. https://doi.org/10.2139/ssrn.4756418.
132. NLCIL. *NLC India Limited* (accessed 23 February 2024). https://www.nlcindia.in/new_website/index.htm.
133. Ray, I., Misra, S., Chen, M., Wang, X. & Das, R. Entrapment of atmospheric particle bound heavy metals by ferns as evidenced by lead (Pb) isotope and MixSIAR: implications for improving air quality. *J. Hazard. Mater.* **469**, 134014, https://doi.org/10.1016/j.jhazmat.2024.134014 (2024).
134. Díaz-Somoano, M. et al. Stable lead isotope compositions in selected coals from around the world and implications for present day aerosol source tracing. *Environ. Sci. Technol.* **43**, 1078–1085, https://doi.org/10.1021/es801818r (2009).
135. Reuer, M. K., Boyle, E. A. & Grant, B. C. Lead isotope analysis of marine carbonates and seawater by multiple collector ICP-MS. *Chem. Geol.* **200**, 137–153, https://doi.org/10.1016/S0009-2541(03)00186-4 (2003).
136. Baker, J., Peate, D., Waight, T. & Meyzen, C. Pb isotopic analysis of standards and samples using a 207Pb–204Pb double spike and thallium to correct for mass bias with a double-focusing MC-ICP-MS. *Chem. Geol.* **211**, 275–303, https://doi.org/10.1016/j.chemgeo.2004.06.030 (2004).
137. White, W. M., Albarède, F. & Télouk, P. High-precision analysis of Pb isotope ratios by multi-collector ICP-MS. *Chem. Geol.* **167**, 257–270, https://doi.org/10.1016/S0009-2541(99)00182-5 (2000).
138. Gelwicks, J. T. & Hayes, J. M. Carbon-isotopic analysis of dissolved acetate. *Anal. Chem.* **62**, 535–539, https://doi.org/10.1021/ac00204a021 (1990).
139. Duce, R. A., Hoffman, G. L. & Zoller, W. H. Atmospheric trace metals at remote northern and southern hemisphere sites: pollution or natural? *Science* **187**, 59–61, https://doi.org/10.1126/science.187.4171.59 (1975).
140. Draxler, R. *An Overview of the HYSPLIT_4 Modelling System for Trajectories, Dispersion, and Deposition*; 1998.
141. NOAA. *GUI Operation* © (accessed 06 September 2024) https://www.ready.noaa.gov/documents/Tutorial_2021/html/test_gui.html.
142. Wang, Y. Q., Zhang, X. Y. & Draxler, R. R. TrajStat: GIS-based software that uses various trajectory statistical analysis methods to identify potential sources from long-term air pollution measurement data. *Environ. Model. Softw.* **24**, 938–939, https://doi.org/10.1016/j.envsoft.2009.01.004 (2009).
143. Longman, J. et al. Quantitative assessment of Pb sources in isotopic mixtures using a Bayesian mixing model. *Sci. Rep.* **8**, 6154, https://doi.org/10.1038/s41598-018-24474-0 (2018).

Acknowledgements

The authors, would like to thank the Centre for Applied Research & Development (CARD) at NLC India Limited (NLCIL) for extending their utmost help and assistance with sample collection. R.D. acknowledges the financial support from Science and Engineering Research Board (Grant no. SPG/2021/002652). S.M.S.N acknowledges the financial support from NLC India Limited (NLCIL) through the industry-sponsored project titled "Development of Mobile EV Based - Real Time Air Quality Monitoring & Modeling for NLCIL" (Project number: RB/1920/CE/270/NLCI/008251). X.W. acknowledges the financial support from the Earth Observatory of Singapore and the Imperial College - Nanyang Technological University Collaboration Fund (INCF-2023-015) and Singapore MOE AcRF Tier 1 (RT22/21). This work comprises Earth

Observatory of Singapore contribution no 633. R.D.'s position is supported by University Grants Commission through the Faculty Recharge Programme (FRP-74) and I.R.'s position is supported by All India Council for Technical Education (AICTE), through the AICTE Doctoral Fellow Programme (S2021280). The Office of Global Engagement, IIT Madras, has provided a scholarship to S.M. through the alumni funding project titled "IITM-NTU JDP" (Project number: SP1920262ALUMDNGLOB) for pursuing his IIT Madras – NTU Singapore Joint Ph.D. Programme. (Guide: Professor S.M.S.N, IIT Madras & Co-guide: Dr. Richard D. Webster, NTU Singapore).

Author contributions

I.R. conducted the sample processing and laboratory analyses, performed data processing, data curation and visualisation and wrote the manuscript. S.M. performed sample collection and edited the manuscript. J.K., and S.Y. conducted laboratory analyses. X.W. supervised and edited the manuscript. S.M.S.N. supervised the sample collection process. R.D. conceived and supervised the research, performed laboratory analyses and edited the manuscript.

Competing interests

The authors declare no competing interests.

Additional information

Supplementary information The online version contains supplementary material available at https://doi.org/10.1038/s41612-024-00836-6.

Correspondence and requests for materials should be addressed to Iravati Ray or Reshmi Das.

Reprints and permissions information is available at http://www.nature.com/reprints

Publisher's note Springer Nature remains neutral with regard to jurisdictional claims in published maps and institutional affiliations.

Open Access This article is licensed under a Creative Commons Attribution-NonCommercial-NoDerivatives 4.0 International License, which permits any non-commercial use, sharing, distribution and reproduction in any medium or format, as long as you give appropriate credit to the original author(s) and the source, provide a link to the Creative Commons licence, and indicate if you modified the licensed material. You do not have permission under this licence to share adapted material derived from this article or parts of it. The images or other third party material in this article are included in the article's Creative Commons licence, unless indicated otherwise in a credit line to the material. If material is not included in the article's Creative Commons licence and your intended use is not permitted by statutory regulation or exceeds the permitted use, you will need to obtain permission directly from the copyright holder. To view a copy of this licence, visit http://creativecommons.org/licenses/by-nc-nd/4.0/.

© The Author(s) 2024

SCHOOL OF ENVIRONMENTAL COMMUNICATIONS

AAETI

ANIL AGARWAL ENVIRONMENT TRAINING INSTITUTE

(A UNIT OF CENTRE FOR SCIENCE AND ENVIRONMENT)

CERTIFICATE OF PARTICIPATION

Global Online Certificate Course

Demystifying Climate Change Data and Maps for Communication in the 21st century

This is to certify that Iravati Ray has participated in the global online certificate course **"Demystifying Climate Change Data and Maps for Communication in the 21st Century"** organised by the School of Environmental Communications, Centre for Science and Environment, India from **December 8 – December 22, 2023**.

With best wishes,

Sunita Narain
Director General

Centre for Science and Environment
Online Course

Centre for Science and Environment
41, Tughlakabad Institutional Area
New Delhi-110 062 INDIA